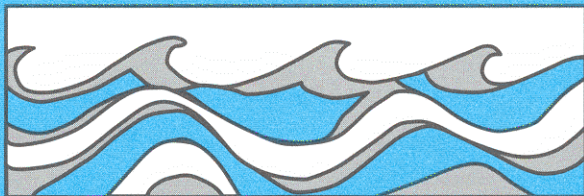University of Washington
Department of Civil and Environmental Engineering

SCOUR IN LOW GRADIENT GRAVEL BED STREAMS: PATTERNS, PROCESSES, AND IMPLICATIONS FOR THE SURVIVAL OF SALMOINID EMBRYOS

Paul DeVries

Seattle, Washington
98195

Department of Civil Engineering
University of Washington
Seattle, Washington 98195

SCOUR IN LOW GRADIENT GRAVEL BED STREAMS: PATTERNS, PROCESSES, AND IMPLICATIONS FOR THE SURVIVAL OF SALMOINID EMBRYOS

Paul DeVries

February 2000

ABSTRACT

A field investigation of scour depth in eleven gravel bed stream reaches between approximately 100 and 300 m long, with slopes between 0.001 and 0.01, showed that scour assessments need to consider two distinct bedload transport mechanisms. Substrate disturbance is caused by (i) bedload layer motion, and (ii) spatial and temporal imbalances in sediment transport rate. This work evaluates both mechanisms in the context of predicting scour depth and salmonid intragravel survival.

Measurements of the maximum depth of substrate disturbed by a moving bedload layer ranged between approximately 1.5 times the 50th (D_{50}) and twice the 90th (D_{90}) percentile particle sizes of the streambed grain size distribution. The upper bound was also approximately equal to 1.5 times the competent grain size, and became independent of flow strength once the largest particles present were mobilized. Disturbance depth did not increase with bedload transport rate because of large stresses needed to mobilize two or more layers of the bed; surface particles may instead move faster to effect a greater transport rate. Reach-average disturbance depth increases with shear stress primarily because a greater bed area becomes active.

Larger magnitude scour depths resulted from three forms of sediment transport rate imbalances. They are, in order of increasing spatial scale: (i) scour and fill of transient, finer grained bedforms located downstream of partial flow obstructions causing differential mobility; (ii) at the pool and riffle scale, where scour depth depends on inter-riffle distances and riffle deposit size and morphology; and (iii) at the reach scale in response to temporal and spatial variability in sediment supply to the channel.

Salmonids may have adapted to these processes by burying eggs greater than 2 to 2.5D_{90} deep, and by constructing redds in locations of the channel least likely to experience significant sediment transport rate imbalances. Adverse effects of floods on intragravel survival may occur indirectly through scour-related fine sediment intrusion, rather than directly through redd scour.

The findings suggest that scour depth in spawning beds is controlled strongly by the size and quantity of gravel and cobble in a reach, and weakly by flood magnitude and duration.

TABLE OF CONTENTS

LIST OF FIGURES

vi

LIST OF TABLES

NOTATION

Symbol	Description	Dimension [1]
a	Long axis diameter of particle	L
A	Area	L^2
b	Intermediate axis diameter of particle	L
c	Short axis diameter of particle	L
c	Flood wave celerity	L/T
c_i	A constant	n
C	Volumetric sediment concentration	n
C_a	Average volumetric sediment concentration of moving layer	n
C_m	Maximum possible volumetric sediment concentration	n
C_o	Static bed volumetric sediment concentration	n
C_δ	Volumetric sediment concentration at top of bedload layer	n
d	Flow (water column) depth	L
d_{cr}	Critical flow depth at incipient motion	L
D	Particle diameter (=b)	L
D_{comp}	Largest particle diameter that the flow can mobilize	L
D_i	i^{th} percentile particle size (e.g., D_{90})	L
D_j	Characteristic particle diameter of size class j	L
D_{1-5}	Scour monitor dimensions (Figure 3-2)	L
e	Coefficient of restitution in a collision	n
f	Darcy-Weisbach friction factor	n
f( )	Function of ( )	v
$\bar{F}$	Froude number = $\sqrt{(U^2/gd)}$	n
g	Acceleration due to gravity	L/T^2
h	Water surface elevation	L
i	Subscript denoting "evaluated for a cell i on a transect"	n
j	Subscript denoting substrate size class j	n
k	Multiple of a particle size	n
k_s	Height of bed surface roughness projections	L
K	A constant	n
L	Control volume length	L
L_j	Distance traveled by size class j	L
L_{xj}	Average distance traveled by size class j during bedload transport	L
m'	Apparent (immersed) weight of sediment	ML/T^2
n	Integer number	n
n	Manning's roughness coefficient	$T/L^{\frac{1}{3}}$
n_s	Number of scour monitor balls moved	n
n_T	Total number of balls on a scour monitor	n
p	Proportion	n

p( )	Probability density function of ( )	n
P	Porosity = (1-C)	n
P_w	Wetted perimeter	L
P_{ws}	Wetted perimeter from nearest bank to scour monitor	L
P_{wt}	Wetted perimeter from nearest bank to channel center of mass	L
Q	Flow rate of water	L^3/T
q	Flow rate of water per unit width	L^2/T
Q_B	Total volumetric bedload transport rate in downstream (x) direction, summed across channel (z direction)	L^3/T
q_B	Bedload mass transport rate per unit width in downstream (x) direction	M/LT
R	Local hydraulic radius = $A/P_w|_{cell}$	L
$\mathbb{R}$	Flow Reynolds number = U/vd	n
$\mathbb{R}_*$	Particle Reynolds number = U_*/vD	n
S	Slope	n
S_b	Bed slope	n
S_f	Energy gradient, or friction slope	n
S_s	Sediment specific gravity = ρ_s/ρ	n
S_w	Water surface slope	n
t	Time	T
T	Duration of competent flow	T
$\bar{T}$	Excess shear stress parameter in Equation 5.15	$M^{1.5}/L^{2.5}T^2$
u	Water velocity at a point	L/T
u_B	Bedload particle velocity at a point	L/T
u_*	Friction (shear) velocity = $\sqrt{(\tau_b/\rho)}$	L/T
U	Depth-averaged water velocity	L/T
U_B	Depth-averaged sediment particle velocity	L/T
W	Width of bedload transport zone across channel	L
W_T	Cumulative effective work done per unit area of bed	M/LT
x	Horizontal axis in direction of flow	L
X	A variable	v
y	Vertical axis perpendicular to flow direction	L
Y	Bed elevation	L
$\dot{Y}$	Fraction of grains that are mobile during a specified time interval	n
z	Horizontal axis perpendicular to flow direction	L

Greek Symbols:

α, α'	A parameter	v
β	A parameter	v
δ	Bedload/bed disturbance thickness/scour depth	L
δ_B	Bedload disturbance depth (static bed)	L
δ_{EX}	Net change in bed elevation (excavation or fill depth)	L

δ_{MB}	Bedload layer thickness (moving bed disturbance depth)	L
$\delta_{MB+SALT}$	Bedload layer thickness + saltation height (moving bed)	L
δ_T	Total bed disturbance/scour depth	L
δ_X	Bedload particle exchange depth in bed	L
Δ	Difference in quantity following symbol	v
ϵ	Error	v
θ	Angle from horizontal	°
θ	Exponential distribution function parameter	1/L
θ_1, θ_2	Angles from vertical in cross- and downstream directions	°
λ	Linear particle concentration	n
ν	Kinematic viscosity	L^2/T
ξ	A parameter	v
ρ	Fluid density	M/L^3
ρ_s	Sediment density	M/L^3
σ_r	Normal stress acting on mobile-immobile particle boundary	M/LT^2
σ_δ	Normal stress acting on bed surface	M/LT^2
τ_b, τ_δ	Shear stress acting at streambed surface	M/LT^2
τ_{cr}	Critical bed shear stress for incipient motion	M/LT^2
τ_r	Resistance to shear motion at mobile-immobile boundary	M/LT^2
τ^*	Dimensionless bed shear stress (Shields parameter) $= \tau_b/[(\rho_s-\rho)gD_{50}]$	n
τ^*_{cr}	Critical dimensionless bed shear stress (for incipient motion)	n
τ^*_g	Dimensionless bed shear stress based on grain size distribution truncated at 8 mm	n
ϕ	Friction angle	°
ϕ_D	Friction angle of stress ratio ($=\tau_r/\sigma_r$)	°
ϕ_i	Critical static internal friction angle	°
ϕ_r	Critical dynamic internal friction angle	°
ω	Stream power per unit area of channel bed	M/T^3
ω_{cr}	Critical stream power per unit area for incipient motion	M/T^3
Ω	Stream power per unit length of channel bed	ML/T^3

$\overline{(\ )}$	Reach average value of ( )
m	Subscript denoting maximum value

[1] - M = Mass
L = Length
T = Time
n = Non-dimensional
v = Variable
° = Angle in degrees

PREFACE

Many who study salmonids for extended periods find themselves facing a dilemma: they get into this field in the first place because they like to catch salmon and trout, and sometimes eat them. But they never seem to have the time to go fishing because they are too busy studying them. A lot of it can be blamed on the fish themselves: just when you think you have them figured out, they go do something that totally throws you. Although humbling, it makes you want to study them more.

About the closest I really get to fishing these days is when I read late at night. I read the following passage a while ago — it struck me as fitting, not only because of the immediate subject, but also because it reminded me of how much one can learn about nature and physical processes from simple observations:

> *He watched them holding themselves with their noses into the current, many trout in deep, fast moving water, slightly distorted as he watched far down through the glassy convex surface of the pool, its surface pushing and swelling smooth against the resistance of the log-driven piles of the bridge. At the bottom of the pool were the big trout. Nick did not see them at first. Then he saw them at the bottom of the pool, big trout looking to hold themselves on the gravel bottom in a varying mist of gravel and sand, raised in spurts by the current.*

> *Ernest Hemingway — Big Two-Hearted River: Part 1 — 1925*

PDV   February 11, 2000

ACKNOWLEDGMENTS

1.0 Introduction

Salmonids (salmon, trout, and charr) select specific spawning sites in gravel bed streams and bury their fertilized eggs within the gravel matrix (Figure 1-1). The location of the egg nest, or redd, reflects streambed characteristics that provide a suitable incubation environment for the developing embryos. One important characteristic is substrate size, which depends in part on adult size and location in the channel (Bjornn and Reiser 1991; Kondolf and Wolman 1993). Other factors that have been linked to selection of spawning sites include water velocity gradients above the bed that lead to downwelling or upwelling through the redd, availability of cover for hiding or resting, sedimentation rates, and possibly groundwater influences. The relative importance of each factor varies with species and location (Bjornn and Reiser 1991).

The selected spawning location may also reflect the stability of the redd with respect to scouring during floods, where substrate and channel characteristics at the redd site influence whether mechanical disturbance of the bed extends down to the elevation of the buried embryos during their incubation period. The large variation found in published egg burial depth data within and between salmonid species reflects differences in spawning substrates, water velocities, and female size (DeVries 1997). It is also possible that stream-specific differences in the prevailing magnitudes and frequencies of scour events also influence egg burial depth. Recent data have indicated distributions of egg burial depth and scour depth that overlap slightly, and it has been inferred that scouring of salmonid redds could control salmonid distributions, population abundance, and reproductive adaptations in gravel bed streams under specific circumstances (Tripp and Poulin 1986; Montgomery et al. 1996; 1999).

Land use activities such as timber harvest, mining, agriculture, and livestock grazing can cause significant changes in sediment delivery and flood characteristics (Meehan 1991). Increased delivery of finer sediment particle sizes and increased frequency of larger flood magnitudes have been hypothesized to be linked to increased scour depths
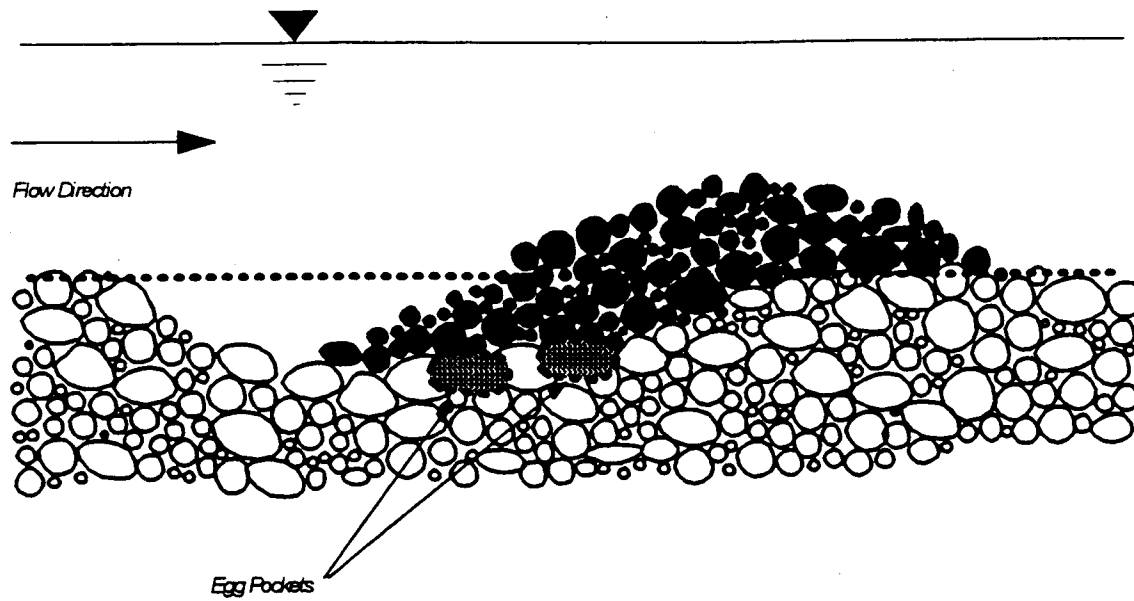
Figure 1-1. A representative salmonid redd, longitudinal cross-section. Depicted are the original bed surface elevation (dashed line), locations of two egg pockets, and disturbed bed material (shaded particles) forming the tailspill.

in the stream channel, with subsequent negative effects on salmonid populations (Tripp and Poulin 1986; Haschenburger 1994; Madej 1996). The ability to estimate past changes and predict potential changes in scour depth resulting from human activities is important for salmonid management. Salmonids serve as an important source of food and income, and provide for significant recreational and cultural needs. They also are critical indicators of good water quality and proper ecosystem and watershed management. Large scale loss of distinct salmonid populations and genetic diversity has already occurred because of extensive destruction and adverse modification of their habitat by land use and water management, overfishing, and long term climatic variation (Nehlsen et al. 1991; Brown et al. 1994; Hare et al. 1999). If scour has a direct effect on population levels, the ability to predict scour depth is a fundamental component of strategies for protection and recovery of stressed salmonid populations.

This dissertation focuses on the scour depth evaluation and prediction problem. There are four principal goals of the research:

(I) To provide fundamental insight into scour mechanisms and the corresponding linkages with bedload transport and hydrology;

(II) To develop relatively simple methods for predicting scour depth magnitudes;

(III) To evaluate linkages between scour, salmonid spawning behavior, and reproductive success; and

(IV) To guide future investigations of scour and its relation to salmonid populations, land use, and water management.

1.1 Definition of Scour Depth

Interpretation of the term 'local scour' varies with context. Its most common meaning in river engineering and geomorphology is taken to be the scour hole that develops around structures (e.g., bridge piers) or in the vicinity of channel constrictions. In that context, local scour represents a change in surface elevation over a discrete area of the bed. This dissertation uses a more restrictive definition that reflects (i) the

smallest relevant measurement scale possible in the field, and (ii) direct influences on salmonid embryos: local scour occurs at a specific point on the streambed. For convenience, the term 'scour depth' is taken to be synonymous with this definition of 'local scour depth' in the remainder of this dissertation, unless stated specifically otherwise.

Scour depth can be considered in terms of mortality mechanisms influencing fertilized eggs and incubating embryos. Mortality resulting from scour may occur in two ways: the eggs/embryos are washed out when the bed elevation lowers to their level, and/or they are crushed mechanically by the moving bedload (e.g., Crisp 1989). Survival is contingent on the depth of physical bed disturbance, where scour depth is defined here to be the thickness of the bed that is disturbed. There is a brief period (~15 days) after fertilization during which the embryos are sensitive to the slightest mechanical shock (Smirnov 1959; Jensen and Alderdice 1983), but it is typically over by the time floods occur. At some point during the intra-gravel life stage, the more developmentally advanced fry ("alevins") may be able to move downwards in the gravel in response to agitation (Bams 1969; Dill 1969; Fast et al. 1981) thereby reducing the probability of mortality from scour.

The terms 'scour and fill' raise a series of questions that are based on the principle of mass conservation:

(I)   Where did the 'scoured' material go to?

(II) Where did the 'fill' material come from? and

(III) What happened during the intervening time?

There are two possible processes that may operate concurrently and that must be evaluated:

(I)   The bed may scour and subsequently fill, which can only occur when there are local imbalances in the sediment transport rate linked to spatial and temporal variability in reach-scale gravel supply and bed shear stress distributions.

(II) The observed scour depth may correspond to the thickness of the moving bedload layer, including underlying particles that are disturbed from rest by

hydraulic and mechanical collision processes. The underlying disturbed particles may be entrained or remain in place. Measurements attributed to 'scour and fill' may be frequently representative of this process instead.

I propose a corresponding partitioning of total scour depth at a location of the streambed, δ_T:

$$\delta_T = \delta_{EX} + \delta_{Bm} \tag{1.1}$$

where: $\quad \delta_{EX} =$ net excavation depth, or difference in bed elevation before and after a flood; and

$\delta_{Bm} =$ maximum disturbance depth caused by a moving bedload layer.
This partitioning relates physical bedload transport and scour processes to distinct mortality mechanisms.

Excavation depth is a result of non-equilibrium sediment transport, as can be seen by considering the control volume in Figure 1-2. A mass transport rate imbalance occurs when the amount of sediment exiting the control volume exceeds the amount entering per unit time, and the streambed surface lowers. The net excavation depth is the time-integrated difference between input and output volumetric transport rates per unit streambed area, adjusted for concentration. The process can be visualized as a successive whisking away of layers of bedload out of the control volume. Data measured in this study are from single thread channels not experiencing extreme changes in form and thalweg location. The net excavation problem is consequently reduced to evaluating streamwise differences in sediment transport rates and storage volumes.

Fill depth is the opposite result. Fill is not likely to have a significant influence on incubation survival except when the deposited material is too thick for successful emergence and the alevins are entombed. How thick a deposit is needed to cause mortality remains to be determined, and is not within the scope of this work. Fill mortality is most likely to be important when extreme channel and bar migration (e.g., in braided reaches) or sudden introductions of large quantities of sediment (e.g., because
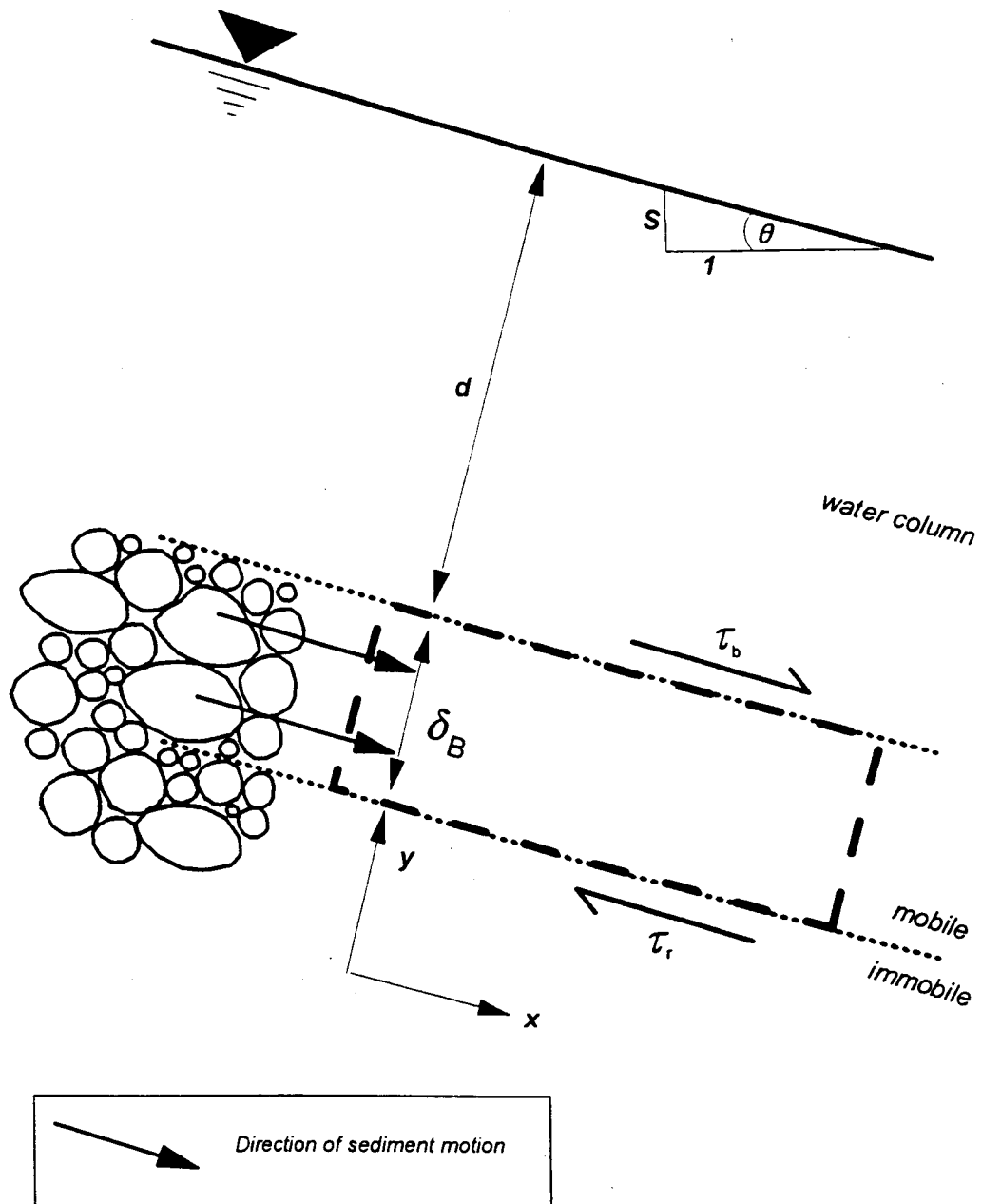
Figure 1-2.   2D control volume for scour depth evaluation.

of a landslide or bank erosion) occur.

Measured scour depth values are most likely to be representative of bedload layer thickness when equilibrium transport conditions prevail (i.e., an adequate sediment supply is present). It has been commonly assumed that the maximum moving bedload layer thickness occurs at or near the maximum boundary shear stress experienced during a flood. In most cases the thickness may be limited to one or two particle layers (e.g., Parker et al. 1982a), but the possibility has been raised for more layers to move as a granular flow under relatively large, applied shear stresses (Hanes and Bowen 1985; Wilson 1987; Haff et al. 1993). The moving bedload layer has been referred to as a 'traction carpet' when flow rates are large and shear stresses are strong enough to mobilize the entire surface armor layer (Hassan 1990; Pitlick 1992).

Bedload layer thickness is defined here as additive to excavation scour depth because it exists at all transport stages. A significant, potential problem with the scour depth partitioning in Equation 1.1 is that the maximum thickness of the moving bedload layer does not occur at the end of transport, which is when the maximum excavation depth occurs according to the equation. Further, excavation depth only partly depends on shear stress. For example, it is possible for 2-year and 10-year peak floods to transport the same total mass of sediment and result in the same net excavation scour depth when the 2-year flood has a sufficiently longer duration. These and related measurement errors are discussed in Chapters 3 and 4.

It is argued in this dissertation that the maximum excavation depth depends more on distribution of the more frequently mobilized gravel and cobble particles in a reach and on duration of flow competence than it does on shear stress magnitude.

1.1.1 *Definition of Active Layer*

The term, 'active layer', has been used in different contexts to describe:

(I) All of the material in the bed that has been disturbed by lowering of the bed
surface elevation (excavation) and/or bedload movement during either a single

flood or multiple floods (δ_T; Borah 1989; Hassan and Church 1994; Lisle 1989; Haschenburger 1996);

(II) All of the material in the bed that has been disturbed by lowering of the bed surface elevation during a single flood or multiple floods, excluding the moving bedload transport layer (Paola and Seal 1995);

(III) The subsurface layer contributing to sediment transport through vertical exchange in a flood (Armanini 1995);

(IV) The layer at the interface of the bed and flow, which is taken to be the moving bedload layer at any time (δ_{Bm}; Borah et al. 1982; Carling 1987; Haff and Jiang 1995; Kelsey 1996); and

(V) The sum of the total scour depth and the total fill depth (Laronne and Duncan 1989).

The first convention (I) is used here, but for individual floods only. Equation 1.1 implies that the moving bedload layer is a component of the active layer.

1.2 Summary of Research Activities

The principal objective of this research is to develop relatively simple predictive tools for assessing potential effects of scour on salmonid reproduction. Two parallel problems are investigated: predicting the thickness of the bedload layer, and predicting net excavation scour depth. This dissertation is directed primarily at defining and resolving the bedload layer thickness problem. The net excavation problem is sufficiently complex that this dissertation cannot evaluate it as thoroughly as the bedload layer thickness problem, but important processes are identified and evaluated to help guide future research.

A fundamental focus of this work is to find the functional relationship of thickness of the moving bedload layer in salmonid spawning beds in terms of basal shear stress or stream power (driving force), and substrate characteristics (resistance to motion). The relative importance of each is evaluated and described. I focus specifically on the

problem of predicting the value of δ_{B_m} (Equation 1.1) in gravel bed streams.

The net excavation scour depth problem is addressed by identifying important variables and their influence on scour depths measured in riffles and in the pool-riffle interface. Riffles are geomorphic features of stream channels where water flow is relatively shallow, steep, and fast compared to other units, and provide the primary spawning habitat for salmonids. Because net excavation scour depth in the study streams is caused primarily by streamwise sediment transport rate imbalances, its magnitude is proposed to be a function of where the redd is located along the length of the riffle and of the dimensions and frequency of riffles. Net excavation scour occurs when there is not enough material arriving from upstream to replace material being transported downstream. I focus specifically on this problem from the perspective of sediment supply.

Laboratory studies have provided fundamental insights into scour mechanisms, but more field-scale data are needed. Existing field data cannot be used to evaluate Equation 1.1 because they are generally descriptive of total scour depth only, over an entire flood season in one or two streams, and because a limited range of substrate characteristics, flow, and stage data were collected that do not facilitate an in-depth evaluation of scour processes.

The work reported here involved extensive field measurement of scour depth and other data needed to elucidate the relations between bedload transport processes and scour depth, over a wide range of physical conditions. A major criticism of field studies is that it is difficult to account for all environmental factors that could contribute to variation in the data. This study was designed specifically to account for dominant sources of variation and minimize unexplainable influences.

The majority of field work occurred over the 1996-97 and 1997-98 flood seasons. A two-year time frame was considered necessary because it can be representative of the characteristic frequency of important channel-forming events in alluvial channels (Wolman and Miller 1960): there is a lower probability that the bed will be mobilized sufficiently and extensively in a single-year study. In illustration, there was extensive and

repeated flooding in the first year, while in the second year minimal flooding occurred. Most data were derived from the first year. Additional data were collected at selected sites in 1998-99 and have been included.

Scour monitors were installed in fifteen stream reaches, with useful data collected in eleven reaches; four were abandoned because of uncontrolled natural or anthropogenic factors (e.g., trees falling into the stream, vandalism, incomplete data, or significant reach-scale aggradation). Study sites were selected to represent a wide range in parameters thought to influence scour depth, including channel size, annual flow characteristics, bed material sizes and composition, channel gradient, and channel confinement. Sites were selected from reaches containing extensive spatial distributions of spawning-size gravel and cobble to minimize local sediment transport rate imbalances. Several sites were established at different locations within a given channel network to evaluate upstream and downstream variation in scour depth and process.

During the first year, scour monitors were placed within each site across one to three transects in riffles containing suitable spawning substrates. The number of transects depended on site characteristics and purpose. In the majority of sites, two transects were located in one 'primary' riffle for intensive data collection. A third transect was located in the immediate upstream riffle to assess mass transport imbalances and differences in scour depth between consecutive riffles. Scour monitors were placed at two or three locations across each transect to assess transverse differences. Scour monitors were also placed during the second year in pools and other intervening channel units throughout three sites to assess longitudinal variation in net excavation scour and bedload disturbance depth.

Bed elevation surveys were conducted before and after floods to measure net excavation depth. Substrate grain size distributions were characterized at each scour monitor location by collecting bulk samples and performing pebble counts; these were done after scour occurred to avoid influencing disturbance depth measurements. Distinctions were made between the surface and subsurface layers in the bulk samples in stratigraphic evaluations of bedload transport processes. Specific gravity was

determined for the substrate in each site. Shear stresses were estimated indirectly because of the danger involved and difficulty of measuring water velocities during floods in most of the study streams.

Where possible, study sites were selected to be near U.S. Geological Survey (USGS) gaging stations so that stage-rating curves could be developed for purposes of shear stress and stream power estimation. Maximum stage was estimated from rating curves, on-site maximum stage recorders, and flood marks. The maximum depth of flow was estimated at each scour location for each flood. Friction slopes were estimated from measured high flow water surface slopes and used to calculate shear stress.

The data were used to examine relationships between bedload layer thickness and shear stress, substrate grain size, and related factors.

1.3 Dissertation Outline

This dissertation (i) identifies and evaluates what is known regarding scour processes, (ii) describes the measurements made in this study, (iii) evaluates the data in terms of bedload disturbance depth and net excavation scour processes, (iv) interprets the relation between the mechanics of scour and salmonid intragravel survival, and (v) provides guidance for future scour research. Chapters 2 through 7 are organized along those lines.

Because relatively little research has been performed regarding salmonid redd scour processes, Chapter 2 reviews previous research on bedload transport and synthesizes the most important features relevant to evaluating total scour depth and its two components. Field, laboratory, and modeling studies were reviewed for information indicating, or suggesting, the most important attributes of scour depth, its measurement, and its interpretation.

Chapter 3 describes the field and laboratory methods used. Measurements are evaluated for potential error sources, and data reduction methods are described. The appendices contain the reduced data and information used in subsequent chapters to

evaluate scour processes.

The two components of total scour depth given in Equation 1.1 are evaluated in separate chapters. Chapter 4 addresses bedload disturbance depth in terms of mobilizing force and the influence of grain size. Specific mechanisms are identified and discussed that may be responsible for the data observed in this and other studies. Chapter 5 identifies the important processes resulting in observed net excavation scour depths, and presents a simplified prediction approach. Both chapters focus on scouring at redd locations in spawning riffles.

The identified scour mechanisms are related to salmonid spawning behavior and survival in Chapter 6. The results of this study provide a context for evaluating intragravel survival explicitly in terms of observed bedload transport processes and resultant scour depths. The relevance of scour to salmonid survival is discussed. Assumptions regarding the linkages between scour and survival are identified and addressed.

Conclusions and recommendations for future scour studies are presented in Chapter 7. Two methods are suggested for approximating maximum scour depth. Future research directions are suggested for developing more accurate predictors of maximum scour depth.

2.0 Review of Bedload Transport and Scour Studies

There is a wealth of information available on sediment transport processes, but there is relatively little known about scour in the context of salmonid survival. Research into specific streambed scour mechanisms has been directed predominantly at scour around abutments and bridge piers (Copp 1988; Richardson and Richardson 1994) and boulders (Klingeman and Huang 1993), scour under submarine pipelines (Chiew 1990), and jet scour (Rajaratnam 1981). Scour depth has been found in these studies to be a function of particle size, dimensions of the flow obstruction, mean approach velocity, and/or Froude number. The most useful predictive relationships that have been developed for these situations have, of necessity, been empirical because of their complex, three dimensional nature. Some of the relations may be relevant when large woody debris settles at, or passes by, salmonid redd locations during flood transport. They may also be relevant to stream reaches where spawning gravel distributions are limited to small accumulations in the immediate vicinity of boulders and other flow obstructions. In such instances, scour is associated primarily with a strongly three dimensional mean velocity field, where local flow concentration, jet action, and/or vortices can give rise to higher local shear stresses than occur at a comparable depth under uniform flow conditions.

Scour associated with meandering processes has also been investigated extensively (Nelson and Smith 1989; Maynord 1996). However, meander scour occurs generally over a longer time scale than flood scour and is subject to relatively subtle three-dimensional effects of the flow field on bed topography (Dietrich 1982). Moreover, meander scour evaluations have focused primarily on pool formation and maintenance rather than on scouring activity in riffle areas where salmonids spawn.

The mechanics of flood scour has generally not been addressed in salmonid spawning beds that occur in riffles and pool tails, and may involve functional relationships that are different from bridge, contraction, jet, or meander scour. Spawning beds consist of an expanse of suitably sized spawning gravel and/or cobble (see review by Kondolf and

Wolman 1993) that extends across the channel bottom. The topography of the bed is relatively smooth. Time-average velocity fields during floods are approximately two-dimensional and vary gradually across the channel. The bed shear stress is proportional to flood depth, and bedload transport mechanisms are simpler than in the other scour processes introduced above. Local scour holes may be present when these flow conditions are not met, but it has been my experience that salmonids generally do not spawn in the vicinity of such areas when spawning beds are present in the stream system.

This dissertation is concerned with the depth of substrate disturbance at specific locations in gravel and cobble deposits that constitute spawning beds. Our understanding of the complex relationships between land and water use, sediment delivery, flood hydrology, fisheries harvest management, and salmonid and stream ecology has advanced significantly over the past several decades, but only recently has a widespread appreciation developed for the potential importance of scour to salmonid populations. As yet, relatively little work has been done on the physics of scour at spawning locations. However, advances have been made in several related branches of bedload transport research that are pertinent to the problem.

This chapter summarizes the literature from the entire bedload transport field, identifies relevant field, flume, analytic, and numeric studies of processes controlling bedload motion, scouring, and bed disturbance depth, and assesses possible prediction approaches. The goal of the review is to distill related research and identify, describe, and understand the mechanisms and characteristics of particle movement during floods in gravel bed streams. Such understanding is critical to developing methods for predicting scour depth.

The review focuses on six themes of bedload transport and scour research. The chapter is organized accordingly into six sections. The first identifies the ways in which a coarse, heterogeneously-sized streambed is mobilized at different levels of flow strength. Such knowledge is important because the composition of the moving bedload reflects streambed composition and flow strength, which should therefore influence bedload disturbance depth. The second section reviews field studies that have measured,

and approaches that have been used to characterize and predict, scour depth. The third section reviews studies of tracer particle movement, the results of which have bearing on the thickness of the bedload layer and the manner in which sediment transport rate imbalances develop at the reach scale. The fourth section reviews the field of granular flow, which has bearing on the potential upper limits to bedload disturbance depths in natural channels. The last two sections review alternative approaches to scour depth prediction, and are distinguished by whether they directly or indirectly evaluate scour depths. The chapter concludes with a synopsis of features of bedload transport and scour processes that are either common or unique to each theme and that are relevant to the scour depth prediction problem.

2.0.1 *Additional Definitions*

The thickness of a moving, non-saltating particle layer δ_B has also been represented in terms of a corresponding static bed disturbance depth. The two are not identical because of dilatancy of the bed material. The bed porosity, P, is needed to convert between units of mass and volume of granular media and varies with dilatancy. It can be shown from mass conservation that:

$$\delta_{B_{static}} C_{static} = \delta_{B_{moving}} C_{moving} \tag{2.1}$$

where the volumetric concentration $C = (1-P)$. The focus of this work is to predict the value of δ_T after salmonids have laid their eggs, which is the value relative to the original static bed surface elevation. It is the static values of δ_T, δ_B and P that are measurable in the field. The symbol δ_B in Equation 1.1 is used from here forward to refer to the equivalent static bed disturbance depth, and δ_{MB} is used to distinguish the thickness of the layer while it is in motion. The thickness of the moving bedload sheet can furthermore be defined either with or without saltating particles. The former is defined here as $\delta_{MB+SALT}$. Saltation heights are typically one to two grain diameters when only the

surface layer is mobilized (Bagnold 1966a; Haff 1991), in which case the value of $\delta_{MB+SALT}$ has been assumed to be two to three grain diameters (Bagnold 1966a).

The magnitude of the left hand side of Equation 2.1 reflects the combined concentration of (i) larger particles that collectively define the streambed elevation by forming a stable, self-supporting structure (the 'framework'; Church et al. 1987), and (ii) finer particles filling the spaces in-between (the 'matrix'; Church et al. 1987). Church et al. (1987) noted that many streambeds are composed of large quantities of fine sediments such that the coarser particles are supported by fine sediments rather than by each other and called such mixtures 'matrix-supported'. A minor modification of these definitions is used here that is more relevant to scour evaluations. Framework particles are those that influence bed elevation, and matrix particles are those that fill the spaces formed by the larger framework particles, irrespective of their absolute size. The distinction between the two is not always clear in the field, however.

2.1 Modes of Coarse Bedload Transport

There are two distinct modes of bedload transport possible in gravel bed streams that are relevant to scour depth prediction. The first mode, 'partial transport', occurs at lower shear stresses and is restricted to motion of a proportion of the sediment available for transport in the surface or armor layer. The thickness of this layer varies with the size of the coarsest particles present in the streambed surface. The maximum thickness of bedload disturbance depth during partial transport should therefore scale with the size of the largest mobile particle, whereas the mean thickness should scale with a smaller size. Partial transport is widely considered to be the dominant mechanism of bedload transport in gravel bed streams (Parker et al. 1982b; Bridge and Dominic 1984; Hassan 1990; Wilcock et al. 1996). For this situation, the surface layer is the primary source of material for bedload transport (Parker 1990a) and thus controls bedload disturbance depth during the more frequently occurring flood flows.

Partial transport involves finer particles moving in greater proportion to their

presence in the streambed than coarser particles (Wilcock 1997a; 1997b). The rates at which coarser particles move increases with shear stress (Parker et al. 1982b; Komar and Shih 1992). The proportion of mobile particles in the bed has been observed to increase rapidly at the beginning of laboratory flume tests used to evaluate partial transport and approaches an asymptotic limiting value (Wilcock 1997a). Additional particles are not entrained, most likely because the excess shear stress (i.e., estimated bed shear stress minus critical shear stress for initiation of motion) is just enough to maintain the limiting rate of motion (Bagnold 1956). It has been determined in flume experiments that a size fraction becomes completely mobilized once the bed shear stress is roughly double the critical stress needed to initiate motion of member particles, and that size class-specific (or, 'fractional') transport rates are independent of the class' characteristic grain size at higher shear stresses and decrease rapidly with size for particles that are not completely mobilized (Wilcock and McArdell 1993; Wilcock and McArdell 1997).

Not all of the bed is in motion at the same time during the partial transport mode. Moving particles originate at the surface, motion is distinctly intermittent, and the larger, partially mobilized particles are thought to control the exchange of particles between the moving surface layer and the layer underneath (Wilcock 1997b; Wilcock and McArdell 1997). It follows that up to the point of simultaneous motion of all bed surface particles, the maximum thickness of the bedload layer is unlikely to be greater than a disturbance depth associated with the largest particle that moves. It also follows that the bed structure should be closer to the static state than the dilated state during partial transport. Deep, local scour holes are unlikely to develop during partial transport once a larger-sized member of the surface grain size distribution vacates its original position because of flow separation within the vacated depression, which reduces the shear stress influencing grain motion at the bottom of the hole; this favors deposition of other moving particles. Turbulent velocity fluctuations influence particles at the edge of the depression, but the maximum depth of exposure is unlikely to increase significantly.

'Equal mobility' is a special case of partial transport that involves all size ranges moving in approximately equal proportion to their presence in the bed. It is largely

associated with sheltering effects and the persistence of a pavement during bedload transport (Parker and Klingeman 1982; Andrews and Parker 1987). The pavement exists as long as bedload involves sporadic motion of individual particles (Parker et al. 1982a); it disappears when the entire surface layer is mobilized simultaneously.

The second mode, 'granular flow', occurs at higher shear stresses and involves motion of all particles within two or more layers of particles. The granular flow state is thought to be rare except in sand bed channels, but has not been completely discounted as a possible phenomenon in gravel bed streams. The term 'traction carpet' refers to simultaneous mobilization of the entire bed surface in a layer that is one or more particles thick, and thus represents an intermediate mode of transport between partial transport and granular flow. It is used here in the strict sense to include the moving surface layer and any particles disturbed in the immediate subsurface layer, until granular flow begins in the sense defined above.

2.1.1 *Structural Phenomena*

Partial transport is a phenomenon that occurs at the particle scale (i.e., at a point). There are three larger scale structural features characteristic of coarse bedload transport that could potentially influence scour depth measurements. The first are particle clusters that promote bed stability and delay onset of motion and bedload transport (Reid and Frostick 1984; Hassan and Reid 1990). Clusters form as part of the armor layer during extended periods of low transport stages when the dimensionless shear stress ratio τ^*/τ^*_{cr} ≤ 2 and are usually found in coarser cobble beds with smaller amounts of gravel present. These structures can reduce sediment transport rates by orders of magnitudes (Church et al. 1998). The largest particles of the surface grain size distribution form the core of cluster structures, the distributions of which depend on the number of largest stones present (Hassan and Reid 1990; Church et al. 1998; Tribe and Church 1999). Clusters are likely to facilitate both (i) deposition of a layer, the thickness of which scales with the size of the largest particles forming clusters, during aggradation, and (ii) local scour

around the cluster perimeter that develops progressively until the clusters finally move. In either case, the thickness of the disturbed layer is likely to be proportional to the size of the largest stones present in the bed surface. The horizontal dimension of clusters has been recorded to be on the order of as much as ten times the diameter of the larger particles forming the cluster (Church et al. 1998). The presence of clusters ought to influence spatial distributions of scour depths.

The other two structural features are bedload sheets, and dune-like bedforms, which constitute related modes of sediment transport that occur over larger spatial scales than particle clusters. They are mentioned here because scour depth has sometimes been assumed to equal the maximum thickness of the sheet or height of the dune bedform. This assumption is evaluated briefly here.

Bedload sheets have been observed visually in field studies performed at low transport rates in channels with predominantly coarse sand and fine gravel beds (Whiting et al. 1988). The thickness of the sheets were one to two times the dimension of the coarsest mobile particles. The sheets were observed to move by the advancement of coarser grains, exposed at the upstream end of the sheet, to the leading (downstream) edge of the sheet where they were buried by finer grains. Where bedload sheets occur, measurements of disturbance depth would be expected to be limited to the thickness of the material contributing to sheet formation.

Dune-like bedforms are analogous to dunes in sand bed channels and generally do not develop to a significant degree in gravel bed streams (Bagnold 1956; Parker and Peterson 1980). Gravel and cobble dunes are not expected in pool-riffle channels because the process depends on a continuous supply of sediment (Simons and Şenturk 1977, pp. 251 ff.), and pools represent a discontinuity in the supply of gravel and cobble material available for bedload transport. Bagnold (1956) determined analytically that small dunes may develop in gravel beds with a limiting slope of about 0.5° when sediment transport rates are small and close to threshold conditions over a sufficiently long period.

Dinehart (1992) inferred the passage of dunes using ultrasonic transducers in the

North Fork Toutle River, a wide, moderately braided channel transporting a large load of sand and fine to medium gravel (bedload sample mean D_{84} ranged between 50 mm and 95 mm; mean diameter = 30 mm). Dune heights were estimated to have ranged between 12 and 45 cm. The depth of disturbance below the original bed elevation caused by their formation was not measured but was likely to have been small because the bed aggraded during the study. The maximum disturbance depth below the original bed elevation is suggested by Dinehart's (1992) data to have been proportional to the diameter of the larger particles present in the bed surface, because the volume of material comprising the dunes appeared to be approximately equal to the volume of the undisturbed bed's surface layer. Wakes downstream of the forming dunes probably limited the disturbance depth in the vicinity of the forming troughs by reducing local bed shear stress. Dinehart (1992) noted that the troughs filled subsequently and inferred that the dunes formed as part of the bed aggradation process. It is unknown whether similar coarse-bedded dune features form during floods when the bed is degrading.

2.2 Field Studies Involving Scour Depth Indicators

Scour depth indicators, or scour monitors, were devised to determine the vertical and horizontal distributions of bed disturbance depth in a stream reach, without influencing the scour depth measurement simply by virtue of their presence (e.g., scour around a sounding weight). Scour monitors indicate the maximum depth of disturbance relative to the original bed elevation. Depending on the device, it may also be possible to distinguish between material that moved initially and material that was deposited later. Numerous devices have been made, including link chains and different versions of movable scour depth indicators. Chapter 3 describes advantages and disadvantages of the various devices.

The earliest intensive field investigations of the physics of scour and fill using scour monitors were conducted in sand bed channels beginning in the late 1950s (e.g., Emmett and Leopold 1965; Colby 1964; Leopold et al. 1995). Variation in scour and fill depths

in sand bed channels has been attributed to the passage of rapidly migrating dune bedforms (Foley 1978), and to the scouring of one stream reach associated with filling in a downstream reach (Leopold et al. 1995). Results from sand beds are not directly transferable to gravel beds, however, because dune-like bedforms in gravel bed channels are of relatively low amplitude (Hassan et al. 1992; Dinehart 1992) and probably do not exist in most coarse beds during floods (Bagnold 1956). Moreover, dimensionless shear stress, which represents the balance between forces inducing motion and forces resisting motion, may be up to two orders of magnitude greater in flooding sand bed streams than in gravel bed streams because of the difference in characteristic particle size (e.g., 1 mm sand versus 50-100 mm stones). Sand is also transported over longer distances than gravel and cobble (Section 2.3).

Fewer field studies have provided physical insights into scouring processes in gravel bed channels than have studies in sand bed channels, in part because of the difficulty installing scour monitors in a coarse, heterogeneous substrate. Of the studies that I could find in the literature, some focused on the correlation between mobilizing force and scour depth, some on the characteristic scour depth in different geomorphic features of a channel reach, and others on the relation between bedload transport rate and associated scour depth. The most quantitative work has involved fitting probability density functions to measured scour depth distributions in a reach. These studies are described below.

2.2.1 *Scour Depth and Mobilizing Force*

Scour and fill depths have been evaluated as either linear or log-linear functions of a characteristic discharge, bed shear stress, and stream power. Haschenburger (1996; 1999) collected scour and fill data using scour monitors in Carnation Creek, British Columbia, and calculated reach average scour depth, fill depth, and active width. Values of each measure increased with discharge and stream power. These results corroborate other findings (Carling 1987; Laronne and Duncan 1989; O'Connor and Harr 1994;

Schuett-Hames et al. 2000) and appear to be explained by (i) the number of zero scour depth observations decreasing as more of the bed surface area becomes exposed to critical shear stresses with rising stage, and (ii) larger particles beginning to move at higher discharges, disturbing a greater depth of the bed locally than could smaller particles.

Haschenburger (1996) fit power functions to (i) mean reach scour depth vs. peak flow per event, and (ii) mean fill depth vs. peak flow. The fits were essentially identical (Haschenburger 1996; p. 49), suggesting that the Carnation Creek study reach as a whole did not experience significant loss or gain of sediment in any individual flood. In contrast, analogous functions for maximum scour depth and fill depth were dissimilar, indicating that local sediment transport imbalances had occurred within the study reach, even though the reach total sediment balance was maintained.

Haschenburger (1996) compared the Carnation Creek results to Leopold et al.'s (1966) results for a sand bed stream in a search for a non-dimensional relationship between reach average scour depth and mobilizing force. Scour depth and peak flow were scaled by a characteristic particle size (D_{50}) and flood flow ($Q_{1.76}$), respectively for each stream. The scaled Carnation Creek scour depth data plotted substantially lower than the sand bed data, most likely because the coarser substrates were not influenced by migrating dune bedforms.

Scatterplots of reach-average scour depth versus discharge or stream power exhibit large variability. Carling (1987) found scour depths to vary by more than an order of magnitude for the same discharge, and his coefficient of determination was low ($r^2 = 0.19$). O'Connor and Harr (1994) found a better fit of mean scour depth vs. excess unit stream power ($r^2 = 0.89$), but used only seven observations, one of which had a strong influence on the slope of the regression. Error about the fitted regression line was also large, ranging between roughly ±30 to 100 percent. Considering that these were results for average scour depth, relationships between local scour depth and discharge, stream power, or shear stress can be expected to exhibit greater variability.

Wilcock et al. (1996) used large tracer gravel installations in spawning reaches of the

Trinity River, California, to evaluate the relationship between depth of bed disturbance and local shear stress. Their data were limited in sample size because of the physical difficulty of gravel sampling, tracer installation and shear stress measurement, but were of high quality. They found that scour to the base of the bed surface layer occurred at a dimensionless shear stress $\tau^*_g \approx 0.035$, where τ^*_g was calculated using a local bed shear stress estimate and the D_{50} of the bed grain size distribution truncated at 8 mm. Entrainment began at $\tau^*_g \approx 0.031$; the bed surface could be disturbed completely with only a thirteen percent increase over the critical shear stress required for initiation of motion.

Wilcock et al. (1996) referred to their measured disturbance depth as the 'exchange depth' because tracer stones were used. They determined that the dimensionless ratio of exchange depth to D_{90} increased rapidly within the range $\tau^*_g \approx 0.031$-0.035, and appeared to level out at higher shear stresses. Their data indicated that the maximum local scour depth for plane bed transport was slightly less than twice the surface layer thickness, or about $1.7D_{90}$. Related flume data showed a limiting value of about $2D_{90}$ (Wilcock and McArdell 1997).

Because it is potentially descriptive of general bedload transport processes, the $2D_{90}$ metric is compared with other study results in the remainder of this chapter and in subsequent chapters.

Wilcock (1997b) fit the following dimensionless relationship between exchange depth, δ_x, and dimensionless shear stress using field and flume data:

$$\frac{\delta_x}{D_{50}} = 7968 \, \tau^{* \, 2.61} \tag{2.2}$$

where δ_x was approximated as the size of the fraction that was 50 percent mobile at a given shear stress.

2.2.2 *Scour Depth and Channel Morphology*

Two studies were identified that evaluated whether variation in measured scour depths was related to the location in the channel reach where the data were collected.

Yee (1981) installed scour chains in a grid pattern throughout three riffles of Prairie Creek, a small coastal stream in California, to determine where deepest scour depths occurred in spawning habitat. In the few floods that occurred, greatest scour depths (6 cm to >24 cm) were measured in the most downstream portion of the riffles where they transitioned into pools. In one site, the lowermost 2.5 meters of the riffle was excavated during a single storm and became part of the pool. Scour depths elsewhere in the three riffles were less than 8 cm, or less than twice the substrate D_{90} (range = approximately 55 to 70 mm), including in the largest storm measured when flows topped the streambanks (Yee 1981).

Schuett-Hames et al. (2000) installed whiffle-ball scour monitors to evaluate the influence of reach-scale channel morphology on the spatial variation of scour depth in Kennedy Creek, Washington. Two different sites were monitored: a straight, narrow, relatively simple channel ('Site A'), and a meandering, structurally complex channel with abundant woody debris ('Site B'). The Site B channel was geomorphically more active, and velocity fields were more strongly three-dimensional and gravel deposits more transient than in Site A. Scour monitors were installed shortly after spawning was completed and scour depths measured in two successive, relatively small floods (1.4 year recurrence interval followed by a smaller, annual event). The bed had been disturbed considerably throughout both reaches by the spawning activity of large numbers of chum salmon (*Oncorhynchus keta*). (I have observed spawning chum salmon to alter the streambed topography of Kennedy Creek completely to the point that even the sides of gravel bars are eroded by fish digging redds wherever they can).

Greatest mean scour depth in the straight reach (Site A) was measured in transient, lateral bar deposits located adjacent to pools. These areas are frequently associated with divergent flow and local eddies during floods that cause changes in pool size, or result in

differential mobilization and deposition of material that is finer than most substrates found in the channel reach. Schuett-Hames et al. (2000) also noted that these areas were influenced by moving woody debris in the study stream. Pool tailout and pool head ("lower riffle") regions exhibited the next greatest mean scour depths, 80 mm and 75 mm respectively. Riffles and glides exhibited the smallest mean scour depths (20 mm in each). Mean scour depth for the reach as a whole was 75 mm. These scour depths were less than twice the characteristic bed surface D_{90} (approximately 50 to 55 mm; Montgomery et al. 1996), and thus may have represented flood disturbance of mostly the surface layer (Wilcock et al. 1996; Wilcock and McArdell 1997).

Similar results were obtained in the more complex Site B, with the exception of pool tailout and glide areas which exhibited greater scour depths than their counterparts in the simpler reach. Depths were slightly greater than twice the reach-average D_{90} in the glide, and four times in the pool tailout. Results in the pool tailout were thought to have been influenced by the greater presence of woody debris and its effect on local three-dimensional flow patterns within the tailout area, and by physical disturbance of the bed by wood passing through the reach (Schuett-Hames et al. 2000).

2.2.3 *Scour Depth and Bedload Transport Rate*

Bedload disturbance depth is related to bedload layer thickness, which is related to bedload transport rate by (one-dimensional) mass conservation:

$$Q_B = U_B \delta_B W(1-P) \qquad (2.3)$$

where Q_B is total volumetric bedload transport rate, U_B is the mean downstream particle velocity of a bedload layer of thickness δ_B, and W is the active width of bedload transport across the streambed. Equation 2.3 provides a means for estimating local bedload layer thickness when the local bedload transport rate and velocity can be measured or estimated (Carling 1987; Montgomery et al. 1996). Equation 2.3 cannot by itself predict

net excavation scour (δ_{Ex}) caused by the layer whisking mechanism because it assumes a single, moving layer of variable thickness. Its use depends on the assumption that the thickness of the bedload layer δ_B equals the total scour depth δ_T, which will be true when the stream reach experiences equilibrium sediment transport rates throughout its length.

Equation 2.3 has been applied most frequently using spatial and temporal averages for parameter values. A time-averaged particle velocity can be estimated relatively easily in the field by measuring distances moved by tracer stones and dividing the distance by the length of time that flows are sufficiently strong (competent) to move them. This time-average has been termed 'virtual' velocity (Einstein 1937; Stelczer 1981). Spatial averages of δ_T can be determined by deploying a large number of scour monitors throughout a reach.

Rennie (1998) estimated a reach average of total scour depth δ_T using virtual bedload velocity and peak bedload transport rate estimates, and compared the results to values measured using scour monitors. The correspondence between predicted and observed was relatively good, suggesting that his total scour depth measurements approximated the bedload disturbance depth, although the result could have been confounded by mixing a time-average quantity (virtual velocity) with an instantaneous measure (peak bedload transport rate). O'Connor and Harr (1994) and Haschenburger (1996) applied Equation 2.3 more consistently using virtual velocity and a reach average δ_T to estimate an average bedload transport rate over the period of flow competence. O'Connor and Harr (1994) believed that their virtual velocity estimates had been underpredicted, whereas Haschenburger (1996) thought that errors in active width had a greater influence on results than virtual velocity.

Carling (1987) estimated a peak local bedload transport rate using Equation 2.3. He let δ equal the average δ_T for the reach and approximated the instantaneous peak bedload velocity by the near-bed water velocity. Peak transport rate estimates were compared to values that were calculated using a stream power-transport rate relationship that had been calibrated specifically to the study stream using high quality bedload trap data. The comparison was poor for lower peak flow magnitudes, where Equation 2.3

overpredicted the bedload transport rate by more than an order of magnitude, but it became better as flow rates approached bankfull. Carling (1987) interpreted this to mean that the entire bed surface layer did not become fully activated until flows approach bankfull.

An alternative explanation is also possible that demonstrates a difficulty in using Equation 2.3 to predict local scour depth. The difficulty stems from uncertainty in estimates of the local, vertically-averaged bedload velocity. There are three ways that bedload transport rate may increase:

(I) More particles situated lower down in elevation become disturbed and entrained (i.e., the bedload layer thickness increases);

(II) More particles become entrained per unit area of streambed; and

(III) Entrained particles move faster.

The influence of (I) on variation in q_B is likely to have been small in Carling's (1987) study relative to the other two. The mean thickness of the moving layer δ_B was estimated by Carling (1987) using scour chains to be about one half the mean bed grain size and was assumed approximately constant for all transport rates. Measurements of maximum local scour depth indicated that the local value of δ_B varied from the mean value by less than a factor of two in the study.

The contribution of (II) was likely to have been important. The estimated magnitude of δ_B was less than the substrate D_{90}, implying that not all of the bed surface was mobilized (i.e., the 'partial transport' mode is implied by Carling's (1987) data — see Section 2.1). Hence, an increase in transport rate with stream power or shear stress would have been associated with an increased number of mobilized particles from the surface, as inferred by Carling (1987). However, the active fraction of the bed surface increases rapidly over a relatively narrow range of shear stress for sizes contributing to the bulk of bedload transport rate (Wilcock and McArdell 1997). Carling's (1987) data represented a wide range of stream power, so it is likely that this mechanism explained some but not all of the observed variation in transport rates predicted by Equation 2.3.

The influence of (III) was likely significant. Carling (1987) may have over-estimated

the bedload transport rate using Equation 2.3 because bedload velocity was approximated by the near-bed water velocity, which must be faster than the particle in order to move it (Bagnold 1956). Carling's (1987) data were evaluated for the contribution of (III) to the calculated value of q_B (determined using the bedload transport rating curve), by re-expressing Equation 2.3 as:

$$q_B = \alpha\left(\xi U_{B_{calculated}}\right)^\beta = \xi U_{B_{corrected}} \tag{2.4}$$

where

$$\xi = \overline{\delta}\rho_s(1-P) \tag{2.5}$$

Equation 2.4 indicates that the true ('corrected') value of bedload velocity is proportional to the β power of the near bed water velocity (which equals the 'calculated' value of U_b). Regression yielded $\beta = 3.09$. Because friction velocity is directly proportional to water velocity, the regression result implies that mean bedload velocity is proportional to approximately the cubed power of friction velocity, or to the 1.5 power of shear stress. Bedload transport rate per unit width (q_B) also increases with the 1.5 power of shear stress (Vanoni 1975; Yalin 1977), indicating that increases in bedload transport rates could be caused in large part by increased particle velocities. Research is evidently needed to evaluate further the relative importance of each of the three ways that bedload transport rate increases with shear stress in gravel bed streams.

2.2.4 Scour Depth and Probability Density Functions

Frequency distributions of total scour depth and fill depth have been identified that integrate over space and time. Hassan and Church (1994) and Haschenburger (1996) determined that local and mean scour (or fill) depth distributions observed throughout a stream reach following a single flood could be described by the one-parameter

exponential probability density function (PDF), $p(\delta)$ as

$$p(\delta) = \theta e^{-\theta \delta} \tag{2.6}$$

where δ is scour (or fill) depth, and the parameter, θ, is the inverse of the distribution mean (Hines and Montgomery 1980). However, significant departures from the exponential PDF occur with increasing magnitude, duration, and frequency of flood flow, when an extensive proportion of the bed participates in repeated movement and scour depth data become more uniformly distributed (Hassan and Church 1994).

Haschenburger (1996) presented frequency distributions of total scour depth for several floods, the largest of which had a return interval of approximately 7 years. Approximately 75 percent of the scour depth measurements made after the largest flood were less than twice the substrate D_{90}. Rennie (1998) also presented frequency distributions of total scour depth, with and without zero values. The largest flood that occurred during his study had a return period of less than two years. Approximately 75 percent of the non-zero measurements after that flood were less than twice the substrate D_{90}.

Haschenburger (1996; 1999) proposed that a generalized model of scour depth distributions could be developed in a form comparable to Equation 2.6 if more information on surface sediment size, structure, and hydrology could be included. Such models would facilitate prediction of an approximate limit to scour depth, or some characteristic scour depth (e.g., the 90th percentile scour depth).

2.3 Field Studies Involving Tracer Particles

Tracer studies have provided valuable information on disturbance depth by measuring initial and final burial depths of tracer stones. They also provide information on distance traveled during a flood and on rates of particle movement. Tracer study results provide insights regarding the motion of individual bedload particles and the

linkages between scour depth measurements and bedload transport rates. Such information is useful for elucidating the relative contributions of δ_{B_m} and δ_{EX} to δ_T in Equation 1.1.

Tracers have included painted rocks, rocks with a distinct lithologic color, and magnetically tagged particles that may or may not be labeled individually. Painted rocks have the disadvantage that the paint wears off. Both painted and colored rocks are impossible to find when they are buried without excavating the entire bed. Magnetically tagged particles have provided greatest insight into scour processes because they have been retrieved when buried to depths of 0.74 meters (Hassan 1990) and their recovery rates may be 90 percent or greater (e.g., Schick et al. 1987; Hassan and Church 1994).

Hassan (1990) identified several possible mechanisms whereby tracer particles may become buried. Burial of smaller particles was thought to be facilitated in part by kinetic sieving through the larger framework particles during bedload transport. Large, immobile particles will develop a scour hole around their base and trap smaller particles that are subsequently covered by fill as flood stage recedes. Deposition of successive streambed layers was thought to be the most common burial mechanism. Hassan (1990) argued that traction carpets were uncommon, and were approximately one particle diameter thick when they occurred.

2.3.1 Depth of Disturbance

Tracer data indicate that particles representative of most of the bed surface grain size distribution are entrained at relatively low transport stages (e.g., $\tau^*/\tau^*_{cr} \approx 1.2$, Andrews and Erman 1986). Leopold and Rosgen (1991) determined that the proportions of each size class moving were similar at flows less than bankfull. The largest particles present in the bed surface may not move until very high transport stages (e.g., $\tau^*/\tau^*_{cr} > 4$, Ashworth and Ferguson 1989), or they may move at smaller peak flood stages (e.g., during annual flood events; Haschenburger 1996). These results are generally consistent with Wilcock et al.'s (1996) observation that disturbance of the surface layer can occur at

relatively small magnitude competent shear stresses.

Published data for mixing depths downstream of tracer release points indicate that the majority of moved particles remain near the bed surface during individual floods, and that the probability that tracer particles move decreases with increased burial depth (Hassan 1990; Hassan and Church 1994). Mean burial depths following individual floods were measured in two ephemeral streams to be between 150 and 220 mm, or approximately 1.3 to 2.0 times the bed surface D_{90} (Hassan 1990; Hassan et al. 1991). Approximately 90 percent of Hassan and Church's (1994) burial depth measurements after a flood in Carnation Creek, a perennial stream, were less than twice the surface substrate D_{90}. Hassan and Church (1994) thought that the majority of their scour depth measurements were representative of mixing within the surface layer during bedload transport, and that the deepest measurements were caused by scour and fill as opposed to a thick traction carpet.

Gamma and exponential distribution models have been used to describe reach-wide variation of tracer stone burial depths following individual, frequently recurring floods (Hassan et al. 1991). As in the case of scour monitor data, these distributions do not fit burial depth data well following a series of floods, or following individual, large recurrence interval floods as particle motion becomes more frequent. This is thought to be in part because the distance traveled approaches the spacing between bars and riffles, where many particles are stored as the flood recedes, such that a systematic, non-random influence occurs (Jackson and Beschta 1982; Kondolf and Graham-Matthews 1986; Hassan et al. 1991; Schmidt and Gintz 1995).

Tracer data have indicated that bars and riffles differ in their total contribution of coarse material to bedload transport. Madej (1996) determined that storage time of individual grains increased with distance across a bar from the active channel bed. Tracer particles trapped on bars have been observed to remain immobile longer on average than particles in the normally wetted channel and not be reactivated until either the bar surface is mobilized extensively during an extreme flood or lateral erosion occurs (e.g., Schick et al. 1987; Newson 1987; Wathen et al. 1997). Deep burial depths are

expected as a result of deposition of successive layers either at the downstream end of a bar in zones of flow divergence (e.g., Prestegaard 1987; Carling 1990) or during the subsiding stages of extreme magnitude (i.e., uncommon) floods as the bar rebuilds. Longer residence times in bars suggests that the majority of coarse material contributing annually to bedload transport originates from the thalweg and surrounding, normally wetted, regions of the channel. This is shown in Chapter 5 to be an important feature of scour and fill processes.

2.3.2 *Particle Travel Distance*

Travel distances of gravel- and cobble-sized tracer particles during individual floods and over the course of the flood season have been determined in some studies to scale with distance between riffles (Mosley 1978; Kondolf and Graham-Matthews 1986; Hassan et al. 1991), and tracers placed by Mosley (1978) in pools were mostly relocated in riffles or on bars. These findings support Jackson and Beschta's (1982) model in which riffles are the dominant starting and ending point for coarse bedload.

In a perennial, unconstrained alluvial gravel bed channel, the spacing between riffles generally ranges between five and seven channel widths (Leopold et al. 1995). Mean travel distances following individual floods in such streams have been measured to be 9 to 21 meters (bankfull width ≈ 55 m; Hattingh and Illenberger 1995) and as much as 265 meters (bankfull width ≈ 60 meters; Mosley 1978). Ashworth (1987; cited in Church and Hassan 1992) measured mean travel distances that varied between 0.22 and nearly 24 meters, in a stream where bankfull width varied between 5 and 15 meters (Ashworth and Ferguson 1989). Mean travel distances were approximately 4 channel widths or greater in some of these studies, although in other studies they were much shorter for comparable flood magnitudes.

2.4 Mechanics of Granular Flow

Granular flow involves motion of a bedload layer that is two or more layers thick within which particles collide with each other and momentum exchange is no longer dominated by fluid-particle interactions. Granular flow theory has been applied to a number of geophysical phenomena including avalanching, debris flows, and to a lesser extent, bedload transport. Most of the relevant research is based originally on the work of Bagnold (1954; 1956; 1966a), which focused predominantly on sand transport but was also relevant to gravel. The granular flow literature provides considerable insight into the processes of bedload transport in gravel bed streams under extreme flood conditions, and is summarized in this section in the context of predicting the maximum thickness of the moving bedload layer as a function of mobilizing force.

Granular flow theory, laboratory flume experiments, and multiparticle computer simulations indicate that a moving sheet flow layer of uniform-sized particles will have a thickness two to three times the particle diameter when the dimensionless shear stress parameter value is on the order of $\tau^* = 0.4$ to 0.5 (Bagnold 1956; Hanes 1986; Nnadi and Wilson 1992; Jiang and Haff 1993; Haff and Jiang 1995; Sumer et al. 1996; Jenkins and Hanes 1998; excludes the height reached by saltating particles). This has been proposed as the approximate transition between the existence of bedforms and sheet flow (Bagnold 1966a; Sumer et al. 1996). Parker et al. (1982b) noted that τ^* rarely exceeds two or three times the critical value in gravel bed streams (which may be between 0.03 and 0.086 depending on bed characteristics and interpretation of incipient motion; Buffington and Montgomery 1997). The surface layer is consequently thought to be the primary source of bedload (Parker 1990a). Results for uniform size should be extendable to heterogenous distributions, where the larger-moving particle sizes dictate layer thickness.

Four approaches to studying granular flow are described below. Each provides insight into scour and fill processes and a potential framework for predicting scour depth. The most basic approach is to approximate the bedload layer as a sliding block

('dynamic Coulomb yield models'). More advanced approaches involve modeling the energy and momentum balance within a moving granular layer. The layer is modeled as either a continuum ('collisional/kinetic energy models') or as a collection of discrete particles ('multiparticle simulation models'). Flume studies provide empirical data but are few in number and quality because of the difficulty tracking individual particles and measuring their speeds and trajectories in a large collection of rapidly and semi-randomly moving objects.

2.4.1 *Dynamic Coulomb Yield Models*

Bagnold (1956, 1966a) applied the principle of solid friction to bedload transport using the dynamic Coulomb yield relation:

$$\tau_r = \sigma_r \tan\phi \qquad (2.7)$$

where the shear stress τ_r resisting the steady state motion of a gravel layer (Figure 1-2) is proportional to the normal stress σ_r by a coefficient of kinetic friction term, $\tan\phi$ (ϕ is called the friction angle). The following review evaluates characteristic magnitudes of each term in Equation 2.7 in moving gravel and cobble bedload layers, with the goal of identifying the maximum predicted thickness of such layers in a natural stream channel.

The appropriate magnitude of the friction angle term is subject to great uncertainty because it can be represented by three distinct values (Hanes and Inman 1985a):

(I) $\phi = \phi_i$ = critical static angle of internal friction, measured as the angle of repose;

(II) $\phi = \phi_r$ = critical dynamic (or residual) angle of internal friction; and

(III) $\tan\phi = \tan\phi_D$ = stress ratio within a shear flow (i.e., Equation 2.7); ϕ_D is greater than or equal to the first two angles by a difference that is explained as an additional fluid frictional component (Bagnold 1966b).

The static angle ϕ_i is greater than or equal to the dynamic angle ϕ_r and differs by 2° to 8° for dry sand (Hanes and Inman 1985a). This range is comparable to the difference

between dynamic and static friction coefficients for sliding blocks, where dynamic coefficients are roughly 67 to 75 percent of static values (Beer and Johnston 1977). This range is also representative of the difference in shear stress magnitudes needed to initiate or maintain sediment motion (e.g., Reid and Frostick 1984; Reid et al. 1985).

Bedload layer thickness increases with decreasing magnitude of $\tan\phi$ for the same shear stress. The critical dynamic angle $\tan\phi_r$ is thus a lower bound on $\tan\phi$ for evaluating the maximum possible thickness of a moving gravel and cobble bedload layer. The value of $\tan\phi_r$ varies with the amount of dilatancy occurring within the shearing layer, which is inversely related to the linear concentration, λ (Bagnold 1954; 1956; Bridge and Dominic 1984; Hanes and Inman 1985a, b):

$$\lambda = \left[\sqrt[3]{\frac{C_m}{C}} - 1 \right]^{-1} \tag{2.8}$$

where C is the volumetric concentration ($= 1 - P$) and C_m is its maximum possible value ($= 0.74$ for uniform spheres). General shearing of uniformly sized spheres becomes possible when the linear concentration decreases to $\lambda \sim 22$ to 17. At $\lambda = 14$ ($C = 0.6$), the particles just clear one another during the time between successive collisions (Bagnold 1956, 1966b). Typical values of $\tan\phi_r$ vary between 0.5 (Savage and Sayed 1984; Hanes and Inman 1985a, b) and 0.63 (Bagnold 1973), although experimental work has determined friction coefficient values to vary by as much as plus or minus sixty percent of $\tan\phi = 0.5$ (Bagnold 1966b; Savage and Sayed 1984; Hanes and Inman 1985a; Campbell 1989). A value of $\tan\phi_r = 0.5$ is used here as a representative value.

The normal stress in Equation 2.7 is, for a layer of uniformly sized grains with diameter D:

$$\sigma_r = m' \cos\theta = D C_o (\rho_s - \rho) g \cos\theta \tag{2.9}$$

where m' is the immersed weight of the grains per unit area of bed, C_o is the at rest volumetric concentration, θ is the angle of the bed from horizontal, and $\cos\theta \approx 1$ for bed

slopes $S_b < 0.1$. Bagnold (1956, 1966a) noted that $C_a \tan\phi_i \approx 0.4$ for a wide range of experimental conditions, and that consequently Equations 2.7 and 2.9 imply that the dimensionless shear stress $\tau^* \approx 0.4$ when the entire surface layer mobilizes and the state of granular flow begins. Bagnold (1966a) reasoned further that the critical value of τ^* for a traction carpet should be between ~0.5 for $D < 0.3$ mm and ~0.25 for $D > 2$ mm.

Bridge and Dominic (1984) argued that $\tau_r = \tau_b - \tau_{cr}$, or the residual (excess) shear stress, where τ_b is the fluid shear stress at the top of the bed, and τ_{cr} is the critical shear stress for incipient motion. The thickness of the layer D was represented as $\delta_{MB+SALT}$, the thickness of the entire moving bedload layer including the saltation zone. Their resulting equation was:

$$\delta_{MB+SALT} = \frac{\tau_b - \tau_{cr}}{(\rho_s - \rho)g C_a \tan\phi_r} = \frac{D(\tau^* - \tau^*_{cr})}{C_a \tan\phi_r} \qquad (2.10)$$

where C_a is the average volumetric concentration of the moving layer. Assuming that $\tan\phi_r \approx 0.5$ and $C_a \approx 0.6$ are representative of moving gravel and cobble bedload layers that just clear one another, Equation 2.10 implies that :

$$\frac{\delta_{MB+SALT}}{D} \approx 3(\tau^* - \tau^*_{cr}) \qquad (2.11)$$

Hanes and Bowen (1985) argued that the normal stress $\sigma_r = m' + \sigma_\delta$, where σ_δ is the normal stress applied at the top of the moving bedload layer due to impacts from saltating grains. They derived the following expression for an assumed linear concentration profile within the moving bedload layer:

$$\delta_{MB} = \frac{2\tau_\delta \Delta\phi}{(\rho_s - \rho)g(C_\delta + C_o)} = \frac{2D\tau^* \Delta\phi}{(C_\delta + C_o)} \qquad (2.12)$$

where $\Delta\phi = (1/\tan\phi_r) - (1/\tan\phi_\delta)$, $\tan\phi_\delta = \tau_\delta/\sigma_\delta$, and τ_δ and C_δ are the applied shear stress and volumetric concentration, respectively, at the surface of the moving bedload layer. Hanes (1986) determined that when the dimensionless shear stress τ^* ranged

between 0.5 and 10, C_δ ranged between 0.06 and 0.16 and $\tan\phi_\delta$ between 0.99 and 1.48.
Substituting $\tau^* = 0.5$, $\tan\phi_r = 0.5$, and $C_o = 0.6$ into Equation 2.12 results in:

$$\frac{\delta_{MB}}{D} \approx 3\tau^* \qquad (2.13)$$

Wilson (1987) developed an analogous relation to Bridge and Dominic (1984) and
argued that $\tau_r \approx \tau_b$ at high shear stresses. He assumed that $\delta_{MB} = 2\delta_B$, $\tan\phi_r = 0.32$, and
$C = 0.625$, resulting in:

$$\frac{\delta_{MB}}{D} \approx 5\tau^* \qquad (2.14)$$

Nnadi and Wilson (1992) recalculated the mean concentration and estimated a new
friction coefficient, resulting in the following relation:

$$\frac{\delta_{MB}}{D} \approx 7.5\tau^* \qquad (2.15)$$

Equation 2.7 and the equations derived from it can be used to estimate the flow
depth required to move a gravel and cobble layer with a thickness $\delta_{MB} = 20$ to 30 cm.
This is a conservative approximation of a minimum egg pocket depth for many salmonids
(DeVries 1997) and allows for dilatancy during bedload transport. Data presented in
Chapter 4 show that this magnitude is also approximately equal to maximum bedload
disturbance depths estimated in this study. Letting $\tau_b \approx \rho g d S_f$ and $\rho_s = 2,650$ kg/m^3
results in required flow depths that are on the order of 10 to 100 meters in spawning
streams like the study streams where friction slopes (S_f) range between 0.01 and 0.001,
respectively. These depths are not observed naturally, and calculated dimensionless
shear stresses are typically less than 0.3 in flooding gravel bed streams (Parker 1978;
Parker et al. 1982b), suggesting that very thick moving gravel and cobble bedload layers
should not occur in natural gravel bed streams.

The limits to δ_{MB} predicted by Equation 2.7 also imply that the bedload layer should

move faster rather than deeper in gravel streambeds as the dimensionless shear stress increases above that required to disturb the entire surface layer. Excess shear stress is more effective in accelerating already moving particles than in mobilizing an underlying layer that is more resistant to motion and contributes relatively little material to bedload (Bagnold 1956).

2.4.2 *Collisional Kinetic Energy Models*

Kinetic theory for rapid grain flow models the physical processes occurring within the moving bedload layer, including momentum exchange through particle collisions. The kinetic, or constitutive modeling approach requires numerical solution of a large system of equations. Models have been derived for uniform and near-uniform grain size distributions but not heterogeneous mixtures because of analytical and computational difficulties, and thus have seen limited application to gravel bed streams. Kinetic models are nonetheless useful for estimating limits to bedload layer thickness and order of magnitude relations to shear stress.

Jenkins and Hanes (1998) developed a model of shearing flows of uniformly sized, nearly elastic spheres. The model was run twice in response to a request by the author for quartz particles 45 and 120 mm in diameter, using a coefficient of restitution $e = 0.85$, a value that is representative of quartz grain collisions (Foerster et al., 1994 determined $e = 0.83$ for glass-aluminum, and 0.97 for glass-glass collisions; Drake, 1990 determined $e = 0.84$ for acetate-acetate collisions). The solutions were similar to those presented in Jenkins and Hanes (1998), and the predicted thickness of the layer approached 5 particle diameters as the magnitude of τ^* decreased down to 0.5. The model experienced computational problems, however, at $\tau^* < 0.5$ that required further investigation (D. Hanes, personal communication, November 14, 1998).

2.4.3 *Multiparticle Computer Simulations*

A critical assumption of kinetic and sliding friction models is that the granular medium can be approximated as a continuum. This assumption is invalid in gravel and cobble beds when the particle dimensions are on the order of the bedload layer thickness. Haff (1995) noted that constitutive models are difficult to scale up to the macroscopic level because of problems in defining appropriate averaging volumes (e.g., when motion is restricted to a relatively thin surface layer; Haff et al. 1993), and observed that the previous history of a granular system strongly affects its subsequent state. These issues are likely of significance to bedload transport modeling, both locally and at the reach scale. Drake (1990) argued that frictional effects were sufficiently important that models based on kinetic theory were incomplete.

Multiparticle (or, 'particle dynamics') simulations provide an alternative model that tracks the trajectories and collisions of individual particles and thus follows the history of the granular medium. The equation of motion is solved for each particle and frictional forces are evaluated directly. The approach is computationally intensive but is useful for inferring particle behavior during bedload transport, and for computing dimensionless relations between layer thickness and shear stress. The approach also allows explicit modeling of mixtures of different grain sizes.

Multiparticle simulations and visual observations indicate that particles present in high concentrations (i.e., as could be the case in gravel and cobble bedload transport) are trapped in a microstructure that prohibits extensive movement relative to neighboring particles (Drake 1990; Campbell 1997). Particles in a layer are restricted to collide with others in the same layer, and with particles in the two adjacent layers immediately above and below (Campbell 1989). Jiang and Haff (1993) calculated that the thickness was restricted to the surface layer when $\tau^* \approx 0.16$. The thickness of the moving layer was approximately equal to $2D_{90}$ in their model at $\tau^* \approx 0.27$. For greater dimensionless shear stresses, Haff and Jiang (1995) determined that the dimensionless thickness of the moving layer increases approximately linearly with τ^*, corroborating kinetic modeling

results:

$$\frac{\delta_{MB+SALT}}{D} = K\tau^*$$ (2.16)

where $K = 6.8$ for coarse sand and $K = 8$ for fine gravel. They recommended using $K = 7.5$ in general applications. Jiang (1995) determined in a later simulation that:

$$\frac{\delta_{MB+SALT}}{D} \approx -1.0 + 9.7\tau^*$$ (2.17)

which is similar to earlier results.

Equations 2.11 through 2.17 indicate that the distinction between δ_B, δ_{MB}, and $\delta_{MB+SALT}$ is inexact and varies with interpretation of the boundaries between the saltating and non-saltating layers and of the magnitude of the static bed porosity. An approximate relation can be determined, however, that allows conversion of Equations 2.11 through 2.17 to the equivalent bedload disturbance depth in a static bed, δ_B. Assuming that the static bed concentration can be approximated by the maximum possible for spheres ($C \approx C_m = 0.74$; Bagnold 1956), Equation 2.1 implies that $\delta_{MB} \approx 1.2\delta_B$ when particles just clear one another between successive collisions (i.e., at $\lambda = 14$, $C = 0.6$; Bagnold 1956). Saltation height has been calculated to be equal to be between one and two grain diameters (Jiang and Haff 1993; Gotoh et al. 1996). Assuming that the average saltation height is one and a half diameters results in the following approximate equality:

$$\delta_{MB+SALT} \approx \delta_{MB} + 1.5D$$ (2.18)

Substituting Equation 2.18 and $\delta_{MB} \approx 1.2\delta_B$ into Equation 2.16 results in the following approximation for estimating the effective depth of disturbance in a static bed (i.e., as measured by scour monitors):

$$\frac{\delta_B}{D} \approx \frac{K\tau^* - 1.5}{1.2}$$ (2.19)

Note that when two layers are disturbed, $\delta_{MB} \geq 2D$ since the layers must just clear each other plus the third layer underneath. Remembering that $\delta_{MB} \approx 1.2\delta_B$, the corresponding disturbance depth in the static bed is approximately $\delta_B \geq 1.7D$, which would be similar to the results of Wilcock et al. (1996) if $D \approx D_{90}$.

2.4.4 *Experimental Studies of Motion at High Shear Stresses*

Measurement problems have limited evaluations of Equations 2.11 through 2.17. The most relevant empirical work is that of Sumer et al. (1996), who performed a series of duct flow experiments using uniform nylon, acrylic, and sand grains. Friction velocity was calculated from $(gRS_f)^{0.5}$ where R was corrected for side wall effects. The acrylic and sand grains behaved differently from the larger, cylindrical plastic particles. They found that suspension began at $\tau^* \approx 2$, supporting Bagnold's (1966a) theoretical result for fully developed suspension. Sheet flow was observed to begin at $\tau^* \approx 0.5$, again supporting Bagnold's (1966a) work. Bedforms developed at lower shear stresses, a result characteristic of small particle sizes (< 1 mm; Bagnold 1956). The thickness of the moving layer increased linearly with dimensionless shear stress, supporting kinetic and multiparticle model predictions. Analyses of video recordings made of particle motion (observed through the glass walls of the flume) resulted in an estimate of $K \approx 6.2$ in Equation 2.16. Vertical profiles of sediment concentration were also measured in the flume. The profiles were extrapolated to the elevation corresponding to a zero concentration to identify the height of the saltating layer, which resulted in a much larger estimate of $K \approx 12$.

2.5 Miscellaneous Scour Depth Prediction Studies

Borah (1989) defined bed scour as the result of an imbalance between sediment transport capacity and the amount of sediment being transported. Building on his earlier work (Borah et al. 1982), he argued that a stream scours material from the bed until the

armor layer grain size distribution is coarse enough to resist further motion. The thickness of the active layer was expressed algebraically in terms of an excavated volume of initially well-mixed material as

$$\delta_T = \frac{D_{armor}}{(1-P)\,p_{armor}}$$ (2.20)

where D_{armor} is the diameter of the smallest non-transportable particle present (assumed to be equal to the thickness of the armor layer), and p_{armor} is the fraction of sizes present in the bed that are of equal or larger size than D_{armor}. The net excavation depth was expressed as $\delta_{EX} = \delta_T - D_{armor}$.

Because the model is based on an initially well-mixed condition, Equation 2.20 is most applicable to the design of a new (constructed) channel or to a newly dammed reach (Borah 1989). In the first case, the flow will remove finer material until a sufficiently coarse armor layer forms that can withstand incipient motion at the highest flow experienced. The scour depth corresponds to the space occupied formerly by the particles carried off by the flow. A similar process happens below dams where sediment supply is suddenly cut off upon dam closure, and the reach eventually develops a static armor layer that is much coarser than for the pre-dam state.

Equation 2.20 predicts that a gravel streambed will ultimately lower to an elevation (determined by the substrate composition) where the surface layer is composed completely of particles that cannot be mobilized by the largest flood expected (Borah 1989). Equation 2.20 predicts the cumulative excavation of available material, but does not predict the excavation rate. Since gravel streambeds are characteristically not armored in this manner and are usually mobilized at least once a year (Richards 1982; Leopold et al. 1995), it is unlikely that the end state predicted by Equation 2.20 is reached under most conditions. Hence, Equation 2.20 has limited utility for predicting scour depth from year to year in natural channels.

Numerical models have been used to simulate and predict erosion and deposition at specified locations along a stream channel. They are most useful in the context of the

present work for evaluating net excavation depth (δ_{EX}). The sediment continuity and Navier-Stokes equations are discretized and analyzed either simultaneously ('coupled' model; e.g., Lyn 1987) or separately ('uncoupled'; e.g., HEC-6, Thomas 1982). Both model types require specification of a bedload transport equation, and their prediction accuracy depends directly on the accuracy of the predicted transport rate. They also require explicit *a priori* specification of a relation describing the thickness of the bedload layer (δ_B), usually assumed to be a multiple of a characteristic particle size (e.g., D_{50}, D_{100}; Kelsey 1996).

Numerical model accuracy is also subject to stability issues and truncation errors associated with the discretization scheme and corresponding magnitudes of the time and space increments used. Uncoupled models are simpler to use than coupled models and are suited for most subcritical flows, when the characteristic time scales of sediment and water motion are significantly different and the bed elevation does not change significantly over the modeled time step. Coupled models become necessary when the mean flow Froude number approaches 1.0 (Lyn 1987). Irrespective of type, numerical models are difficult to use to simulate short term changes in bed elevation associated with a single flood because of the difficulty in determining the initial and boundary conditions, and because model errors may be on the order of measured disturbance depths. They perform best when applied to longer term and larger scale evaluations of long profile development, where the magnitude of model error is small relative to the overall change in bed elevation.

2.6 Indirect Evaluations of Scour

Given the absence of explicit scour depth prediction models, assessments of the potential effects of scour on salmonid intragravel survival have been based instead on indirect approaches. The Washington State Watershed Analysis Methodology assumes that scour influences salmonids adversely when the "pre-development" five-year flood becomes a two-year flood in the "post-development" state (WFPB 1994). The

assumption is based on two other critical assumptions: (i) the magnitude and frequency of scour depth increases with magnitude and frequency of floods; (ii) a two-year peak flood will not scour out eggs and developing embryos, but a five year flood will. These assumptions remain to be evaluated using scour depth and egg burial depth data.

2.7 Synopsis

Conclusions drawn from the literature review are summarized below.

Bedload transport in gravel bed streams exhibits several possible modes of particle motion. They are, in order of increasing bed shear stress:

(I)   Partial transport ($\delta_B < 1$ layer);

(II) Traction carpet (1 layer $\leq \delta_B < 2$ layers); and

(III) Fully developed granular flow ($\delta_B \geq 2$ layers).

Partial transport, where a fraction of the bed surface is mobilized at the same time, is the most common transport mechanism and generally involves motion within the surface layer only. Scour extending down several layer thicknesses during partial transport must therefore be associated with the layer whisking scour process. Bedforms and particle clusters are structural features related to partial transport whose influence on scour depth appears to be limited to disturbance of the surface layer. Disturbance down to the bottom of the surface layer has been determined in the field to occur at dimensionless shear stresses as small as $\tau^*_g \approx 0.035$.

Analytic and particle simulation models suggest that the thickness of a traction carpet is approximately equal to the bed surface substrate D_{90} at a dimensionless bed shear stress $\tau^* \approx 0.2$ to 0.25, and may reach $2D_{90}$ when $\tau^* \approx 0.4$ to 0.5. At higher dimensionless shear stresses, models and laboratory data indicate that the thickness of the moving layer increases linearly, and at a greater rate, with shear stress. Gravel bed streams rarely, if ever, experience flood depths and shear stresses of the magnitude that appear to be required for granular flow, which suggests that measured scour depths that

are greater than twice the local D_{90} are a product of non-equilibrium sediment transport rates.

The majority of total bed disturbance depths measured in scour monitor and tracer studies have been less than the $2D_{90}$ bound suggested by Wilcock and McArdell (1997). Relationships that show a well-defined increase in reach-average scour depth with shear stress or stream power likely reflect more of the bed, and larger particles, being mobilized as shear stress increases. There is no clear, comparable relationship between local scour depth and either shear stress or stream power, and local scour depth measurements exhibit extremely large variability (as much as an order of magnitude; e.g., Carling 1987) for the same bed shear stress.

The bulk of transported coarse material appears to move from riffle to riffle, where it is stored between floods. Relatively little is stored in pools compared to riffles. Point bars appear to contribute relatively little material to bedload transport over riffles during individual floods because they are longer-term storage locations compared to material stored in the normally wetted channel. The appropriate length scale for evaluating the relationship between non-equilibrium sediment transport rates and local scour depth may therefore be the distance between successive riffles.

There is room for improvement with respect to predicting local scour depth at a salmonid redd location. Methods that have been used to predict reach and time-averaged quantities do not appear to be transferable to local, instantaneous quantities because:

(I)   The variability observed in both total scour depth and the thickness of the bedload layer may preclude identifying simple functional relationships with either shear stress or stream power.

(II) The one-dimensional continuity equation ($Q_B = A U_B$) may be ineffective for predicting the thickness of the bedload layer locally because it requires a relation between local bedload velocity and shear stress (or stream power) that is not well defined. Increases in bedload transport rates may reflect increases in mean particle velocity of the bedload layer more strongly than increases in the layer

thickness, probably because of frictional attributes of granular flow.

(III)   Gamma and exponential probability density functions are restricted presently to descriptions of reach-scale distributions of scour depth caused by low magnitude floods and do not facilitate prediction of local scour depth.

Prediction methods based on granular flow appear to be restricted to uncommon, extreme flood conditions in gravel bed streams. Other approaches and information are needed. Chapter 3 describes methods that were used in this study to collect the type of data needed for an improved understanding of scour processes and scour depth prediction.

3.0 Methods

It was a favorite saying of ... Dwight Eisenhower, that in war, before the battle is joined, plans are everything, but once the shooting begins, plans are worthless. The same aphorism can be said about exploration....what cannot be predicted is what is around the next bend in the river or on the other side of the hill. The planning process, therefore, is as much guesswork as it is intelligent forecasting of the physical needs of the expedition. It tends to be frustrating, because the planner carries with him a nagging sense that he is making some simple mistakes that could be easily corrected in the planning stage, but may cause a dead loss when the mistake is discovered midway through the voyage.

Stephen Ambrose — Undaunted Courage: Meriwether Lewis, Thomas Jefferson, and the opening of the American West — 1996.

Measuring physical processes in the field is difficult, especially in natural gravel bed streams. Variation observed in a measured outcome (e.g., scour depth) may be explained by the correct analysis of either a deterministic or stochastic process, or it may be a consequence of some unexplained phenomenon or oversight. The latter is often attributed to measurement error, uncontrolled events, and/or "natural variation" (Hurlburt's, 1984 "demonic intrusion" is a fitting term). A defensible field research program should attempt to minimize these two sources of variation as much as possible. It is crucial that the field research program be designed according to the following questions:

(I)   What is the fundamental process resulting in the phenomenon (dependent variable) of interest?

(II) Have all important process (independent) variables and parameters been identified and represented?

(III) What is an appropriate method of measurement for each variable, and is the resulting interpretation correct? ("Am I measuring what I think I'm measuring?")

The possibility of collecting insufficient data, the wrong data, or data including

unexplained variation that is subsequently mis-attributed to the process under study must be acknowledged and addressed by the study design as much as possible. This fundamental idea was a guiding philosophy behind selection and design of methods for this study.

Scour depth is the dependent variable in this study and is proposed to consist of two parts: the thickness of the moving bedload layer, and net excavation depth. The primary independent variables that are hypothesized to be important include local shear stress and grain size distribution characteristics that represent motive and resistive forces. Direct evaluation of each during floods cannot be accomplished safely. Indirect measurements were needed from which motive and resistive forces could be estimated, and with which sediment continuity could be evaluated. To accomplish this, ten specific measurement problems needed to be resolved, including:

(I) Selection of suitable study sites;

(II) Selection of a durable scour monitor design that would not provide false readings;

(III) Development and fabrication of a practical and effective tool for inserting scour monitors without significantly disturbing the streambed;

(IV) Identification of surveying techniques that provide consistent measures of bed elevation so that differences between successive surveys reflect net changes in elevation rather than measurement error;

(V) Identification of a method for estimating local shear stress;

(VI) Identification of practical and effective means for measuring maximum stage;

(VII) Relation of stage at a transect to that at a nearby stream gage;

(VIII) Measurement of water surface elevation and calculation of friction slopes;

(IX) Identification of relevant grain size distribution statistics and determination of accurate measurement techniques; and

(X) Quantification of spatial distributions of gravel available for bedload transport.

These and related measurement issues are described in the remainder of this chapter. Field measurement procedures are described first, followed by field data reduction

approaches. This chapter focuses on measurement and estimation of the dependent and independent variables so that subsequent chapters can focus specifically on the scour depth problem.

3.1 Study Stream/Site Selection

In contrast with laboratory flume studies, field investigations are subject to a large set of variables that are difficult to control experimentally. However, judicious choice of several study sites can lead to minimizing unexplained sources of variation and maximizing variation in the physical characteristics that are thought to be important. Goals and criteria for selecting appropriate study sites are described below in rough order of importance to the study. Candidate study streams were chosen after discussions with forestry, geomorphology, and fisheries professionals, and examining previously compiled channel classification and spawning survey data (Washington Department of Natural Resources and U.S. Forest Service watershed analyses, and Washington Department of Fish and Wildlife reports).

Two different channel types, "plane bed" and "pool-riffle", with reach slopes less than 0.03 (Montgomery and Buffington 1997), were sought to capture a range of morphologic channel units typically used by spawning salmonids. The class of gravel bed stream considered in this study is that where channel morphology and gravel/cobble distributions are not controlled to a significant extent by bedrock or large individual clasts, and gradually varied flow conditions prevail such that water surface slopes approximate friction slopes at flood stage.

Study streams and sites were selected to characterize a wide range of scour depths and independent variables. The purpose was to increase the applicable range of scour depth predictors and facilitate larger scale testing of dimensionless variables. Ways to accomplish this included selecting for variation in stream sizes and location in the channel network (i.e., upstream vs. downstream). Stream size and location correspond to a range of shear stresses, and flood magnitudes and duration. Selecting for variation

in stream gradient was expected to influence the range of shear stress or stream power available for bedload transport. A range of substrate particle sizes and material types was necessary to capture variability in the characteristics that influence resistance to motion.

Known scour and/or bedload transport history figured prominently in stream and site selection. Streams and sites were preferred that had a relatively high likelihood of bedload transport activity relative to all streams in the sampling set, based on flood history and field observations of others. In the event that the study period encompassed a series of low flow years, a scour data set might still be obtainable.

Stream reaches were identified that had extensive spawning gravel deposits in riffles and that were used consistently by a number of different salmonid species. Such deposits were generally associated with appreciable bedload transport activity across the normally wetted portions of the bed. Substrate sizes were targeted that were suitable for salmonid spawning, with D_{50} ranging between roughly 15 and 80 mm (cf. Kondolf and Wolman 1993). In addition, slightly larger substrate sizes were also targeted to expand the variability explained by the data set. Different areas were selected with different salmonid species to evaluate species distribution differences and the relation between scour depth and egg burial depth.

Sites were selected to contain either a series of pool-riffle sequences with abundant gravel, or a relatively long, straight riffle. For the former, the upstream riffle was anticipated to contain an abundant supply of gravel that was sufficient to replace material transported out of the primary study riffle. The latter channel morphology was reasoned to exhibit close to equilibrium sediment transport because of limited local transport rate imbalances existing along the length of the reach. The reach length was assumed *a priori* to correspond to typical particle travel distances based on tracer stone data reported in the literature for individual and multiple floods (generally less than 100 m; see Section 2.3.2). Selection of sites to represent different channel forms was a practical means for comparing and contrasting hypothesized scour mechanisms.

Streams were selected that represented different degrees of flood flow confinement,

in consideration of the possibility that unconfined streams might exhibit shallower scour depths than confined streams by virtue of overbank flow and its imposed limit to shear stress.

Preferred sites had a continuous-recording stream gage located nearby that provided an accurate and complete stage/flow history which could be related directly to flood stage at scour monitor locations. This was considered superior to selecting sites where use of maximum stage recorders (less information) or relying on flood marks (less accurate) would be necessary.

The candidate study streams and sites were selected to have features that would minimize unexplained variation in scour depth as much as possible. Streams with extensive loading of large woody debris were avoided since it would not be possible to differentiate between scour induced by fluid stress associated with flow depth versus physical ploughing or short term scour hole development around the object as it moved downstream. Deposition of large woody debris in the vicinity of scour monitors would also complicate results. Relatively straight reaches were preferred, to limit meander bend scour associated with secondary currents and channel migration, avoid strong cross-stream differences in water surface elevation, and minimize local roughness effects and asymmetric shear stress distributions induced by channel curvature. Reaches were also selected to have limited potential for contraction, jet, or vortex scour so that the mechanism of scour could be restricted to that induced by shear stress associated with the mean flow depth. Sites with significant bedform and boulder roughness were avoided. Sites with patches of spawning gravel interspersed with boulders were also avoided since scour would likely be associated with three dimensional velocity fields around flow obstructions.

Logistical considerations were also important. Relative ease of access to streams and sites influenced selection, permitting a relatively large number of sites to be visited quickly and safely during floods. However, preferred sites also had limited public access, or were accessed primarily by more respectful anglers, because vandalism and interference are significant concerns in field studies.

Forty-eight candidate reaches/sites were identified in twenty-four streams. All sites were visited in the field in June and July, 1996. Of these, fifteen sites were selected and instrumented in the fall of 1996. Four sites were later abandoned because of uncontrolled circumstances or because they did not provide much useful data. One site (South Fork Snoqualmie River at Edgewick; downstream of study site) was discontinued because a large tree fell directly across the upstream transect in the study riffle, affecting the results through subsequent scour hole development and downstream deposition. Another site, Trap Creek (tributary to Willapa River), was discontinued because of vandalism: all of the scour monitors were pulled early in the study by fishermen before enough useful data could be collected. A third site, South Fork Stillaguamish River near Granite Falls, was discontinued because of access problems and loss of scour monitors. The fourth site, Mill Creek (also tributary to Willapa River), experienced fill.

The general physical characteristics of the remaining eleven sites (Figure 3-1) are summarized in Table 3-1. The streams satisfied most of the criteria discussed above. Scour monitor deployment was increased in the Raging River, Issaquah Creek, and South Fork Snoqualmie River sites over the 1997-98 flood season. The other sites were discontinued after the first year so that more time could be spent on the three remaining sites and on data analysis.

Site locations, photographs, and maps are provided in Appendix A.

3.2 Field Data Collection

3.2.1 *Scour Monitor*

Numerous devices have been developed and tested in streams to measure scour depth. The relevant problem here was to select an appropriate device based on practical application and measurement considerations. All devices have been based on burial in the streambed, subsequent relocation after a flood or floods, and noting changes in the original device configuration that indicate scour depth. Chains (Leopold et al. 1995)
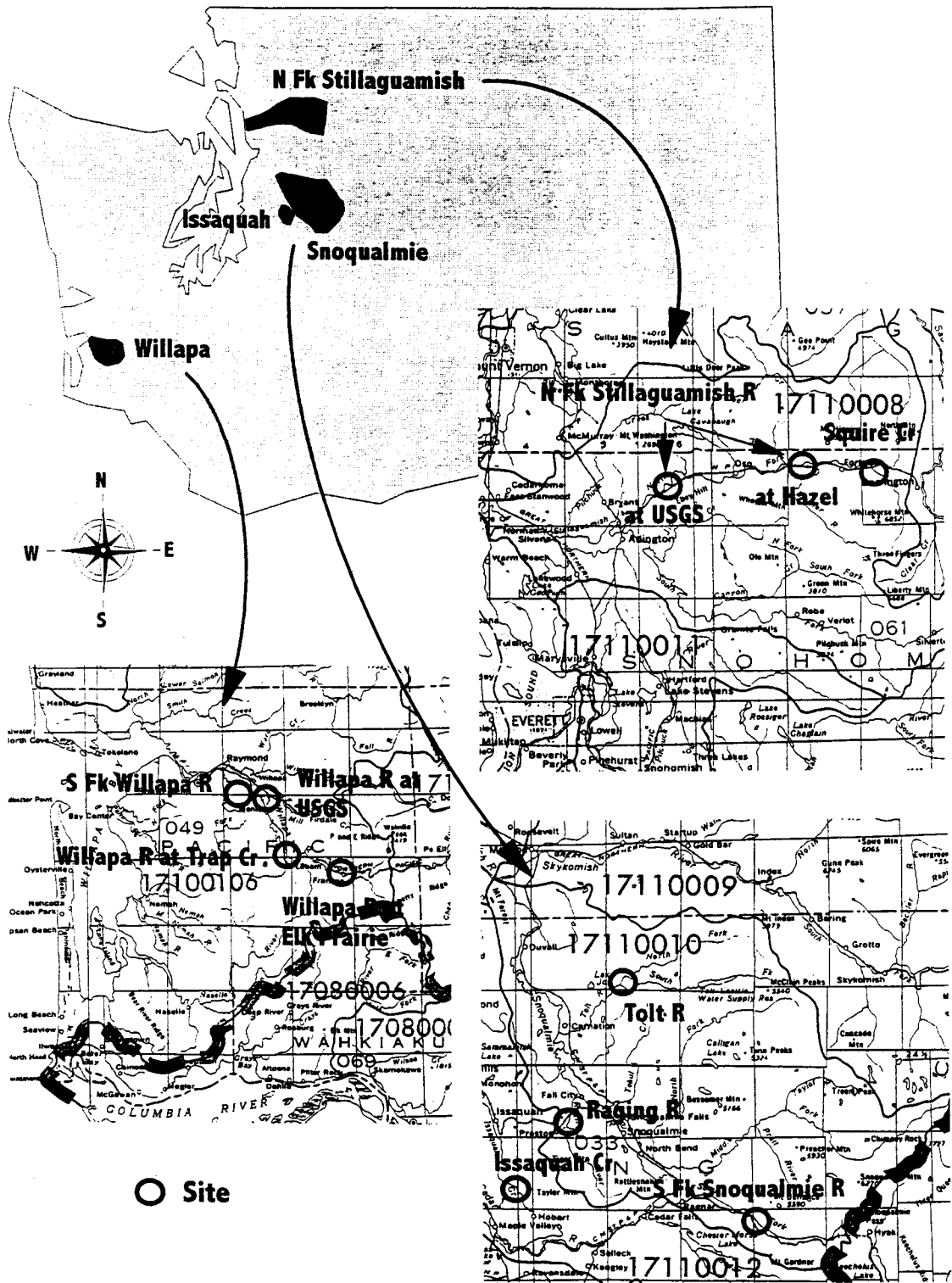
Figure 3-1. Location of study basins, streams, and sites.

Table 3-1. Study site characteristics.

Study Reach	River km	Drainage Area (km²)	Stream Reach Slope on 7.5 Minute Topo	Estimated Friction Slope [i]	Range of Surface Grain Sizes (mm) D84	D50	Mean Annual Flow (m³/s)[ii]	Peak Flow on Record (m³/s)[ii]
Issaquah Creek	16.6	46	0.0125	0.0051	67-76	41-44	1.38	38.51
N Fk Stillaguamish River at Hazel	35.7	347	0.0031	0.0032	80-117	34-59	na	na
N Fk Stillaguamish River at USGS	10.3	679	0.0015	0.0013	123-171	79-91	53.88	1039
Raging River	6.9	73	0.0200	0.0099	109-150	56-83	3.77	176.1
S Fk Snoqualmie River	27.4	118	0.0043	0.0040	50-151	35-85	8.55	239.2
S Fk Willapa River	8.0	89	0.0030	0.0014	32-62	22-35	4.78	92.87
Squire Creek	2.1	52	0.0083	0.0029	90-93	53-55	5.27	182.3
Tolt River	14.0	211	0.0083	0.0090	35-70	21-35	16.45	492.6
Willapa River at Elk Prairie	59.5	51	0.0020	0.0017	95	44	na	na
Willapa River at Trap Cr	47.8	220	0.0021	0.0031	36-128	33-48	na	na
Willapa River at USGS	28.6	337	0.0014	0.0013	73-85	39-56	17.87	419.0

[i] - See Section 3.3.4

[ii] - Italics = discontinued gage; "na" = no gage located nearby

indicate scour depth as the point at which the originally vertical chain bends away from its initial position towards the horizontal. Fill is measured as the depth of residual material above the scour depth point. Chains have been used extensively (e.g., Emmett and Leopold 1965; Carling 1987; Laronne and Duncan 1989; Lisle 1989; Nawa and Frissell 1993; Laronne et al. 1994; Madej 1996). The devices have been found to be relatively reliable, although installation may not always ensure that the links are extended completely because of their weight, and some judgement may be needed to identify the location of the bend. Foley (1978) used 3 mm diameter nylon cord in a sand bed stream that differed from a chain in that the nylon was almost neutrally buoyant and bent more markedly at the scour depth. Both techniques require subsequent relocation and excavation of the device to determine scour depth, and are thus essentially single-use methods. Relocation of a buried device and its excavation are also laborious and difficult in a gravel or cobble streambed.

A variation of the scour chain method was tested by Duncan and Ward (1985) in which a chain was attached to an L-shaped rod that was free to slide down a shaft which in turn was driven into the streambed. The device was designed to slide as far down as scour occurred. The device turned out to be susceptible to damage and interference by debris floating downstream.

An alternative approach that resolves most problems of scour chain-type devices involves burial of an indicator that is mobilized by excavation or movement of gravel around it. McNeil (1962) and Moring (1975) buried stacked ping pong balls in the streambed and measured scour by excavating after floods and counting the number of balls remaining. Tracer stones have been employed more extensively than balls (e.g. Hassan 1990; Hassan and Church 1994; Wilcock et al. 1996). Crisp (1989) used artificial fish eggs to determine washout depth. Drawbacks to this approach are that the indicators are not retained and cannot be reused if they are not relocated, excavation is still required to measure scour depth, and measurement accuracy is influenced when indicators are missed during retrieval.

Sliding indicators, attached to a guide line that is anchored in the streambed, have

been used extensively in recent years. Upon bed mobilization, the indicator slides along the line to its free end as it is entrained by moving gravel and fluid drag. Designed correctly, the indicator should move all the way to the end of the line, which will remain above the streambed in most cases except when extensive fill occurs. The indicator should be sufficiently durable to withstand the rough environment of the mobile gravel layer and not be destroyed or torn from the line. When these conditions are met, the sliding indicator method facilitates rapid determination of scour depth without extensive excavation (as long as there is negligible net fill that the monitor is not buried). Depending on practical aspects of flow depth and depth of scour measured, the monitors may be reset for measuring another event.

Tagart (1976) used ping pong balls on a monofilament fishing line. The device was anchored into the streambed by a lead weight and had a cork attached to the other end. Potential problems with this type of device included fragility of ping pong balls and buoyancy of the cork increasing the susceptibility of the device to be snagged by passing debris. Nawa and Frissell (1993) used sliding beads and found them to work relatively well. The bead size was relatively small compared to ping pong balls and thus reduced scour depth measurement error. Beads may be crushed by large moving particles and are difficult to count under all but low flow conditions.

The precursor to the device used in this study consisted of plastic practice golf balls (also known as "whiffle" balls, approximately 4 cm in diameter) strung on a nylon monofilament line. This device was designed during research work conducted on the Queen Charlotte Islands in the early to mid 1980's (Tripp and Poulin 1986; Klassen and Northcote 1986; M. Church, personal communication). Haschenburger (1996) used a similar device, with 25 balls per monitor. A potential drawback to this configuration is that the nylon line might become kinked near the water column-streambed junction, and confirmation of scour depth might then have to wait until the device was excavated. Alternatively, the line can be severed by moving gravel (Haschenburger 1996) or cut through the indicator ball.

The primary drawback to the use of whiffle balls is the magnitude of the associated

measurement error. A scour monitor ball should generally not move when the pivot angle between the ball and the scour depth elevation is greater than 180 degrees because substrate particles hold the ball in place. Scour of a single ball will occur when the disturbance depth falls below one half of the ball diameter and the pivot angle becomes less than 180 degrees. The next ball underneath should not move until the scour depth reaches its half-diameter depth. The scour depth measurement error of a single monitor is thus expected to be plus or minus half the ball diameter, or ±2 cm (range = 4 cm).

The device used in this study is similar to that used by Montgomery et al. (1996) (Figure 3-2). A thin stainless steel "aircraft cable" wire was used instead of a monofilament line. Galvanized wire was not used because it is less flexible and kinks more easily than stainless steel. Corrosion of the wire was prevented by use of 'sacrificial' zinc fender washers. The size of the wire was a balance between low weight, high durability, high flexibility, and low propensity to slice through the plastic golf balls. A 1.6 mm ($^1/_{16}$") diameter wire was used. The brand of practice golf balls used, Gold Eagle, was found to be particularly durable and resistant to crushing. Six, eight, ten, or twelve balls were used per monitor, the number depending on expected scour depth and/or depth to bedrock. Aluminum crimps were used to fasten the ends of the wire and hold the balls at a fixed position during insertion into the streambed.

A wooden dowel was used as an inexpensive bottom anchor (suggested by N.P. Peterson, Simpson Timber Co.). I confirmed in a jar of water that the dowel became neutrally buoyant within a few months of submersion such that it was unlikely to influence the measured scour depth during bedload transport. Buoyancy was not a problem, however, because the surrounding gravel always held the anchor firmly in place after installation. The anchor was situated only a few centimeters from the bottom crimp, which worked well in most cases. There were a few exceptions to this, however, in smaller substrates (D_{90} ≤ 80 mm) when the active bed elevation lowered to the last or next-to-last ball. At that point, the anchor resistance was overcome by drag forces acting on the already-moved balls and the scour monitor was lost (2 monitors were recovered downstream in Issaquah Creek as evidence of this). The problem has been

58
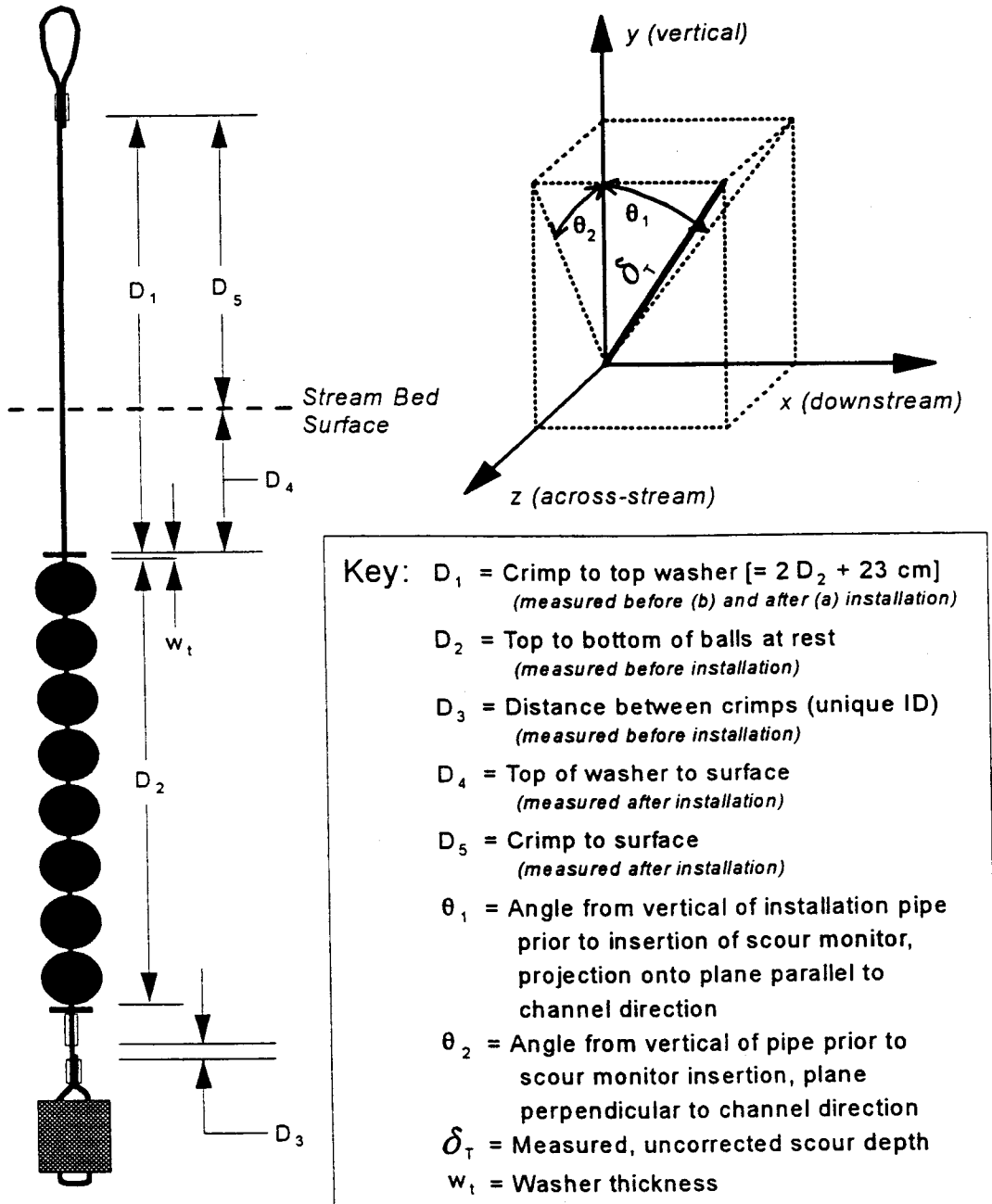
Figure 3-2. Scour monitor and installation dimensions.

noted in other studies (e.g., S. Hilton, personal communication August 1998). Based on the relevant dimensions of the present devices and observed instances of corresponding monitor loss, future scour monitors should be constructed with the anchor situated at least 10 cm below the lowest indicator ball to preclude monitor loss before all of the balls have moved. Alternatively, a heavy weight could be used.

The scour monitor device depicted in Figure 3-2 works well; the number of balls ending up at the end of the line is a reliable measure of scour depth. Excavations of a large number of monitors in this work showed that the indicator balls moved completely to the end of the cable without stopping prematurely within the gravel layer. Remaining, undisturbed balls were found consistently to be stacked in their original configuration.

3.2.2 *Scour Monitor Installation*

The scour monitors were inserted into the streambed using a tube installation device that is driven into the streambed and creates a space to be occupied by the monitor (Figure 3-3). The installation device was designed specifically for this research and represents an improvement in driving efficiency over previously used systems. The device consists of an inner tube with a well point head, and an outer tube and driving cap. The entire assembly was driven into the bed using first a fence post pounder and then a 4.5 kg sledge hammer (details on the device and its use are presented in Appendix B).

A number of scour monitor dimensions were measured during installation (Figure 3-2). The distance from the top crimp to the top washer (D_1 in Figure 3-2) was measured both before and after installation to ensure that the indicator balls were seated properly without any gaps occurring between balls. The combined height of the indicator balls (D_2 in Figure 3-2) was measured before installation because the dimension it represents is always greater than the multiple of number and average diameter of balls because of manufacturing and surface irregularities. The distance between the lower two crimps (D_3 in Figure 3-2) was measured before installation as a unique identifier of each scour
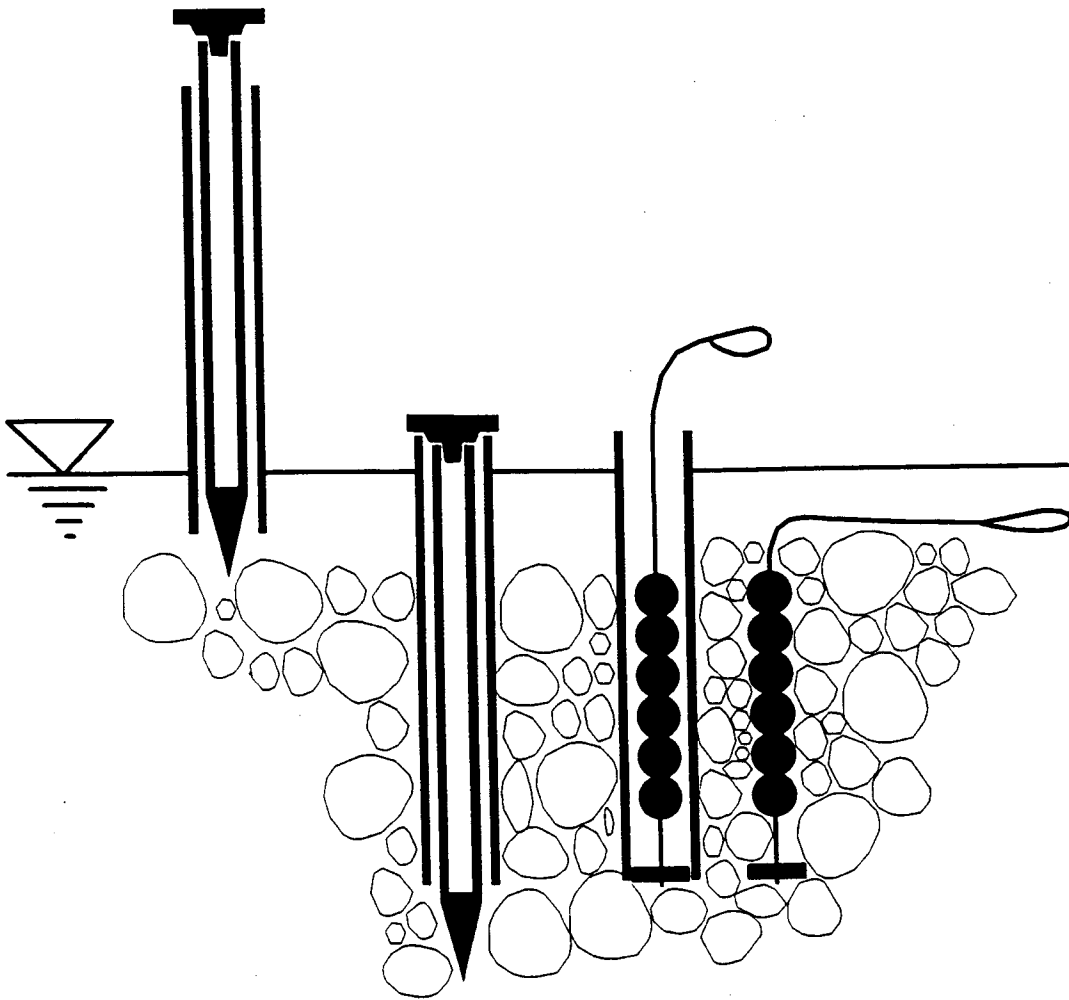
Figure 3-3. Schematic of method of scour monitor installation into the streambed.

monitor for contingency purposes (e.g., if the monitor was later recovered downstream); the value varies slightly between monitors during construction. The distance from the streambed elevation to the top washer and to the top crimp (D_4 and D_5, respectively, in Figure 3-2) were measured to distribute potential error inherent in defining the level of the streambed surface (see Section 3.3.1).

The inner tube was removed and the scour monitor inserted as far as possible into the outer tube until the anchor met resistance. The monitor was held in place with a 1.5 m-long threaded (for easier grip) steel rod with an eye-hook fastened at the lower end. The top end of the scour monitor cable was threaded through the hook, which maintained the indicator balls in their installed position as the outer tube was lifted and removed (Appendix B).

The rod was then removed, and the streambed excavated down to the first ball to check whether the balls had separated, by comparing the D_1 measurement before (D_{1b}) and after (D_{1a}) installation. The largest substrate particles present were set aside, and the remaining excavated material placed into a bucket. Typically, only the top ball lifted slightly during installation, but this was corrected by either (i) pushing and working the ball down until it contacted the next ball, or (ii) pulling gently on the monitor cable to bring all of the balls together snugly and ensure that the top ball was sitting at the desired depth below the bed surface. The elevation of the top ball was typically set within the lower half of the surface armor layer. The D_4 measurement was made, where the threaded steel rod was placed across the hole to define an average bed surface elevation. The excavated substrate was then replaced and covered with the larger original surface particles. The D_5 measurement was made subsequently, again using the threaded rod to define a bed surface elevation. Finally, the free end of the scour monitor cable was placed on the bed pointing in the downstream direction, and concealed among the larger surface rocks to reduce the potential for vandalism.

3.2.3 Transect Selection and Placement of Scour Monitors

At most of the 1996-97 sites, two transects were located across a riffle containing suitable spawning habitat. Transect ends were defined on both banks by stakes, steel reinforcng bar (rebar), or nails in trees. The transects crossed regions of the streambed where salmonid spawning was judged likely to occur according to observed substrate sizes and hydraulic conditions. A third transect was placed upstream, in either the next riffle if the primary riffle was relatively short, or in the same riffle/pool unit if it was several channel widths long, relatively prismatic, and had a relatively flat bed. The lower two transects provided most of the detailed data for this study. The third transect provided information on sediment transport mass imbalances: substantially different scour depth measurements between the lower two and upper transects indicated net transport rate imbalances in the reach.

Scour monitors were placed in Autumn of 1996 (during low flow) in pairs across each of the lower two transects. Monitor pairs were placed at two or three locations across each transect to measure cross-channel variation. Pairing of monitors was intended to reduce measurement error through replication: the original study design called for averaging the two scour depths at a location before proceeding with shear stress and other analyses. Pairing also increased the probability of getting useful data: one of the two monitors would likely remain if the other was pulled by a curious fisherman. Unfortunately, scour monitors were pulled in many cases before useful data could be collected, and thus replication was abandoned and the results for each scour monitor were treated as unique observations for consistency.

Two or three scour monitors were also placed in Autumn 1996 across the upstream transect. Monitors were not placed in pairs since the upstream transect was originally not intended for detailed evaluations of scour depth and mobilizing force. Measured scour depths across the upstream transect were compared to values measured downstream to assess spatial patterns of scour in a reach. The data were later integrated with the main riffle results to increase the number of observations given problems of

scour monitor loss.

Additional transects were established in Autumn 1997 in the Raging River, South Fork Snoqualmie River, and Issaquah Creek sites (depicted on site maps in Appendix A). One transect in each site was located across a pool and/or run (shallower and faster than a pool, deeper and slower than a riffle). Two of the transects in the Raging River site were located across a low gradient cascade. Transect locations were generally selected to measure the longitudinal variation in scour depth in a riffle-cascade-run-riffle sequence in the Raging River, a riffle-pool-riffle sequence in the South Fork Snoqualmie River site, and a pool-riffle-run-riffle sequence at the Issaquah Creek site. Scour monitors were installed in pairs at one, two, or three locations across each transect. The number of locations depended on the extent of the transect width that was likely to be mobile under most flood conditions, or in the case of pools, a single pair was located near the thalweg. Table 3-2 lists the number of transects and scour monitors installed in each of the fifteen original sites in 1996 and 1997.

3.2.4 *Surveying of Bed Topography*

Numerous surveying benchmarks were established at each site for redundancy in case some were lost or shifted in elevation (which occurred at many sites). Steel reinforcing bar (rebar), large nails, and the highest elevation of immobile, angular boulders were used. Survey level loops were done frequently to track and correct for changes in benchmark elevations, to ensure the same survey datum.

Consistent surveying of bed elevations in natural channels containing gravel and cobble substrates is subject to measurement error because the rod-person may place a leveling rod between individual bed particles one time, and on top of a particle the next time. This influence of surface microtopography on the measurement decreases with increasing rod base diameter. Conversely, the influence of bedform topography increases with rod base diameter, as does the effect of drag in moving water on the maneuverability of the survey rod.

Table 3-2. Numbers of transects and scour monitors installed in Autumn 1996 and 1997.

Study Reach	1996		1997	
	Number of Transects	Number of Monitors Per Transect	Number of Transects	Number of Monitors Per Transect
Sites Yielding Scour Data:				
Issaquah Creek	2	4, 4	7	2, 2, 3, 3, 2, 2, 2
N Fk Stillaguamish River at Hazel	3 (+1 redd)	6, 5, 6, (7 at redd)	na	na
N Fk Stillaguamish River at USGS	3	4, 6, 2	na	na
Raging River	3	6, 6, 3	6	4, 4, 2, 2, 2, 2
S Fk Snoqualmie River	3	6, 5, 3	6	6, 2, 2, 2, 4, 2
S Fk Willapa River	3	4, 4, 4	na	na
Squire Creek	3	6, 6, 4	na	na
Tolt River	4	6, 6, 2, 2	na	na
Willapa River at Elk Prairie	3	4, 4, 2	na	na
Willapa River at Trap Cr	3	4, 6, 2	na	na
Willapa River at USGS	2	6, 6	na	na
Discontinued Sites:				
Mill Creek	1	4	na	na
S Fk Snoqualmie at Edgewick	3	6, 4, 4	na	na
S Fk Stillaguamish at Granite Falls	2	4, 2	na	na
Trap Creek	1	4	na	na

A field test was conducted in Autumn 1996 to identify an appropriately sized yet practical leveling rod base diameter that minimized bed elevation measurement errors induced by microtopography and bedform influences. Ten transects with different substrates were surveyed using a range of rod base diameters. A 127 mm (5 inch) diameter was found to be most suitable for making consistent bed surveys over a wide range of bed roughness, and was consequently used in this study. Details supporting this choice are given by DeVries and Goold (1999).

Bed elevations were surveyed in two ways. In the first approach, cross-section

elevation measurements were made immediately after scour monitor installation, periodically over the winter when feasible to track bed changes due to individual large floods, and in the spring at the time of monitor retrieval. Scour depths and hydraulic parameters were calculated at each monitor location using the measured cross-section geometry.

In the second approach, topographic surveys were conducted in selected sites in Autumn 1996 using a surveying total station and prism. The 127 mm leveling rod base was fixed to the base of a prism rod. Ten to twenty measurements were made at approximately 0.5 m to 3 m intervals across the channel, on transects spaced 1 to 5 meters apart, with resolution depending on channel size. Greater resolution was needed across the channel than along the channel because of concomitant differential variation in bed elevation. Greatest resolution was required in the vicinity of abrupt changes in bed elevation and around large, isolated boulders. The topographic surveys were repeated at the end of the 1996-97 flood season. Surveys were not repeated at the end of the 1997-98 season because negligible flooding and bed mobilization occurred that year. Comparisons of bed elevations before and after a flood season were made to identify local net sediment losses and gains in the site that were subsequently evaluated together with the distributions of measured scour depths.

3.2.5 *Stage, Water Depth, and Water Surface Slope Measurements*

Water surface elevation data were needed to estimate the flood flow depth at a location and the longitudinal water surface slope. Flood elevations were measured usually along one bank in as many safely accessible locations as possible, although occasionally it was possible to wade out slightly into the channel and mark water surface elevations on trees, boulders, or stout shrubs. Flood stages were typically marked with nails, rebar, string, or flagging and surveyed later when the flood had subsided and access was possible. A ruler or other straight-edge implement was used to judge the surrounding, average water surface elevation in cases of runup against a flow obstruction

or of rapid local fluctuations in water level due to turbulence. The latter were often relatively large during floods, on the order of 5 cm or more. Elevations were also measured against previous, known elevation marks or nearby survey control points using either a builder's hand level or a carpenter's level. Flood marks were used to estimate the maximum stage at both gaged and non-gaged sites after each major flood. Maximum stage was noted by flood deposits, wash lines, and melted snow lines.

At sites near continuously recording U.S. Geological Survey (USGS) gaging stations, stage was surveyed at a number of flood flows at each transect. Rating curves were developed that related transect stage to stage at the gaging station (Appendix C). Fifteen-minute stage data were obtained for the station from the USGS office in Tacoma, Washington. The time of each water surface elevation measurement was recorded to compare with 15-minute stream gage data. This allowed more accurate prediction of maximum stage at each transect compared to flood forensic measurements.

Maximum stage recorders were installed at sites in streams without USGS gages, or where the site was not immediately adjacent to the gage (the North Fork Stillaguamish River at Hazel, the Raging River, in Squire Creek, the South Fork Snoqualmie River, the South Fork Willapa River, and the Trap Creek and Elk Prairie sites on the Willapa River). Flexible, clear polyethylene tubing was tried first, with floating powdered cork inside. The maximum stage was to be indicated by cork residue stuck to the inside of the tubing after the flood waters receded. The tubing was fastened to trees, pilings, clay cliff faces, or other suitable surfaces. The method did not work very well due to the relatively small diameter of the tubing, development of cork plugs, siltation, and freezing. The recorders were difficult to read accurately, and often a single grain of cork located above a larger collection of cork corresponded better with other measures of maximum stage.

An idea for a better maximum stage recorder originated while looking for flood deposits. Moss on tree trunks trapped floating debris, notably conifer needles and filamentous material. Moss also trapped sediment particles, which supported additional moss growth. Strips of white velcro tape (available in fabric stores) were stapled against

tree trunks located near the bankfull channel margin. Both the hook half and the cloth half were fastened side by side. The hook half of the velcro tape was expected to trap filamentous material, while the cloth half was expected to trap fine sediment material. All trapped material was expected to show up readily against the white strips. Velcro maximum stage recorders were installed at a number of sites during the winter after the failure of the cork recorders. The maximum stage mark was found to show clearly, with an interpretation error of roughly +/- 1.5 cm (the elevation of the line matched other high flow marks nearby to within a few centimeters). The data generally did not need to be corrected for runup on the trunk, which was estimated (using $U^2/2g$) to be typically 3 cm or less according to visual estimates of surface velocities near the recorder location. The error was smaller than errors associated with deducing stage from flood deposits and was relatively small compared to the water depth over the scour monitor during flood flow.

Most elevations surveyed were slightly higher than that of the main channel because of cross-channel velocity head differences. However, for purposes of energy slope calculations, the error appeared to be relatively consistent along the length of the channel based on observed surface water velocity distributions and thus likely had little influence on the result.

Water depth was calculated for each scour monitor as the difference between stage and the elevation of the bed at the monitor location before the flood. The pre-flood bed elevation was selected arbitrarily as the basis for depth calculations because (i) a large number of transect cross-section and stage data had to be processed, and (ii) the differences in bed elevations before and after the flood generally did not change substantially at the scour monitor location such that the attendant error was small. Additional error was introduced by the moving bed in that a well defined flow boundary did not exist. However, dilatation is relatively small when only one to two layers are involved, and friction losses of static and mobile beds should be similar because the largest grains are moving much slower than the fluid such that the effect is likely to be of minor importance (Whiting and Dietrich 1990).

Longitudinal water surface slopes were calculated from the measured water surface elevations. Longitudinal stationing was measured using a tape on one or both banks between marked survey points. The study sites were relatively straight so that corrections to stationing for channel curvature were small.

Cross-channel variation in water surface elevation caused by channel curvature may have introduced unexplained error to the estimates of flow depth at scour monitor locations. The variation was not measured because only one side of the channel was readily accessible at flood stage. The sites were relatively straight so that the error was likely small. Equation 7.15 in Henderson (1966) can be used for making a rough estimate: maximum mean velocities were approximately 3 m/s, and the radius of curvature was at least ten times the channel width, so that the error may have been at most between about 10 to 20 cm (or, approximately 10 percent of the flow depth), depending on stream size. I did not notice significant cross-channel variation in stage in the vicinity of the scour monitors during flood flows.

3.2.6 *Water Temperature Measurement*

Water temperatures were measured during floods to estimate kinematic viscosity and density of the flood waters. Water temperatures ranged between 3°C and 10°C across all sites.

3.2.7 *Substrate Characteristics*

Particle size frequency distributions were measured at scour monitor locations in the spring following the 1996-97 flood season; measurements were not made before the flood season since they could have influenced subsequent bedload transport and scouring processes in the vicinity of the scour monitor. It was assumed that the final deposit around each monitor was representative of composition and conditions before scour occurred; this was later judged visually in the field to be appropriate in almost all cases

except in the Tolt River where the primary riffle deposit was scoured out. Photographs were taken of a ruler and the substrate around each scour monitor location after installation for contingency (in case there were future problems with substrate sampling; e.g., in the Tolt River).

Two methods were used to determine grain size distributions: pebble counts (Wolman 1954) were conducted at all scour monitor locations, and bulk samples were collected at most locations using a 30.48 cm (12 inch) diameter McNeil sampler (McNeil and Ahnell 1960). The two methods were selected because they gave independent, equivalent estimates of surface grain size distributions (Kellerhals and Bray 1971; Diplas and Sutherland 1988). An exception to equivalency is when there is a large proportion of particles finer than 8 to 15 mm present, at which point the pebble count becomes limited by finger width and may thus be less accurate (Fripp and Diplas 1993; Kondolf 1997). This error influences predominantly the finer tail of the distribution, which is less important for evaluating scour in coarse streambeds. The larger particles that form the bed framework structure are most relevant.

Pebble counts were conducted over patches that appeared visually to be texturally-homogeneous and that extended upstream and/or downstream of each scour monitor pair along expected sediment transport paths. Streamwise patch counts were conducted instead of transect counts because of textural cross-channel variation. Transect pebble counts are incapable of accurately characterizing local grain size distributions and require prohibitively large sample sizes when the condition of textural homogeneity is not met throughout the area sampled (Dunne and Leopold 1978; Wolcott and Church 1991; Kondolf 1997). In some cases, the count was performed over a homogeneous patch extending streamwise between scour monitor pairs on two transects, and the results applied to both pairs.

Rice and Church (1996) determined that marginal improvements in precision were greatest when sample size was increased to 300 to 400 stones. They consequently recommended sampling 400 stones to reduce confidence interval size about pebble count percentile size estimates to a more satisfactory level. However, sample size was limited

in this study by logistics since a large number of sites had to be sampled over a large geographic area, and other data had to be collected as well. In a compromise between speed and accuracy (Kellerhals 1967), counts were comprised initially of 100 stones. This sample size yields reasonably precise particle percentile estimates depending on sorting and relative size (Wolman 1954; Rice and Church 1996). The count was divided into two 50-stone samples, each collected by a different person to reduce observer bias (Wolman 1954; Hey and Thorne 1983).

Pebble count sample sizes were expanded in summer 1997 and summer 1998 to 200 to 350 stones in coarser, more poorly sorted substrates when comparisons with bulk sample results suggested inaccuracy caused by too small a pebble count sample size or bulk sample weight. Pooling of the 1997 and 1998 samples from the same patch location was done because only minor bedload transport occurred over the winter of 1997-98 (according to stream gage, tracer study, and scour monitor observations).

Bulk substrate samples were collected at scour monitor locations. When the scour monitor was missing or buried, it was relocated by triangulation. Layers of the streambed were excavated and sieved separately, including the surface armor layer which is characteristically coarser than the underlying substrate. The existence of distinct subsurface layers has been noted in previous studies (e.g., Diplas and Fripp 1992) and may provide stratigraphic evidence of bedload transport history through vertical and spatial variation in layer grain size distributions. Layers were defined by first excavating out the larger stones felt by hand, followed by the surrounding finer material down to the top of the next large, immobile particle encountered. The beginning of the next layer could generally be distinguished clearly in all but the finest mixtures. The surface layer thickness was defined generally by the short ("c") axis dimension of the largest surface particle present within the sampler, but sometimes extended below the bottom of that particle. In very coarse substrates, this was not always the same as the surrounding bed's average armor layer thickness, approximated as the distribution's D_{90} (Parker and Sutherland 1990) or D_{95} (Ettema 1984). The thickness of each subsequent subsurface layer appeared to correspond roughly to a value between the short and intermediate

("b") axis dimensions of the largest particle defining the layer. Excavation continued down to approximately 25-30 cm depth, a limitation imposed by the McNeil sampler. Two to four layers typically were sampled.

The results from McNeil samplers approximate the true substrate composition better than other excavation techniques (Young et al. 1991). However, bulk samples are subject to more stringent sample size limitations than pebble counts. The sample weight required increases to impractical levels as the substrate sample coarsens and becomes more poorly sorted (Church et al. 1987; Ferguson and Paola 1997). Bulk sampling may be biased if excavated layer thicknesses are less than twice the geometric mean diameter of the coarsest particles present, and the surface bulk sample weight may be too small for accurate characterization of the true grain size distribution in larger substrates (Diplas and Fripp 1992). As noted above and described in Section 3.3.2, single sample weights in larger substrates ($D_{90} > 100$ mm) were too small to meet such accuracy requirements. In lieu of using a larger diameter sampler (e.g., Klingeman and Emmett 1982; Milhous et al. 1995), sample weights were increased later the same or following summer by collecting additional samples to coincide with expanded pebble counts. Samples were collected adjacent to the previous sample locations.

Size distributions were determined by wet-sieving of individual size fractions (Table 3-3) in the laboratory. The sieved material was dried and weighed. Particles smaller than 2 mm were considered as a single size class since they are transported relatively easily, and they do not represent a significant influence on the gravel framework structure and scour depth. Particles larger than the 128 mm sieve size were measured using a metal template with square holes (Hey and Thorne 1983), which is analogous to sieving.

Specific gravity was determined for substrate mixtures in each site in the laboratory at room temperature, using a volumetric displacement technique. The material was weighed dry and then placed in a graduated cylinder. Samples from the Willapa system contained a mixture of lighter sedimentary rocks composed of fine clay particles, with denser volcanic rocks; densities were determined for each type of rock.

Table 3-3. Sieve sizes used to define particle size distribution.

Size of Squared Opening (mm)	Equivalent Phi Size [i]	US Standard/ASTM Sieve Mesh No.
254	- 8.0	10 "
180	- 7.5	7 1/4 "
127	- 7.0	5 "
88.9	- 6.5	3 ½ "
63.5	- 6.0	2 ½ "
44.3	- 5.5	1 3/4 "
31.8	- 5.0	1 1/4 "
22.2	- 4.5	7/8 "
15.9	- 4.0	5/8 "
11.1	- 3.5	7/16 "
7.90	- 3.0	5/16 "
4.00	- 2.0	# 5
2.00	- 1.0	# 10

[i] $Phi = -log_2 D$ where D is in mm

3.3 Field Data Reduction

The following quantities were estimated from the field data:

(I)   Total scour depth, net excavation depth, and maximum bedload disturbance depth;

(II)   Substrate grain size distribution percentiles, porosity, and specific gravity;

(III)   Instantaneous and maximum local shear stress, unit stream power, and dimensionless shear (Shields) stress occurring during individual floods;

(IV)   Bedload transport rates and average particle velocities; and

(V)   Spatial distributions and quantities of sediment available for bedload transport.

Considerable time was spent on data reduction to determine whether estimates of the dependent and independent variables were relevant and accurate. It was important that the results not be influenced by significant, unexplained variation. The local scour depth signal needed to be related to the local forces inducing and resisting sediment motion, and the larger scale controls on sediment transport.

The remainder of this chapter summarizes the development of each estimate, identifies the appropriate measurements, and discusses measurement accuracy. Subsequent chapters discuss the resulting observed relations between scour depth and hydraulics and geomorphology of the study streams.

3.3.1 Scour Depth

Total scour depth, δ_T, at the monitor location was indicated by the number of balls disturbed and moved to the end of the cable. It was measured as the distance down to the top of the first undisturbed ball from the original bed elevation (Figure 3-2). In cases where the scour monitor was unavoidably installed at an angle, the measured scour depth was corrected using the notation in Figure 3-2 by:

$$\delta_{T_{corrected}} = \sqrt{\frac{\left(\delta_{T_{measured}}\right)^2}{1 + \tan^2\theta_1 + \tan^2\theta_2}}$$ (3.1)

The measured value of δ_T was calculated from:

$$\delta_T = \frac{n_s}{n_T}\left[D_2 + (D_{1b} - D_{1a})\right] + D_4 + \frac{\left[D_{1a} - (D_5 + D_4)\right]}{2} + wt$$ (3.2)

where wt is the washer thickness (= 2 mm). Equation 3.2 distributes the total inter-ball spacing error equally among all balls, and splits the error between the D_4 and D_5 measurements to determine the elevation of the top of the first ball relative to the streambed surface, which is not well defined (Figure 3-2; DeVries and Goold 1999).

Net excavation scour depth, δ_{EX}, was calculated as the magnitude of the negative change in the surveyed bed elevation at a monitor location before and after a flood (Figure 3-4; net fill depth was calculated as the positive change in bed elevation).

Maximum bedload disturbance depth, δ_{Bm}, was estimated as the difference between the total and net excavation scour depths (Equation 1.1; Figure 3-4). A critical assumption is that the bed surface elevation did not proceed beyond the limits defined by its pre- and post-flood level (i.e., no additional excavation scour followed by fill; Figure 3-4). Instances of local degradation or aggradation were assumed to be uni-directional, affected by reach-scale loss or gain of sediment (e.g., through downstream translation and diffusion of a mass of sediment originating from upstream), or by slight shifts in thalweg location due to limited meander migration. Differences between δ_T and δ_{EX} were thus attributed solely to δ_{Bm}. This assumption and the magnitude of other potential errors are examined in Chapter 4 in more detail.

Measurement error in δ_T was equal to the dimensions of the balls and taken to be uniformly distributed within ±2 cm. Measurement error in net excavation depth using the 127 mm (5 inch) leveling rod base was approximately within ±1 cm; this was derived from the difference in average bed elevation measurements presented in Table 1 of DeVries and Goold (1999) as being statistically similar to that obtained using the 127 mm base. The standard deviation of δ_{Bm} was therefore equal to approximately 1.3 cm (determined by propagating variance in Equation 1.1). Assuming the error in δ_{Bm} to be normally distributed, 90 percent of measurements of δ_{Bm} were likely within ±2 cm of the correct value. The error in δ_{Bm} would have been greater if the standard leveling rod base (i.e, as-purchased) had been used to survey bed elevations (DeVries and Goold 1999).

Unexplained measurement error could have been introduced in δ_{Bm} when the bed surface elevation defined by the 127 mm leveling rod base and by the slender steel rod (used to measure the D_4 and D_5 scour monitor dimensions) differed by the error quantity $\epsilon_{surface\ datum}$, such that:

$$\delta_T = \delta_{EX} + \delta_{Bm} + \epsilon_{surface\ datum} \qquad (3.3)$$
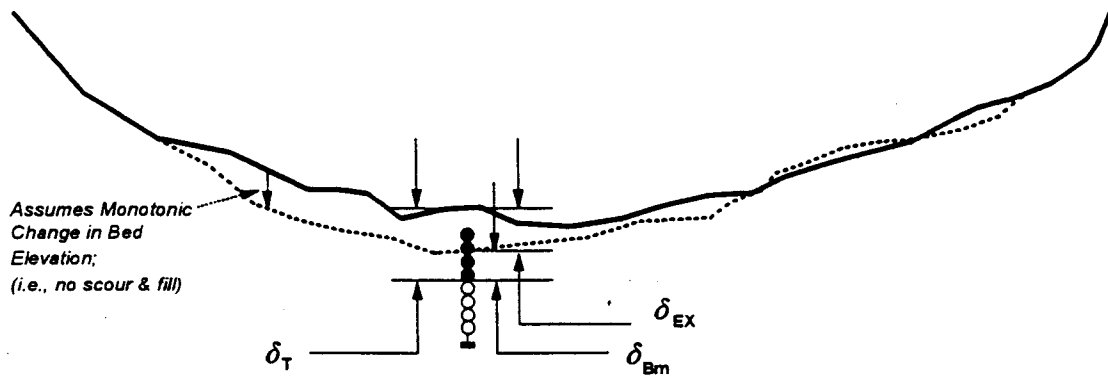
Figure 3-4. Depiction of how total scour depth (δ_T), net excavation scour depth (δ_{EX}), and maximum bedload disturbance depth (δ_{Bm}) are estimated for Equation 1.1, assuming that no scour and fill occurred. The pre-flood bed elevation is depicted by the solid profile, the post-flood elevation by the dashed profile; no scour and fill occurs below the lower of the two lines. The dark circles indicate scour monitor balls that were disturbed and moved to the end of the monitor cable.

The value of $\epsilon_{surface\ datum}$ was judged visually in the field to be negligible: the steel rod rested on top of the majority of particles at approximately the same elevation defined by the 127 mm diameter survey rod base.

All of the scour depth, bed elevation, and related data analyzed here are presented in Appendix D. Table D-1 indicates for which monitors scour depths and bed elevations could be determined and attributed to a single, large flood.

3.3.2 *Grain Size Distributions*

Pebble count results are presented in Appendix E. Grain size distributions were calculated for McNeil bulk samples based on the whole sample, and on a sample truncated at 8 mm with finer material excluded. McNeil sample data and results are presented in Appendix F. The 8 mm limit was selected for three reasons:

(I) Particles finer than 8 mm in the bulk samples typically comprised between 20 and 30 percent of the total sample weight. This range is comparable in magnitude to the range of porosities estimated for the samples. Eight millimeters consequently approximated the smallest effective grain size that formed the gravel framework and determined the bed elevation. Smaller sizes constituted primarily matrix material filling the pore spaces between the framework particles. Wilcock et al. (1996) made similar observations.

(II) To compare with Wilcock et al.'s (1996) field study, in which they argued further that particles smaller than 8 mm were mobilized more readily at low shear stress (i.e., were more transient) than coarser fractions in their study sites, which were of comparable texture to the present study sites (i.e., gravel-cobble beds).

(III) Eight millimeters is about the smallest particle size that can be picked up manually in pebble counts without significant bias. Fripp and Diplas (1993) recommended that a truncation smaller than 15 mm results in bias since the limit corresponds approximately to a human finger width. Smaller sizes were found to be under-represented in their samples. Others have suggested a lower limit

between 2 and 8 mm (Kellerhals and Bray 1971; Dunne and Leopold 1978; Kondolf 1997). This is a bigger concern when the majority of particles are on the order of 15 mm. In coarser substrates, the probability of picking up a particle smaller than 8-15 mm is reduced substantially and the coarse tail of the distribution is essentially unaffected. This was confirmed in initial analyses in the present work. Moreover, the tip of the finger is rounded and capable of feeling a particle smaller than 15 mm and picking it up. Eight millimeters was a compromise for making direct comparisons of bulk grain size distributions with pebble count results.

The independent pebble count and bulk sample percentile results were plotted against each other. This was more instructive than overlaying entire distributions and applying nonparametric distribution tests. The D_{50}, D_{75}, D_{84}, D_{90}, and D_{95} particle sizes were compared (Appendix G), and a general limit to bulk sample accuracy was inferred. The data scatter in the plots was relatively uniform and narrow about the 1:1 line except for samples with D_{90} larger than approximately 100 mm, at which point errors became considerable.

The errors were thought initially to be attributable to insufficient sample weight in the bulk samples and too small a pebble count sample size. The average weight of material collected in bulk samples from each layer ranged generally between 8 and 20 kg. The largest stone accounting for five percent of these sample weights corresponds to a diameter of approximately 70-90 mm (cf. Figure 3.9 in Church et al. 1987). In contrast, Church et al. recommended that the largest stone account for no more than $\frac{1}{1000}$th (0.1 %) of the sample weight. Accuracy was evidently low for the coarser substrates sampled.

Additional bulk samples were collected for those samples greatest in error and the corresponding pebble count was expanded at the same time. Pebble count percentile estimates did not change substantially with increased sample size, whereas bulk sample estimates did. With increased sample weights, the largest stone accounting for five percent of the sample weight was closer to 90-100 mm in diameter. The scatter could

not be reduced sufficiently without collecting prohibitively large bulk samples, even if Church et al.'s (1987) requirement were to be relaxed to a less restrictive two or five percent criterion.

Since the pebble count percentiles did not change substantially or consistently with increased sample size, it was inferred that all corresponding pebble count percentile estimates (i.e., D_{50} to D_{95}) were likely to be more accurate than the equivalent bulk sample's when the former's D_{90} value was larger than about 100 mm. The larger diameter percentile estimates (i.e., D_{84}, D_{90}, D_{95}) were found to be equally acceptable between pebble count and bulk samples when the corresponding pebble count D_{90} was smaller than 100 mm.

Bulk samples were more appropriate for D_{50} calculations in substrates with $D_{90} <$ 100 mm because (i) the sample weights more closely matched accuracy requirements (pebble count sample size remained at 100 stones), and (ii) the pebble count D_{50} may have been more susceptible to measurement error associated with methodologic truncation at 8 or 15 mm (item 3 above).

The question was also addressed whether or not to convert bulk sample percentile particle sizes to correspond to pebble count intermediate axis diameter measurements, since the two will not be the same if the b-c axis projection is non-circular (Komar and Cui 1984; Church et al. 1987). Average values for particle c-axis/b-axis ratios were on the order of 0.65-0.75 in the study streams. The corresponding ratio of sieve diameter to b-axis diameter is on the order of 0.84-0.88 (Church et al. 1987), which is also close to the general result for natural sand grains determined by Komar and Cui (1984) (~0.83 for any given size fraction). The plots comparing pebble count to bulk sample percentiles indicated no need for a corresponding magnitude correction of sieve size to equivalent pebble count diameter in this study (Appendix G).

For consistency, the pebble count and bulk sample estimates were not averaged because not all pebble counts had a commensurate bulk sample. Consequently, one or the other method was selected based on consistency, accuracy, and relevance as detailed below.

After considering these methodological issues related to sampling and size measurement, the following grain size distribution percentiles were determined to be relevant:

(I) The surface layer D_{90} is an appropriate scaling parameter for active bedload layer thickness because it approximates the armor layer thickness, which in turn controls the exchange of particles between the bed and bedload (Parker et al. 1982a; Parker and Sutherland 1990). Selection of the 90th percentile is a matter of convenience (e.g., compared to selecting the 84th or 95th percentiles) because it has been used in this context before (e.g., Parker and Sutherland 1990; Wilcock et al. 1996). It is a more robust estimator than coarser percentiles (e.g., D_{95}; Ettema 1984) in poorly sorted substrates (Rice and Church 1996; Ferguson and Paola 1997). The 84th percentile has been applied commonly in hydraulics and sediment transport because the grain size distribution has been assumed to be approximately lognormal, and thus may have statistical convenience rather than any physical importance.

(II) The combined surface and proximate subsurface layer D_{50} was relevant for estimating an appropriate Shields parameter, τ^*. The median particle size provides reasonable representation of the entire grain size distribution in bedload transport calculations (Wilcock 1997b). The two layers were combined because the largest surface layer particles frequently protruded into the next layer underneath, and vice versa, such that the resistance to motion of the surface layer was influenced by the immediate subsurface layer.

The D_{90} values were estimated consistently from the pebble counts. They also gave similar results to bulk surface samples truncated at 8 mm when the respective D_{90} was smaller than 100 mm. The correspondence was even closer when the bulk surface and adjacent subsurface layers were combined (Appendix G). This result was likely because (i) of the protrusion of the largest particles between adjacent layers in many if not most bulk samples, and (ii) the sample weight was increased accordingly, resulting in greater statistical accuracy. The D_{90} estimates were also similar between the truncated and non-

truncated distributions derived from the bulk samples, suggesting that the coarser tail of the distribution was insensitive in this study to sampling error induced by finger width (cf. Diplas and Fripp 1993).

The D_{50} values were estimated by the more accurate pebble counts when the sample D_{90} was >100 mm and by truncated, combined (surface+adjacent subsurface) layer bulk samples otherwise. In addition to representing material potentially contributing to bedload transport, combining the two layers was also consistent with Wilcock et al. (1996), who used a similarly-sized sampler in similarly-sized substrates ($85 \leq D_{90} \leq 120$ mm). Truncation/layer-combination was further justified when it was found that the resulting D_{50} corresponded more closely to pebble count values than either truncated or non-truncated samples of the surface layer alone (Appendix G). Non-truncated, combined-layer D_{50} estimates were smaller than pebble count values due to the inclusion of the finer subsurface material.

3.3.3 Substrate Porosity and Specific Gravity

Static porosity in natural streambed sediments varies substantially with particle size, shape, and mixture properties (Komura 1963; Carling and Reader 1982; Brayshaw et al. 1996). Porosity could not be determined in the field because of data collection logistics and thus had to be estimated. Mean porosity was estimated for each substrate sample using Komura's (1963) empirical relation,

$$P = 1 - \frac{2}{S_s} + \frac{0.229}{S_s \, D_{50}^{0.21}} \tag{3.4}$$

where D_{50} is in centimeters. Carling and Reader's (1982) relation was not selected because it included only a particle size term. Although the influence of specific gravity, S_s, in Komura's (1963) equation is opposite of the expected trend in gravel beds (porosity generally increases with decreasing specific gravity; e.g., Onoda and Liniger 1990), the equation predicts Carling and Reader's (1982) data relatively well using their

measured specific gravities which were approximately 2.15-2.20. It also predicts the porosity well for the denser substrates found in the study streams, where specific gravities are on the order of 2.6 to 2.8 (Komura 1963) (Table 3-4; Figure 3-5).

Particle density was calculated as the dry weight in kilograms divided by the volume of water displaced at room temperature in cubic meters. Specific gravity was calculated as the ratio of particle density to the density of water consistent with the temperature measured during flood conditions (Table 3-4).

Table 3-4. Measured specific gravities of study streambed substrates.

Study Reach	Specific Gravity
Issaquah Creek	2.71
N. Fk. Stillaguamish River at Hazel	2.71
N. Fk. Stillaguamish River at USGS	2.80
Raging River	2.73
S. Fk. Snoqualmie River	2.72
S. Fk. Willapa River	2.60
Squire Creek	2.66
Tolt River	2.63
Willapa River at Elk Prairie	2.71
Willapa River at Trap Creek	2.69
Willapa River at USGS	2.78

3.3.4 *Shear Stress Estimation*

Evaluation of scour depth at a specific location of the streambed necessitated estimating local shear stress during flooding conditions. The channel average shear stress does not provide information on the lateral distribution of local shear stress and underestimates the forces acting on the most active portions of the stream channel.

82
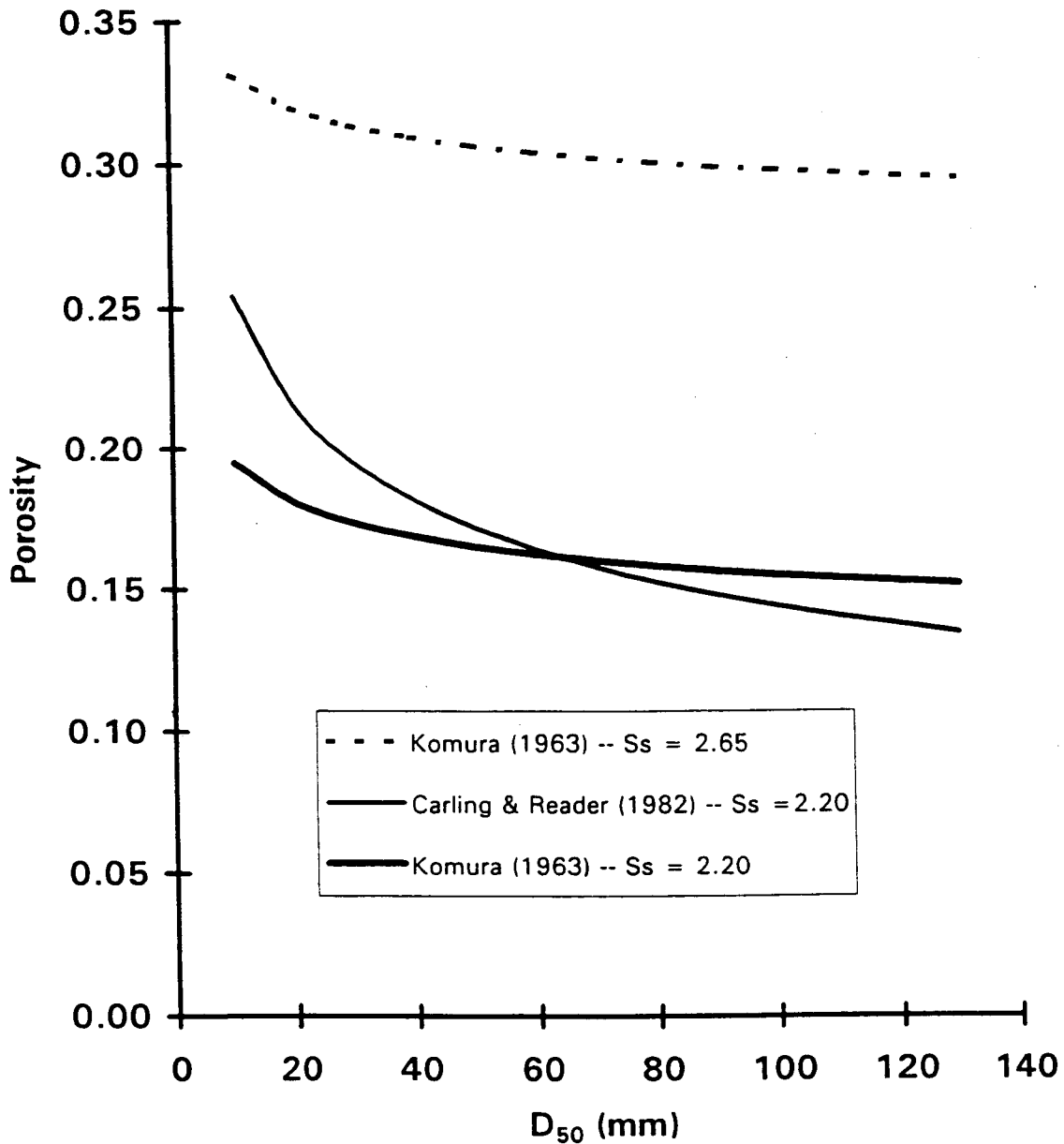
Figure 3-5. Calculation of substrate porosity for a range of gravel mixtures of increasing median particle size and different specific gravities, using the relations of Komura (1963) and Carling and Reader (1982).

There are few practical methods available for estimating local shear stress in an irregular, natural channel using field data (Knight et al. 1994; ASCE 1998). The simplest methods that exist include the momentum and empirical flow resistance equations. More complex methods (e.g., Wiberg and Smith 1991; Shiono and Knight 1991) were infeasible since their information requirements could not be satisfied. Flood conditions further limit the number of methods that can be used because it is increasingly difficult and hazardous, if not impossible to measure relevant parameters.

Neither velocity profiles nor mean column velocities could be measured practically and safely in the study streams under flood conditions. Surface velocity could be measured only in the smallest channels using cork floats, and yielded variable results because of the difficulty of dividing the channel into more than a few cells across a transect and determining to which cell the float belonged. Hence a roughness relation could not be employed consistently to estimate friction velocity (e.g., as done by Wilcock 1996).

A uniform flow, wide channel approximation of bed shear stress τ_b was used (Henderson 1966):

$$\tau_b = \rho g R S_f \tag{3.5}$$

using the local hydraulic radius R, calculated for a cell i from detailed surveys of the cross-section at low flow and the water surface elevation at flood flow, and channel mean friction slope S_f, which could be estimated more readily than local mean column velocity for all study streams. The wide channel approximation is valid when the channel aspect ratio (water surface width/depth) is sufficiently large. All study streams were characterized by bankfull aspect ratios that were greater than the critical range of 5 to 10 suggested by Nezu and Nakagawa (1993) to be the lower limits for making the approximation.

Water surface slopes were used to estimate S_f at flood flows. The value of S_f depends on the magnitude of the steady and unsteady flow terms in the equation of motion, which can be written as (Henderson 1966):

$$\frac{\partial}{\partial x}\left(h + \frac{U^2}{2g} \right) + \frac{1}{g}\frac{\partial U}{\partial t} = -S_f \qquad (3.6)$$

The longitudinal water surface slope ($S_w = \partial h/\partial x$) at flood flow approaches the energy gradient for a reach because velocity head differences become smaller between successive transects as the water level rises. Longitudinal water surface profiles also smooth out across riffles and pools with increasing stage and asymptotically approach the reach slope, which approximates friction slope at high flows (Leopold et al. 1995).

The unsteady flow accelerative term ($1/g \; \partial U/\partial t$) was negligible for the study streams. This can be shown by rewriting the term using $q=Ud$ and the product rule as:

$$\frac{1}{g}\frac{\partial U}{\partial t} = \frac{1}{g}\left(\frac{1}{d}\frac{\partial q}{\partial t} - \frac{q}{d^2}\frac{\partial d}{\partial t} \right) \qquad (3.7)$$

This term was estimated in the gaged study streams to be two or more orders of magnitude smaller than the slope of the hydraulic grade line (water surface elevation), using USGS gage data (e.g., approximately 0.00001 versus 0.0051, respectively, in Issaquah Creek). Loop effects on rating curves and shear stress were thus negligible. The term is also assumed to be negligible in the ungaged study streams on the basis that they have similar channel slopes to the gaged ones (Henderson 1966). The maximum shear stress was therefore estimated as the value corresponding to maximum local hydraulic radius and the estimated friction slope. The maximum bedload layer thickness δ_{Bm} was assumed to occur with the maximum shear stress.

Friction slopes were difficult to estimate in many of the study stream reaches. Water surface slopes were computed for each study reach (i) at a transect location, (ii) over the length of a single geomorphic channel unit (e.g., a riffle), and/or (iii) over the reach length, depending on the number of measurements which was limited by accessibility and the quality of flood marks. Slopes were determined from linear regressions of plots of

elevation against distance. Identification of the water surface elevation was problematic because of rapidly fluctuating ('choppy') local water surfaces during flood flows and uncertainty in interpreting flood marks later. Subsequent data reduction indicated that flood marks provided the least accurate data for estimating slopes (conversely, the error in measured hydraulic radius was relatively small). Estimated slopes were plotted against water surface elevation at a selected transect to check slope changes with discharge. Plots of water surface elevation vs. longitudinal (streamwise) distance (Appendix H) were used to identify potentially erroneous water surface elevation data and to help interpret observed variation in slopes with discharge.

The friction slope was calculated as (i) an average graphical intersection point between the reach and local water surface slopes on the slope-water surface elevation plot (South Fork Willapa River; Willapa River at Elk Prairie), (ii) the average of the higher measured reach and local water surface slopes when they were approximately similar in magnitude (North Fork Stillaguamish River at Hazel, Raging River), or (iii) an asymptotic, average reach slope at higher flood stages (Issaquah Creek, North Fork Stillaguamish River at USGS, South Fork Snoqualmie River, Squire Creek, Willapa River at Trap Creek and at USGS). All relevant plots are presented in Appendix H for each site. Friction slope estimates are listed in Table 3-1.

Scour monitors were placed away from the streambanks, in the central half of the channel, to minimize the influence of side wall effects on local bed shear stress. Shear stress partitioning was assumed to be unnecessary because the study sites were selected to be free of sources of significant local- and reach-scale form drag and other losses (e.g., large woody debris, boulders, prominent channel transitions, and sinuosity).

In a crude evaluation of shear stress estimates, cross-sectional surface velocity distributions were estimated in the Raging River using painted cork floats, at a flood flow rate of approximately 30 m³/s. The channel was divided into six lanes, and the mean surface velocities for each lane were converted to mean column velocity using the channel average Manning's n calculated for the sampled flow rate, and the law of the wall velocity profile (Equation 2 in Wilcock 1996). The resulting mean velocity

estimates were approximately within 10 percent of values predicted using the local $\rho g R S_f$ shear stress estimates and the law of the wall, supporting the plausibility of the local shear stress estimates.

Equation 3.5 yields a time-averaged shear stress. The actual shear stress at the moment a particle begins to move can be larger than the mean shear stress because of turbulence. However, the time-averaged stress is appropriate for evaluating general bedload motion and scour depth in coarse beds for a number of reasons. First, the magnitude of turbulent velocity fluctuations is completely characterized by the time-averaged shear stress when flows are approximately uniform because the fluctuations scale with the friction velocity (Nezu and Nakagawa 1993; Nelson et al. 1995). The study sites all experienced relatively uniform flow conditions during flooding. Second, local disturbances in shearing granular materials die out quickly with distance from the disturbance (Passman et al. 1980). Local turbulent fluctuations in shear stress would therefore be expected to influence only a restricted area and depth of a gravel/cobble bed. Third, each region of the bed should experience a similar fluctuation at different times, until all of the bed area subject to a given mean shear stress has experienced comparable maximum instantaneous shear stress magnitudes. As corroboration, Keshavarzy and Ball (1996) determined in a rough bed flume that, although particle entrainment occurred at a lower critical shear stress than that predicted using an average shear stress, general bedload motion characteristics were best described by average shear stress. Based on these observations, Equation 3.5 appears to be appropriate for evaluating scour depths at the study sites.

3.3.5 *Dimensionless Shear Stress Parameter*

The dimensionless shear stress, or Shields parameter, represents the balance between motive and resistive forces and was calculated as:

$$\tau^*_{\,j} \; = \; \frac{\tau_b}{(\rho_s - \rho)\, g\, D_j} \qquad\qquad (3.8)$$

where the subscript j is specific to grain size distribution percentile. For $\tau^*_{\,j} = \tau^*_{\,g}$, $D_j =$ D_{50} calculated from a grain size distribution truncated at 8 mm (see Section 3.3.2).

3.3.6 *Stream Power Estimation*

Bagnold (1956) showed that the bedload transport rate could be expressed in terms of the rate of work done in transporting bedload material, which could also be expressed as the product of total power available to transport sediment times an efficiency factor. Bagnold (1966a) noted that the total available (stream) power per unit length of stream, Ω, could be expressed as

$$\Omega \; = \; \rho g Q S_w \qquad\qquad (3.9)$$

where Q is the total stream discharge rate and S_w is the water surface slope. This result follows directly from the Reynolds Transport Theorem for steady, uniform flow (Street et al. 1996). Available stream power is analogous to the time rate of energy increase for a fluid system. Stream power is dissipated through changes in internal energy and heat, turbulent energy production, and any useful work done. The latter may be achieved through bedload transport. The quantity of stream power expended in transporting bedload is equal to the product of Ω and a bedload efficiency factor. Although bedload efficiency factors are difficult to estimate and may vary considerably, Bagnold (1966a) reasoned that plots of transport rates versus stream power and related empiricisms were useful predictors of bedload transport rate and the corresponding work done, which can influence local scour depth.

Because it has been used extensively by others in similar contexts, stream power per unit area, ω, was calculated for each stream as:

$$\omega \;=\; \rho g q S_w \;\approx\; \rho g R S_f U \;=\; \tau_b U \qquad (3.10)$$

where q is the flow rate per unit width of channel. The local mean column velocity was calculated using:

$$U \;=\; \sqrt{8gRS_f}\left[1.16 \;+\; 2\,\log\left(\frac{R}{D_{84}}\right)\right] \qquad (3.11)$$

which is a combination of Manning's equation:

$$U \;=\; \frac{1}{n}\,R^{\frac{2}{3}}\,\sqrt{S_f} \qquad (3.12)$$

and Limerinos' (1970) D_{84}-based relation:

$$\frac{1}{\sqrt{8g}}\,\frac{R^{\frac{1}{6}}}{n} \;=\; \frac{1}{\sqrt{f}} \;=\; 1.16 \;+\; 2\,\log\left(\frac{R}{D_{84}}\right) \qquad (3.13)$$

Equation 3.11 was used because a local hydraulic radius and D_{84} could be estimated more accurately than inferring a local Manning's n from measured flow rates.

The maximum stream power was assumed to occur at the maximum stage of a flood. Any potential loop rating influence on stream power was tested by evaluating the following expression (Henderson 1966):

$$\frac{Q_{max,\ unsteady}}{Q_{max,\ uniform}} \;\approx\; \sqrt{1 \;+\; \frac{1}{S_w c}\,\frac{\partial d}{\partial t}} \qquad (3.14)$$

where c is the flood wave speed and is of order $1.2U$ to $1.7U$ (Rantz et al. 1982). The ratio in Equation 3.14 ranged between 0.99 and 1.01 and was thus negligible.

3.3.7 Bedload Transport Rates and Mean Particle Velocities

Bedload transport rate predictions were used to estimate maximum bedload layer thickness using the continuity equation:

$$\delta_{Bm} = \frac{q_{Bm}}{U_{Bm} \, \rho_s \, (1 - P)}$$

(3.15)

where q_B is the bedload mass transport rate per unit width, U_B is the particle velocity averaged over δ_{Bm}, and the subscript m refers to maximum value during a flood (assumed to occur simultaneously with maximum shear stress and stream power).

Bedload transport rates could not be measured directly in this study because of logistics and cost. Rates were estimated using:

(I)   Parker's (1990a; 1990b) surface-based equation, which was derived from Oak Creek bedload transport data and channel mean shear stress (Milhous 1973); and

(II) Bagnold's (1980) average stream power relation, which was derived from a variety of sand and gravel bed streams.

The two methods were selected for comparative purposes because no single bedload transport relation is able to predict rates accurately in all streams (Gomez and Church 1989).

Parker's (1990a) relation was selected as a representative shear stress-based estimator because (i) Oak Creek is similar in physical character to several of the study streams, (ii) a relation based on surface substrate characteristics is preferred over one that is subsurface based (e.g., Parker et al. 1982b), since it is exclusively the surface layer that supplies bedload material at lower transport stages (Parker et al. 1982a; Parker 1990a), and (iii) it has been determined to be a satisfactory predictor of bedload transport rates in other gravel bed streams (e.g., Chang 1994).

Bagnold's relation was selected as a representative stream power-based estimator because (i) it is simple to apply, and (ii) its predictive accuracy is better than other stream power methods (Gomez and Church 1989).

Parker's (1990a) and Bagnold's (1980) relations predict similar transport rates in the study streams at intermediate shear stresses as shown in Figure 3-6. At higher and lower shear stresses, they diverge markedly. The divergence over the lower range is likely due in large part to Parker's (1990a) relation representing grain size distributions truncated at 2 mm, whereas Bagnold's (1980) represents the entire distribution and thus predicts higher transport rates at low shear stresses (Figure 3-6).

Parker (1990a) argued that the 2 mm truncation was useful because smaller particles become suspended in gravel bed streams at high shear stresses. Transport capacity is usually sufficient to move the finer material at low transport stages, prior to significant disturbance of the armor layer. Material finer than 2 mm generally accounts for less than five percent of the surface, and fifteen percent of the subsurface layer sample weights, respectively, in the study streams (Appendix F). Following arguments similar to those in Section 3.3.2 regarding porosity and streambed structure, material finer than 2 mm should have a negligible effect on bed structure in the study streams; it fits within the matrix space associated with the larger sized material present. Parker's (1990a) bedload transport relation should therefore be better suited conceptually to estimating bedload layer thickness than Bagnold's (1980) because it ignores the finer matrix material.

The problem of estimating mean particle velocity was ill-posed. The vertical limits of integration to calculate a mean value depend on specifying the unknown value of δ_{Bm}, which in any case is not defined clearly for a heterogenous mixture. A continuum approximation cannot be applied until the bedload layer thickness is considerably thicker than the characteristic particle size. Little is known about the fluid-particle interactions and stresses that exist when moving bedload particles originate in the surface and immediate subsurface layers. Consider further the bounds on U_B, which include saltation velocity and a virtual velocity as maximum and minimum limits, respectively. The limits span roughly two orders of magnitude and the correct answer lies somewhere between. Measurements of particle velocities in flumes and streams reflect this range.

Sand and finer gravel fractions aside, larger individual particles move in an intermittent manner in gravel bed streams under common flood magnitudes (e.g., Hassan
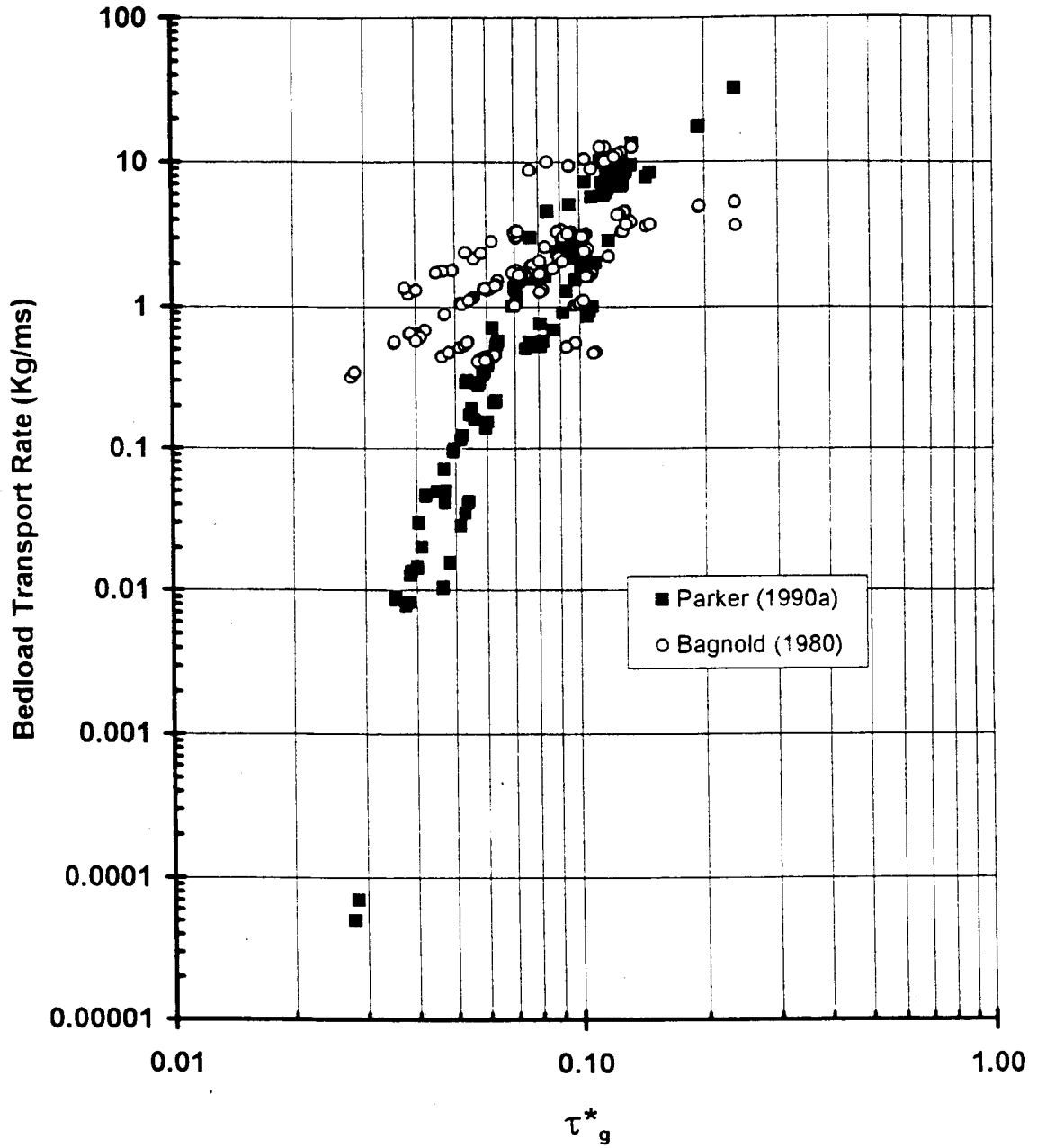
Figure 3-6. Estimated bedload transport rates per unit stream width in the
vicinity of each scour monitor at the time of peak stage, calculated
using Bagnold's (1980) and Parker's (1990a) equations.

et al. 1991). The period of rest decreases with increasing transport rate and decreasing particle size. Virtual velocity estimates represent an integration of this intermittent start-and-stop motion over the time period when the stream is capable of transporting material. The difference between virtual velocity and actual velocity during motion increases with particle size because the period over which transport is possible decreases due to selective transport effects. Larger particles move shorter distances than smaller ones, especially during the state of partial transport (Wilcock 1997a). Moreover, intermittency of motion implies that virtual velocity is not temporally synchronized with maximum bedload transport rate and layer thickness. Virtual velocity is therefore not a good basis for estimating local maximum bedload layer thickness.

Hassan et al.'s (1992) empirical relation was used here to identify the lower bound of mean particle velocity:

$$U_B = 0.00188 \ (\omega - \omega_{cr})^{1.62} \tag{3.16}$$

where ω is flood peak stream power per unit area of bed and ω_{cr} is the value of stream power at the threshold of movement. Since the study stream grain size distributions were unimodal, the threshold power was estimated as (Bagnold 1980):

$$\omega_{cr} \approx 290 \ D_{50}^{1.5} \ \log_{10}(12d/D_{50}) \tag{3.17}$$

Corresponding estimates of virtual velocity were on the order of 0.001-0.01 m/s.

Saltation velocities represent the maximum possible particle velocity during bedload transport. They are relatively well understood and represent an extension of suspended sediment theory. However, they can also vary in magnitude considerably depending on application, and significantly overestimate mean particle velocities of denser bedload aggregations. Bagnold (1956; 1966a) and Bridge and Dominic (1984) developed expressions for velocity of a single particle over a fixed bed as a function of excess shear velocity. Calculated magnitudes were consequently quite high (on the order of 0.1-1.0

m/s in Bridge and Dominic, 1984).

Ippen and Verma (1955) determined a relatively simple empirical expression for single, saltating particles:

$$\frac{U}{U_B} = 1 + \frac{1}{12} (S_s - 1) \frac{k_s}{D} \frac{1}{S_w}$$ (3.18)

where $k_s=2.85D_{84}$ and $D=D_{50}$. Ippen and Verma (1955) suggested that the relation could also be re-expressed using a near bed velocity instead of mean column velocity, after appropriate logarithmic profile conversion. Carling (1987), citing this and related work by Abbott and Francis (1977), extrapolated measured velocity profiles down to a near-bed reference height equal to 0.5 times his estimated mean bedload layer thickness, which was measured to be approximately equal to $0.55D_{50}$. This resulted in a near-bed reference height equal to $0.275D_{50}$. Carling argued that this value approximated the mean particle velocity.

The velocity at $0.275D_{50}$ was calculated in this study using the law of the wall (cf. Wilcock 1996) and compared with Ippen and Verma's (1955) equation and the results of Bridge and Dominic (1984). The three estimates were comparable in magnitude and thus defined the approximate upper bound of particle velocities (generally between 0.1 and 0.5 m/s for the peak flood stage). The calculated velocity at $0.275D_{50}$ is negative when $D_{50}/D_{84} < 0.345$, however, and could not describe velocity fields in study streams where more poorly sorted streambed substrates had ratios less than 0.345.

To apply Equation 3.15 consistently, it was necessary to estimate an intermediate mean bedload velocity that reflected the whole moving layer, no matter how thick or thin it was. An expression was needed that described the mean velocity at any time while the bed was physically in motion during flooding. No such experimentally- or empirically-derived relation could be found in the literature for gravel bed streams. It may be appropriate to apply a theoretical granular flow relation, assuming that most particles during large floods are moving in a nearly continuous state at around the time the peak shear stress occurs, when the bed may approach traction carpet conditions. The relevant

literature was reviewed, but most velocity expressions were not transferable to this study since they required more information than could be obtained in the field, or they were embedded in a model that could not be solved analytically (e.g., Jenkins and Hanes 1998).

A dynamic Coulomb yield model expression was developed by Hanes and Bowen (1985), and re-evaluated by Hanes (1986), that could be applied more readily to field data than other granular flow-based equations:

$$u_B(y) = \frac{3 \, u_* \, \tau^* \, C_m \, f_1[\lambda(y)] \, \Delta\phi}{\sqrt{c_i \, S_s} \, (C_0^2 - C_\delta^2)} \tag{3.19}$$

where the linear particle concentration λ (Equation 2.8) is evaluated for $C=C(y)$, which is the volumetric concentration evaluated at a height y above the mobile-immobile bed boundary and is assumed to follow the linear profile:

$$C(y) = C_0 - \frac{y}{\delta} (C_0 - C_\delta) \tag{3.20}$$

c_i is a constant characterizing material properties including elasticity (assumed equal to 0.013; Hanes and Bowen 1985); C_m is the maximum possible volumetric concentration of the material (assumed equal to 0.65; Hanes and Bowen 1985). The at rest volumetric concentration, C_o, is slightly less than C_m (Hanes and Bowen 1985) and is effectively equivalent to $(1-P)_{static}$; C_δ is assumed equal to 0.05 at $\tau^*_{50} = 0.15$ (cf. Figure 2 in Hanes 1986); $tan\phi_r$ is approximately equal to 0.5 (Hanes and Inman 1985a) and $tan\phi_\delta$ is assumed equal to 0.90 (cf. Figure 2 in Hanes 1986); and:

$$f_1(\lambda) = \frac{\lambda + \frac{1}{3}}{(1 + \lambda)^3} \tag{3.21}$$

The maximum velocity is that of the surface layer, determined by evaluating Equation 3.19 at $f_1(\lambda_\delta)$:

$$u_B(\delta) \;=\; \frac{3\,u_*\,\tau^*\,C_m\,f_1[\lambda_\delta]\,\Delta\phi}{\sqrt{c_i\,S_s}\,(C_0^2 - C_\delta^2)} \tag{3.22}$$

The mean velocity of the moving layer can be estimated by integrating Equation 3.19 over $y = 0, \delta$:

$$U_B \;=\; \frac{1}{\delta}\int_0^\delta u_B(y)\,dy \;=\; \left[\frac{3\,u_*\,\tau^*\,C_m\,\Delta\phi}{\sqrt{c_i\,S_s}\,(C_0^2 - C_\delta^2)}\right]\int_0^\delta f_1[\lambda(y)]\,dy \tag{3.23}$$

resulting in:

$$U_B \;=\; \left[\frac{3\,u_*\,\tau^*\,C_m\,\Delta\phi}{\sqrt{c_i\,S_s}\,(C_0^2 - C_\delta^2)}\right]\left[\frac{C_m + C_0 + C_\delta}{3C_m} + \frac{0.6\,(C_\delta^{5/3} - C_0^{5/3})}{(C_0 - C_\delta)\,C_m^{2/3}}\right] \tag{3.24}$$

Use of Equation 3.24 depends on choice of volumetric concentrations. Hanes and Bowen (1985) assumed the static concentration to be $C_0 = 0.60$, resulting in:

$$U_B \;=\; 0.28 U_\delta \;\approx\; \frac{2.4\,u_*\,\tau^*}{\sqrt{S_s}} \tag{3.25}$$

Porosity estimates for my sites were estimated to be between 0.30 and 0.35, resulting in C_0 values ranging between 0.65 and 0.70. Following Hanes and Inman (1985a) where $C_m \approx C_0 + 0.05$:

$$U_B \;\approx\; \frac{2.1\,u_*\,\tau^*}{\sqrt{S_s}} \;\rightarrow\; \frac{2.2\,u_*\,\tau^*}{\sqrt{S_s}} \tag{3.26}$$

The predicted mean bedload velocity is relatively insensitive to differences in static

porosity, which makes intuitive sense since the static porosity has little meaning once the bed dilates and becomes mobile. Based on this result, the mean bedload velocity was estimated for all of the study streams using a single coefficient equal to 2.2; i.e.:

$$U_B \approx \frac{2.2\,u_*\,\tau^*}{\sqrt{S_s}} \qquad (3.27)$$

Calculated values generally ranged between 0.01 to 0.08 m/s in the study sites.

3.3.8 *Spatial Distributions of Sediment Available for Bedload Transport*

Changes in bed topography correspond to spatial and temporal changes in sediment storage. The topographic survey data were used to identify where net scour and fill occurred within each study reach. The data were recorded in Cartesian coordinates, and the axes were adjusted so that the coordinates of surveyed benchmarks were approximately the same for the 1996 and 1997 surveys. A small amount of error resulted from slight leaning of the prism rod and occasional inability to sight the total station laser on the center of the prism because of riparian vegetation. However, horizontal spatial measurement errors were calculated to be within ±0.03 m (absolute) by comparing the coordinates of the benchmarks from each year's survey, and were thus neglible. Vertical measurement error was determined to be less than 0.009 m based on comparisons with level loop surveys determined using an autolevel.

The adjusted data were contour-plotted using Surfer® (Golden Software Inc.). The axes were rotated so that the longitudinal profile of the channel was parallel to the horizontal axis. A rectangular grid was established that extended over the majority of the channel bottom, with a resolution approximately half the cross-stream survey measurement resolution. The Surfer® Kriging gridding algorithm was used with standard program settings, and the resulting elevation contours matched the data well; in a few instances small depressions or hills were calculated at isolated grid points between

transects, but their influence on the results was unimportant.

Identical grids were used for both the 1996 and 1997 data. The grid data were exported, and the 1996 elevation subtracted from the 1997 elevation. The differenced data were re-imported into Surfer® and contour plots created showing net scour (negative values) and fill (positive values). The difference plots were compared to the bed elevation plots, and evaluated for reach-wide patterns influencing the scour monitor measurements.

3.4 Data Analyses

The basic data identified in this chapter are analyzed in depth in the next two chapters. Chapter 4 uses the majority of data to identify the maximum disturbance depths caused by a moving bedload layer and to evaluate the corresponding bedload transport mechanisms. Chapter 5 presents additional data and analyses related to predicting net excavation scour depth.

4.0 Disturbance Depth Caused by a Moving Bedload Layer

This chapter presents evidence that the disturbance depth caused by moving bedload is restricted to a thin layer in gravel bed streams. The maximum thickness of the disturbed layer is found to scale with the streambed surface grain size distribution, vary spatially in a stochastic manner, and be less than or equal to approximately twice the bed D_{90} or one and a half times the diameter of the largest particle mobilized. The constraints to disturbance depth are demonstrated in three ways. I present evidence that (i) mobilizing forces that occur in natural gravel bed channels are insufficient to cause a bedload disturbance depth that is deeper than approximately $2D_{90}$, irrespective of flood magnitude; (ii) disturbance depth does not correlate significantly with bedload transport rate, which is correlated with flow strength; and (iii) the $2D_{90}$ constraint applies to all regions of the channel bed after accounting for scour and fill. Supporting stratigraphic evidence is also presented that indicates the presence of thin bedload layers in gravel bed streams.

The results indicate the nature of the scouring process in salmonid spawning beds, and provide crucial context for evaluating net excavation scour (Chapter 5) and the influence of scour on salmonids (Chapter 6). The chapter concludes with a discussion of the physical mechanism by which bedload disturbs the streambed.

The explicit relationship between disturbance depth, exchange depth (Wilcock et al. 1996), and thickness of the moving bedload layer is also discussed at the end of this chapter. Scour depth has historically been interpreted as all of these depths. The term 'bedload disturbance depth' reflects the mode of measurement and is used here to represent the parameter δ_{Bm}. The conclusions of this work depend critically on correctly measuring bedload disturbance depth. I show in the next section that there may be a systematic measurement error in some of the data presented, but that this error is insufficient to influence the conclusions of this and subsequent chapters.

4.1 Measurement Errors of Maximum Bedload Disturbance Depth

Chapters 1 and 3 identified the critical assumption stemming from the definition of Equation 1.1 that, after partitioning out the contribution of net excavation, the remaining component of total scour depth approximates the maximum local disturbance depth caused by bedload transport during a flood. There are two potential sources of error that are excluded in Equation 1.1, but there was no way to identify their magnitude explicitly using the methods of this study. Necessary information included the temporal change in bed surface elevation during the study floods, where the only means to obtain such data practically would have involved the use of hydroacoustics (e.g., Dinehart 1989); this was not feasible given the scale of sampling effort and the available budget. The order of magnitude of the error was evaluated indirectly instead by identifying the possible bedload transport processes involved and assessing their influence on the data.

The first error is where scour and fill occurs, and some of the data appear to have been influenced by this phenomenon. Specifically, total scour depths measured in: the Tolt River (all scour monitors); across a fine grained bar deposit on Transect 2 of the South Fork Willapa River; Transect 1 of the Willapa River below Trap Creek; and Transects 4, 6, and a fine grained bar deposit on Transect 2 of the South Fork Snoqualmie River; were all likely to have been influenced significantly by a scour and fill cycle, based on geomorphologic and/or sediment continuity evidence discussed in Chapter 5. Those data have been excluded from analyses of bedload disturbance depth in this chapter.

The remaining δ_{Bm} data are assumed to be associated with negligible scour and fill, for three reasons. First, the data were collected in reaches containing extensive quantities of gravel and cobble available for transport during floods. There was consequently little opportunity for significant sediment transport rate imbalances to develop such that a significant scour and fill cycle likely did not occur.

Second, the study reaches and transects were plane bed in character because pools were present in limited numbers and surface area, or were not well defined. Significant

shifting of the thalweg location was not evident in successive cross-section surveys (see plots in Appendix D) and was highly unlikely.

Third, net changes in bed elevation were generally consistent in direction (i.e., net scour or net fill) in all study sites instrumented with multiple transects, as determined by before- and after-flood cross-sectional surveys (presented in Appendix D). The topographic surveys also showed a net scour or net fill throughout the length of each reach where such data were collected (discussed in Chapter 5). It is unlikely that the entire reach experienced additional scour and fill during the floods in the study because the phenomenon would have required all of the surface layer material in the reach to be transported downstream, and be replaced later in time by new material arriving from upstream. Tracer stone data collected in this study (see Chapter 5) and reported in the literature (see Section 2.3) suggest that most of the coarser particles present did not move far enough (i.e., approximately one-half to one pool-riffle wavelength) during the floods in the study for reach-wide scour and fill to occur. The net effect of these three circumstances is that a significant scour and fill signal was unlikely in the bedload disturbance depth data analyzed in this chapter.

The other source of error is inherent in the definition of Equation 1.1, which assumes that the maximum bedload disturbance depth occurs near the time that the bed elevation change begins (in the case of net fill) or ends (net excavation). Net scour and net fill occur over the entire period of sediment transport. The maximum bedload disturbance depth should occur nearer the peak flow, however, between the beginning and end of transport. Equation 1.1, therefore, is biased when significant bed degradation or aggradation occurs. The bias will be negligible when near-equilibrium sediment transport prevails in a reach because the bed elevation does not change significantly, and the calculated value of δ_{B_m} will then be an accurate estimate of the disturbance depth caused by the peak shear stress during a flood.

In the case of net scour, though, the bed surface elevation is higher at the time of maximum shear stress than when sediment transport ceases. If one assumes that the lowest elevation of bed disturbance occurs at the same time as peak shear stress, the

calculated value of δ_{Bm} will be less than or equal to the disturbance depth that would have been calculated had the bed surface elevation remained unchanged, for the same flood hydrograph. In the case of net fill, the bed elevation is lower at the time of maximum shear stress than when sediment transport ceases. Because net fill is ignored when evaluating Equation 1.1, the calculated value of δ_{Bm} will also be less than or equal to the disturbance depth that would have been measured had the bed surface elevation remained unchanged. Maximum bedload disturbance depths may therefore be underestimated using Equation 1.1 when the bed elevation changes in either direction (up or down) during a flood.

The effect of this measurement bias was evaluated by comparing estimated values of δ_{Bm} measured at locations where:

  (I)   Net fill occurred;

  (II) Bed elevations were essentially static (i.e., changed less than $\pm$ 1 cm, which was approximately the surveying measurement error); and

  (III) Net excavation occurred.

Although sample sizes were too small to test for significant differences, Table 4-1 indicates that this source of variation exists in the data. Estimates of δ_{Bm} were larger on average when there was no net change in bed elevation at the measurement location than when the location experienced either net excavation or net fill. This is consistent with the error mechanism described here.

Fortunately, there were enough measurements made at locations that did not experience significant changes in bed elevation (δ_{EX}) that the bounds of δ_{Bm} could be evaluated using data that were representative of equilibrium sediment transport (see next section). Further, most locations experienced bed elevation changes (δ_{EX}) that were less than 6 cm in magnitude (see data in Appendix D), which corresponds to the maximum combined surveying and scour monitor measurement error (Section 3.3.1). A large proportion of those locations experienced less than a 4 cm change in bed elevation. Assuming that the combined surveying/scour monitor measurement error was random and normally distributed about zero, 95 percent of bedload disturbance depth

Table 4-1. Average values of estimated maximum bedload disturbance depth, δ_{Bm}, and sample size for (a) net excavation, (b) no significant change in the bed elevation, and (c) net fill during a flood.

Stream	Flood Date	Average Value of δ_{Bm} in Meters (Sample Size), Associated With:		
		(a) Net Excavation	(b) No Net Change in Bed Elevation	(c) Net Fill
Issaquah Creek	1/1/97 and 11/25/98 [1]	0.11 (9)[2]	0.18 (1)	0.11 (7)
Raging River	11/27/96	0.18 (9)	0.28 (2)	na
	1/1/97	0.13 (6)	0.23 (2)	na
S Fk Snoqualmie River	2/14/97	0.12 (3)	0.16 (2)	na
Squire Creek	1/1/97	0.10 (7)	0.17 (1)	0.10 (2)

[1] *- Floods with similar peak magnitudes*
[2] *- (9) = Number of scour monitors*

measurements would be accurate to within ±2 standard deviations (±2 cm), or on the order of ±10 to 20 percent of the mean values in Table 4-1 [under the maximum ignorance assumption that the data follow a uniform distribution, the standard deviation of the data would equal $[(4^2 + 2^2)/12]^{0.5} = 1.3$ cm, in which case approximately 90 percent of the data would be within ±2 cm].

4.2 Mobilizing Force and Bedload Disturbance Depth

The data measured in this work indicate that the maximum bedload disturbance depth in a gravel and cobble streambed increases with flow strength until the largest particles present are mobilized, at which point disturbance depth becomes asymptotic to an upper limit. I show this here in three ways. The most direct evidence is seen in plots of disturbance depth versus estimates of the shear force applied at the streambed surface in the downstream direction. I also provide indirect evidence that the thickness of the

bedload layer does not increase significantly with bedload transport rate, which increases with flow strength. There is furthermore no apparent relation between the maximum bedload disturbance depth estimate and the respective location in a reach.

4.2.1 *Shear Stress and Stream Power*

Data were collected for a wide range of estimated peak shear stresses (20 to 190 Pa) and flood recurrence intervals (one- to twelve-year, with most less than the three-year flood; Table 4-2). Figure 4-1 depicts scatterplots of bedload disturbance depths measured in each stream against estimated shear stress at the scour monitor location. The scatter is comparable to the variability recorded by others who have measured total scour depth distributions (e.g., Hassan and Church 1994; Haschenburger 1996; Rennie 1998).

Komar's (1996) average flow competence relation:

$$\tau_{cr} = \tau^*_{cr}(\rho_s - \rho)gD_{50}^{0.6}D_{comp}^{0.4} \qquad (4.1)$$

is also depicted in Figure 4-1 for each stream, where the two curves are defined by the critical dimensionless shear stress τ^*_{cr} equal to 0.031 as a lower bound (Wilcock et al. 1996), and 0.08 as a rough upper bound (Buffington and Montgomery 1997). The values of 0.031 and 0.08 also respectively define approximate lower and upper envelopes to the data Komar (1996) used for evaluating Equation 4.1. The curves are terminated at the maximum particle size present that the equation predicts could be transported during the largest flood sampled, and delineate estimates of the largest particle size that the stream is capable of transporting at smaller magnitudes of local shear stress.

Exponents of the D_{50} term in Equation 4.1 can take values other than 0.6. For example, Milhous' (1973) data are fit by an exponent value of 0.43, whereas other data are fit better by values of 0.8 and larger (Komar 1996) including in this study (see Chapter 5). Larger exponents result in the curves rising more rapidly and higher. The

Table 4-2. Frequency characteristics of floods for which scour depth data were collected, at gaged sites.

Study Reach	Flood Date	Peak Flow Rate (m³/s)	Estimated Return Period (Years) [1]
Issaquah Creek	01/01/97	22.2	2.5
	10/30/97	8.64	1.2
	11/25/98	21.0	2.3
N Fk Stillaguamish River at USGS	03/19/97	934	12
Raging River	11/27/96	57.8	2.4
	01/01/97	52.5	1.9
	02/14/97	42.4	1.4
S Fk Snoqualmie River	02/14/97	59.0	1.2
	03/19/97	100	1.7
	10/04/97	50.7	1.1
	10/30/97	114	2.0
S Fk Willapa River [2]	01/01/97	57.1	3.2
Squire Creek [2]	10/04/96	17.4	~ 1
	10/22/96	33.5	~ 1
	01/01/97	62.1	1.3
	01/30/97	40.1	~ 1
	03/19/97	90.0	2.5
Tolt River	11/27/96	155	1.5
	03/19/97	207	2.5
Willapa River at USGS	01/01/97	286	4.0

[1] - Flood return periods estimated from at-site fitted Generalized Extreme Value Distribution
[2] - Estimated using gages discontinued ca. 1970

lines depicted in Figure 4-1 define a range of average flow competence relations that might be observed in the study streams. Exceptions are possible depending on unaccounted-for, site-specific characteristics that influence determination of the exponent.

Four features are apparent in Figure 4-1. First, the bedload disturbance depth data in all streams except the lower North Fork Stillaguamish River (USGS site) are approximately bounded to the left in the plots by the competent grain size curve defined by $\tau^*_{cr} = 0.031$, or by an analogous curve defined by $0.031 < \tau^*_{cr} < 0.08$, suggesting that
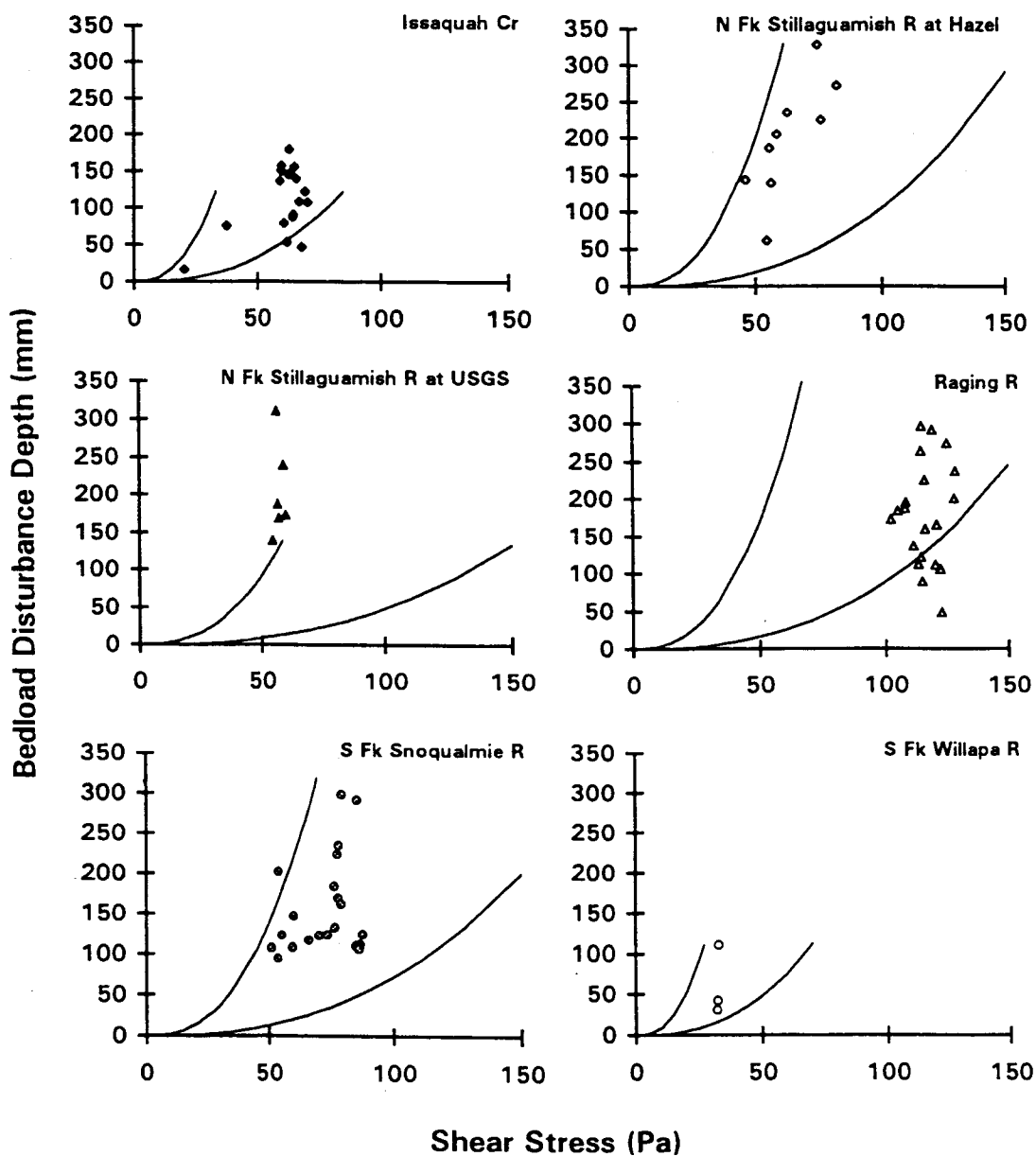
Figure 4-1. Variation of maximum measured bedload disturbance depths with local bed shear stress at scour monitor locations in the study streams. Measurements thought to have been influenced by scour and fill are not shown. The curves delineate competent grain sizes predicted using Komar's (1996) relation (Equation 4.1) with $\tau^*_{cr} = 0.031$ (left curve) and $\tau^*_{cr} = 0.08$ (right).
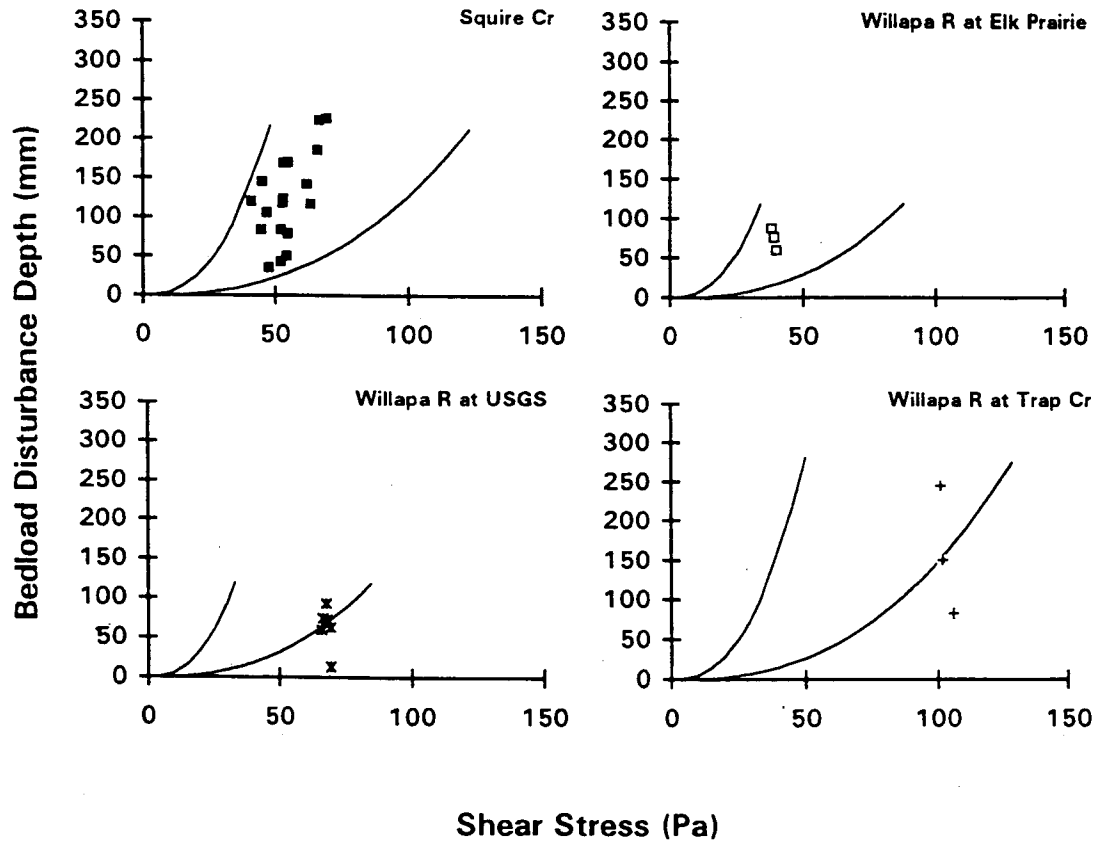
Figure 4-1. Continued.

bedload disturbance depth reflects in part the size of the largest mobile particle. It is plausible that the North Fork Stillaguamish site-specific D_{50}-exponent in Equation 4.1 is larger than 0.6, in which case the data would also be bounded to the left by the competent grain size curve defined by $\tau^*_{cr} = 0.031$; also, the bed was locally steeper than the longitudinal water surface gradient such that τ^*_{cr} could have been smaller than 0.031 (Fernandez Luque and van Beek 1976), resulting in larger predicted competent particle sizes than depicted.

Second, data from several streams are to the right of one or both curves, and do not appear to be bounded by the characteristic shape of a flow competence relation. This suggests that in those streams, shear stresses were well above critical levels required to mobilize all members of the bed surface layer. The appearance of a bound in the other streams may be misleading, because the data represent scour depths measured at the flood peak. Incipient motion of the largest particles may have occurred prior to the peak flood stage.

Third, the unbounded bedload disturbance depth measurements do not exhibit a clear distribution with increasing shear stress and appear to be distributed approximately uniformly within each site. This result differs from those of previous studies, where gamma or exponential distributions have been shown to fit disturbance depth data (Hassan and Church 1994; Haschenburger 1996; Rennie 1998). The difference likely occurs because the data in Figure 4-1 were measured closer to the thalweg than to the channel margin, in the region of the cross-section that experiences the greatest bedload transport activity. The best fits of exponentially decaying, gamma-type distributions include zero (or non-detected) and near-zero disturbance depths measured nearer the channel margin and on bars. The data measured in this study may constitute a subset of a larger scale (i.e., reach-wide) spatial probability distribution.

Fourth, the maximum bedload disturbance depths do not substantially exceed competent particle sizes. One interpretation of this and the other three features is that maximum bedload disturbance depth increases with shear stress until the largest competent particle size present is mobilized, after which there is no clear trend.

Similar observations were made when maximum stream power, expressed either as total or excess, was substituted in the analysis for bed shear stress.

4.2.1.1 *Removing the Influence of Scale*

Particle size and other stream-specific attributes of scale influence the observed disturbance depth-shear stress relationships in Figure 4-1. Dimensionless representation of disturbance depth and shear stress standardizes the data to similar geometric and dynamic scales. The thickness of the streambed surface layer defines an appropriate length scale for non-dimensionalizing disturbance depth because the surface is the first layer to move during a flood, and influences mobilization of the next layer underneath. The thickness is usually defined by a characteristic particle size. The local D_{90} was used here, in large part because Wilcock et al. (1996) and others have used it in similar contexts for a number of physical and statistical reasons (see Section 3.3.2).

Shear stress was non-dimensionalized as the Shields parameter (Equation 3.8), which represents the ratio of motive to resistive stresses acting on the bed surface particles. It was calculated here using grain size distributions that were truncated at 8 mm either deliberately (McNeil samples) or effectively (pebble counts) (Section 3.3.2). Stream power was not evaluated in this context because it is difficult to non-dimensionalize in a physically meaningful way, and is subject to additional unexplained variation because the requisite efficiency factor (Bagnold 1966a) cannot be determined readily (making it difficult to apportion how much of the energy is dissipated in bedload transport). It is more convenient and physically meaningful to non-dimensionalize mobilizing force using the Shields parameter.

Figure 4-2 shows that non-dimensionalizing bedload disturbance depth and shear stress results in reducing data scatter, but not substantially. In some sites the scatter increases (e.g., Raging River, North Fork Stillaguamish River at Hazel), but the same general patterns remain as seen in Figure 4-1. In all cases there is wide scatter in bedload disturbance depth for the same dimensionless shear stress. Data from Issaquah
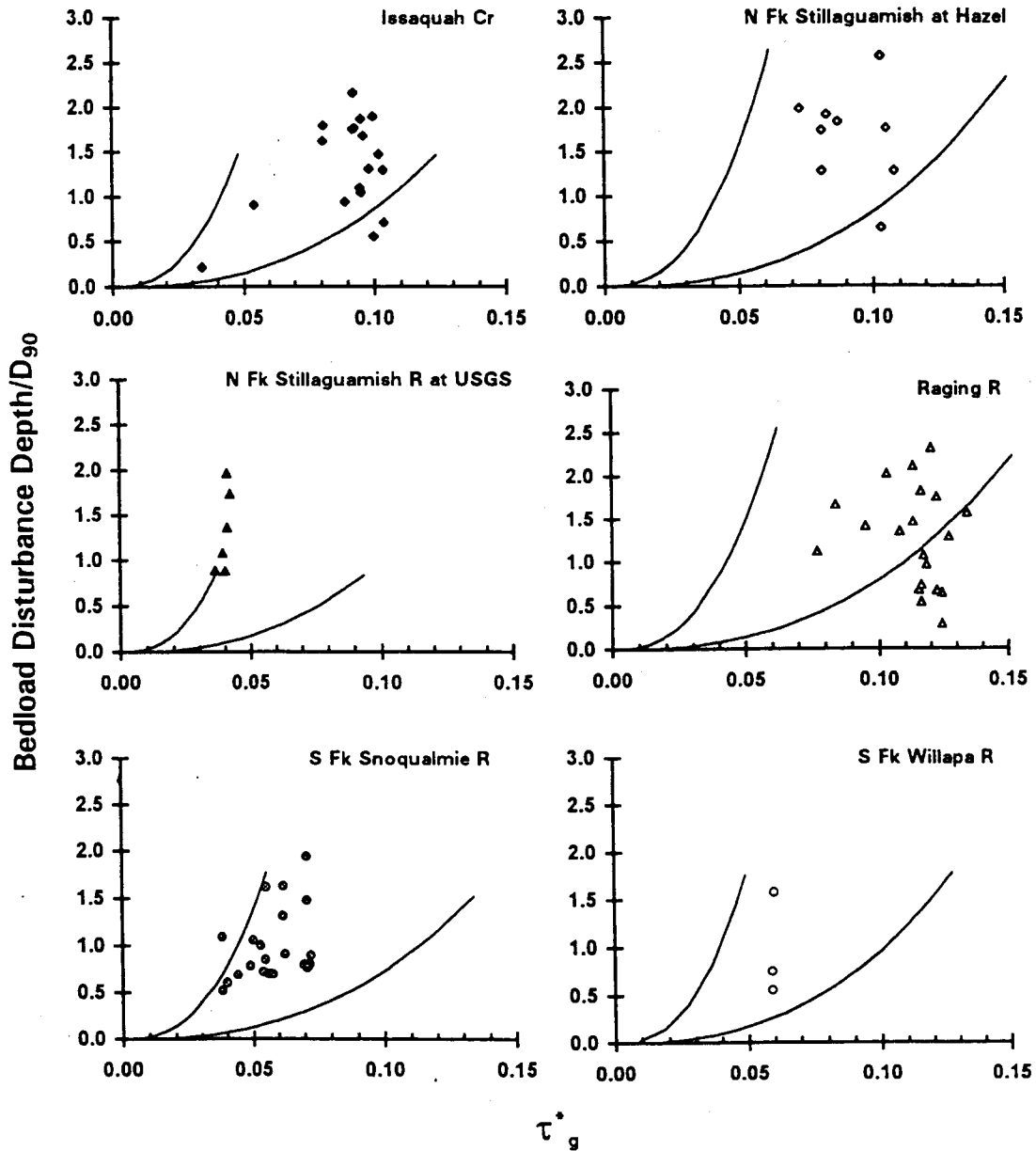
Figure 4-2. Variation of maximum measured dimensionless bedload disturbance
depths with local dimensionless bed shear stress at scour monitor
locations in the study streams. Measurements thought to have been
influenced by scour and fill are not shown. The curves delineate
competent grain sizes predicted using Komar's (1996) relation
(Equation 4.1) with $\tau^*_{cr} = 0.031$ (left curve) and $\tau^*_{cr} = 0.08$ (right).
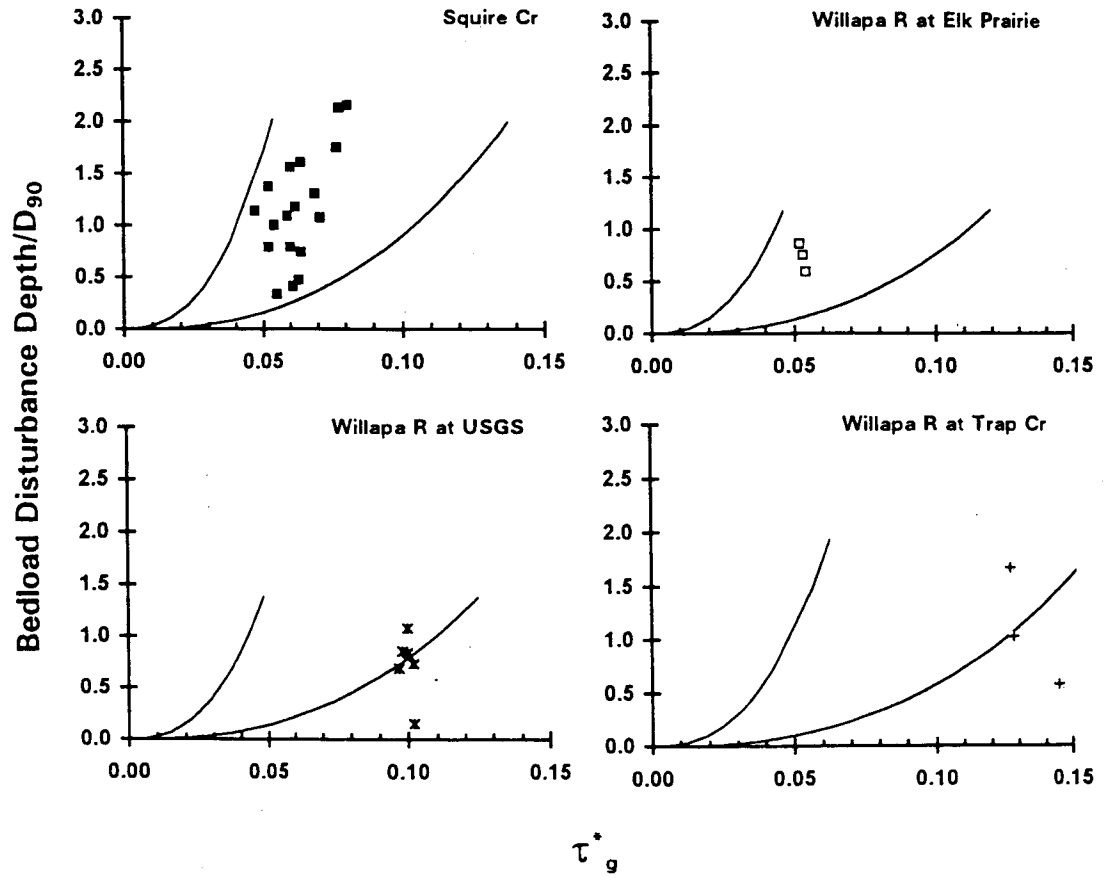
Figure 4-2. Continued.

Creek, the South Fork Snoqualmie River, and Squire Creek could be interpreted to represent a trend between average disturbance depth and shear stress, but data from the other streams generally can not. The wide scatter and relatively small range in estimated shear stresses preclude confirmation of trends in any given stream. Because the most important stream-specific effects of scale on disturbance depth geometry, flow strength, and resistance to motion have been accounted for in the axes of Figure 4-2, it is not clear that additional dimensionless variables would reduce the scatter, or explain differences between sites, sufficiently that a universal trend would emerge.

There were too few data to evaluate fully the relationship (or lack of one) between shear stress and bedload disturbance depth in each stream. Assuming that the selected dimensionless variables are appropriate, the alternative approach was to plot the corresponding results for the different streams on the same graph. Figure 4-3 shows all of the dimensionless data from Figure 4-2 plotted together. Figure 4-3a also shows estimates from locations that experienced scour and fill for comparison. As described earlier, there was geomorphic evidence for rejecting those data from this analysis. The majority of data in Figure 4-3b are bounded by two lines proposed in the work of Wilcock et al. (1996) and Wilcock and McArdell (1997) to represent the approximate limits to exchange depth and bedload layer thickness (horizontal line, $\delta_{Bm}/D_{90} = 2$) and the shear stress at which the bed is mobilized down to the bottom of the armor layer (vertical line, $\tau^*_g = 0.035$). A single scour monitor observation from Issaquah Creek falls within the narrow range $\tau^*_g = 0.031$ to 0.035 that Wilcock et al. (1996) proposed was the transition from general immobility of the bed surface framework to disturbance of the bed surface layer. During that flood, the other scour monitors remained undisturbed, and the single observation represents disturbance that occurred during partial transport.

Measurement bias in δ_{Bm} caused by net excavation or net fill (Section 4.1) does not appear to have influenced the data scatter in Figure 4-3 substantially. Measurement bias was evaluated in two ways. In the first, the data were classified according to whether the location experienced net excavation, no net change, or net fill. Figure 4-4a shows that a large number of data below the $\delta_{Bm} \approx 0.8D_{90}$ line were associated with net
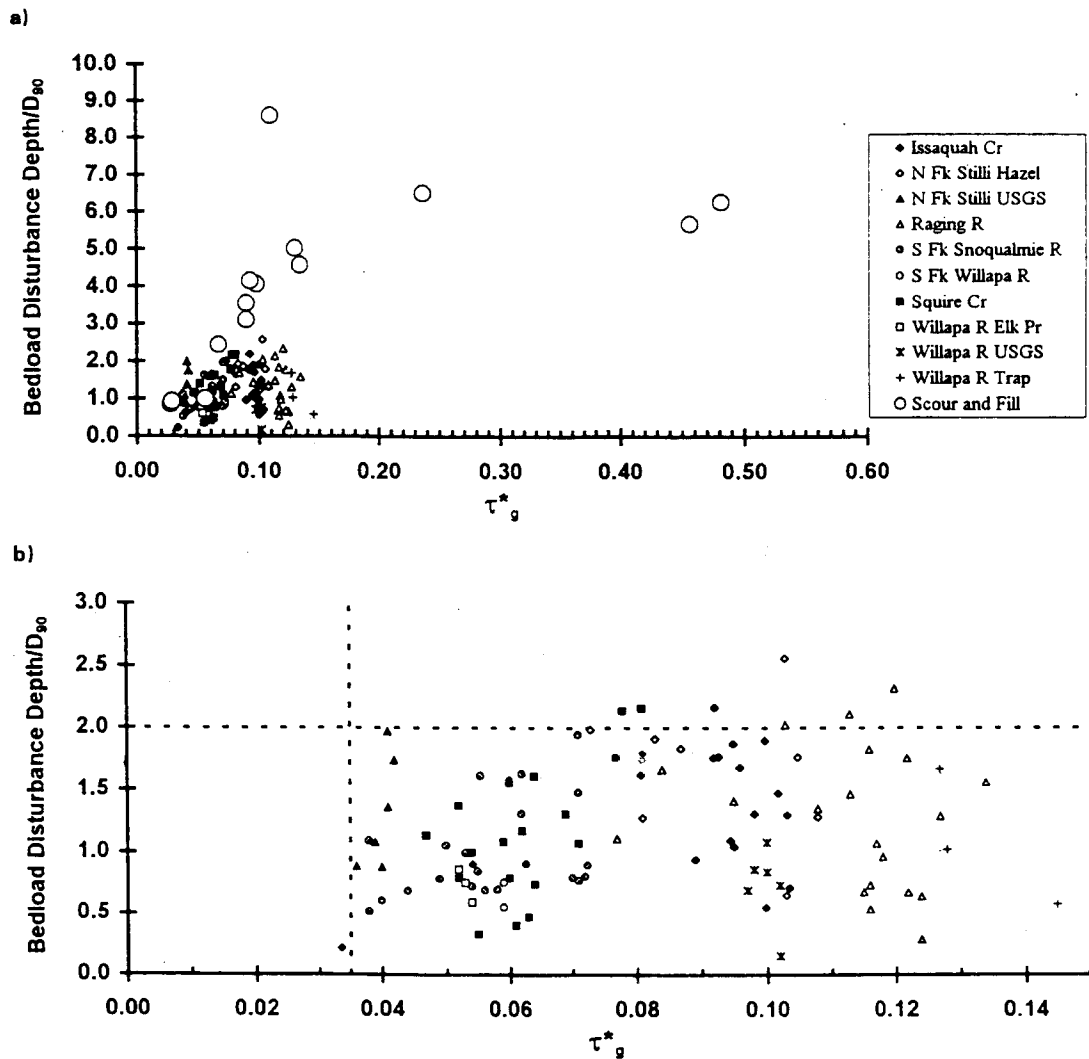
Figure 4-3. Variation of measured local dimensionless bedload disturbance depths calculated using Equation 1.1, with estimated local dimensionless bed shear stress: (a) all data, including measurements thought to be influenced by scour and fill; (b) scour and fill data removed. The horizontal dashed line represents $\delta_{Bm} = 2D_{90}$; the vertical line is for $\tau^*_g = 0.035$.

a)

b)
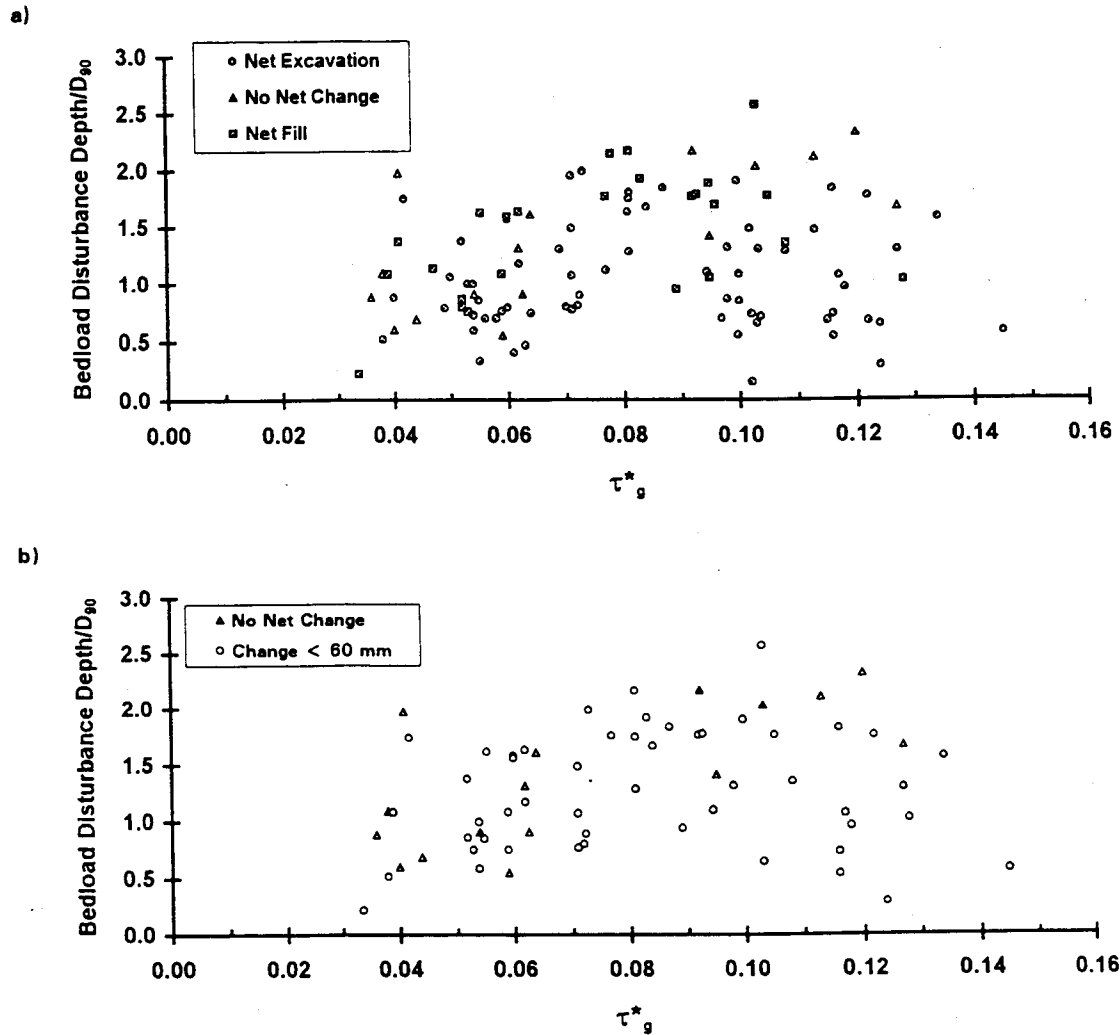
Figure 4-4. Evaluation of measurement bias related to the formulation of Equation 1.1: a) the data in Figure 4-3b are classified according to the net change in local bed elevation after the measured flood; b) the data are classified by whether the bed experienced no net change, or the change was within measurement error.

excavation and consequently may be underestimates of the maximum bedload disturbance depth. However, filtering out all data where net excavation or fill were determined by pre- and post-flood bed elevation surveys to exceed 60 mm (i.e., greater than measurement error in δ_{Bm}) results in a data scatter that is not substantially different from that of the entire data set. The $\delta_{Bm} = 2D_{90}$ and $\tau^*_g = 0.035$ lines bound the filtered data equally well in Figure 4-4b compared with Figure 4-3b. Regression of the data in Figure 4-4b indicates a slope that is only slightly significantly different from zero at the 95 percent confidence level, but the data do not have any obvious trend. Figure 4-4 indicates that there is no clear, systematic effect of bias on the distribution of disturbance depth data that would change the conclusions of this analysis.

In the second approach, the bias in Equation 1.1 was approximated by assuming that bed elevation changes occurred linearly with time during a flood, and that the maximum shear stress occurred halfway between the beginning and ending of bedload transport. Equation 1.1 could then be rewritten as:

$$\delta_{Bm} \approx \delta_T - \frac{\delta_{EX}}{2} \tag{4.2}$$

where δ_{EX} is the absolute value of the net change in bed elevation. This expression is supported by the data in Table 4-1. Bedload disturbance depths were recalculated using Equation 4.2 and are plotted in Figure 4-5. Most of the data remain bounded by the $2D_{90}$ line, and all but three measurements are bounded by the $2.2D_{90}$ line. There is no apparent significant measurement bias.

To evaluate the influence of non-systematic measurement error on precision, the uncertainty variance was estimated for each measurement using a first order approximation (Benjamin and Cornell 1970):

$$Variance\,[f(X_1, X_2, \ldots, X_n)] \approx \sum_{i=1}^{n} \left(\frac{\partial f}{\partial X_i} \right)^2 Variance\,[X_i] \tag{4.3}$$

The first order uncertainty variance was computed for δ_{Bm}/D_{90} and τ^*_g. The independent
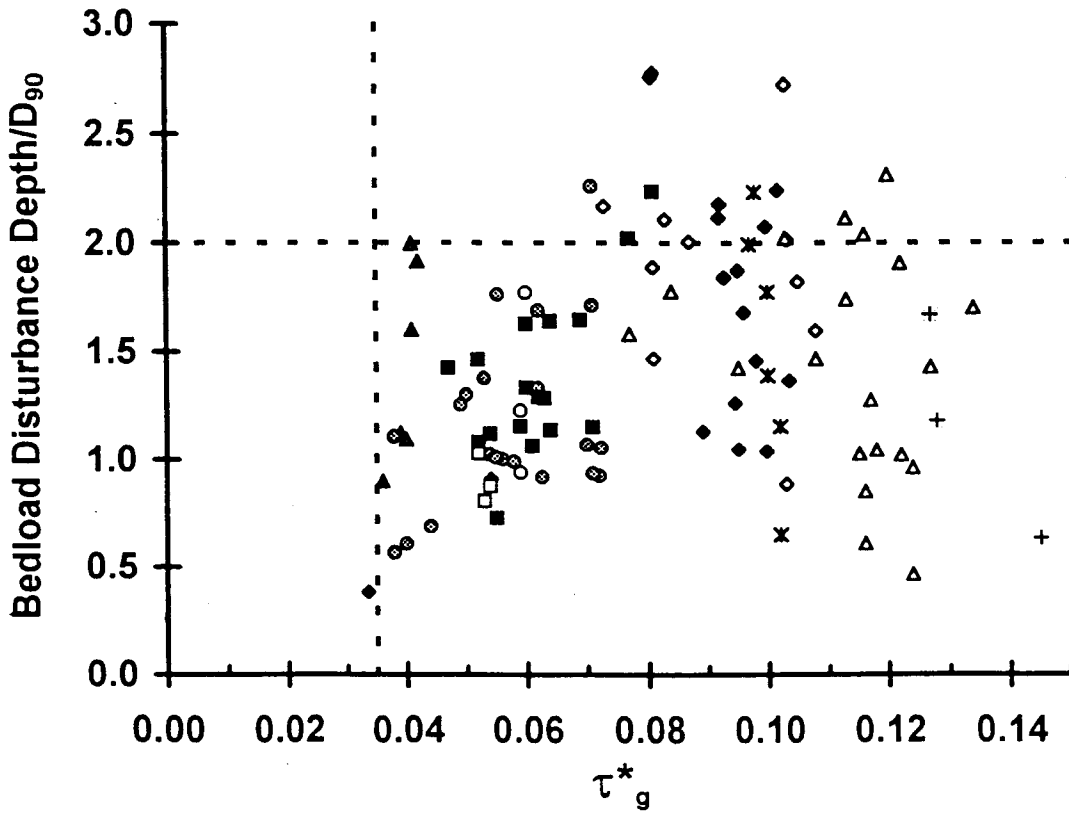
Figure 4-5. Evaluation of measurement bias related to the formulation of Equation 1.1. The data in Figure 4-3b were recalculated to approximate an unbiased estimate of δ_{Bm} using Equation 4.2.

stochastic (X_i) variables included δ_{Bm}, D_{90}, D_{50}, R, and S_f. The standard deviation of disturbance depth was estimated above as 0.013 m. The uncertainty variance in hydraulic radius and friction slope were assumed to be distributed uniformly (i.e., maximum ignorance assumption) over the ranges ± 0.05 m and ± 10 percent, respectively. The D_{90} and D_{50} percentile particle size standard deviations were approximated as 0.5ϕ and 0.79ϕ, respectively, following bootstrap simulations by Rice and Church (1996) where $\phi = -2 \log_2 D_i$. Figure 4-6 indicates that only two observations may be significantly greater than the $2D_{90}$ line.

The possibility was also considered that the shear stress estimates depicted in Figures 4-1 through 4-6 might include the contribution of other, unexplained losses (e.g., side wall effects, local form drag) that influenced the data scatter. Several study streams afforded measurement of scour depth and bed elevation changes at the same location over two or three floods. Unexplained bias in shear stress estimates should be experienced to a similar degree at a specific location over the range of flows monitored. Hence, each monitor should exhibit a consistent positive trend between bed shear stress and disturbance depth if a deterministic relationship exists. Figure 4-7 shows that there was no consistent, positive relationship between the dimensionless bedload disturbance depth and shear stress estimates: some scour monitors exhibited a positive, some a negative, and others no relation. The lack of a consistent, positive trend could not be explained by evaluating the data according to whether (i) the bed was worked by a previous flood during the 1996-97 season (temporal sequence of measurements is indicated in the figure by the arrows), and (ii) the data were influenced by measurement bias per Section 4.1.

Two observations from the North Fork Stillaguamish River (USGS site) have a disproportionately large influence in Figures 4-3b and 4-4: they approximately define the intersection location of the $\tau^*_g = 0.035$ and $2D_{90}$ lines, and there are no other observations with as large a dimensionless disturbance depth until $\tau^*_g \approx 0.07$. The plotting positions are valid, however, because: (i) it has been established that the measured values of δ_{Bm} are less than or equal to the 'true' value, and Figure 4-5 suggests
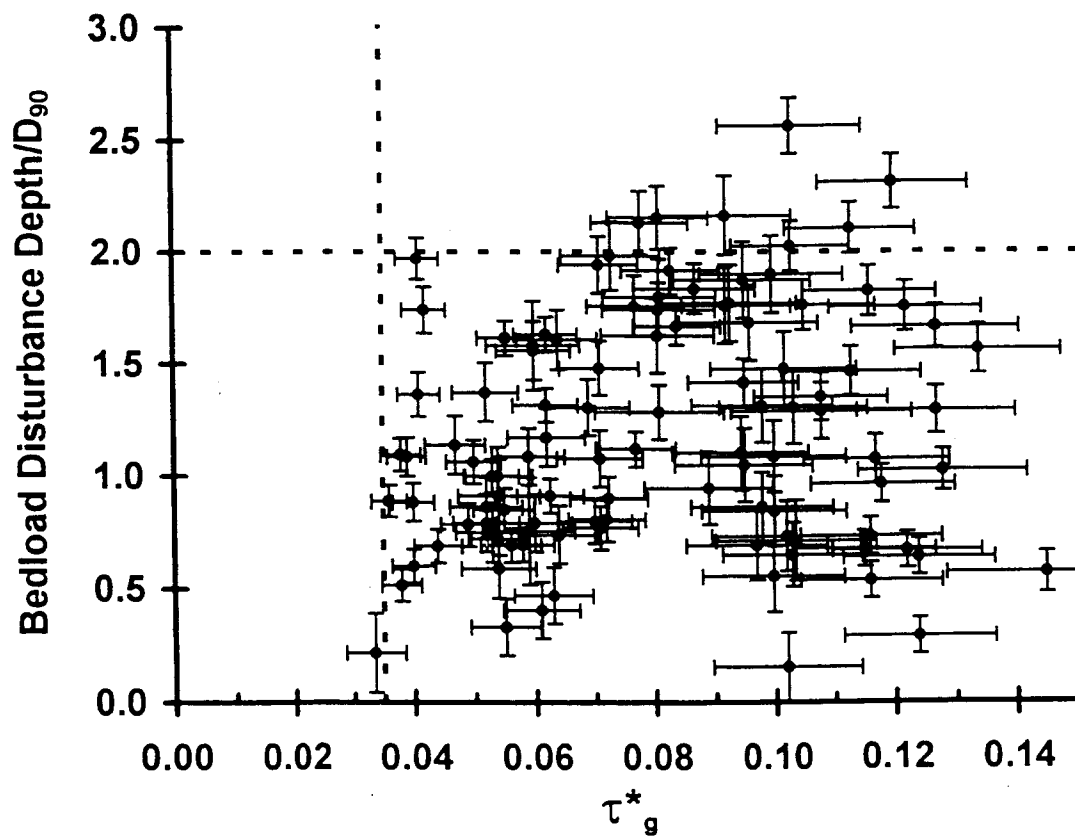
Figure 4-6. The influence of measurement errors on the dimensionless bedload disturbance depth and shear stress data. Error bars were approximated using Equation 4.3.
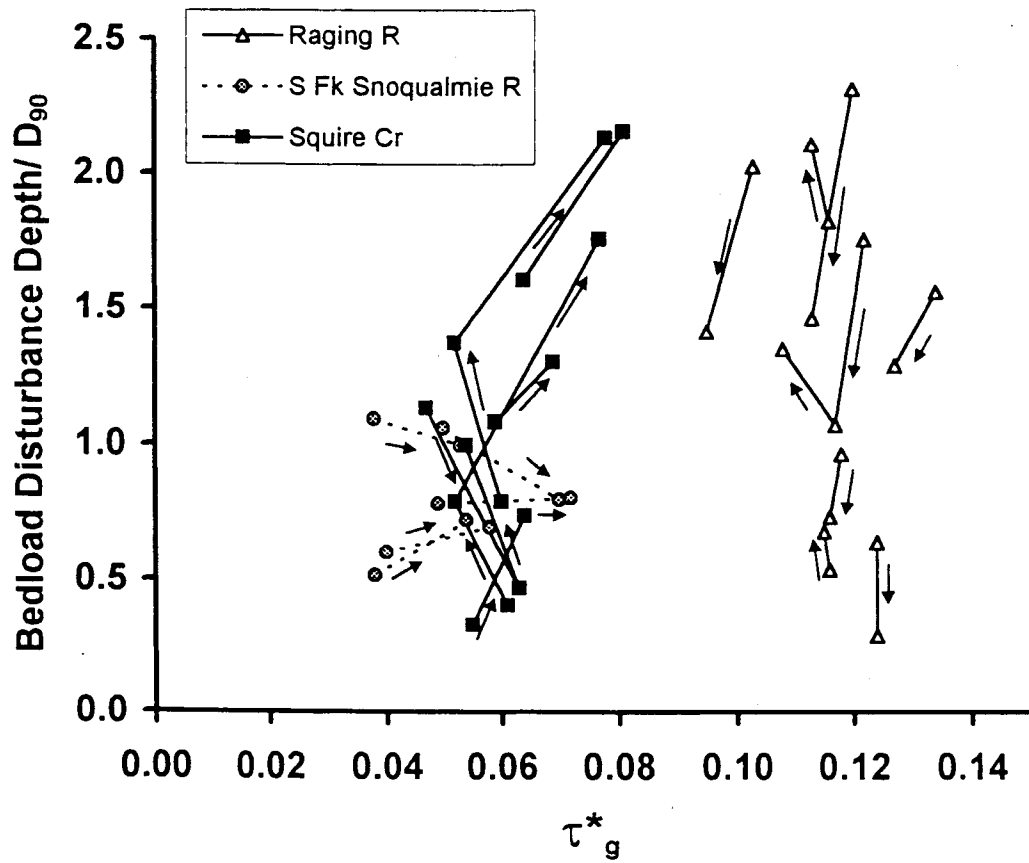
Figure 4-7. Evaluation of scour monitor-specific relations between dimensionless bedload disturbance depths and dimensionless shear stresses, at selected study sites. Measurements made by the same scour monitor are linked by solid lines and the temporal sequence of measurements is indicated by the arrows.

that the bias was negligible; (ii) the larger of the two dimensionless bedload disturbance depths (triangle in Figure 4-4b) was calculated using a coarser D_{90} (158 mm) than the smaller one (circle; 138 mm), and is also the better estimate of δ_{Bm} because the bed elevation did not change; and (iii) the friction slope estimate was one of the best in the study; it was not influenced significantly by sidewall or other effects because the channel was wide and nearly uniform, the scour monitors were located near the thalweg, and the water surface slope used to approximate the friction slope was asymptotic to the reach slope at an intermediate flood stage (Figure H-6; Appendix H). Plotting issues (i) and (ii) indicate that the ordinate (δ_{Bm} /D_{90}) values of the two observations should not be substantially lower than shown in Figure 4-3b and 4-4. Plotting issue (iii) indicates that the abscissa (τ_g^*) values should not be substantially different than shown. Hence, there are no grounds for rejecting the two observations.

The results presented in Figures 4-3 through 4-7 indicate that, over the sampled range of $0.035 \leq \tau_g^* \leq 0.15$, there was no consistent positive trend between shear stress and maximum bedload disturbance depth, which was less than approximately $2D_{90}$ or $2.2D_{90}$ depending on measurement accuracy and precision. This interpretation is based on considering all of the site data together in lieu of having comparable data from one stream. Future work should evaluate this in individual streams over at least a five year period, to obtain a suitably wide range of shear stresses.

4.2.1.2 Bedload Disturbance Depth at Higher Dimensionless Shear Stress ($\tau_g^* > 0.15$)

This work presents data for $\tau_g^* \leq 0.15$, where most floods had a recurrence interval of less than three years. What happens at greater shear stresses during larger floods? I am unaware of any published work describing bedload disturbance depth of a bed with substrate size and mixture characteristics of typical salmonid spawning beds at higher dimensionless shear stresses. Granular flow theory, computer simulations, and flume data indicate that the thickness of a moving bed consisting of uniformly sized particles exceeds twice the particle size when the dimensionless shear stress approaches 0.4 to 0.5

(see Section 2.4). Similar results have been determined for mixtures in which the largest particle is roughly twice the size of the smallest particle (e.g., Haff and Jiang 1995; Sumer et al. 1996), indicating that uniform sphere results may be extendible to moderately-sorted mixtures. It is unclear whether similar results hold for a coarser, more heterogeneous bed, although a plausible analogy can be made based on certain assumptions described below. Alternatively, a greater dimensionless shear stress may be required than 0.5 to result in granular flow in a gravel and cobble bed. A medium of uniform-sized particles is relatively easier to shear than a heterogeneous one because there is less interlocking of particles and fewer frictional contact points when particles are approximately the same size.

Several equations were identified in Chapter 2 that describe the thickness of a granular flow layer as a function of applied surface shear stress. The equations were modified here to predict the static bed disturbance depth δ_B using the relation $\delta_{MB} \approx 1.2\delta_B$ (see Section 2.4.3). Figure 4-8 shows that the granular flow-based predictions of bedload disturbance depth in a uniformly-sized medium define a band that is less than $2D$ wide. It is not clear *a priori* whether the appropriate scaling size D for a heterogeneously-sized medium should be the mixture D_{50}, D_{90}, or another percentile. The mixture D_{50} has been used commonly to non-dimensionalize shear stress when evaluating bedload transport rates, but Figure 4-8a shows that using it to scale bedload disturbance depths results in values that are substantially greater than the granular flow predictions. Figure 4-8b shows that using the mixture D_{90} as a non-dimensionalizing length scale results in measured values that correspond more closely to the magnitude of granular flow-based predictions of dimensionless bedload disturbance depth, and have a similar vertical scatter. The mixture D_{90} also has a physical significance because it approximates the thickness of the surface layer, which is defined by D for a uniformly-sized mixture. Hence, making an analogy to the results of granular flow work is plausible when bedload disturbance depth is scaled by the mixture D_{90}.

Assuming that the granular flow predictions can be compared with the data measured here, I hypothesize from Figure 4-8b that the maximum bedload disturbance depth in a

a)

b)
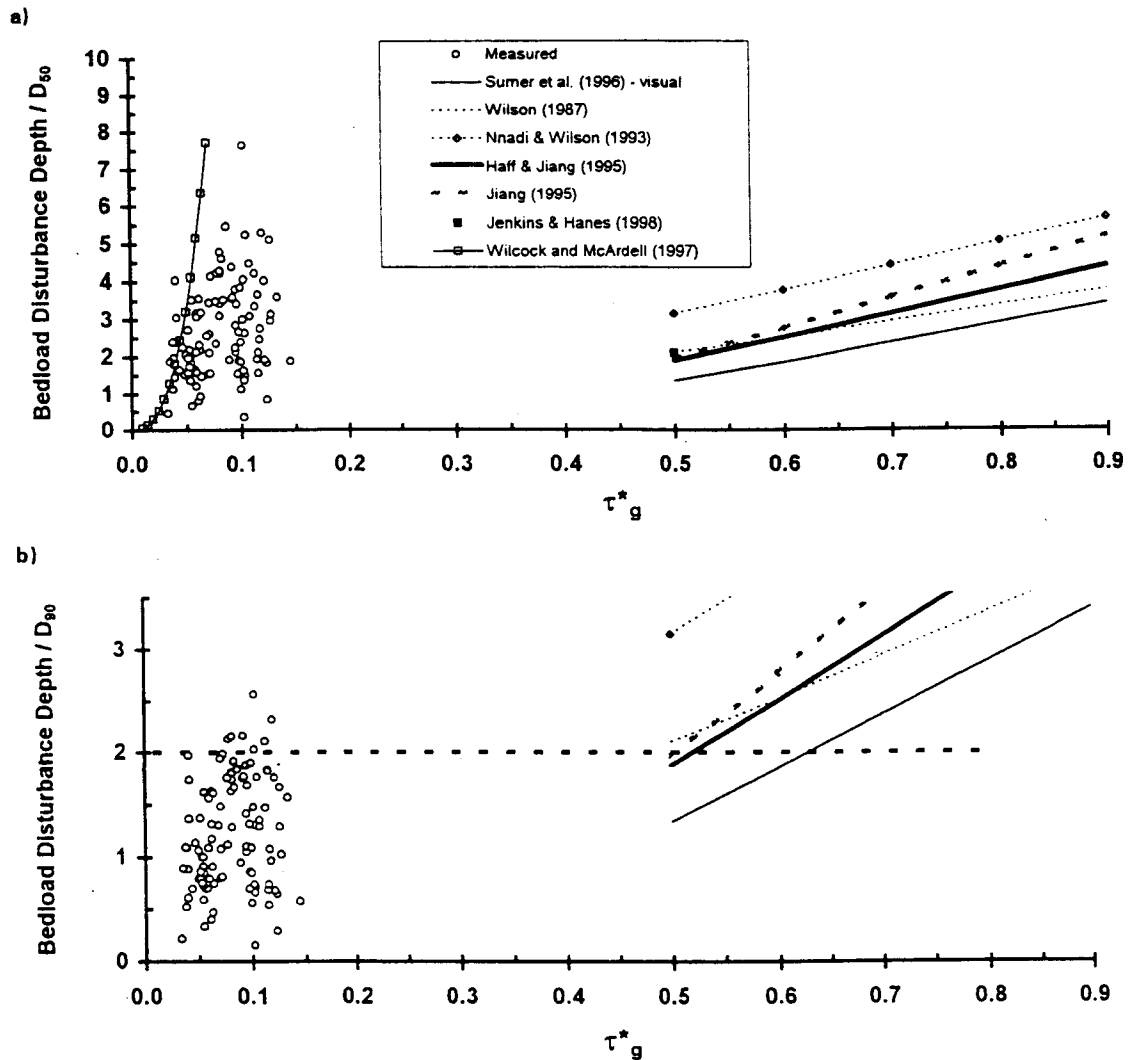
Figure 4-8. Comparison of dimensionless bedload disturbance depths measured in this work with depths predicted by granular flow and partial transport relationships reported in the literature.

gravel bed stream continues to be approximately $2D_{90}$ as dimensionless shear stress increases over the range $0.15 < \tau^*_g < 0.5$. More data are needed from that range to test this hypothesis.

Figure 4-8a also shows that Wilcock's (1997b) exchange depth relation (Equation 2.2) approximately bounds the measured bedload disturbance depths when they are scaled by the mixture D_{50}. Equation 2.2 appears to be useful for estimating the maximum bedload disturbance depth when the bed shear stress is smaller than that needed to disturb a depth of $2D_{90}$.

4.2.2 *Estimated Bedload Transport Rates and Disturbance Depth*

Figure 4-9 shows that Equation 3.15 does not predict bedload disturbance depths measured in the study streams using either Parker's (1990a) or Bagnold's (1980) bedload transport rate equations. Equation 3.15 generally underpredicts dimensionless disturbance depth (Figure 4-9a), and the error increases with disturbance depth magnitude (Figure 4-9b). The horizontal scatter in Figure 4-9b indicates that the difference between predicted and observed depths cannot be adjusted by a multiplicative correction factor.

Part of the reason for the prediction failure is that bedload transport equations are highly variable in terms of statistical precision and the way in which bedload transport processes are represented. Figures 3-5 and 4-9a show that, although Bagnold's (1980) and Parker's (1990a) equations result in similar bedload transport rate and dimensionless thickness estimates when τ^*_g ranges between 0.07 and 0.15, the range in transport rate estimates spans nearly an order of magnitude for the same dimensionless shear stress, which is not an uncommon occurrence (e.g., Gomez and Church 1989). A systematic error may have been introduced because both relations were derived from measurements of channel average transport rates and shear stress or stream power (Milhous 1973; Gomez and Church 1988). The equations were used here to estimate bedload transport rates in regions of the bed where shear stress is larger than the channel average.

Figure 4-9. Comparisons of bedload disturbance depths estimated using
Equation 3.15: a) variation with dimensionless shear stress;
b) predicted versus observed. Bedload transport rate was estimated
using Parker's (1990a) or Bagnold's (1980) equations; bedload
velocity was estimated using Hanes and Bowen's (1985)/Hanes'
(1986) equation.

The transport rate estimates diverge significantly when τ^*_g is less than 0.07 and greater than 0.15 because of the assumptions and data used to develop each transport equation. Parker (1990a, p.419) derived a transport rate function, called $G(\phi)$, that distinguishes between selective transport and equal mobility of different size fractions. The transport rate function is formulated such that the transition to a mobile armor layer occurs when the dimensionless shear stress $\tau^* \geq 0.077$ (the equation predicted transport of essentially all size fractions in my study sites when τ^*_g exceeded about 0.07-0.08). Parker's (1990a) model also ignores sediments finer than 2 mm in size. Conversely, Bagnold's (1980) equation models the entire mixture as a mobile armor layer with an effective thickness determined by the total material mass flow rate. The correspondence between the two bedload transport rate equations for $\tau^*_g \geq 0.07$ occurs because Parker's (1990a) work directly, and Bagnold's (1980) relationship effectively, models a mobile armor layer.

For ($0.15 < \tau^*_g < 0.25$), bedload layer thickness predictions based on Bagnold's (1980) equation were similar in magnitude to predictions made for lower values of τ^*_g. Predictions based on Parker's (1990a) equation increased exponentially and appear to overestimate disturbance depth when $\tau^*_g > 0.2$. These predictions are not shown in Figure 4-9 because measured disturbance depth data were not available, but are described here to provide additional detail on the predictive ability of Equation 3.15.

There is another reason for the predictive failure of Equation 3.15: the mean bedload velocity was probably over-estimated using Equation 3.27. Bedload velocities were back-calculated using measured disturbance depths and estimated bedload transport rates to evaluate their approximate magnitude in the study streams. Figure 4-10 indicates that the power function expressions of Hanes and Bowen (1985) and Hassan et al. (1992) likely over- and under-estimate mean bedload velocity, respectively.

The following power functions were fit in arithmetic space (by minimizing sums of squares; log-linear fits were visually poorer when plotted in Figure 4-10) to the bedload velocities back-calculated using Parker's (1990a) bedload transport relation ($r^2 = 0.47$):
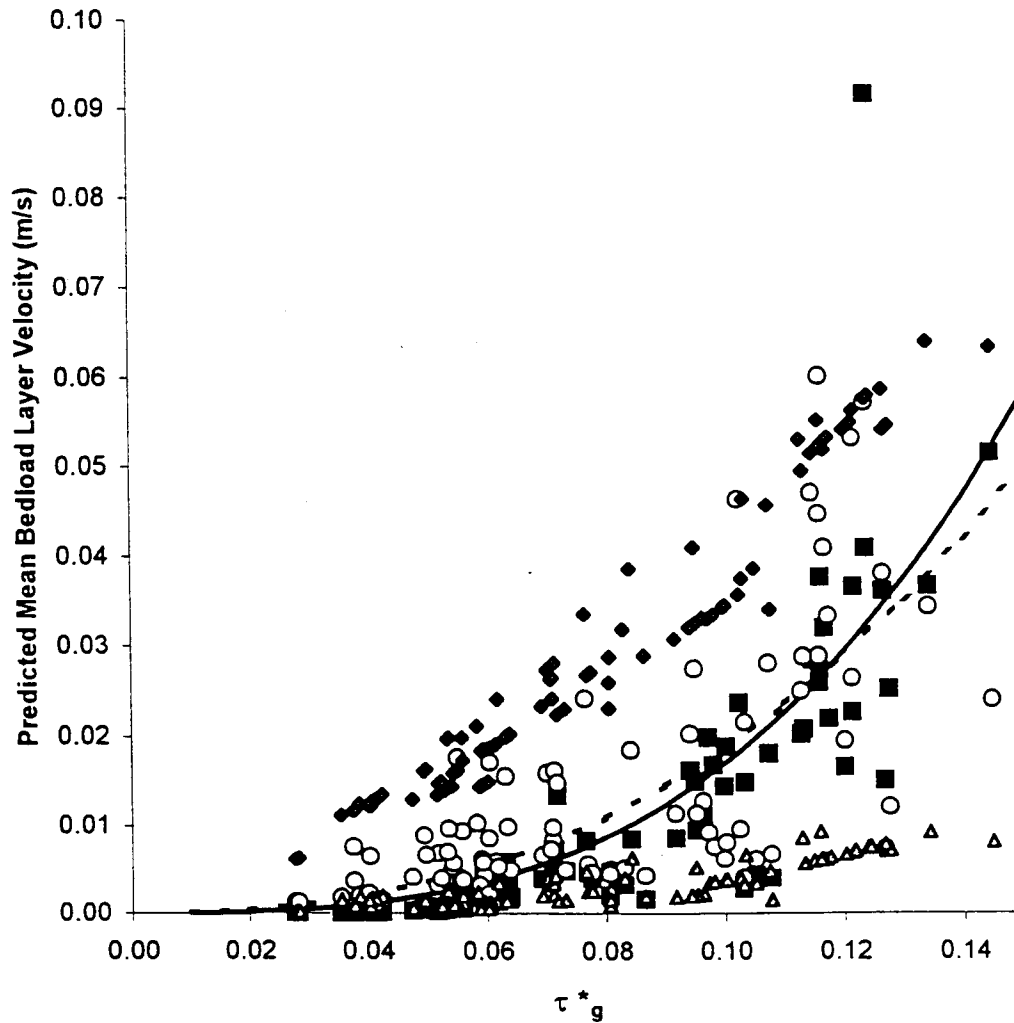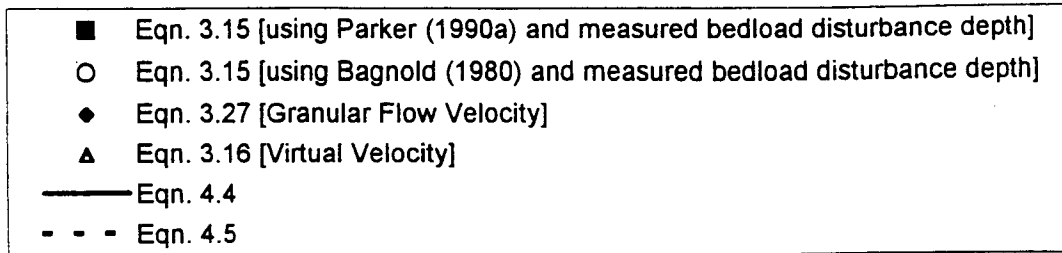
Figure 4-10. Comparison of bedload layer velocity predictions, and their variation with dimensionless shear stress.

$$U_B = 18 \, \tau^*_g{}^{3.0} \tag{4.4}$$

and using Bagnold's (1980) relation ($r^2 = 0.40$):

$$U_B = 4.7 \, \tau^*_g{}^{2.4} \tag{4.5}$$

where $\tau^*_g < 0.15$. Both equations indicate that bedload velocity increases rapidly with shear stress which could explain why disturbance depth appears to be generally insensitive to shear stress in the study streams. Equation 4.5 is closer to the theoretical result of Hanes and Bowen (1985) and Hanes (1986) (Equation 3.27) and the empirical data of Carling (1987) (Section 2.2.3), and does not rise with shear stress as sharply as Equation 4.4 in Figure 4-10. Figure 4-10 shows that neither regression fit is particularly good, however, because of the wide, non-Gaussian scatter and heteroscedasticity in the data. Consequently, neither equation can be used as a predictive tool.

The closer dependence of bedload transport rates on bedload velocity than on layer thickness, and the ill-posed nature of predicting the vertical mean of bedload velocity argue against using bedload transport rates to predict the local thickness of the bedload layer (or vice versa). Additionally, features related to net excavation scour (Chapter 5) and salmonid spawning behavior relative to maximum bedload disturbance depth (Chapter 6) indicate that Equation 3.27 is inappropriate for evaluations of the effects of scour on salmonids.

4.2.3 *Influence of Location in Channel*

There were no systematic influences of location in the channel on shear stress estimates that could have influenced their plotting position in Figures 4-1 through 4-8 and thus the conclusions reached here. This was determined in two ways.

First, the possibility that shear stresses could have been over-estimated because of

unexplained side-wall roughness was evaluated quantitatively by calculating a wetted

perimeter ratio representing the relative distance of a scour monitor from the channel

margin to a characteristic channel midpoint. Figure 4-11 illustrates how the ratio P_{ws}/P_{wt}

was determined. The midpoint was defined by dividing the channel into two equal areas

[the midpoint generally occurred near the thalweg of the study streams, where shear

stresses and bedload transport rates were estimated to be greatest]. The ratio P_{ws}/P_{wt}

was nearer one for scour monitors located near the mid-point and zero near the water's

edge.

Figure 4-12 shows a contour plot of dimensionless bedload disturbance depth as a

function of wetted perimeter ratio and dimensionless bed shear stress. Only those data

where net bed elevation changes were less than or equal to 4 cm were included to

minimize confounding effects of measurement error on δ_{Bm} (Section 4.1). The

dimensionless shear stress was normalized by 0.15 (approximately the largest value

estimated for the data in the figure) to a new scale between zero and one, to minimize

the effect of scale bias on grid interpolations. Any systematic influence of scour monitor

location would be indicated by the existence of a series of diagonal contour bands, where

the greatest dimensionless disturbance (darkest shade) would be expected to occur in the

upper right hand corner (near the channel center, large shear stress), and the smallest

(lightest) in the lower left hand corner of the plot (near the channel margin, small shear

stress). No such trend exists in the data. There does not appear to be any systematic

bias in the shear stress estimates caused by the channel sidewall proximity.

A similar outcome (not shown) resulted when the local aspect ratio P_{ws}/d (where d is

the water depth at the scour monitor location) was substituted for P_{ws}/P_{wt} in Figure 4-12.

The value of P_{ws}/d exceeded 4.0 for all but three of the scour monitor locations.

Experiments reported by Knight et al. (1994) indicate that sidewall roughness effects

become significant at smaller local aspect ratios.

The second possibility that was evaluated was that the bedload disturbance depth

measurements could be influenced by longitudinal location along the channel.

Differential mobility of the bed surface layer could depend on longitudinal variation in
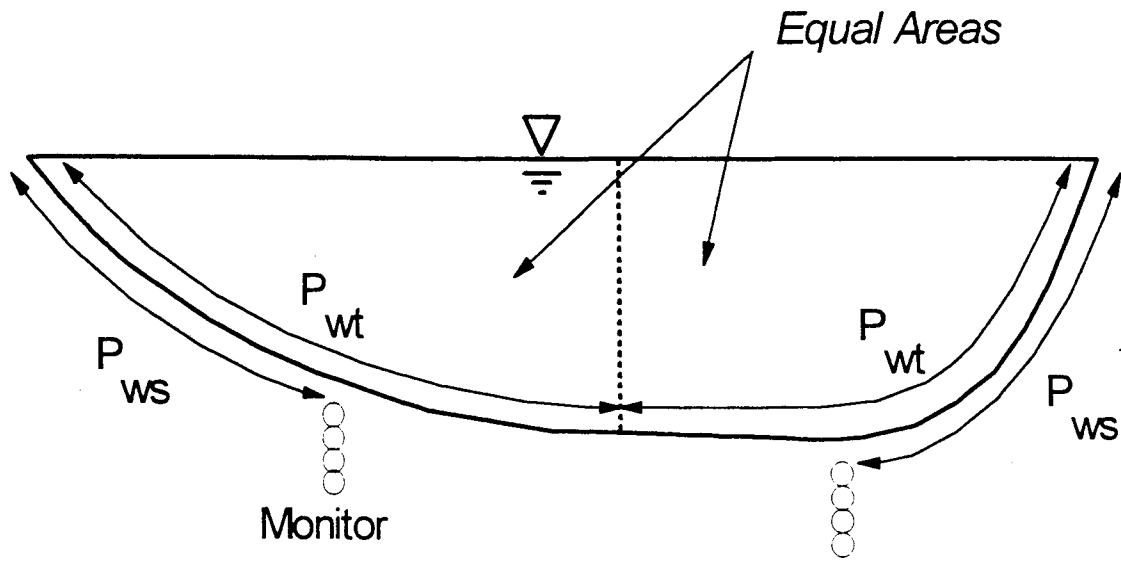
Figure 4-11. Procedure for defining the location of a scour monitor at a channel cross-section for evaluating the potential influence of side-wall effects on shear stress estimates. The wetted perimeters quantify the location relative to the nearest streambank and the channel center, which is defined here as the point on the bed dividing the total wetted cross-section area into two equal areas.
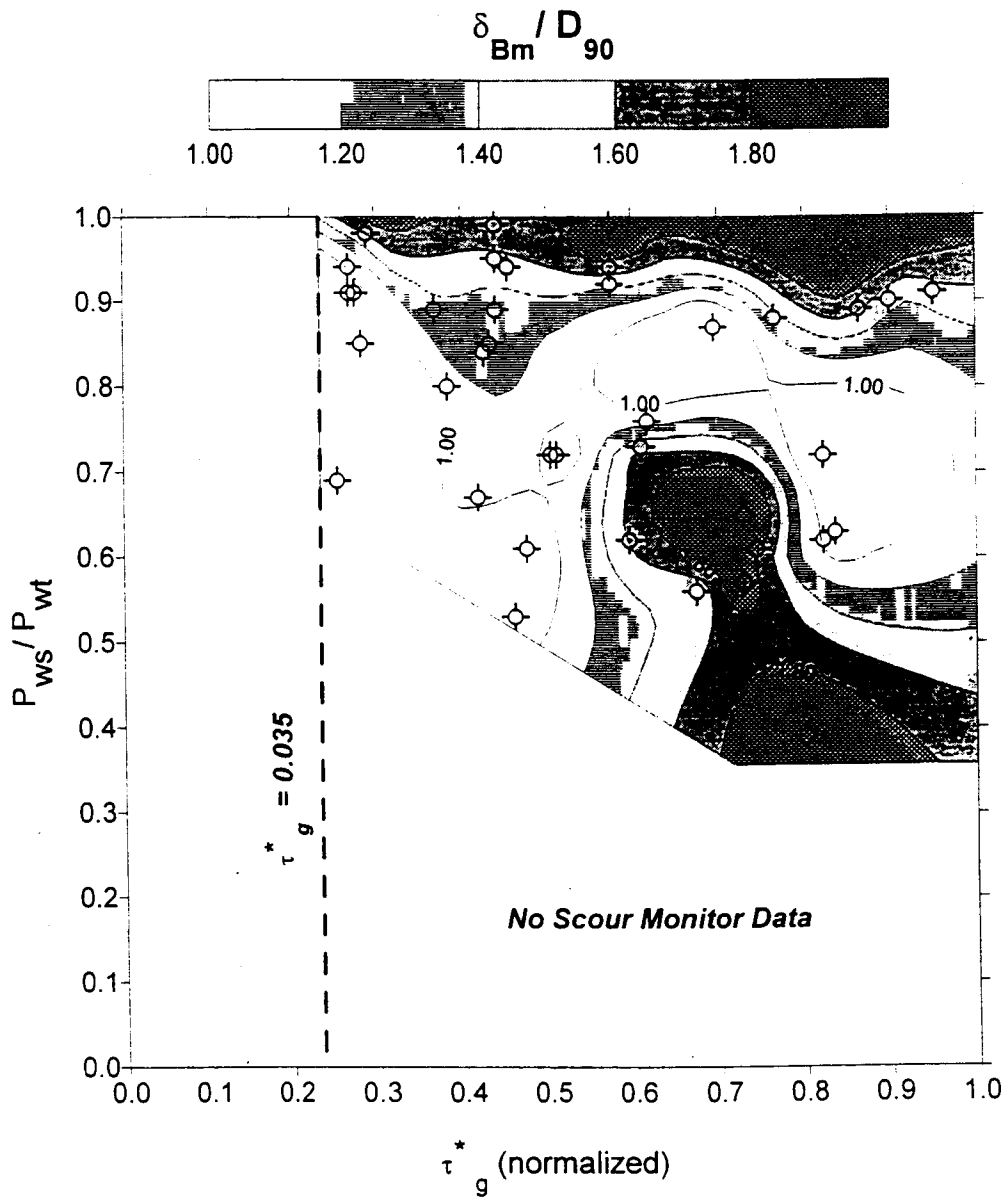
Figure 4-12. Contour plot of wetted perimeter ratio versus dimensionless shear stress, normalized by a value of 0.15. Only those data measured at locations experiencing minor net changes in bed elevation were analyzed and displayed. P_{ws}/P_{wt} values near 0.0 correspond to locations near the channel margin, values near 1.0 are near the channel centerline. The normalized $\tau_g^* = 0.035$ line is indicated.

shear stress, grain size distributions, and availability of transportable material. For example, error could have been introduced to bed shear stress estimates in the event of significant, unexplained longitudinal variation in friction slope magnitude and form drag effects. Such variation is most likely to be evident in shear stress comparisons between pools and riffles, which are characterized by the greatest slope differences in the study streams at lower flows.

The longitudinal profile of a typical pool-riffle sequence was arbitrarily divided into six regions according to hydraulic and gravel deposit features as depicted in Figure 4-13. The data of Figure 4-3b were classified accordingly and replotted in Figure 4-14. The new distinction made in Figure 4-13 between pool tail and pool edge reflects net excavation scour processes; both have previously been called the pool tail. The distinction is important to make (Chapter 5) because the pool edge experiences scour and fill, whereas the pool tail does not. Exactly where the division occurs cannot be determined through visual observation of bed and channel morphology, however, and scour depth measurements are needed.

Figure 4-14 shows no systematic trend in the data scatter. Bedload disturbance depths in riffles, riffle crests, and pool tails exhibited similar distributions over the range of estimated dimensionless shear stresses. The largest dimensionless scour depth above the $\delta_{Bm}=2D_{90}$ line was located in the pool tail/edge region, and may thus have experienced unexplained scour and fill.

These analyses indicate that no obvious systematic error was introduced to the results by virtue of where the scour monitor was located in the channel, with the possible exception of the pool tail/edge region where scour and fill may have occurred.

4.3 Grain Size Distribution and Bedload Disturbance Depth

My interpretation of the data in Section 4.2 is that maximum bedload disturbance depth is independent of dimensionless shear stress in the study streams once the largest grain size can be mobilized. The reason for this interpretation is linked to the preferential
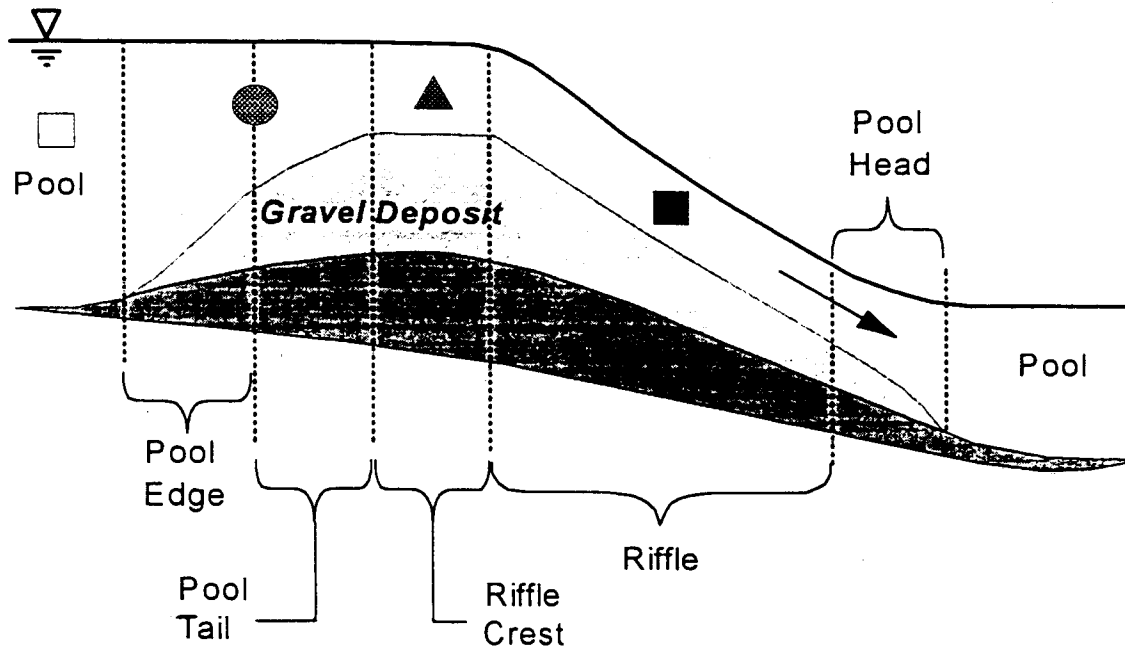
Figure 4-13. Classifications used to identify the relative longitudinal position of a scour monitor in a pool-riffle sequence, for evaluating form drag effects on shear stress estimates and relation of scour depth measurements to geomorphic processes.
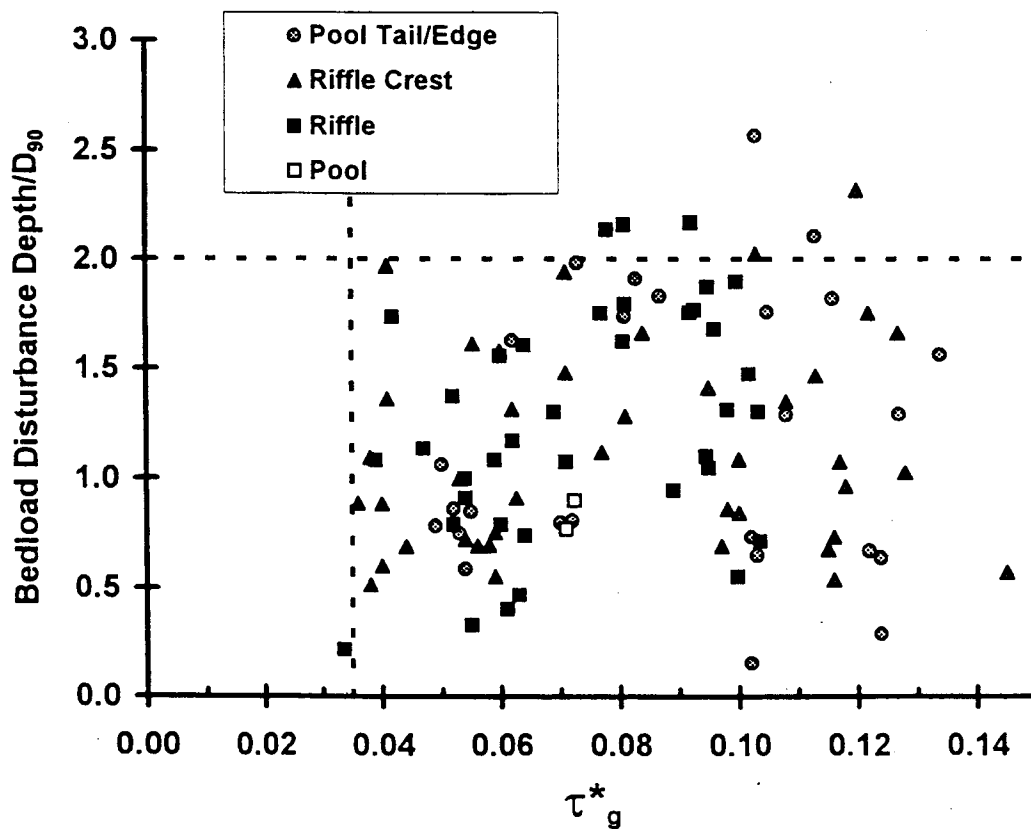
Figure 4-14. Variation of dimensionless bedload disturbance depths with dimensionless local bed shear stress, where data are classified according to longitudinal position in a pool-riffle-sequence. The horizontal dashed line represents $\delta_{Bm} = 2D_{90}$; the vertical line is for $\tau^*_g = 0.035$.

increase in bedload velocity over layer thickness with greater shear stresses. On the basis that the maximum depth is related to the largest particle size present in the surface layer that the flood is capable of mobilizing (the 'competent particle size', or D_{comp}), it is plausible that bedload disturbance depth distributions reflect the mobile bed grain size distribution. This possibility is also supported by the work of Wilcock et al. (1996) and Wilcock and McArdell (1997), in which they determined exchange depth to be a function of grain size.

Can a bedload disturbance depth limit be defined as a multiple of a characteristic grain size? Figure 4-15a indicates that the $2D_{90}$ line envelopes most of the disturbance depth data and that the $2.1D_{90}$ line envelopes data from all but the two locations suggested by Figure 4-14 to have experienced scour and fill. Subjectivity is involved in selecting an appropriate limit because there is no good, physically-based reason why 2 is better than 2.1 as a multiplier of D_{90}. Wilcock and McArdell's (1997) approximate limit of $2D_{90}$ is consistent with the data collected here.

Figure 4-15b indicates that the bedload disturbance depth limit may also be expressed as kD_{comp}, where the competent size is estimated using Komar's (1996) average relationship (Equation 4.1; limited by the largest size present in the bed surface). This expression is more appropriate from a physical perspective than $2D_{90}$ or $2.1D_{90}$ because it relates maximum disturbance depth to the maximum size of particle potentially moving past the scour monitor location. The value $k = 1$ is insufficient to explain a large proportion of the observations; $k = 2$ is too heavily influenced by only two measured values; $k = 1.5$ bounds almost all of the data. The value $k \approx 1.5$ is therefore proposed pending future data collection.

Figure 4-16 shows the data from Figure 4-15 adjusted for measurement bias using Equation 4.2. The upper graph shows that the adjusted data are bounded by approximately the $2.2D_{90}$ line, whereas $1.5D_{comp}$ remains a good fit. There is no evidence to suggest that the $2D_{90}$ line should not be used as an approximate bound to bedload disturbance depth.

Despite the physical merit of $1.5D_{comp}$, the D_{90}-based bound is proposed to be more
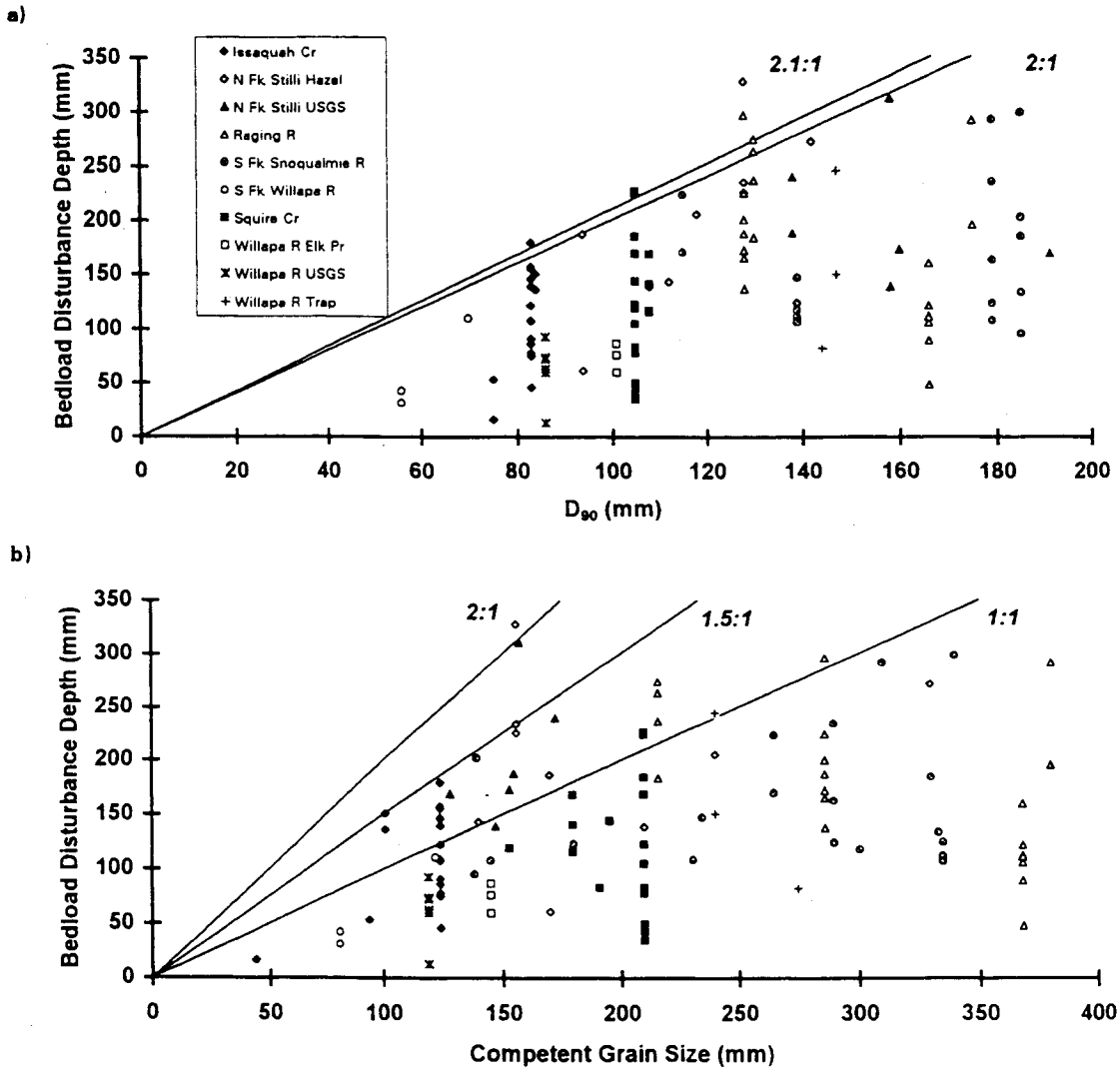
Figure 4-15. Measured bedload disturbance depths versus a) local D_{90}, and
b) local competent grain size predicted using Equation (5-18) and
$\tau^*_{cr} = 0.031$, $\beta = 0.6$ (Komar 1996). Particle dimensions are for the
b-axis diameter.
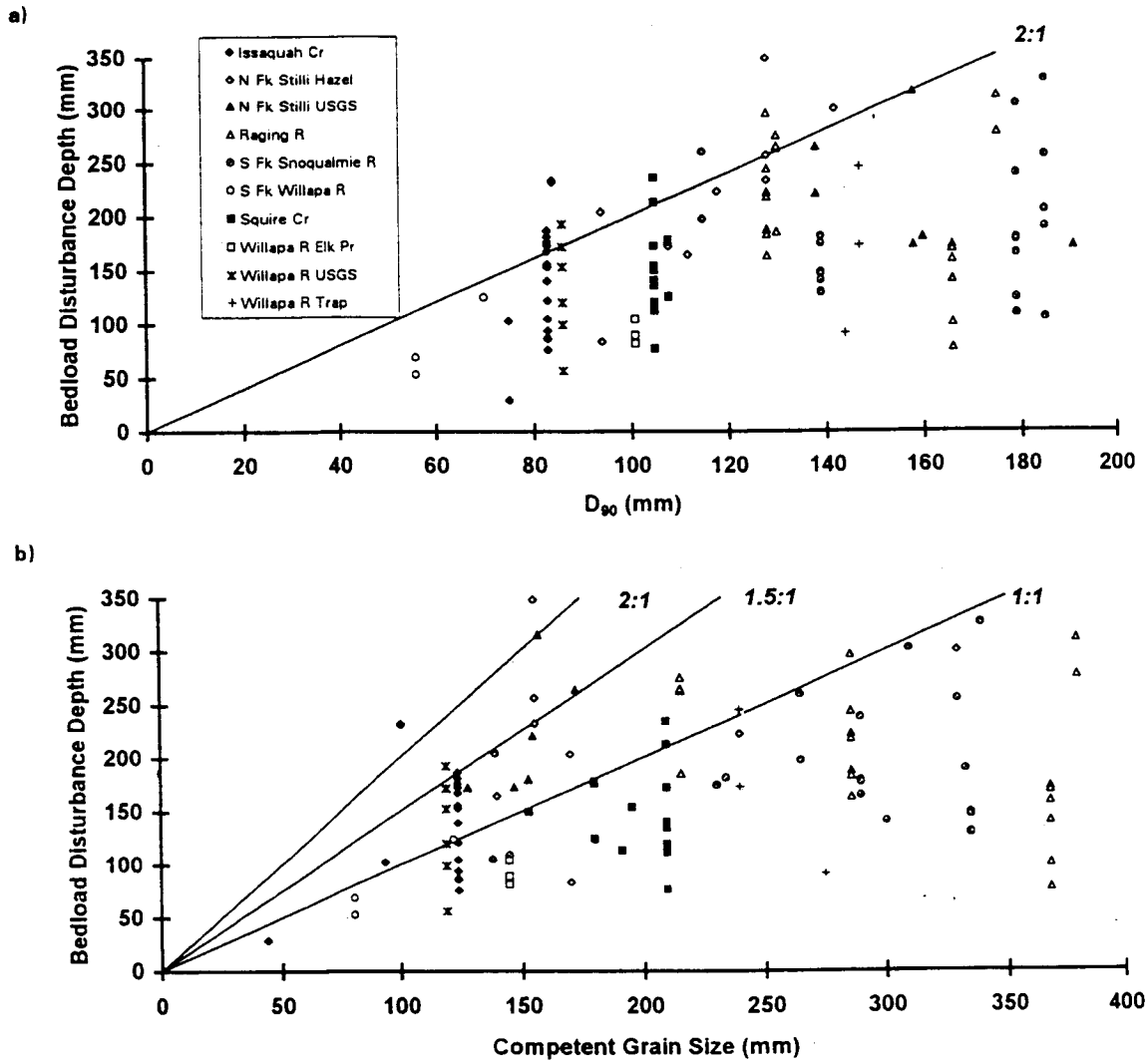
Figure 4-16. Measured bedload disturbance depths in Figure 4-15, adjusted for approximate measurement bias using Equation 4.2.

practical and appropriate because general competence relations are subject to considerable uncertainty related to determining when incipient motion occurs (Buffington and Montgomery 1997), and the D_{100} of a grain size distribution sample is not a robust estimator. The $2D_{90}$ estimator is more robust statistically, and Figures 4-15 and 4-16 indicate that it envelopes the data as well as does the $1.5D_{comp}$ estimator.

4.4 Stratigraphic Evidence of a Bedload Layer Thickness Limit

The bulk sediment (McNeil) samples collected near the scour monitor locations provided stratigraphic records of distinct layers in the bed and of spatial patterns in sediment transport. Differences in grain size distributions between successive layers were interpreted as corresponding to different bedload layers. Because the sample layer thicknesses were defined by the largest particle present in each layer, the existence of layers with distinctly different grain size distributions supports the proposition that bedload layer thicknesses and disturbance depths are relatively thin.

The grain size distributions for each sampled layer were truncated at 8 mm and at 127 mm. The truncations were designed to reduce the influence of sampling errors on grain size distribution comparisons. Particles smaller than 8 mm in diameter settled disproportionately in the bottom layer sample because they could not be collected completely by hand, and were underrepresented in the surface armor layer regardless of sampling efficiency. The fine particle size tail of the non-truncated grain size cumulative probability distribution of each layer is biased accordingly, where successively deeper layers would always be finer. Particles larger than 127 mm could not be collected in sufficient weight to meet sample size constraints on accuracy. The remaining particle size classes could be collected efficiently with a 30 cm diameter McNeil sampler, and their individual weights accounted for comparable proportions of the total truncated sample weight.

Evidence in support of a thin bedload layer (i.e., where layer-whisking is dominant) was inferred by meeting either of two criteria:

(I)   Different truncated grain size distributions between successive subsurface layers
      at a scour monitor location (the surface armor layer is typically coarser); and

(II) Truncated grain size distributions that are similar for analogous subsurface layers
      from samples that are located proximally and upstream and downstream from
      each other.

The bulk substrate sampling data indicated that grain size distributions were
frequently significantly different between layers. Figure 4-17 shows this for Issaquah
Creek, the bed of which was finer than most of the other study streams and which was
therefore less likely to exhibit stratification. Layers in streams with coarser beds than
Issaquah Creek were defined by larger particles and more extensive sediment transport
may have been required to develop successive strata through a degradation-aggradation
cycle, with a corresponding greater probability of each stratum representing differences
in reach-scale sediment delivery and transport characteristics and therefore having
different grain size distributions.

Figure 4-17a shows truncated grain size distributions of three layers collected at the
location of scour monitor 2 in Issaquah Creek. The three distributions were significantly
different from each other (Chi-square test, $p > 0.99$). As expected, the surface armor
layer is coarser than the subsurface layers, whose distributions are also significantly
different from each other.

Figure 4-17b shows grain size distributions for samples collected from the same
subsurface layer at two upstream locations (scour monitors 5 and 9) in Issaquah Creek.
The three distributions were statistically similar to each other ($p < 0.8$), suggesting that
they were from a stratigraphic layer that extended in the stream-wise direction (i.e., the
direction of gravel motion).

Significant ($p > 0.99$) cross-stream variation was noted between scour monitors 5
and 7 (Figure 4-17b), which were located on the same transect. The difference in grain
size distributions may have been representative of progressive building of a finer-grained,
depositional bar along the left side of the channel, in the vicinity of scour monitor 7 (see
Figure A-2, Appendix A and pebble count grain size distributions in Appendix E), and

a)

Issaquah Creek:
Scour Monitor 2, Truncated Sample

b)

Issaquah Creek:
Subsurface Layer 2, Truncated Sample
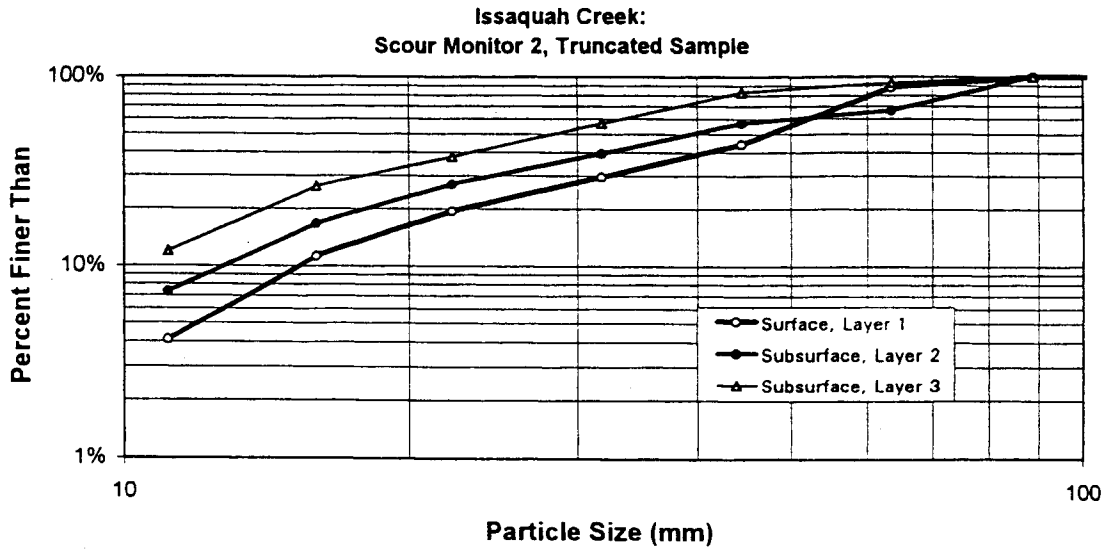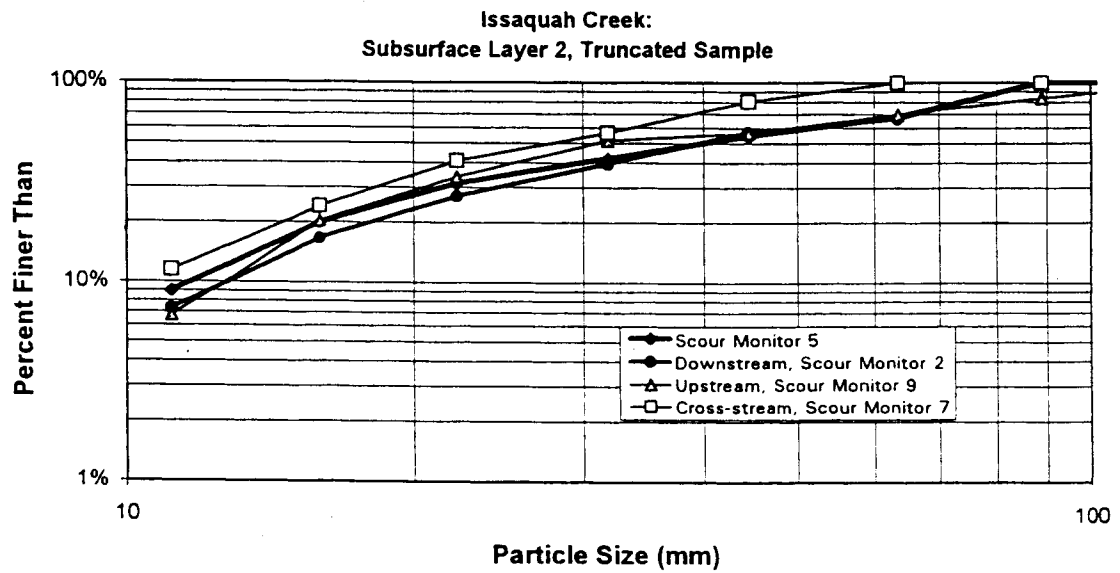
Figure 4-17. Cumulative grain size distributions of different McNeil samples collected a) from different streambed substrate layers at the same scour monitor location, and b) from the same subsurface layer at different scour monitor locations. The distributions were calculated after truncating the sieve sizes at 8 mm and 127 mm to minimize methodological bias.

of cross-channel textural variation in general.

Upstream-downstream similarity in layer grain size distributions was observed in other study streams, including at the North Fork Stillaguamish River at Hazel, Raging River, and Willapa River at USGS sites. Cross-stream similarity was observed in the North Fork Stillaguamish River at USGS, South Fork Snoqualmie River, and Squire Creek sites. Appendix I shows these and other distribution comparisons. The plots in Figure 4-17 and Appendix I provide, collectively, support for the existence of distinct thin layers in coarse streambeds.

The existence of different subsurface grain size distributions at a location is indirect evidence of limited vertical mixing occurring between subsurface layers. Limited vertical mixing implies that layer whisking is the dominant mechanism of scour and fill. Since each subsurface layer was generally defined in the McNeil sample by the largest particle or particles present, the thickness of the bedload layer during the formation of successive layers may have also been defined by those same particles. These results support the observations in previous sections regarding bounds on bedload disturbance depth, and are consistent with Hassan and Church's (1994) observations that the most active vertical mixing during individual floods occurred in the layers closest to the bed surface (layer thickness was defined as equal to the substrate D_{50}).

4.5 Discussion

The results presented here indicate that bedload transport in the study streams is associated with the disturbance of a relatively thin layer of the bed surface. The maximum bedload disturbance depth appears to be proportional to the competent grain size when shear stress is less than that required to mobilize the largest particle present in the spawning bed. At higher shear stress, the limiting disturbance depth of the bedload layer appears to be approximately twice the surrounding substrate D_{90}, or 1.5 times the largest grain size present when dimensionless shear stress τ^*_g is less than 0.15. Granular flow study results indicate that two or more layers are mobilized simultaneously when τ^*_g

exceeds approximately 0.4 to 0.5. It is proposed here that the maximum bedload disturbance depth remains approximately twice the bed D_{90} for intermediate values of τ^*_g.

In one stream, the maximum bedload disturbance depth was approximately $2D_{90}$ when $\tau^*_g \approx 0.035$, a result that is consistent with the findings of Wilcock et al. (1996). It is possible, since the bedload disturbance depth data could only be determined for the estimated bed shear stress at peak flood stage, that the beds in many of the other streams may have been disturbed to the base of the surface layer at similarly low dimensionless shear stresses, at lower flood stages.

Dimensionless shear stresses equal to 0.4 and 0.5 are atypical of gravel bed streams in general, and may only occur in highly confined channels under catastrophic flood conditions. With the exception of the Tolt River site, which was confined between two steep, high ridges, the study sites were all situated within channels that possessed active floodplains or old floodplain terraces (Leopold et al. 1995) that provide an asymptotic limit to flow depth. Flow depths defined by the bankfull and floodplain terrace elevations differed by no more than a factor of two in Issaquah Creek, the North Fork Stillaguamish River (both sites), the Raging River, and the Willapa River (Elk Prairie and USGS sites). They were less than a factor of four for the remaining sites. A value of $\tau^*_g = 0.4$ corresponds to flood depths that are more than twice and as many as ten times the depth required to inundate the study site floodplain terraces, or, more than four times bankfull flow depths. These flow depths exceed the range measured at the respective USGS gaging stations. The highly confined Tolt River site would require a flow depth of approximately 6-7 m to result in $\tau^*_g = 0.4$ for the coarser, commonly transported, spawning-sized material present. These flow depths are not achieved in any of the study streams with stream gages by a 500-year event, according to extrapolations of flood frequency data using at-site, fitted Generalized Extreme Value distributions. The result holds for all distributions used commonly to evaluate extreme floods.

Because the study reaches represent a wide range of hydraulic conditions and substrates, it is plausible that these findings can be extended to other gravel bed streams

with gradients less than or equal to 0.01. Deep scour measurements made in very coarse cobble beds ($D_{90} > 127$ mm) can probably be explained completely by this mechanism (e.g., in the Dungeness River, Washington; Orsborn and Ralph 1994). Measurements reported in the literature as representing scour and fill are in many cases more likely to have been measurements of bedload disturbance depth.

The data of this study indicate that much of the bed surface area was disturbed to a depth less than $2D_{90}$ for a given bed shear stress in a given stream. The variation in maximum bedload disturbance depths for a given shear stress depicted in Figures 4-1 and 4-2 cannot be explained deterministically by variation in bed shear stress alone.

Stochasticity in bedload disturbance depth can be introduced in a number of ways. Random turbulent fluctuations in bed shear stresses represent one means, but it has already been argued in Section 3.3.4 that a corresponding, significant influence on disturbance depth is unlikely in gravel beds. An exception may be when the flood flow magnitude only slightly exceeds the condition for incipient motion throughout its duration and particle motion is largely intermittent. The data from this study were collected for conditions of more intense bedload transport where incipient motion considerations were likely to have been less important.

Unexplained variation due to random or systematic measurement errors has also been accounted for and cannot explain the magnitude of the observed variation in dimensionless bedload disturbance depth. The only remaining potentially significant influence is the bed grain size distribution. This has been shown to influence the maximum possible value of bedload disturbance depth in a reach. Smaller values of maximum bedload disturbance depths observed elsewhere in the reach are a consequence of the mechanism whereby particles move. It is plausible that the bed grain size distribution influences the mechanism whereby individual particles move during bedload transport, and therefore influences the bedload disturbance depth distribution. Some candidate mechanisms are described and evaluated in the remainder of this chapter.

4.5.1 *Conceptual, Limiting Bed Disturbance Mechanisms*

There are two alternative conceptual models of particle motion that define the hypothetical bounds of bedload disturbance depth distributions at a specific location of a gravel streambed. The first (Model I) is that the disturbance depth is proportional to the largest sized particle passing by a location. The larger particles in motion typically roll, tumble, and/or slide, and may occasionally saltate slightly as they move downstream. The smaller moving particles are more likely to saltate than larger ones (Vanoni 1975; Parker et al. 1982a). The smaller particles should therefore have less influence on disturbance depth than larger ones on this basis alone. Smaller particles also present a smaller profile than larger particles when they roll or slide. The Model I disturbance depth results from a combination of two possible mechanisms:

(I)   Mechanical disturbance of particles underneath and to the side by the larger moving particle, caused by collisions, ploughing, and downward loading; and

(II) Fluid shear and drag forces, associated with water passing around the larger moving particle, that mobilize smaller particles in the vicinity, including beneath the larger moving particle.

The velocity of moving particles may be too small in magnitude to dislodge imbricated particles in most collisions because of the retarding influence of fluid drag (Bagnold 1951) and because imbricated particles are locked in place in a heterogenous mixture by a large number of frictional contact points. The dislodgement of formerly static particles through collisions cannot be discounted completely (Carling 1990). Although the disturbance depth appears to be greater than the b-axis dimension, it is unlikely that the depth reflects the a-axis dimension directly because the larger mobile particles present are more inclined to move with their a-axis oriented perpendicular to the downstream direction (Rust 1972; Martini 1977). The a-axis should therefore influence the plan area of bed disturbance more than it would the depth. Moving particles are not uniquely oriented with the a-axis perpendicular to the flow, thus an elliptical particle could disturb a greater depth of the bed than a sphere of radius equal to

the ellipsoid's *b*-axis dimension. It is plausible that these features, together with fluid action, could disturb a depth greater than the subject particle's *b*-axis diameter.

The corresponding cumulative distribution function (CDF) of maximum bedload disturbance depth posited for Model I is depicted in Figure 4-18a. The cumulative grain size distribution of the bed surface is also depicted in the figure for comparison, where the grain size has been multiplied by 1.5 to reflect the relation between competent grain size and bedload disturbance depth that is indicated by my data. The disturbance depth CDF approaches a step function when the flow remains competent for long enough that the monitor location will experience passage of all mobiles sizes. The step occurs at the maximum possible disturbance depth, which is expected to be approximately equal to the limiting disturbance depth ($2D_{90}$ or $1.5D_{100}$) when all sizes present in the bed are mobilized, based on the results of this work. Assuming that the disturbance depth limit scales down linearly, the step is posited to occur at roughly $1.5D_{comp}$ when the largest particles present are not mobilized.

The second conceptual model ('Model II') is that the bedload disturbance depth is proportional to the dimension of the particles present in the bed, where disturbance occurs directly in association with the mobilization of surface stones. The disturbance mechanism during initial entrainment of a particle involves the progressive mining of smaller particles (the size of which increases with shear stress) around the larger particle, which may either join the bedload immediately from its original position or may settle downwards initially by local scouring and undermining until the flow strength is sufficient to move it. Entrainment of a particle also facilitates the entrainment of smaller grains underneath it resulting in disturbance of the bed at an elevation below its original undersurface elevation (Parker et al. 1982a). As transport ceases, larger particles settle out first and the flow continues to excavate around and/or undermine the particle, disturbing the surrounding bed accordingly.

The disturbance depth at the cessation of mobility is likely to be smaller than the depth at the time of incipient motion because the particle is simply deposited. A greater scouring depth likely occurs during initial entrainment, as a particle is dug out and
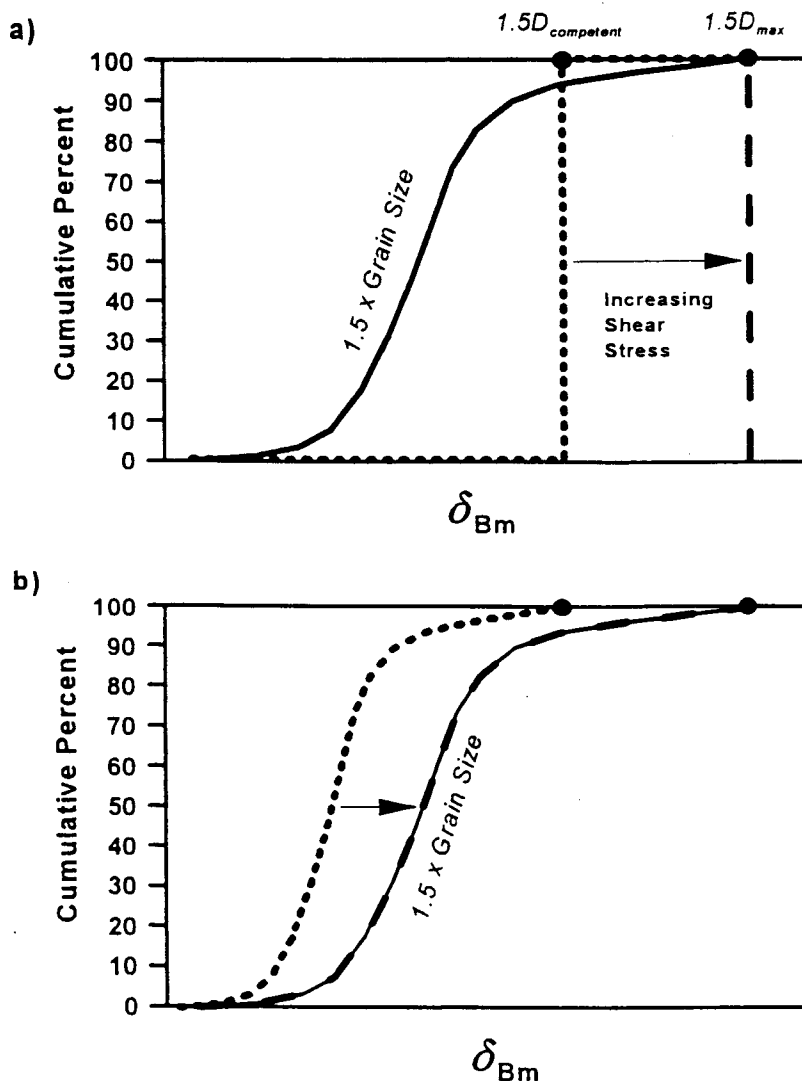
Figure 4-18. Hypothetical cumulative distribution functions (CDFs) of bedload disturbance depths measured over an area of bed composed of gravel and cobble. Graphs a) (Model I) and b) (Model II) are for conceptually different, limiting bedload disturbance mechanisms. The solid line depicts the grain size distribution of the bed surface, where the particle sizes have been multiplied by a factor of 1.5. The dashed lines depict candidate disturbance depth CDFs and their variation with shear stress, which increases as indicated by the arrows. The larger dashed line depicts the hypothetical limiting state; the filled circles the deepest disturbance depths possible. See text for explanation.

mobilized, than at any other time during a flood. The model thus assumes that disturbance depths caused during deposition are negligible compared to depths caused during initial entrainment. During transport, the model requires that the particles do not disturb the bed substantially underneath as they roll, slide, and/or saltate in an overpassing bedload sheet.

The hypothetical CDF for maximum bedload disturbance depth posited for Model II is shown in Figure 4-18b. Model II describes a peeling away of the bed surface layer either in portions or simultaneously, with disturbance occurring underneath as the layer is removed. The conceptual Model II CDF is accordingly a function of the static bed grain size distribution CDF. The corresponding limiting case for Model II is complete mobility of all bed surface framework particle sizes, where the bedload disturbance depth CDF is assumed to be equal to the static bed grain size CDF truncated at 8 mm (i.e., ignoring matrix material) and multiplied (or, shifted to the right) by a factor k. The magnitude of k is unknown but, following a similar argument for Model I, may equal approximately 1.5. This assumes a characteristic undermining or subsurface-layer entrainment depth equal to half the entrained surface particle's b-axis diameter. The model assumes that disturbance depth CDFs are located to the left of the limiting case CDF when flows are too small to mobilize all grain sizes present, as indicated in Figure 4-18b. This is because the bedload grain size CDF is always to the left of or equal to the static bed CDF.

A possibility exists in the Model II formulation for the shifted bedload grain size CDF to approximate the disturbance depth CDF when the bedload is finer than the static bed; i.e., during selective transport. Testing such a possibility requires sampling bedload and could form the basis for future work.

4.5.2 *Testing the Conceptual Limiting Mechanisms*

The data collected here permit evaluation of the two hypothetical limiting cases. The bedload disturbance depth data were filtered such that only measurements from locations where the net bed elevation change was 4 cm or less were used to make comparisons of

disturbance depth and grain size distributions. A 4 cm criterion was selected as a compromise between minimizing bias from Equation 1.1 and having enough data to evaluate the candidate models; it is less than the maximum possible measurement error (6 cm). Only four streams provided enough filtered data measured in a single flood. Figure 4-19 shows that, although represented by a small sample size, the filtered data indicated consistently that disturbance depth distributions were neither (i) a strict step function (Model I), nor (ii) a direct, linear function of the grain size distribution (Model II) in the four streams with enough data to explore this issue.

The most data for a single event were collected in Issaquah Creek, which experienced a 2.3-year flood that slightly exceeded bankfull flow. These data are presented in Figure 4-19a as the connected symbols. All scour monitors were disturbed and local dimensionless shear stresses (τ^*_g) exceeded 0.08, from which I infer that the bed armor was mobilized completely (Parker 1990a; Section 4.2.2). Shear stresses were competent for long enough that the largest grain sizes present were estimated to have moved more than 100 m on average (see Chapter 5). This distance is sufficient that the probability of the largest particle present in the static bed passing by a scour monitor location can be assumed to be equal to 1.0. Accordingly, the absence of a distinct step function in the disturbance depth CDF indicates that the hypothesized Model I mechanism alone is not representative of bedload motion.

Figure 4-19a shows that the largest disturbance depth measured in Issaquah Creek was approximately the same dimension as 1.5 times the largest, competent grain size present in the bed surface. The bedload grain size CDF was predicted by Parker's (1990a) transport equation to be only slightly finer than the bed surface CDF; i.e., all members of the bed were likely to have been entrained. The lack of fit between disturbance depth and shifted grain size CDFs suggests that the Model II disturbance mechanism alone is also not representative of bedload motion. A blend of Models I and II may be the mechanism effecting bedload disturbance depth, with emphasis placed on the larger mobile (and immobile) particles present.

Wilcock and McArdell (1997) attributed a shift toward larger sizes in the bedload
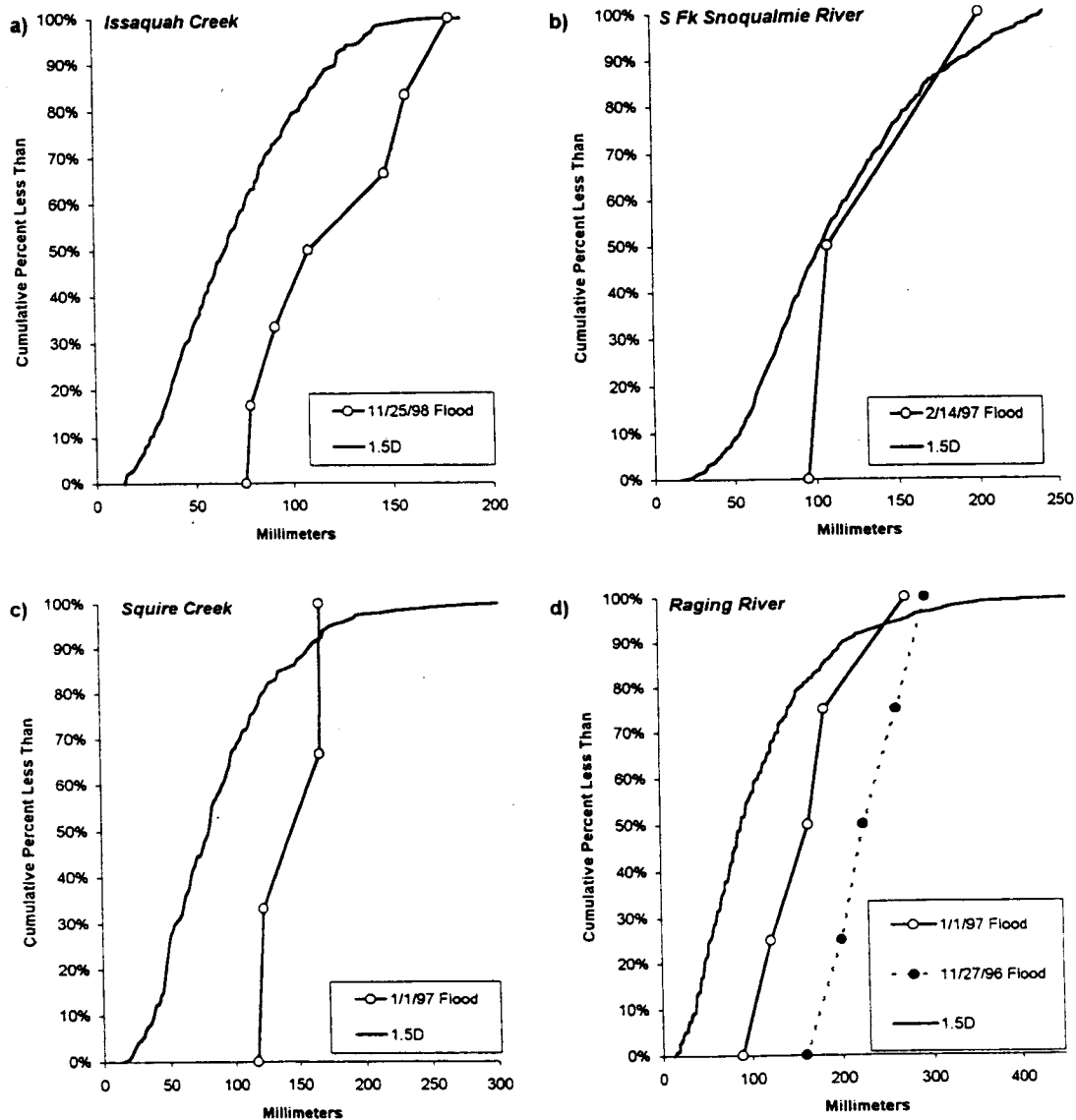
Figure 4-19. Measured cumulative distribution functions (CDF) of bedload
disturbance depths measured in four study sites (= lines with
symbols). The solid line without symbols is the grain size
distribution of the patch truncated at 8 mm (CDF in graph [b] was
also truncated at 163 mm, the predicted competent particle size),
where the particle sizes have been multiplied by 1.5.

grain size CDF with increasing shear stress to a progressive mining of finer sizes from the subsurface as the entrained proportion of coarse grains increases. They noted in their flume studies that the actively transported grains collected in migrating grain-scale bed forms passing over the immobile bed. Figure 4-19d provides an example where such a mining and transport process may also be responsible for the observed bedload disturbance depth distributions in the Raging River, which similarly suggest a shift toward larger sizes with increasing shear stress.

4.5.3 *Proposed Bedload Disturbance Mechanism*

The process proposed below involves a blend of both mechanisms. The Model II mechanism occurs first for a specified maximum mobile particle size, as shear stresses approach and exceed the level required for its mobility. The Model I mechanism acts (i) concurrently through the previously initiated motion of smaller particles (but their corresponding disturbance depth is also smaller), and (ii) subsequently once the subject particle size is in motion. The Model I disturbance depth occurring during particle motion may additionally reflect a combined influence of particles moving in grain-scale bedforms on the stability of the underlying layer. The Model II mechanism can act at each intermediate step taken by the larger mobile particles, but probably does not result in as deep a disturbance depth as that occurring near the initial step: the particles probably do not stay immobile long enough for the small-scale equivalent of a local scour hole to develop around them. The Model II mechanism acts in the presence of particle clusters that collectively form a structure resistant to motion and that effect a small-scale scour hole, analogous to an immobile, erratic boulder. The Model II mechanism is likely to be the primary influence on the deepest bedload disturbance depths, and both mechanisms influence the variance of the disturbance depth distribution.

The disturbance depth CDFs presented in Figure 4-19 indicate that (i) the coarser mobile particles present in the bed are the primary influence on bedload disturbance depth distributions (they disturb the bed deeper than smaller particles); and (ii) the lower

limit to the disturbance depth CDF may be approximately 1.5 times the bed D_{50}. In other words, particles smaller than the bed D_{50} may not influence disturbance depth distributions substantially. This result reflects the hiding phenomenon of incipient motion and bedload transport (Parker et al. 1982b; Diplas 1987; Parker 1990a), where smaller particles are sheltered by larger particles and thus their mobility is much less selective than expected on the basis of uniform-sized sediment. The lack of dependence on particles finer than the bed D_{50} is also consistent with previous observations that the armor layer, which is defined by the larger sizes present, controls the thickness of the bedload layer and bedload transport processes in general in gravel bed streams (e.g., Parker and Sutherland 1990).

The $1.5D_{comp}$ limit in Issaquah Creek reflects the Model II mechanism applied to the largest mobile particle (Figure 4-19a). Too few data were collected to evaluate the limit in this manner in the other streams (Figure 4-19b, 4-19c and 4-19d). Many of the deeper bedload disturbance depth measurements in coarser beds were associated with visual field observations of the transport of small boulders and large cobbles. Several such particles were observed to have moved from, and/or come to rest at locations that were on top of (Figure 4-20a) or adjacent to (Figure 4-20b) scour monitors in the Raging River, Willapa River, and the South Fork Snoqualmie River.

There were also too few data to test the hypothesis that the onset of motion is associated with a deeper disturbance depth than the cessation of transport. Visual field observations provide some indirect support. For example, one scour monitor in Squire Creek recorded a bedload disturbance depth of 180 mm and total fill depth of 240 mm next to a deposited particle with dimensions of 410 x 340 x 300 mm (Figure 4-20b). The particle had settled out and the bed had filled in around it. The disturbance depth was less than the particle's b-axis dimension, suggesting that local scour around the deposited particle was minimal. Another scour monitor in the same stream recorded smaller total scour when a small boulder (approximately 350-400 mm in size; estimated from a photograph) settled on top of it, than in the next flood (1/1/97) when the stone moved downstream. Although these large particles were present in small numbers and may be

a)
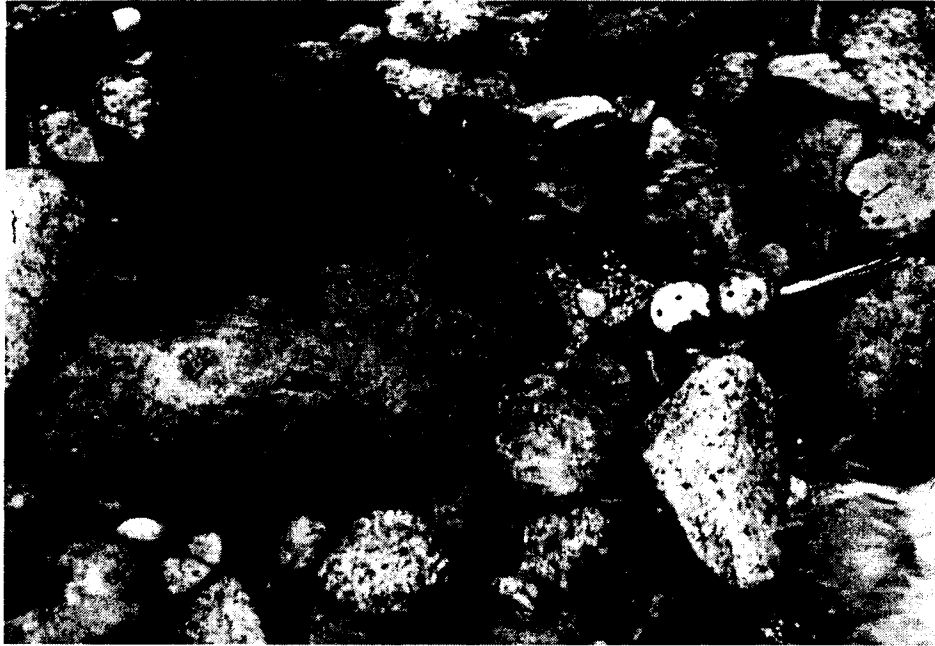
b)

Figure 4-20. Examples of small boulders settling a) on top of, and b) adjacent to scour monitors. Two balls were triggered in the top photograph, and four in the bottom (visible in lower left hand corner). The beds are predominantly cobble/coarse gravel mixtures.

mobilized predominantly by fluid drag, they were essentially flush with the bed surface and participated in bedload transport. These observations may be representative of bedload disturbance processes associated with the larger members (e.g., $>D_{90}$) of the bed grain size distribution when they stop moving.

A speculation on the basis of these observations and the results presented in this chapter is that a similar outcome to Figure 4-19a (i.e., maximum disturbance depth $\approx$ $1.5D_{comp}$) would have been observed in Figures 4-19b, 4-19c, and 4-19d if a larger number of bedload disturbance depth data had been collected in those streams.

Figure 4-21 shows three hypothesized CDFs for $\delta_{Bm,}$ and the bed surface grain size CDF shifted to the right by the multiplication factor $k = 1.5$. The bedload disturbance depth CDFs are inferred from the results presented in Figure 4-19. I hypothesize on the basis of the results presented in this chapter and the findings of Hassan and Church (1994) that the disturbance depth distribution in the most active region of the streambed is approximately uniform, and that the upper limit corresponds to one and a half times the b-axis diameter of the largest competent particle. Under the hypothesis, the entire distribution shifts to larger sizes with increased shear stress until the largest particle present is mobilized. The distribution then remains essentially unchanged, as indicated by the far right CDF curve in Figure 4-21, until the shear stresses are sufficient to mobilize the next layer completely underneath and granular flow begins. Since such high shear stresses are suggested by the results of this work, granular flow studies, and other researchers (e.g., Parker et al. 1982b) to be extremely rare, the hypothesis implies that a natural limit exists to the thickness of the moving bedload layer in gravel bed streams. Consequently, increases in shear stress are not expected to result directly in significant increases in scour depth due to increased bedload layer thicknesses, and deep scour must be effected through some other mechanism.

The proposed disturbance mechanism may shed light upon the connection between bedload disturbance depth, exchange depth, and thickness of the moving bedload layer. Bedload disturbance depth will be greater than exchange depth when bed particles underneath are disturbed mechanically by the entrained particle and/or by water moving
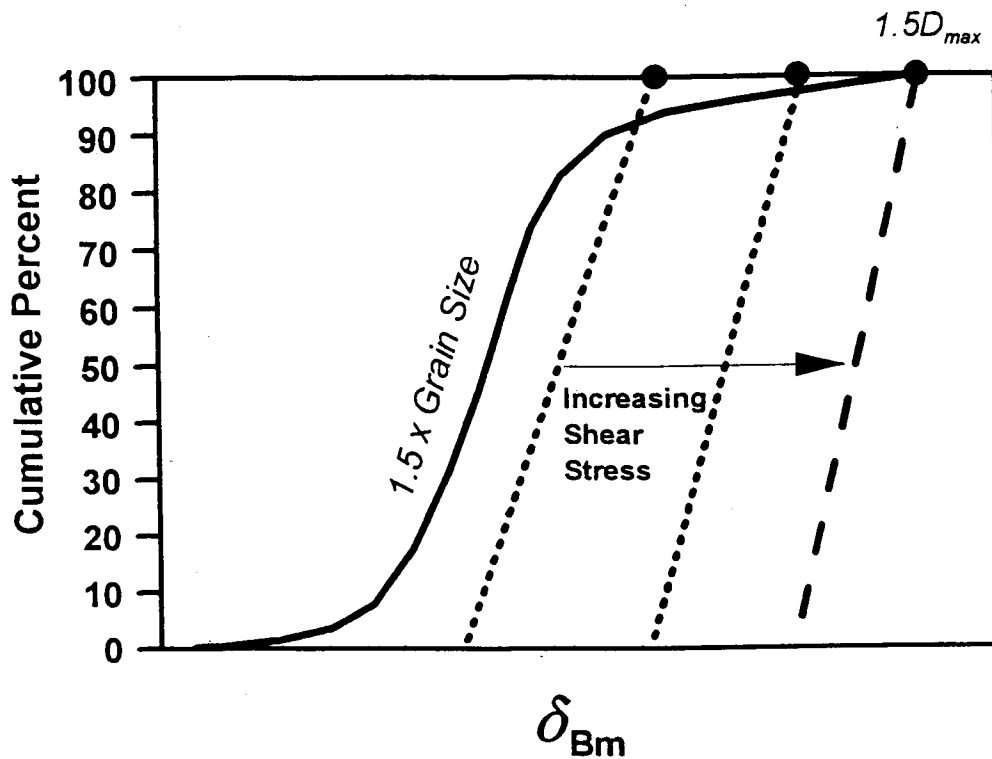
Figure 4-21. Hypothesized cumulative distribution function (CDF) of bedload
disturbance depths measured over an area of bed composed of gravel
and cobble. The solid line depicts the grain size distribution of the
bed area, where the particle sizes have been multiplied by a factor of
1.5. The dashed lines depict the variation of disturbance depth
CDFs with shear stress, which increases as indicated by the arrow.
The larger dashed line depicts the hypothetical limiting state; the
filled circles the deepest disturbance depths possible.

around it but are not entrained themselves. In this case, bedload disturbance depth is not representative of the moving bedload layer thickness because not all particles that are disturbed contribute to the transport rate. The bedload disturbance depth is representative of material contributing to bedload transport only if smaller particles underneath the larger particle are exchanged, or entrained (Parker et al. 1982a).

Wilcock and McArdell (1997) approximated the magnitude of the exchange depth as the dimension of the size fraction that is fifty percent mobile at a given flow strength; for example, an exchange depth said to be equal to D_{90} corresponds to at least fifty percent of the D_{90} size class being in motion. Wilcock and McArdell (1997) found that the exchange depth approaches $2D_{90}$ when the entire bed surface is mobilized. This is the same approximate limit observed for bedload disturbance depth in this study. Based on my findings, it is likely that the maximum exchange depth is approximately the same as the maximum bedload disturbance depth.

Figure 4-19 indicates that the median thickness of the bedload layer is less than $2D_{90}$ and appears to be closer to between D_{90} and $1.5D_{90}$. Parker and Sutherland's (1990) bed armor model assumed that the characteristic surface layer thickness contributing directly to bedload transport was approximately equal to D_{90}. The data presented in Figure 4-19 support Parker and Sutherland's (1990) assumption. However, the average bedload layer thickness does not represent all of the bed particles contributing to bedload transport, and sediment transport models that track disturbance depths must account for exchange with the subsurface. Local bedload disturbance depths approximate local exchange depths, and their maximum values appear to be approximately twice the average thickness of the moving bedload layer.

5.0 Net Excavation Scour

A conclusion of Chapter 4 is that the maximum thickness of the moving bedload layer in gravel bed streams is approximately twice the bed surface D_{90}. Consequently, larger magnitude scour depths (e.g., as much as $53D_{84}$ in Redwood Creek, California; Lisle 1995) must be due to net excavation scour, which is caused by local sediment transport rate imbalances and layer whisking, rather than to large shear stresses and thick bedload layers. Data collected in this study do not permit a detailed evaluation of transport rate imbalances in the study reaches (e.g., using a two- or three-dimensional numerical model). However, it is possible to use the data to identify and evaluate some of the more important hydraulic and sediment transport processes that may influence net excavation scour and intragravel survival of salmonids.

Figure 5-1 shows that total scour depths were generally less than 350 mm in all study streams and, like bedload disturbance depth, did not exhibit a clear relation with shear stress. Figure 5-2 indicates that location in the channel has a much greater influence on total scour depth than shear stress. With few exceptions, total scour depths within the riffle and riffle crest regions of the study sites (see Figure 4-13) were approximately $2.5D_{90}$ or less. This result reflects the availability of sufficient gravel and cobble located immediately upstream of the scour monitor location, and within the length of the reach, to preclude significant sediment transport rate imbalances occurring at either scale.

Figure 5-2 shows that the most extreme outliers above the $2.5D_{90}$ line and to the left of the $\tau^*_g = 0.035$ line were located in the pool tail/edge region (see Figure 4-13). The outliers included scour and fill measured in transient, small scale deposits that were finer-grained than substrates found in the majority of the channel. The deposits were small in area, occupied a fraction of the channel width, and likely exhibited delayed initiation and early cessation of bedload motion during the rising and falling stages of a flood, respectively, because of temporally variable and locally divergent velocity fields associated with flow obstructions located upstream. One such deposit occurred as a side
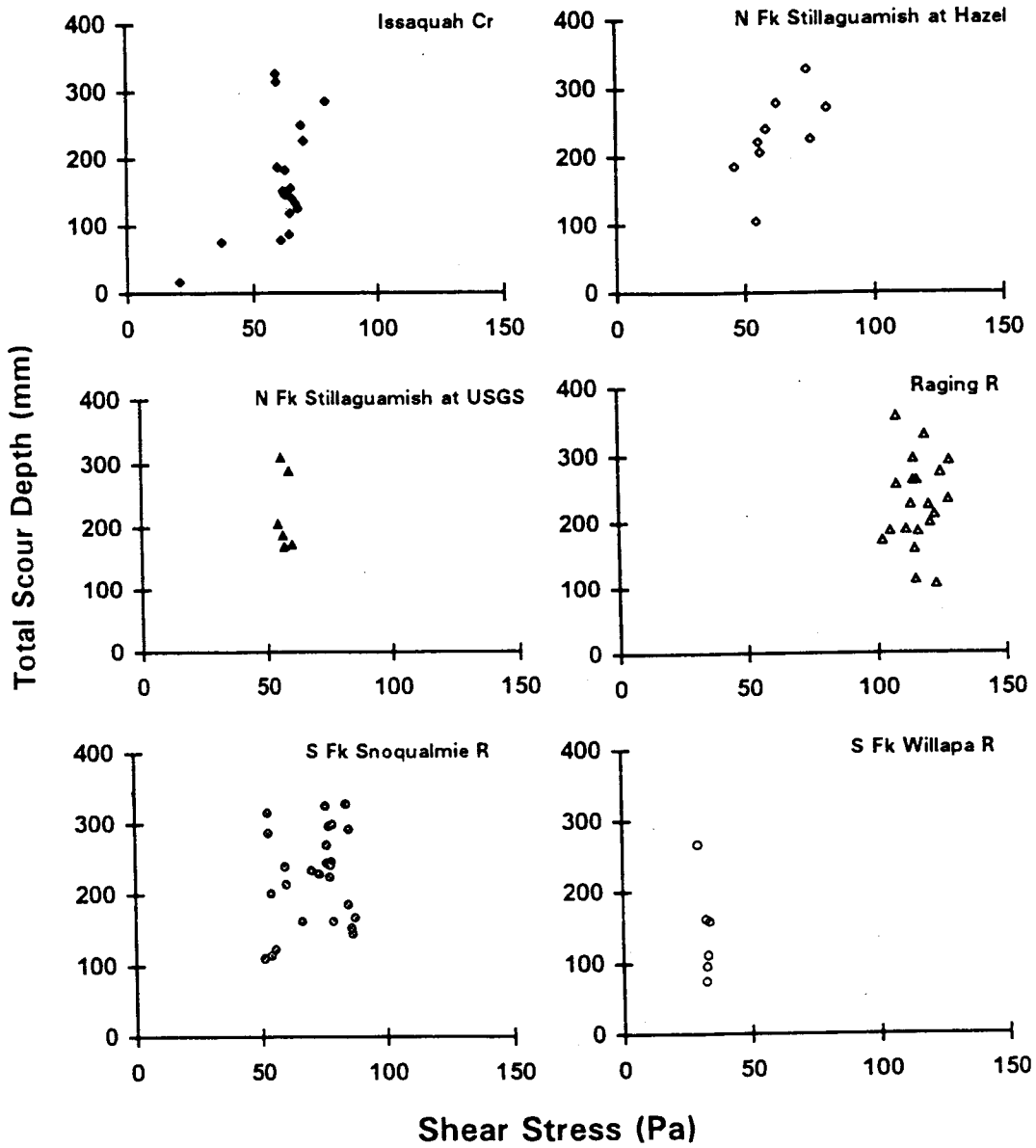
Figure 5-1. Variation of total measured scour depths with local bed shear stress at scour monitor locations in the study streams.
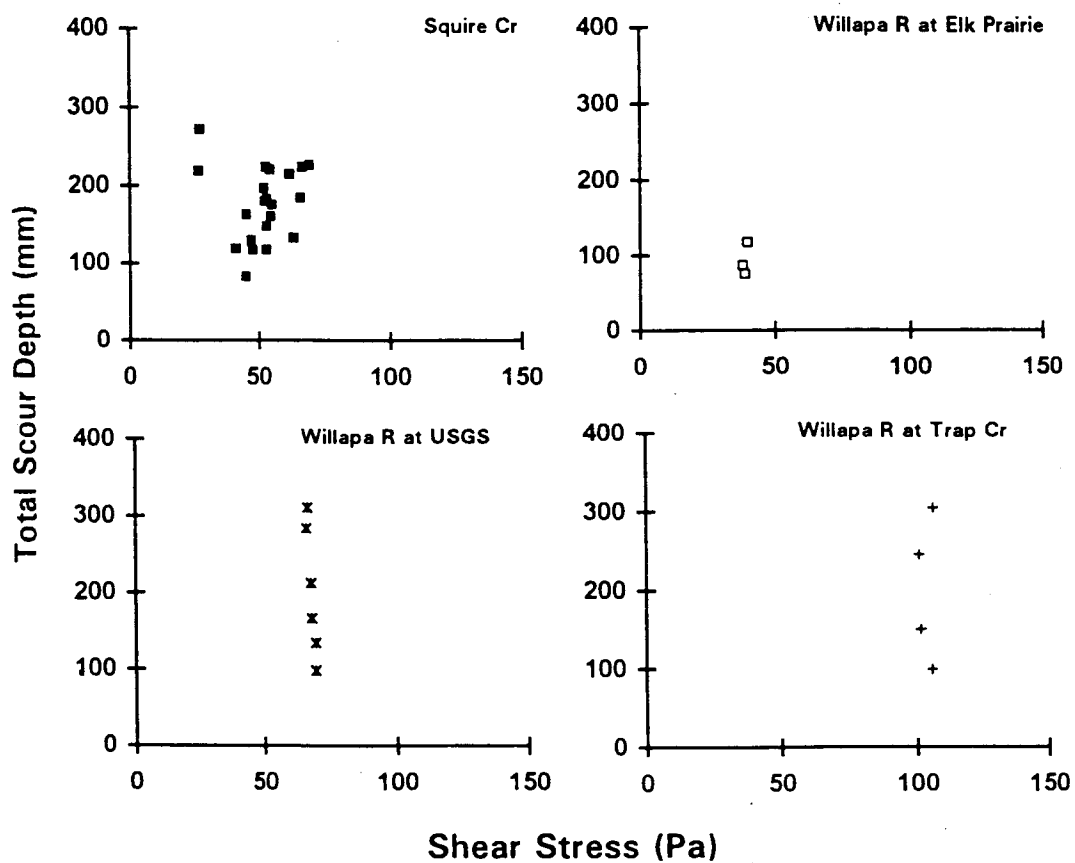
Figure 5-1. Continued.
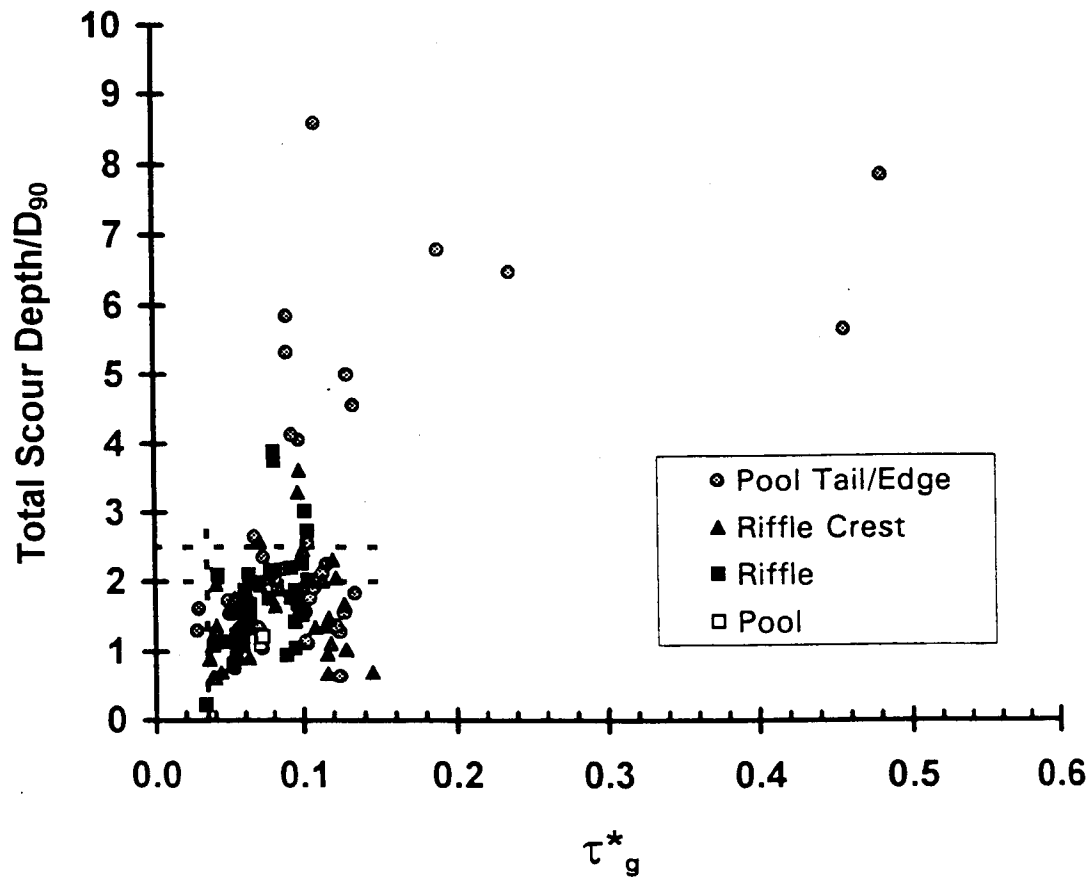
Figure 5-2. Variation of dimensionless local total scour depths with dimensionless local bed shear stresses, where data are classified according to longitudinal position in a pool-riffle-sequence. The horizontal dashed lines represent $\delta_{Bm} = 2D_{90}$ and $\delta_{Bm} = 2.5D_{90}$; the vertical line is for $\tau^*_g = 0.035$.

bar on the left side of Transect 2 of the South Fork Snoqualmie River site (Figure A-10, Appendix A). Another deposit was observed as a bar that had formed downstream of a junction with a high flow channel, on Transect 2 of the South Fork Willapa River site (Figure A-12). A third example was a small side bar located downstream of a bedrock outcropping, on the right side of Transects 2 and 3 of the Tolt River site (Figure A-16). Scour depth measurements made at these three locations reflected small-scale sediment transport rate imbalances that were primarily a function of unsteady flow and local hydraulic conditions.

The outliers in Figure 5-2 also include scour depths measured in pool tail/edge regions or in riffles that were relatively short in length and infrequent in spacing, where sediment transport rate imbalances appear to have developed in relation to stream-wise variation in the distribution of gravel and cobble at the riffle-pool scale. An extreme example was observed on Transects 1, 2, and 3 of the Tolt River site (Figures A-16, D-21 through D-23), which nearly scoured out completely. Scour data for the Tolt River site are not shown in Figure 5-2 because the scour monitors were not recovered. The transects were located across a riffle that was unusual in the sense that the majority of the bed in the environs of the reach was much coarser, with boulders scattered throughout. There was relatively little gravel and cobble material upstream of the riffle that was available to replace material being transported out of the study riffle, which scoured out as a result.

A less extreme example of sediment transport rate imbalances at the pool-riffle scale was apparent on Transect 1 of the Willapa River at the Trap Creek site (Figure A-20), which was located across the last gravel riffle downstream of Trap Creek, and below which the streambed became predominantly bedrock again (the bed was mostly bedrock upstream of the confluence; the tributary was the primary source of gravel and cobble to the reach). Most of the bars in the reach were vegetated with brush and willows, and did not appear to erode significantly during the study floods. There was a long bedrock pool spanning the distance between Transect 1 and the next riffle upstream where the bed was also significantly coarser (see grain size distributions in Figure E-5, Appendix E for scour

monitor numbers 1-4 on Transect 1, and numbers 7-12 on Transect 2).

A third possible example was observed on Transect 6 of the South Fork Snoqualmie River site (Figure A-10), which was the only transect in the reach where a scour depth deeper than $2D_{90}$ was measured over the 1997-1998 flood season, after a flood with a return interval of approximately 2 years (scour monitor #21 in Table D-1, Appendix D; scour monitor #22 was buried and was not recovered). The depth of bed disturbance was much deeper than had been measured in the rest of the channel after larger floods. Elsewhere, scour depths were less than $2D_{90}$ and were shallowest in the lower pool (the two 'pool' data in Figure 5-2).

The data indicate that specific areas in the channel vary in terms of total scour depth. Areas that differ geomorphically should therefore be identified and evaluated separately for important controls on net excavation scour. Areas of finer grained, transient deposits will not be treated here because they are generally small in plan area, distributed sporadically, and are generally not used for spawning except possibly in high gradient channels, which are not the subject here. The processes involved in erosion and re-formation of fine grained deposits are relatively well understood: their morphology is contingent on the bed location being sheltered from competent flows during lower flood stages, when bedload transport is occurring elsewhere in the channel, and mobilizing at higher stages.

There are two major geomorphic areas in low gradient channels used predominantly by salmonids for spawning that will be evaluated separately below. They reflect different scales of net excavation scour, and are the pool-riffle interface, and the riffle proper.

5.1 Net Excavation Scour Depth in the Pool-Riffle Interface

Riffles serve as the primary storage location for material contributing to bedload transport. As described in Chapter 2, bars are longer term storage locations for gravel and cobble than the riffle bed because they are primarily a depositional feature, and thus appear to contribute relatively little material annually to bedload transport over riffles

and redd locations. Jackson and Beschta (1982) proposed the transport process to be a 'leap-frogging' of bed material downstream from riffle to riffle. They argued that bedload at lower transport rates consisted of finer material originating primarily from pools. All material was observed to be routed efficiently through pools during higher flood stages. Campbell and Sidle (1985) noted a similar occurrence. Lisle (1979) proposed that this could be linked to temporal variation in shear stresses between pools and riffles during floods.

I propose on the basis of mass conservation that this discontinuity in the distribution of commonly transported gravel and cobble must be an important cause of deep scour and fill (i.e., $>>2D_{90}$) in the pool-riffle interface region, and that scour and fill occurs predominantly at the upstream edge of a riffle deposit in the 'pool edge' region (cf. Figure 4-13). This is because there must be a finite time interval during which material from the next upstream deposit is transported downstream before it reaches the pool edge region. During that interval, material arrives from upstream at a rate that is insufficient to replace material being transported from the upstream edge of the deposit, and the deposit erodes at its head.

Finer grained material that may be stored in the pool when sediment supply is high is transported away at lower flood stages before significant transport of the coarser riffle deposit material occurs (Lisle and Hilton 1999). This process likely continues until an underlying, coarser lag layer is exposed in the pool bottom that does not mobilize extensively, except under catastrophic flooding conditions (Richards 1982). Such lag layers were observed in pools of four of the study streams (Raging River, South Fork Snoqualmie River, Squire Creek, and Tolt River). An implication is that scour depth in pools is large only when there is a transient, finer grained deposit present during low flows. Otherwise, scour depth in pools could be limited during most floods to a relatively shallow disturbance depth caused by incomplete mobilization of the coarser lag layer. In either case, salmonids generally do not spawn in pools.

At higher flood stages, the riffle deposit must ultimately erode, beginning at the upstream end first. The process is depicted in Figure 5-3. There is a moving bedload
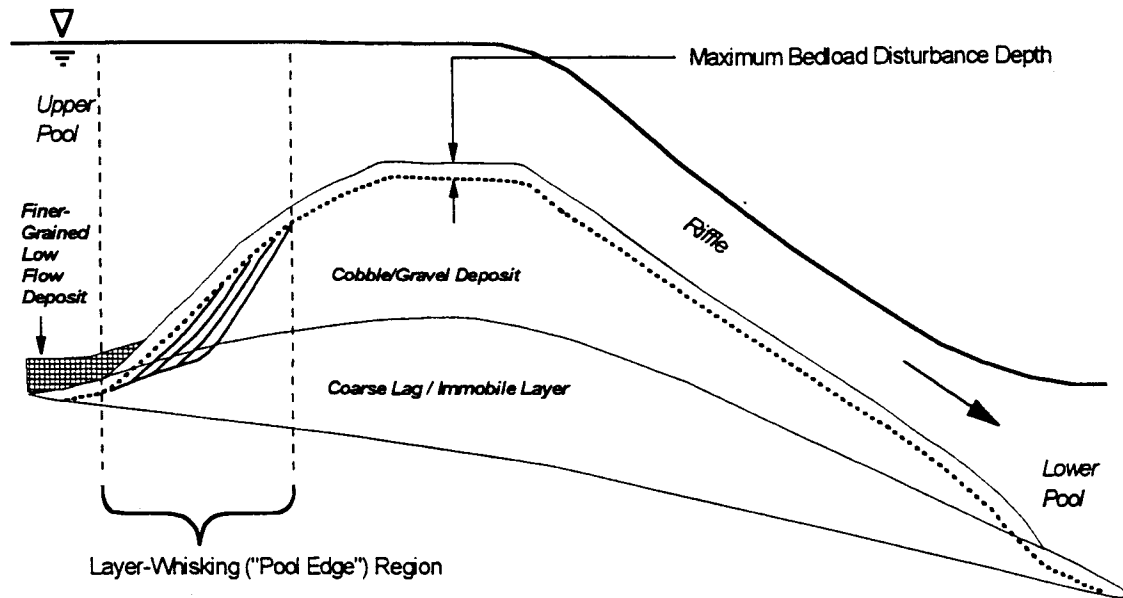
Figure 5-3. Longitudinal vertical profile depicting the progressive scouring process in the pool edge region. The series of solid lines in the "layer whisking region" indicate successive elevations of bedload disturbance depths as layers are whisked away by the flow.

layer occurring throughout the riffle and pool complex. The thickness of the moving layer in the pool may reflect the lag layer grain size distribution and competence of the flood to mobilize it, and in the riffle it is limited to approximately $2D_{90}$ or less (according to the results of Chapter 4). Successive layers are whisked away from the pool edge region until replacement material arrives at a sufficient rate from upstream to cause erosion to stop. Fill is assumed to occur when the flood subsides, whereby material already traveling through the pool collects on the pool edge face and shear stresses become too small for the material to be transported over an adverse bed gradient up to the riffle crest. An additional hypothesis is that, because the recession period of the descending limb of the flood hydrograph is longer than the duration of the ascending limb and because lower shear stresses are required to continue bedload transport than to initiate it, there is time for mobilized material within the pool to be transported to the pool-edge region as the flood stage subsides.

5.1.1 Developing a Predictor of Net Excavation Scour Depth

The distance between riffle deposits is probably not the only cause of sediment transport rate imbalances in the pool-riffle interface. The hydraulics and plan-view morphology of the pool-riffle interface may facilitate a diverging sediment transport field in the pool edge and tail region, for some period during a flood. Divergence (in the mathematical sense) of sediment transport rate should be associated with excavation scour. To see this, it is instructive to review the sediment continuity (Exner) equation, which can be expressed per unit stream width (z-axis) and unit stream length (x-axis) as:

$$\frac{\partial y}{\partial t} = \frac{-1}{\rho_s (1-P)} \nabla \cdot \vec{q}_B(x,z) = \frac{-1}{\rho_s (1-P)} \left[\frac{\partial q_{B_x}}{\partial x} + \frac{\partial q_{B_z}}{\partial z} \right] \qquad (5.1)$$

The left hand side of Equation 5.1 represents the rate of change in the depth of sediment storage. The right hand side represents the difference between input and

output bedload transport rates. A positive divergence of the sediment transport rate vector (the bracketed terms in Equation 5.1) results in a drop in bed elevation, or net excavation scour. Equation 5.1 is usually approximated numerically because of analytic intractabilities and cannot be evaluated directly with the data collected here.

Equation 5.1 is derived from the Reynolds Transport Theorem (RTT), which may be reduced to a simpler expression that can be evaluated here. The RTT is applied to the conceptual control volume shown in Figure 5-4, which is a simplified 2-D representation of the pool-riffle interface region. The bed elevation is assumed in the following conceptual model derivation to rise and fall uniformly (in the y-direction) across the plan area of the control volume.

For constant density, and the control volume (cv) and surface (cs) depicted in Figure 5-4, the RTT states that for mass conservation:

$$\frac{\partial}{\partial t} \iiint_{cv} \rho \, dx \, dy \, dz = -\oint_{cs} \rho \, \vec{U}_B \cdot d\vec{A} \tag{5.2}$$

The length of the model control volume, L is constant. The active width of the bed is assumed to be proportional to the width of the channel between the left and right bank bottoms and is approximately constant while significant transport activity occurs. This assumed behavior is inferred from the results of Haschenburger (1996) and Haschenburger and Church (1998). The widths W_1 and W_2 of the control volume represent the active widths at the upstream and downstream boundaries, respectively. The channel bed may be wider than the control volume but water flow is not deep or fast enough to mobilize the bed extensively on either side of it. Letting the height of the control volume extend from 0 to the average bed elevation Y, the left hand side of Equation 5.2 can be rewritten using the average width as:

$$\frac{\partial}{\partial t} \iiint_{cv} dx \, dy \, dz \approx L \left(\frac{W_1 + W_2}{2} \right) \frac{\partial}{\partial t} \int_{0_{cv}}^{Y} dy = L \left(\frac{W_1 + W_2}{2} \right) \frac{\partial Y}{\partial t} \tag{5.3}$$
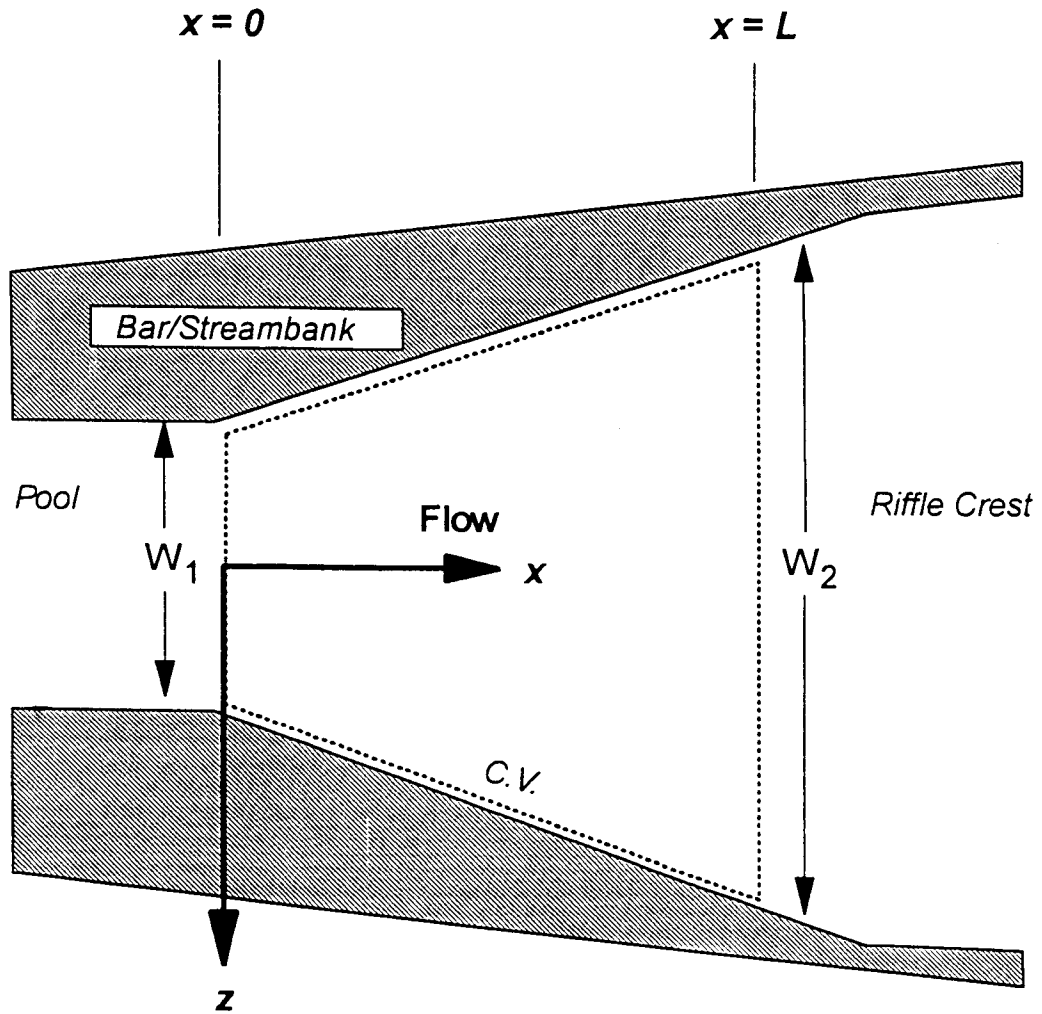
Figure 5-4. Plan view of control volume used to develop an estimator of net excavation scour depth in the pool-riffle interface.

The right hand side of Equation 5.2 is evaluated at the left and right vertical faces of the control volume of Figure 5-4 only (since the active width is assumed to be fixed, no material enters or leaves the control volume from or to either bank, respectively):

$$\oint_{cs} \vec{U}_B \cdot d\vec{A} = \int\int U_B \, dy \, dz \Big|_{x=L} - \int\int U_B \, dy \, dz \Big|_{x=0} \tag{5.4}$$

Assuming that U_B is an average value and $\neq f(y,z)$, and letting δ_B be the average bedload layer thickness (which is assumed to be approximately constant and equal to D_{90}):

$$\oint_{cs} \vec{U}_B \cdot d\vec{A} = \delta_B U_B \int dz \Big|_{x=L} - \delta_B U_B \int dz \Big|_{x=0}$$
$$= Q_B \Big|_{x=L} - Q_B \Big|_{x=0} \tag{5.5}$$

where Q_B is the total downstream volumetric bedload transport rate (m^3/s) across each control surface.

The Reynolds Transport Theorem now becomes:

$$0 \cong L \left(\frac{W_1 + W_2}{2} \right) \frac{\partial Y}{\partial t} + Q_B \Big|_{x=L} - Q_B \Big|_{x=0} \tag{5.6}$$

or alternatively:

$$\frac{\partial Y}{\partial t} \cong \frac{-2}{L(W_1 + W_2)} \left(Q_B \Big|_{x=L} - Q_B \Big|_{x=0} \right) \tag{5.7}$$

The total volumetric sediment transport rate across each control surface can be expressed in terms of the mass transport rate per unit width q_b (kg m^{-1}s^{-1}) as:

$$Q_B = \frac{q_b W}{\rho_s (1-P)} \tag{5.8}$$

Integrating from the beginning of flow competence at time t_1, to time t_2 when

material arrives at a sufficient rate from the next riffle upstream (when excavation is assumed to stop):

$$\int_{t_1}^{t_2} \frac{\partial Y}{\partial t} dt \; = \; \delta_{EX} \; \cong \; -2 \int_{t_1}^{t_2} \frac{\left[(q_B W)_2 - (q_B W)_1 \right]}{L(W_1 + W_2) \, \rho_s \, (1-P)} \, dt \qquad (5.9)$$

Equation 5.9 is an approximate expression for predicting maximum net excavation scour depth during a flood. If the bedload transport rates can be estimated accurately over the course of the flood, Equation 5.9 may predict the value of δ_{EX} that can be used in Equation 1.1 to predict total scour depth.

The conceptual model represented by Equation 5.9 suggests attributes of the pool-riffle interface that may influence scour in the pool edge region. It is beyond the scope of the data collected in this study to determine the extent to which the mechanism acts, including confirming when t_1 and t_2 occur and precisely where the boundaries of the control volume are best evaluated, but it can be seen from the equation that there can be certain morphologic and hydraulic features of the pool-riffle interface that promote excavation there at some time during a flood.

For example, shear stresses during the initial competent stages of a flood can be higher in the riffle than in the pool (Keller 1971; Lisle 1979; Carling 1991; Clifford and Richards 1992). Extension of the control volume upstream into the pool and downstream to the riffle crest is associated with a corresponding sediment transport rate imbalance across the control surface. This may also be influenced by differences in the grain size of riffle and pool beds, which is not accounted for in the example. The bedload transport rate per unit width across the downstream end of the control volume may consequently be greater than across the upstream end, resulting in a negative value for δ_{EX} in Equation 5.9 (i.e., the interface scours). As the flood stage increases, shear stresses in the pool and riffle become comparable (Carling 1991; Clifford and Richards 1992). The transport rates per unit width then also converge, but at that point the magnitude of δ_{EX} may still be negative as $(q_b W)_1$ can still be less than $(q_b W)_2$ because of

the difference in widths. The riffle needs to supply material leaving the control volume, and "steals" from itself to satisfy mass conservation. Hence, the plan-view, active bed morphology of the pool-riffle interface could favor the occurrence of net excavation scour for a certain period during a flood according to the conceptual model. This needs to be evaluated further with field measurements of spatial and temporal variation in local shear stresses and bedload transport rates in a pool-riffle unit.

Equation 5.9 also predicts that as the active width W_1 becomes progressively narrower than W_2, with all else remaining equal, the length of time it takes to achieve the same value of scour depth may decrease such that the inter-deposit distance required to preclude a greater scour depth becomes shorter. The model also predicts that for a long stream reach containing abundant gravel throughout, where L may be relatively large and W_1 and W_2 similar in magnitude, δ_{EX} is approximately equal to zero; i.e. equilibrium transport is approximated.

5.1.2 *Predicting Scour Depth and Effects on Intragravel Survival*

The conceptual model of Equation 5.9 was tested for its ability to estimate of the threshold for net excavation scour effects on embryo survival. This was done using data from the Raging River by specifying a total scour depth that approximated an egg burial depth, and letting δ_{EX} equal the difference between that and maximum bedload disturbance depth (from Chapter 4) using Equation 1.1. The length L was set equal to the streamwise distance from the upstream edge of the study riffle deposit to Transect 1, where salmon redds were observed. W_1 and W_2 were set equal to the width of the active channel, as determined from surveys of cross-section profiles and field observations of bed activity, at the upstream edge of the deposit and at the transect location, respectively. The time that it took for the bed to lower by δ_{EX} was estimated by stepping through the integral in Equation 5.9 until the equality was satisfied. This time was then compared with an estimate of the average time taken by different particle sizes to move to the head of the riffle deposit from the immediate upstream deposit.

The remainder of this section focuses first on estimating travel time for any particle size as a function of shear stress, for purposes of estimating the total travel distance during any flood. I then evaluate Equation 5.9 as a predictor of net excavation scour depth, including whether there is a characteristic particle size that can be used in the analysis.

5.1.2.1 *Estimating Particle Travel Distances Between Riffle Deposits During a Flood*

Travel distance is the product of average particle step length (which increases with shear stress magnitude) and the number of steps (which increases with shear stress and total duration of flow competence; Wilcock 1997a). A consistent expression for travel distance therefore considers the temporal variation of shear stress during a flood. It should be possible to predict the total distance traveled during a time interval by identifying a relationship between travel distance and shear stress and then integrating that relationship over the period of flow competence. This approach differs from earlier methods that represent total travel distance as a function of maximum stream power (e.g., Hassan et al. 1991; Haschenburger 1996) or maximum shear stress (Ferguson and Wathen 1998), which do not differentiate between floods with similar peak magnitudes but different durations.

A simple expression for average travel distance of particles of a size class D_j originating from the bed surface is, to first order (Wilcock 1997a):

$$L_{x_j} = \frac{q_{B_j} T_j}{[\pi/6]\rho_s p_j D_j \acute{Y}_j} \tag{5.10}$$

where T_j is the duration of flow competence for particle size class D_j (which comprises $100 p_j$ percent of the overall surface grain size distribution), and $\acute{Y}_j$ is the proportion of grains in size class j entrained over T_j ($\acute{Y}_j = 1.0$ when the fraction is fully mobile). This expression can be modified to represent travel distance over a small differential element

of time as:

$$dL_j = \frac{q_{B_j}(t)\,dt}{[\pi/6]\rho_s p_j D_j \dot{Y}_j(t)} \tag{5.11}$$

which on integration becomes:

$$L_{x_j} = \int_0^{L_{x_j}} dL_j = \int_{t_1}^{t_2} \frac{q_{B_j}(t)}{[\pi/6]\rho_s p_j D_j \dot{Y}_j(t)}\,dt \tag{5.12}$$

where t_1 and t_2 represent the beginning and end times, respectively, of flow competence for size class j.

Equation 5.12 can be solved explicitly if the bedload transport rate is known (i.e., measured). Alternatively, when the transport rate is unknown, the equation can be re-expressed for sediments with similar densities as:

$$L_{x_j} \approx f\left(\frac{1}{p_j D_j} \int_{t_1}^{t_2} (\tau_b(t) - \tau_{cr_j})^{1.5}\,dt\right) = f\left(\mathcal{T}_j\right) \tag{5.13}$$

because the average transport rate of size fraction j is proportional to $(\tau_b - \tau_{cr_j})^{1.5}$ (Yalin 1977). The excess shear stress calculation and integration are depicted in Figure 5-5. Equation 5.13 is consistent with the work of Bagnold (1956; 1966a), who argued that if the entire excess shear stress $(\tau_b - \tau_{cr})$ is applied to bedload transport, the effective work done per unit area in moving bedload should also be related to excess shear stress, rather than to τ_b alone. Work done is a product of the force applied and the distance moved in the direction of the force.

Equation 5.13 is approximate in the sense that excess shear stress depends on the value of τ_{cr_j}, which varies between a static, incipient motion condition and a dynamic one. The relation between the two remains to be determined by future research. Equation 5.13 is also subject to unexplained variation because it ignores (i) the
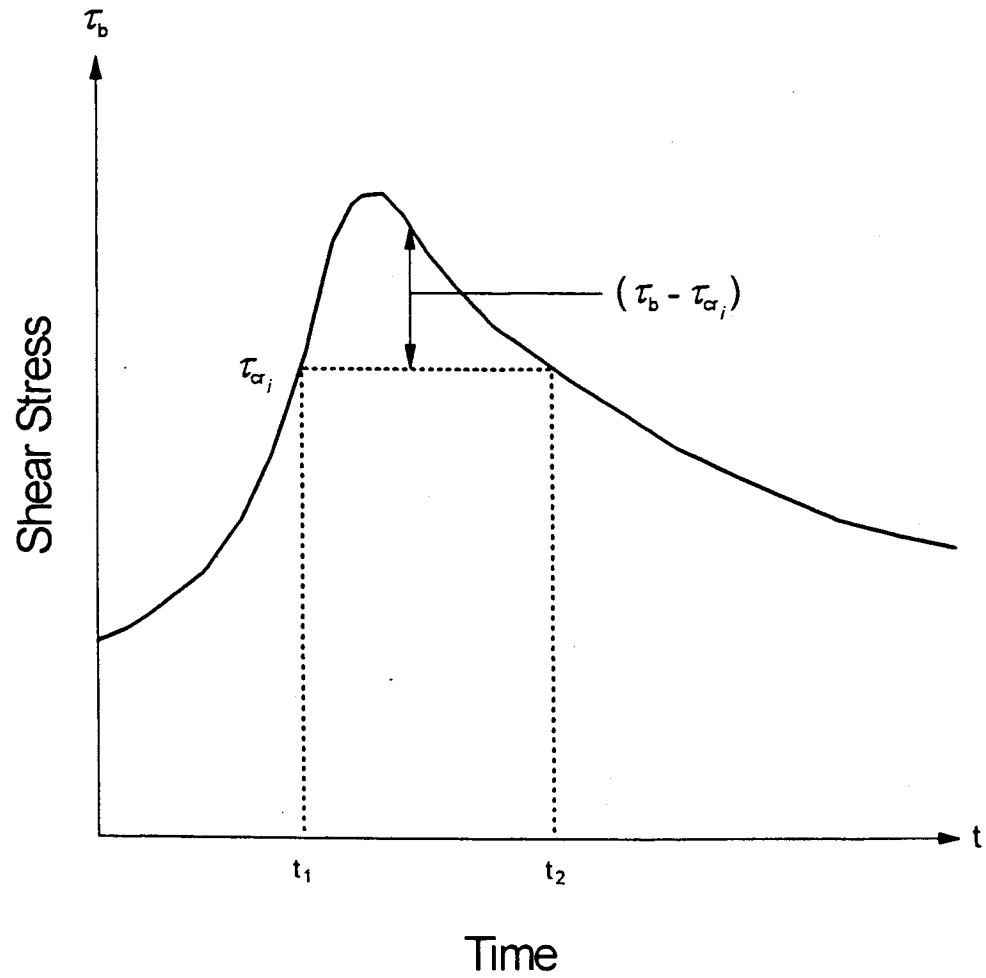
Figure 5-5. Schematic of the calculation of excess shear stress at a time t during the period of flow competence for grain size class j that extends between times t_1 and t_2.

contribution of the subsurface layer to bedload transport (e.g., during surface particle entrainment; Parker et al., 1982a), and (ii) the fraction of surface size class j not participating in transport when the bed experiences partial mobility (Wilcock 1997a). The contribution of the subsurface material was ignored, to first order, because considerably fewer particles from the subsurface layer participate in bedload transport than do surface particles (Parker 1990a; Hassan and Church 1992; Wilcock 1997a). The mobility fraction $\acute{Y}_j$ has been omitted from Equation 5.13 because it is unknown; $\acute{Y}_j \approx 1.0$ for almost fully, and fully mobile fractions.

Equation 5.13 indicates that the average distance traveled by a size class j (L_{xj}) is a function of $\mathcal{T}_j$. There should be an approximately linear relationship between L_{xj} and $\mathcal{T}_j$ for fully mobile fractions, and a non-linear relation for partially mobile fractions (that tends to zero with average travel distance). Equation 5.13 and $\mathcal{T}_j$ may represent a convenient, empirical averaging approach. This hypothesis was tested using tracer data collected over the 1997-98 flood season in two of the study streams.

Equation 5.13 was discretized and Equation 3.5 was used to estimate shear stress, resulting in the approximation:

$$\int_{t_1}^{t_2} (\tau_b(t) - \tau_{cr_j})^{1.5} dt \approx (\rho g S_j)^{1.5} \sum_{t=t_1}^{t_2} (d(t) - d_{cr_j})^{1.5} \cdot \Delta t \qquad (5.14)$$

where the hydraulic radius term in Equation 3.5 was approximated by a depth d, which was evaluated as the difference between the water surface elevation and the average bed elevation of the active portion of the channel across a selected transect.

Tracer data were collected in the Raging River and Issaquah Creek reaches following a small flood in each. Both floods had about a 1.1 year recurrence interval, based on a Generalized Extreme Value distribution fit to gage data (using a computer program courtesy of Y. Alila, University of British Columbia). The gravel samples collected earlier in the study were painted three different colors. Each color sample was placed in a patch approximately 1 m in diameter near the thalweg, on three different transects in

each reach (Transects 3, 5, and 6 in Issaquah Creek, and Transects 1, 3, and 6 in the Raging River; see Figures A-2 and A-8 in Appendix A). Tracer stones were 22.2 mm and larger (sieve sizes are listed in Table 3-3). One of the colors was placed in a small pool in Issaquah Creek, but the location experienced fill from an adjacent, steep-sloped, aggrading point bar before a significant number of rocks were mobilized. They were later uncovered and several particles mobilized during a flood in the following year. Those data were discarded.

The sites were revisited after the floods subsided, and the *b*-axis diameter and distance traveled were measured for each tracer stone recovered. Because the floods were moderate in magnitude and duration, net excavation scour was negligible and consequently tracers remained within the surface layer. Recovery rates were correspondingly high: >90% for the smaller and 100% for the larger size classes. Scatter plots of distance traveled versus grain size were comparable between the different colors within a stream, so the data were pooled to increase sample size. Figure 5-6 indicates that each color group, and the pooled data, were distributed similarly. The data were distributed approximately as exponential distributions, consistent with earlier work by Hassan et al. (1991), Hassan and Church (1992), and Haschenburger (1996), where the probability density function of travel distance is:

$$p(L_{x_j}) = \theta e^{-\theta L_{x_j}} \tag{5.15}$$

The exponential distribution was fit here by calculating the mean distance traveled for each size class *j*, and inverting it to obtain the distribution parameter θ (Hines and Montgomery 1980). Figure 5-7 shows the measured and fitted CDFs of distance moved for each size class. Fits are poorest for the two smallest size classes, but overall the distribution visually fit the data relatively well. A characteristic particle size was calculated for each size class as the geometric mean of the size class limits. Figure 5-8 shows the average distance traveled by each class. The trends are similar to the data of Hassan and Church (1992) and Haschenburger (1996).

a)

b)
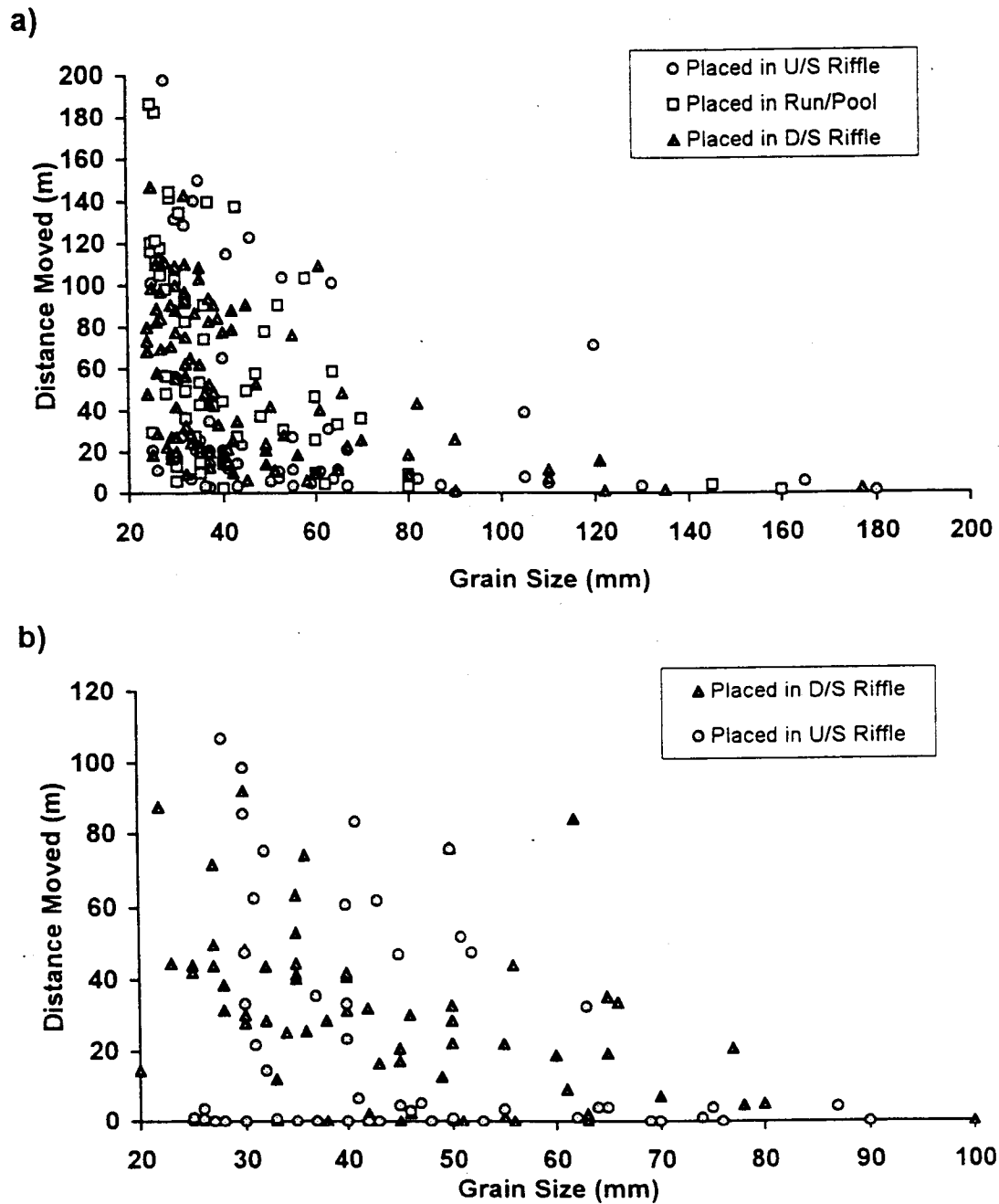
Figure 5-6. Distances traveled by different tracer stone grain sizes during a flood in the a) Raging River and b) Issaquah Creek study reaches. Data are distinguished by where in the reach they were placed originally.

a)

b)
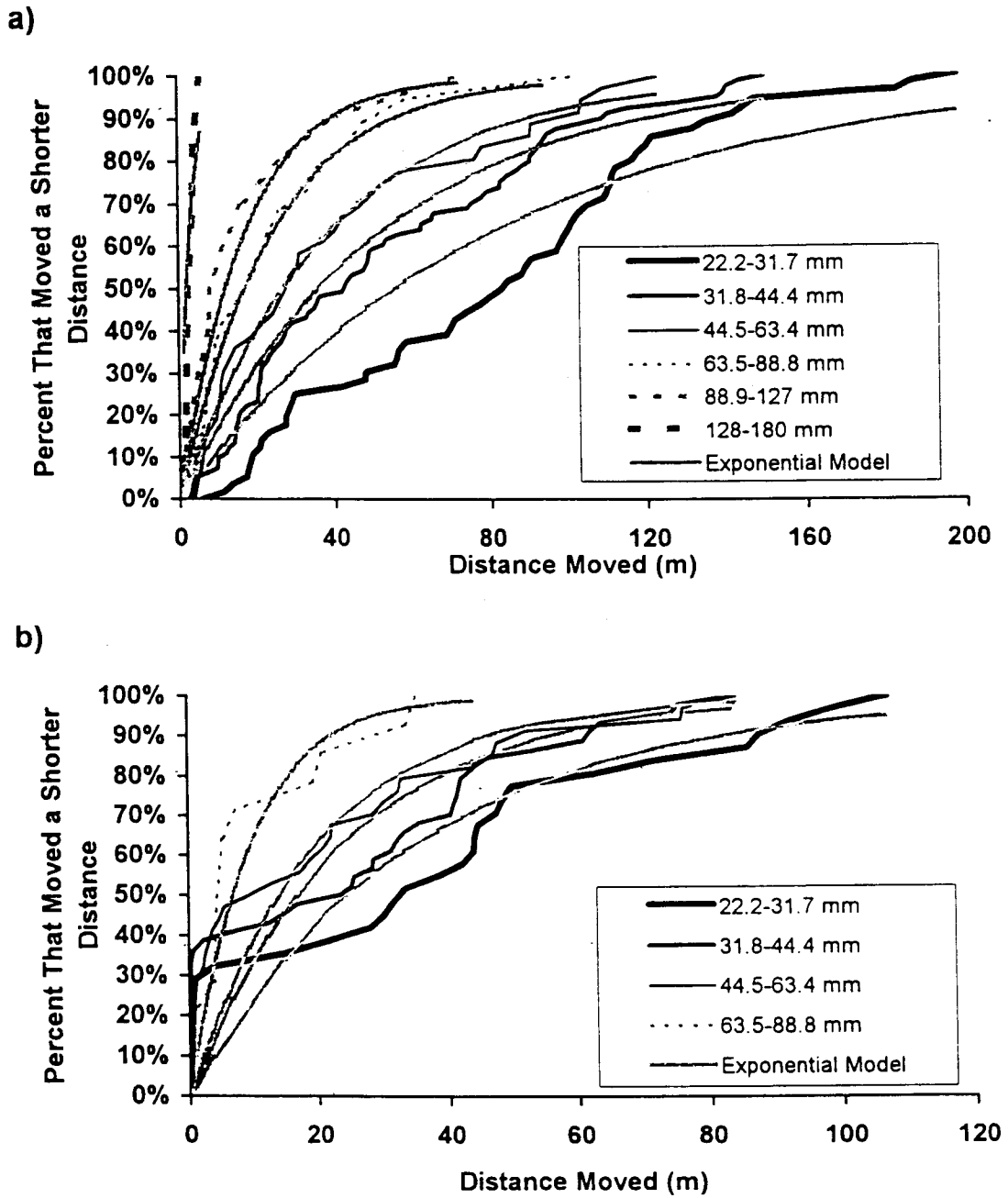
Figure 5-7. Empirical cumulative distribution functions (CDFs) of travel
distances measured in the a) Raging River and b) Issaquah Creek
study reaches for different tracer stone size classes, and fitted
exponential CDFs.
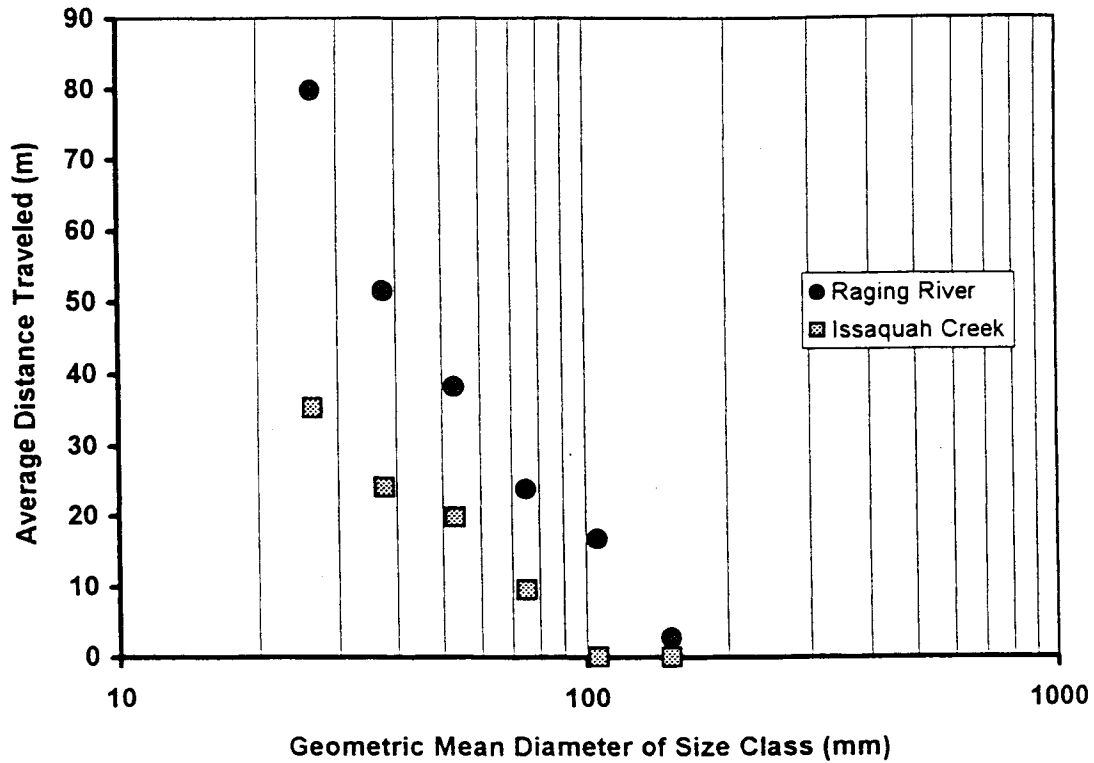
Figure 5-8. Average distance traveled by tracer stones placed in the Raging River and in Issaquah Creek, plotted against the geometric mean diameter of each size class.

Water surface elevations and discharges were estimated using nearby USGS gages in both reaches. The mean depth over the active bed portion of the channel $d(t)$ was calculated using the rating curves presented in Appendix C that relate stage at different transects at the sites to stage at the gage. Transect 1 was assumed to be representative for each reach, and a corresponding $d(t)$ calculated relative to the average bed elevation across the active portion of the channel width. This assumption was satisfied best for the Issaquah Creek reach, which possessed a nearly uniform channel. The channel morphology in the Raging River reach was more irregular, where maximum depth along the thalweg ranged between 0.8 and 1.3 m, averaged 1.1 m, and was approximately 0.95 m at Transect 1 at the peak flow rate (estimated from cross-section and topographic surveys, and water surface elevations presented in Appendix H). The cross-section profile of the transect was relatively flat across the active portion of the bed, however (Figure D-5, Appendix D).

The flow depth at which each size class was mobilized (d_{cr} in Equation 5.14) was calculated by fitting the following flow competence relation (Komar 1996) to each reach:

$$\tau_{cr} = \tau^*_{cr}(\rho_s - \rho)g D_{50}^{\beta} D_{comp}^{(1-\beta)} \tag{5.16}$$

where the parameters τ^*_{cr} and β were specific to each stream. Equation 5.16 was fit to two points:

(I)   The lower point was determined from a smaller magnitude flood that occurred several weeks earlier in which only a few members of the smallest tracer size class moved a few meters or less in both streams.

(II)   The upper point was determined from the largest immobile tracer particles during the primary flood. In Issaquah Creek, this corresponded to the 106 mm size class, whereas in the Raging River the size was determined by extrapolating the data in Figure 5-8 to the abscissa (x-) axis.

Figure 5-9 shows pooled pebble counts from which the D_{50} value was determined for each reach.
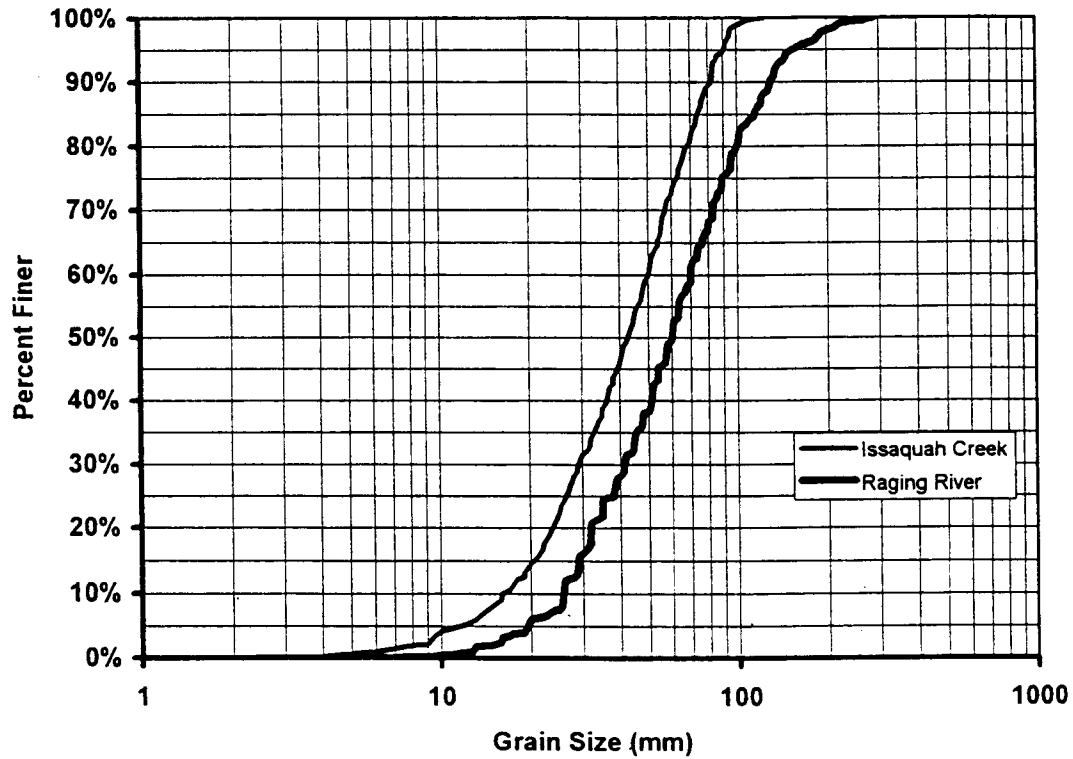
Figure 5-9. Cumulative grain size distributions of mobilized areas of the bed in the Raging River and Issaquah Creek study reaches, derived from pebble counts. The distributions were obtained by pooling pebble count data collected for different scour monitor locations.

The resulting flow competence relation determined for the Raging River reach was:

$$\tau_{cr_j} = 0.080(\rho_s - \rho)gD_{50}^{0.89}D_{comp_j}^{0.11} \qquad (5.17)$$

The relation determined for the Issaquah Creek reach was:

$$\tau_{cr_j} = 0.031(\rho_s - \rho)gD_{50}^{0.85}D_{comp_j}^{0.15} \qquad (5.18)$$

The two relations have similar magnitude exponents (β), but substantially different estimates of τ_{cr}^*. The difference can be explained in terms of influences on incipient motion specific to each stream. The estimate for the Raging River reach is relatively large in magnitude ($\tau_{cr}^* = 0.080$, near the upper end of the typical range, 0.030-0.086; Buffington and Montgomery 1997) because the substrate was relatively large, well imbricated and cemented, and particle clusters were present. The peak flow rate in the Raging River was small (return period = 1.1 years) and the flood was the first of the season to move particles larger than the bed D_{50} size. Increased resistance to motion of an unworked, imbricated cobble-gravel bed during the first flood is well known (e.g., Laronne and Carson 1976; Hassan and Reid 1990; Kirchner et al. 1990; Buffington and Montgomery 1997), as is the retarding influence of particle clusters on incipient motion (Church et al. 1998). Conversely, the substrate in Issaquah Creek was more sorted, relatively loose, and easily mobilized, and the critical dimensionless shear stress estimate is therefore smaller in magnitude.

The USGS fifteen-minute time increment stage data were used to estimate depths and the excess shear stress was accordingly calculated every fifteen minutes and summed over the period of flow competence for each size class j using Equation 5.14. The average distance traveled by each size class was plotted against T_j for both streams. Figure 5-10 shows that the data can be described well by a single curve. A linear relationship describes travel distances for values of T_j greater than about 30,000 $Pa^{1.5}$ hr m^{-1}. Travel distances for smaller values of T_j appear to follow a nonlinear
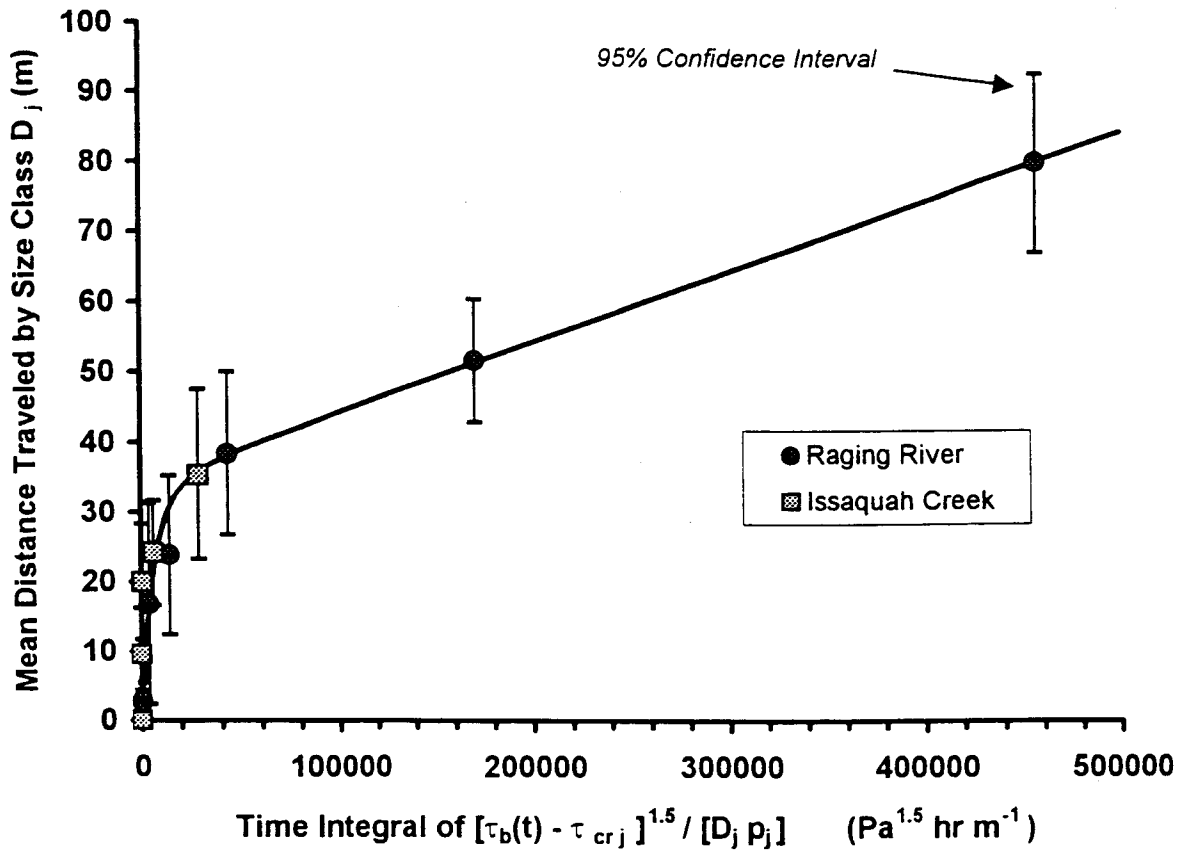
Figure 5-10. Relationship between mean distance traveled and the time integral of excess shear stress divided by grain size and proportion in bed for size class *j*. The line (Equation 5.19) was fit by eye to the pooled data from the Raging River and Issaquah Creek.

relationship down to $\mathcal{T}_j = 0$, rather than a second linear (or series of linear) relationship(s) with an appropriate match point(s).

The following equation was fit visually to the data and describes the measured travel distances L_{x_j} in meters relatively well:

$$L_{x_j} = 1.00 x 10^{-4} \mathcal{T}_j + 34.1 \left[1 - \left(3.33 x 10^{-5} \mathcal{T}_j + 1 \right)^{-5} \right] \qquad (5.19)$$

It is not possible without corresponding bedload transport data to explain completely the shape of Equation 5.19. One possible explanation alluded to earlier during development of the relation is that the linear portion represents size fractions experiencing full mobility (i.e., the finer sizes in the Raging River), whereas the nonlinear portion represents partial mobility. Wilcock (1997a) showed that the data of Hassan and Church (1992) and Haschenburger (1996) were generally representative of partial transport. The similarity indicated earlier between Figure 5-10 and their results could indicate that most of the size classes here also experienced partial mobility. Equation 5.19 could be modified by including the $\acute{Y}_j$ term in $\mathcal{T}_j$ to represent the fraction of the size class experiencing mobility (Wilcock 1997a); inclusion of the $\acute{Y}_j$ term should influence only the non-linear portion of Equation 5.19. Future research is needed that must also include collecting bedload transport data as done by Wilcock and McArdell (1993; 1997) to elucidate this issue. More data are especially needed that are representative of fully mobile size fractions.

5.1.2.2 *Testing the Ability of Equation 5.9 to Predict δ_{EX}*

Equation 5.19 provides a means for estimating the distance traveled by a characteristic size class and the time it takes to travel between riffle deposits in the Raging River and Issaquah Creek. This time can be compared to the time predicted by Equation 5.9 for net excavation scour depth to reach a specific magnitude. In the conceptual model, scouring of embryos would be indicated by Equations 5.9 and 5.19 as occurring when the predicted travel time between riffle deposits exceeds the predicted

time for net excavation scour to reach the threshold value. At that point, the embryos may become vulnerable to crushing by the moving bedload, followed by washing out as the bed elevation continues to lower.

Of the two streams with tracer data, the Raging River reach should provide better data for testing Equations 5.9 and 5.19 because the reach was more irregular in shape than the Issaquah Creek reach (which was approximately uniform in shape) and contained gravel/cobble deposits that were more distinctly separated in space. Tracer data collected from the Raging River reach also defined the shape of Equation 5.19 over a greater range of integrated shear stresses than data from Issaquah Creek.

A remaining problem in applying the conceptual model was to determine a relevant particle size (or sizes) that could be used to index travel time between riffles. Insufficient data were collected here to determine the answer experimentally; bedload transport data are needed to address this issue. The bed D_{50} has been found to be a suitable means for characterizing mobility of the entire mixture in general (Wilcock 1997b). Particles finer than the bed D_{50} are relatively easily entrained (Wilcock and McArdell 1997) and do not appear to influence bedload disturbance depth according to the data in Chapter 4. On the basis of typical porosity ranges (between approximately 0.28 and 0.35; Brayshaw et al. 1996), particles whose diameters are on the order of D_{28} (or D_{35}) and smaller are also unlikely to be important because they fill the interstices between the larger particles and thus may not influence bed surface elevation significantly. Which particle size percentile is the best index of travel time is unclear. The bed D_{50} is proposed for the purpose of evaluating the predictive ability of Equation 5.9 to first order.

The test of Equation 5.9 involved predicting the time in which the entire surface layer would be whisked out of the control volume during the November 27-28, 1996 flood, and comparing the result to the time predicted by Equation 5.19 for the D_{50} grain size to travel an average distance equal to the inter-riffle spacing. The thickness of the surface layer was assumed to be equal to the bed D_{90} (i.e., $\delta_{EX} = 0.13$ m; corresponding egg burial depth $\approx 3D_{90}$; see Chapter 6). The active width W_2 was estimated to be approximately 13 m (i.e., between stations 4 and 17 of Transect 1; Figure D-5, Appendix

D). The active width, W_l, at the upstream edge of the riffle deposit was estimated to be between 9 and 10 m based on visual post-flood observations of bed disturbance from 1996 to 1998. The intervening control volume length L (Figure 5-4) was estimated to be about 30 m based on field observations of streambed surface textures and from the topographic surveying data. Sediment density and bed porosity were estimated to be 2,730 kg/m^3 (Table 3-4), and 0.32 (using Equation 3.4), respectively.

In the absence of bedload transport measurements, or data describing the spatial and temporal variation in friction slope in the reach, an additional simplifying approximation was made that bedload transport rate per unit width was the same across the upstream and downstream faces of the control surface and could be represented by calculations for Transect 1. This assumption made excavation scour depth a function of active channel bed width differences. Bedload transport rates estimated at Transect 1 and at the upstream control surface from shear stress estimates differed by 50 percent at the peak flow rate, suggesting that unknown errors may have been introduced to the analysis.

Bedload transport rates were computed on an hourly basis using Parker's (1990a) relation. Transport rates were summed from the beginning of flow competence (for the D_{50} particle size) over the course of the November 27-28, 1996 flood, whose hydrograph is depicted in Figure 5-11. Equation 5.9 was satisfied when $(t_2 - t_l) \approx 4$ or 5.5 hours depending on the value of W_l. Over that same time interval, the calculated value of T_j was between 13,000 and 26,000 Pa$^{1.5}$ hr m^{-1}, for which the predicted average travel distance of the D_{50} particle size was between 30 and 35 m using Equation 5.19. This is roughly half the riffle to riffle distance at the site, which was between 55 and 60 m. The model therefore predicted that the surface layer would be eroded away before sufficient replacement material arrived from upstream. This is incorrect since the average net excavation scour depth across Transect 1 was measured to be approximately 0.04 m (Figure D-5, Appendix D). In other words, Equation 5.9 failed the test and overpredicted net excavation scour depth.

There are several potential reasons for the apparent failure of Equation 5.9 to predict net excavation scour depth. The conceptual model relies on input variables that are
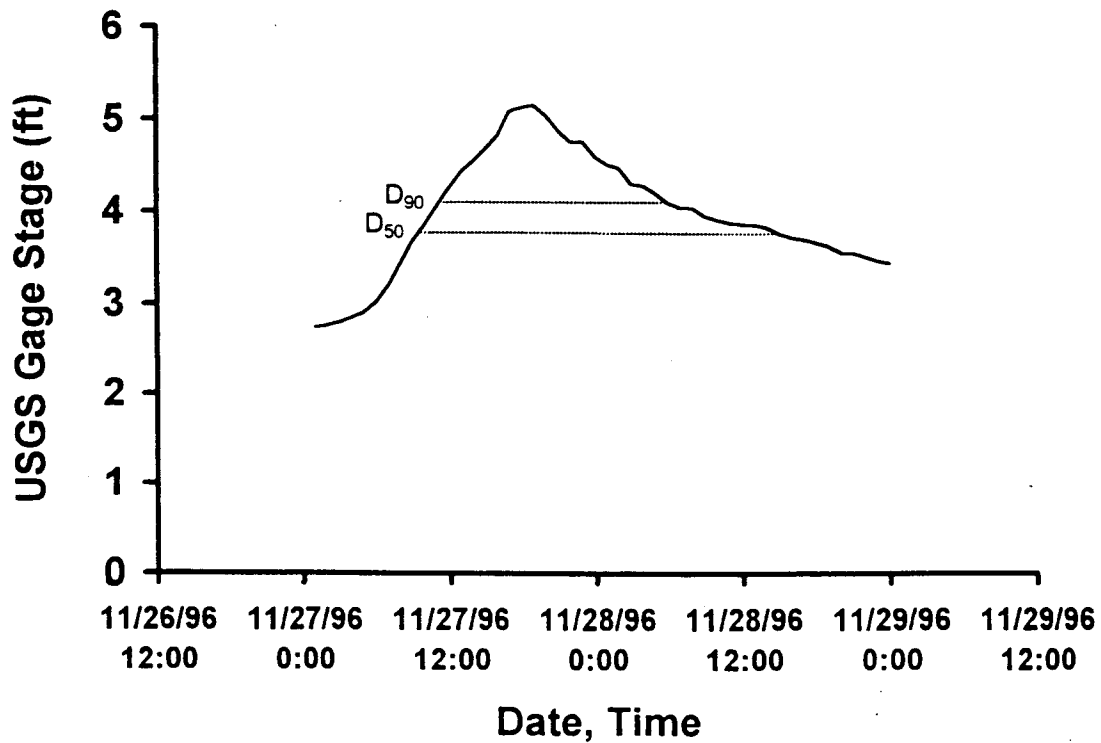
Figure 5-11. November 1996 flood hydrograph for Raging River, used in evaluating Equations (5.9) and (5.19). The periods of flow competence for the D_{50} and D_{90} particle sizes are indicated by the dotted lines.

insufficiently precise. The largest error sources include uncertainty in the bedload transport estimates, which can easily exceed a factor of two for the same shear stress as shown in Figure 3-6, and uncertainty in specifying W_1, W_2, and L. Two important assumptions influenced the application of Equation 5.9 that may not have been correct: (i) a size fraction smaller than the D_{50} (e.g., D_{35}) may have been a more appropriate index grain size for the model; and (ii) the bedload transport rates per unit width at $x = 0$ and $x = L$ were likely to have been significantly different during the initial competent stages of the flood and may have been similar for a much shorter time during the flood than was modeled.

These issues need to be explored in future work by collecting bedload transport and more detailed channel morphology and hydraulic data. Such information is critical for describing the influences of temporal and spatial variation in shear stress and bedload transport rate on net excavation scour. Because it represents a practical means for predicting δ_{EX} compared to the alternative approach of numerical modeling, Equation 5.9 merits further study.

5.2 Net Excavation Scour Depth in Riffles, Riffle Crests, and Pool Tails

Based on the analysis framework presented in Section 5.1, the data in Figure 5-2 suggest that net excavation scour depths in the pool tail, riffle crest, and riffle regions were relatively small in the study streams compared to scour depths in the pool edge region. Scour depth in the riffle and pool tail may, therefore, be influenced by a different process from that influencing scour depth in the pool edge region. This is indicated by the topographic surveying data collected at six sites in 1996 and again in 1997, which shows that net excavation scour or net fill occurred throughout the length of each reach.

Figure 5-12 shows that the Issaquah Creek reach experienced net fill throughout its length over the course of the 1996-97 flood season. The fill averaged 0.086 m over the area depicted in the upper plot of the figure, and was distributed relatively uniformly throughout the reach.
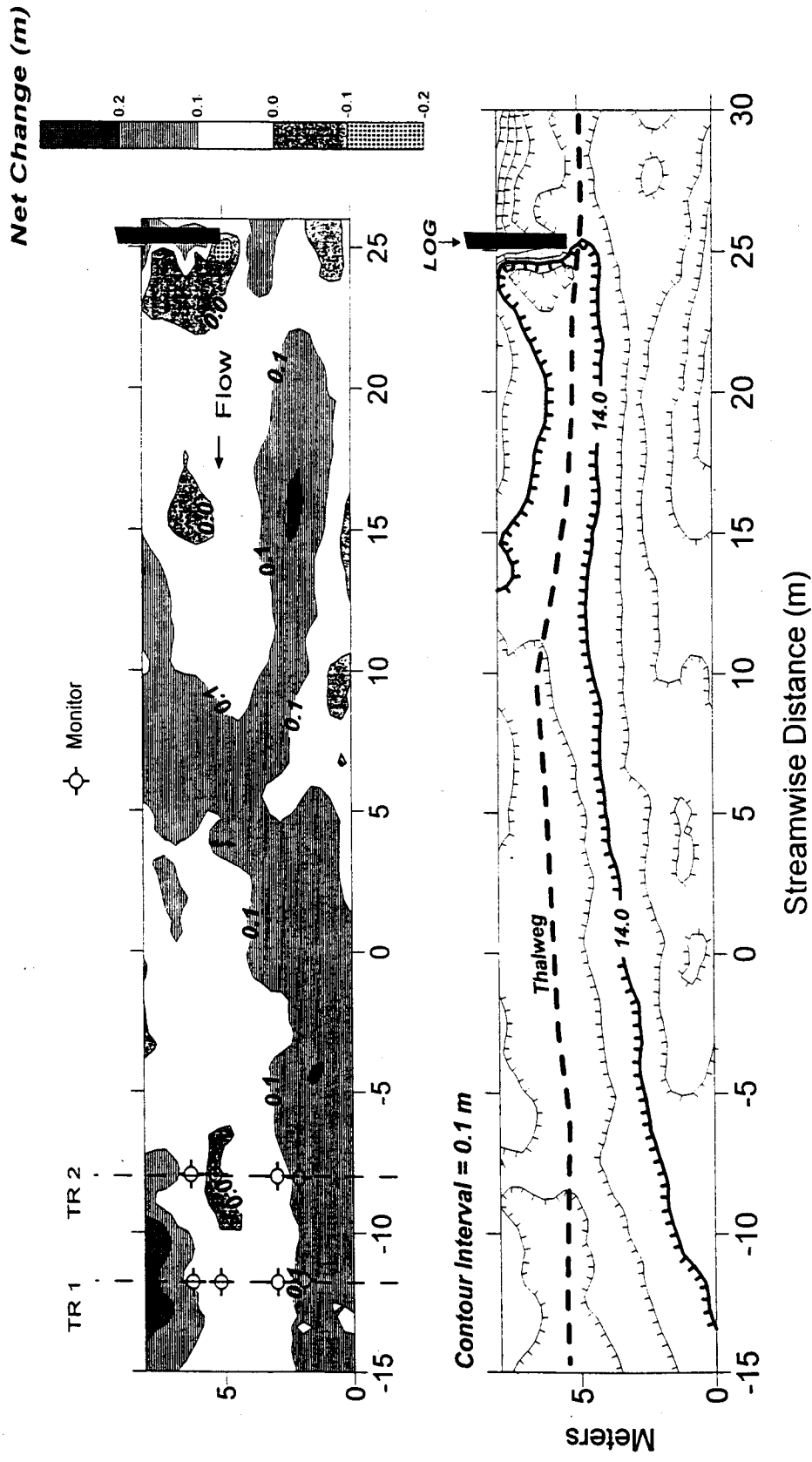
Figure 5-12. Net bed elevation changes in the Issaquah Creek study reach between 1996 and 1997 (top), and 1997 bed elevation contour plot (bottom).

Figure 5-13 shows that the North Fork Stillaguamish River reach at the USGS gage experienced net excavation scour over some areas of the channel bed and net fill over others. The reach as a whole experienced minor net fill that averaged 0.009 m. Scour along the upstream half of the thalweg appeared to be balanced by fill further downstream and on the right-side (looking downstream) bar. However, less can be inferred from the topographic survey of this site compared to the other sites because the surveyed reach was short relative to the channel width (approximately 2 channel widths long).

Figure 5-14 shows that the North Fork Stillaguamish River reach at Hazel experienced net excavation scour over most of the channel bottom area, where the bed elevation dropped an average of 0.025 m over the area surveyed. A smaller area of the bed filled in the vicinity of a pool formed by a debris jam when the jam washed out during one flood. A large maple tree subsequently fell into the channel immediately downstream of the jam location and caused local fill upstream and downstream of it. The maple also caused erosion further out in the channel and formation of a secondary thalweg around its periphery. The maple tree disappeared the next fall, and the reach continued to experience net scour in subsequent flood seasons (1997-98 and 1998-99) as evidenced by noticeable erosion around small, isolated clumps of in-channel riparian vegetation located about 100 meters downstream of the reach. The bed appeared to have degraded around the vegetation clumps at a rate of around 0.06 to 0.08 m per year.

Figure 5-15 shows that the two riffles in the Raging River reach each experienced net excavation scour of a similar magnitude. The bed elevation dropped an average of 0.052 m over the area surveyed most intensively. Coarser resolution surveying within the intervening length of stream indicated some fill had occurred in association with a bar deposit forming along the left bank of the low gradient cascade unit (see Figure A-8).

Figure 5-16 shows that the thalweg region of both riffles in the South Fork Snoqualmie River reach experienced net excavation scour. The bed elevation dropped an average of 0.069 m over the lower riffle area. Although the bed rose an average of 0.007 m in the upper riffle, fill occurred there primarily over the right half of the channel,
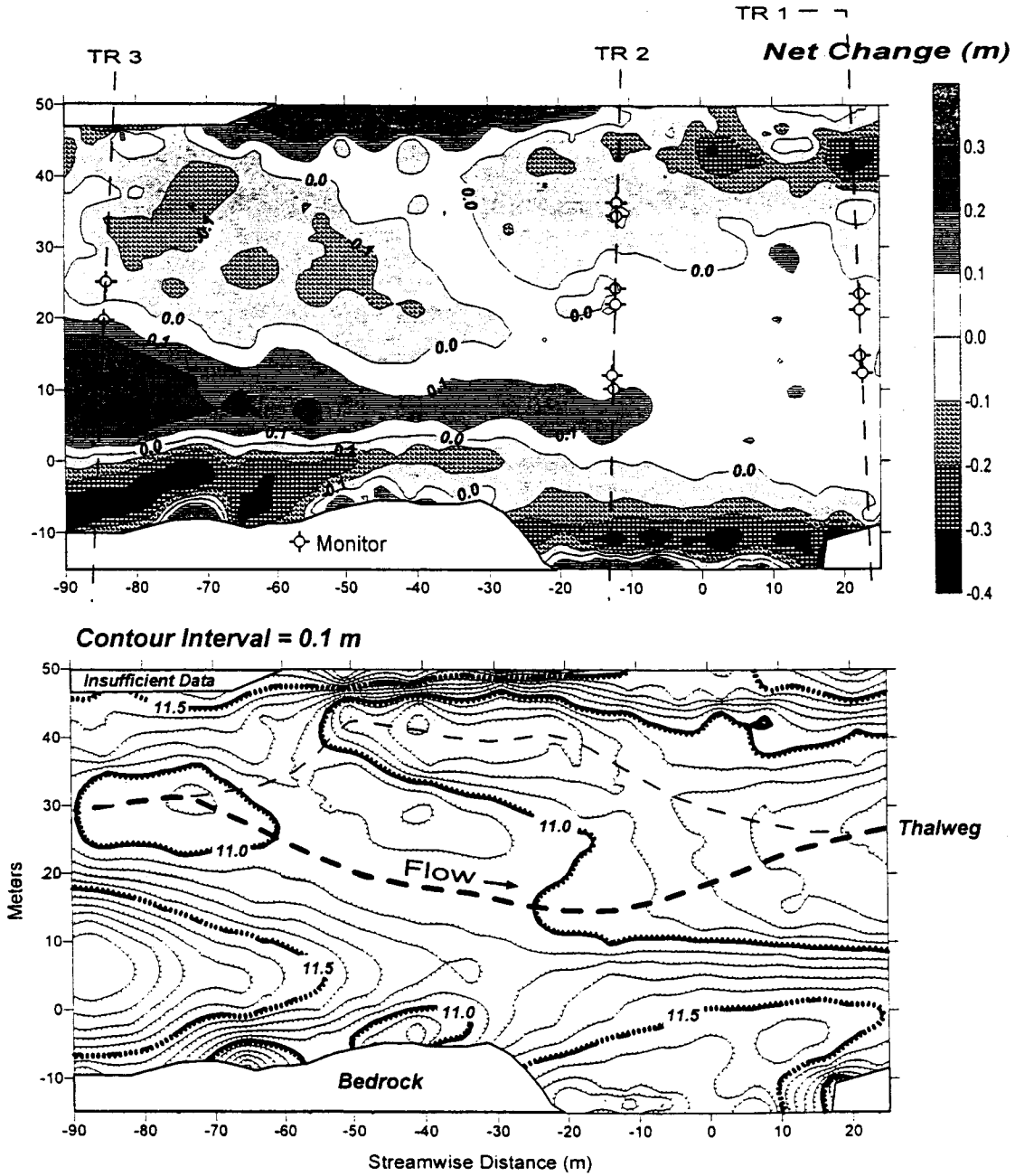
Figure 5-13. Net bed elevation changes in the North Fork Stillaguamish River at the USGS gage study reach between 1996 and 1997 (top), and 1997 bed elevation contour plot (bottom).
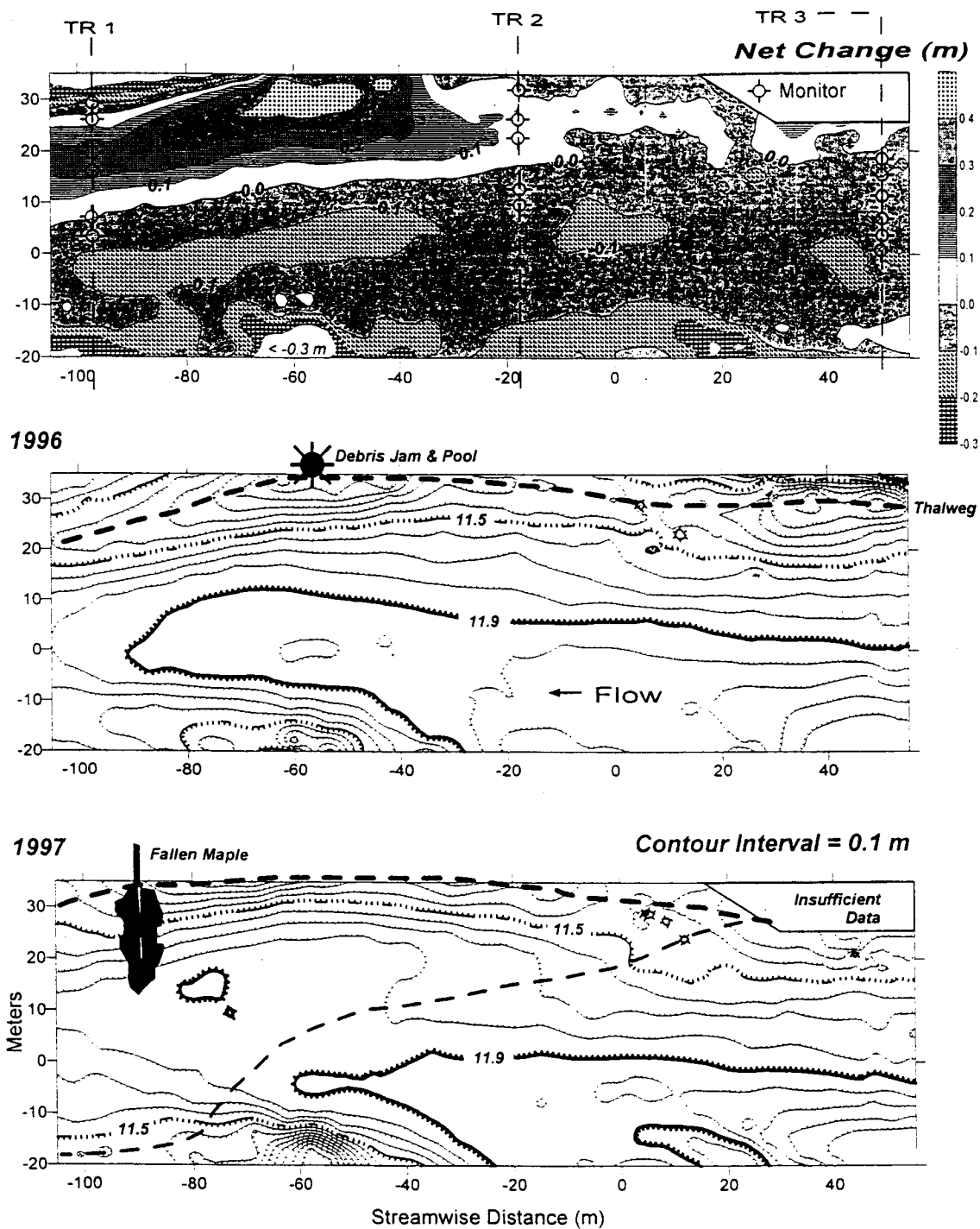
Figure 5-14. Net bed elevation changes in the North Fork Stillaguamish River at Hazel study reach between 1996 and 1997 (top), and 1996 (middle) and 1997 bed elevation contour plots (bottom).
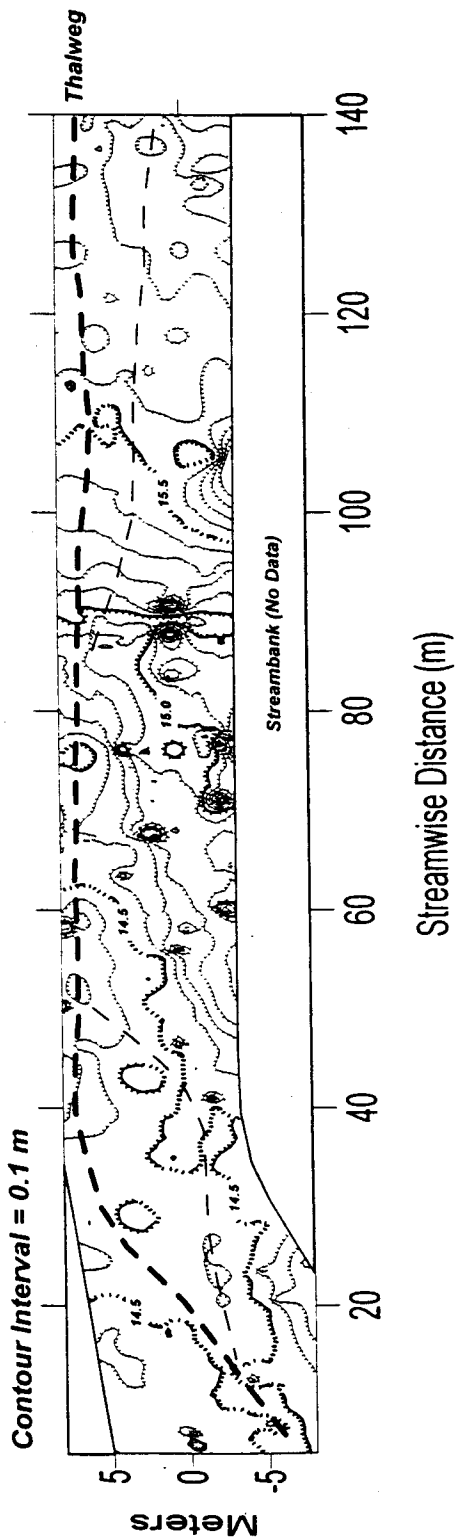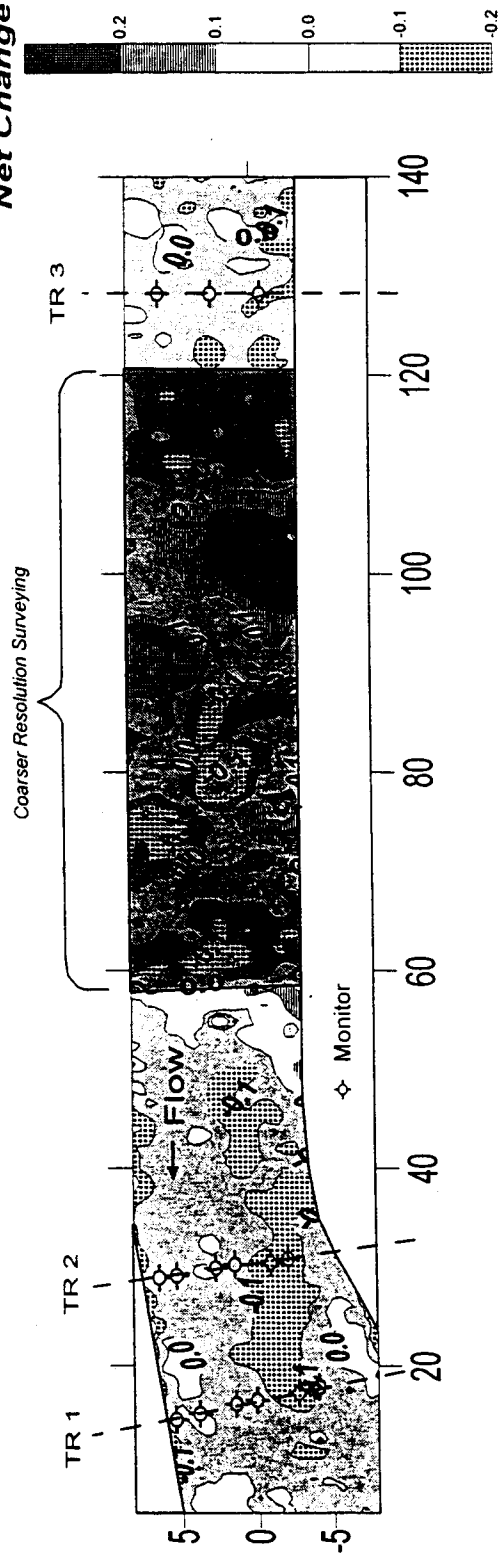
Figure 5-15. Net bed elevation changes in the Raging River study reach between 1996 and 1997 (top), and 1997 bed elevation contour plot (bottom).

190
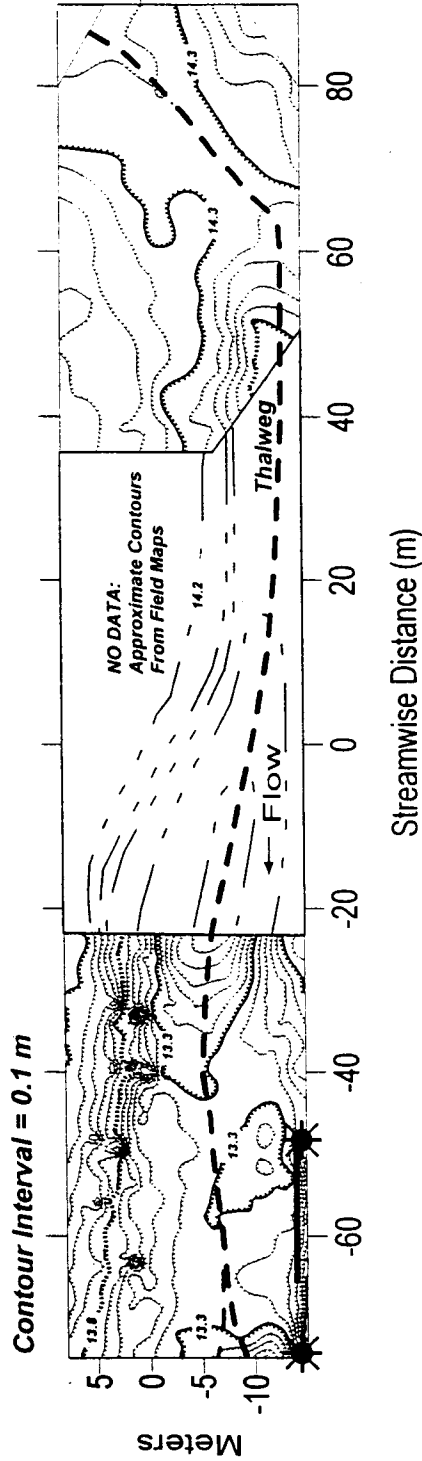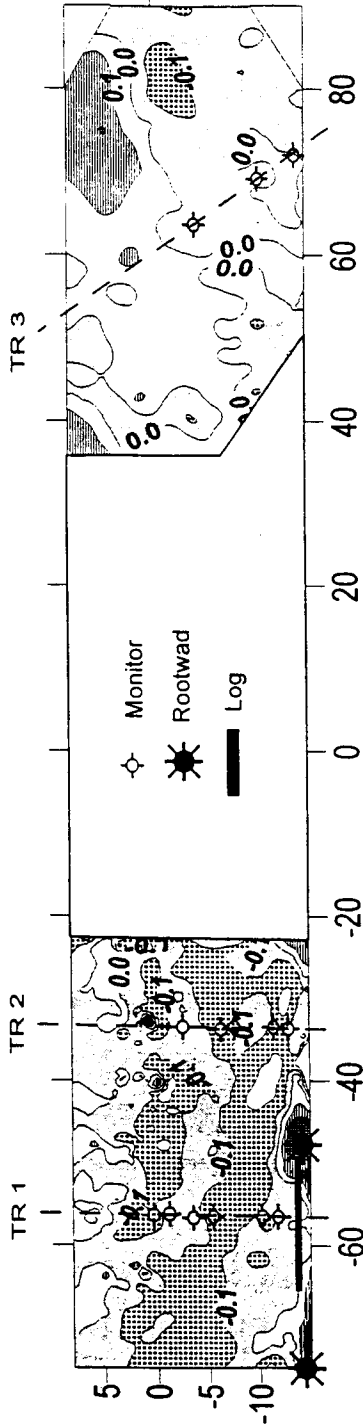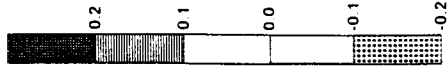
Figure 5-16. Net bed elevation changes in the South Fork Snoqualmie River study reach between 1996 and 1997 (top), and 1997 bed elevation contour plot (bottom).

in a relatively shallow area. The bed elevation dropped approximately 0.035 m on average over the left half of the channel.

A large tree was scoured out and fell into the middle of the channel upstream of the Squire Creek reach, resulting in the rapid erosion of the right bank and of a large bar deposit located on the left bank, and subsequent introduction of substantial quantities of gravel and cobble to the study reach. Figure 5-17 shows that the reach experienced net fill, and most of the scour monitors were buried by the spring of 1997 as a result. The bed elevation rose 0.106 m on average. The mid-channel bar depicted in the lower left corner of the bottom contour plot formed around the downstream end of the fallen tree. The scour monitors were recovered the following year as the gravel and cobble slug dispersed downstream and the bed degraded again.

In all of these cases, except the North Fork Stillaguamish River reach at the USGS gage (which was probably too short to infer anything), net excavation or net fill occurred over a distance that was as long as, or longer than, the study reach. The topographic and scour monitor data indicate that the rate at which the average elevation of the more active areas of the channel bed changed was approximately ±0.1 m per year or less in the study reaches. The cause could not be identified conclusively for all sites using the available data, but was more likely associated with temporal and spatial variation in sediment supply to the channel than with the pool-riffle scour and fill dynamics described in Section 5.1. This is because the six reaches described above contained relatively large quantities of gravel and cobble such that local sediment transport rate imbalances of the form influencing scour and fill in the pool-riffle interface could not have developed over most of the reach area.

It is plausible that the observed reach-scale variation reflected slugs or pulses of sediment that could have originated from a tributary, from a landslide or debris flow, or from localized channel avulsion or bank erosion (Nicholas et al. 1995; Beechie 1998; Wathen and Hoey 1998). As such, the slugs represent a temporary change in supply relative to transport capacity, which may be the way in which a transport rate imbalance is induced. In Squire Creek, the sediment pulse appeared to have originated from local
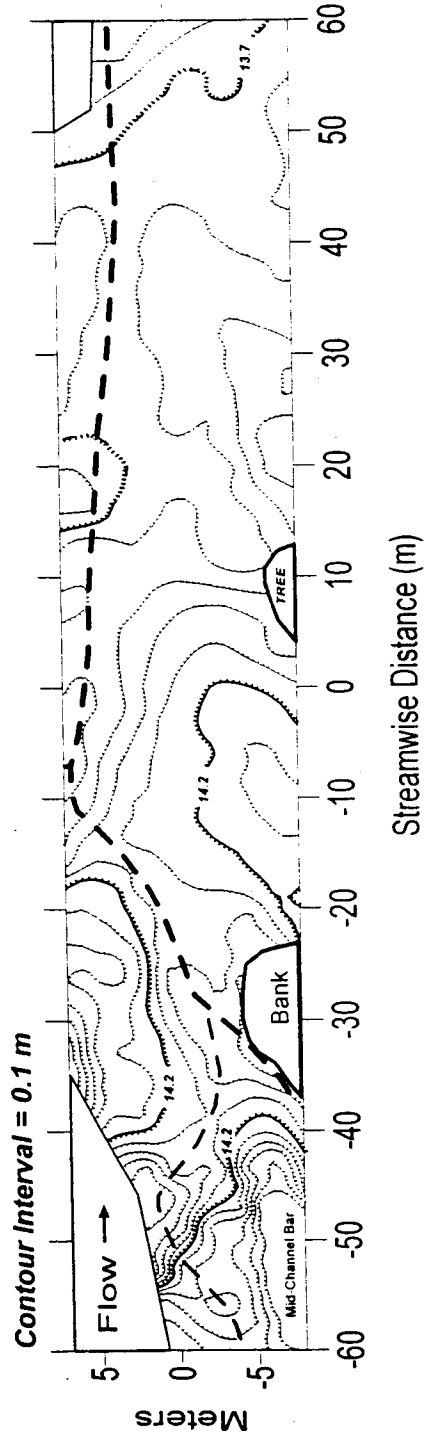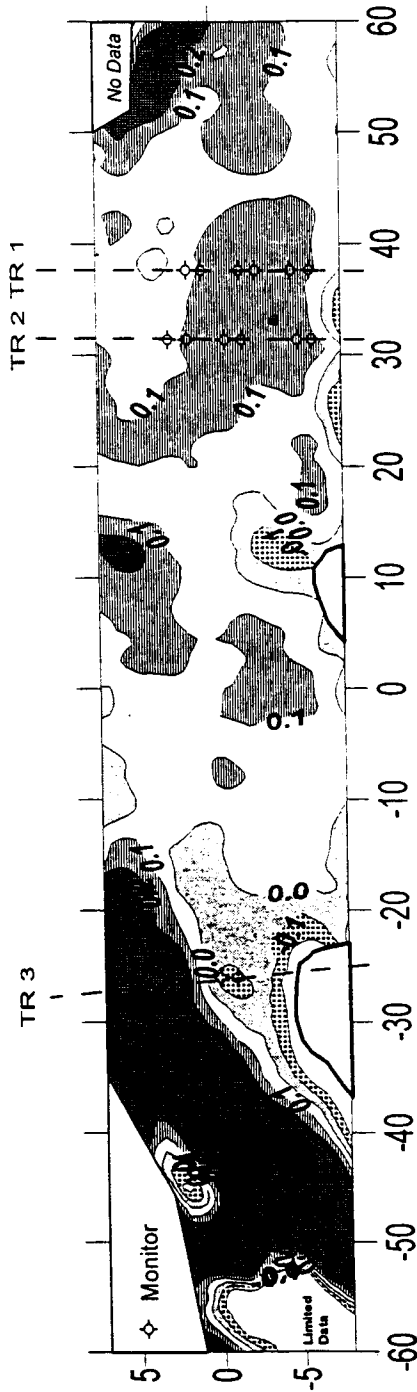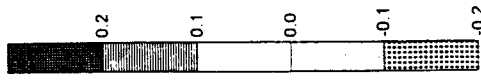
Figure 5-17. Net bed elevation changes in the Squire Creek study reach between 1996 and 1997 (top), and 1997 bed elevation contour plot (bottom).

bank erosion, extended over a short distance (about 200 meters), and dispersed downstream relatively quickly (in about two years). Larger sediment slugs may have been present in the other streams based on the length of reach affected. Large scale introductions of sediment have resulted in pulses that extended over distances of several thousand meters and more in other streams (Nicholas et al. 1995; Lisle et al. 2000).

Reaches experiencing sediment pulses may be associated with riffle deposits that experience net fill (aggradation) throughout their length as a pulse approaches from upstream or is introduced locally, followed by net excavation scour (degradation) as it disperses, analogous to the ascending and descending limbs of a wave. The magnitude of excavation depends on the sediment pulse amplitude, wavelength, celerity, and diffusion coefficient (Lisle et al. 1997; 2000). A detailed evaluation of these factors appears to be critical to predicting net excavation scour depth in riffles but is beyond the scope of this dissertation. The data indicate that they could be important influences on net excavation scour depth and salmonid intragravel survival.

5.3 Summary of Net Excavation Scour Mechanisms Likely to Influence Survival

The data collected in this study suggest that net excavation scour at salmonid redd locations is associated with sediment transport rate imbalances that occur over varying spatial and temporal scales. The imbalances appear to be related to (i) the spatial discontinuity in gravel and cobble distributions inherent in pool-riffle morphology, and (ii) temporal changes in sediment supply to the channel relative to its transport capacity. Deepest scour depths in this study were associated with the first mechanism. Temporal changes in supply may result in temporary aggradation or degradation throughout a riffle, but the data and inferences about bedload transport processes suggest that associated net excavation scour depths are less severe with respect to salmonid intragravel survival than scour depths linked with pool-riffle maintenance mechanisms.

I infer from the results in this chapter that when gravel and cobble are abundant in a low gradient reach, redd locations in the pool tail region and downstream in the riffle are

unlikely to experience significant local sediment transport rate imbalances related to pool-riffle dynamics because the location receives material excavated from upstream in the same deposit. This protection against deep scour likely diminishes as the reach becomes supply-poor, where the distance to the immediate upstream riffle becomes greater than a certain threshold value such that the entire riffle can experience deep scour and fill, as occurred in the Tolt River site. The magnitude of this threshold distance needs to be determined in future work, but may reflect the observation that pool-riffle spacing in alluvial channels is generally five to seven channel widths in magnitude (Leopold et al. 1995). Assuming this characteristic represents an approximate state of equilibrium at the pool-riffle scale in low gradient alluvial channels, longer spacing may be associated with an increased area of the pool tail and riffle that scours and fills. The risk to embryos of scouring would then increase with pool and riffle spacing. This hypothesis could be evaluated by measuring spatial scour depth distributions in different riffles over a range of riffle-to-riffle spacings.

Less is known about characteristic magnitudes of net excavation scour depth associated with temporal changes in supply. This is because the mechanism of dispersal is not well understood, the supply changes can occur over a wide range of spatial scales, and because there are relatively few scour depth data available that have been linked directly to this process. The data collected as a part of this work suggest that the magnitude is on the order of 0.1 m per year or less in the study streams, but it remains to be determined whether this is characteristic of other streams as well. Redds constructed on a sediment slug, pulse, or wave are hypothesized to have a higher likelihood of being influenced by scour than redds constructed in the same reach when the pulse is absent, because the additional sediment may disperse and translate downstream, resulting in bed degradation (Lisle et al. 2000). The rise and fall in bed elevations observed over a several year period in some of the study streams suggests that when the pulse is well defined, redds constructed further upstream on the pulse may be influenced by deeper net excavation scour than redds constructed downstream. Additional field research is needed to explore these possibilities.

6.0 Implications for Salmonid Spawning and Intragravel Survival

Salmonid embryo survival could be more influenced by scour and other physical changes to the streambed than the early life stage survival of other riverine fish species because of their relatively protracted intragravel residence time. Scour-induced mortality to this phase of the salmonid life cycle could limit population size directly if the substrate is excavated to, or mobilized at, the depth of developing embryos (McNeil 1966; Seegrist and Gard 1972; Erman et al. 1988; Lisle 1989; Kondolf et al. 1991). Scour also facilitates and accelerates fine sediment intrusion (Lisle 1989; Scrivener and Brownlee 1989) and may thus influence survival indirectly because increased concentrations of fine sediments in redds are linked to decreased survival to emergence (Chapman and McLeod 1987).

Several studies have compared estimates of egg-to-fry survival or smolt production with peak flow rate during the incubation period, and have correlated larger floods with lower apparent survival rates (e.g., Lister and Walker 1966; Thorne and Ames 1987; Scrivener and Brownlee 1989; Seiler and Kishimoto 1997; Seiler et al. 1998; Seiler 1999). Gangmark and Bakkala (1960) noted that adult chinook salmon returns were smaller for year classes that experienced heavy freshets during the incubation life history stage. Stober et al. (1978a; 1978b) found fewer eggs and embryos within the gravel after floods than before. These observers inferred that direct scour effects were the primary mortality mechanism, but coincident egg burial depth and scour depth data were unavailable for confirmation. Stober et al.'s sampling efficiency may have been compromised by fill and difficult instream working conditions. The inference appeared reasonable considering that only a small fraction of the eggs laid by a female salmonid typically emerge from the gravel as fry (e.g., 4 percent on average in the studies of Gangmark and Bakkala, 1960), and washed out eggs and embryos have been found after floods (e.g., Hutchison and Shuman 1942; Withler 1952; Gangmark and Bakkala 1960; McNeil 1966; Elliot 1976). It remains to be confirmed, however, whether scour mechanisms represent a significant direct source of intragravel mortality in low gradient ($S \leq 0.01$) gravel bed streams, or influence survival

indirectly through other processes.

This chapter integrates the results of the previous chapters to address this issue. This work has obtained direct information and data regarding scour and bedload transport processes that permit closer inspection than before of linkages between scour and salmonid reproductive behavior and intragravel survival. A number of hypotheses and interpretations that were plausible given available data and information on scour depths and processes at the time are reexamined. Several are supported by this work, and revised or alternate interpretations are proposed for several others. I argue that the primary mechanism of scour-induced mortality of the intragravel life stage in low gradient gravel bed streams is more likely to be expressed through indirect effects such as fine sediment intrusion, rather than through direct, mechanical washing out or crushing of embryos.

6.1 General Relations Between Scour and Salmonids

Great significance has been attributed in the literature to the potential influences of scour on salmonid individual and population-level adaptations. There appear to be six reproductive strategies that salmonids are most likely to display in response to scour influences that could represent adaptations to selective pressures:

(I) Selection and modification of substrate characteristics influencing local bed stability;

(II) Redd form topography influencing bed stability;

(III) Egg burial depth;

(IV) Redd location in the channel at the geomorphic unit (i.e., pool-riffle) scale;

(V) Redd location in the channel network; and

(VI) Timing of spawning.

Spawning of multiple age classes and repeat spawning by iteroparous species also represent potential reproductive strategies. Almost all salmonid species exhibit one or both, with the exception of pink salmon (*O. gorbuscha*). These features represent a degree of resiliency to the effects of scour because reproductive effort is spread out over

more than one year, increasing the odds of reproductive success. These strategies are likely to be evolutionary adaptations to the gravel bed stream environment in general, where disturbance is a characteristic ecological feature experienced by all life stages (Resh et al. 1988), rather than to mechanical scouring per se.

The six strategies listed above are most likely to be important when populations are smaller in size and thus more vulnerable to adverse influences on reproductive success. The results presented in Chapters 4 and 5 are pertinent to the first four strategies. The fifth and sixth strategies are not addressed here since the data collected as part of this work are restricted to gravel bed streams with gradients of 0.01 and less. More and better scour data are needed from higher gradient streams to address the issues of redd location in the channel network and reproductive timing.

6.2 Redd Substrate Characteristics, Redd Morphology, and Bed Stability

Physical changes to the streambed structure and topography caused by spawning activity are thought to contribute to a lower probability of disturbance and scour through surface coarsening and sheltering of the bed from higher shear stresses by redd bedforms (Montgomery et al. 1996). Coarsening occurs because smaller particles are washed downstream and larger particles remain as the female constructs the redd. Coarsening increases resistance to motion because the mean size of the mixture increases. Sheltering by bedforms (often referred to as "form drag"; e.g., Nelson and Smith 1989) may help reduce the magnitude of mobilizing forces acting on grains. The results of my work indicate that such benefits are restricted predominantly to the condition of incipient motion, and scouring of embryos should not occur if the larger particles situated above and around them are not mobilized by a flood. The benefits afforded by either coarsening, or bedform drag, appear to be lost once the larger member particles in the bed are mobilized.

It has been shown here and by Wilcock et al. (1996) that the bed can be mobilized to the base of the armor layer at relatively low dimensionless shear stresses ($\tau_g^* \approx 0.035$), and

that the maximum depth of scour due to moving bedload is a function of the bed grain size distribution and is equal to approximately $2D_{90}$. Although the grain size distribution in the redd is coarser than the surrounding bed (Kondolf et al. 1993), the largest particles in the redd are similar in size to the largest particles in the surrounding bed. It is likely that such particles move in the redd once the flow is strong enough to move them in the surrounding bed. The maximum depth of scour is thus expected to be similar in the two locations, and scour depth data collected by Rennie (1998) support this conjecture. Moreover, salmonid embryos appear to be buried well below the elevation of the base of the armor layer in general (Section 6.3), which should protect them from scour during conditions of incipient motion and partial transport when not all members of the bed surface are mobilized. Hence, processes controlling incipient motion of the armor layer do not appear to be representative of processes controlling the eventual scour depth. It is when the largest particles are mobilized in the spawning bed armor layer that scour should begin to be a potential direct or indirect influence on the intragravel survival of embryos and fry.

Redd construction could increase the probability of incipient motion of the coarser surface particles remaining in the redd compared to that of similarly-sized particles in the surrounding, undisturbed bed, because the bed is loosened (Montgomery et al. 1996) and the number of frictional contact points are reduced as the substrate is cleaned of finer particles. The shear stresses required to mobilize a granular layer can be smaller for a more sorted mixture than for a less sorted mixture because there are fewer frictional contact points between particles in the better sorted mixture (redd superimposition appears to take advantage of this feature: redds can be constructed more easily in the cleaned out, looser substrate).

Post-spawning reinfiltration of fines, particularly particles smaller than pea gravel, returns the egg pocket environment to approximately pre-spawning conditions. The rate can be gradual (Peterson and Quinn 1996) or rapid (Kondolf et al. 1993) depending on flood and sediment transport characteristics. This process acts to reverse the influence of substrate coarsening or cleaning (Kondolf et al. 1993), and can happen during relatively small floods because the reinfiltrating particles are mobilized more completely at lower

shear stresses than the larger particles that constitute the bed framework (Wilcock and McArdell 1997). It remains to be determined how quickly the stability of the bed is influenced.

Alteration of the substrate grain size distribution during redd construction may protect embryos from scour in another way that is unrelated to surface coarsening and its effects on incipient motion. The coarsest particles remaining in the egg pocket centrum (Chapman 1988) may not move during intense bedload transport because they have settled in elevation during redd construction and can be embedded partially in an immobile, lower layer. Smaller, surrounding particles may be entrained, but the embedded particles can be held in place by a large number of frictional contact points as long as the net friction angle with other immobile particles is sufficient to prevent their motion. Embryos may thereby be protected against bedload transport-induced mortality because the eggs settle to the base of the larger particles forming the egg pocket centrum (Vronskii 1972; Chapman 1988). Salmonids may therefore take advantage of the thin-layer nature of the sediment transport mechanism in heterogeneous coarse beds by lowering the elevation of the largest stones in the egg pocket during redd construction so they can be anchored in place by the undisturbed subsurface layer.

Benefits attributed to redd bedform drag appear to be temporary, because the redd topography smooths out in floods and it is unusual to find distinct remnants of its morphologic footprint afterwards. This occurs because the tailspill is exposed to the highest shear stresses, material is transported away and not replaced, and the tailspill surface elevation subsequently lowers (Hobbs 1937; Stuart 1953; Rennie 1998). The pits are zones of flow separation and thus should fill relatively quickly upon the initiation of bedload transport. The fill material may be relatively fine at first, but eventually it will be replaced by larger particles that arrive intermittently and that are less likely to move until the entire surrounding bed is mobilized. A similar argument can be applied to the case where bedform drag is promoted by concentrated spawning activity of large numbers of adults. As for bed coarsening, the primary influence of redd topography in both instances appears to be a temporary increased resistance to initial motion. The resistance should

decrease during a flood as the bedforms disappear, and grain size, location in the channel, and reach-scale gravel and cobble distributions likely influence scour depth more than the initial bed state. The benefits of redd surface topography therefore appear to be temporary and may primarily reflect other influences on intragravel survival such as water exchange (Vaux 1962; Alonso et al. 1988), and flow separation keeping deposited eggs within the pit until they are fertilized and buried.

The thin-layer nature of bedload transport indicated in this study has other biological implications with respect to redd construction. Methods involving the use of the caudal fin to lift particles through suction, or physically sweep and push particles downstream, are unlikely to be primary redd construction techniques because they use considerable energy and relatively little effective work is done on the bed. Moreover, it would not take very long before the tail is ground to a stub in the case of sweeping or pushing. Spawning salmonids have a fixed amount of energy reserves available, which can be critical for salmon and steelhead that migrate from several hundred to more than a thousand kilometers to reach their spawning grounds. It is likely that they excavate their redds as efficiently as possible, using the excavation mechanism proposed below.

Salmonids usually can excavate their redds only a few stones at a time. It can be inferred from the results of Chapter 4 that this is due to the larger shear stresses required to mobilize a heterogeneous sediment mixture. A spawning female must first remove smaller particles before a larger particle can be broken free. The largest particles forming the egg pocket centrum are probably too large for the fish to move effectively. Next to substrate size and bed morphology, the redd location and egg depths reflect the water velocity at the time of spawning, which falls within a characteristic range for each species (Bovee 1978; Bjornn and Reiser 1991; DeVries 1997). The apparent reason is that salmonids have evolved to take maximum advantage of their spawning environment and are efficient 'hydraulic miners'. In digging, they appear to use their body and tail to redirect and accelerate higher momentum fluid from the rapidly moving water column down towards the bed. The resulting directed flow and vortices rapidly and effectively scour away first the smaller particles and then the larger particles, with minimal effort on

the part of the fish, and influence final redd configuration (Tautz and Groot 1975). There should be an increased advantage with velocity that is eventually offset by the increased energy demand for a fish to remain in place over the redd, resulting in observed velocity utilization patterns where larger fish can use faster water for spawning (Beamish 1978; Webb 1978; Bovee 1978; Beland et al. 1982). It follows that a salmonid could construct a redd without physically touching the bed surface, and it would be interesting to see in the field if the condition of the caudal fin and peduncle improves with depth of water over the redd, when the fish becomes less constrained by the water surface boundary (after factoring out substrate size and velocity as co-variates).

6.3 Egg Burial Depths and Location of Redd in a Channel Reach

The depth to which salmonid eggs are buried influences survival to emergence as fry directly because embryos located at shallower depths are at greater risk of being influenced by bedload transport and intruding sediments than deeper buried embryos (Lisle 1989). This risk may be reduced during later stages of development, when alevins are capable of moving downwards in the gravel after hatching in response to agitation and other cues (Bams 1969; Dill 1969; Dill and Northcote 1970; Fast et al. 1981), but for a fixed amount of time the embryos are vulnerable to mechanical scouring. Montgomery et al. (1996) measured scour depths throughout a reach of Kennedy Creek, a small Puget Sound stream, and determined that the scour depths were generally shallower than, or near the smaller values of, depths to the top of chum salmon (*Oncorhynchus keta*) egg pockets during frequent, bankfull flows. It was proposed that the egg burial depths reflected an adaptation to typical scour depths occurring in that stream, and that this was an adaptive mechanism characteristic of salmonids in general. Data collected here and in other studies suggest the basis for such a mechanism, as described below.

Published egg burial depth data exhibit a wide range, even for a single species (DeVries 1997). Sources of variation include differences in measurement methodology, spawning behavior, microhabitat selection, fish size, the presence of excavation barriers,

and the occurrence of unmeasured scour or fill. Differences in measurement methodology and elevation datum are particularly significant sources of variation. For purposes of scour assessments, the depth from the original bed elevation down to the top of the main egg pocket(s) is a critical parameter that determines the threshold of significant scour impacts. This measure of egg burial depth can be scaled by the substrate D_{90} to compare with dimensionless bedload disturbance and net excavation scour depth data.

Egg burial depth data described in DeVries (1997) were examined accordingly and, where possible, compared against the substrate D_{90} present either prior to redd construction, adjacent to the redd site, or of the redd itself. Few of the documents reviewed provided the requisite information directly. In some cases, only the finer half to three-quarters of the grain size distribution was presented, and the D_{90} was estimated by extrapolating the cumulative distribution on log-log plots. In other cases, the D_{90} was approximated by extrapolating from nearby quantiles (e.g. D_{84}, D_{100}), or in a few instances as the size for which the 'majority' of particles were reported as being smaller than. I estimate that the approximations are within ±20% of the correct value, based on analogous extrapolations of substrate grain size data measured here and in several of the reports. The estimated D_{90} values are presented with relevant egg burial depth information in Table 6-1. Included is an observation from Issaquah Creek, where a pair of spawning chinook salmon disturbed two scour monitors that were located at the tail end of the redd; the egg burial depth reported for Issaquah Creek in Table 6-1 is an underestimate because the eggs almost certainly settled to a lower elevation than that indicated by the scour monitor balls.

Table 6-1 shows that the shallowest eggs and egg pockets were generally buried at a depth that was $2D_{90}$ or greater below the original bed surface elevation. Eggs were buried approximately $3.7D_{90}$ on average. Values where egg depths were reported relative to the overlying gravel datum are likely to be underestimates of egg depth relative to the original streambed elevation (cf. bottom of Table 6-1; Figure 2 in DeVries 1997; Steen and Quinn 1999). The two egg depth-to-D_{90} ratios in Table 6-1 that are less than 2.0 were probably influenced by this bias. Furthermore, the lowest ratio (1.4) was based on a D_{90} estimated

Table 6-1. Ratio of egg burial depths reported in the literature to estimated D_{90} of spawning substrates.

Species/ Author(s)	Datum [i]	Portion of Pocket [i]	Egg Depth (mm) Mean	Egg Depth (mm) Shallowest	D_{90} (mm)	Egg Depth/D_{90} Mean	Egg Depth/D_{90} Shallowest Eggs
Brown Trout							
Hobbs (1940)	Original Level	Discrete Eggs	200	200	64		3.1
Hobbs (1937)	Original Level	Top	200		64	3.1	
Reiser and Wesche (1977)	Overlying Gravel	Discrete Eggs	105		64	1.6	
Witzel and MacCrimmon (1983)	Overlying Gravel	Discrete Eggs		130	43		3.0
Grost et al. (1991)	Overlying Gravel	Discrete Eggs	110		46	2.4	
Grost et al. (1991)	Overlying Gravel	Discrete Eggs	120		46	2.6	
Grost et al. (1991)	Overlying Gravel	Top	90		46	2.0	
Bull Trout							
Shepard et al. (1984)	Overlying Gravel	Top		100	50		2.0
Chinook Salmon							
Hobbs (1937)	Original Level	Top		150	76		2.0
Hobbs (1937)	Original Level	Top		200	76		2.6
Vronskii (1972)	Overlying Gravel	Top	210		100	2.1	
Chapman et al. (1986)	Overlying Gravel	Top	190		135	1.4	
This Study (Issaquah Creek)	Original Level	Top		>150	83		>1.8
Chum Salmon							
Montgomery et al. (1996a)	Original Level	Top	230		50	4.6	
Cutthroat Trout							
Kiefling (1978)	Overlying Gravel	Top		150	64		2.3

204

Table 6-1. (continued).

Species/ Author(s)	Datum [i]	Portion of Pocket [i]	Egg Depth (mm) Mean	Egg Depth (mm) Shallowest	D_{90} (mm)	Egg Depth/D_{90} Mean	Egg Depth/D_{90} Shallowest Eggs
Dolly Varden Trout							
Blackett (1968)	Original Level	Top		150	50		3.0
Golden Trout							
Knapp and Vredenburg (1996)	Original Level	Bottom [ii]		40	20		2.0
Pink Salmon							
Rukhlov (1969)			320		100	3.2	
Rainbow Trout							
Hobbs (1937)	Original Level	Top	200		64	3.1	
Hooper (1973)	Original Level	Top	150		38	3.9	
Hobbs (1940)	Original Level	Discrete Eggs		390	130		3.0

Averages:		
Original Level	3.7	2.6
Overlying Gravel	2.0	2.5

i - See DeVries (1997)
ii - Assuming thin egg pocket

by extrapolating the cumulative grain size distribution from a lower percentile. The D_{90} would have been overestimated if the actual grain size distribution variance was smaller than assumed.

The egg depth-to-D_{90} ratios presented in Table 6-1 indicate that salmonids bury their eggs below the $2D_{90}$ zone that was shown in Chapter 4 to be influenced by bedload disturbance. This zone may be an intrinsic feature influencing scour depth in spawning beds, and probably represents the most significant selective pressure imposed by bedload transport processes on egg burial depth in low gradient ($S \leq 0.01$) gravel bed streams.

The ratios in Table 6-1 suggest that egg burial depths also include a 'buffer' zone that may be an adaptation to typical net excavation scour depths caused by reach scale sediment transport rate imbalances, integrated over the duration of the incubation period of 2 to 8 months (Scott and Crossman 1973; Groot and Margolis 1991). The average shallowest reported egg burial depths were estimated to be 2.6 times the local D_{90} (Table 6-1). The majority of total scour depth data measured in suitable spawning locations in this study were less than 2.5 times the local D_{90} (Figure 5-1), including in streams where net excavation scour occurred along the length of the reach. This approximate correspondence may be indicative of such an adaptation in the respective streams in which the egg burial depth data of Table 6-1 were collected. Studies in the future should measure egg burial depths, substrate size, and net excavation scour depth to evaluate this possibility further.

Table 6-1 and the results of Chapters 4 and 5 have significant implications. Most importantly, embryos in redds that are constructed in low gradient spawning beds do not appear to be vulnerable to deep scour when spawning-sized material is abundant in a reach, because there appears to be an approximate physical limit to scour depth that is imposed by the principle of mass conservation. This implication was first hinted at by Parker et al. (1982a), who proposed that eggs may be relatively safe from mechanical crushing mortality because the bed rarely mobilized below the surface layer in their flume experiments.

Furthermore, the data collected and reviewed here suggest that redds constructed in

low gradient spawning beds may not experience deep scour associated with typical temporal imbalances in reach-scale supply, if the annual rates of bed change observed in the study streams are representative of other streams with similar hydraulic and geomorphic processes. There is some indirect support for this in the literature. Although the height of a transient gravel pulse resulting from temporal variation in supply may frequently exceed 1 m, the wavelength is typically several orders of magnitude greater (Lisle et al. 2000) and the time between peak bed elevation and residual elevation as the pulse disperses may be at least several years and often longer (Nicholas et al. 1995; Beechie 1998). The magnitude of net excavation during each distinct incubation period is thus likely to be a fraction of the total height of the transient mass. Research is needed to identify characteristic rates at which streambed elevations drop as a transient mass of gravel disperses, in terms of meters per flood season and incubation period. The results can then be compared with the data in Table 6-1 to address this issue more thoroughly.

Given the apparent bounds on bedload disturbance depth (δ_{B_m} in Equations 1.1 and 4.2), the principle of natural selection predicts that the redd location should be where net excavation scour (δ_{EX}) is most likely to be negligible. Salmonids spawning in gravel bed streams possessing slopes similar to the study streams (i.e., $S \leq 0.01$) typically spawn in reaches where gravel and/or small cobble are present in abundance, and particularly in riffles and in the pool tail region (Figure 4-13) where the bulk of regularly transported bed framework material is stored. These locations are suggested by this work to experience relatively small net excavation scour depths because sufficient 'buffer' material is stored at the upstream edge of the deposit (i.e., in the pool edge region) to offset the bedload transport rate occurring at the redd location until new material arrives at a similar rate from the immediate upstream deposit.

Within the same streams, areas of the bed where total scour depths are most likely to exceed $2.5D_{90}$ are indicated by this work to include the pool edge region (Figure 4-13; Figure 5-2), locally fine and transient bar deposits, and riffles that are relatively short in length and infrequent in longitudinal spacing. It has been my experience that salmonids generally do not build redds in these locations unless population size is so large that fish

are spawning virtually everywhere in the channel and there is extensive competition for redd sites. Some fish may then be forced to use less desirable locations after encountering more aggressive redd defenders. In those circumstances, redds constructed in the less suitable locations are more susceptible to scour (e.g., in the transient bar deposits adjacent to flow obstructions that were observed by Schuett-Hames et al. 1999), but it is debatable whether this could have a significant influence on reproductive success overall given large escapement numbers.

Another, significant implication of this work is that scour depths in low gradient spawning reaches are influenced more strongly by sediment supply and distribution characteristics than by flow strength. Hence, flood magnitudes, duration, or frequency may have a negligible influence on direct scour mortality, whereas patterns in, and changes to, sediment supply and distribution within the spawning reach are likely to be critical influences on scour depth and survival.

6.3.1 *Female Size and Scour Survival*

Commercial and sport fisheries have helped reduce the average size of anadromous salmonids because there has been a historic trend of selectively catching larger and older fish (Ricker et al. 1978; Wright 1999). Reduced body size affects survival negatively for a number of reasons unrelated to scour. Evidence that smaller fish bury their eggs at shallower depths than larger fish has been used to infer that smaller members of a spawning population are also more susceptible to scour-induced mortality than larger fish (van den Berghe and Gross 1984; Holtby and Healey 1986; Tripp and Poulin 1986; Scrivener and Brownlee 1989; Kitano and Shimazaki 1995; DeVries 1997; Steen and Quinn 1999). However, direct evidence remains to be collected that includes long term, concurrent data describing egg burial depth, fish size, substrate size, and scour depth at redd locations.

A selective scour-based pressure against smaller females would require at least two conditions to be met, including (i) that a characteristic scour depth exists initially that is

less than the mean egg burial depth achieved by the smaller females; and (ii) that the characteristic scour depth increases just enough to reach the offspring of smaller females but not enough to reach the offspring of larger females. The scour depth data collected here and Table 6-1 suggest that the smaller-bodied members of a spawning population also bury their eggs below $2D_{90}$, and possibly $2.5D_{90}$, such that the first condition could be true in general.

There is no evidence that the second condition is met in low gradient gravel bed streams. A phenotypic pressure against smaller females is not exhibited when they contribute annually to escapement. If they were more susceptible to scour, there should be evidence of predominantly larger females returning to spawn from brood years experiencing larger magnitude floods; I am unaware of any such published evidence. The results of this work suggest that redd location and the thin-layer nature of bedload transport in low gradient gravel bed streams may act to protect the offspring of smaller females from scour as well as the offspring of larger females. If there is any advantage to size, it appears to act through other ways.

Additional data are needed before it is possible to conclude that there is a phenotypic relationship between fish size, egg burial depth, and survival. The results of this work indicate the need to collect and evaluate concurrently: (i) frequency distributions of egg depths relative to the original bed elevation, (ii) frequency distributions of total scour depth, net excavation scour depth, net fill depth, and maximum bedload layer thickness at spawning locations (and not elsewhere in the reach); (iii) grain size distributions; (iv) female size data; (v) data representing the location of the redd and scour monitors relative to channel morphology; and (vi) data describing the reach-scale abundance of spawning-sized substrates.

6.4 Scour and Fine Sediment Intrusion

The suitability of spawning habitat is obviously not contingent on stability alone. Another important influence is spawning substrate quality, which is characterized primarily

by the size of the substrate framework where the embryos live, and by the degree to which the spaces within the substrate framework are filled by fine sediments (Carling and McCahon 1985). The best substrate frameworks for salmonids comprise gravel and small cobble, the mix varying with species (Kondolf and Wolman 1993). Redd construction activity results in the removal of fine sediments from the spaces of the framework. The rate and amounts at which fine sediments intrude back into a newly cleaned redd are of interest because if they are too high, permeability may be reduced or the fry become physically entombed (Chapman and McLeod 1987; Chapman 1988). The finer sediments influence permeability and exchange of oxygen and metabolic waste products across the embryonic surface, while coarser sediments are more responsible for entrapment (Everest et al. 1987; Alonso et al. 1988; Scrivener and Brownlee 1989).

Sediment deposition and intrusion processes into clean gravel substrates are well known. At low water discharges, the suspended load infiltrates into the gravel matrix at a rate that is directly proportional to the suspended sediment concentration. This material is sufficiently fine that it will infiltrate to the bottom of an excavated redd and fill the voids of the substrate from the bottom up to the bed surface. The concentration of suspended sediments is generally small during low flow periods in gravel bed streams. At higher discharges sand-sized materials begin moving and infiltrate into the gravel matrix until they are impeded by small crevices or bridging, and form a drape. Sand moves at relatively low flows while the rest of the bed is immobile: for example, sand was observed to nearly fill several excavated holes in the North Fork Stillaguamish River within one week during early fall when dimensionless shear stresses were on the order of $\tau^* \approx 0.03$ (based on untruncated grain size distribution) and $\tau^*_g \approx 0.02$ (grain size distribution truncated at 8 mm). A progressive filtering of finer material occurs until a sand-silt seal is created. The depth at which the seal forms depends on several factors including the size of the infiltrating grains, the size composition of the gravel matrix, and the magnitudes of the main channel and intragravel flows (Einstein 1968; Beschta and Jackson 1979; Lisle 1980; Carling 1984; Carling and McCahon 1985; Diplas and Parker 1985; Scrivener and Brownlee 1989).

A sediment seal restricts the rate of fine sediment intrusion to the level of incubating salmonid eggs until it is disturbed. The means for this to occur would be for the bed to be mobilized at the elevation of the seal (Lisle 1989; Scrivener and Brownlee 1989). During partial transport, only a proportion of the bed surface is mobilized at any instant, influencing the local rate of fine sediment intrusion correspondingly (Wilcock and McArdell 1997), but a large area of the bed can be disturbed nonetheless with a flood of sufficient duration. The average depth of the seal depends predominantly on the bedload disturbance depth. In low gradient channels, the maximum depth of disturbance scales with the largest particle mobilized in the vicinity of the redd location.

The question posed in the context of scour processes and survival to emergence of salmonid embryos is whether the level of disturbance is sufficient to result in intrusion-related mortality. Three previous studies indicate the answer. Lisle (1989) determined that the seal generally formed near the bed surface and was up to several centimeters thick. The seal was facilitated by the heterogeneity of the bed substrates because spaces between larger particles were filled by smaller particles. Deeper scour measurements were generally associated with deeper sediment intrusion. Similarly, Scrivener and Brownlee (1989) noted that seal depths determined in freeze core samples increased with the return period of freshet. They also noted that the percent of fines concentrations increased with depth and proposed that this was because cleaning frequency decreased accordingly. Survival to emergence was related more strongly to substrate composition than to peak flow magnitude. In a flume study, Beschta and Jackson (1979) determined that sand particles intruded approximately ten centimeters or less below a stable bed surface. Deepest intrusion depths were facilitated by framework particles that rocked back-and-forth in place because of flow stresses but did not move downstream.

One inference from these studies is that scour is the primary mechanism facilitating fine sediment intrusion to the level of the eggs. Fine sediments intrude deeper than the scour depth because the particles are able to settle through the framework interstices. Consequently, if scouring influences incubation survival in low gradient channels, it is plausible that the primary mechanism of mortality is through intruded sediments rather

than the physical scouring action itself. Embryos that are buried shallower than $2D_{90}$ are also likely to be influenced by direct scour as the armor layer becomes mobilized. Embryos that are buried deeper should survive bed mobilization and scour in general when fine sediments do not reach the egg pocket in significant quantities, provided that the amount and sizes of fines are such that alevins can still emerge successfully.

Effects of increased flood frequency and duration on intragravel survival in low gradient channels may therefore be manifest by increased quantities and depths of intruded sediments, rather than by increased scour depth. Scouring mainly facilitates the adverse effects of fine sediment intrusion. Increasing flood magnitude cannot cause intrusion below the limiting depth imposed by typical bedload disturbance and net excavation scour depths, and should thus influence survival predominantly in terms of a corresponding increase in intrusion rates and not through an increase in scour depth. This needs to be evaluated more fully using studies measuring scour depth, fine sediment intrusion rates, and survival to emergence.

A testable hypothesis is that streams with salmonid spawning habitat containing less than approximately 20 percent by weight of sediments finer than 6.4 mm should not exhibit a significant change in survival to emergence with changes in flood frequency and duration characteristics, all other factors remaining the same (e.g., no increased stream bank erosion rates or landslide inputs). Under the hypothesis, increased magnitude, frequency, and duration of flooding can occur without influencing survival if fine sediment levels in the redd remain below this 20 percent threshold (Chapman and McLeod 1987).

Conversely, spawning beds with high embeddedness levels (usually associated with a large fine sediment loading) may or may not exhibit significant changes in survival to emergence with hydrologic change depending on the levels of fine sediments present in the streambed and in the redd prior to flood disturbance. Hydrologic changes will not result in significant changes in survival to emergence when fine sediment (< 6.4 mm) levels in the redd exceed approximately 45 percent because survival to emergence is very low (Chapman and McLeod 1987) and further declines in survival to emergence are unmeasurable in the field. Changes may occur in survival to emergence when particles

smaller than 6.4 mm constitute between approximately 20 and 45 percent of the bed material, the range that is associated with a rapid decline in survival (Chapman and McLeod 1987). In that case, increased bed mobilization should result in increased rates of fine sediment intrusion down to the embryo elevation, and egg pocket concentrations should approach adverse levels more rapidly than in a bed that is less frequently and extensively disturbed by flooding.

6.5 Summary

Salmonids appear to have adapted to general scouring mechanisms that act during floods in low gradient ($S \leq 0.01$) gravel bed streams. Different species and stocks exhibit similar adaptations to characteristic scour depths. Most notably, they include egg burial depth, and locating the redd within reaches containing abundant gravel deposits (and cobble, depending on species), and in specific regions of the channel that are least likely to scour. Redd construction may influence initial bed stability during a flood, but does not appear to be important with respect to the eventual scour depth.

The results of this study indicate that bedload disturbance depths are less than or equal to approximately $2D_{90}$. This represents the strongest selective scour pressure acting on salmonids, and may be universal to all gravel bed streams if the range of hydraulic and geomorphic conditions measured here are representative. Total scour depths associated with reach-scale transport rate imbalances that occur during the incubation period appear to be on the order of $2.5D_{90}$ and less at the spawning locations monitored in this study, and include the maximum disturbance depth associated with bedload transport. There is indirect evidence that salmonids have adapted to both, based on characteristic egg burial depths reported in the literature.

The relationship between female size and egg burial depth may not influence scouring of embryos in low gradient gravel bed streams that contain an abundant supply of spawning substrate. This is because egg burial depths appear to exceed twice to two-and-a-half times the substrate D_{90}., which is suggested by this work to be an approximate

bound to scour depths in spawning locations within such streams. Low gradient reaches with a limited supply of spawning substrate-sized material are generally not used for spawning. Those that are used are suggested by the results of this work to experience scour depths that are likely to influence the offspring of all sizes of females.

The strongest influence of scour processes on salmonid survival to emergence appears to be through sediment intrusion depths. The primary mortality mechanism potentially linked to scour depth is therefore an indirect one. Larger magnitude, more frequent, and longer duration floods facilitate greater total fine sediment intrusion to the egg pocket, rather than influence scouring of embryos per se. In low gradient ($S \leq 0.01$) channels, the influence of floods on survival appears to be ultimately constrained by fine sediment supply and bed composition characteristics.

7.0 Conclusions and Recommendations

7.1 Conclusions Regarding Scour Mechanisms and Effects on Intragravel Survival

I have shown through this work that assessments of scour depth in gravel bed streams and its effects on salmonid intragravel survival need to include consideration of the specific, physical mechanisms of bedload transport. Direct scour mortality occurs to developing embryos when the bed is disturbed down to their elevation. The term 'scour depth' in this context is synonymous with bed disturbance depth. Disturbance is caused by two characteristically different mechanisms: movement of the bedload layer, and sediment transport rate imbalances. It is necessary to differentiate between the two before making inferences regarding cause and effect.

For example, a significant inference had been made previously that a direct relationship exists between local scour depth and flow strength, where larger floods scour a greater depth of the gravel streambed than smaller ones, resulting in greater salmonid embryo losses. The inference appears to be incorrect, however, because it was based on correlations of reach-average values of disturbance depth. Reach average values increase significantly with shear stress because of a significantly greater area of the bed becoming active, rather than because of a significantly greater local disturbance depth.

Local scour depth in gravel bed streams appears to be a function of bed shear stress near the condition of incipient motion only, when local disturbance depth increases with size of particle mobilized. The depth of disturbance caused by the moving bedload appears to have a mechanical upper limit in gravel bed streams that is independent of flow strength once the largest particles present in the spawning bed are mobilized (excepting erratics and other uncommonly large, immobile particles). Greater bedload disturbance depths appear to be beyond the capability of natural stream systems under all but extremely rare, catastrophic conditions (e.g., >500-year peak flood magnitude in the

study streams).

The data measured in this work indicate that the bounds to bedload disturbance depth are approximately twice the b-axis diameter of the bed surface D_{90} particle, or one and a half times the b-axis diameter of the largest competent particle. The thickness of the bedload layer does not appear to increase significantly with bedload transport rates. Increased bedload transport rate per unit width is likely associated with faster particle movement instead.

Only a fraction of the active gravel bed surface area experiences the $2D_{90}$ or $1.5D_{comp}$ bound. Much of the bed surface experiences smaller bedload disturbance depth limits, and the data indicate that the median disturbance depth limit in the study streams was between approximately one and one-and-a-half times the D_{90} dimension once the bed was fully mobile. Maximum bedload disturbance depths at a location appear to be distributed approximately uniformly throughout a reach and are influenced predominantly by mobilized particles that are larger than the bed D_{50}.

The data reported here indicate that the mechanism of disturbance is a combination of (i) excavation of particles, and (ii) movement downstream of particles comprising the largest sized fractions. A bedload disturbance depth model based on particle entrainment probabilities is insufficient to describe the bedload disturbance depth distribution in a stream reach since it only describes the first mechanism. The relevant dominant size fractions for each mechanism are unknown. A complete model must identify these, and also include a mechanical component that describes the probability that a particle of a specific size moving downstream will disturb a specific depth. The information needed to support such a model does not exist.

Large magnitude scour depths in low gradient ($S \leq 0.01$) gravel bed streams result from sediment transport rate imbalances. Major scour can occur in three ways in such channels. First, at the smallest scale, deep scour occurs in transient bedforms that are finer-grained than substrates found in the majority of the channel. These bedforms exhibit delayed initiation, and early cessation, of mobility during a flood because of temporally variable influences of flow obstructions on local velocities. Salmonids

generally avoid such areas when spawning.

In the second, transport rate imbalances may occur in the pool edge region through a combination of (i) the distance between riffle deposits influencing travel times of particles between spawning substrate deposits, and (ii) the pool-riffle channel morphology promoting a diverging sediment transport field in the pool edge and tail regions at some point during a flood. Salmonids spawning in the pool tail are most susceptible to deep scour from this process. Scour depths in the study streams significantly exceeded bedload disturbance depths at the upstream end of the riffle deposit, particularly in the pool edge region. The data support a postulated mechanism whereby excavation scour continues until sufficient material arrives from the nearest upstream riffle deposit to establish equilibrium sediment transport locally. Intervening geomorphic channel units (e.g., pools, runs) and bars may contribute to bedload transport, but not as extensively as the riffle deposits. The affected length of the pool edge region likely depends on the geometry of the riffle deposit and the distance to the next deposit upstream. Tracer data indicate that the distance traveled by particles between deposits varies with the time integral of excess shear stress, and can be the same for a smaller (e.g., 2-year) and a larger (e.g., 10-year) flood if the smaller flood is of sufficiently long duration.

The influences of flood magnitude, duration, and frequency on total scour depth appear to be minor compared to the influence of how gravel and cobble are distributed in the reach. Increased flow strength results in increased bedload velocity, which reduces the travel time for particle movement between deposits. Since the bulk of coarse bedload transport during a flood is from riffle to riffle, observed riffle frequencies and amplitudes may reflect a balance of bedload transport rates between and over riffle deposits that is influenced by prevailing hydrography, channel slope, and sediment size and supply characteristics.

The third mechanism involves transport rate imbalances that occur over longer distances than the reach length. Such imbalances are likely responses to temporal and spatial variation in supply of gravel and cobble to the channel, which results in a

sediment pulse that subsequently disperses. The entire reach experiences net scour and/or net fill depending on the dimensions and location of the pulse front, crest, and back. A redd constructed nearer the upstream limit of the pulse distribution likely experiences deeper total scour depth than one constructed nearer the downstream limit, or than one in a reach without a significant gravel pulse present.

7.1.1 *Biologic and Geomorphic Implications of Study Results*

Salmonids appear to have adapted to the dominant features of bedload transport and scour identified above. Available data indicate that egg burial depths are typically greater than 2 to $2.5D_{90}$, which in the study streams reflected a combination of disturbance depths associated with bedload motion and net excavation scour. Eggs buried shallower than 2 to $2.5D_{90}$ may be scoured, but most eggs and embryos appear to be buried deeper and are suggested by this work to be generally safe from scouring in low gradient gravel bed streams when there is abundant material available for bedload transport. The probability of reproductive success is increased further by selecting redd locations in areas of the channel where deep excavation scour depths are least likely to occur. There is also evidence that the more developmentally advanced alevins are able to move downwards within the substrate to avoid direct scour mortality.

The primary importance of scour to intragravel survival may be through fine sediment intrusion into egg pockets. Fine sediments are typically prevented from reaching developing embryos in large quantities because of the formation of a fine sediment seal above the elevation at which the fertilized eggs were deposited. Deeper bed disturbance results in breaking up of an existing seal and reformation of a new seal at a deeper level. The elevation of the seal is below the boundary between mobile and immobile bed framework particles and can be similar to that of the embryos. Survival can thus be influenced indirectly by scour through sediment intrusion, without the embryos directly experiencing a mobile bed.

The results of this work suggest that land and water resource management-induced

increases in flood magnitudes, duration, and frequency should not influence salmonid embryo survival in low gradient gravel bed streams in the near term (i.e., within a one to five year time frame, which is the time scale important to scour-related effects), except in channels where (i) particles smaller than 6.4 mm constitute between approximately 20 and 45 percent of spawning bed substrates (a critical range within which intragravel survival changes rapidly), or (ii) the change in flood hydrology results in erosion of stream banks, delivery of fine sediments, and increases in percent fines composition of the bed to adverse levels. Changes in flood hydrography appear unlikely to cause increases in scour depth that would influence survival significantly.

Hydrologic change is important over the long term when it influences the overall sediment transport regime of the channel such that the balance between annual net transport and supply volumes of gravel and cobble material is upset. A long term decline in spawning habitat availability results when the bed degrades and coarsens, unless there are compensatory increases in the supply of gravel and cobble sediments to the channel. Limits to salmonid population size would then be caused by (i) reduced spawning habitat quantity and (ii) increased susceptibility to scour of the pool tail region as riffle spacing becomes greater.

Anthropogenic changes in quantity and quality of spawning habitat appear to be more important influences on flood-related scour mortality in low gradient gravel bed streams than changes in hydrology, where the total depth of scour in spawning beds is controlled strongly by the quantity and size of gravel and cobble in a reach, and weakly by flood magnitude and duration. Adverse effects of floods during the incubation period are thus more likely to occur indirectly through other processes such as fine sediment intrusion than directly through redd scour. Fining of spawning bed gravel may consequently be detrimental to survival primarily because of increases in fine sediment levels available for intrusion. Bed fining should not lead to significantly deeper scour depths in typical spawning-sized substrates because it is the larger framework particles present that determine scour depth in spawning substrates, not the smaller-sized matrix material. Too strong a fining may result in avoidance by spawning salmonids, precluding

potential scour effects.

Consideration of sediment mass conservation for a channel reach suggests that anthropogenic mass wasting or other large scale form of delivery may indirectly reduce scour depths in spawning beds temporarily because of the increased quantities of material that become available for bedload transport, thereby reducing the potential for riffle-to-riffle scale transport rate imbalances to develop. Conversely, increased scour depths may occur temporarily over the longer term as the transient input material disperses. This may help explain the results of Tripp and Poulin (1986), who measured deeper scour depths in streams influenced by landslides and debris flows that had occurred between six and ten years earlier than in streams with relatively little mass wasting activity.

More complete and accurate egg burial depth data are needed to address these issues. Scour measurements are presently interpreted using a database that contains too much unexplained variability, and it has often been concluded that direct scouring effects on embryos have occurred without having an accurate estimate or measure of egg burial depths.

7.2 Recommended Approach for Scour Field Studies

Schuett-Hames et al. (1996) recommended a monitoring approach for assessing scour impacts on salmonids in gravel bed streams. Sample size requirements (i.e., number of scour monitors) were proposed for different levels of precision and confidence in measurements of total scour depth. They also recommended (i) surveying the bed elevation before and after major storm events to document changes, (ii) conducting 100-pebble counts across each monitoring transect to determine the grain size distribution D_{50}, and (iii) calculating or estimating peak discharge.

The results and conclusions of this work generally support the recommended approach. Based on the results of this work, the following modifications and additional measurements appear necessary for improved interpretation of scour depth measurements:

(I)   Bed elevations should be surveyed using a 127 mm (5 inch) diameter leveling rod base to minimize the influence of bed microtopography on measurements of the magnitude of net excavation or fill.

(II) Scour monitor measurements should be made in the manner depicted in Figure 3-2 to prevent error caused by indicators not being seated snugly, and to address potential errors in defining the surface elevation of a rough bed.

(III) Either a pebble count of the surface material or a bulk (McNeil) sample of the surface and immediate subsurface layers appears to be appropriate for characterizing bed grain size distributions in scour studies. Pebble counts should be conducted in longitudinal patches that are in line upstream and downstream with the scour monitor location, because bedload transport characteristics are influenced by cross-channel variation in bed texture. Results should be evaluated for accuracy when minimum sample size requirements proposed by Rice and Church (1996) or Ferguson and Paola (1997) are not met (collecting 300 to 400 stones results in an unbiased pebble count percentile estimate; bulk sampling volume accuracy is determined by substrate sorting, median grain size, and desired percentile).

(IV) The substrate D_{90} should be used for scaling scour depth because it approximates the thickness of the armor layer and half the maximum bedload disturbance depth. Grain size distributions should be truncated at 8 mm prior to calculating D_{90} and other percentile particle sizes to characterize the substrate framework structure, which determines bed elevation.

(V)   The peak water level stage is better than the peak flow rate (recommended by Schuett-Hames et al. 1996) for evaluating the effects of scour on survival because it can be more closely linked to mobilizing force. Continuous recording gage data are best because they permit determining the magnitude and duration of shear stresses that are competent to move different particle size classes. Tracer stones can be used to calibrate a site-specific relation determining the critical stage and shear stress at which each particle size class is mobilized.

[Note: measurement of peak stage or flow rate does not appear to be critical to scour assessments because maximum scour depth is independent of shear stress, and reach average scour depth is unsuitable for evaluating salmonid survival.]

(VI) Scour depth measurements should be classified spatially according to where in the channel they were collected, both across and along the channel, and whether the location is subject to obstructions at higher flows that may influence erosion and deposition patterns locally. This information is needed to identify the scouring process that occurred.

Scour depth measurements should be evaluated according to Equation 1.1:

$$\delta_T = \delta_{EX} + \delta_{Bm} \tag{1.1}$$

When interpreting bedload layer thickness, data should be rejected where the net change in bed elevation is greater than the scour monitor device measurement error. Alternatively, Equation 4.2 may be useful for estimating the corresponding unbiased value:

$$\delta_{Bm} = \delta_T - \frac{\delta_{EX}}{2} \tag{4.2}$$

The scour depth data should be scaled by the local D_{90} to determine if the observed scour depth exceeds $2D_{90}$. Observed scour depths are representative of disturbance of the surface layer alone when the total scour depth is less than $2D_{90}$. Scour depth measurements that exceed $2D_{90}$ should be evaluated for the relative importance of scour and fill, shifts in thalweg location, and reach-scale changes in bed elevation.

Published egg burial depth data suggest that scouring of embryos may not occur until the total scour depth exceeds $2.5D_{90}$ or more. Scour depth measurements should be scaled by the substrate D_{90} and compared to this criterion to determine whether incubating embryos may have been influenced by scouring.

7.3 Predicting Scour Depth at Redd Locations

An important goal of scour monitoring studies is to provide fisheries managers with information regarding whether existing redds have been scoured out. This can be assessed directly by installing scour monitors next to redds and evaluating the data in the manner described in Section 7.2. Scour monitor installation is labor intensive and involves carrying heavy equipment, which limits scour measurements to more accessible reaches. The ability to monitor scour depth decreases with increasing remoteness of spawning area. A method for predicting scour depth that is based on more easily and efficiently collected data would be of great utility. Two approaches are suggested in sections 7.3.1 and 7.3.2 for predicting the maximum possible redd scour depth, $\delta_{T\,max}$, at potential spawning locations in the channel when stream gradients are less than 0.01.

The actual scour depth will frequently be smaller than $\delta_{T\,max}$ because not all locations experience the maximum bedload disturbance depth. An estimate of the probability that a redd will experience a specific scour depth (e.g., depth to 90 percent of all egg pocket ceilings) is required. Pending more accurate identification of distributions of δ_{Bm} and δ_T in the future, the probability distribution of redd scour depth, $p(\delta_T)$, is estimated, to first order, using Equation 2.6 (the exponential distribution; Haschenburger 1999). The distribution parameter is estimated assuming that approximately 90 percent of total scour depths in areas used by spawning salmonids are less than $2.5D_{90}$ (based on Figure 5-1, in which the nine largest scour depths were in channel locations typically not used by spawning salmonids and were therefore not included). The cumulative distribution function of Equation 2.6 is accordingly:

$$0.9 \;=\; 1 - e^{(-\theta\; 2.5 D_{90})} \tag{7.1}$$

resulting in:

$$\theta \;=\; \frac{\ln(10)}{2.5 D_{90}} \;\approx\; \frac{0.92}{D_{90}} \tag{7.2}$$

Equations 2.6 and 7.2 give a first order approximation of the probability that a redd will be scoured down to a specific depth. The maximum possible scour depth is estimated by one of the two approaches described in Sections 7.3.1 and 7.3.2.

7.3.1 *Predicting $\delta_{T\,max}$ When the Bed Elevation Cannot be Surveyed*

It is assumed here that the combination of maximum bedload disturbance depth and net excavation scour measured in the study streams apply to other streams with similar hydraulic and geomorphic characteristics. Four situations need to be considered:

(I) *Redd located in the vicinity of the riffle crest or in the riffle:* The maximum total scour depth is approximately 2.5 times the local D_{90} of the undisturbed bed in the vicinity of the redd.

(II) *Redd located in the pool tail:* Maximum total scour depth may equal or exceed 2.5 times the local D_{90} when pool-riffle spacing exceeds a value of seven bankfull channel widths.

(III) *Redd located in the vicinity of a partial high flow obstruction:* Total scour depth during a flood may exceed 2.5 times the local D_{90} when the redd is constructed in a transient deposit that is notably finer grained than the substrate found further out in the main channel. When the redd is constructed in a deposit that is as coarse as the main bed, scour greater than 2.5 times the local D_{90} is only likely if case (II) or (IV) is also applicable.

(IV) *Redd located in the vicinity of immobile large woody debris:* This situation was not evaluated directly in this work. Scour depth may be estimated, however, using bridge pier or abutment scour methods, where the dimension of the obstruction is approximated as an equivalent pier diameter or abutment thickness. Scour will adversely affect embryos when the redd location is within the estimated perimeter of the scour hole that develops around the structure during high flow. (Reaches with abundant large woody debris could be more susceptible to scouring effects if debris is mobilized during a flood and passes over the redd

location. Whether and how much scour occurs is totally unpredictable and requires scour depth measurements to quantify it).

The approach is based on three principal observations made in this study: (i) total scour depth depends on where in the channel the redd is located, (ii) there appears to be a physical limit to bedload layer thickness in gravel bed streams, and (iii) net excavation scour depths associated with reach-scale sediment transport rate imbalances may have a characteristic magnitude such that total scour depth usually does not exceed roughly 2.5 times the local D_{90}.

The approach is also based on the assumption that reaches with a pool-riffle spacing greater than seven channel widths are more likely to exhibit significant sediment transport rate imbalances and net excavation scour in the pool-riffle interface than channels with smaller distances between riffles. Seven channel widths was reported by Leopold et al. (1995) to be an upper limit to typical longitudinal spacing of riffle deposits; an equilibrium condition may be implied in which riffle spacing and particle travel distances are balanced against each other. If true, a longer riffle to riffle spacing would exceed typical particle travel distances during a flood, thereby facilitating significant scour in the riffle deposits. Additional research is needed to examine this assumption further).

7.3.2 Predicting $\delta_{T\,max}$ When the Channel Bed Can be Surveyed

This approach takes advantage of the direct knowledge gained when the bed elevation can be surveyed in the vicinity of a redd before and after a flood. The maximum potential scour depth in the redd is estimated using Equation 4.2 when excavation has occurred, and as twice the local D_{90} when fill has occurred. However, the accuracy likely decreases with increasing change in bed elevation. Cases (III) and (IV) in Section 7.3.1 cannot be evaluated in this manner.

7.4 Future Research

This work has identified several avenues for additional research into the scour depth prediction problem. The six most important topics are repeated here:

(I) More theoretical and experimental work are needed to refine the empirical form of the bedload disturbance depth distribution depicted in Figure 4-21. The predominant grain sizes influencing disturbance depths through (i) particle entrainment and (ii) particle motion need to be determined. The characteristic distribution of disturbance depths caused by moving particles from different size classes also needs to be determined. This work would be done best in a wide flume where it is easier to control grain size distribution and follow the motion of a large number of particles. A probability-based model of bedload disturbance depth can be developed by combining the resulting information with a suitable fractional mobility function, $\acute{Y}$ (Wilcock 1997a, 1997b). The resulting model could be used to predict bedload disturbance depths in a gravel bed stream as a function of shear stress. Empirical field and flume data are needed to evaluate the empirical model proposed in Figure 4-21, and to help develop and validate the probabilistic model.

(II) Net excavation depth depends more strongly on the spatial distributions of substrate framework material in a reach than on flood strength. Previous work has focused primarily on flood strength. A method needs to be developed that includes direct consideration of riffle deposit spacing, storage volumes of commonly mobilized framework material, and bedload velocities and transport rates. These factors all influence sediment transport rate imbalances, and thus net excavation scour depth, throughout a reach. Equations 5.9, 5.12, and 5.19 are offered as starting points for further investigation.

(III) Gravel pulses likely influence scour depths as they disperse within and downstream of a reach. They appear to be a significant feature of gravel bed streams influencing the susceptibility of salmonid embryos to scour effects. The

effect could last one to ten, or more years depending on the nature of the supply imbalance and flood characteristics. Research activities should focus on developing methods for identifying their presence, identifying where the redd is located on the waveform, and on predicting dispersion rates. Scour studies should attempt to identify the presence or absence of such pulses since they can confound interpretations of the cause of observed scour depths.

(IV) The results of this study suggest that direct deleterious scour effects are unlikely in low gradient gravel bed streams with slopes less than 0.01 unless sediment supply is low and fish are forced to spawn in transient deposits. However, this conclusion is based in part on reported egg burial depth data that are subject to large unexplained variation. Much of that variation could be reduced through more rigorous field work identifying the distribution of egg burial depths relative to the original bed elevation in terms of substrate size, water velocity, and female size and species.

(V) The relationship between scour depth and fine sediment intrusion rate may be the most important influence of bed mobility on intragravel survival of salmonid embryos, but relatively little work has been done on the subject. Research is needed to elucidate this relationship.

(VI) Future investigations of the relationship between flooding and survival need to evaluate all possible mortality mechanisms. It should not be assumed that scouring of embryos is the primary source of flood-related mortality without obtaining confirming data. Other mortality mechanisms may have a higher likelihood of being important, and should be considered for all life history stages.

8.0 References

Abbott, J.E., and J.R.D. Francis. 1977. Saltation and suspension trajectories of solid grains in a water stream. Phil. Trans. Roy. Soc. Lon. A, 284: 225-254.

Alonso, C.V., F.D. Theurer, and D.W. Zachman. 1988. Tucannon River offsite study: sediment intrusion and dissolved oxygen transport model. US Department of Agriculture, Agricultural Research Service, Hydro-Ecosystem Research Group, Fort Collins, Colorado.

Andrews, E.D., and D.C. Erman. 1986. Persistence in the size distribution of surficial bed material during an extreme snowmelt flood. Water Resour. Res. 22: 191-197.

Andrews, E.D., and G. Parker. 1987. Formation of a coarse surface layer as the response to gravel mobility. Ch. 11 in: C.R. Thorne, J.C. Bathurst, and R.D. Hey [Eds.]. Sediment transport in gravel-bed rivers. John Wiley & Sons, New York.

Armanini, A. 1995. Non-uniform sediment transport: dynamics of the active layer. J. Hydraulic Res. 33: 611-622.

ASCE Task Committee on Hydraulics, Bank Mechanics and Modeling of River Width Adjustment. 1998. River width adjustment; I: Processes and mechanisms. J. Hydraulic Engin. 124: 881-902.

Ashworth, P.J., and R.I. Ferguson. 1989. Size-selective entrainment of bed load in gravel bed streams. Water Resour. Res. 25: 627-634.

Bagnold, R.A. 1951. The movement of a cohesionless granular bed by fluid flow over it. Brit. J. Appl. Phys. 2: 29-34.

Bagnold, R.A. 1954. Experiments on a gravity-free dispersion of large solid spheres in a Newtonian fluid under shear. Proc. Roy. Soc. Lon. Ser. A Vol 225: 49-63.

Bagnold, R.A. 1956. The flow of cohesionless grains in fluids. Phil. Trans. Roy. Soc. Lon. A, 249: 235-297.

Bagnold, R.A. 1966a. An approach to the sediment transport problem from general physics. U.S. Geol. Surv. Prof. Pap. 422-I. 37 p.

Bagnold, R.A. 1966b. The shearing and dilatation of dry sand and the 'singing' mechanism. Proc. R. Soc. Lond. A, 295: 219-232.

Bagnold, R.A. 1973. The nature of saltation and of 'bed-load' transport in water. Proc. R. Soc. Lond. A, 332: 473-504.

Bagnold, R.A. 1980. An empirical correlation of bedload transport rates in flumes and natural rivers. Proc. Royal Soc. London A, 372: 453-473.

Bams, R.A. 1969. Adaptations in sockeye salmon associated with incubation in stream gravels. pp. 71-87 in: Northcote, T.G. [Ed.]. Symposium on salmon and trout in streams. H.R. MacMillan Lectures in Fisheries. Inst. Fish., Univ. Brit. Col., Vancouver.

Beamish, F.W.H. 1978. Swimming capacity. Ch. 2 in: Hoar, W.S., and D.J. Randall [Eds.]. Fish physiology, Volume VII: Locomotion. Academic Press, New York NY.

Beechie, T. 1998. Rates and pathways of recovery for sediment supply and woody debris recruitment in northwestern Washington streams, and implications for salmonid habitat restoration. Ph.D. Dissertation, University of Washington, Seattle. 199 p.

Beer, F.P., and E.R. Johnston. 1977. Vector mechanics for engineers: Statics. Third ed. McGraw Hill, Inc. New York, NY. 448 p.

Beland, K.F., R.M. Jordan, and A.L. Meister. 1982. Water depth and velocity preferences of spawning Atlantic salmon in Maine rivers. N. Am. J. Fish. Manag. 2: 11-13.

Benjamin, J.R., and C.A. Cornell. 1970. Probability, statistics, and decision for civil engineers. McGraw-Hill Co., New York, NY. 684 p.

Beschta, R.L., and W.L. Jackson. 1979. The intrusion of fine sediments into a

stable gravel bed. J. Fish. Res. Bd. Can. 36: 204-210.

Bjornn, T.C., and D.W. Reiser. 1991. Habitat requirements of trout, char and salmon in North America. p. 83-138 in: W.R. Meehan [Ed.]. Influences of forest and rangeland management on salmonid fishes and their habitats. Am. Fish. Soc. Spec. Publ. 19. Bethesda, MD.

Blackett, R.F. 1968. Spawning behavior, fecundity and early life history of anadromous Dolly Varden in southeastern Alaska. Alaska Dept. Fish Game Res. Rep. 6.

Borah, D.K., C.V. Alonso, and S.N. Prasad. 1982. Routing graded sediments in streams: Formulations. J. Hydraul. Div. ASCE, 108: 1486-1503.

Borah, D.K. 1989. Scour depth prediction under armoring conditions. J. Hydraul. Engin. 115: 1421-1425.

Bovee, K.D. 1978. Probability-of-use criteria for the family Salmonidae. U.S. Fish and Wild. Serv. FWS/OBS-78-07.

Brayshaw, A.C., G.W. Davies, and P.W.M. Corbett. 1996. Depositional controls on primary permeability and porosity at the bedform scale in fluvial reservoir sandstones. Ch. 11 in: P.A. Carling, and M.R. Dawson [Eds.]. Advances in fluvial dynamics and stratigraphy. John Wiley & Sons, New York, NY.

Bridge, J.S., and D.F. Dominic. 1984. Bed load grain velocities and sediment transport rates. Water Resour. Res. 20(4): 476-490.

Brown, L.R., P.B. Moyle, and R.M. Yoshiyama. 1994. Historical decline and current status of coho salmon in California. N. Am. J. Fish. Manag. 14: 237-261.

Buffington, J.M., and D.R. Montgomery. 1997. A systematic analysis of eight decades of incipient motion studies, with special reference to gravel bed rivers. Water Resour. Res. 33: 1993-2029.

Campbell, A.J., and R.C. Sidle. 1985. Bedload transport in a pool-riffle sequence of a coastal Alaska stream. Water Resour. Bull. 21: 579-590.

Campbell, C.S. 1989. The stress tensor for simple shear flows of a granular

material. J. Fluid Mech. 203: 449-473.

Campbell, C.S. 1997. Self-diffusion in granular shear flows. J. Fluid Mech. 348: 85-101.

Carling, P.A. 1984. Deposition of fine and coarse sand in an open-work gravel bed. Can. J. Fish. Aquat. Sci., 41: 263-270.

Carling, P.A. 1987. Bed stability in gravel bed streams, with reference to stream regulation and ecology. Ch. 13 in: K. Richards [Ed.]. River Channels: Environment and process. Inst. Brit. Geog. Spec. Publ. Ser., Oxford U.K.

Carling, P.A. 1990. Particle over-passing on depth-limited gravel bars. Sedimentology 37: 345-355.

Carling, P.A. 1991. An appraisal of the velocity-reversal hypothesis for stable pool-riffle sequences in the River Severn, England. Earth Surf. Proc. Land. 16: 19-31.

Carling, P.A., and N.A. Reader. 1982. Structure, composition and bulk properties of upland gravel streams. Earth Surf. Proc. Land. 7: 349-365.

Carling, P.A., and C.P. McCahon. 1985. Natural siltation of brown trout (Salmo trutta L.) spawning gravels during low flow conditions. P. 229-244 in: Craig, J.F. and J.B. Kemper [Eds.]. Regulated streams: Advances in ecology. 3rd Intl. Sym. on Regul. Streams. Plenum Press, N.Y., N.Y. 430 p.

Chang, H.H. 1994. Selection of gravel-transport formula for stream modeling. J. Hydraul. Engin. 120: 646-651.

Chapman, D.W. 1988. Critical review of variables used to define effects of fines in redds of large salmonids. Trans. Am. Fish. Soc. 117(1): 1-21.

Chapman, D.W., D.E. Weitkamp, T.L. Welsh, M.B. Dell, and T.H. Schadt. 1986. Effects of river flow on the distribution of chinook salmon redds. Trans. Am. Fish. Soc. 115: 537-547.

Chapman, D.W., and K.P. McLeod. 1987. Development of criteria for fine sediment in the northern Rockies ecoregion. Final report prepared for EPA Region 10, Work assignment 2-73. Battelle Columbus Laboratories. EPA

910/9-87-162. 279 p.

Chiew, Y. 1990. Mechanics of local scour around submarine pipelines. J. Hydraulic Engin. 116: 515-529.

Church, M.A., D.G. McLean, and J.F. Wolcott. 1987. River bed gravels: Sampling and analysis. Ch. 3 in: Thorne, C.R., J.C. Bathurst, and R.D. Hey [Eds.]. Sediment transport in gravel-bed rivers. John Wiley and Sons, New York, NY. 995 p.

Church, M., and M.A. Hassan. 1992. Size and distance of travel of unconstrained clasts on a streambed. Water Resour. Res. 28: 299-303.

Church, M., M.A. Hassan, and J.F. Wolcott. 1998. Stabilizing self-organized structures in gravel-bed stream channels: Field and experimental observations. Water Resour. Res. 34: 3169-3179.

Clifford, N.J., and K.S. Richards. 1992. The reversal hypothesis and the maintenance of riffle-pool sequences: A review and field appraisal. Ch. 2 in: P.A. Carling and G.E. Petts [Eds.]. Lowland floodplain rivers: Geomorphological perspectives. John Wiley and Sons, New York, N.Y.

Colby, B.R. 1964. Scour and fill in sand-bed streams. USGS Prof. Paper 462-D.

Copp, H.D. 1988. Scour at bridge piers. Final report. Res. Proj. GC8287, Task 4. Washington State Dept. Transportation.

Crisp, D.T. 1989. Use of artificial eggs in studies of washout depth and drift distance for salmonid eggs. Hydrobiologia 178: 155-163.

DeVries, P.E. 1997. Riverine salmonid egg burial depths: Review of published data and implications for scour studies. Can. J. Fish. Aquat. Sci. 54: 1685-1698.

DeVries, P.E., and D.J. Goold. 1999. Leveling rod base required for surveying gravel river bed surface elevations. Water Resour. Res. 35: 2877-2879.

Dietrich, W.E. 1982. Flow, boundary shear stress, and sediment tranport in a river meander. Ph.D. dissertation, Univ. of Washington, Seattle. 261 p.

Dill, L.M. 1969. The sub-gravel behavior of Pacific salmon larvae. P.89-99 in: Northcote, T.G. [Ed.]. Symposium on salmon and trout in streams. H.R.

MacMillan Lectures in Fisheries. Inst. Fish., Univ. Brit. Col., Vancouver.

Dill, L.M., and T.G. Northcote. 1970. Effects of gravel size, egg depth, and egg density on intragravel movement and emergence of coho salmon (*Oncorhynchus kisutch*) alevins. J. Fish. Res. Bd. Can. 27: 1191-1199.

Dinehart, R.L. 1989. Dune migration in a steep, coarse-bedded stream. Water Resour. Res. 25: 911-923.

Dinehart, R.L. 1992. Evolution of coarse bed forms: Field measurements at flood stage. Water Resour. Res. 28: 2667-2689.

Diplas, P. 1987. Bedload transport in gravel-bed streams. J. Hydraul. Engin. 113: 277-292.

Diplas, P., and Parker, G. 1985. Pollution of gravel spawning grounds due to fine sediment. Project Report No. 240. St. Anthony Falls Hydraulic Lab., University of Minnesota, 145 p.

Diplas, P., and A.J. Sutherland. 1988. Sampling techniques for gravel sized sediments. J. Hydraul. Engin. 114: 484-501.

Diplas, P., and J.B. Fripp. 1992. Properties of various sediment sampling procedures. J. Hydraul. Engin. 118: 955-970.

Drake, T.G. 1990. Structural features in granular flows. J. Geophys. Res. 95(B6): 8681-8696.

Duncan, S.H., and J.W. Ward. 1985. A technique for measuring scour and fill of salmon spawning riffles in headwater streams. Water Resour. Bull. 21: 507-511.

Dunne, T., and L.B. Leopold. 1978. Water in environmental planning. W.H. Freeman and Co. San Francisco, CA.

Einstein, H.A. 1937. Bedload transport as a probability problem (Translation of original Ph.D. dissertation). Appendix C in : Shen, H.W. [Ed.]. Sedimentation. Published by H.W. Shen, 1972. Fort Collins, CO.

Einstein, H.A. 1968. Deposition of suspended particles in a gravel bed. J. Hydraul. Div., ASCE, 94(5):1197-1205.

Elliot, J.M. 1976. The downstream drifting of eggs of brown trout, *Salmo trutta* L. J. Fish Biol. 9: 45-50.

Emmett, W.W., and L.B. Leopold. 1965. Downstream patterns of riverbed scour and fill. Paper No. 46, p. 399-409 in: Proc. Fed. Inter-Agency Sed. Conf. 1963. Misc. Publ. No. 970, U.S. Dept. Ag., Washington, D.C.

Erman, D.C., E.D. Andrews, and M. Yoder-Williams. 1988. Effects of winter floods on fishes in the Sierra Nevada. Can. J. Fish. Aq. Sci. 45: 2195-2200.

Ettema, R. 1984. Sampling armor-layer sediments. J. Hydraulic Engin. 110: 992-996.

Everest, F.H., R.L. Beschta, J.C. Scrivener, K.V. Koski, J.R. Sedell, and C.J. Cederholm. 1987. Fine sediment and salmonid production — a paradox. p. 98-142 in: Salo, E.O., and T.W. Cundy [Eds.]. Streamside management: Forestry and fisheries interactions. Coll. For. Resour., University of Washington, Seattle, WA.

Fast, D.E., Q.J. Stober, S.C. Crumley, and E.S. Killebrew. 1981. Survival and movement of chinook and coho salmon alevins in hypoxic environments. p. 51-60 in: Brannon, E.L., and E.O. Salo [Eds.]. Proceedings of the Symposium on Salmon and Trout Migratory Behavior. Univ. Washington, Seattle.

Ferguson, R.I., and C. Paola. 1997. Bias and precision of percentiles of bulk grain size distributions. Earth Surf. Proc. Land. 22: 1061-1077.

Ferguson, R.I., and S.J. Wathen. 1998. Tracer-pebble movement along a concave river profile: Virtual velocity in relation to grain size and shear stress. Water Resour. Res. 34: 2031-2038.

Fernandez Luque, R., and R. van Beek. 1976. Erosion and transport of bedload sediment. J. Hydraulic Res. 14: 127-144.

Foerster, S.F., M.Y. Louge, H. Chang, and K. Allia. 1994. Measurements of the collision properties of small spheres. Phys. Fluids 6: 1108-1115.

Foley, M.G. 1978. Scour and fill in steep, sand-bed ephemeral streams. Geol. Soc.

Am. Bull. 89: 559-570.

Fripp, J.B., and P. Diplas. 1993. Surface sampling in gravel streams. J. Hydraul. Engin. 119: 473-490.

Gangmark, H.A., and R.G. Bakkala. 1960. A comparative study of unstable and stable (artificial channel) spawning streams for incubating king salmon at Mill Creek. Calif. Fish Game 46: 151-164.

Gomez, B., and M. Church. 1988. A catalogue of equilibrium bedload transport data for coarse sand and gravel-bed channels. Department of Geography, University of British Columbia, Vancouver Canada. August. 90 p.

Gomez, B., and M. Church. 1989. An assessment of bed load sediment transport formulae for gravel bed rivers. Water Resour. Res. 25: 1161-1186.

Gotoh, H., T. Tsujimoto, and H. Nakagawa. 1996. Discrete probabilistic model of bed-load layer as granular assemblies. J. Hydrosci. Hydraulic Engin. 14: 13-23.

Groot, C. and L. Margolis [Eds.]. 1991. Pacific salmon life histories. UBC Press, Vancouver, Canada.

Grost, R.T., W.A. Hubert, and T.A. Wesche. 1991. Description of brown trout redds in a mountain stream. Trans. Am. Fish. Soc. 120: 582-588.

Haff, P.K. 1991. Basic physical models in sediment transport. p. 1-14 in: Kraus, N.C., K.J. Gingerich, and D.L. Kriebel [Eds.]. Coastal sediments '91. Proceedings of a specialty conference on quantitative approaches to coastal sediment processes. Seattle, WA June 25-27. ASCE, New York, NY.

Haff, P.K. 1995. Constitutive laws and prediction in granular systems. p. 786-789 in: Sture, S. [Ed.]. Engineering mechanics: Proceedings of 10th conference, Engin. Mech. Div. ASCE. Boulder, CO, May 21-24. ASCE, New York, NY.

Haff, P.K.,Z. Jiang, and S.B. Forrest. 1993. Transport of granules by wind and water: Micromechanics to macromechanics in geology and engineering. Mech. Mater. 16: 173-178.

Haff, P.K., and Z. Jiang. 1995. Vertical mixing of grains during bedload transport. p. 931-933 in: Sture, S. [Ed.]. Engineering mechanics: Proceedings of 10th conference, Engin. Mech. Div. ASCE. Boulder, CO, May 21-24. ASCE, New York, NY.

Hanes, D.M. 1986. Grain flows and bed-load sediment transport: Review and extension. Acta Mech. 63: 131-142.

Hanes, D.M., and A.J. Bowen. 1985. A granular-fluid model for steady intense bed-load transport. J. Geophys. Res. 90(C5): 9149-9158.

Hanes, D.M., and D.L. Inman. 1985a. Experimental evaluation of a dynamic yield criterion for granular fluid flows. J. Geophys. Res. 90(B5): 3670-3674.

Hanes, D.M., and D.L. Inman. 1985b. Observations of rapidly flowing granular-fluid materials. J. Fluid Mech. 150: 357-380.

Hare, S.R., N.J. Mantua, and R.C. Francis. 1999. Inverse production regimes: Alaska and West Coast Pacific salmon. Fisheries 24: 6-14.

Haschenburger, J.K. 1994. Models for scour and fill depths in salmonid streams in the Pacific Northwest. p. A-505, Abstracts with programs, Geol. Soc. Am. Ann. Meet., October 24-27. Seattle, Wa.

Haschenburger, J.K. 1996. Scour and fill in a gravel-bed channel: Observations and stochastic models. Ph.D. Dissertation, Dept. of Geog., Univ. Brit. Colum. 144 p.

Haschenburger, J.K. 1999. A probability model of scour and fill depths in gravel-bed channels. Water Resour. Res. 35: 2857-2869.

Haschenburger, J.K., and M. Church. 1998. Bed material transport estimated from the virtual velocity of sediment. Earth Surf. Proc. Land. 23: 791-808.

Hassan, M.A. 1990. Scour, fill, and burial depth of coarse material in gravel bed streams. Earth Surf. Proc. Land. 15: 341-356.

Hassan, M.A., and I. Reid. 1990. The influence of microform bed roughness elements on flow and sediment transport in gravel bed rivers. Earth Surf. Proc. Land. 15: 739-750.

Hassan, M.A., M. Church, and A.P. Schick. 1991. Distance of movement of coarse particles in gravel bed streams. Water Resour. Res. 27: 503-511.

Hassan, M.A., and M. Church. 1992. The movement of individual grains on the streambed. Ch. 8 in: P. Billi, R.D. Hey, C.R. Thorne, and P. Tacconi [Eds.]. Dynamics of gravel-bed rivers. John Wiley and Sons, New York.

Hassan, M.A., M. Church, and P.J. Ashworth. 1992. Virtual rate and mean distance of travel of individual clasts in gravel-bed channels. Earth Surf. Proc. Land. 17: 617-627.

Hassan, M.A., and M. Church. 1994. Vertical mixing of coarse particles in gravel bed rivers: A kinematic model. Water Resour. Res. 30: 1173-1185.

Hattingh, J., and W.K. Illenberger. 1995. Shape sorting of flood-transported synthetic clasts in a gravel bed river. Sed. Geol. 96: 181-190.

Henderson, F.M. 1966. Open channel flow. MacMillan Publ. Co., Inc., New York.

Hey, R.D., and C.R. Thorne. 1983. Accuracy of surface samples from gravel bed material. J. Hydraul. Engin. 109: 842-851.

Hines, W.W., and D.C. Montgomery. 1980. Probability and statistics in engineering and management science. 2nd ed. John Wiley and Sons, New York, NY. 634 p.

Hobbs, D.F. 1937. Natural reproduction of quinnat salmon, brown and rainbow trout in certain New Zealand waters. N.Z. Mar. Dept. Fish. Bull. No. 6.

Hobbs, D.F. 1940. Natural reproduction of trout in New Zealand and its relation to density of populations. N.Z. Mar. Dept. Fish. Bull. No. 8. 93 p.

Holtby, L.B., and M.C. Healey. 1986. Selection for adult size in female coho salmon (Oncorhynchus kisutch). Can. J. Fish. Aquat. Sci. 43: 1946-1959.

Hooper, D.L. 1973. Evaluation of the effects of flows on trout stream ecology. Dept. Engin. Res., Pac. Gas Elec. Co, Emeryville, Calif. 97 p.

Hurlburt, S.H. 1984. Pseudoreplication and the design of ecological field experiments. Ecol. Monographs 54(2): 187-211.

Hutchison, S.J., and R.F. Shuman. 1942. Reproduction of pink salmon at Little Port Walter, 1941-42. Pac. Fisherman 40(14): 29-31.

Ippen, A.T., and R.P. Verma. 1955. Motion of particles on bed of a turbulent stream. Trans. ASCE 120: 921-938.

Jackson, W.L., and R.L. Beschta. 1982. A model of two-phase bedload transport in an Oregon coast range stream. Earth Surf. Proc. Land. 7: 517-527.

Jenkins, J.T., and D.M. Hanes. 1998. Collisional sheet flows of sediment driven by a turbulent fluid. J. Fluid Mech. 370: 29-52.

Jensen, J.O.T, and D.F. Alderdice. 1983. Changes in mechanical shock sensitivity of coho salmon (*Oncorhynchus kisutch*) eggs during incubation. Aquaculture 32: 303-312.

Jiang, Z. 1995. The motion of sediment-water mixtures during intense bedload transport: computer simulations. Sedimentology 42: 935-945.

Jiang, Z., and P. Haff. 1993. Multiparticle simulation methods applied to the micromechanics of bed load transport. Water Resour. Res. 29: 399-412.

Keller, E.A. 1971. Areal sorting of bed-load material: The hypothesis of velocity reversal. Geol. Soc. Am. Bull. 82: 753-756.

Kellerhals, R. 1967. Stable channels with gravel-paved beds. J. Waterways Harbors Div. ASCE 93: 63-83.

Kellerhals, R., and D.I. Bray. 1971. Sampling procedures for coarse fluvial sediments. J. Hydraul. Div. ASCE 97: 1165-1180.

Kelsey, A. 1996. Modelling the sediment transport process. Ch. 7 in: Carling, P.A., and M.R. Dawson [Eds.]. Advances in fluvial dynamics and stratigraphy. John Wiley & Sons, New York.

Keshavarzy, A., and J.E. Ball. 1996. The influence of the turbulent shear stress on the initiation of motion in an open channel flow. p. 191-197 in: Tickle, K.S., and four others [Eds.]. Stochastic hydraulics '96. A.A. Balkema, Rotterdam, Netherlands.

Kiefling, J.W. 1978. Studies on the ecology of the Snake River cutthroat trout.

Wyoming Game Fish Dept. Fish. Tech. Bull. No. 3, Cheyenne. 198 p.

Kirchner, J.W., W.E. Dietrich, F. Iseya, and H. Ikeda. 1990. The variability of critical shear stress, friction angle, and grain protrusion in water-worked sediments. Sedimentology 37: 647-672.

Kitano, S., and K. Shimazaki. 1995. Spawning habitat and nest depth of female Dolly Varden *Salvelinus malma* of different body size. Fish. Science 61: 776-779.

Klassen, H.D., and T.G. Northcote. 1986. Stream bed configuration and stability following gabion weir placement to enhance salmonid production in a logged watershed subject to debris torrents. Can. J. For. Res. 16: 197-203.

Klingeman, P.C., and W.W. Emmett. 1982. Gravel bedload transport processes. Ch. 7 in: Hey, R.D., J.C. Bathurst, and C.R. Thorne [Eds.]. Gravel-bed rivers. John Wiley and Sons, New York, NY.

Klingeman, P.C., and C. Huang. 1993. Scour development at isolated river-bed obstacles. pp. 989-994 in: Shen, H.W., S.T. Su, and F. Wen [Eds.]. Hydraulic Engineering '93. Conf. Proc., San Francisco, CA, July 25-30. ASCE, New York, NY.

Knapp, R.A., and V.T. Vredenburg. 1996. Spawning by California golden trout: characteristics of spawning fish, seasonal and daily timing, redd characteristics, and microhabitat preferences. Trans. Am. Fish. Soc. 125: 519-531.

Knight, D. W., K.W.H. Yuen, and A.A.I. Al-Hamid. 1994. Boundary shear stress distributions in open channel flow. Ch. 4 in: K. J. Beven, P. C. Chatwin, and J. H. Milbank, [Eds]. Mixing and transport in the environment. John Wiley and Sons, Ltd., Chichester, England.

Komar, P.D. 1996. Entrainment of sediments from deposits of mixed grain sizes and densities. Ch. 4 in: Carling, P.A., and M.R. Dawson [Eds.]. Advances in fluvial dynamics and stratigraphy. John Wiley & Sons, New York.

Komar, P.D., and B. Cui. 1984. The analysis of grain-size measurements by sieving

and settling-tube techniques. J. Sed. Petrol. 54: 603-614.

Komar, P.D., and S.M. Shih. 1992. Equal mobility versus changing bedload grain sizes in gravel bed streams. Ch. 5 in: P. Billi, R.D. Hey, C.R. Thorne, and P. Tacconi [Eds.]. Dynamics of gravel-bed rivers. John Wiley and Sons. New York, N.Y.

Komura, S. 1963. Discussion of sediment transportation mechanics: introduction and properties of sediment. J. Hydraul. Div. ASCE 89: 263-266.

Kondolf, G.M. 1997. Application of the pebble count: Notes on purpose, method, and variants. J. Am. Water Resour. Assoc. 33: 79-87.

Kondolf, G.M., and W.V. Graham-Matthews. 1986.. Transport of tracer gravels on a coastal California river. J. Hydrol. 85: 265-280.

Kondolf, G.M., G.F. Cada, M.J. Sale, and T. Felando. 1991. Distribution and stability of potential salmonid spawning gravels in steep boulder-bed streams of the eastern Sierra Nevada. Trans. Am. Fish. Soc. 120: 177-186.

Kondolf, G.M., and M.G. Wolman. 1993. The sizes of salmonid spawning gravels. Water Resour. Res. 29: 2275-2285.

Kondolf, G.M., M.J. Sale, and M.G. Wolman. 1993. Modification of fluvial gravel size by spawning salmonids. Water Resour. Res. 29: 2265-2274.

Laronne, J.B., and M.A. Carson. 1976. Interrelationships between bed morphology and bed-material transport for a small, gravel-bed channel. Sedimentology 23: 67-85.

Laronne, J.B., and M.J. Duncan. 1989. Constraints on duration of sediment storage in a wide, gravel-bed river, New Zealand. p. 165-172 in: R.F. Hadley, and E.D. Ongley [Eds.]. Sediment and the environment. Proc. of the Baltimore Symp., May 1989. IAHS Publ. No. 184.

Laronne, J.B., D.N. Outhet, P.A. Carling, and T.J. McCabe. 1994. Scour chain employment in gravel bed rivers. Catena 22: 299-306.

Leopold, L.B., W.W. Emmett, and R.M. Myrick. 1966. Channel and hillslope processes in a semiarid area, New Mexico. USGS Prof. Paper 252.

Leopold, L.B., and D.C. Rosgen. 1991. Movement of bed material clasts in mountain streams. p. 4-183 - 4-188 in: Proc. Fifth Fed. Interagency Sed. Comm., March 18-21. Federal Energy Regulatory Commission.

Leopold, L.B., M.G. Wolman, and J.P. Miller. 1995. Fluvial processes in geomorphology. Republication. Dover Publications, Inc. New York, N.Y. 522 p.

Limerinos, J. T. 1970. Determination of the Manning coefficient from measured bed roughness in natural channels. U.S. Geol. Surv. Water Supply Paper 1898-B.

Lisle, T. 1979. A sorting mechanism for a riffle-pool sequence: Summary. Geol. Soc. Am. Bull. 90: 616-617.

Lisle, T. 1980. Sedimentation of spawning areas during storm flows, Jacoby Creek, North Coastal California. Presented at the fall meeting of the American Geophysical Union, San Francisco, December 8, 10 p.

Lisle, T.E. 1989. Sediment transport and resulting deposition in spawning gravels, north coastal California. Water Resour. Res. 25: 1303-1319.

Lisle, T.E. 1995. Particle size variations between bed load and bed material in natural gravel bed channels. Water Resour. Res. 31: 1107-1118.

Lisle, T.E., J.E. Pizzuto, H. Ikeda, F. Iseya, and Y. Kodama. 1997. Evolution of a sediment wave in an experimental channel. Water Resour. Res. 33: 1971-1981.

Lisle, T.E., and S. Hilton. 1999. Fine bed material in pools of natural gravel bed channels. Water. Resour. Res. 35: 1291-1304.

Lisle, T.E., Y. Cui, G. Parker, and J.E. Pizzuto. 2000. The dominance of dispersion in the evolution of bed load pulses in gravel bed rivers. Submitted to Earth Surf. Proc. Land. *In review.*

Lister, D.B., and C.E. Walker. 1966. The effect of flow control on freshwater survival of chum, coho, and chinook salmon in the Big Qualicum River. Can. Fish Cult. 37: 3-25.

Lyn, D.A. 1987. Unsteady sediment-transport modeling. J. Hydraulic Engin. 113: 1-15.

Madej. M.A. 1996. Changes in channel-stored sediment, Redwood Creek, northwestern California, 1947 to 1980. Geomorphic processes and aquatic habitat in the Redwood Creek basin, northwestern California. U.S. Geol. Surv. Prof. Pap. 1454-O. 27 p.

Martini, I.P. 1977. Gravelly flood deposits of Irvine Creek, Ontario, Canada. Sedimentology 24: 603-622.

Maynord, S.T. 1996. Toe-scour estimation in stabilized bendways. J. Hydraul. Engin. 122: 460-464.

McNeil, W.J. 1962. Mortality of pink and chum salmon eggs and larvae in southeast Alaska streams. Ph.D. Diss. Univ. Wash., Seattle.

McNeil, W.J. 1966. Effect of the spawning bed environment on reproduction of pink and chum salmon. Fish. Bull. 65: 495-523.

McNeil, W.J., and W.H. Ahnell. 1960. Measurement of gravel composition of salmon stream beds. Fish. Res. Inst. Circ. 120. Univ. Wash., Seattle WA. 7 p.

Meehan, W.R,. 1991. Influences of forest and rangeland management on salmonid fishes and their habitat. Am. Fish. Soc. Spec. Publ. 19. Bethesda, MD.

Milhous, R.T. 1973. Sediment transport in a gravel-bottomed stream. Ph.D. Thesis, Oregon State Univ., Corvallis OR. 232 p.

Milhous, R.T., S.A. Hogan, S.R. Abt, and C.C. Watson. 1995. Sampling river-bed material: the barrel sampler. Rivers 5: 239-249.

Montgomery, D.R., J.M. Buffington, N.P. Peterson, D. Schuett-Hames, and T.P. Quinn. 1996. Stream-bed scour, egg burial depths, and the influence of salmonid spawning on bed surface mobility and embryo survival. Can. J. Fish. Aq. Sci. 53: 1061-1070.

Montgomery, D.R., and J.M. Buffington. 1997. Channel-reach morphology in mountain drainage basins. GSA Bull. 109: 596-611.

Montgomery, D.R., E.M. Beamer, G.R. Pess, and T.P. Quinn. 1999. Channel type and salmonid spawning distribution and abundance. Can. J. Fish. Aq. Sci. 56: 377-387.

Moring, J.R. 1975. The Alsea watershed study: Effects of logging on the aquatic resources of three headwater streams of the Alsea River, Oregon. Part II - Changes in Environmental conditions. Fish. Res. Rep. No. 9, Or. Dept. Fish Wild. Corvallis. 26 p.

Mosley, M.P. 1978. Bed material transport in the Tamaki River near Dannevirke, North Island, New Zealand. N.Z. J. Sci. 21: 619-626.

Nawa, R.K., and C.A. Frissell. 1993. Measuring scour and fill of gravel streambeds with scour chains and sliding-bead monitors. N. Am. J. Fish. Manag. 13: 634-639.

Nehlsen, W., J.E. Williams, and J.A. Lichatowich. 1991. Pacific salmon at the crossroads: stocks at risk from California, Oregon, Idaho, and Washington. Fisheries 16: 4-21.

Nelson, J.M., and J.D. Smith. 1989. Flow in meandering channels with natural topography. p. 69-102 in: Ikeda, S., and G. Parker [Eds.]. River meandering. AGU Water Resour. Mono. No. 12. Washington, D.C.

Nelson, J.M., R.L. Shreve, S.R. McLean, and T.G. Drake. 1995. Role of near-bed turbulence structure in bed load transport and bed form mechanics. Water Resour. Res. 31: 2071-2086.

Newson, M.D. 1987. Discussion. p. 639-640 in: Thorne, C.R., J.C. Bathurst, and R.D. Hey [Eds.]. Sediment transport in gravel-bed rivers. John Wiley and Sons, New York, NY. 995 p.

Nezu, I., and Y. Nakagawa. 1993. Turbulence in open-channel flows. IAHR Monograph. A.A. Balkema, Rotterdam, Netherlands. 281 p.

Nicholas, A.P., P.J. Ashworth, M.J. Kirkby, M.G. Mackin, and T. Murray. 1995. Sediment slugs: Large-scale fluctuations in fluvial sediment transport rates and storage volumes. Prog. Phys. Geog. 19: 500-519.

Nnadi, F.N., and K.C. Wilson. 1992. Motion of contact-load particles at high shear stress. J. Hydraulic Engin. 118: 1670-1684.

O'Connor, M., and R.D. Harr. 1994. Bedload transport and large organic debris in steep mountain streams in forested watersheds on the Olympic Peninsula, Washington. Final report to Timber/Fish/Wildlife, Sediment, Hydrology and Mass Wasting Steering Comm. and the State of Wa. Dept. Nat. Resour., Olympia. October 31.

Onoda, G.Y., and E.G. Liniger. 1990. Random loose packings of uniform spheres and the dilatancy onset. Phys. Rev. Let. 64: 2727-2730.

Orsborn, J.F., and S.C. Ralph. 1994. An aquatic reosurce assessment of the Dungeness River system: Phase II - Physical channel analysis, hydrology and hydraulics and Phase III - Fisheries habitat survey. Report prepared for the Jamestown S'Klallam Tribe, Sequim WA.

Paola, C., and R. Seal. 1995. Grain size patchiness as a cause of selective deposition and downstream fining. Water Resour. Res. 31: 1395-1407.

Parker, G. 1978. Self-formed straight rivers with equilibrium banks and mobile bed. Part 2. The gravel river. J. Fluid Mech. 89: 127-146.

Parker, G. 1990a. Surface-based bedload transport relation for gravel rivers. J. Hydraul. Res. 28: 417-436.

Parker, G. 1990b. The "ACRONYM" series of Pascal programs for computing bedload transport in gravel rivers. External Memo. No. M-220. St. Anthony Falls Hydraulic Lab., Univ. Minn. Minneapolis. February.

Parker, G., and A.W. Peterson. 1980. Bar resistance of gravel-bed streams. J. Hydraul. Div. ASCE 106: 1559-1575.

Parker, G., and P.C. Klingeman. 1982. On why gravel bed streams are paved. Water Resour. Res. 18: 1409-1423.

Parker, G., S. Dhamotharan, and H. Stefan. 1982a. Model experiments on mobile, paved gravel bed streams. Water Resour. Res. 18: 1395-1408.

Parker, G., P.C. Klingeman, and D.L. McLean. 1982b. Bedload and size

distribution in paved gravel-bed streams. J. Hydraul. Div. ASCE 108: 544-571.

Parker, G., and A.J. Sutherland. 1990. Fluvial armor. J. Hydraul. Res. 28: 529-544.

Passman, S.L., J.W. Nunziato, P.B. Bailey, and J.P. Thomas, Jr. 1980. Shearing flows of granular materials. J. Engin. Mech. Div. ASCE 106: 773-783.

Peterson, N.P., and T.P. Quinn. 1996. Persistence of egg pocket architecture in redds of chum salmon, *Oncorhynchus keta*. Env. Biol. Fishes 46: 243-253.

Pitlick, J. 1992. Flow resistance under conditions of intense gravel transport. Water Resour. Res. 28: 891-903.

Prestegaard, K.L. 1987. Sediment transport and deposition zones in braided streams. p. 411-412 in: Beschta, R.L., T. Blinn, G.E. Grant, F.J. Swanson, and G.G. Ice [Eds.]. Erosion and sedimentation in the Pacific rim. IAHS Publ. No. 165.891-903.

Rantz, S.E., and others. 1982. Measurement and computation of streamflow: Volume 1, measurement of stage and discharge, and Volume 2, computation of discharge. USGS Water Supply Paper 2175. Washington D.C. 631 p.

Rajaratnam, N. 1981. Erosion by plane turbulent jets. J. Hydraul. Res. 19: 339-358.

Reid, I., and L.E. Frostick. 1984. Particle interaction and its effect on the thresholds of initial and final bedload motion in coarse alluvial channels. p. 61-68 in: Koster, E.H., and R.J. Steel [Eds.]. Sedimentology of gravels and conglomerates. Can. Soc. Pet. Geol. Mem. 10.

Reid, I., L.E. Frostick, and J.T. Layman. 1985. The incidence and nature of bedload transport during flood flows in coarse-grained alluvial channels. Earth Surf. Proc. Land. 10: 33-44.

Reiser, D.W., and T.A. Wesche. 1977. Determination of physical and hydraulic preferences of brown and brook trout in the selection of spawning locations. Water Resour. Ser. No. 64, Water Resour. Res. Inst., Univ. Wyoming,

Laramie. 100 p.

Rennie, C.D. 1998. Bed mobility of gravel rivers: Mobilization (scour) depth of
chum salmon redds, and equilibrium bedload transport. M.A.S. Thesis, Univ.
British Columbia, Vancouver. 168 p.

Resh, V.H., and others. 1988. The role of disturbance in stream ecology. J. N.
Am. Benthol. Soc. 7: 433-455.

Rice, S., and M. Church. 1996. Sampling surficial fluvial gravels: the precision of
size distribution percentile estimates. J. Sed. Res. 66: 654-665.

Richards, K. 1982. Rivers: Form and process in alluvial channels. Methuen,
London. 361 p.

Richardson, E.V., and J.R. Richardson. 1994. Practical method for calculating
contraction scour. p. 6-10 in: Cotoneo, G.V. and R.R. Rumer [Eds.].
Hydraulic Engineering '94. Conf. Proc., Buffalo, New York, August 1-5.
ASCE, New York, NY.

Ricker. W.E., H.T. Bilton, and K.V. Aro. 1978. Causes of the decline in size of
pink salmon (*Oncorhynchus gorbuscha*). Fish. Mar. Serv. Tech. Rep. 820,
Dept. of Fish.and the Envir.,Canada.

Rukhlov, F.N. 1969. Materials characterizing the texture of bottom material in the
spawning grounds and redds of the pink salmon [*Oncorhynchus gorbuscha*
(Walbaum)] and the autumn chum salmon [*Oncorhynchus keta* (Walbaum)] on
Sakhalin. J. Ichthy. 9: 636-644.

Rust, B.R. 1972. Pebble orientation in fluvial sediments. J. Sed. Petrol. 42: 384-
388.

Savage, S.B., and M. Sayed. 1984. Stresses developed by dry cohesionless granular
materials sheared in an annular shear cell. J. Fluid Mech. 142: 391-430.

Schick, A.P., J. Lekach, and M.A. Hassan. 1987. Bed load transport in desert
floods: observations in the Negev. Ch. 20 in: Thorne, C.R., J.C. Bathurst,
and R.D. Hey [Eds.]. Sediment transport in gravel-bed rivers. John Wiley
and Sons, New York, NY. 995 p.

Schmidt, K.H., and D. Gintz. 1995. Results of bedload tracer experiments in a mountain river. Ch. 3 in: E.J. Hickin [Ed.]. River Geomorphology. John Wiley and Sons, New York.

Schuett-Hames, D., B. Conrad, A. Pleus, and K. Lautz. 1996. Literature review and monitoring recommendations for salmonid spawning gravel scour. TFW Ambient Monitoring Program TFW-AM-9-96-001. Olympia WA. 23 p.

Schuett-Hames, D.E., N.P. Peterson, R. Conrad, and T.P. Quinn. 2000. Effects of gravel scour and fill on salmonid incubation habitat. N. Am. J. Fish. Manag. *In review.*

Scott, W.B., and E.J. Crossman. 1973. Freshwater fishes of Canada. Fish. Res. Bd. Can. Bull. 184.

Scrivener, J.C., and M.J. Brownlee. 1989. Effects of forest harvesting on spawning gravel and incubation survival of chum (*Oncorhynchus keta*) and coho salmon (*O. kisutch*) in Carnation Creek, British Columbia. Can. J. Fish. Aquat. Sci. 46: 681-696.

Seegrist, D.W., and R. Gard. 1972. Effects of floods on trout in Sagehen Creek, California. Trans. Am. Fish. Soc. 101(3): 478-482.

Seiler, D., L. 1999. 1999 wild coho forecasts for Puget Sound & Washington coastal systems. Wash. Dept. Fish and Wild., Olympia WA.

Seiler, D., and L. Kishimoto. 1997. Annual Report: 1997 Cedar River sockeye salmon fry production evaluation. Wash. Dept. Fish and Wild., Olympia WA. April.

Seiler, D., L. Kishimoto, and S. Neuhauser. 1998. Annual Report: 1997 Skagit River wild 0+ chinook production evaluation. Wash. Dept. Fish and Wild., Olympia WA. April.

Shepard, B.B., K. Pratt, and P.J. Graham. 1984. Life histories of westslope cutthroat and bull trout in the upper Flathead River basin, Montana. Mont. Dept. Fish, Wild. Parks, Kalispell.

Shiono, K., and Knight, D. W. 1991. Turbulent open channel flows with variable

depth across the channel. J. Fluid Mech., 222, 617-646.

Simons, D.B., and F. Şentürk. 1977. Sediment transport technology. Water Resources Publications, Fort Collins, CO.

Smirnov, A.I. 1959. The effect of mechanical agitation on developing eggs of the pink salmon *Oncorhynchus gorbuscha* (Walbaum). Salmonidae. Fish. Res. Bd. Can. Trans. Ser. No. 231. 5 p.

Steen, R.P., and T.P. Quinn. 1999. Egg burial depth by sockeye salmon (*Oncorhynchus nerka*): Implications for survival of embryos and natural selection on female body size. Can. J. Zool. 77: 836-841.

Stelczer, K. 1981. Bed-load transport: Theory and practice. Water Resources Publication, Littleton CO. 295 p.

Stober, Q.J., R.E. Narita, and A.H. Hamalainen. 1978a. Instream flow and the reproductive efficiency of sockeye salmon. Fish. Res. Inst., Univ. of Washington, Seattle WA. FRI-UW-7808. 124 p.

Stober, Q.J., S.Crunley, and R.L. McComas. 1978b. Prespawning mortality and the reproductive efficiency of Cedar River sockeye salmon. Fish. Res. Inst., Univ. of Washington, Seattle WA. FRI-UW-7809. 53 p.

Street, R.L., G.Z. Watters, and J.K. Vennard. 1996. Elementary fluid mechanics, 7th ed. John Wiley and Sons, New York, NY. 757 p.

Stuart, T.A. 1953. Spawning migration, reproduction and young stages of Loch trout (*Salmo trutta* L.). Fresh. Sal. Fish. Res. No. 5, Scottish Home Dept., Edinburgh. 39 p.

Sumer, B.M., A. Kozakiewicz, J. Fredsøe, and R. Deigaard. 1996. Velocity and concentration profiles in sheet-flow layer of movable bed. J. Hydraulic Engin. 122: 549-558.

Tagart, J.V. 1976. The survival from egg deposition to emergence of coho salmon in the Clearwater River, Jefferson County, Washington. M.Sc. Thesis, Univ. Wash., Seattle. 101 p.

Tautz, A.F., and C. Groot. 1975. Spawning behavior of chum salmon

(*Oncorhynchus keta*) and rainbow trout (*Salmo gairdneri*). J. Fish. Res. Bd. Can. 32: 633-642.

Thomas, W.A. 1982. Mathematical modelling of sediment movement. Ch. 18 in: Hey, R.D., J.C. Bathurst, and C.R. Thorne [Eds.]. Gravel-bed rivers. John Wiley and Sons, New York, NY.

Thorne, R.E., and J.J. Ames. 1987. A note on variability of marine survival of sockeye salmon (*Oncorhynchus nerka*) and effects of flooding on spawning success. Can. J. Fish. Aquat. Sci. 44: 1791-1795.

Tribe, S., and M. Church. 1999. Simulations of cobble structure on a gravel streambed. Water Resour. Res. 35: 311-318.

Tripp, D.B., and V.A. Poulin. 1986. The effects of logging and mass wasting on salmonid spawning habitat in streams on the Queen Charlotte Islands. B.C. Min. For. Lands, Land Manag. Rep. No. 50. 29 p.

van den Berghe, E.P., and M.R. Gross. 1984. Female size and nest depth in coho salmon (*Oncorhynchus kisutch*). Can. J. Fish. Aquat. Sci. 41: 204-206.

Vanoni, V.A. 1975. Sedimentation engineering. ASCE Man. and Rep. on Engin. Prac. No. 54. ASCE, New York, NY. 745 p.

Vaux, W.G. 1962. Interchange of stream and intergravel water in a salmon spawning riffle. U.S. Fish Wild. Serv. Spec. Sci. Rept. Fish. 405. 11 p.

Vronskii, B.B. 1972. Reproductive biology of the Kamchatka River chinook salmon [*Oncorhynchus tshawytscha* (Walbaum)]. J. Ichthy. 12: 259-273.

Washington Forest Practices Board (WFPB). 1994. Standard methodology for conducting watershed analysis. Version 2.1 Olympia, WA.

Wathen, S.J., T.B. Hoey, and A. Werrity. 1997. Quantitative determination of the activity of within-reach sediment storage in a small gravel-bed river using transit time and response time. Geomorphology 20: 113-134.

Wathen, S.J., and T.B. Hoey. 1998. Morphological controls on the downstream passage of a sediment wave in a gravel-bed stream. Earth Surf. Proc. Land. 23: 715-730.

Webb, P.W. 1978. Hydrodynamics: Nonscombroid fish. Ch. 3 in: Hoar, W.S., and D.J. Randall [Eds.]. Fish physiology, Volume VII: Locomotion. Academic Press, New York NY.

Whiting, P. J., W.E. Dietrich, L.B. Leopold, T.G. Drake, and R.L. Shreve. 1988. Bedload sheets in heterogeneous sediment. Geol. 16: 105-108.

Whiting, P. J., and W.E. Dietrich. 1990. "Boundary shear stress and roughness over mobile alluvial beds." J. Hydraulic Engin. 116(12), 1495-1511.

Wiberg, P. L., and Smith, J. D. 1991. Velocity distribution and bed roughness in high-gradient streams. Water Resour. Res. 27(5), 825-838.

Wilcock, P.R. 1996. Estimating local bed shear stress from velocity observations. Water Resour. Res. 32: 3361-3366.

Wilcock, P.R. 1997a. Entrainment, displacement and transport of tracer gravels. Earth Surf. Proc. Land. 22: 1125-1138.

Wilcock, P.R. 1997b. The components of fractional transport rate. Water Resour. Res. 33: 247-258.

Wilcock, P.R., and B.W. McArdell. 1993. Surface-based fractional transport rates: Mobilization thresholds and partial transport of a sand-gravel sediment. Water Resour. Res. 29: 1297-1312.

Wilcock, P.R., A.F. Barta, C.G. Shea, G.M. Kondolf, W.V.G. Matthews, and J. Pitlick. 1996. Observations of flow and sediment entrainment on a large gravel-bed river. Water Resour. Res. 32: 2897-2909.

Wilcock, P.R., and B.W. McArdell. 1997. Partial transport of a sand/gravel sediment. Water Resour. Res. 33: 235-245.

Wilson, K.C. 1987. Analysis of bed-load motion at high shear stress. J. Hydraulic Engin. 113: 97-103.

Withler, F.C. 1952. Sockeye reproduction in a tributary of Babine Lake, 1950-51. Fish. Res. Bd. Can. Prog. Rep. Pac. Coast Stns. 91: 13-17.

Witzel, L.D., and H.R. MacCrimmon. 1983. Redd-site selection by brook trout and brown trout in southwestern Ontario streams. Trans. Am. Fish. Soc. 112:

760-771.

Wolcott, J., and M. Church. 1991. Strategies for sampling spatially heterogeneous phenomena: The example of river gravels. J. Sed. Pet. 61: 534-543.

Wolman, M.G. 1954. A method of sampling coarse river-bed material. Trans. Am. Geophys. Union 35: 951-956.

Wolman, M.G., and J.P. Miller. 1960. Magnitude and frequency of forces in geomorphic processes. J. Geol. 68: 54-74.

Wright, S. 1999. Critical fish population management elements that are necessary for the future recovery of at-risk chinook salmon (*Oncorhynchus tschawytscha*) stocks. Report prepared for Washington Trout, Duvall, WA.

Yalin, M.S. 1977. Mechanics of sediment transport. Pergamon Press, Oxford. 298 p.

Yee, C.S. 1981. Scour and fill of spawning gravels in a small coastal stream of northwestern California. Coop. Res. Proj. Final Report, Pac. SW. For. Range Expt. Stn, and Humboldt St. Univ. Arcata, CA. 29p.

Young, M.K., W.A. Hubert, and T.A. Wesche. 1991. Biases associated with four stream substrate samplers. Can. J. Fish. Aq. Sci. 48: 1882-1886.

Appendix A

SITE LOCATIONS, PHOTOGRAPHS AND MAPS
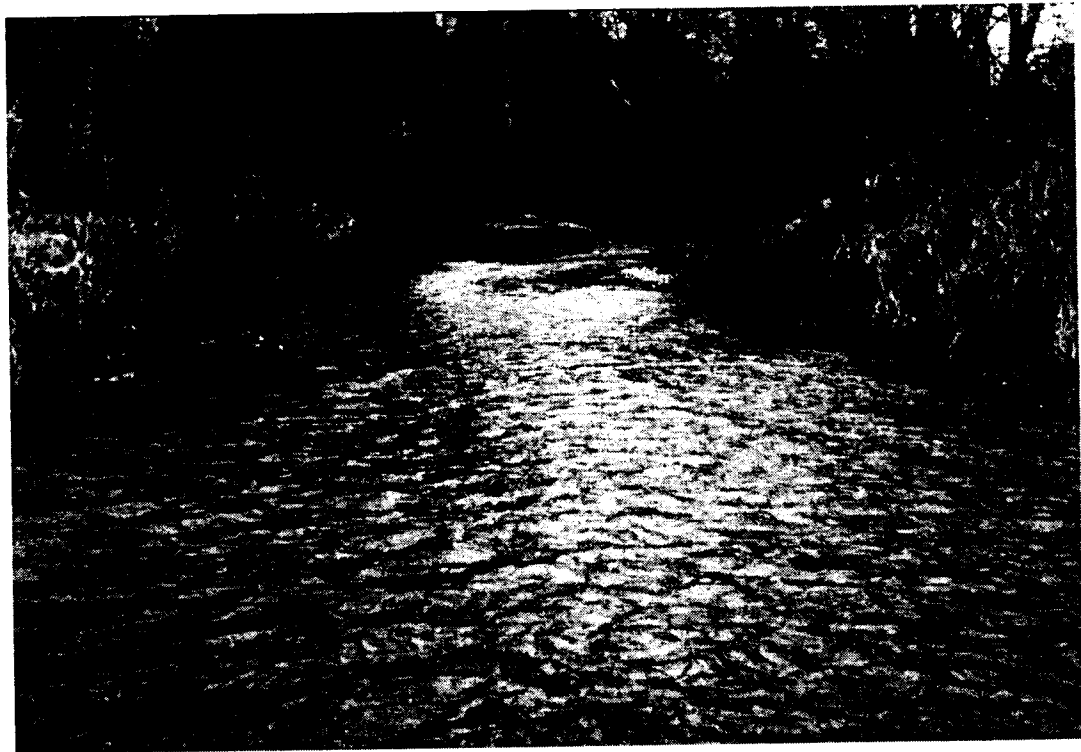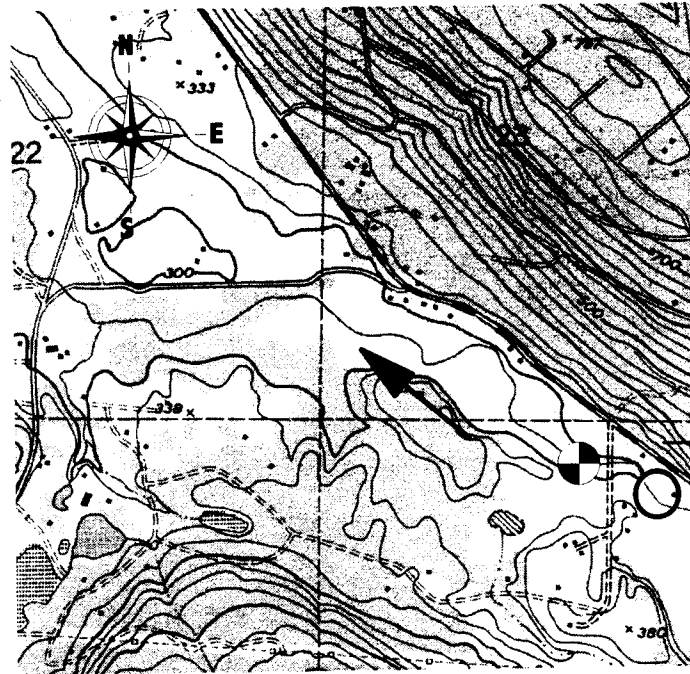
Figure A-1. Location and representative photograph of the Issaquah Creek study
site. The site (circled), USGS gage, and flow direction are indicated
on the map. Photograph looks upstream at site: 1996-97 transects are
located near the center of the picture; 1997-98 transects are
distributed throughout visible length of stream.
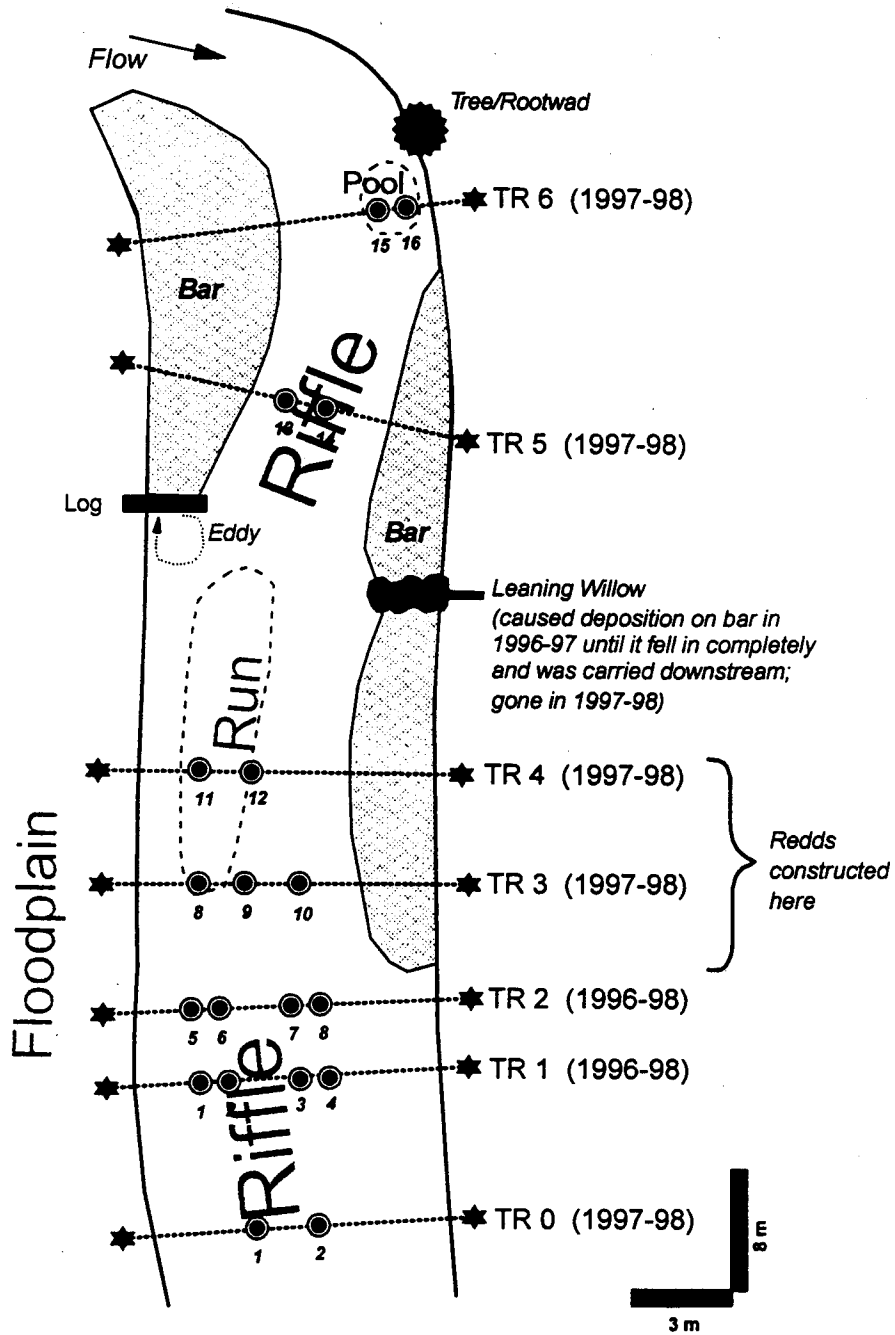
Figure A-2. Issaquah Creek study site map. Scour monitor locations and identification numbers are depicted; transects are labeled according to year(s) sampled. Scale is approximate.
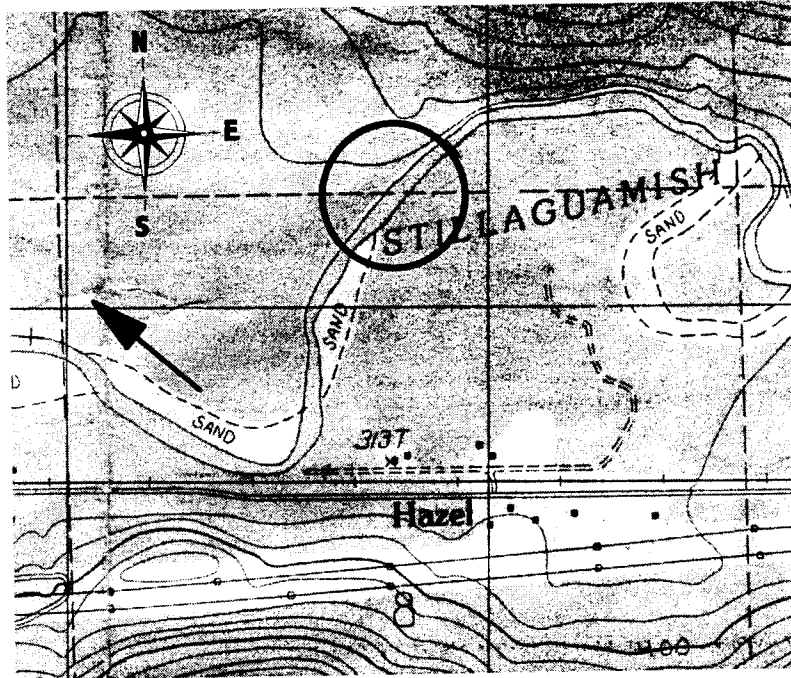
Figure A-3. Location and representative photograph of the North Fork Stillaguamish River at Hazel study site. The site (circled) and flow direction are indicated on the map. Photograph looks downstream at site: Transect 3 is located near downstream end of bar, Transect 1 is near the leaning trees on right bank.
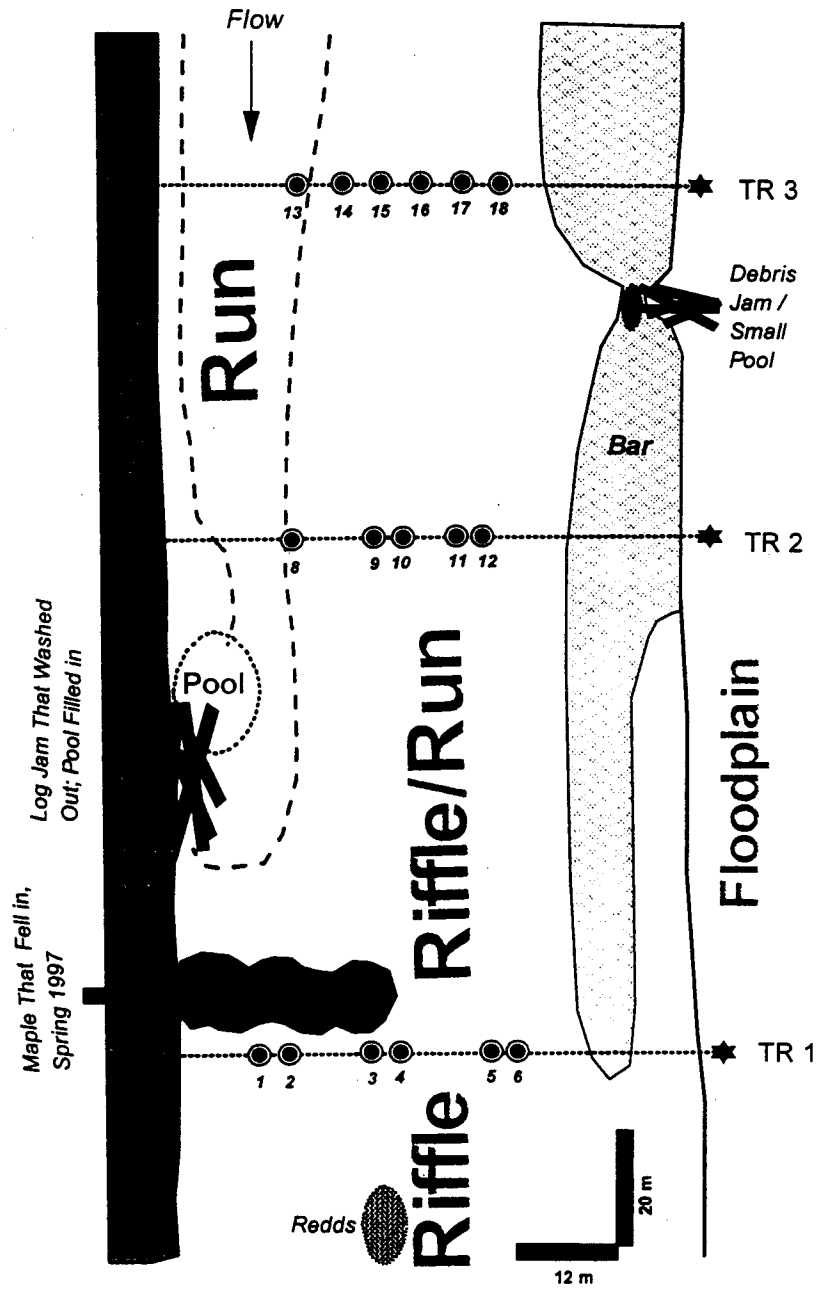
Figure A-4. North Fork Stillaguamish River at Hazel study site map. Scour monitor locations and identification numbers are depicted. Scale is approximate.
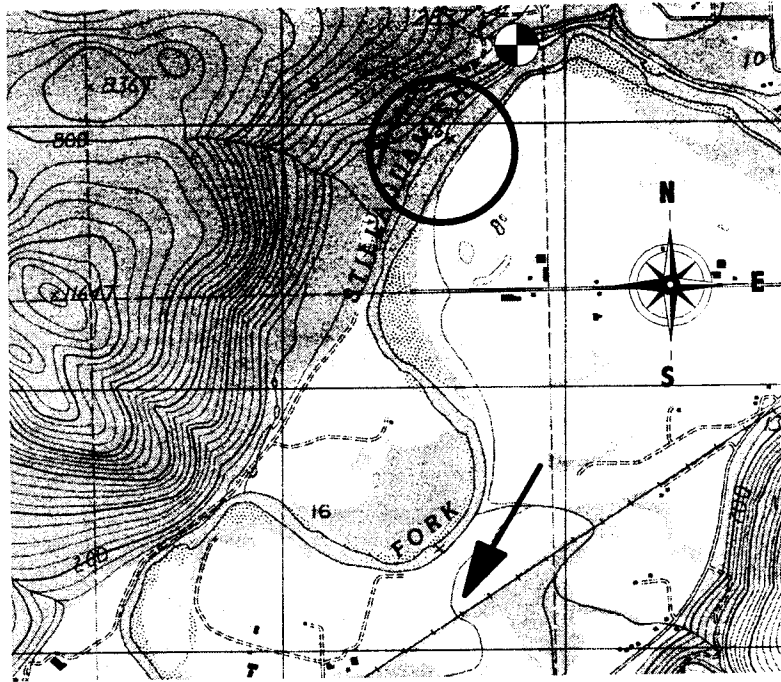
Figure A-5. Location and representative photograph of the North Fork Stillaguamish River USGS study site. The site (circled), USGS gage, and flow direction are indicated on the map. Photograph looks upstream at site: Transects 1 and 2 are located across the bar in the foreground; Transect 3 is located across bar in background.
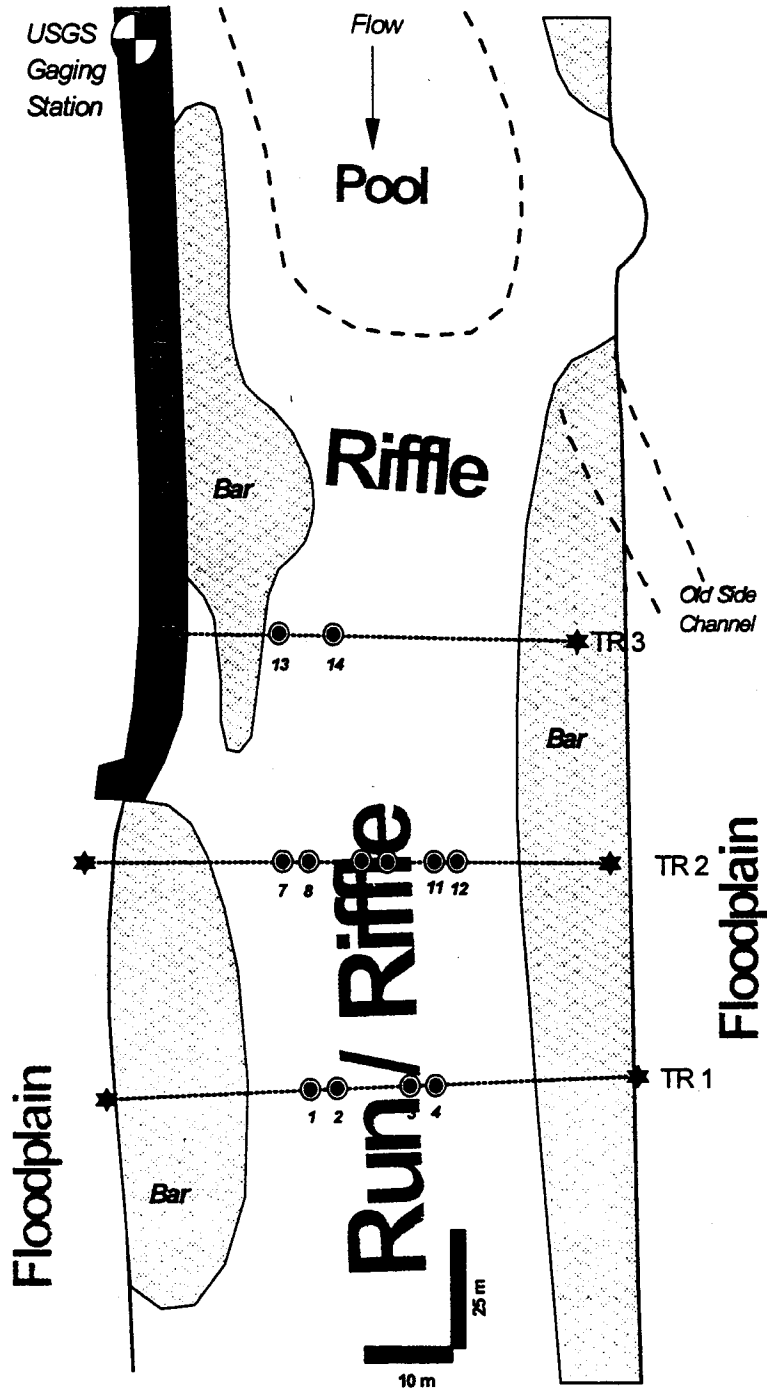
Figure A-6. North Fork Stillaguamish River at USGS study site map. Scour monitor locations and identification numbers are depicted. Scale is approximate.
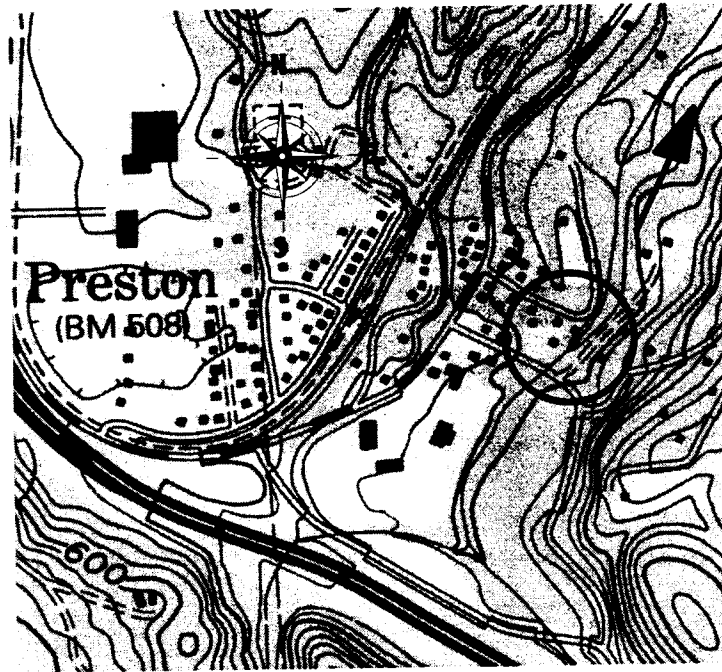
Figure A-7. Location and representative photograph of the Raging River study
site. The site (circled) and flow direction are indicated on the map.
Photograph looks upstream at site: Transects 1 and 2 are located at
and above the riffle crest in foreground; upstream riffle is just visible
upstream of bridge; additional 1997-98 transects are located between
the riffles.
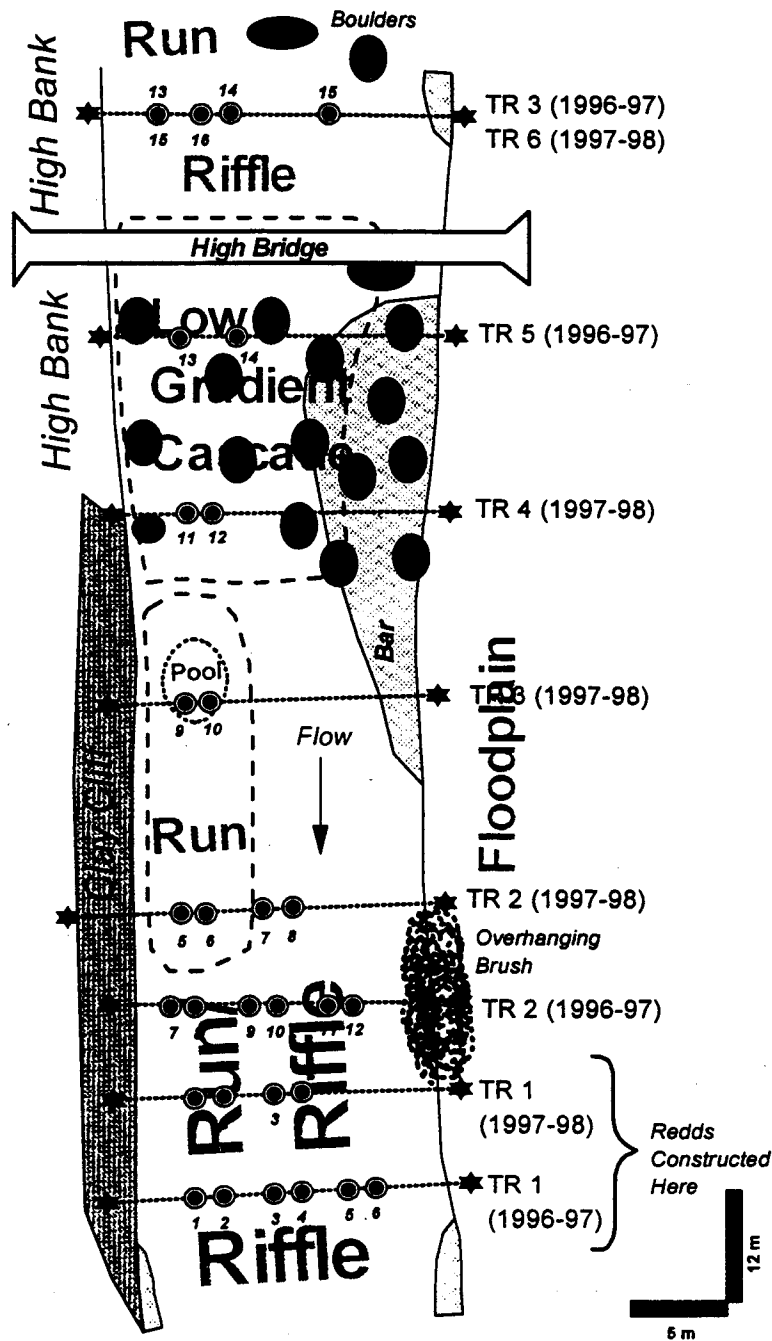
Figure A-8. Raging River study site map. Scour monitor locations and identification numbers are depicted; transects are labeled according to year(s) sampled. Scale is approximate.

260
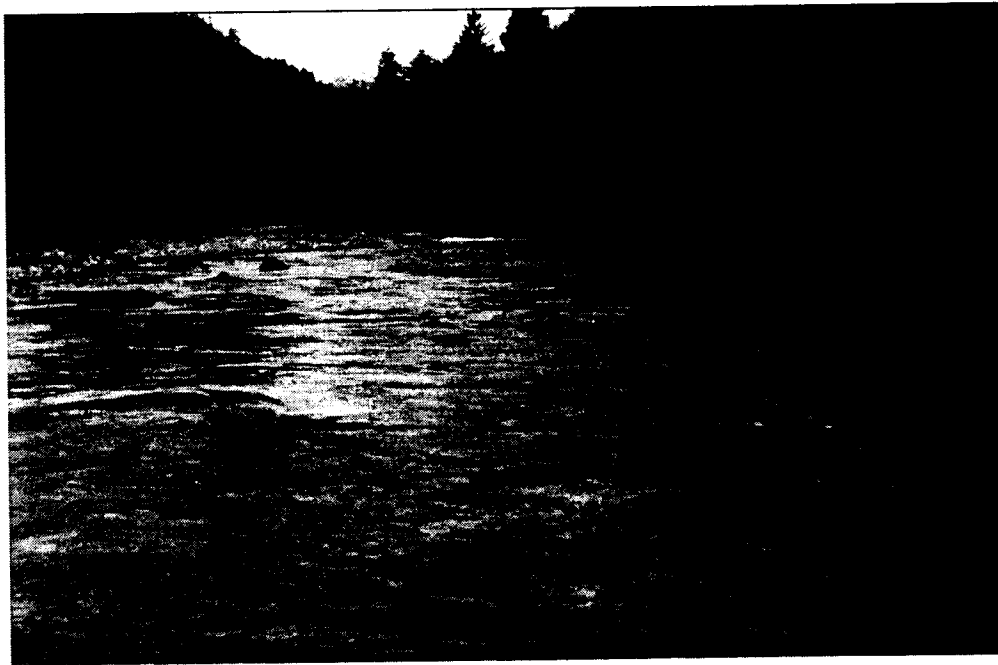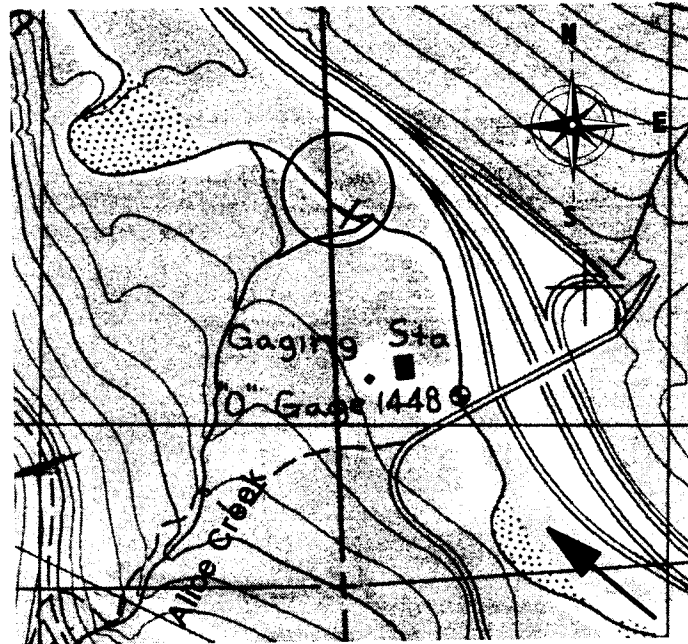
Figure A-9. Location and representative photograph of the S. Fk. Snoqualmie River study site. The site (circled), USGS gage, flow direction, and new channel location of Alice Creek are indicated on map. Photograph looks upstream at site: Transects 1 and 2 are located near center of photo; upstream riffle is above bar; extra 1997-98 transects are located between riffles and at upstream edge of upper riffle, below Alice Creek.
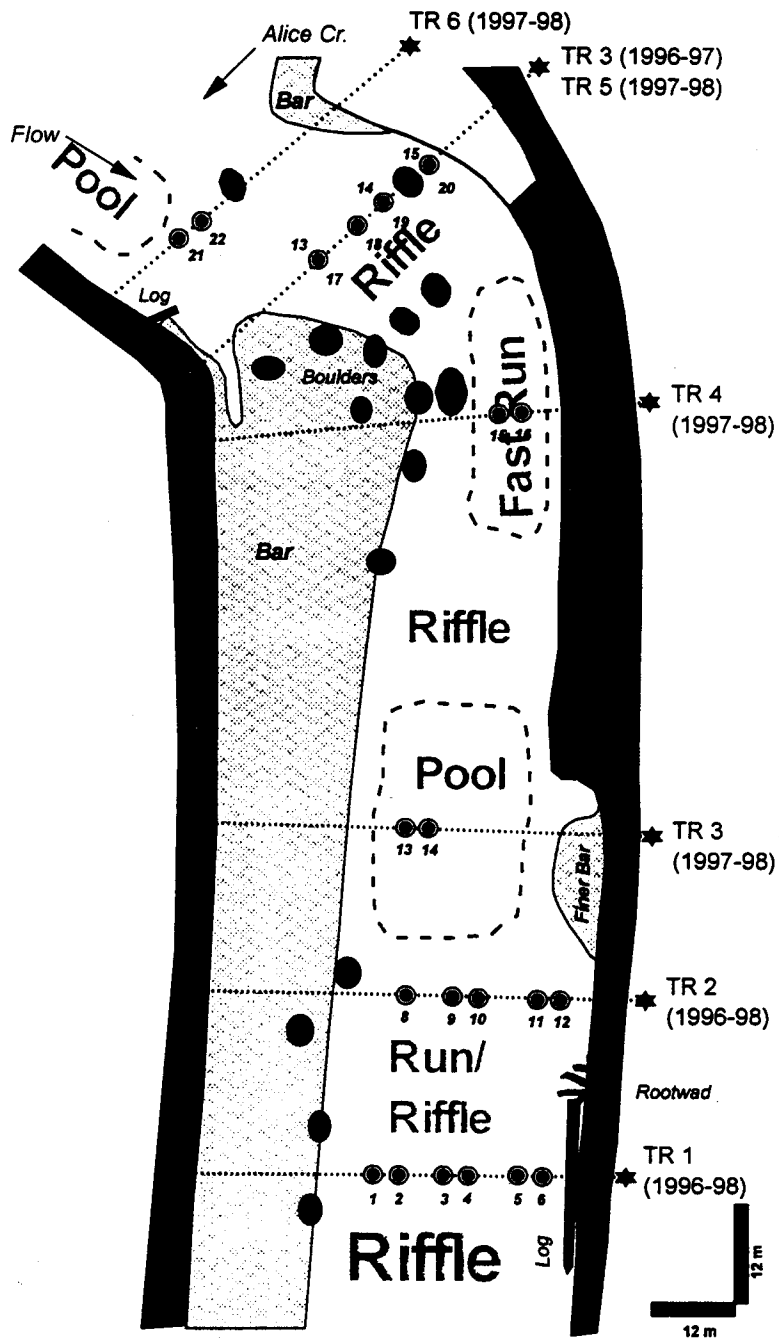
Figure A-10. South Fork Snoqualmie River study site map. Scour monitor locations and identification numbers are depicted; transects are labeled according to year(s) sampled. Scale is approximate.
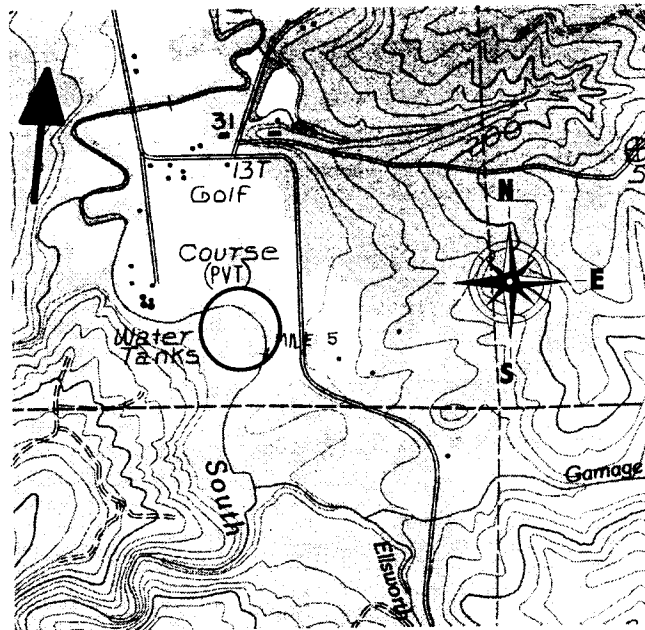
Figure A-11. Location and representative photograph of the South Fork Willapa
River study site. The site (circled) and flow direction are indicated on
map. Photograph looks downstream at lower riffle: Transect 1 is
located near riffle crest in background, and Transect 2 is located
across bar in center of photograph.
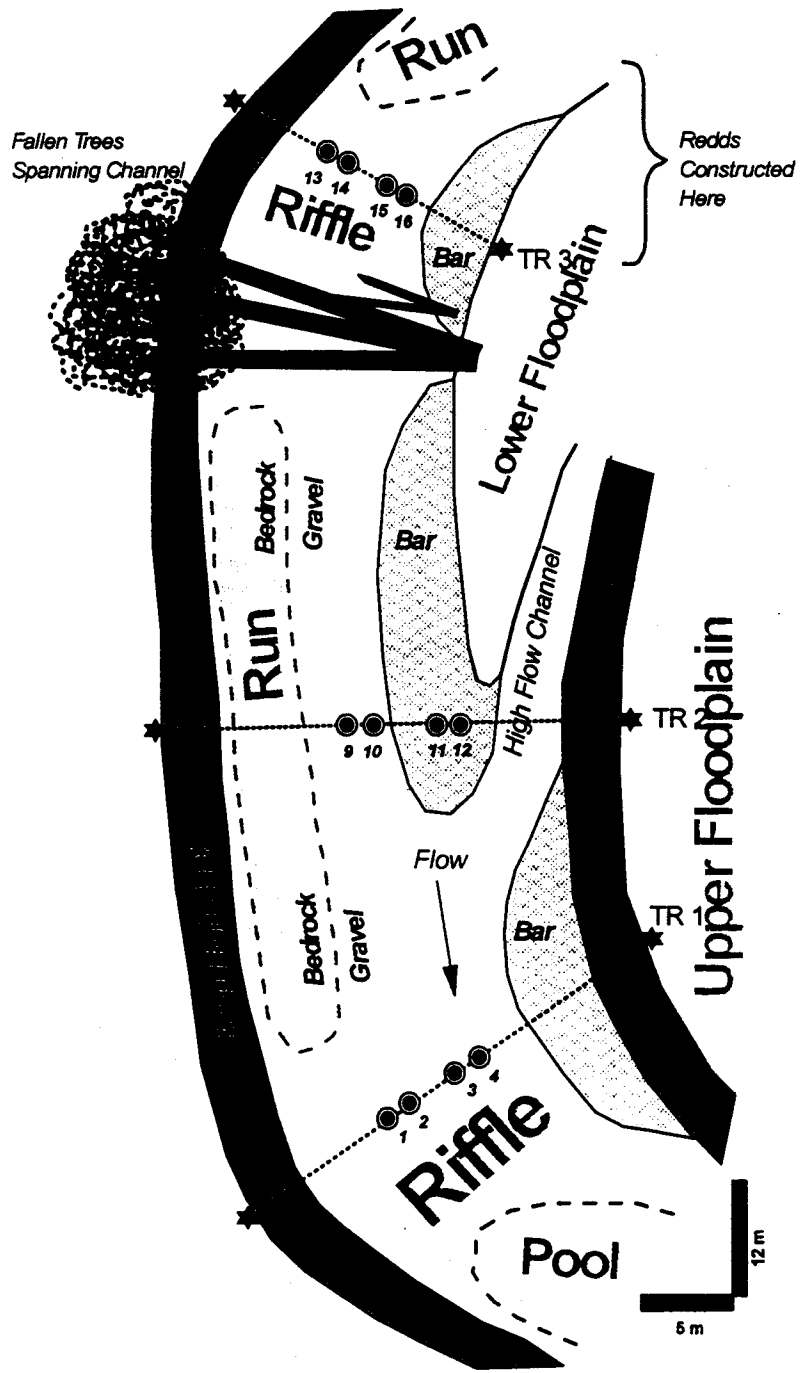
Figure A-12. South Fork Willapa River study site map. Scour monitor locations and identification numbers are depicted. Scale is approximate.
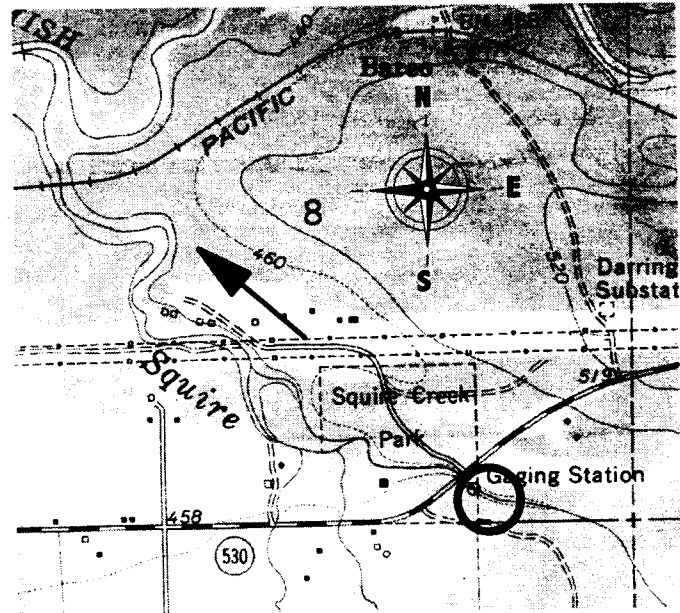
Figure A-13. Location and representative photograph of the Squire Creek study
site. The site (circled), discontinued USGS gage, and flow direction
are indicated on map. Photograph looks downstream at site:
Transects 1 and 2 are located in downstream riffle; Transect 3 is
located in pool tail, above upstream riffle that is visible in foreground.
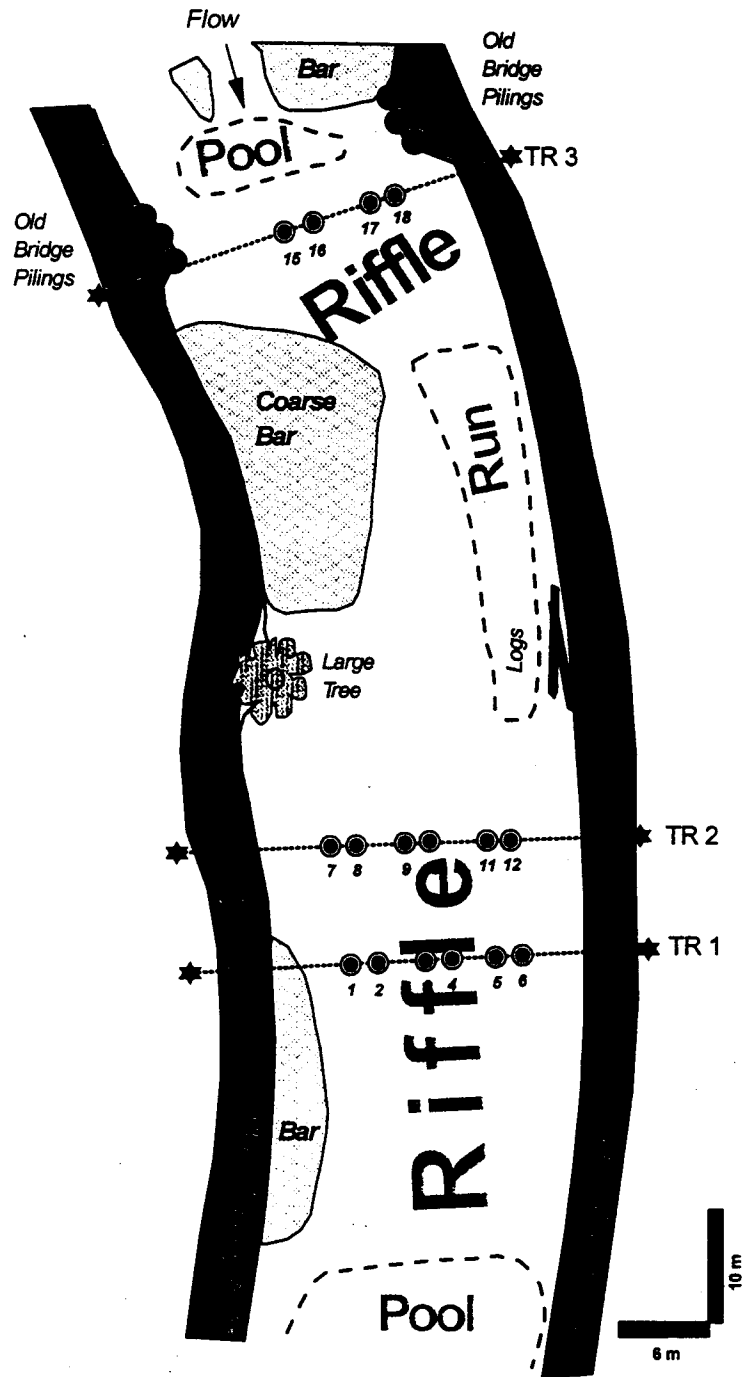
Figure A-14. Squire Creek study site map. Scour monitor locations and identification numbers are depicted. Scale is approximate.
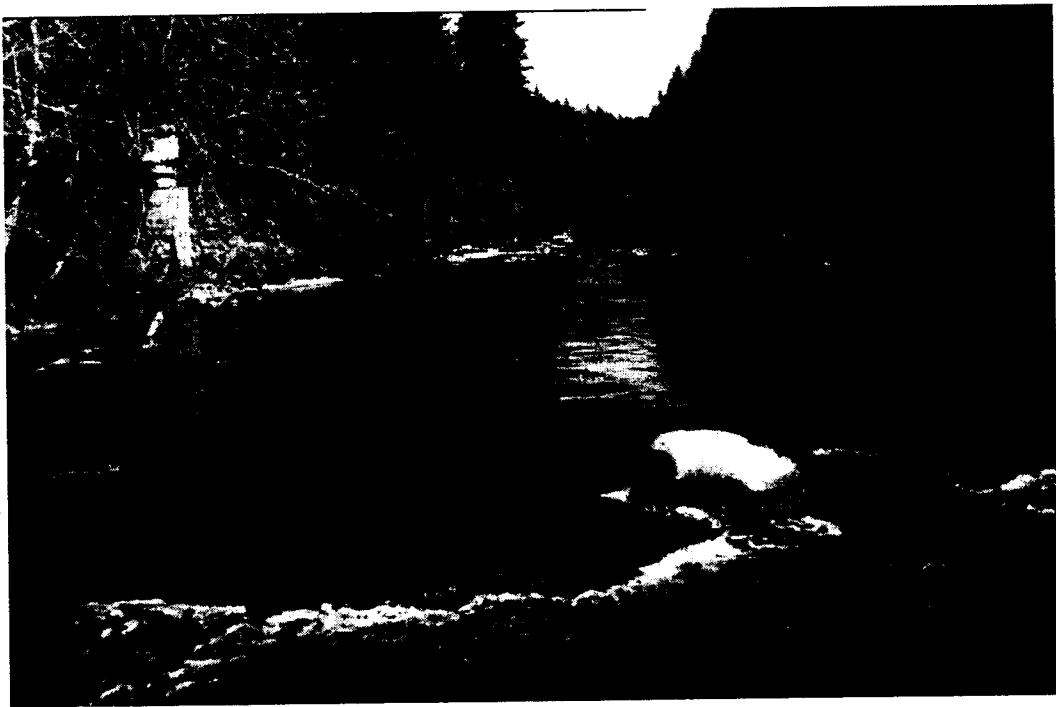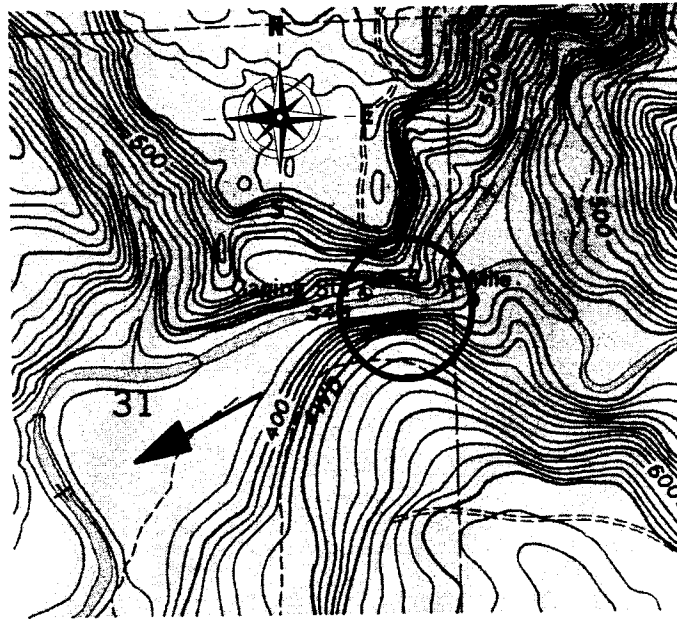
Figure A-15. Location and representative photograph of the Tolt River study site. The site (circled), USGS gage, and flow direction are indicated on map. Photograph looks upstream at site: Transects 1, 2 and 3 are located near riffle crest and in pool tail, at center of photo; USGS gaging station, visible at left, is located between Transects 2 and 3. Upstream riffle is located above low gradient cascade in background, below forks.
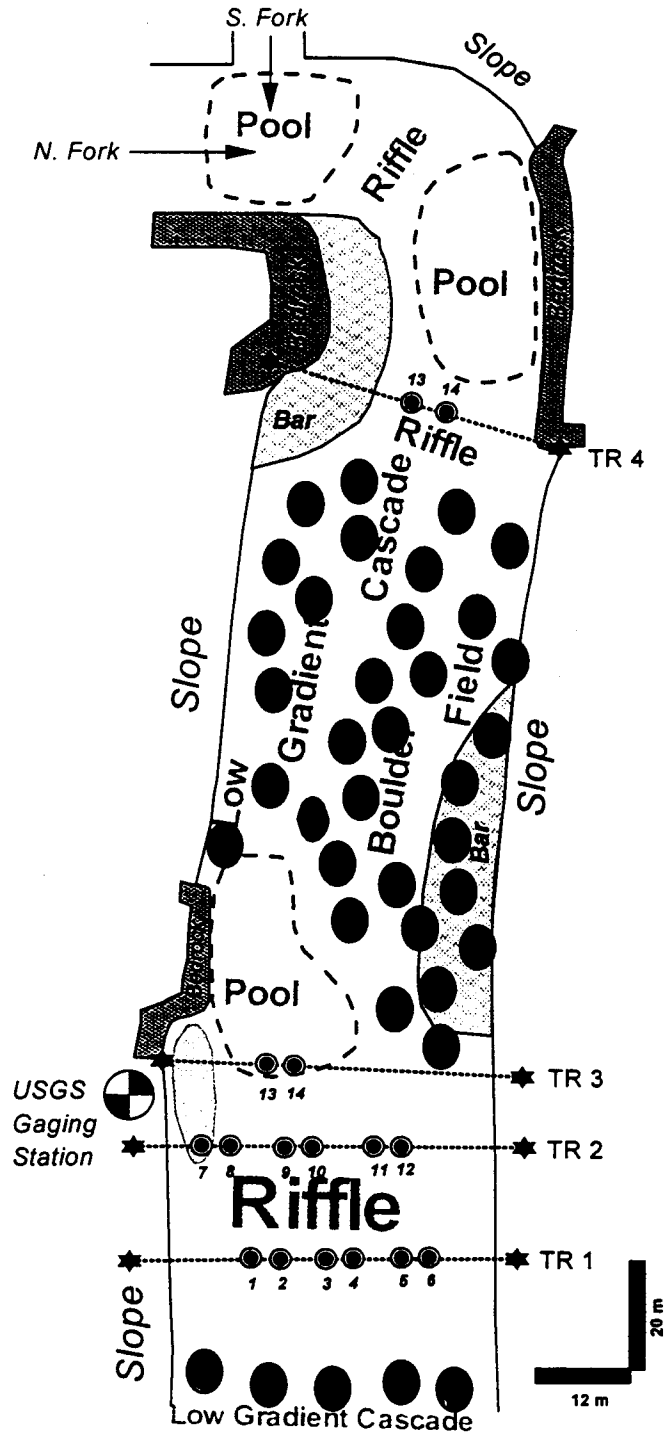
Figure A-16. Tolt River study site map. Scour monitor locations and identification numbers are depicted. Scale is approximate.
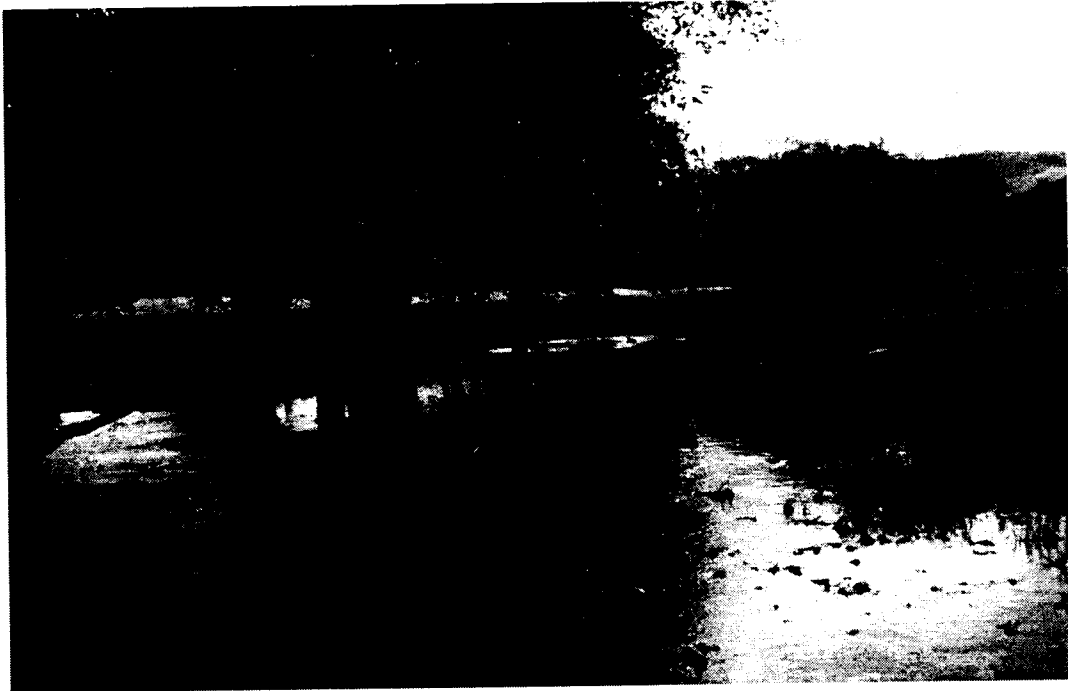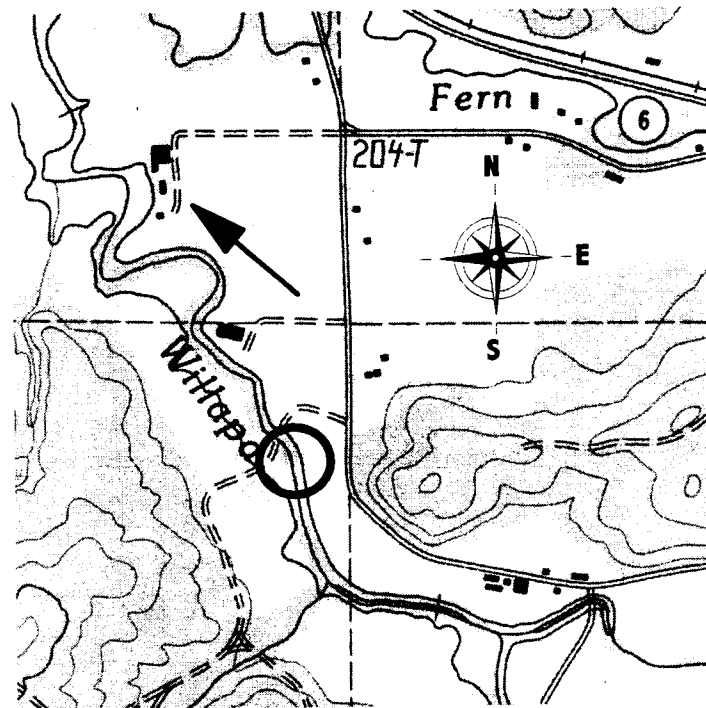
Figure A-17. Location and representative photograph of the Willapa River at Elk
Prairie study site. The site (circled) and flow direction are indicated
on map. Photograph looks downstream at lower riffle: Transects 1
and 2 are located at and above riffle crest near center of photograph.
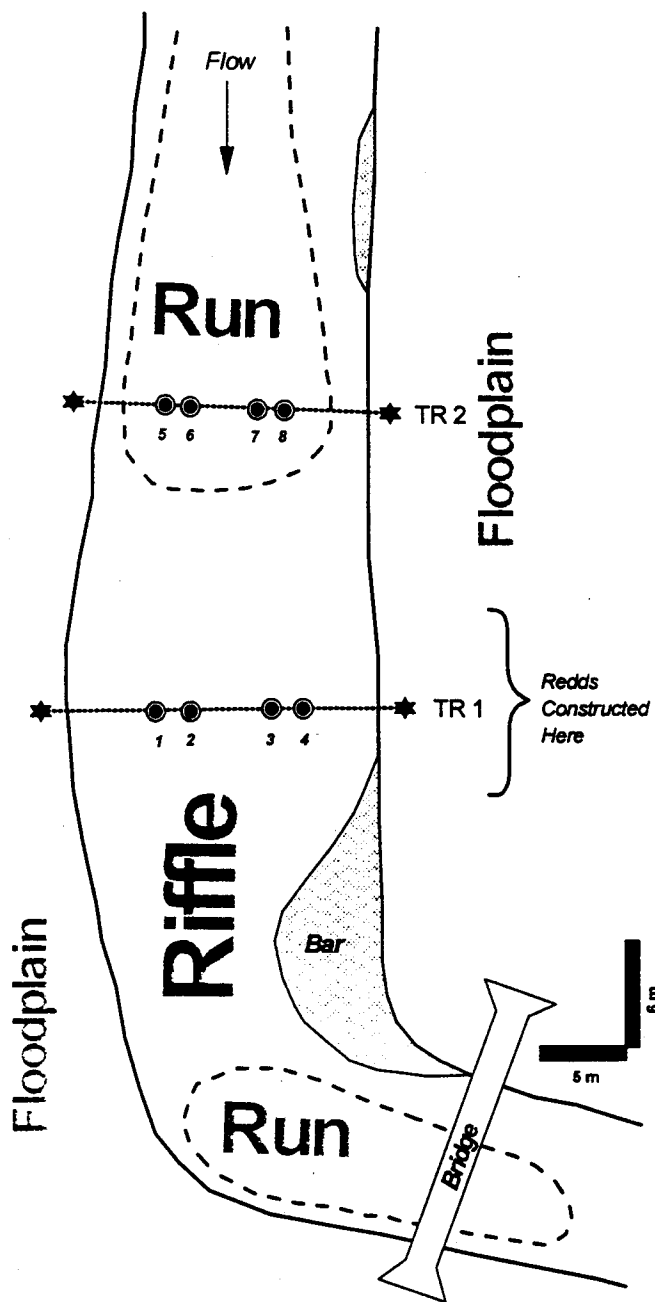
Figure A-18. Willapa River at Elk Prairie study site map. Scour monitor locations and identification numbers are depicted. Scale is approximate.
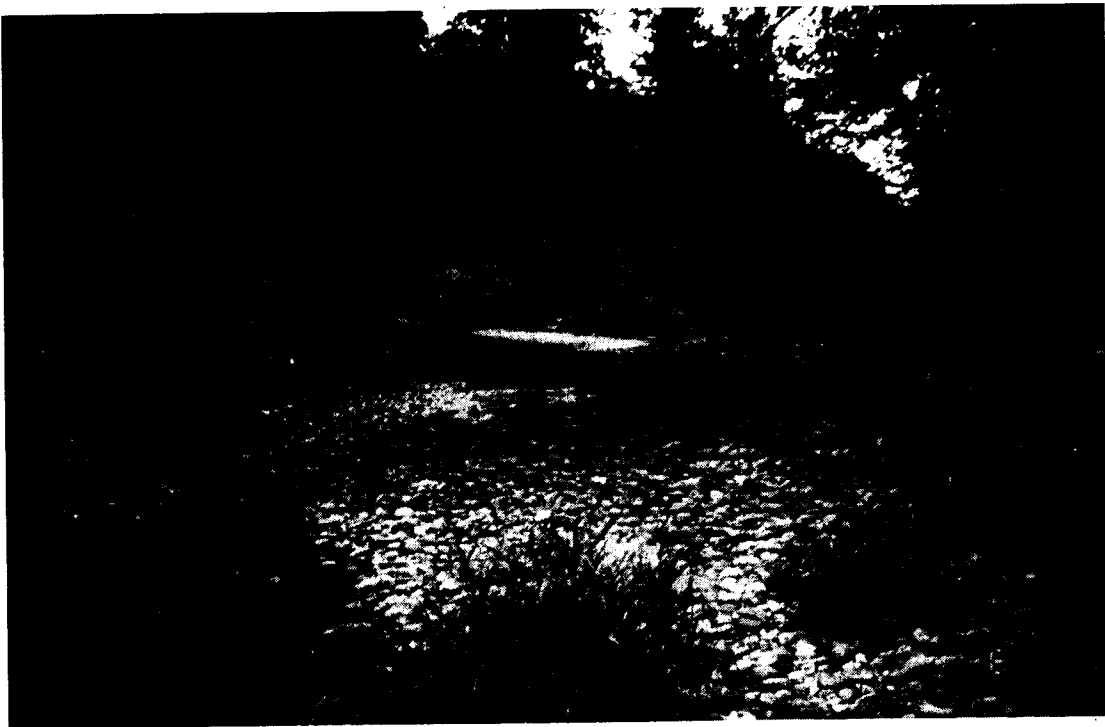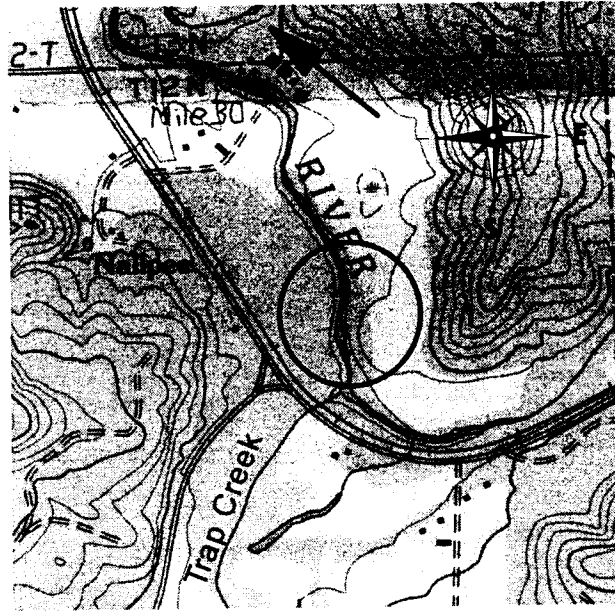
Figure A-19. Location and representative photograph of the Willapa River at Trap
Creek study site. The site (circled) and flow direction are indicated on
map. Photograph looks upstream at Riffle 1; Transect 1 is located
above riffle crest at center of photo; Riffle 2 is located upstream,
around the corner and out of sight in the photograph.
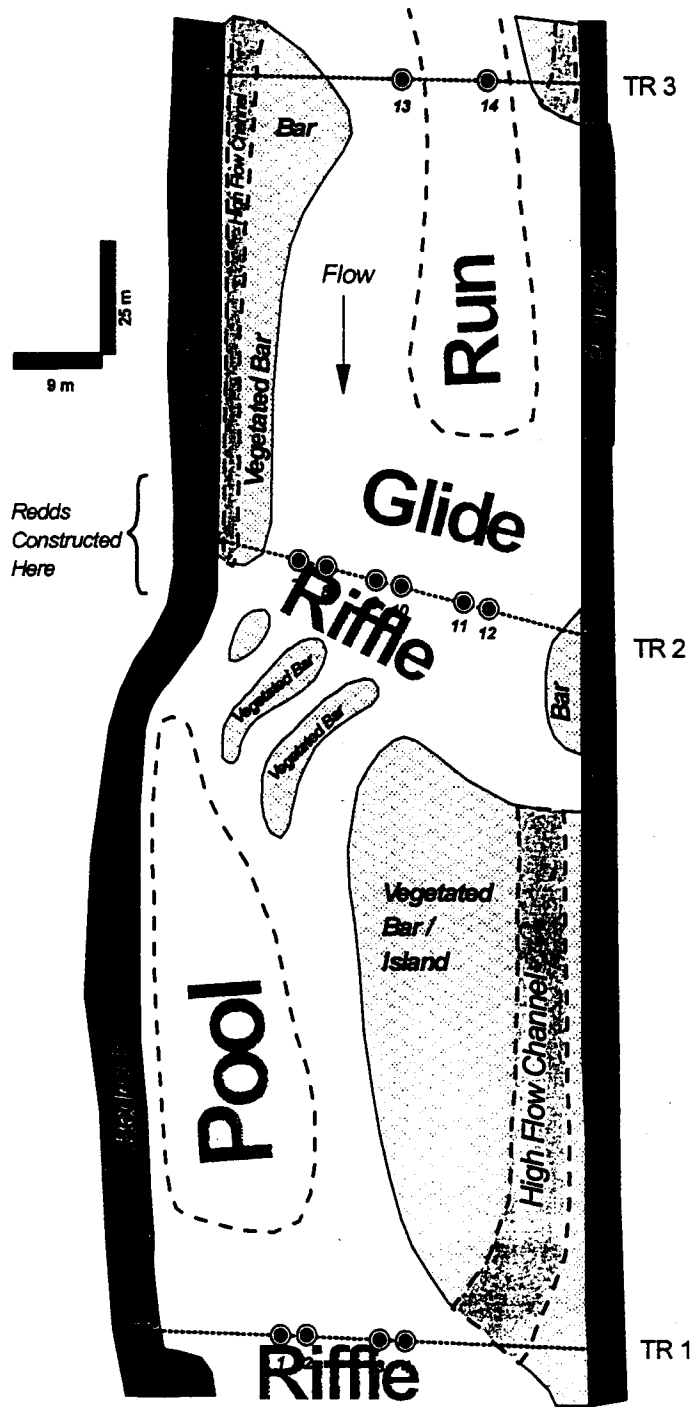
Figure A-20. Willapa River at Trap Creek study site map. Scour monitor locations and identification numbers are depicted. Scale is approximate.
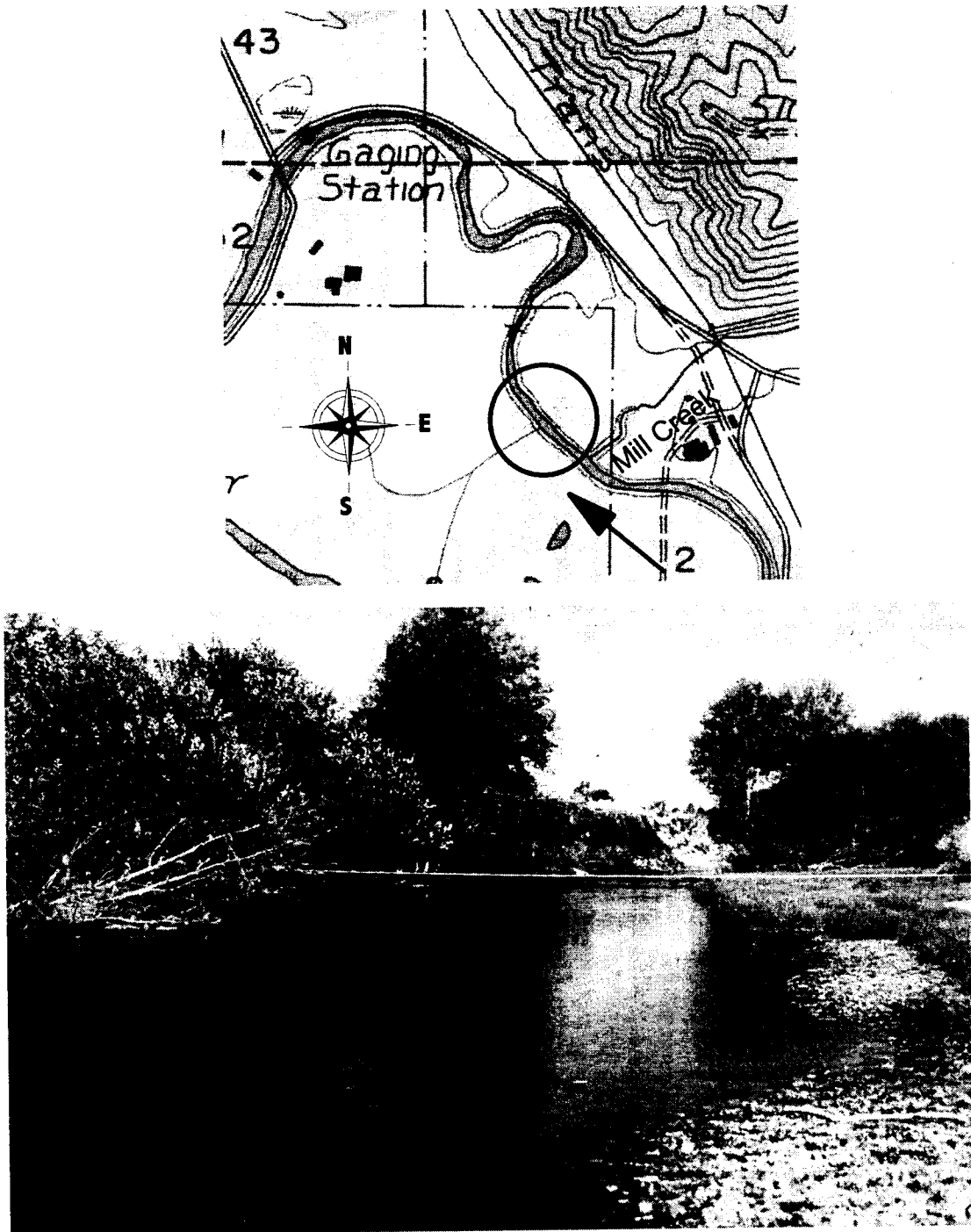
Figure A-21. Location and representative photograph of the Willapa River at USGS study site. The site (circled), USGS gage, and flow direction are indicated on the map. Photograph looks downstream at Riffle; the tape is strung across Transect 1, and Transect 2 is located across bar in foreground. Mill Creek enters roughly 200 meters upstream.
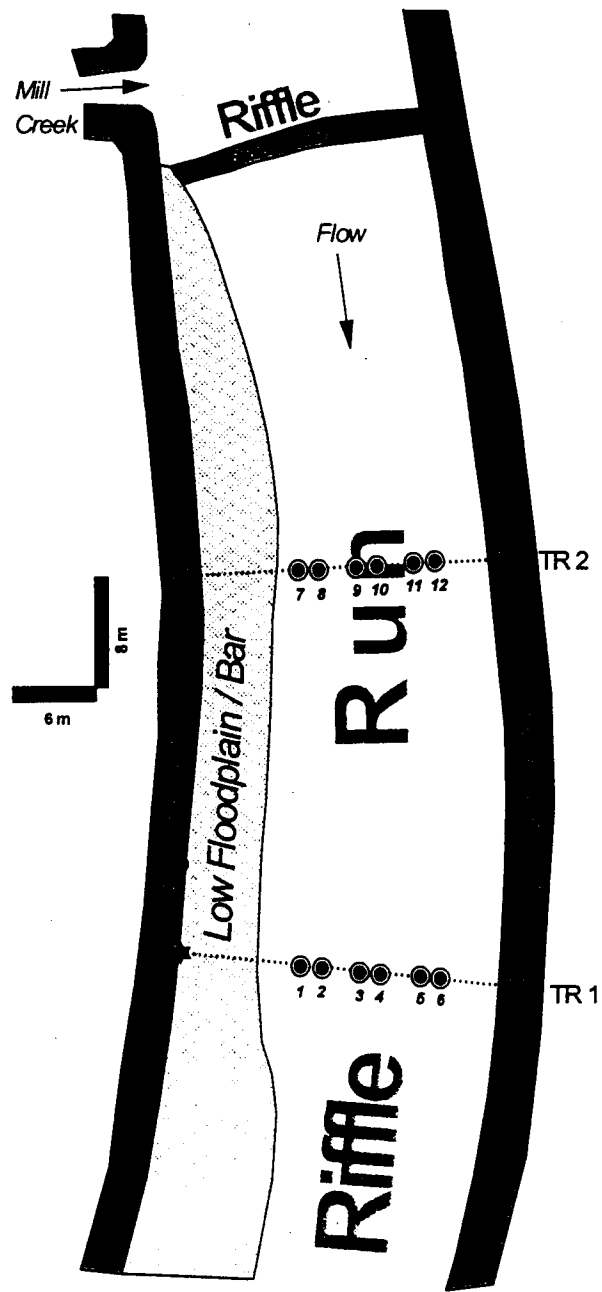
Figure A-22. Willapa River at USGS study site map. Scour monitor locations and identification numbers are depicted. Scale is approximate.

SCOUR MONITOR INSTALLATION DEVICE

A schematic of the monitor insertion device is presented in Figure B-1. The device was designed to be constructed using commercially-available cast iron well point heads that are used specifically for driving into gravel aquifers. The well point head comes with a standard pipe thread and is screwed onto the inner pipe, which is machined accordingly. The head requires minor lathe work to ensure a smooth fit inside the outer pipe. The head can be replaced easily if it breaks. Several additional, backup devices can be constructed at the same time for a small marginal labor cost.

Both outer and inner tubes are made from 1020 carbon steel that meets American Society for Testing and Materials standard ASTM A513. The inner tube needs to be thicker walled than the outer tube because it absorbs most of the impact energy. The inner and outer tubes combined weigh about 10 kg per meter length, or 7 kg less than analogous solid steel variations. A standard pipe thread is machined onto the lower end of the inner tube to fit the well point head. Both tubes are of moderate strength and hardness (minimum tensile strength 586,000 kPa; 165 Brinell hardness), but are much harder than cheaper, standard galvanized steel plumbing pipe, which failed rapidly in an initial prototype. The tubes eventually bell outward at the upper, impact end after being used to insert approximately 25 to 30 scour monitors in cobble (50 or more in fine-coarse gravel mixtures) and then need to be trimmed by approximately 1 cm. This drawback was of negligible importance compared to the alternatives of using even harder steel tube (more expensive material that will still bell and possibly fracture) or using an inner solid steel rod (heavier). At the lower end, the tapering on the outer tube guides rocks away from the gap between the inside of

Cap: tool steel, tapered inserts:

20 mm

7 mm — 51 mm Dia.

5°

15 mm — 30 mm Dia.

1.5°

Inner tube: seamless carbon steel tubing
43.13 mm O.D. (29.85 mm I.D.)
Standard pipe thread at bottom

1.2 to 1.5 m

Outer tube: seamless carbon steel tubing
57.15 mm O.D. (51.05 mm I.D.)
Tapered at bottom

Machined to 50.17 mm O.D.

50.80 mm (2") octagonal well point head
Cast iron, standard pipe thread
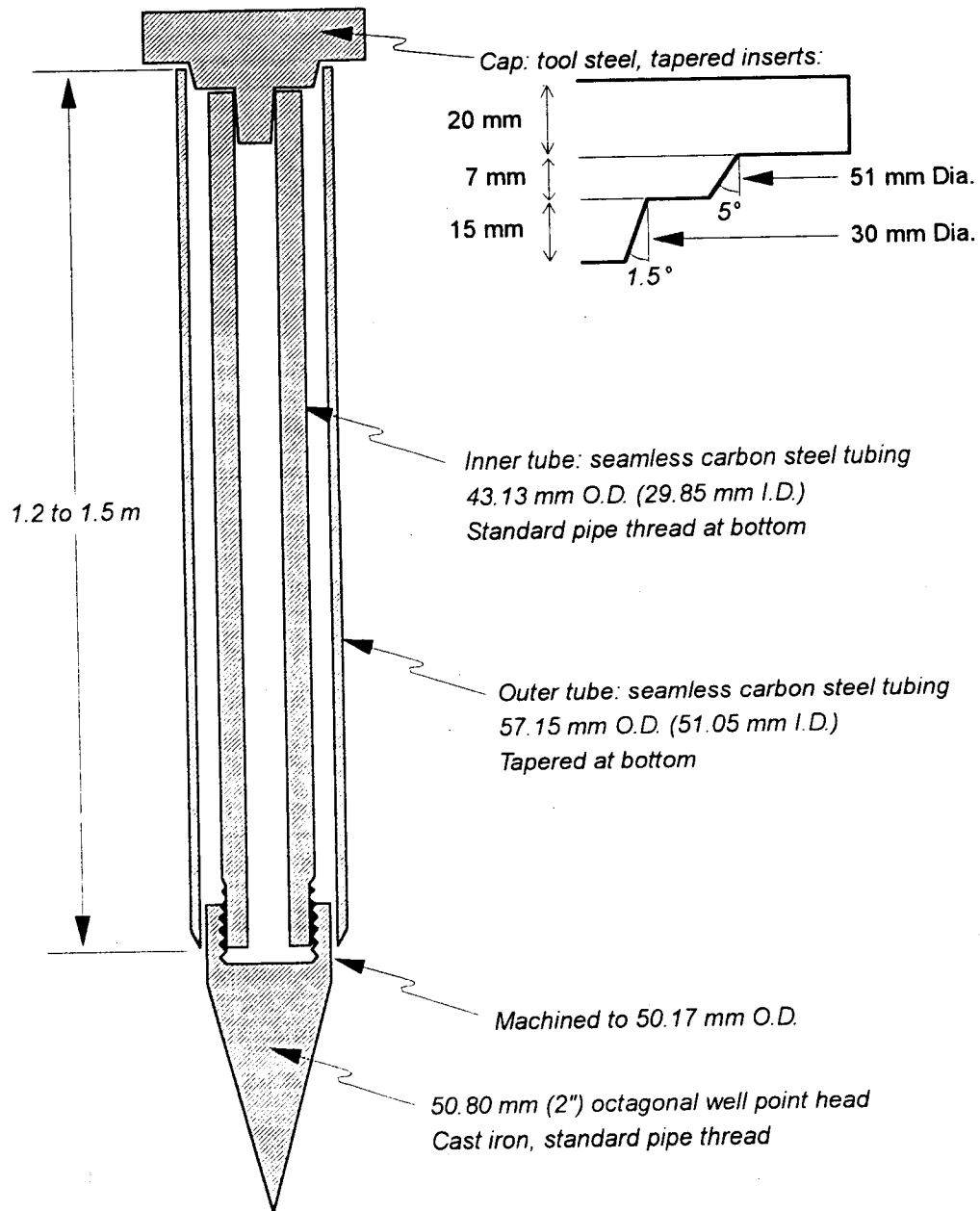
Figure B-1. Schematic of scour monitor installation tube device.

the tube and the well point head, thereby preventing wedging of small particles.

A tool steel cap transmits the impact from a driving tool, such as a sledge hammer, to both inner and outer tubes. The tapering on the cap directs the two tubes to bell outward, thereby preventing them from closing in and jamming. During impact, the cap should be hit squarely from above or else a small asymmetry can develop, and as a result the tube will have to be trimmed after a few monitors have been installed. The assembly is driven into the stream bed first by a large fence-post pounder (a large diameter steel pipe with a welded end cap and handles, weighing approximately 9 kg) until the cap is at an elevation at which a 4.5 kg sledge hammer can be used safely.

Once the device is driven to the desired depth, a few additional impacts may be required until the top end of the outer tube is slightly below that of the inner tube. As a result, the well point head is not wedged tightly and removal of the inner tube is relatively easy. The cap is removed and a custom-designed extractor is inserted into the inner tube (Figure B-2a) and wedged by driving the steel sleeve between the tapered nut and the inside of the tube (Figure B-2b). Relatively little force should be used when dropping the steel block to wedge the sleeve, or else the sleeve and nut may be wedged so tightly that the extractor can only be removed at a machine shop. An optional, larger diameter ring (not shown in Figure B-2) can be welded onto the upper end of the sleeve that prevents accidental wedging of the entire sleeve inside the inner tube, which can make extraction difficult to impossible. The internal tube and extractor assembly are then freed by a light ramming of the steel block upwards on the end nut, and the assembly is lifted (Figure B-2c).

The outer tube remains in the stream bed while the scour monitor is placed. The extractor is freed from the inner tube by a downward impact to the end nut that forces the tapered nut down and out of the steel sleeve, which is then no longer wedged tight against the inner tube (Figure B-2d). The extractor weighs between 3 and 5 kg depending on shaft length and on the size of the steel block.

A scour monitor is inserted through the outer tube, which is subsequently
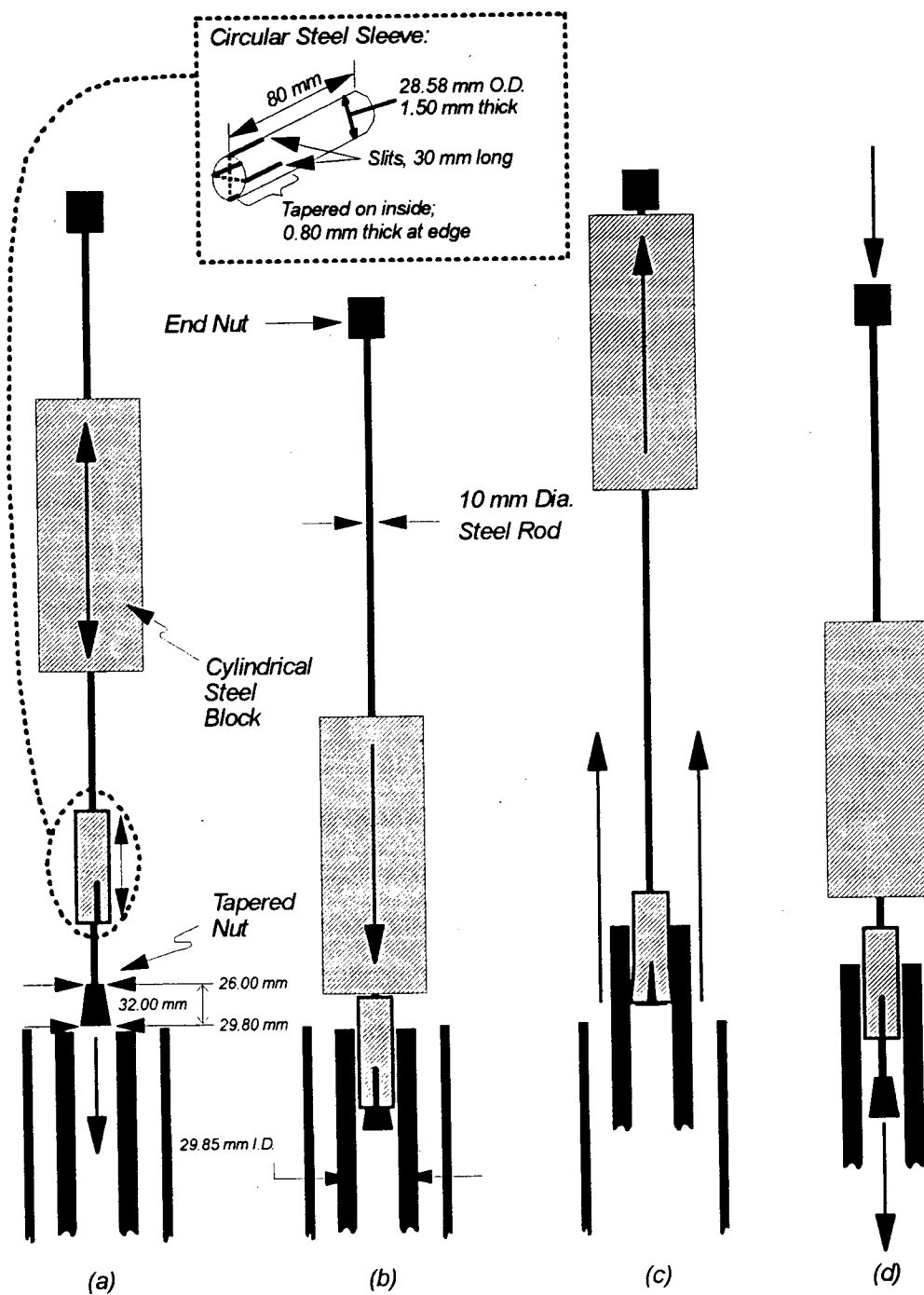
Figure B-2. Schematic of device for extracting inner tube of scour monitor installer. See text for explanation.

removed. A long, slender steel rod with an eye-hook at the end can be used to retain the whiffle balls in their installed position while the outer tube remains in contact with the gravel; this prevents significant separation of the balls during outer tube removal.

The stream bed should be excavated down to the first ball to confirm whether the balls have separated by comparing the distance between the top ball and the upper end of the scour monitor cable before and after installation. Typically, only the top ball lifts slightly as the slender retaining rod is removed. This can be corrected by pushing and working the ball down until it contacts the next ball. Alternatively, pulling gently on the monitor cable will bring all of the balls together snugly, plus ensure that the top ball is sitting at the desired depth below the bed surface (which varies with grain size distribution characteristics and study objective).

A scour monitor can be installed and appropriate measurements made typically within about five minutes in fine gravel, or 10 to 15 minutes in larger cobble. The well point heads are extremely effective at working their way down through a gravel/cobble bed. Occasionally the tube leans at a small angle as the well point head works around a large cobble and a correction to the measured scour depth is necessary.

The components are sufficiently lightweight that they can be carried over long distances. Weight is not only important for portability, however. It also influences the useful work, or energy used, in driving the tube assembly into the stream bed. A lighter tube assembly will have a lower impedance, or resistance to impulsive motion, than a heavier one for the same applied force. Impedance limits the force that can be transmitted to the stream bed and thus the useful work done (Fragaszy et al. 1985; Massarsch 1992). Hence, a lighter tube assembly can be driven deeper for each blow of a sledge hammer than a heavier tube assembly, with a concomitant increase in efficiency. However, reduced impedance is also linked to increased vibration amplitude in the surrounding stream bed (Massarsch 1992), resulting in a trade-off.

In field applications of the device, visual observation of individual stream bed particles at the surface and sensation of vibration transmitted to the feet did not

indicate that a substantial radius of high amplitude vibration occurs within the surrounding stream bed during impact. The advantages of lighter weight appeared to be more important than the potential disadvantage. These aspects of impact physics had not been considered by previous investigators and motivated the present design.

The issue of disturbance to the stream bed has not been discussed in depth within the scour measurement literature. It has been assumed *a priori* in previous studies, without any supporting justification, that the disturbance is sufficiently small and unimportant that scour monitor installation does not influence the scour depth measurement. I conducted a literature review of pile driving research to assess the issue. The review indicated that disturbance to the surrounding stream bed during tube driving is restricted to a small radius because cohesionless substrates are typically compacted and rearranged by displacement and vibration (Poulos and Davis 1980; Broers and Dieterman 1992; Shublaq 1992).

Driving of single piles in sands disturbs the substrate radially over a distance between 3 to 6 times the pile diameter, the multiplier depending on the degree of original substrate compaction. The radius of influence is greater for denser, more compacted sands (Hartikainen 1972; Poulos and Davis 1980; Shublaq 1992). The most significant displacement of sands appears to be limited to within 1 to 2 pile diameters, however.

Similar limited zones of disturbance can be expected for gravel beds. The radius of significant disturbance will correspond to at least the diameter of the largest particle contacted, although I have found that there is a point with increasing particle size at which the tube is displaced laterally instead of the particle. Bed excavation indicated that this happens for subsurface contacts with particles larger than about 150-180 mm (intermediate axis diameter). Smaller particles tend to shift and compact more than the largest particles present. I have observed upward heaving at the bed surface only within a 1 to 2 tube-diameter radius from the edge of the outside tube. After removal of the outer tube, the bed surface elevation was similar to its undisturbed state as the compacted material partially loosened again and closed back

in on the installed scour monitor.

Installing scour monitors changes stream bed structure. Surface friction angle is likely to be reduced, thus increasing local mobility. This can be minimized by removing the largest particles in the armor layer prior to insertion and replacing them afterwards. Subsequent reworking of the stream bed occurs as particles begin rocking at higher stages and they settle into more stable positions. Reinfiltration of finer material at lower stages reduces mobility because of increased contact area and interlocking between substrate matrix and framework particles. The area of disturbance is small relative to the area mobilized during bedload transport, and it is unlikely that a local scour hole will initiate at such a small scale. Significant scour should occur only when larger areas of the bed experience substantial bedload transport. Hence, scour monitor installation using the device is unlikely to disturb the bed sufficiently to cause premature or increased scour in a river reach, and whiffle ball scour measurements probably do not experience methodologic error that could be introduced by their installation.

Previous installation devices have been smaller in diameter. This could possibly represent a disadvantage of the present device, which has a relatively large internal diameter (51.05 mm) compared to that of a plastic practice whiffle ball (38.10 mm). The diameter is dictated by the sizes of well point heads that are available; the head used was selected because it was inexpensive, durable, and effective for driving into gravel and cobble deposits. Devices could be specially fabricated with a smaller internal diameter that is closer to 38.10 mm, but it has been my experience that a relatively large clearance between whiffle ball and tube is desired. Otherwise, the scour monitor can snag during installation on small irregularities at the tube end that develop with use, or become wedged against the tube interior by sand particles that may become suspended during installation. The incremental difference in tube diameter furthermore should not result in marginally greater disturbance to the surrounding river bed, because the amplitude of the disturbance of a pile driven into non-cohesive soils decreases relatively quickly with distance from the pile due to both

geometric and material damping effects (Massarsch 1992).

Literature Cited

Broers, H., and H.A. Dieterman. 1992. Environmental impacts of pile driving. p.61-68 in: Barends, F.B.J., editor. Application of stress wave theory to piles. Balkema. Rotterdam, Netherlands.

Fragaszy, R.J, J.D. Higgins, and E.C. Lawton. 1985. Development of guidelines for construction control of pile driving and estimation of pile capacity (Phase I). Washington State Department of Transportation, Olympia WA. WA-RD-68.1. 83p.

Hartikainen, J. 1972. On the distribution of pile loads in a friction pile foundation. Acta Universitatis Ouluensis Ser. C, Technica No. 3, Mechanica No. 2. 36p. University of Oulu, Finland.

Massarsch, K.R. 1992. Keynote lecture: Static and dynamic soil displacements caused by pile driving. p.15-24 in: Barends, F.B.J., editor. Application of stress wave theory to piles. Balkema. Rotterdam, Netherlands.

Poulos, H.G., and E.H. Davis. 1980. Pile foundation analysis and design. John Wiley and Sons, New York, NY. 397p.

Shublaq, E.W. 1992. Soil disturbance due to installation of model piles and pile groups. Soils and Foundations 32(4): 17-26.

US GEOLOGICAL SURVEY STREAM GAGE STAGE VS. STUDY TRANSECT STAGE: STAGE-STAGE RATING PLOTS

The following plots depict stage measurements made at selected transects (y-axis) in sites near USGS gages versus the official stage measured at the same time at the gage (x-axis). The dashed lines connect the data in the temporal order that they were measured to show possible changes in bed elevation at either the gage or the transect (i.e., rating shifts).

Site-Specific Notes:

Issaquah Cr: The bed elevation rose approximately 0.1m during the 1/1/97 flood; this can be also seen in the cross-section plots that follow later in this document. There is a change in slope at higher flows as the water surface approaches and exceeds bankfull elevation in the site (upper four points in plots). ·

Raging R: No significant shift occurred in rating plots; data scatter due to measurement errors in determining the water surface elevation at the site (caused by very rough, rapidly fluctuating water surface during floods)

S. Fk. Snoqualmie R: A rating shift occurred during the 1/1/97 flood, apparently due to a bed elevation change at the control for Transects 1 and 2. The rating stayed about the same for most the remainder of the study, and water surface elevation measurement error was probably the primary source of the observed variation during that period. The rating changed back to its original location in the fall of 1998, possibly indicating the passage of a gravel slug through the reach.
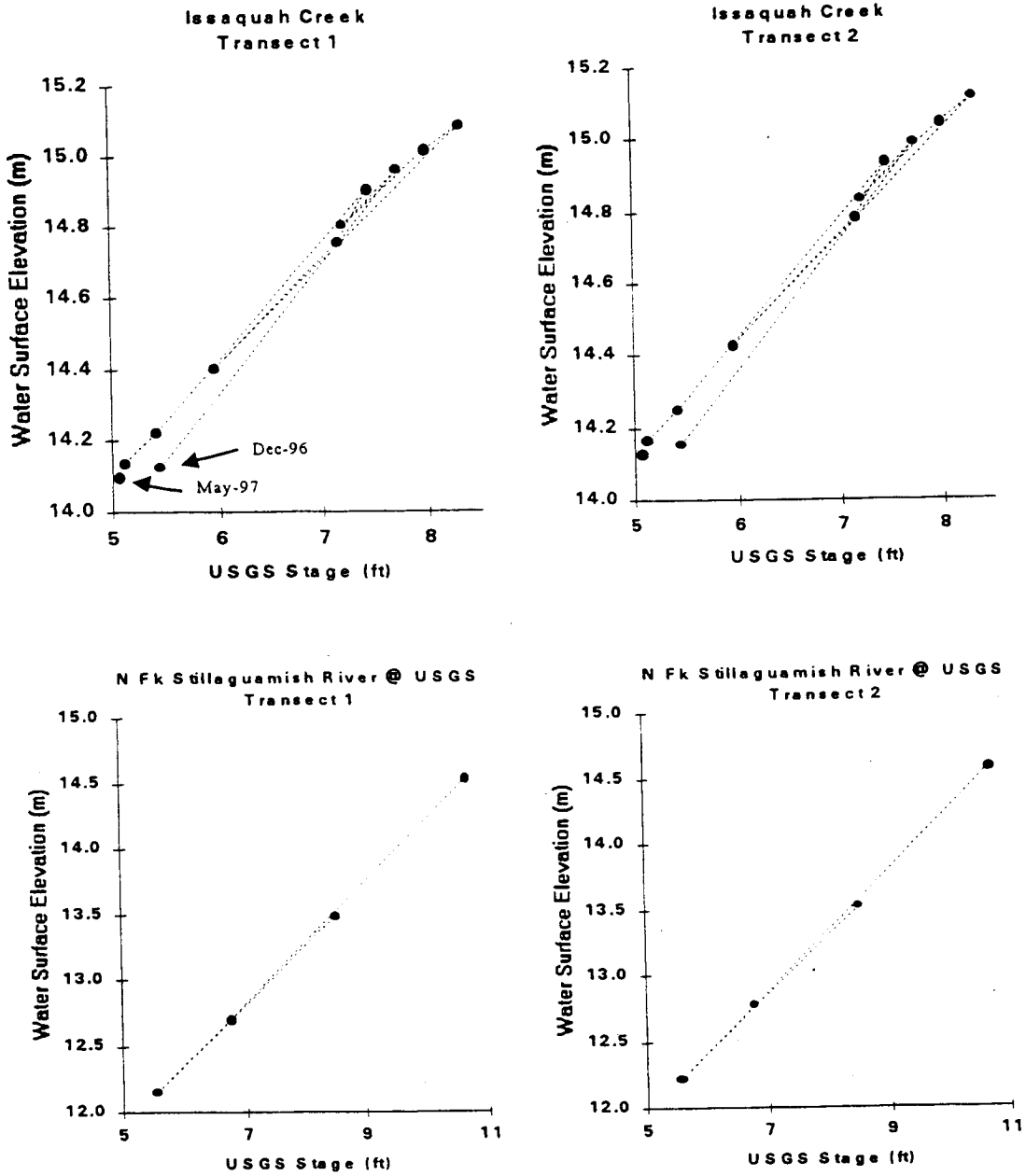
Figure C-1. Rating plots linking stage at selected transects to stage at USGS gage.
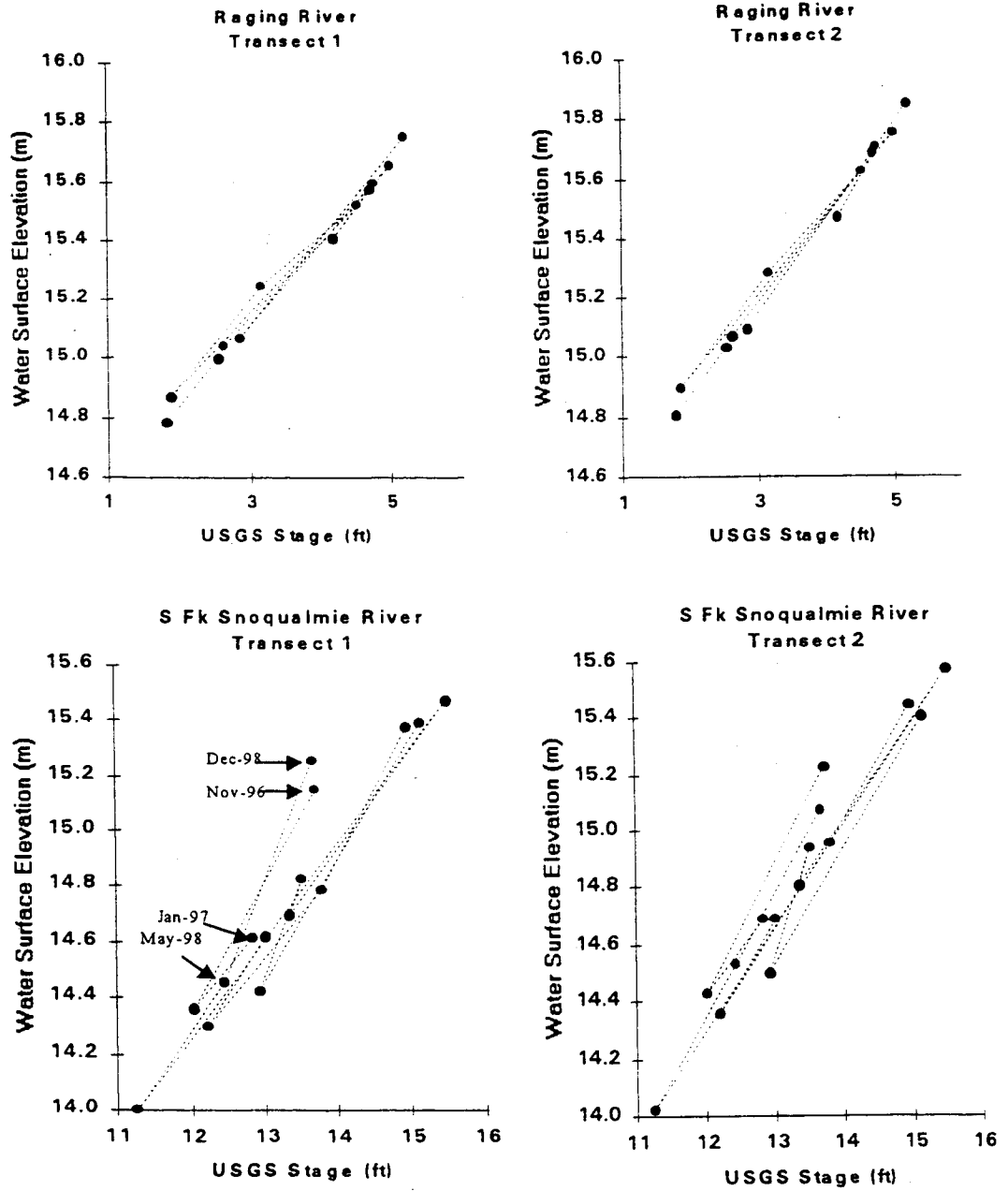
Figure C-2. Rating plots linking stage at selected transects to stage at USGS
gage.

285
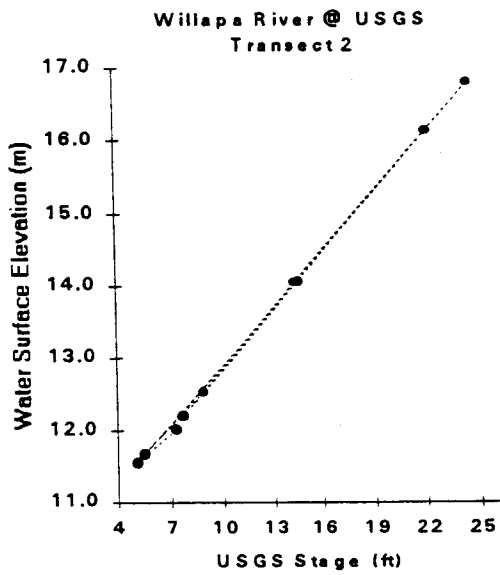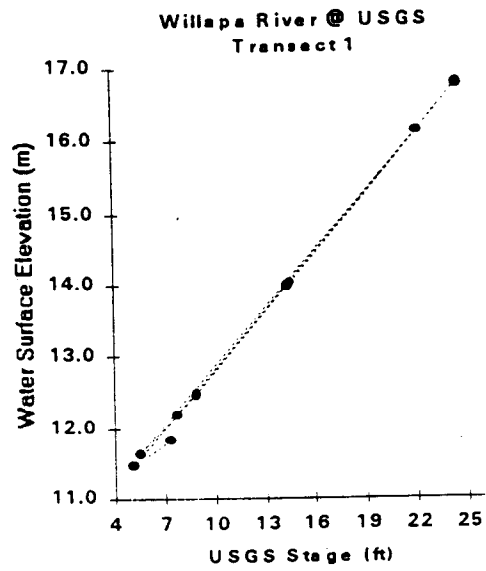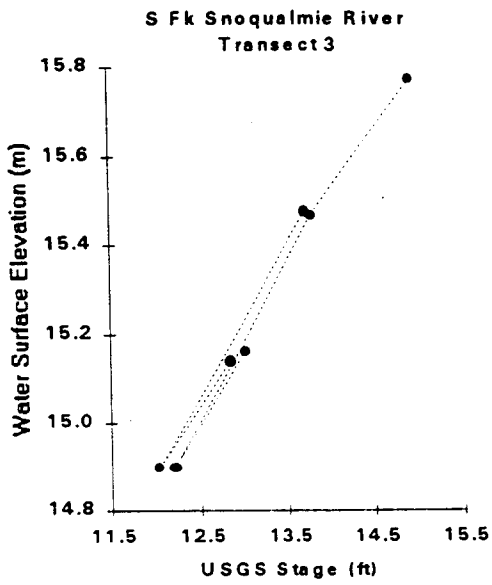
Figure C-3. Rating plots linking stage at selected transects to stage at USGS gage.

BED ELEVATION PLOTS AND
SCOUR DEPTH DATA

Scour monitor identification numbers indicated on Figures D-1 to D-15 match identification numbers in Table D-1 and the site maps in Appendix A. The depicted position of the top ball in the plots is that prior to bed disturbance in the Autumn of 1996. The diameter of each ball is drawn to scale (0.04 m) relative to the vertical axis. Subsequent bed profiles are indicated by the dates and arrows. Numbers in boldface italics in the total scour depth column of Table D-1 indicate monitors that were not triggered: bedload disturbance was not measured because it occurred above the elevation of the top ball and the numbers are thus maximum possible values.
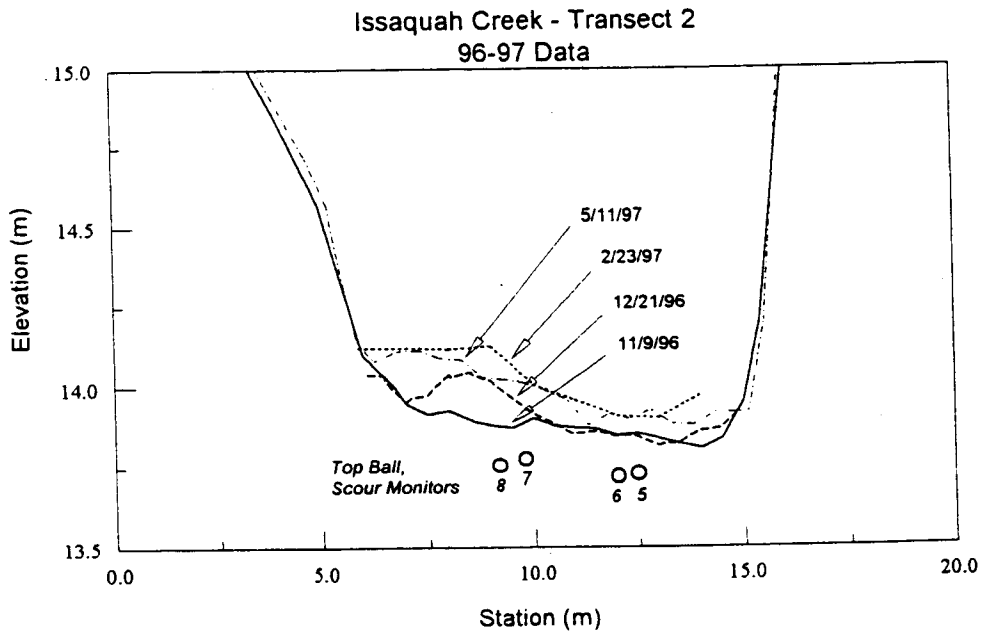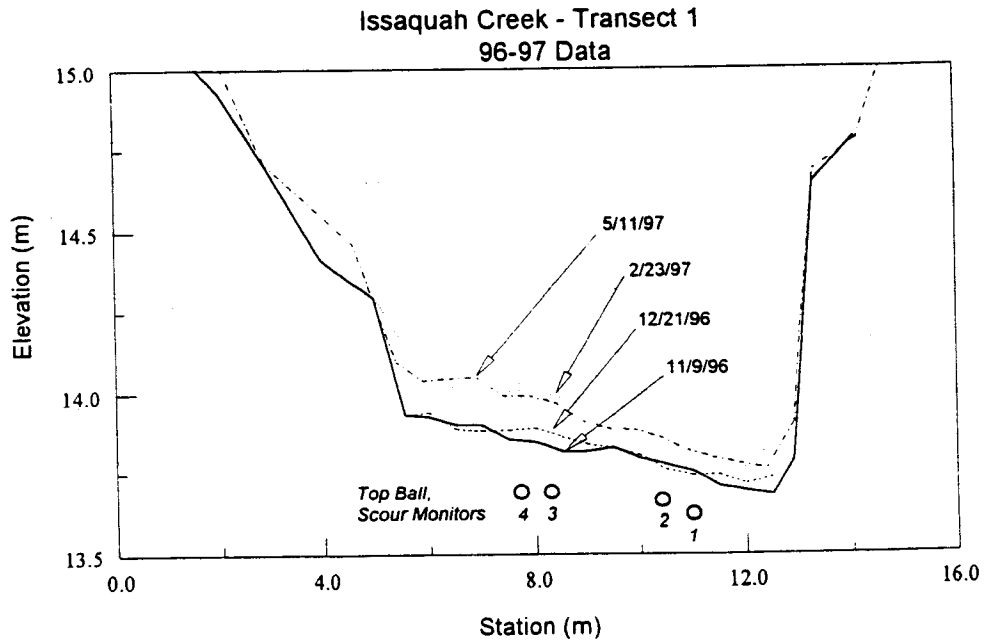
Figure D-1. Surveyed cross-sections and locations of scour monitors, Issaquah Creek, Transects 1 and 2; 1996-97 flood season.

N Fk Stillaguamish River at USGS - Transect 1
96-97 Data

N Fk Stillaguamish River at USGS - Transect 2
96-97 Data
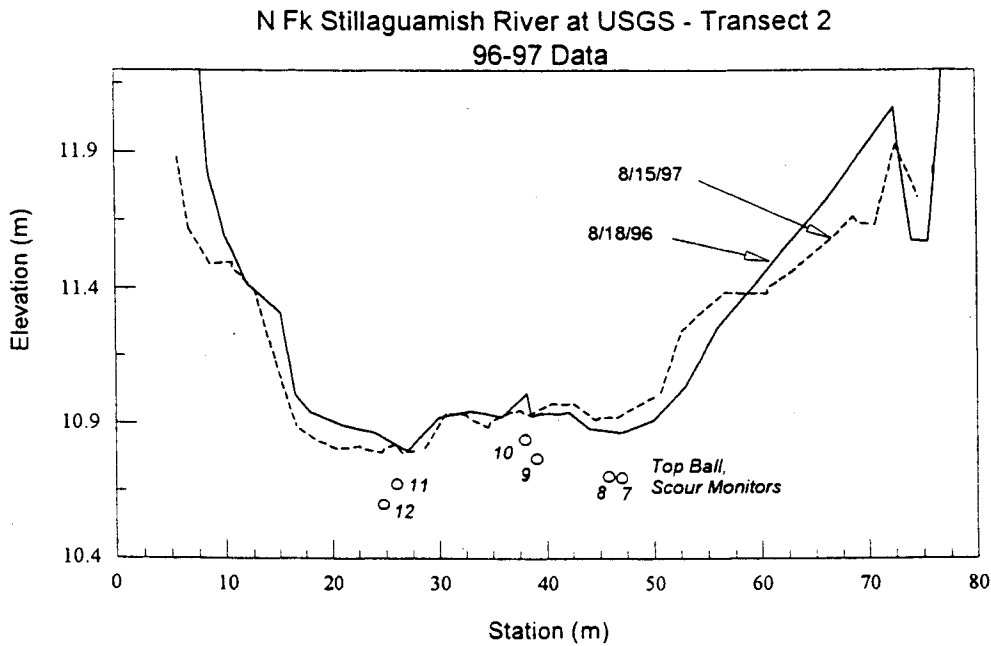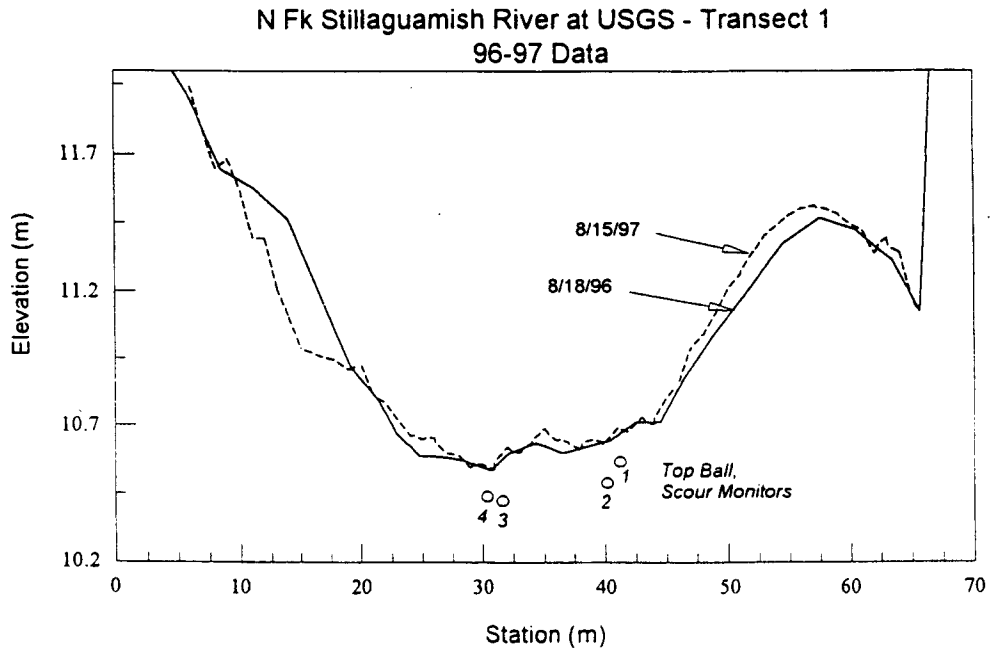
Figure D-2. Surveyed cross-sections and locations of scour monitors, North Fork Stillaguamish River at USGS, Transects 1 and 2; 1996-97 flood season.
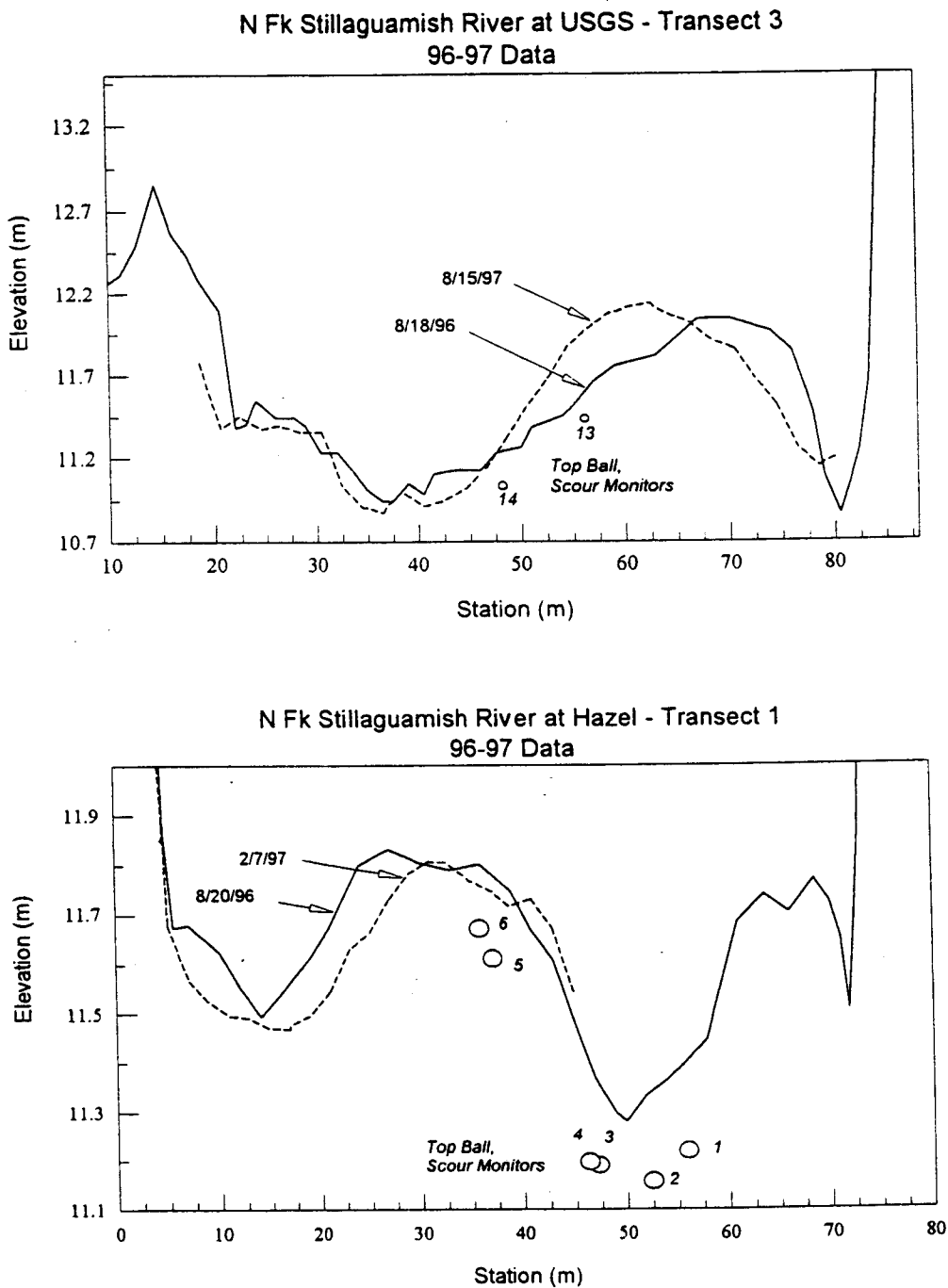
Figure D-3. Surveyed cross-sections and locations of scour monitors, North Fork Stillaguamish River at USGS, Transect 3, and North Fork Stillaguamish River at Hazel, Transect 1; 1996-97 flood season.

N Fk Stillaguamish River at Hazel - Transect 2
96-97 Data

N Fk Stillaguamish River at Hazel - Transect 3
96-97 Data
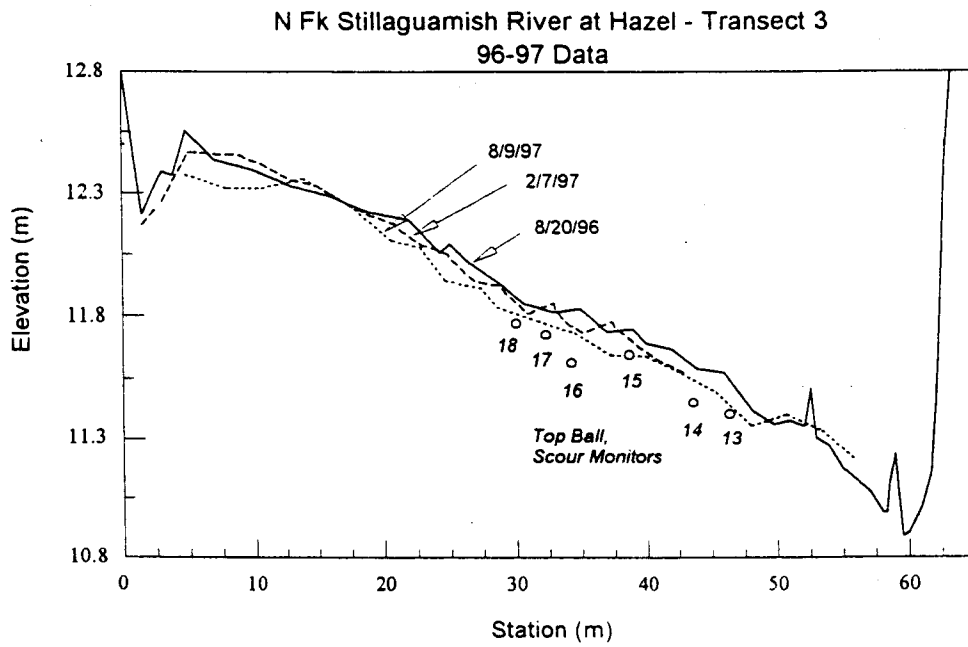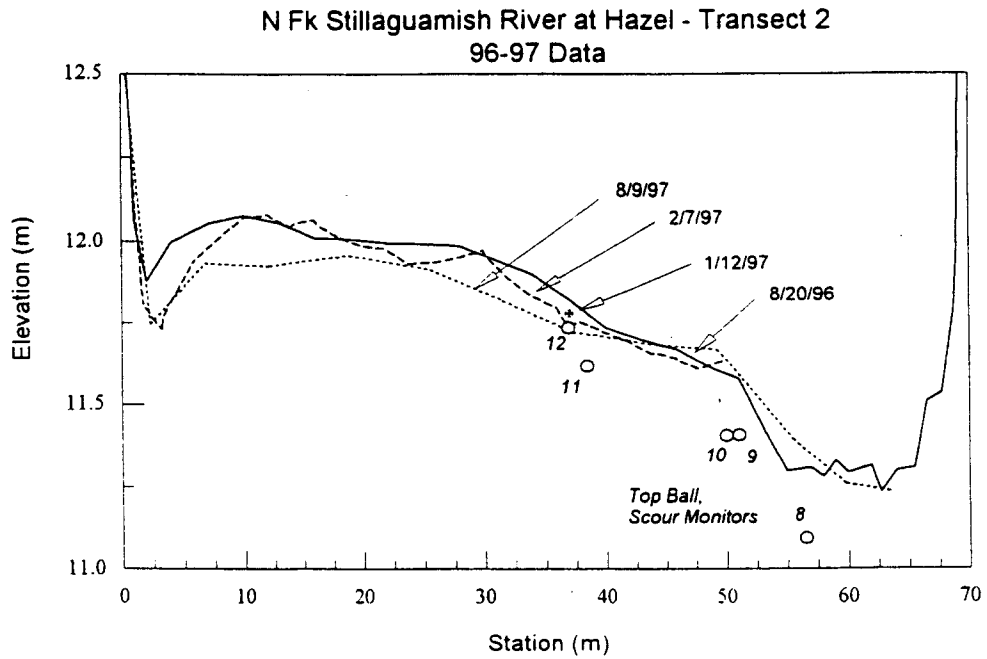
Figure D-4. Surveyed cross-sections and locations of scour monitors, North Fork Stillaguamish River at Hazel, Transects 2 and 3; 1996-97 flood season.
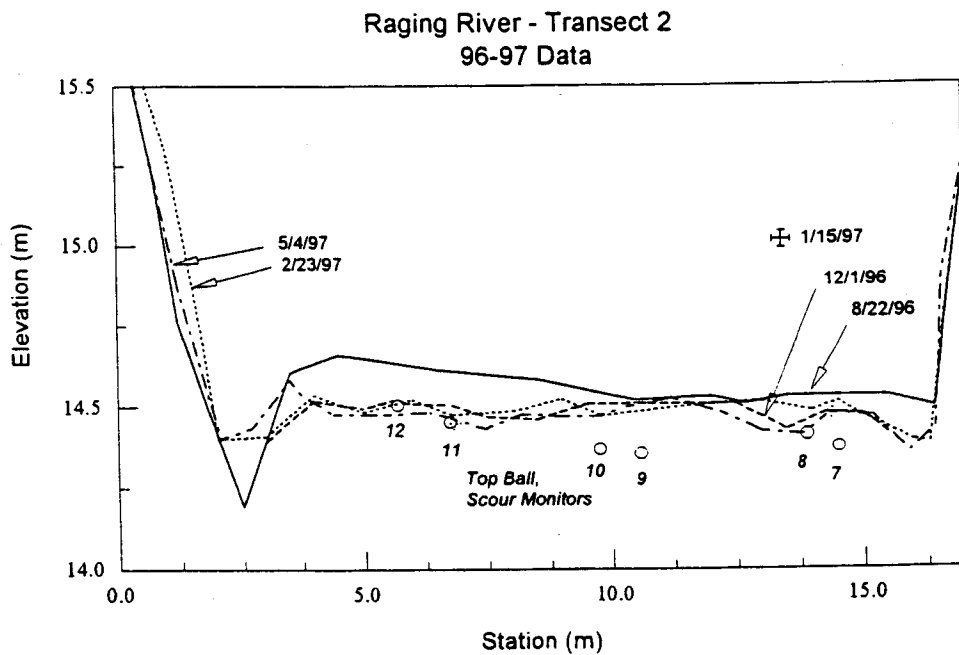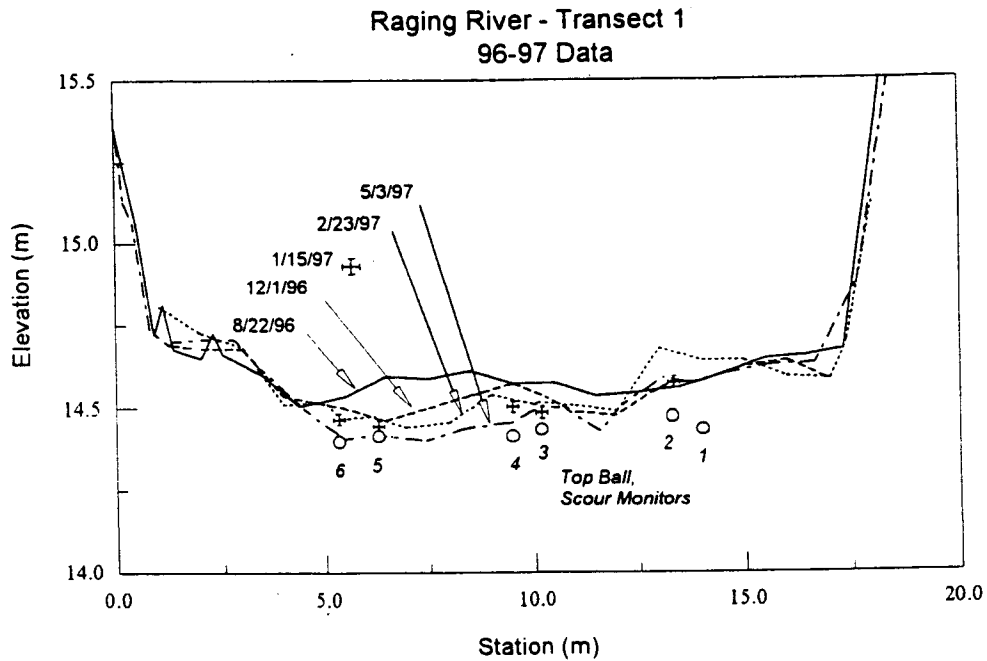
Figure D-5. Surveyed cross-sections and locations of scour monitors, Raging River, Transects 1 and 2; 1996-97 flood season.

Raging River - Transect 3
96-97 Data

S Fk Snoqualmie River at Alice Creek - Transect 1
96-97 Data
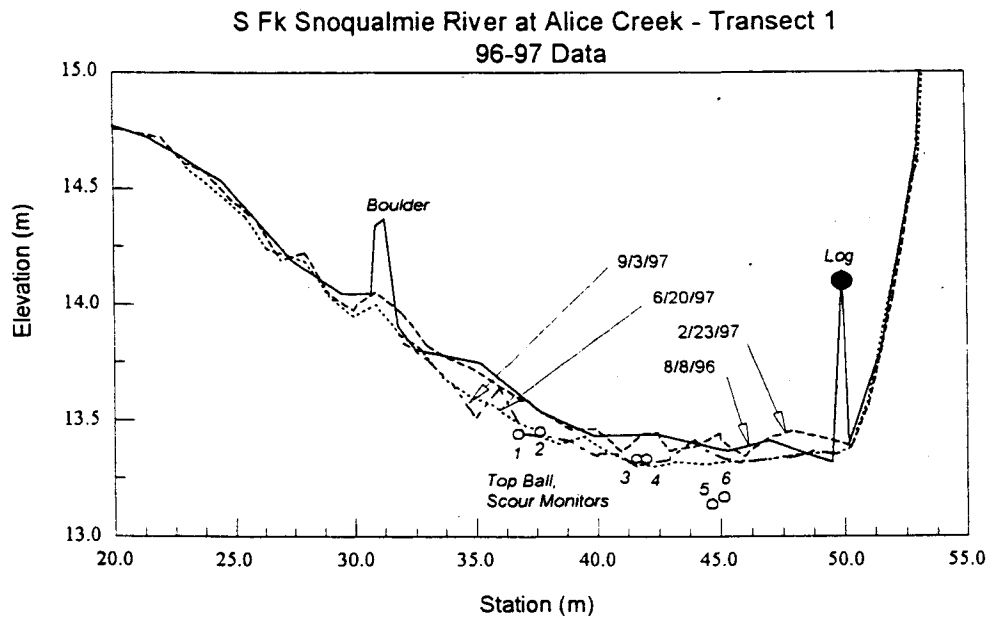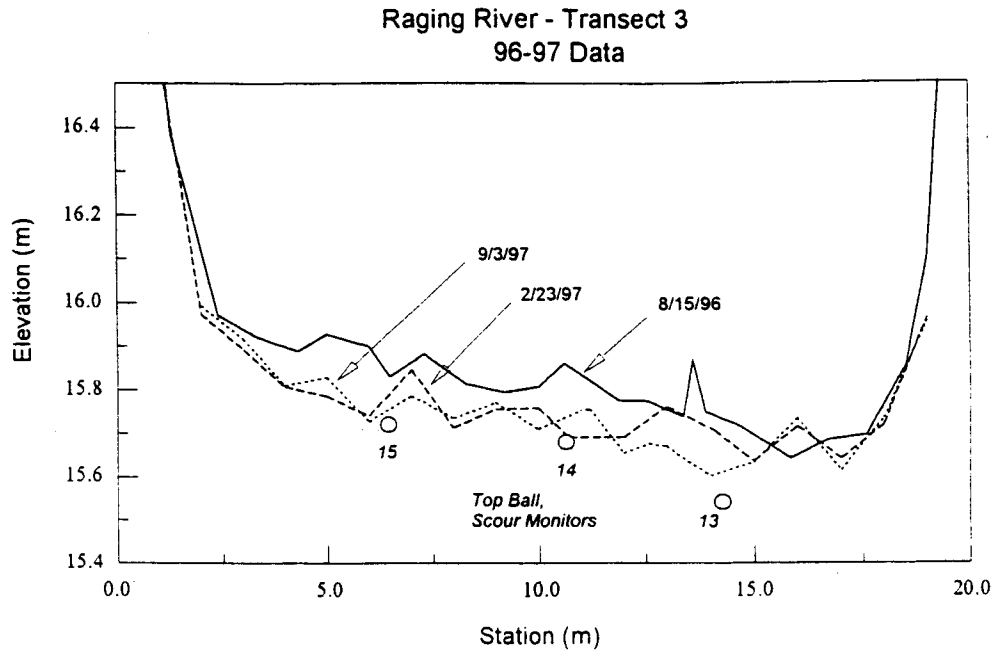
Figure D-6. Surveyed cross-sections and locations of scour monitors, Raging River, Transect 3, and South Fork Snoqualmie River, Transect 1; 1996-97 flood season.
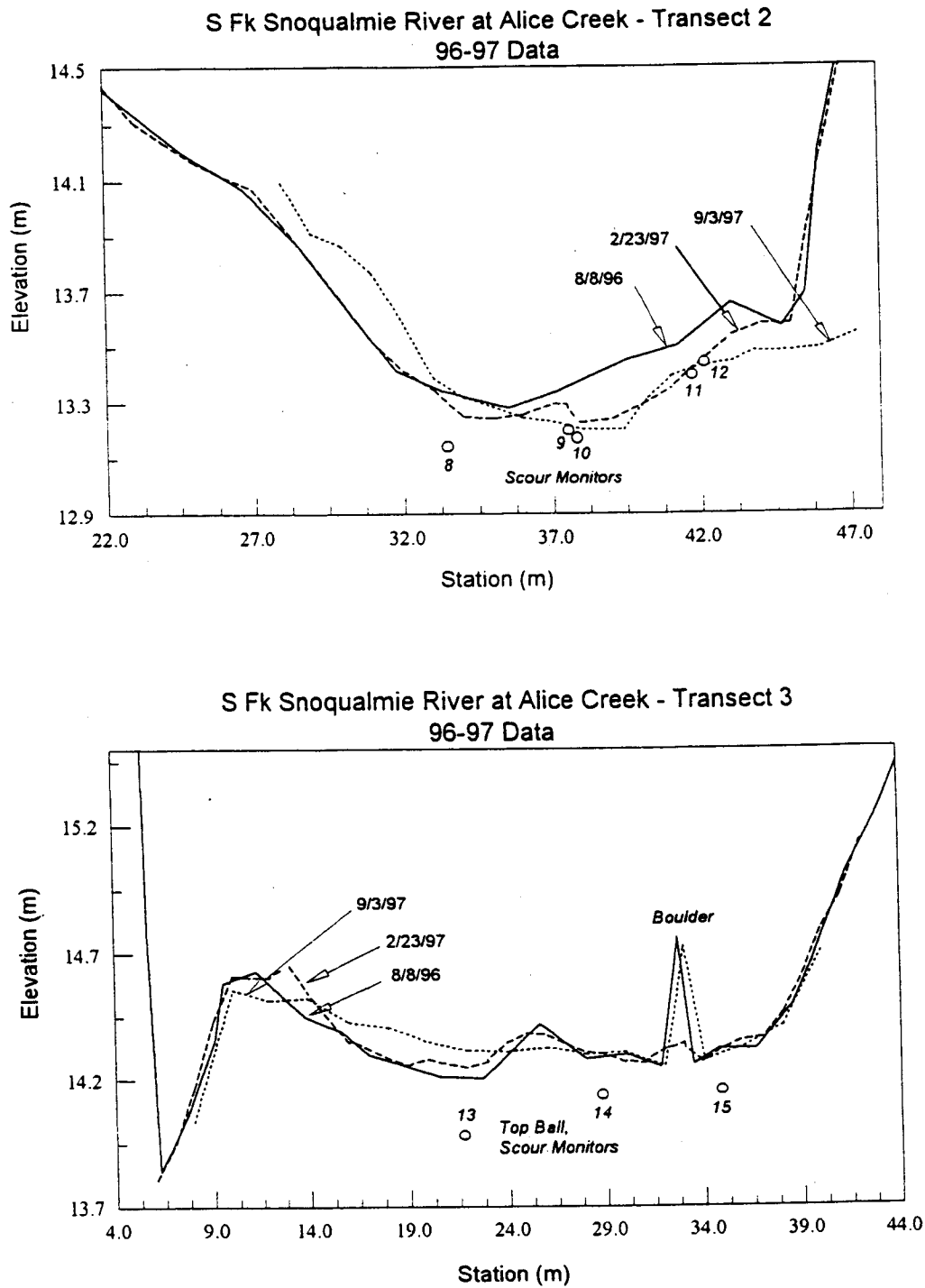
Figure D-7. Surveyed cross-sections and locations of scour monitors, South Fork Snoqualmie River, Transects 2 and 3; 1996-97 flood season.
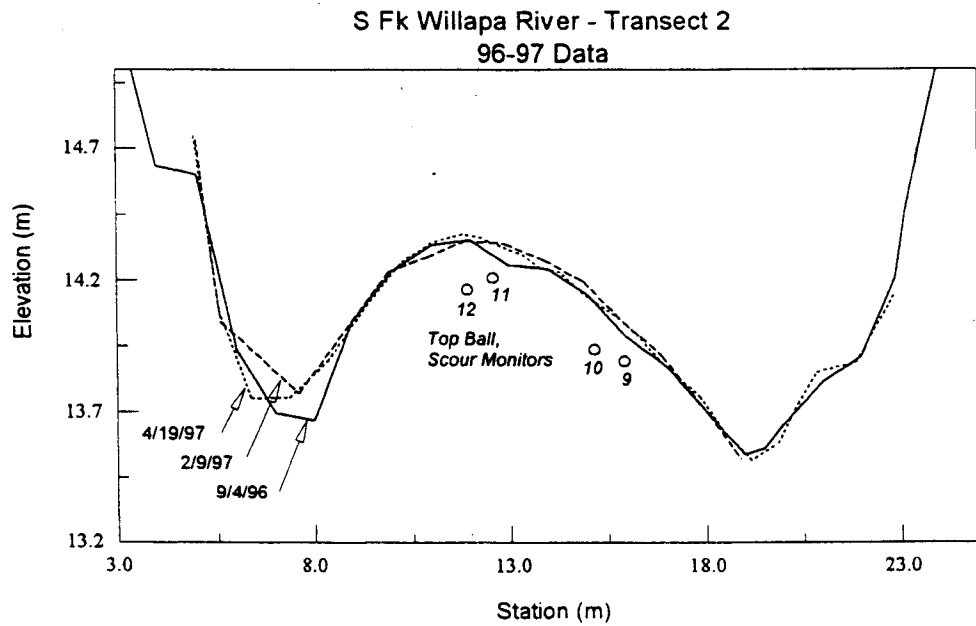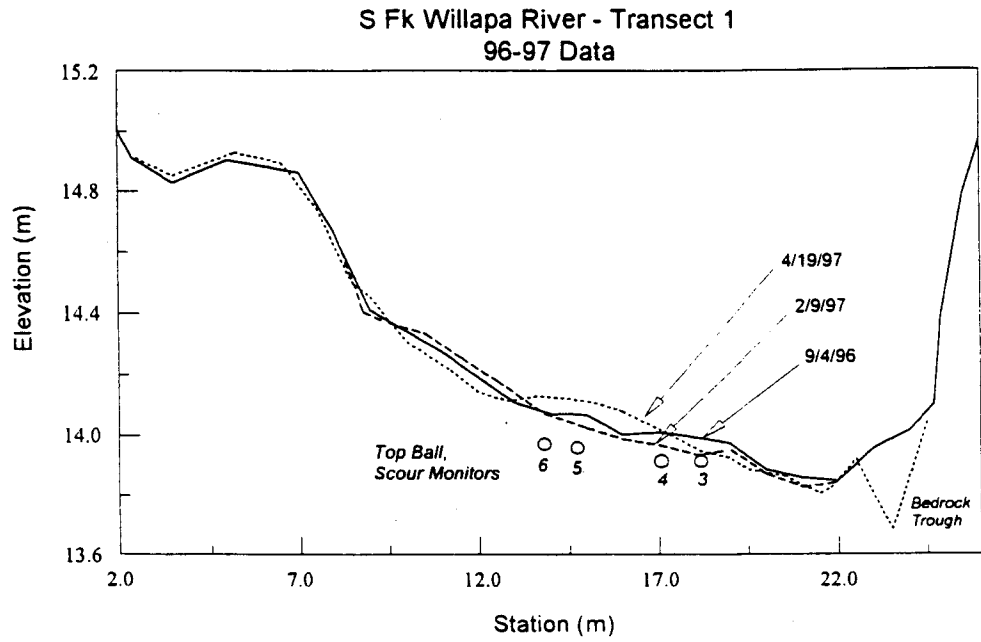
Figure D-8. Surveyed cross-sections and locations of scour monitors, South Fork Willapa River, Transects 1 and 2; 1996-97 flood season.
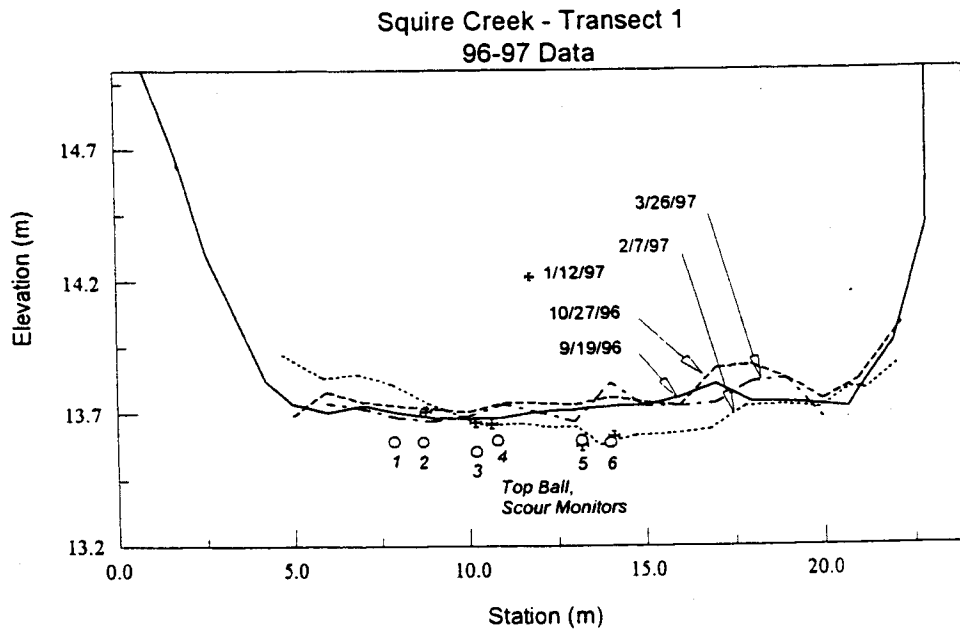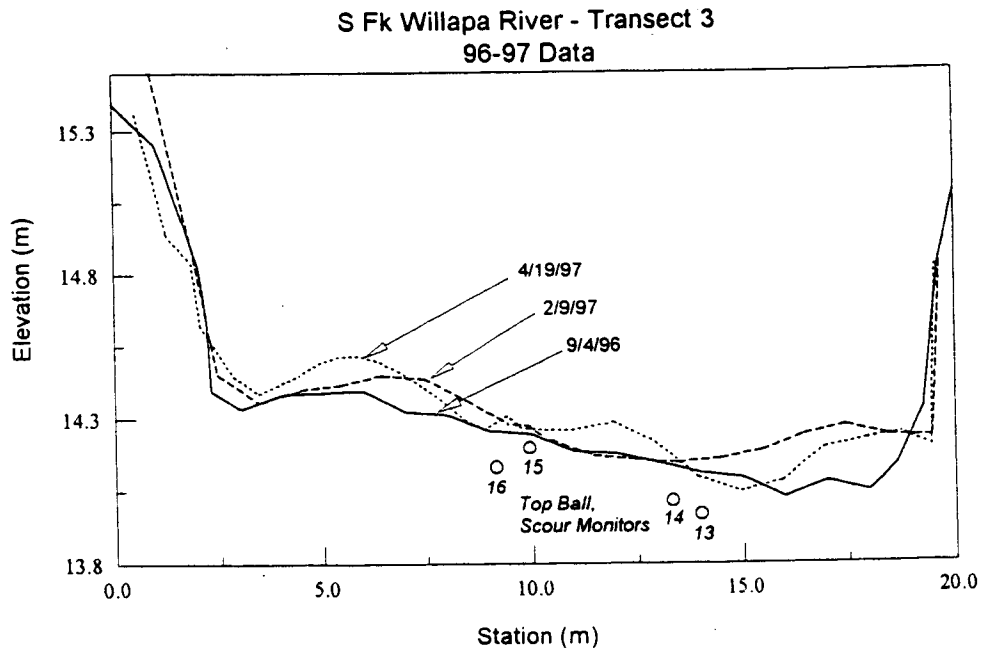
Figure D-9. Surveyed cross-sections and locations of scour monitors, South Fork Willapa River, Transect 3, and Squire Creek, Transect 1; 1996-97 flood season.

Squire Creek - Transect 2
96-97 Data

Squire Creek - Transect 3
96-97 Data
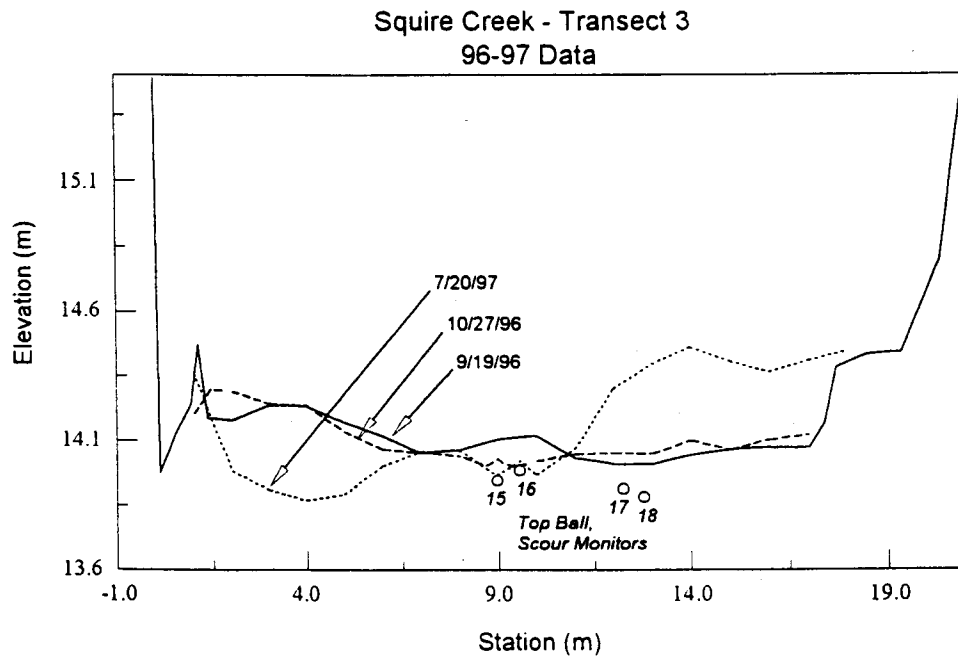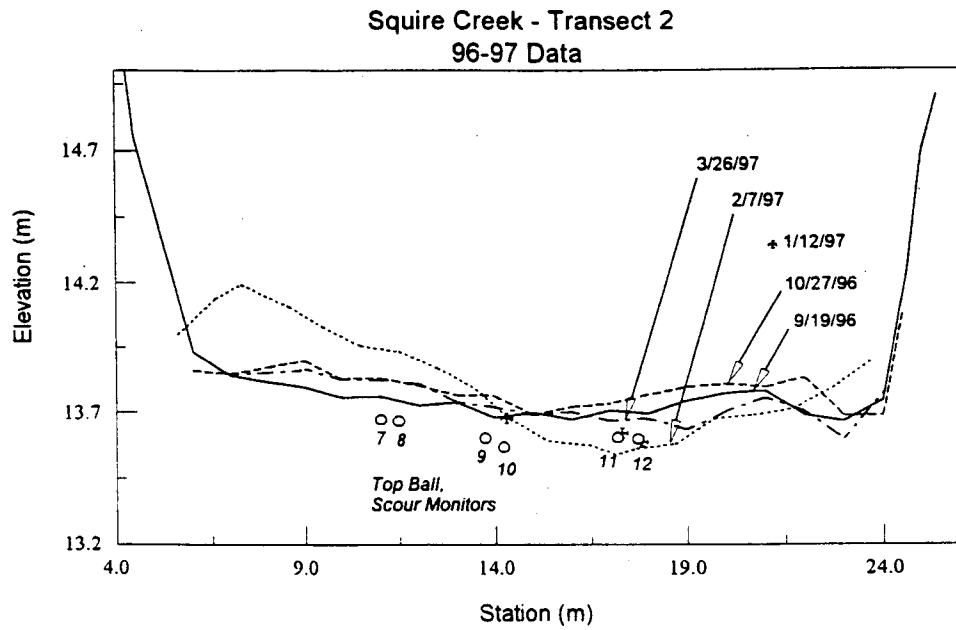
Figure D-10. Surveyed cross-sections and locations of scour monitors, Squire Creek, Transects 2 and 3; 1996-97 flood season.
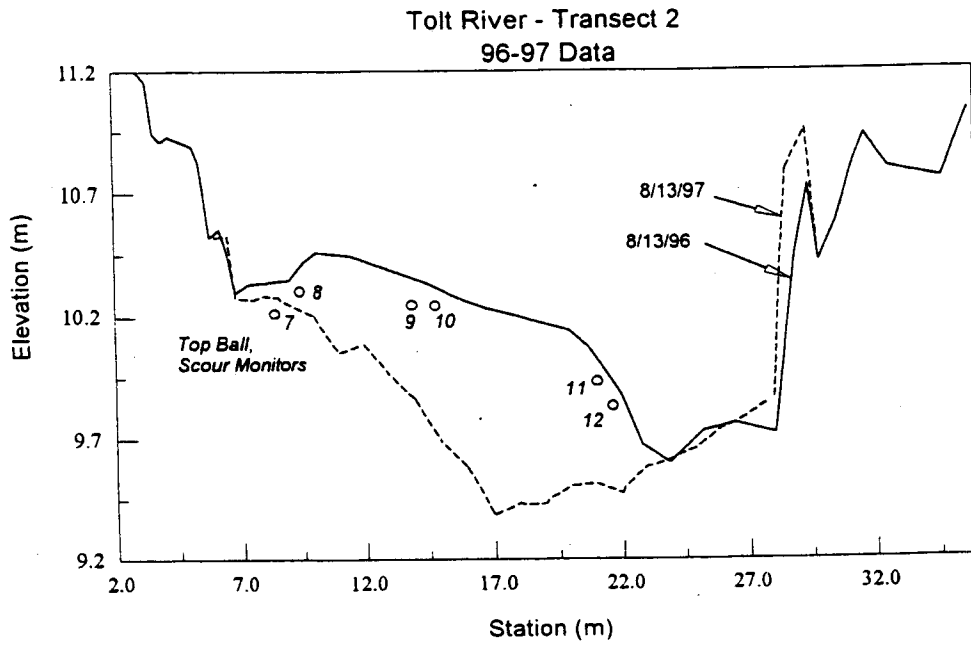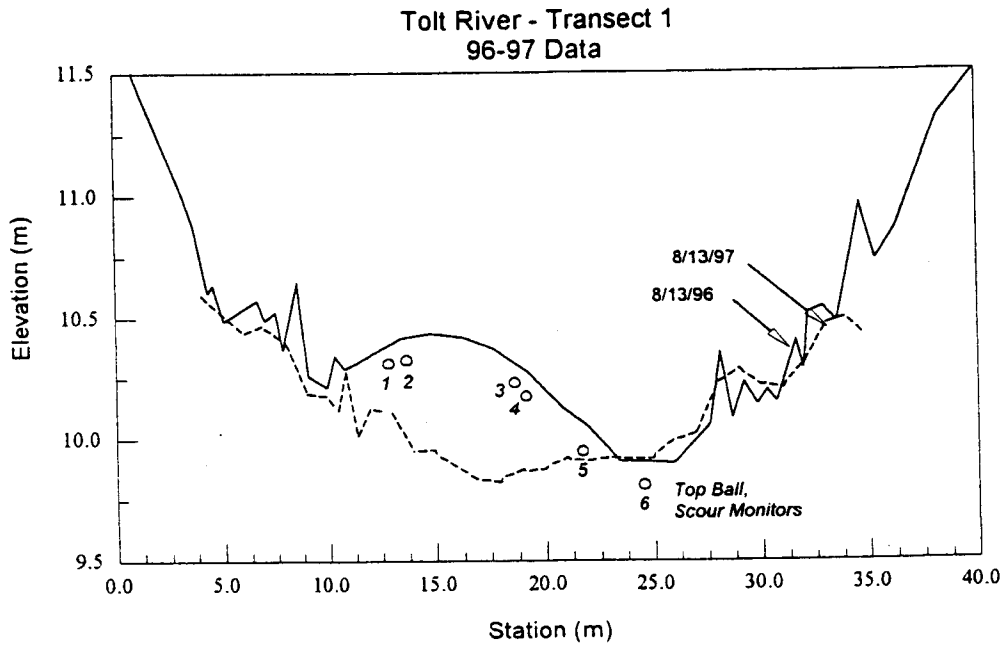
Figure D-11. Surveyed cross-sections and locations of scour monitors, Tolt River, Transects 1 and 2; 1996-97 flood season.
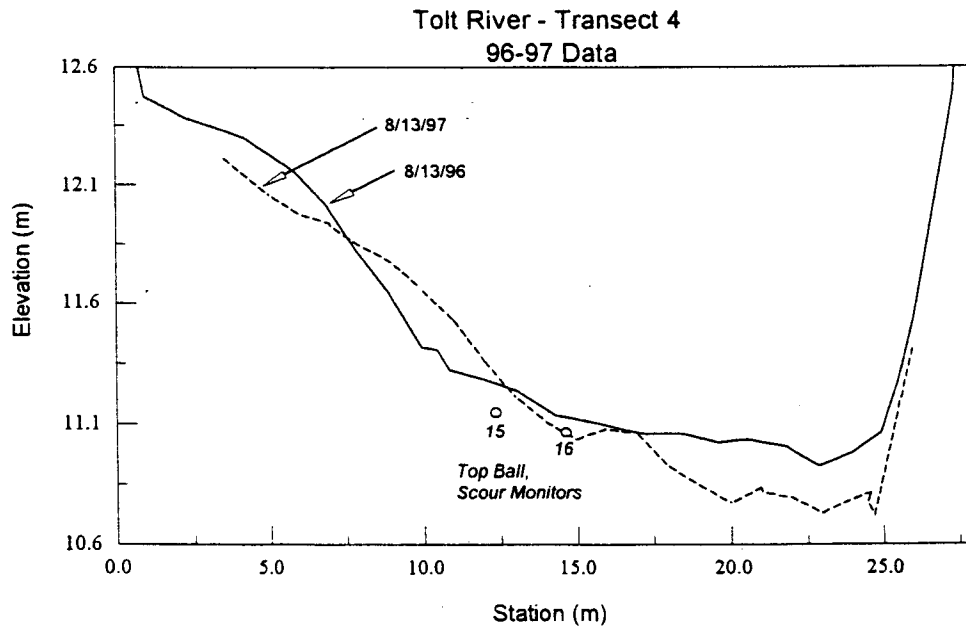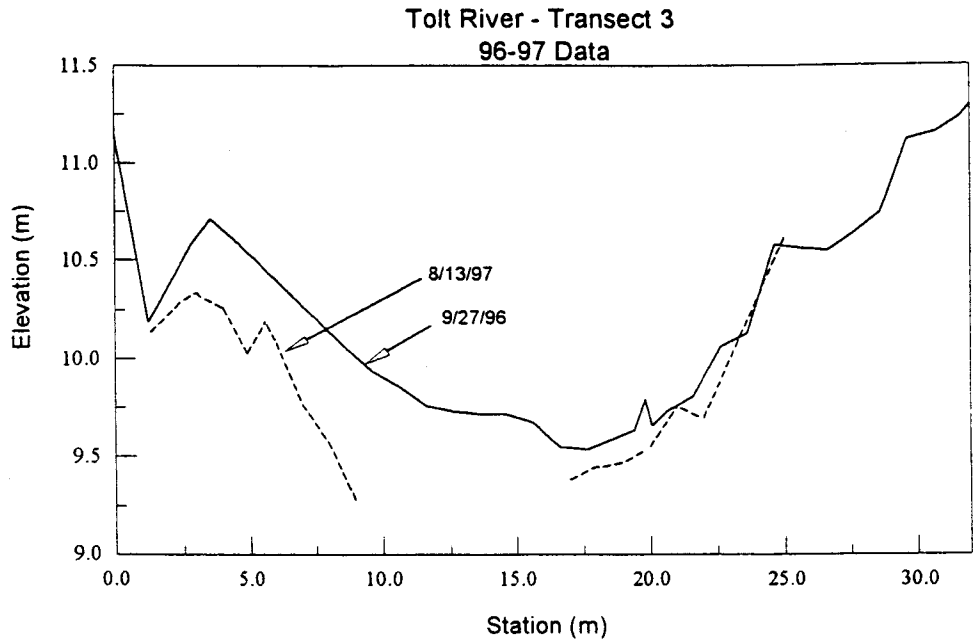
Figure D-12. Surveyed cross-sections and locations of scour monitors, Tolt River, Transects 3 and 4; 1996-97 flood season.
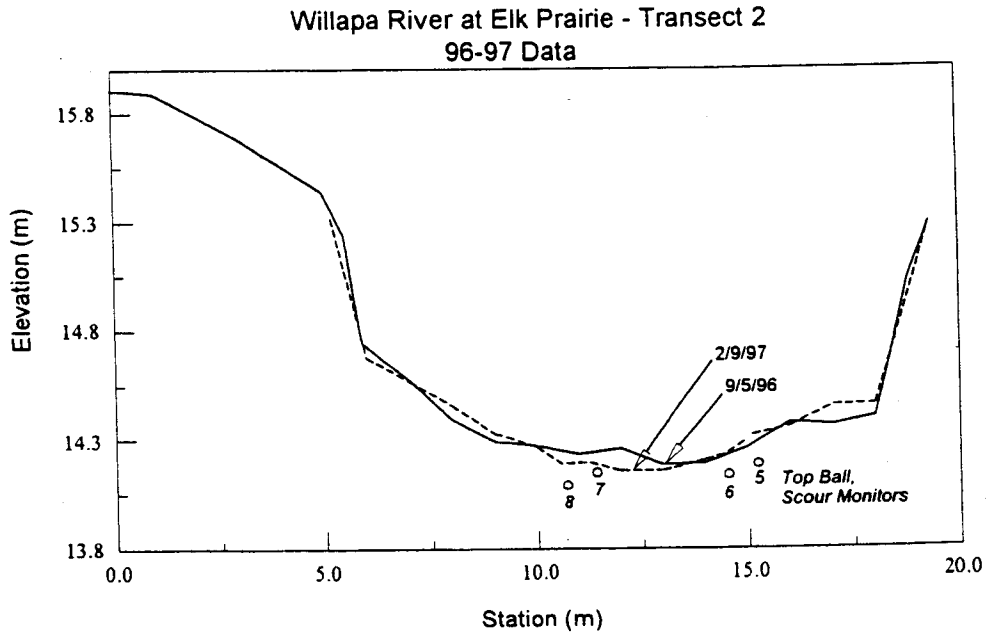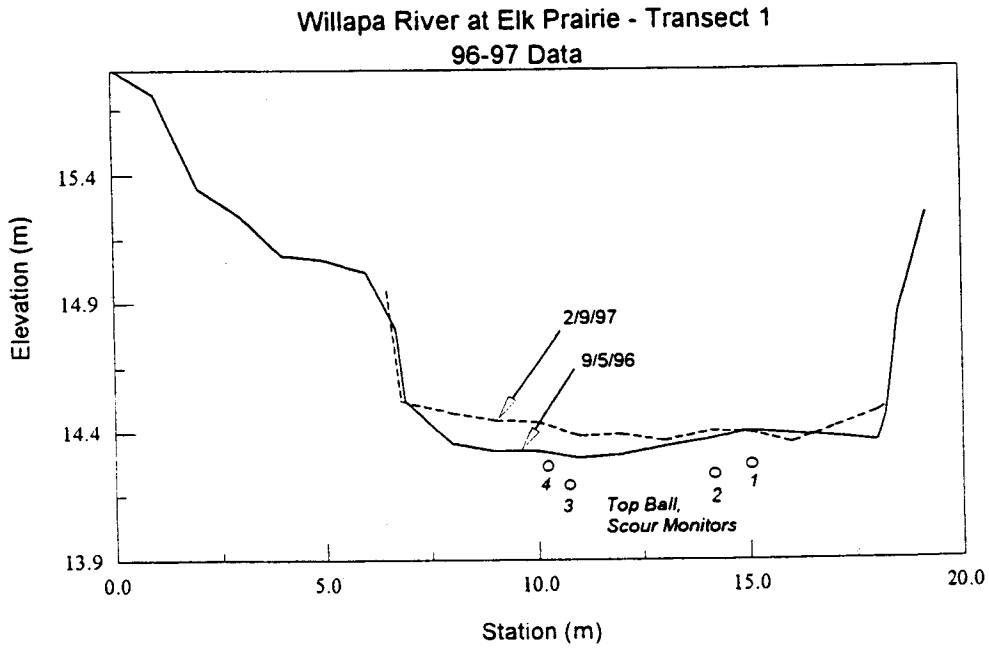
Figure D-13. Surveyed cross-sections and locations of scour monitors, Willapa River at Elk Prairie, Transects 1 and 2; 1996-97 flood season.
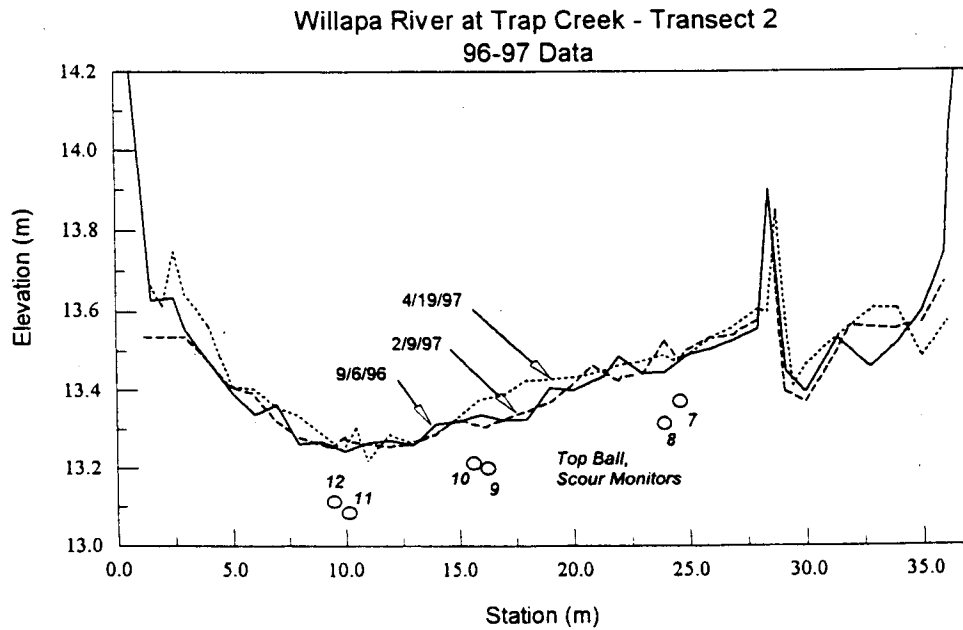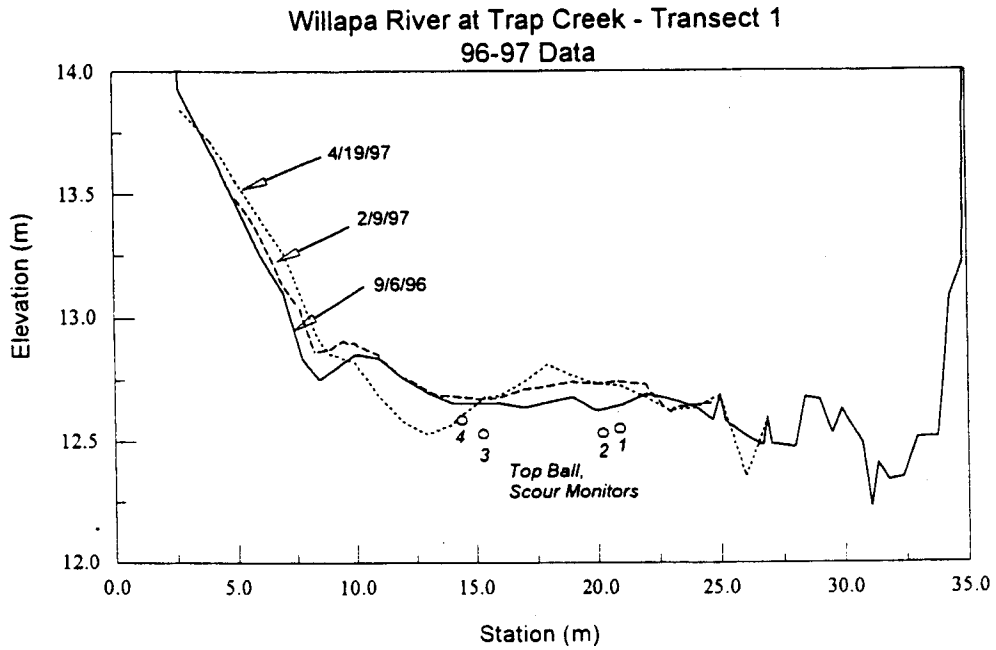
Figure D-14. Surveyed cross-sections and locations of scour monitors, Willapa River at Trap Creek, Transects 1 and 2; 1996-97 flood season.
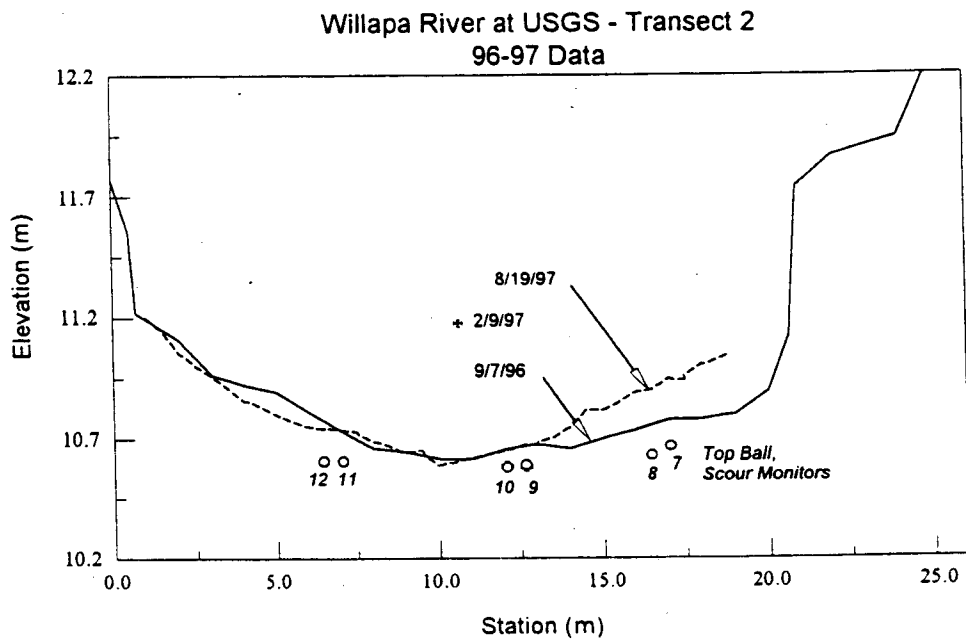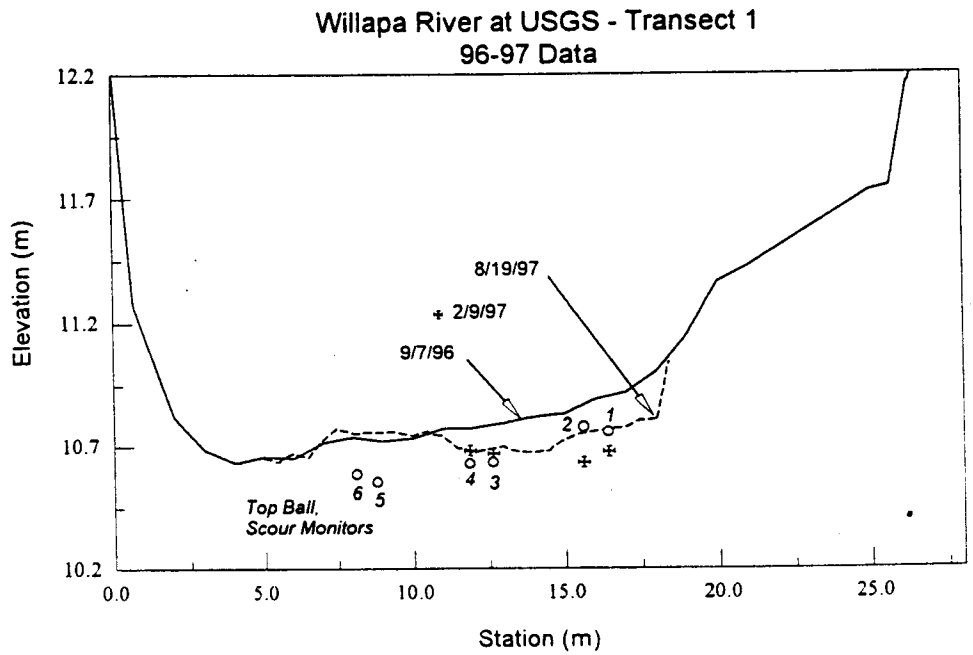
Figure D-15. Surveyed cross-sections and locations of scour monitors, Willapa River at USGS, Transects 1 and 2; 1996-97 flood season.

Table D-1. Scour Depth and Related Data

Site	Date Installed / Reset	Habitat [1]	Transect	Scour Monitor ID #	Bed: Before	Bed: After	Top of Undisturbed Bed	Total	Net Excavation	Bedload Layer Thickness	Net Fill Depth (m)	Flood Date	Maximum Bed Shear Stress (Pa)	Shields Parameter	Excess Stream Power (W/m2)	D_{max} (mm)	D_{90} (mm)	D_{50} (mm)	$D_{competent}$ (mm)
Issaquah Creek	11/09/96	RF1	1	2	13.777	13.859	13.682	0.095	0.000	na	na	01/01/97	63.1	0.092	154	124	83	41	124
Issaquah Creek	11/09/96	RF1	1	3	13.828	13.970	13.708	0.120	0.000	na	na	01/01/97	66.3	0.096	169	124	83	41	124
Issaquah Creek	11/09/96	RF1	1	4	13.850	13.990	13.709	0.141	0.000	na	na	01/01/97	65.5	0.095	165	124	83	41	124
Issaquah Creek	11/09/96	RF1	2	5	13.852	13.909	13.749	0.103	0.000	na	na	01/01/97	64.8	0.095	162	124	83	41	124
Issaquah Creek	11/09/96	RF1	2	6	13.847	13.907	13.701	0.146	0.000	0.146	0.060	01/01/97	60.3	0.100	150	124	83	41	101
Issaquah Creek	11/09/96	RF1	2	7	13.889	14.011	13.794	0.095	0.000	na	na	01/01/97	59.9	0.081	144	101	84	44	101
Issaquah Creek	11/09/96	RF1	3	9	na	na	na	0.140	0.000	0.140	>0	01/01/97	59.6	0.081	143	101	84	44	101
Issaquah Creek	11/09/96	RF1	3	10	na	na	na	0.166	0.000	0.156	>0	01/01/97	61.3	0.089	148	124	83	41	124
Issaquah Creek	11/09/96	RF1	4	11	na	na	na	0.087	0.000	0.087	>0	01/01/97	37.2	0.054	60	124	83	41	109
Issaquah Creek	09/10/97	RF1	0	2	13.828	13.798	13.640	0.188	0.030	0.158	0.000	11/25/98	20.3	0.034	19	94	75	36	41
Issaquah Creek	09/10/97	RF1	1	3	14.035	13.871	13.720	0.315	0.164	0.151	0.000	11/25/98	62.5	0.104	160	94	75	36	94
Issaquah Creek	09/10/97	RF1	1	4	14.063	13.873	13.737	0.326	0.190	0.136	0.000	11/25/98	63.8	0.093	160	124	83	41	124
Issaquah Creek	09/10/97	RF1	2	5	13.849	13.880	13.771	0.078	0.000	0.078	0.031	11/25/98	65.0	0.095	165	124	83	41	124
Issaquah Creek	11/08/97	RF1	2	6	13.871	13.871	13.796	0.075	0.000	0.075	0.000	10/30/97	63.4	0.092	161	124	83	41	124
Issaquah Creek	09/10/97	RF1	2	7	13.837	13.862	13.821	0.016	0.000	0.016	0.025	12/16/97	71.0	0.103	193	124	83	41	124
Issaquah Creek	09/10/97	RF1	2	7	13.932	13.834	13.781	0.151	0.098	0.053	0.000	11/25/98	70.0	0.102	188	124	83	41	124
Issaquah Creek	11/08/97	RN	3	8	13.837	13.849	13.690	0.147	0.000	0.147	0.012	11/25/98	67.5	0.098	177	124	83	41	124
Issaquah Creek	11/08/97	RN	3	9	13.849	13.822	13.731	0.118	0.027	0.091	0.000	11/25/98	68.6	0.100	182	124	83	41	124
Issaquah Creek	11/08/97	RN	3	10	13.837	13.834	13.654	0.183	0.003	0.180	0.000	11/25/98	79.7	0.190		124	83	41	124
Issaquah Creek	09/10/97	RN	4	11	13.862	13.743	13.635	0.227	0.119	0.108	0.000					124	83	41	124
Issaquah Creek	09/10/97	RN	4	12	13.868	13.740	13.618	0.250	0.128	0.122	0.000					124	83	41	124
Issaquah Creek	09/10/97	RF2	5	13	14.105	13.972	13.972	0.133	0.024	0.109	0.000					124	83	41	124
Issaquah Creek	09/10/97	RF2	5	14	14.118	13.992	13.992	0.126	0.080	0.046	0.000					94	42		
Issaquah Creek	09/10/97	PO	6	16	13.828	na	13.534	0.285	na	na	na								
N Fk Stillaguamish @ Hazel	10/01/96	REDD1	na	1	na	na	na	0.330	na	na	na						*142*		
N Fk Stillaguamish @ Hazel	10/01/96	REDD1	na	2	na	na	na	0.271	na	na	na						*142*		
N Fk Stillaguamish @ Hazel	10/01/96	REDD1	na	4	na	na	na	0.273	na	na	na						*142*		
N Fk Stillaguamish @ Hazel	10/01/96	REDD2	na	6	na	na	na	0.272	na	na	na						*142*		
N Fk Stillaguamish @ Hazel	10/01/96	REDD2	na	7	na	na	na	0.263	na	na	na					140	112	34	140
N Fk Stillaguamish @ Hazel	08/20/96	RF1	1	6	11.801	11.759	11.616	0.185	0.042	0.143	0.000	01/01/97	46.0	0.081	91	330	142	59	330
N Fk Stillaguamish @ Hazel	08/20/96	RF1	2	8	11.306	11.362	11.034	0.272	0.000	0.272	0.056	03/19/97	82.3	0.083	238	156	128	43	156
N Fk Stillaguamish @ Hazel	08/21/96	RF1	2	9	11.572	11.587	11.347	0.225	0.000	0.225	0.015	03/19/97	75.8	0.105	214	156	128	43	156
N Fk Stillaguamish @ Hazel	08/21/96	RF1	2	10	11.594	11.635	11.266	0.328	0.000	0.328	0.041	03/19/97	74.3	0.103	206	170	94	45	170
N Fk Stillaguamish @ Hazel	08/20/96	RF1	2	11	11.778	11.743	11.557	0.221	0.035	0.186	0.000	03/19/97	55.3	0.073	133	170	128	45	170
N Fk Stillaguamish @ Hazel	08/21/96	RF1	2	12	11.821	11.777	11.716	0.105	0.044	0.061	0.000	01/01/97	54.3	0.103	128	170	94	45	170
N Fk Stillaguamish @ Hazel	08/21/96	RF1	3	14	11.601	11.557	11.322	0.279	0.044	0.235	0.000	01/01/97	62.5	0.087	152	156	128	43	156
N Fk Stillaguamish @ Hazel	10/12/96	RF1	3	15	11.747	11.712	11.507	0.240	0.035	0.205	0.000	01/01/97	58.2	0.081	136	240	118	43	230
N Fk Stillaguamish @ Hazel	08/21/96	RF1	3	16	11.823	11.756	11.617	0.206	0.067	0.139	0.000	01/01/97	56.0	0.108	132	210	108	31	210

Table D-1. Scour Depth and Related Data

Site	Date Installed / Reset	Habitat	Transect	Scour Monitor ID #	Bed: Before	Bed: After	Top of Undisturbed Bata	Total	Net Excavation	Bedload Layer Thickness	Net Fill Depth (m)	Flood Date	Maximum Bed Shear Stress (Pa)	Shields Parameter	Excess Stream Power (W/m2)	Dmax (mm)	D90 (mm)	D60 (mm)	Dcompeten (mm)
N Fk Stillaguamish @ USGS	08/21/96	RF1	1	2	10.641	10.592	10.352	0.289	0.049	0.240	0.000	03/19/97	59.1	0.042	156	200	138	79	137
N Fk Stillaguamish @ USGS	08/21/96	RF1	1	3	10.576	10.589	10.403	0.173	0.000	0.173	0.013	03/19/97	60.1	0.039	153	215	160	88	130
N Fk Stillaguamish @ USGS	08/21/96	RF1	2	7	10.864	10.930	10.676	0.188	0.000	0.188	0.066	03/19/97	56.6	0.041	144	200	138	79	127
N Fk Stillaguamish @ USGS	08/21/96	RF1	2	9	10.535	10.930	10.620	0.311	0.000	0.311	0.009	03/19/97	56.1	0.041	138	265	158	77	127
N Fk Stillaguamish @ USGS	08/25/96	RF1	2	10	10.931	10.940	10.801	0.206	0.067	0.139	0.005	03/19/97	54.6	0.040	131	265	158	77	121
N Fk Stillaguamish @ USGS	08/25/96	RF1	2	11	11.007	10.822	10.648	0.169	0.000	0.169	0.000	03/19/97	57.1	0.036	133	370	191	91	116
N Fk Stillaguamish @ USGS	08/25/96	RF1	2	12	10.845	10.793	10.669	*0.172*	0.052	*na*	*na*	03/19/97	57.3	0.036			191		
Raging River	08/15/96	RF1	1	2	14.578	14.578	14.315	0.263	0.000	0.263	0.000	11/27/96	114.0	0.103	325	216	130	65	216
Raging River	12/21/96	RF1	1	2	14.578	14.576	14.391	0.187	0.003	0.184	0.000	01/01/97	104.9	0.095	280	216	130	65	216
Raging River	08/22/96	RF1	1	3	14.574	14.535	14.310	0.264	0.039	0.225	0.000	11/27/96	115.5	0.122	337	286	128	56	286
Raging River	12/21/96	RF1	1	3	14.535	14.483	14.346	0.189	0.052	0.137	0.000	01/01/97	111.1	0.117	314	286	128	56	286
Raging River	08/15/96	RF1	1	3	14.483	14.513	14.310	0.173	0.000	0.173	0.030	02/14/97	102.1	0.108	269	286	128	56	286
Raging River	12/21/96	RF1	1	4	14.572	14.572	14.276	0.296	0.000	0.296	0.000	11/27/96	114.3	0.120	330	286	128	56	286
Raging River	08/15/96	RF1	1	4	14.572	14.502	14.315	0.257	0.070	0.187	0.000	01/01/97	107.7	0.113	297	368	166	58	368
Raging River	12/21/96	RF1	1	5	14.582	14.467	14.355	0.227	0.115	0.112	0.000	11/27/96	113.1	0.115	299	368	166	58	368
Raging River	08/22/96	RF1	1	5	14.467	14.444	14.355	0.112	0.023	0.089	0.000	01/01/97	114.5	0.116	307	368	166	58	368
Raging River	12/21/96	RF1	1	6	14.529	14.503	14.343	0.186	0.026	0.160	0.000	11/27/96	115.7	0.118	312	368	166	58	368
Raging River	08/15/96	RF1	1	6	14.503	14.465	14.343	0.160	0.038	0.122	0.000	01/01/97	114.2	0.116	304	216	130	65	216
Raging River	12/21/96	RF1	1	7	14.535	14.479	14.242	0.293	0.056	0.237	0.000	01/01/97	127.9	0.116	402	216	130	65	216
Raging River	08/22/96	RF1	2	7	14.479	14.477	14.203	0.276	0.002	0.274	0.000	01/01/97	124.5	0.113	375	286	128	56	286
Raging River	08/22/96	RF1	2	10	14.544	14.474	14.209	0.235	0.035	0.200	0.000	11/27/96	127.6	0.134	404	286	128	56	286
Raging River	12/21/96	RF1	2	10	14.509	14.505	14.309	0.200	0.035	0.165	0.000	01/01/97	120.5	0.127	364	368	166	58	368
Raging River	08/22/96	RF1	2	11	14.611	14.447	14.399	0.212	0.106	0.106	0.000	11/27/96	122.0	0.124	344	368	166	58	368
Raging River	12/21/96	RF1	2	11	14.506	14.518	14.399	0.106	0.058	0.048	0.000	01/01/97	122.4	0.124	346	368	166	58	368
Raging River	08/22/96	RF1	2	12	14.633	14.447	14.407	0.226	0.115	0.111	0.000	11/27/96	120.0	0.122	333	368	166	58	368
Raging River	08/22/96	RF2	1	13	15.732	15.692	15.401	0.331	0.040	0.291	0.000	11/27/96	118.7	0.084	318	380	175	83	380
Raging River	08/22/96	RF2	1	14	15.858	15.695	15.500	0.358	0.163	0.195	0.000	11/27/96	108.0	0.077	266	380	175	83	380
S Fk Snoqualmie River	08/11/96	RF1	1	1	13.615	13.595	13.460	*0.155*	0.020	*na*	*na*	02/14/97	48.8	0.039	157		179	75	211
S Fk Snoqualmie River	08/11/96	RF1	1	1	13.595	13.485	13.361	0.234	0.110	0.124	0.000	03/19/97	70.7	0.056	84	290	179	75	119
S Fk Snoqualmie River	08/08/96	RF1	1	2	13.539	13.537	13.429	0.110	0.002	0.108	0.000	02/14/97	51.1	0.040	170	290	179	75	227
S Fk Snoqualmie River	08/08/96	RF1	1	2	13.537	13.432	13.308	0.229	0.105	0.124	0.000	03/19/97	73.8	0.058	91	290	179	75	120
S Fk Snoqualmie River	08/11/96	RF1	1	3	13.436	13.417	13.322	0.114	0.019	0.095	0.000	02/14/97	54.0	0.038	179	340	185	85	222
S Fk Snoqualmie River	08/11/96	RF1	1	3	13.417	13.306	13.173	0.244	0.111	0.133	0.000	03/19/97	76.8	0.054	91	340	185	85	120
S Fk Snoqualmie River	08/08/96	RF1	1	4	13.437	13.442	13.235	0.202	0.000	0.202	0.005	02/14/97	54.2	0.038	179	340	185	85	220
S Fk Snoqualmie River	08/08/96	RF1	1	4	13.442	13.301	13.117	0.325	0.141	0.184	0.000	03/19/97	76.5	0.063	213	340	185	85	265
S Fk Snoqualmie River	08/11/96	RF1	1	5	13.384	13.311	13.088	0.296	0.073	0.223	0.000	03/19/97	77.7	0.071		265	115	65	

Table D-1. Scour Depth and Related Data

Site	Date Installed/Reset	Habitat[1]	Transect	Scour Monitor ID #	Bed: Before	Bed: After	Top of Undisturbed Bals	Total	Net Excavation	Bedload Layer Thickness	Net Fill Depth (m)	Flood Date	Maximum Bed Shear Stress (Pa)	Shields Parameter	Excess Stream Power (W/m2)	D_{max} (mm)	D_{90} (mm)	D_{60} (mm)	$D_{component}$ (mm)
S Fk Snoqualmie River	08/08/96	RF1	1	6	13.372	13.318	13.148	0.224	0.054	0.170	0.000	03/19/97	78.0	0.071	214	265	115	65	265
S Fk Snoqualmie River	08/11/96	RF1	2	8	13.336	13.357	13.045	0.291	0.000	0.291	0.021	03/19/97	85.6	0.062	223	310	179	82	276
S Fk Snoqualmie River	08/08/96	RF1	2	9	13.358	13.291	13.144	0.214	0.067	0.147	0.000	02/14/97	60.4	0.050	126	335	139	72	165
S Fk Snoqualmie River	08/08/96	RF1	2	9	13.291	13.216	13.105	0.186	0.075	0.111	0.000	03/19/97	85.2	0.070	239	335	139	72	302
S Fk Snoqualmie River	08/11/96	RF1	2	10	13.372	13.241	13.132	0.240	0.131	0.109	0.000	02/14/97	60.0	0.049	125	335	139	72	163
S Fk Snoqualmie River	08/11/96	RF1	2	10	13.241	13.208	13.096	0.145	0.033	0.112	0.000	03/19/97	86.9	0.072	247	335	139	72	312
S Fk Snoqualmie River	08/08/96	RF1	2	11	13.545	13.425	13.258	0.287	0.120	0.167	0.016	02/14/97	53.2	0.090		88	54	35	88
S Fk Snoqualmie River	08/11/96	RF1	2	11	13.425	13.441	13.179	0.246	0.000	0.246	0.000	03/19/97	78.8	0.134		88	54	35	88
S Fk Snoqualmie River	08/11/96	RF1	2	12	13.581	13.457	13.266	0.315	0.124	0.191	0.024	02/14/97	52.9	0.090		88	54	35	88
S Fk Snoqualmie River	08/11/96	RF1	2	12	13.457	13.481	13.187	0.270	0.000	0.270	na	03/19/97	76.9	0.130		88	54	35	88
S Fk Snoqualmie River	08/11/96	RF2	1	1	14.207	14.250	14.061	0.146	0.000	na	na	03/19/97	57.1	0.045	199	290	124	75	252
S Fk Snoqualmie River	08/11/96	RF2	1	5	14.322	14.316	14.175	0.147	0.006	0.235	0.000	10/30/97	78.3	0.062	105	290	179	75	139
S Fk Snoqualmie River	09/04/97	RF1	1	7	13.496	13.490	13.255	0.241	0.006	0.123	0.000	10/04/97	55.7	0.044	204	290	179	75	258
S Fk Snoqualmie River	09/04/97	RF1	1	2	13.426	13.426	13.303	0.123	0.000	0.163	0.003	10/30/97	79.3	0.063	201	340	179	85	235
S Fk Snoqualmie River	09/04/97	RF1	1	3	13.426	13.426	13.263	0.163	0.000	0.298	0.055	10/30/97	79.4	0.055		335	185	72	196
S Fk Snoqualmie River	09/04/97	RF1	1	5	13.389	13.444	13.091	0.298	0.000	na	na	03/19/97				335	139	72	308
S Fk Snoqualmie River	09/04/97	RF1	1	6	13.365	13.359	13.090	0.275	na	na	0.000	10/04/97	66.7	0.055	161	335	139	72	319
S Fk Snoqualmie River	09/04/97	RF1	2	9	13.331	13.350	12.988	0.343	0.045	0.118	na	10/04/97				165	139	75	165
S Fk Snoqualmie River	09/04/97	RF1	2	10	13.203	13.158	13.040	0.163	na	na	0.000	10/04/97	86.3	0.071	257		124		81
S Fk Snoqualmie River	09/04/97	PO	3	13	12.804	12.758	12.651	0.228	0.046	0.107	na	10/04/97	87.9	0.072	266				81
S Fk Snoqualmie River	09/04/97	PO	3	14	12.746	12.703	12.578	0.153	0.043	0.125	na	10/04/97							81
S Fk Snoqualmie River	09/04/97	RN	4	15	13.337	13.331	12.998	0.339	na	na	na	10/04/97							81
S Fk Snoqualmie River	09/04/97	RN	4	16	13.322	13.292	12.986	0.351	na	na	na	10/30/97							81
S Fk Snoqualmie River	09/04/97	RF2	5	19	14.301	14.252	14.130	0.171	na	na	na	10/30/97	84.7	0.067	249				112
S Fk Snoqualmie River	09/04/97	RF2	5	20	14.243	14.240	14.132	0.111	na	na	na								
S Fk Snoqualmie River	09/20/97	RN/PO	6	21	14.023	13.996	13.695	0.328	0.027	0.301	0.000					165			
S Fk Willapa River	09/04/96	RF1	1	3	13.989	13.936	13.894	0.095	0.053	0.042	0.000	01/01/97	32.6	0.059	70	81	124	75	165
S Fk Willapa River	09/04/96	RF1	1	4	14.009	13.966	13.935	0.074	0.043	0.031	0.000	01/01/97	32.3	0.059	69	81	56	35	81
S Fk Willapa River	09/04/96	RF1	1	5	14.067	14.116	13.979	0.088	0.000	na	na	01/01/97	31.3	0.057		81	56	35	81
S Fk Willapa River	09/04/96	RF1	1	6	14.078	14.072	13.991	0.087	0.006	na	na	01/01/97	33.8	0.098		81	56	22	
S Fk Willapa River	09/04/96	RF1	2	9	13.992	14.040	13.834	0.158	0.000	0.168	0.048	01/01/97	32.2	0.093		81	39	22	81
S Fk Willapa River	09/04/96	RF1	2	10	14.116	14.119	13.955	0.161	0.000	0.161	0.003	01/01/97	29.3	0.110		81	39	17	81
S Fk Willapa River	09/04/96	RF2	2	11	14.295	14.342	14.029	0.266	0.000	0.266	0.047	01/01/97	34.7	0.063			31		
S Fk Willapa River	09/04/96	RF2	1	13	14.112	14.093	14.001	0.111	0.019	na	na	01/01/97				70			
S Fk Willapa River	09/04/96	RF2	1	14	14.133	14.166	14.040	0.092	0.000	na	na	01/01/97							
S Fk Willapa River	09/04/96	RF2	1	15	14.246	14.273	14.135	0.111	0.000	0.111	0.027	01/01/97	33.1	0.060	69	122	70	35	112

Table D-1. Scour Depth and Related Data

Site	Date Installed/Reset	Habitat	Transect	Scour Monitor ID #	Elevations (m) Bed: Before	Bed: After	Bed: Top of Undisturbed	Scour Depths (m) Total	Net Excavation	Bedload Layer Thickness	Net Fill Depth (m)	Flood Date	Maximum Bed Shear Stress (Pa)	Shields Parameter	Excess Stream Power (W/m2)	D max (mm)	D90 (mm)	D60 (mm)	D comparison (mm)
Squire Creek	09/19/96	RF1	1	1	13.705	13.688	13.572	0.133	0.017	0.116	0.000	03/19/97	63.7	0.071	165	180	108	55	180
Squire Creek	09/19/96	RF1	1	2	13.690	13.705	13.573	0.117	0.000	0.117	0.015	01/01/97	53.0	0.059	119	180	108	55	171
Squire Creek	02/07/97	RF1	1	2	13.748	13.674	13.533	0.215	0.074	0.141	0.000	03/19/97	62.1	0.069	158	180	108	55	180
Squire Creek	09/19/96	RF1	1	3	13.680	13.665	13.497	0.183	0.015	0.168	0.000	01/01/97	53.3	0.060	120	180	108	55	173
Squire Creek	09/19/96	RF1	1	4	13.684	13.659	13.536	0.148	0.025	0.123	0.000	01/01/97	53.1	0.062	120	210	105	53	176
Squire Creek	09/19/96	RF1	1	5	13.715	13.577	13.535	0.180	0.138	0.042	0.000	01/01/97	52.3	0.061	115	210	105	53	172
Squire Creek	09/19/96	RF1	1	5	13.577	13.638	13.494	0.083	0.000	0.083	0.061	01/30/97	44.7	0.052	87	210	105	53	130
Squire Creek	09/19/96	RF1	1	5	13.638	13.694	13.454	0.184	0.000	0.184	0.056	03/19/97	66.4	0.077	180	210	105	53	210
Squire Creek	02/07/97	RF1	1	6	13.724	13.610	13.527	0.197	0.114	0.083	0.000	01/01/97	52.1	0.060	114	210	105	53	171
Squire Creek	09/19/96	RF1	1	6	13.610	13.591	13.447	0.163	0.019	0.144	0.000	01/30/97	45.1	0.052	89	210	105	53	132
Squire Creek	09/19/96	RF1	1	6	13.591	13.893	13.367	0.224	0.000	0.224	0.302	03/19/97	67.0	0.078	183	210	105	53	210
Squire Creek	09/19/96	RF1	1	10	13.684	13.677	13.508	0.176	0.007	0.169	0.000	01/01/97	55.2	0.064	129	210	105	53	189
Squire Creek	02/07/97	RF1	2	10	13.695	13.712	13.469	0.226	0.000	0.226	0.017	03/19/97	69.7	0.081	196	210	105	53	210
Squire Creek	09/19/96	RF1	2	11	13.702	13.619	13.541	0.161	0.083	0.078	0.000	01/01/97	54.8	0.064	127	210	105	53	186
Squire Creek	09/19/96	RF1	2	11	13.619	13.536	13.501	0.118	0.083	0.035	0.000	01/30/97	47.5	0.055	98	210	105	53	145
Squire Creek	09/19/96	RF1	2	11	13.696	13.577	13.577	0.119	0.000	0.119	0.061	10/22/96	40.9	0.047	74	210	105	53	112
Squire Creek	09/19/96	RF1	2	12	13.767	13.757	13.537	0.220	0.171	0.049	0.000	01/01/97	54.5	0.063	125	210	105	53	185
Squire Creek	09/19/96	RF1	2	12	13.586	13.586	13.456	0.130	0.025	0.105	0.000	01/30/97	46.9	0.054	95	210	105	53	142
Squire Creek	09/19/96	RF2	2	13	13.586	14.026	13.884	0.219	0.077	0.142	0.000	10/04/97	26.4	0.028		365	168	58	48
Squire Creek	09/19/96	RF2	1	13	14.103	13.967	13.803	0.223	0.059	0.164	0.000	01/01/97	52.8	0.056		365	168	58	163
Squire Creek	09/19/96	RF2	1	14	14.112	13.994	13.840	0.272	0.118	0.154	0.000	10/04/97	26.9	0.029		365	168	58	50
Tolt River	08/13/96	RF1	1	6	9.906	9.916	9.685	0.221	0.000	*0.221*	0.010	11/27/96	182.5	0.457		60	39	25	60
Tolt River	08/13/96	RF1	2	7	10.345	10.282	10.038	0.307	0.063	*0.244*	0.000	03/19/97	161.9	0.482		60	39	10	60
Willapa River @ Elk Prairie	09/05/96	RF1	1	1	14.400	14.395	14.291	*0.109*	0.005	na	na	01/01/97	34.3	0.046		145	101	44	108
Willapa River @ Elk Prairie	09/05/96	RF1	1	2	14.374	14.403	14.254	*0.120*	0.000	na	na	01/01/97				145	101	44	112
Willapa River @ Elk Prairie	09/05/96	RF1	1	3	14.304	14.395	14.209	*0.095*	0.000	na	na	01/01/97				145	101	44	117
Willapa River @ Elk Prairie	09/05/96	RF1	1	4	14.318	14.424	14.285	*0.033*	0.000	na	0.034	01/01/97					101		
Willapa River @ Elk Prairie	09/05/96	RF1	2	5	14.291	14.325	14.204	0.087	0.000	0.087	0.011	01/01/97	38.1	0.052	78		101		
Willapa River @ Elk Prairie	09/05/96	RF1	2	6	14.231	14.242	14.155	0.076	0.000	0.076	0.000	01/01/97	39.0	0.053	80				
Willapa River @ Elk Prairie	09/05/96	RF1	2	7	14.245	14.187	14.128	0.117	0.058	0.059	na	01/01/97	39.9	0.054	84				
Willapa River @ Elk Prairie	09/05/96	RF1	2	8	14.245	14.189	14.107	*0.138*	0.056	na	na	01/01/97	39.7	0.054					
Willapa River @ USGS	09/07/96	RF1	1	1	10.901	10.677	10.617	0.284	0.224	0.060	0.000	01/01/97	66.2	0.097	224	119	86	39	119
Willapa River @ USGS	09/07/96	RF1	1	2	10.868	10.631	10.557	0.311	0.237	0.074	0.000	01/01/97	66.8	0.098	227	119	86	39	119
Willapa River @ USGS	09/07/96	RF1	1	3	10.786	10.667	10.574	0.212	0.119	0.093	0.000	01/01/97	68.0	0.100	234	119	86	39	119
Willapa River @ USGS	09/07/96	RF1	1	4	10.774	10.680	10.608	0.166	0.094	0.072	0.000	01/01/97	68.2	0.100	235	119	86	39	119
Willapa River @ USGS	09/07/96	RF1	1	5	10.723	10.755	10.576	*0.147*	0.000	na	na	01/01/97							
Willapa River @ USGS	09/07/96	RF1	1	6	10.735	10.762	10.607	*0.128*	0.000	na	na	01/01/97							

Table D-1. Scour Depth and Related Data

Site	Date Installed/Reset	Habitat¹	Transect	Scour Monitor ID #	Elevations (m) Bed: Before	Bed: After	Top of Undisturbed Bells	Scour Depths (m) Total	Net Excavation	Bedload Layer Thickness	Net Fill Depth (m)	Flood Date	Maximum Bed Shear Stress (Pa)	Shields Parameter	Excess Stream Power (W/m2)	Dmax (mm)	D90 (mm)	D50 (mm)	Dcompetent (mm)
Willapa River @ USGS	09/07/96	RF1	2	9	10.670	10.585	10.572	0.098	0.085	0.013	0.000	01/01/97	69.8	0.102	244	119	86	39	119
Willapa River @ USGS	09/07/96	RF1	2	10	10.657	10.585	10.522	0.135	0.072	0.063	0.000	01/01/97	69.8	0.102	244	119	86	39	119
Willapa River @ USGS	09/07/96	RF1	2	11	10.729	10.735	10.628	0.101	0.000	na	na	01/01/97	69.3	0.071			95		
Willapa River @ USGS	09/07/96	RF1	2	12	10.776	10.741	10.627	0.149	0.035	na	na	01/01/97	68.7	0.070			95		
Willapa River @ Trap Creek	09/06/96	RF1	1	3	12.657	12.673	12.353	0.304	0.000	0.304	0.016	01/01/97	106.3	0.237		103	47	27	103
Willapa River @ Trap Creek	09/06/96	RF2	2	7	13.474	13.475	13.229	0.245	0.000	0.245	0.001	01/01/97	101.0	0.127		240	147	48	240
Willapa River @ Trap Creek	09/06/96	RF2	2	8	13.444	13.489	13.294	0.150	0.000	0.150	0.045	01/01/97	101.6	0.128		240	147	48	240
Willapa River @ Trap Creek	09/06/96	RF2	2	9	13.333	13.306	13.219	0.114	0.027	na	na	01/01/97	105.9	0.145			144		
Willapa River @ Trap Creek	09/06/96	RF2	2	10	13.332	13.315	13.233	0.099	0.017	0.082	0.000	01/01/97	105.8	0.145		275	144	44	275
Willapa River @ Trap Creek	09/06/96	RF2	2	11	13.247	13.264	13.105	0.141	0.000	na	na	01/01/97	108.1	0.148		144			
Willapa River @ Trap Creek	09/06/96	RF2	2	12	13.255	13.258	13.133	0.122	0.000	na	na	01/01/97					144		

¹ RF1, RF2 = Riffle; RN = Run; PO = Pool; REDD1, REDD2 = adjacent salmon egg nests

Appendix E

PEBBLE COUNT GRAIN SIZE DISTRIBUTIONS

Table E-1. Pebble Count Summary Statistics

Site	1996-97 Scour Monitor (SM) No.	n	Particle Size (mm)				
			D_{50}	D_{75}	D_{84}	D_{90}	D_{95}
Issaquah Cr	1, 2	100	40	64	72	84	93
	3, 4, 7, 8	100	44	57	67	75	82
	5, 6, 9, 10, 11	200	41	64	76	83	86
N Fk Stillaguamish R @ Hazel	1, 2, 8	100	59	100	117	142	165
	3, 4	100	47	85	106	126	172
	5, 6	100	34	57	85	112	119
	9, 10, 13, 14	100	43	82	101	128	136
	11, 12	100	23	62	80	94	133
	15	100	43	79	99	118	149
	16, 17, 18	100	31	70	88	108	150
N Fk Stillaguamish R @ USGS	1, 2, 7, 8	300	79	109	123	138	158
	3, 4	100	88	130	147	160	175
	9, 10	300	77	117	138	158	178
	11, 12	300	91	153	171	191	219
Raging R	1, 2, 7, 8	250	65	94	109	130	151
	3, 4, 9, 10	350	56	89	111	128	157
	5, 6, 11, 12	350	58	105	131	166	202
	13, 14	200	83	120	150	175	232
S Fk Snoqualmie R	1, 2	200	75	121	151	179	199
	3, 4	200	85	124	155	185	236
	5, 6	200	65	87	99	115	148
	8	200	82	137	163	179	216
	9, 10	300	72	103	113	139	171
	11, 12	100	34	43	50	54	59
	13, 14	100	75	105	110	124	147
Squire Cr	1, 2, 3, 7, 8, 9	100	55	78	93	108	123
	4, 5, 6, 10, 11, 12	100	53	75	90	105	117
	15, 16	200	58	92	133	168	211
S Fk Willapa R	3, 4, 9, 10	100	21	27	34	41	48
	13, 14, 15, 16	100	34	57	62	70	75
Tolt R	7, 8	100	25	32	35	39	44
Willapa R @ Elk Prairie	All	100	53	78	90	101	120
Willapa R @ Trap Cr	1, 2	100	28	39	44	51	63
	3, 4	100	17	29	36	47	59
	7, 8	100	48	80	128	147	163
	9, 10, 11, 12	100	44	86	124	144	239
Willapa R @ Mill Cr/USGS	1, 2, 3, 4, 7, 8, 9, 10	100	44	63	73	86	101
	5, 6, 11, 12	100	57	76	85	95	108
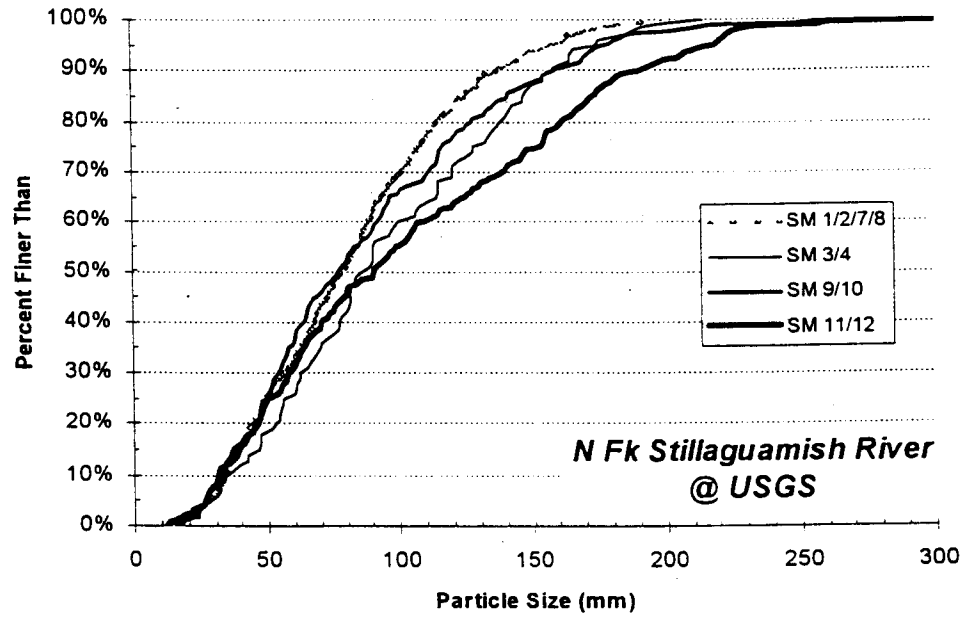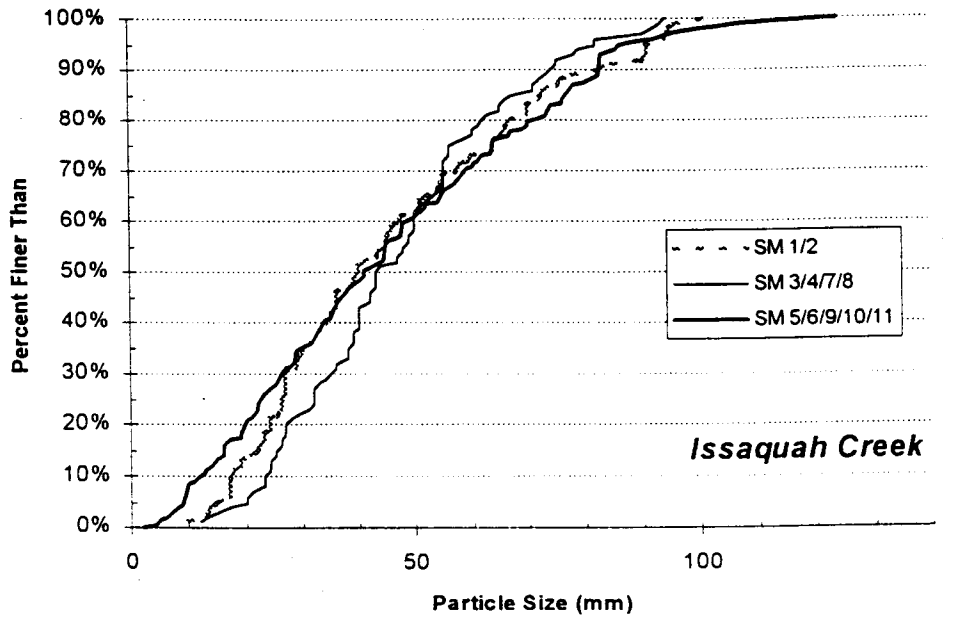
Figure E-1. Pebble count grain size distributions for the Issaquah Creek and North Fork Stillaguamish River at USGS sites.
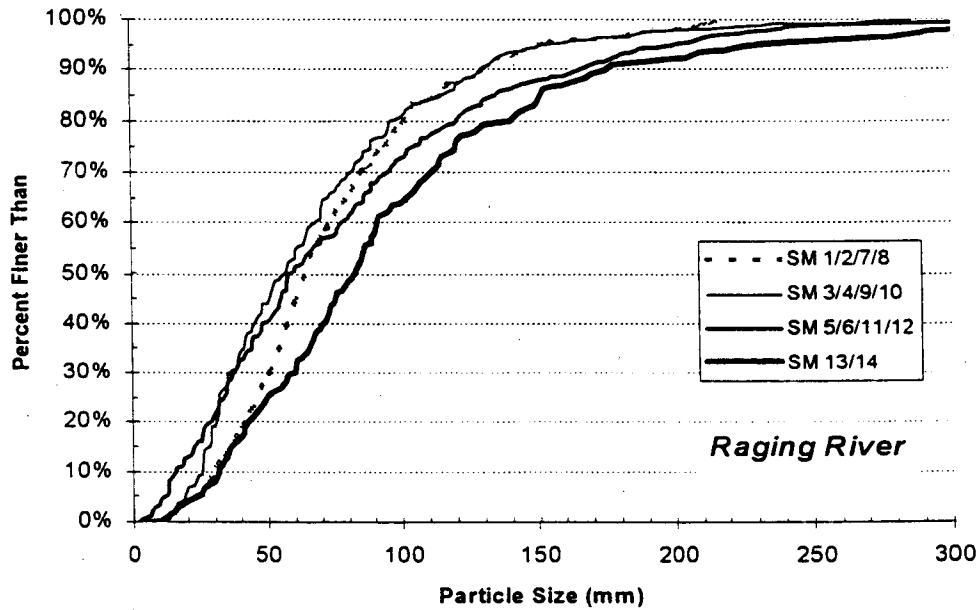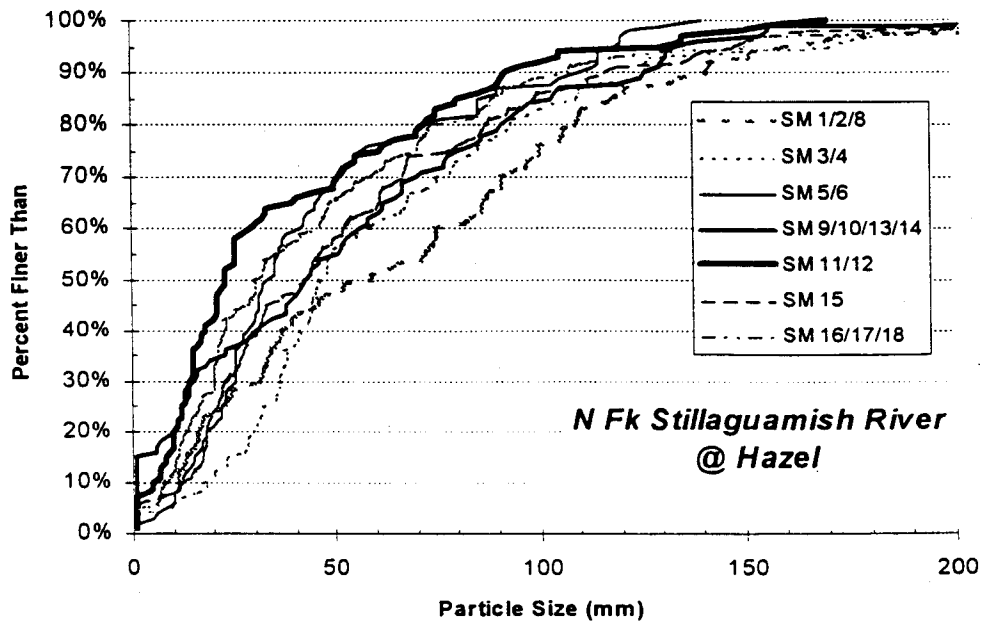
Figure E-2. Pebble count grain size distributions for the North Fork Stillaguamish River at Hazel and Raging River sites.
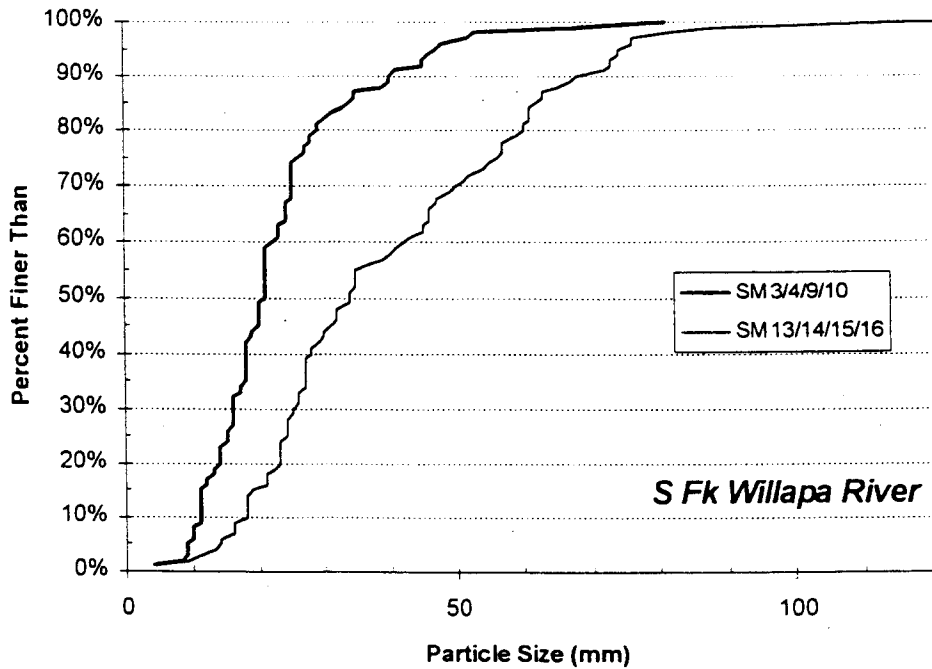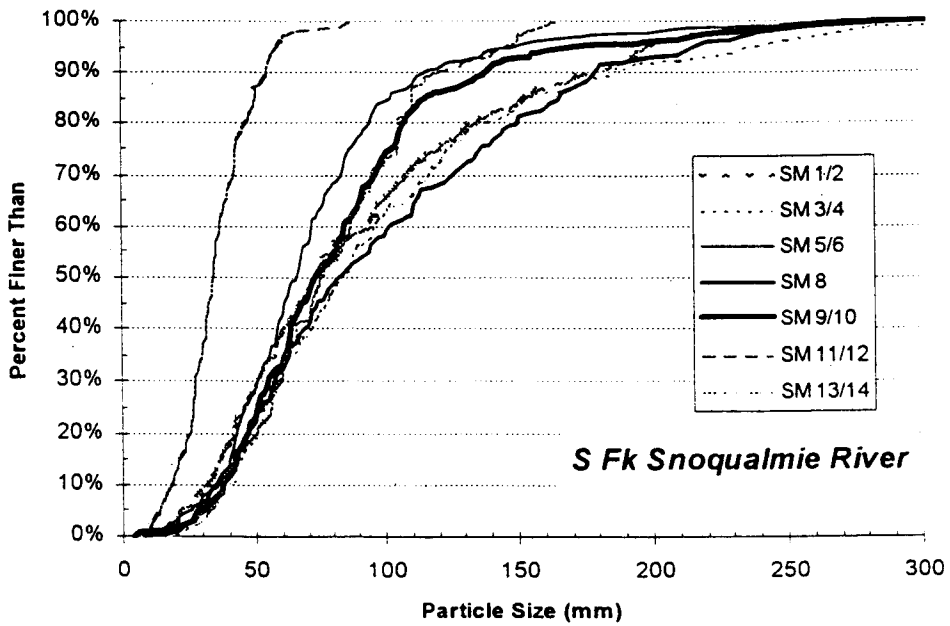
Figure E-3. Pebble count grain size distributions for the South Fork Snoqualmie
River and South Fork Willapa River sites.
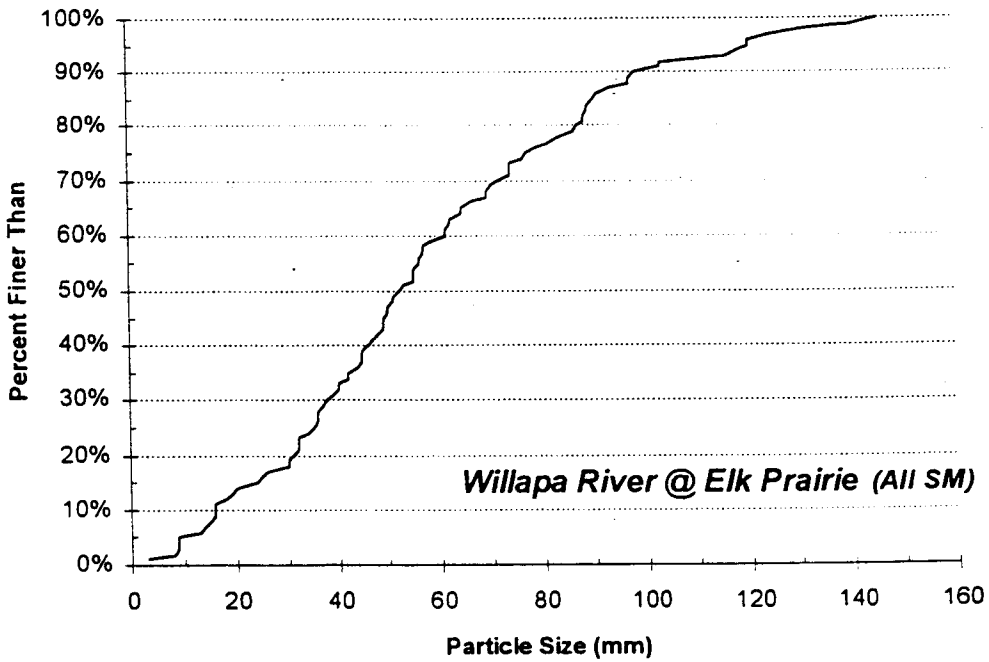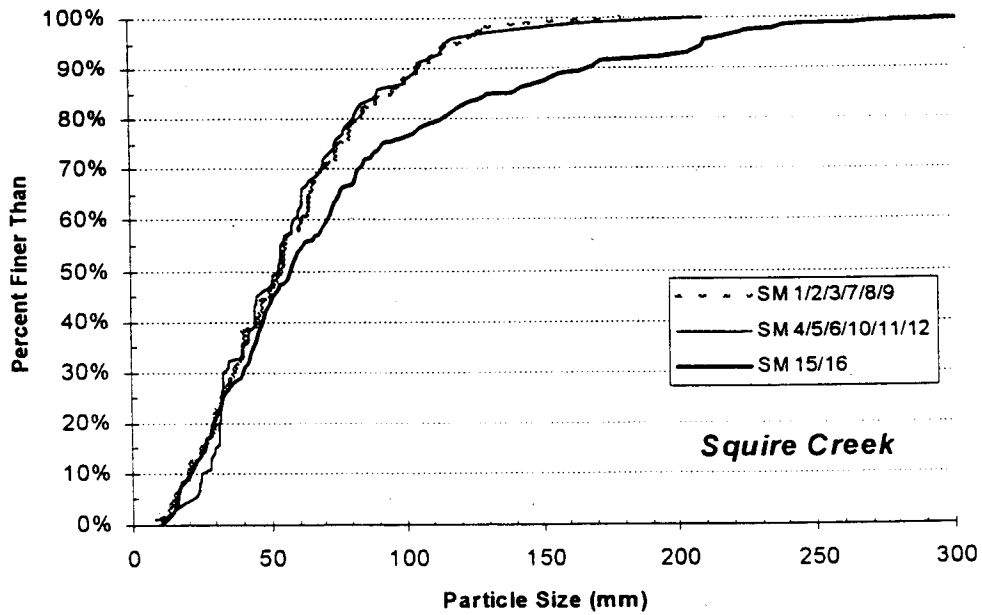
Figure E-4. Pebble count grain size distributions for the Squire Creek and
Willapa River at Elk Prairie sites.
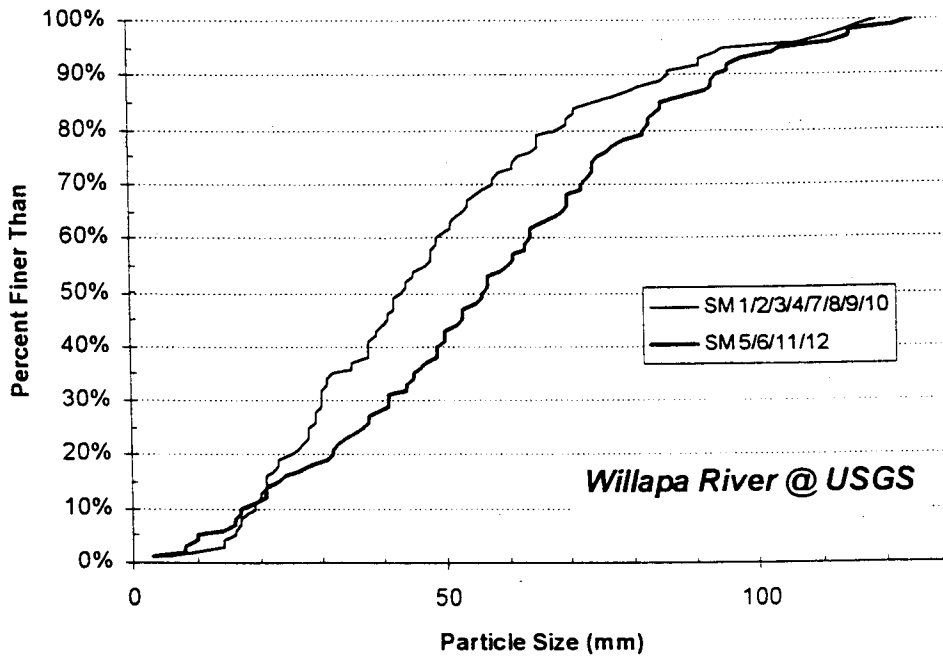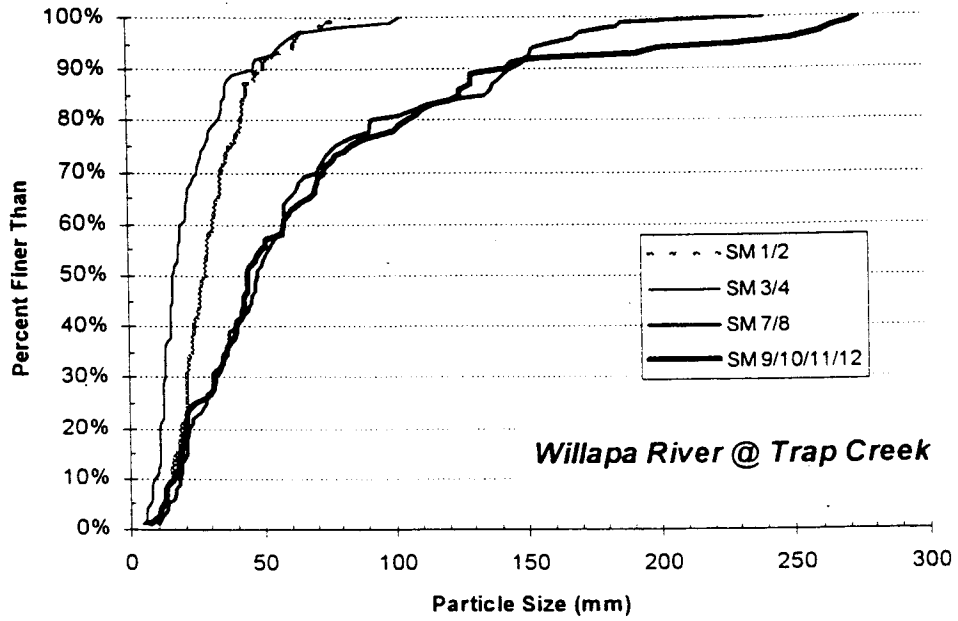
Figure E-5. Pebble count grain size distributions for the Willapa River at Trap Creek and USGS sites.

MCNEIL (BULK) GRAVEL SAMPLES:
RAW DATA AND
SELECTED GRAIN SIZE DISTRIBUTION QUANTILES

Layers are defined in the order excavated, from top (L1 = surface) to bottom (lowest elevation subsurface layer). Quantiles are presented first for the entire, untruncated distribution, followed by the distribution truncated at 8 mm.

Table F-1.   Issaquah Creek McNeil Data — Mass (kg) Retained by Sieve Size

Sieve Size (mm)	Scour Monitor 2				Scour Monitor 5			
	Surface (1)	SubSurf (2)	SubSurf (3)	SubSurf (4)	Surface (1)	SubSurf (2)	SubSurf (3)	SubSurf (4)
181.0	0.0000	0.0000	0.0000	0.0000	0.0000	0.0000	0.0000	0.0000
128.0	0.0000	0.0000	0.0000	0.0000	0.0000	0.0000	0.0000	0.0000
88.9	0.0000	0.0000	0.0000	0.0000	1.2231	0.0000	0.0000	0.0000
63.5	0.8001	2.0228	0.5804	0.0000	0.5110	2.2943	0.0000	0.3744
44.5	2.7429	0.5716	0.3547	0.4630	1.5996	0.9344	0.8611	0.5790
31.8	0.9263	1.0500	0.9949	1.1864	1.0746	0.8784	0.8640	0.7763
22.2	0.6430	0.7359	0.4141	1.1964	0.9303	0.7565	1.1025	0.6587
15.9	0.5172	0.6298	0.3937	0.5678	0.4538	0.8143	0.8392	0.4248
11.1	0.4501	0.5536	0.5141	0.6813	0.3601	0.7735	0.6228	0.4427
7.9	0.2610	0.4401	0.4327	0.5616	0.1829	0.6393	0.4605	0.2920
4	0.3009	0.6370	0.6265	0.9259	0.1316	0.9896	0.6664	0.5966
2	0.1197	0.4695	0.4703	0.8785	0.0464	0.6554	0.4733	0.5547
<2	0.1000	0.8132	0.9424	1.7129	0.0448	1.1100	1.0262	1.0789

Sieve Size (mm)	Scour Monitor 7				Scour Monitor 9		
	Surface (1)	SubSurf (2)	SubSurf (3)	SubSurf (4)	Surface (1)	SubSurf (2)	SubSurf (3)
181.0	0.0000	0.0000	0.0000	0.0000	0.0000	0.0000	0.0000
128.0	0.0000	0.0000	0.0000	0.0000	0.0000	0.0000	0.0000
88.9	0.0000	0.0000	1.0948	0.0000	0.0000	1.1793	0.0000
63.5	1.3752	0.0000	0.0000	0.6421	0.8051	1.0580	1.4941
44.5	0.8254	0.9284	0.5982	1.9975	1.9270	0.9649	1.5314
31.8	1.8397	1.1902	1.0566	0.9342	2.5754	0.3660	0.7273
22.2	0.5828	0.7521	0.6778	0.9411	0.7072	1.3000	0.6241
15.9	0.4852	0.8083	0.8745	0.9560	0.4135	1.0040	0.8398
11.1	0.2389	0.6085	0.8569	0.8978	0.3160	0.9995	0.7006
7.9	0.1229	0.5551	0.5697	0.5483	0.1648	0.4988	0.4286
4	0.0993	0.6486	0.6870	0.7253	0.1344	0.7141	0.6482
2	0.0572	0.6729	0.7558	0.7381	0.0675	0.4360	0.5050
<2	0.0147	0.6865	0.9747	1.0852	0.0982	0.7239	0.8502

Table F-2. North Fork Stillaguamish River at Hazel McNeil Data — Mass (kg) Retained by Sieve Size

Sieve Size (mm)	Scour Monitor 6			Scour Monitor 9			Scour Monitor 11		
	Surface (1)	SubSurf (2)	SubSurf (3)	Surface (1)	SubSurf (2)	SubSurf (3)	Surface (1)	SubSurf (2)	SubSurf (3)
181.0	0.0000	0.0000	0.0000	0.0000	0.0000	21.4030	0.0000	0.0000	0.0000
128.0	0.0000	0.0000	5.4856	0.0000	3.7910	0.0000	0.0000	0.0000	0.0000
88.9	4.7552	0.0000	0.0000	0.0000	2.3346	0.0000	3.2207	0.0000	0.0000
63.5	0.5438	3.5950	2.5177	1.5613	0.7253	2.8432	0.4727	0.0000	0.5563
44.5	1.5102	1.3177	1.1787	2.6458	1.9645	0.8338	1.1800	1.7645	0.0000
31.8	1.7627	0.5709	1.9153	1.0191	1.8979	0.7749	1.8785	0.4580	1.0439
22.2	1.3707	1.2508	0.9993	0.5254	1.7555	0.5524	0.9735	0.5731	1.6091
15.9	0.8408	1.0633	0.7822	0.3556	1.5737	0.6756	0.6218	0.3549	1.2855
11.1	0.7980	0.8992	0.7890	0.3383	2.0243	0.5094	0.4500	0.3816	1.0478
7.9	0.6436	0.7717	0.6861	0.1624	1.3978	0.4889	0.4899	0.3126	0.7096
4	0.8884	1.2136	1.0901	0.2214	1.7986	0.8385	0.6723	0.5776	1.0478
2	0.6602	0.9432	0.7485	0.0856	1.2113	0.6314	0.6104	0.5108	0.7620
<2	0.7943	2.2638	1.8486	0.0475	1.4138	0.7694	1.0217	0.9894	1.2086

Sieve Size (mm)	Scour Monitor 15			Scour Monitor 16		
	Surface (1)	SubSurf (2)	SubSurf (3)	Surface (1)	SubSurf (2)	SubSurf (3)
181.0	0.0000	0.0000	0.0000	0.0000	0.0000	0.0000
128.0	0.0000	0.0000	0.0000	8.4511	9.1640	0.0000
88.9	4.5810	0.0000	0.0000	4.4028	3.8620	3.6632
63.5	0.7209	1.0862	1.5303	1.6388	0.5512	1.9586
44.5	1.6176	0.9986	1.1268	3.5306	2.2611	0.1975
31.8	1.7303	1.5511	1.1094	2.9720	2.0038	0.7777
22.2	0.4874	0.9750	0.8476	1.9468	1.8275	1.0534
15.9	0.5207	0.9059	0.5486	1.2194	1.7630	0.9446
11.1	0.4135	0.8846	0.7181	1.2029	1.8154	1.1031
7.9	0.2698	0.6884	0.5942	0.7688	1.3619	0.7479
4	0.3707	1.1629	1.0416	0.9753	2.2057	1.2528
2	0.2367	0.8626	0.7977	0.5366	1.4313	0.9355
<2	0.4813	1.8952	2.3003	0.8759	2.3633	1.9890

Table F-3. North Fork Stillaguamish River at USGS McNeil Data — Mass (kg) Retained by Sieve Size

Sieve Size (mm)	Scour Monitor 2		Scour Monitor 7		Scour Monitor 9		Scour Monitor 11	
	Surface (1)	SubSurf (2)	Surface (1)	SubSurf (2)	Surface (1)	SubSurf (2)	Surface (1)	SubSurf (2)
181.0	0.0000	0.0000	0.0000	0.0000	0.0000	0.0000	0.0000	0.0000
128.0	4.4600	4.0580	0.0000	5.3608	3.5181	3.7910	4.7201	2.8083
88.9	4.9377	2.5335	3.7613	1.7636	0.0000	2.3346	0.0000	1.6211
63.5	2.1742	0.6374	2.8492	1.4014	2.3367	0.7253	0.0000	0.0000
44.5	1.6322	0.4036	2.3658	1.2918	2.1089	1.9645	2.4103	0.9869
31.8	0.7462	1.3471	1.1732	1.5094	2.1402	1.8979	1.2241	0.9791
22.2	0.3730	1.3296	0.9577	1.5566	1.2399	1.7555	0.6145	0.7396
15.9	0.3050	1.0330	1.1795	1.2883	0.9723	1.5737	0.5355	0.7751
11.1	0.1308	0.9058	0.7305	1.5667	0.8604	2.0243	0.3124	0.6228
7.9	0.0703	0.6005	0.4268	1.1286	0.5513	1.3978	0.2436	0.4192
4	0.0757	0.8363	0.6183	1.8016	0.7402	1.7986	0.3399	0.7755
2	0.0277	0.5741	0.4577	1.3668	0.4623	1.2113	0.1784	0.6623
<2	0.0489	0.8112	0.7450	1.3601	0.5190	1.4138	0.2768	1.2620

Table F-4.   Raging River McNeil Data — Mass (kg) Retained by Sieve Size

Sieve Size (mm)	Scour Monitor 1				Scour Monitor 2			Scour Monitor 5	
	Surface (1)	SubSurf (2)	SubSurf (3)	SubSurf (4)	Surface (1)	SubSurf (2)	SubSurf (3)	Surface (1)	SubSurf (2)
181.0	0.0000	0.0000	0.0000	0.0000	22.6570	0.0000	0.0000	0.0000	0.0000
128.0	4.0967	0.0000	7.5640	0.0000	9.8820	0.0000	0.0000	0.0000	6.1173
88.9	0.0000	1.1565	0.0000	3.6908	0.0000	0.0000	0.0000	2.6190	2.7244
63.5	0.8280	2.8071	2.0399	0.8890	0.0000	0.5453	0.0000	1.4420	0.4650
44.5	2.7172	0.4883	0.7279	0.5096	0.8884	1.3859	0.8030	1.4888	1.7940
31.8	1.0095	0.5895	0.6324	1.5745	1.1150	0.6088	0.9811	0.6262	0.3969
22.2	0.7517	0.4148	0.7939	1.4634	1.0414	0.8904	0.9022	0.3873	1.2258
15.9	0.2093	0.5449	1.1498	1.3565	0.5884	0.4971	0.7655	0.1854	1.0900
11.1	0.0647	0.5441	1.0338	1.5613	0.3472	0.6311	0.9394	0.2197	1.3750
7.9	0.0045	0.2342	0.9294	1.3711	0.2081	0.4696	0.7796	0.1976	1.2020
4	0.0000	0.2126	1.3500	1.9802	0.1639	0.7137	1.2547	0.3041	2.1789
2	0.0000	0.0775	0.5398	1.3004	0.0625	0.4374	0.9458	0.2534	1.7958
<2	0.0000	0.0470	1.2990	1.7148	0.0472	0.5411	1.3934	0.1742	2.5725

Sieve Size (mm)	Scour Monitor 4			Scour Monitor 7		Scour Monitor 10		Scour Monitor 11	
	Surface (1)	SubSurf (2)	SubSurf (3)	Surface (1)	SubSurf (2)	Surface (1)	SubSurf (2)	Surface (1)	SubSurf (2)
181.0	21.3930	0.0000	20.1850	28.4910	0.0000	0.0000	0.0000	0.0000	0.0000
128.0	18.8742	7.1840	0.0000	8.0730	0.0000	0.0000	0.0000	6.5480	0.0000
88.9	0.0000	2.5179	0.0000	7.2172	0.0000	5.0876	6.9530	5.7553	0.0000
63.5	2.7505	0.7778	0.9049	7.7922	0.8990	1.0310	0.8770	2.0177	1.4041
44.5	1.9935	2.7326	0.0000	2.3607	0.7411	2.3114	2.4369	2.0145	2.5031
31.8	1.4635	2.3135	0.8328	4.3828	0.8194	1.9051	0.8920	1.9509	1.1212
22.2	1.7209	1.8531	1.5031	3.3245	1.0103	1.7981	0.8317	1.3586	1.5386
15.9	1.5691	1.7289	1.2744	2.5169	0.8822	1.8939	0.9218	0.9918	1.0221
11.1	1.2348	1.8772	1.3615	2.2122	1.1151	1.4068	0.7856	0.7628	0.8546
7.9	1.0482	1.5172	1.0424	1.5846	0.8009	1.1416	0.8142	0.6122	0.5769
4	1.2104	2.4957	2.1755	2.3651	1.5170	2.0410	1.5701	0.9300	0.9823
2	0.8413	2.0974	2.1384	1.4194	1.1864	1.9024	1.4239	0.7045	0.6727
<2	0.9410	2.9485	3.9554	1.7403	1.9601	2.0983	2.1346	0.9268	1.0398

Table F-5. South Fork Snoqualmie River McNeil Data — Mass (kg) Retained by Sieve Size

Sieve Size (mm)	Scour Monitor 2 Surface (1)	Scour Monitor 2 SubSurf (2)	Scour Monitor 4 Surface (1)	Scour Monitor 4 SubSurf (2)	Scour Monitor 6 Surface (1)	Scour Monitor 6 SubSurf (2)	Scour Monitor 8 Surface (1)	Scour Monitor 8 SubSurf (2)
181.0	0.0000	0.0000	0.0000	0.0000	0.0000	0.0000	0.0000	0.0000
128.0	0.0000	0.0000	0.0000	16.3650	0.0000	2.4049	0.0000	0.0000
88.9	3.0366	1.2153	8.3050	2.9588	2.1549	1.5021	0.0000	0.0000
63.5	0.4054	0.7364	0.0000	0.0000	1.0620	1.4896	2.9127	1.3553
44.5	2.5156	0.7730	1.1762	1.9117	1.8590	0.1934	1.9556	0.9537
31.8	0.8862	1.6801	0.4580	1.6928	0.5684	1.5023	1.4581	0.5756
22.2	0.7900	1.3289	0.8478	1.0506	0.7980	0.9622	0.9540	0.6315
15.9	0.3766	0.9047	0.3552	1.1435	0.4054	1.0247	0.7197	0.7890
11.1	0.2245	0.6839	0.2425	0.9970	0.4082	0.8413	0.6714	0.7034
7.9	0.1560	0.5062	0.1166	0.7649	0.2774	0.6617	0.3347	0.4930
4	0.2211	0.9737	0.1477	1.5029	0.3616	1.0533	0.3897	0.8779
2	0.1263	1.0176	0.0688	1.2749	0.2665	0.8834	0.2867	0.7765
<2	0.1750	1.7244	0.0399	1.0755	0.3921	1.4724	0.3754	0.8158

Sieve Size (mm)	Scour Monitor 9 Surface (1)	Scour Monitor 9 SubSurf (2)	Scour Monitor 11 Surface (1)	Scour Monitor 11 SubSurf (2)	Scour Monitor 11 SubSurf (3)
181.0	11.2870	0.0000	0.0000	0.0000	0.0000
128.0	0.0000	0.0000	0.0000	0.0000	0.0000
88.9	6.1322	4.3446	0.0000	0.0000	0.0000
63.5	4.2610	3.2986	0.4632	0.6656	0.9714
44.5	2.5542	2.0095	0.9146	1.5581	0.3246
31.8	2.4957	1.5644	1.5005	1.1689	0.4047
22.2	2.0355	1.7436	1.1579	1.1530	1.0155
15.9	1.4172	1.4047	0.6065	0.7039	0.4508
11.1	1.1075	1.2888	0.3406	0.5495	0.4133
7.9	0.7906	0.8436	0.2412	0.4118	0.3133
4	1.1239	1.3881	0.3479	0.7535	0.6200
2	0.9142	1.2411	0.2467	· 0.6859	0.6209
<2	1.2827	2.0143	0.3479	1.1265	1.0106

Table F-6. South Fork Willapa River McNeil Data — Mass (kg) Retained by Sieve Size

Sieve Size (mm)	Scour Monitor 3	Scour Monitor 9	Scour Monitor 11
181.0	0.0000	0.0000	0.0000
128.0	0.0000	0.0000	0.0000
88.9	0.0000	0.0000	0.0000
63.5	0.0000	0.0000	0.0000
44.5	1.3738	0.1385	0.0000
31.8	1.6441	0.7660	0.3807
22.2	0.7925	1.4221	0.9976
15.9	0.7331	1.0372	1.3799
11.1	0.4361	0.9092	1.2321
7.9	0.2344	0.4769	0.9094
4	0.1981	0.4572	1.3940
2	0.0072	0.1803	0.8166
<2	0.0635	0.2193	1.6933

Table F-7. Squire Creek McNeil Data — Mass (kg) Retained by Sieve Size

Sieve Size (mm)	Scour Monitor 2			Scour Monitor 4				Scour Monitor 5	
	Surface (1)	SubSurf (2)	SubSurf (3)	Surface (1)	SubSurf (2)	SubSurf (3)	SubSurf (4)	Surface (1)	SubSurf (2)
181.0	0.0000	0.0000	0.0000	0.0000	0.0000	0.0000	0.0000	0.0000	0.0000
128.0	0.0000	0.0000	0.0000	0.0000	0.0000	0.0000	4.4679	0.0000	0.0000
88.9	1.1692	0.0000	0.0000	0.0000	0.0000	0.0000	1.3440	5.6265	2.8122
63.5	1.7423	0.6787	0.0000	0.8441	0.5979	1.2991	0.0000	0.9470	1.0940
44.5	1.3953	0.6991	0.7139	2.4909	0.1579	0.9790	0.0000	2.3101	1.6415
31.8	1.7247	0.9736	1.8887	1.3847	0.6619	0.5692	0.6806	1.1616	2.0232
22.2	1.2027	0.4349	1.3030	0.8624	0.8282	0.2407	0.2870	1.0321	2.0928
15.9	0.6926	0.6907	0.8669	0.4787	0.6476	0.2340	0.5049	0.5369	1.2502
11.1	0.5047	0.3476	0.8748	0.3339	0.7276	0.3719	0.4291	0.2936	1.1400
7.9	0.2813	0.1857	0.5807	0.1982	0.5585	0.1492	0.3008	0.1498	0.7233
4	0.3173	0.2860	0.9930	0.1818	0.7686	0.2305	0.5573	0.1275	0.9661
2	0.1986	0.1591	0.6756	0.0853	0.6090	0.1799	0.5080	0.0370	0.6823
<2	0.3078	0.2772	1.6588	0.1378	1.7700	0.5681	1.3798	0.0276	1.4110

Sieve Size (mm)	Scour Monitor 8			Scour Monitor 10			Scour Monitor 12	
	Surface (1)	SubSurf (2)	SubSurf (3)	Surface (1)	SubSurf (2)	SubSurf (3)	Surface (1)	SubSurf (2)
181.0	0.0000	0.0000	0.0000	0.0000	0.0000	0.0000	0.0000	0.0000
128.0	7.3050	0.0000	0.0000	0.0000	5.1219	0.0000	0.0000	0.0000
88.9	3.5644	0.0000	0.0000	1.5391	0.0000	2.8419	0.0000	0.0000
63.5	2.6819	0.0000	1.1372	0.0000	1.6772	0.7164	7.3080	1.3765
44.5	1.0244	0.7415	0.8607	3.2870	0.8114	0.7066	3.3005	1.5786
31.8	0.9562	0.5729	0.7064	2.6402	0.9707	0.5927	1.9218	0.7824
22.2	0.6778	0.8958	0.9133	0.9712	0.9300	0.4589	1.5136	0.6467
15.9	0.4786	0.8340	0.7634	0.8719	0.8577	0.3619	0.9653	0.7759
11.1	0.2933	0.7149	0.7004	0.4021	0.9681	0.5077	0.7635	0.5958
7.9	0.1940	0.5566	0.6382	0.1965	0.7157	0.5354	0.4386	0.4664
4	0.2148	0.8160	1.0205	0.1814	1.1546	0.9289	0.6125	0.7470
2	0.1050	0.5835	0.8318	0.0797	0.9293	0.8247	0.3740	0.5198
<2	0.1273	0.7899	1.3231	0.1463	2.3306	1.7801	0.6025	0.7600

Table F-8. Willapa River at Elk Prairie McNeil Data — Mass (kg) Retained by Sieve Size

Sieve Size (mm)	Scour Monitor 6		Scour Monitor 7	
	Surface (1)	SubSurf (2)	Surface (1)	SubSurf (2)
181.0	0.0000	0.0000	0.0000	0.0000
128.0	0.0000	0.0000	0.0000	0.0000
88.9	0.0000	0.0000	1.9912	0.0000
63.5	0.0000	0.0000	1.7397	0.0000
44.5	1.9600	1.4320	0.6557	1.1519
31.8	0.7313	0.6422	1.0320	0.7798
22.2	0.4211	0.7169	0.4469	1.0228
15.9	0.3560	0.3880	0.2862	0.5037
11.1	0.2329	0.3095	0.1126	0.5056
7.9	0.0978	0.3593	0.0573	0.3860
4	0.1115	0.5903	0.0500	0.5228
2	0.0589	0.3833	0.0170	0.4071
<2	0.0923	0.7845	0.0224	1.1787

Table F-9. Willapa River at Trap Creek McNeil Data — Mass (kg) Retained by Sieve Size

Sieve Size (mm)	Scour Monitor 2			Scour Monitor 3			Scour Monitor 7	
	Surface (1)	SubSurf (2)	SubSurf (3)	Surface (1)	SubSurf (2)	SubSurf (3)	Surface (1)	SubSurf (2)
181.0	0.0000	0.0000	0.0000	0.0000	0.0000	0.0000	0.0000	0.0000
128.0	0.0000	0.0000	0.0000	0.0000	0.0000	0.0000	0.0000	0.0000
88.9	0.0000	0.0000	0.0000	0.0000	0.0000	0.0000	0.0000	0.0000
63.5	0.7705	0.0000	1.9477	0.0000	0.8589	1.6939	0.0000	0.4519
44.5	1.0629	0.3173	1.3918	0.3333	0.2708	0.5666	1.1915	0.8250
31.8	0.6900	0.9302	0.9764	0.7754	0.2209	0.2824	0.9837	0.8342
22.2	0.6002	0.8010	0.8436	0.5891	0.3418	0.3741	0.7904	0.8258
15.9	0.4299	0.5885	0.4756	0.6122	0.3747	0.3908	0.4319	0.8645
11.1	0.2835	0.3559	0.3516	0.5195	0.3222	0.3832	0.2376	0.7045
7.9	0.1255	0.2286	0.2041	0.3065	0.2832	0.2872	0.1051	0.6007
4	0.0433	0.1496	0.1905	0.3687	0.4476	0.5337	0.1688	0.9902
2	0.0021	0.0266	0.0859	0.2371	0.4182	0.4861	0.1053	0.6313
<2	0.0027	0.1321	0.5463	0.3592	0.8926	1.1379	0.1195	1.0567

Table F-10. Willapa River at USGS McNeil Data — Mass (kg) Retained by Sieve Size

Sieve Size (mm)	Scour Monitor 2			Scour Monitor 3		Scour Monitor 5	
	Surface (1)	SubSurf (2)	SubSurf (3)	Surface (1)	SubSurf (2)	Surface (1)	SubSurf (2)
181.0	0.0000	0.0000	0.0000	0.0000	0.0000	0.0000	0.0000
128.0	0.0000	0.0000	0.0000	0.0000	0.0000	0.0000	0.0000
88.9	0.0000	0.0000	0.0000	2.2473	0.0000	0.0000	1.6414
63.5	0.6872	0.0000	0.6617	0.0000	0.0000	1.6477	0.4547
44.5	0.3346	0.4785	0.7591	0.3956	0.5427	1.9046	1.4484
31.8	0.7075	0.5266	0.2896	0.6848	1.1197	0.5819	0.3583
22.2	0.7468	0.7949	0.3868	0.2807	1.0706	0.2563	0.2224
15.9	0.4787	0.6729	0.3184	0.2333	0.6523	0.2460	0.1548
11.1	0.3032	0.5355	0.2950	0.2072	0.5537	0.2874	0.2370
7.9	0.0568	0.2872	0.2754	0.1345	0.4399	0.2093	0.2205
4	0.0241	0.2387	0.3280	0.1989	0.7985	0.2577	0.4027
2	0.0017	0.0805	0.1567	0.1270	0.5502	0.1199	0.2371
<2	0.0014	0.1371	0.3231	0.1065	0.5222	0.0939	0.2465

Sieve Size (mm)	Scour Monitor 10		Scour Monitor 11	
	Surface (1)	SubSurf (2)	Surface (1)	SubSurf (2)
181.0	0.0000	0.0000	0.0000	0.0000
128.0	0.0000	0.0000	0.0000	0.0000
88.9	0.0000	0.0000	0.0000	0.0000
63.5	1.4246	1.4626	0.9585	1.8373
44.5	0.1195	1.1517	1.7950	0.1595
31.8	0.6556	0.6442	0.3291	0.1163
22.2	0.6008	0.7040	0.5343	0.2536
15.9	0.3831	0.4625	0.3569	0.2262
11.1	0.1365	0.5374	0.2984	0.3229
7.9	0.1300	0.4692	0.2184	0.3792
4	0.0839	0.7081	0.3267	0.6854
2	0.0175	0.3271	0.1546	0.4037
<2	0.0427	0.6987	0.1360	0.6104

ENTIRE MCNEIL SAMPLE

Site: ISSAQUAH CREEK

Scour Monitor # 2

	Total	Surf	SubSurf	Surf+L2	L2	L3	L4
D50.	23.	45.	17.	36.	27.	15.	11.
D75.	46.	58.	39.	58.	64.	38.	28.
D84.	58.	62.	51.	67.	73.	45.	35.
D90.	67.	67.	67.	75.	79.	64.	40.
D95.	78.	77.	78.	82.	84.	76.	46.

Scour Monitor # 5

	Total	Surf	SubSurf	Surf+L2	L2	L3	L4
D50.	24.	45.	18.	34.	22.	17.	15.
D75.	49.	68.	41.	63.	60.	32.	36.
D84.	62.	94.	55.	76.	71.	41.	45.
D90.	75.	106.	67.	85.	78.	48.	56.
D95.	87.	116.	78.	100.	83.	55.	69.

Scour Monitor # 7

	Total	Surf	SubSurf	Surf+L2	L2	L3	L4
D50.	23.	41.	19.	31.	18.	17.	21.
D75.	44.	63.	41.	45.	36.	40.	47.
D84.	56.	72.	51.	56.	43.	56.	55.
D90.	65.	78.	59.	66.	49.	98.	60.
D95.	83.	84.	83.	77.	56.	112.	70.

Scour Monitor # 9

	Total	Surf	SubSurf	Surf+L2	L2	L3	L4
D50.	33.	41.	24.	35.	24.	25.	
D75.	56.	54.	58.	56.	62.	56.	
D84.	67.	60.	72.	69.	81.	66.	
D90.	79.	66.	83.	82.	96.	74.	
D95.	88.	77.	98.	99.	111.	81.	

Scour Monitor # 5+9

	Total	Surf	SubSurf	Surf+L2	L2	L3	L4
D50.	28.	42.	21.	34.	23.	21.	15.
D75.	53.	59.	49.	59.	61.	45.	36.
D84.	65.	69.	63.	73.	74.	56.	45.
D90.	77.	86.	75.	84.	83.	63.	56.
D95.	88.	104.	85.	100.	95.	75.	69.

ENTIRE MCNEIL SAMPLE

Site: N FK STILLI HAZEL

Scour Monitor # 6

	Total	Surf	SubSurf	Surf+L2	L2	L3	L4
D50.	37.	41.	35.	31.	21.	47.	
D75.	83.	98.	78.	74.	64.	136.	
D84.	110.	109.	130.	90.	73.	152.	
D90.	134.	115.	148.	103.	79.	163.	
D95.	156.	121.	164.	115.	84.	171.	

Scour Monitor # 9

	Total	Surf	SubSurf	Surf+L2	L2	L3	L4
D50.	78.	50.	111.	38.	30.	209.	
D75.	204.	62.	211.	76.	99.	234.	
D84.	222.	71.	227.	112.	131.	242.	
D90.	234.	77.	237.	139.	148.	247.	
D95.	244.	83.	246.	159.	164.	250.	

Scour Monitor # 11

	Total	Surf	SubSurf	Surf+L2	L2	L3	L4
D50.	23.	38.	16.	33.	19.	15.	
D75.	47.	93.	32.	59.	48.	27.	
D84.	63.	105.	43.	94.	53.	33.	
D90.	95.	113.	53.	106.	57.	40.	
D95.	110.	120.	61.	116.	60.	67.	

Scour Monitor # 15

	Total	Surf	SubSurf	Surf+L2	L2	L3	L4
D50.	30.	59.	15.	36.	16.	15.	
D75.	62.	104.	41.	74.	39.	45.	
D84.	83.	112.	55.	97.	50.	60.	
D90.	99.	118.	68.	108.	63.	71.	
D95.	112.	123.	78.	117.	75.	80.	

Scour Monitor # 16

	Total	Surf	SubSurf	Surf+L2	L2	L3	L4
D50.	53.	67.	40.	58.	49.	25.	
D75.	124.	135.	116.	136.	136.	89.	
D84.	144.	151.	138.	152.	152.	102.	
D90.	157.	162.	153.	162.	162.	111.	
D95.	169.	171.	166.	171.	171.	119.	

Scour Monitor # 11+16

	Total	Surf	SubSurf	Surf+L2	L2	L3	L4
D50.	40.	56.	28.	49.	41.	19.	
D75.	107.	119.	96.	122.	127.	65.	
D84.	131.	139.	124.	143.	146.	87.	
D90.	149.	154.	144.	156.	158.	101.	
D95.	164.	167.	161.	168.	169.	114.	

ENTIRE MCNEIL SAMPLE

Site: N FK STILLI USGS

Scour Monitor # 2

	Total	Surf	SubSurf	Surf+L2	L2	L3	L4
D50.	94.	105.	49.				
D75.	133.	136.	131.				
D84.	150.	152.	148.				
D90.	161.	162.	160.				
D95.	171.	171.	170.				

Scour Monitor # 7

	Total	Surf	SubSurf	Surf+L2	L2	L3	L4
D50.	47.	55.	37.				
D75.	100.	88.	127.				
D84.	123.	102.	146.				
D90.	143.	111.	158.				
D95.	161.	119.	169.				

Scour Monitor # 9

	Total	Surf	SubSurf	Surf+L2	L2	L3	L4
D50.	38.	47.	30.				
D75.	93.	85.	99.				
D84.	136.	142.	131.				
D90.	152.	156.	148.				
D95.	166.	168.	164.				

Scour Monitor # 11

	Total	Surf	SubSurf	Surf+L2	L2	L3	L4
D50.	52.	58.	39.				
D75.	141.	151.	124.				
D84.	155.	162.	144.				
D90.	164.	169.	158.				
D95.	172.	174.	169.				

Scour Monitor # 2+7

	Total	Surf	SubSurf	Surf+L2	L2	L3	L4
D50.	65.	79.	41.				
D75.	119.	114.	129.				
D84.	139.	125.	147.				
D90.	154.	143.	159.				
D95.	167.	161.	170.				

ENTIRE MCNEIL SAMPLE

Site: RAGING RIVER

Scour Monitor # 1

	Total	Surf	SubSurf	Surf+L2	L2	L3	L4
D50.	50.	66.	38.	67.	68.	70.	19.
D75.	115.	150.	102.	123.	84.	150.	69.
D84.	141.	161.	132.	145.	89.	161.	98.
D90.	156.	168.	149.	158.	103.	168.	108.
D95.	168.	174.	164.	169.	115.	174.	118.

Scour Monitor # 2

	Total	Surf	SubSurf	Surf+L2	L2	L3	L4
D50.	161.	197.	15.	183.	23.	11.	
D75.	213.	229.	35.	222.	48.	27.	
D84.	228.	238.	47.	234.	56.	36.	
D90.	238.	244.	54.	242.	62.	43.	
D95.	246.	249.	61.	248.	72.	53.	

Scour Monitor # 4

	Total	Surf	SubSurf	Surf+L2	L2	L3	L4
D50.	142.	165.	55.	138.	34.	192.	
D75.	201.	208.	194.	180.	122.	226.	
D84.	220.	225.	216.	206.	144.	237.	
D90.	233.	236.	230.	224.	157.	243.	
D95.	244.	245.	242.	239.	169.	249.	

Scour Monitor # 5

	Total	Surf	SubSurf	Surf+L2	L2	L3	L4
D50.	51.	65.	33.				
D75.	115.	98.	130.				
D84.	137.	109.	148.				
D90.	152.	116.	160.				
D95.	166.	121.	170.				

Scour Monitor # 7

	Total	Surf	SubSurf	Surf+L2	L2	L3	L4
D50.	97.	126.	11.				
D75.	200.	208.	29.				
D84.	220.	225.	43.				
D90.	233.	236.	58.				
D95.	243.	245.	73.				

Scour Monitor # 10

	Total	Surf	SubSurf	Surf+L2	L2	L3	L4
D50.	33.	26.	48.				
D75.	94.	74.	100.				
D84.	106.	99.	110.				
D90.	114.	110.	117.				
D95.	120.	118.	122.				

ENTIRE MCNEIL SAMPLE

Site: RAGING RIVER

Scour Monitor # 11

	Total	Surf	SubSurf	Surf+L2	L2	L3	L4
D50.	53.	89.	27.				
D75.	110.	130.	52.				
D84.	133.	148.	60.				
D90.	150.	160.	67.				
D95.	165.	170.	78.				

Scour Monitor # 1+2+7

	Total	Surf	SubSurf	Surf+L2	L2	L3	L4
D50.	86.	159.	23.	129.	22.	28.	19.
D75.	186.	212.	71.	202.	57.	133.	69.
D84.	210.	228.	99.	221.	72.	150.	98.
D90.	226.	238.	131.	234.	81.	161.	108.
D95.	240.	246.	154.	244.	88.	171.	118.

Scour Monitor # 4+10

	Total	Surf	SubSurf	Surf+L2	L2	L3	L4
D50.	91.	131.	51.	80.	39.	192.	
D75.	182.	187.	171.	158.	105.	226.	
D84.	207.	211.	204.	183.	124.	237.	
D90.	225.	227.	222.	209.	142.	243.	
D95.	239.	240.	238.	231.	161.	249.	

Scour Monitor # 5+11

	Total	Surf	SubSurf	Surf+L2	L2	L3	L4
D50.	52.	79.	29.				
D75.	112.	120.	91.				
D84.	135.	137.	132.				
D90.	151.	153.	149.				
D95.	165.	166.	164.				

ENTIRE MCNEIL SAMPLE

Site: S FK SNOQUALMIE

Scour Monitor # 2
```
        Total   Surf   SubSurf Surf+L2   L2      L3      L4
--------------------------------------------------------------
D50.    37.     56.     22.
D75.    69.     99.     43.
D84.    97.     109.    67.
D90.    108.    116.    91.
D95.    117.    122.    108.
```

Scour Monitor # 4
```
        Total   Surf   SubSurf Surf+L2   L2      L3      L4
--------------------------------------------------------------
D50.    111.    104.    131.
D75.    146.    117.    158.
D84.    159.    121.    166.
D90.    167.    123.    172.
D95.    173.    125.    176.
```

Scour Monitor # 6
```
        Total   Surf   SubSurf Surf+L2   L2      L3      L4
--------------------------------------------------------------
D50.    41.     53.     33.
D75.    93.     89.     98.
D84.    114.    103.    130.
D90.    130.    112.    148.
D95.    154.    119.    164.
```

Scour Monitor # 8
```
        Total   Surf   SubSurf Surf+L2   L2      L3      L4
--------------------------------------------------------------
D50.    33.     43.     18.
D75.    62.     67.     50.
D84.    72.     75.     65.
D90.    78.     80.     73.
D95.    83.     85.     81.
```

Scour Monitor # 9
```
        Total   Surf   SubSurf Surf+L2   L2      L3      L4
--------------------------------------------------------------
D50.    67.     87.     37.
D75.    116.    196.    81.
D84.    194.    217.    97.
D90.    216.    231.    108.
D95.    235.    243.    117.
```

Scour Monitor # 11
```
        Total   Surf   SubSurf Surf+L2   L2      L3      L4
--------------------------------------------------------------
D50.    24.     30.     21.     27.     23.     17.
D75.    43.     43.     43.     44.     45.     37.
D84.    54.     52.     55.     53.     54.     63.
D90.    63.     60.     66.     61.     61.     72.
D95.    75.     71.     77.     71.     71.     80.
```

ENTIRE MCNEIL SAMPLE

Site: S FK SNOQUALMIE

Scour Monitor # 2+8

	Total	Surf	SubSurf	Surf+L2	L2	L3	L4
D50.	35.	50.	20.				
D75.	64.	76.	46.				
D84.	79.	89.	66.				
D90.	92.	102.	79.				
D95.	109.	114.	96.				

Scour Monitor # 4+9

	Total	Surf	SubSurf	Surf+L2	L2	L3	L4
D50.	88.	95.	71.				
D75.	136.	126.	138.				
D84.	164.	204.	153.				
D90.	188.	222.	163.				
D95.	219.	238.	172.				

ENTIRE MCNEIL SAMPLE

Site: S FK WILLAPA

Scour Monitor # 3

	Total	Surf	SubSurf	Surf+L2	L2	L3	L4
D50.	34.						
D75.	45.						
D84.	51.						
D90.	56.						
D95.	60.						

Scour Monitor # 9

	Total	Surf	SubSurf	Surf+L2	L2	L3	L4
D50.	19.						
D75.	28.						
D84.	32.						
D90.	37.						
D95.	42.						

Scour Monitor # 11

	Total	Surf	SubSurf	Surf+L2	L2	L3	L4
D50.	10.						
D75.	18.						
D84.	22.						
D90.	27.						
D95.	31.						

ENTIRE MCNEIL SAMPLE

Site: SQUIRE CREEK

Scour Monitor # 2

	Total	Surf	SubSurf	Surf+L2	L2	L3	L4
D50.	29.	41.	20.	38.	31.	16.	
D75.	47.	71.	38.	64.	49.	33.	
D84.	62.	83.	44.	77.	61.	39.	
D90.	75.	95.	53.	86.	71.	43.	
D95.	89.	110.	63.	103.	80.	50.	

Scour Monitor # 4

	Total	Surf	SubSurf	Surf+L2	L2	L3	L4
D50.	34.	43.	28.	26.	11.	41.	105.
D75.	74.	57.	93.	48.	27.	65.	150.
D84.	118.	62.	137.	57.	36.	74.	161.
D90.	144.	67.	152.	64.	47.	79.	169.
D95.	161.	78.	166.	76.	73.	84.	174.

Scour Monitor # 5

	Total	Surf	SubSurf	Surf+L2	L2	L3	L4
D50.	46.	75.	30.				
D75.	95.	107.	63.				
D84.	107.	115.	92.				
D90.	114.	119.	105.				
D95.	121.	123.	116.				

Scour Monitor # 8

	Total	Surf	SubSurf	Surf+L2	L2	L3	L4
D50.	50.	111.	15.	77.	14.	15.	
D75.	116.	149.	33.	136.	28.	40.	
D84.	141.	161.	47.	152.	37.	57.	
D90.	155.	168.	58.	163.	47.	69.	
D95.	168.	174.	71.	171.	55.	78.	

Scour Monitor # 10

	Total	Surf	SubSurf	Surf+L2	L2	L3	L4
D50.	39.	43.	32.	41.	36.	26.	
D75.	91.	58.	105.	88.	138.	93.	
D84.	119.	63.	135.	135.	153.	105.	
D90.	141.	101.	151.	151.	163.	113.	
D95.	160.	113.	165.	165.	172.	120.	

Scour Monitor # 12

	Total	Surf	SubSurf	Surf+L2	L2	L3	L4
D50.	47.	54.	26.				
D75.	70.	74.	55.				
D84.	77.	80.	64.				
D90.	81.	83.	73.				
D95.	85.	86.	81.				

ENTIRE MCNEIL SAMPLE

Site: SQUIRE CREEK

Scour Monitor # 2+8

	Total	Surf	SubSurf	Surf+L2	L2	L3	L4
D50.	36.	80.	17.	53.	20.	16.	
D75.	80.	131.	36.	108.	39.	35.	
D84.	111.	148.	45.	135.	48.	43.	
D90.	138.	160.	56.	151.	57.	54.	
D95.	158.	170.	68.	165.	67.	68.	

Scour Monitor # 4+10

	Total	Surf	SubSurf	Surf+L2	L2	L3	L4
D50.	37.	43.	30.	35.	22.	33.	105.
D75.	82.	57.	101.	62.	79.	77.	150.
D84.	119.	62.	136.	91.	140.	94.	161.
D90.	142.	82.	152.	137.	155.	106.	169.
D95.	160.	104.	166.	157.	167.	116.	174.

Scour Monitor # 5+12

	Total	Surf	SubSurf	Surf+L2	L2	L3	L4
D50.	46.	60.	29.				
D75.	77.	83.	59.				
D84.	88.	94.	78.				
D90.	102.	106.	94.				
D95.	114.	116.	110.				

ENTIRE MCNEIL SAMPLE

Site: TOLT RIVER

Scour Monitor # 7

	Total	Surf	SubSurf	Surf+L2	L2	L3	L4
D50.	10.	17.	7.				
D75.	22.	30.	19.				
D84.	28.	36.	25.				
D90.	33.	41.	29.				
D95.	40.	46.	35.				

ENTIRE MCNEIL SAMPLE

Site: WILLAPA @ ELK PRAIRIE

Scour Monitor # 6

	Total	Surf	SubSurf	Surf+L2	L2	L3	L4
D50.	31.	43.	22.				
D75.	50.	54.	45.				
D84.	55.	58.	51.				
D90.	58.	60.	56.				
D95.	61.	62.	60.				

Scour Monitor # 7

	Total	Surf	SubSurf	Surf+L2	L2	L3	L4
D50.	38.	72.	19.				
D75.	71.	96.	37.				
D84.	88.	107.	46.				
D90.	102.	115.	52.				
D95.	114.	121.	58.				

Scour Monitor # 6+7

	Total	Surf	SubSurf	Surf+L2	L2	L3	L4
D50.	35.	53.	20.				
D75.	56.	79.	40.				
D84.	65.	95.	49.				
D90.	85.	106.	54.				
D95.	104.	116.	59.				

ENTIRE MCNEIL SAMPLE

Site: WILLAPA @ TRAP CR

Scour Monitor # 2

	Total	Surf	SubSurf	Surf+L2	L2	L3	L4
D50.	36.	41.	34.	32.	26.	42.	
D75.	57.	59.	56.	48.	37.	66.	
D84.	67.	68.	67.	57.	41.	74.	
D90.	75.	75.	75.	64.	44.	80.	
D95.	82.	82.	82.	76.	52.	84.	

Scour Monitor # 3

	Total	Surf	SubSurf	Surf+L2	L2	L3	L4
D50.	17.	19.	17.	17.	14.	20.	
D75.	45.	33.	61.	36.	46.	66.	
D84.	65.	39.	72.	47.	68.	74.	
D90.	74.	43.	78.	64.	75.	80.	
D95.	81.	51.	84.	76.	82.	84.	

Scour Monitor # 7

	Total	Surf	SubSurf	Surf+L2	L2	L3	L4
D50.	22.	33.	15.				
D75.	41.	47.	34.				
D84.	49.	53.	45.				
D90.	56.	57.	55.				
D95.	62.	60.	67.				

ENTIRE MCNEIL SAMPLE

Site: WILLAPA a USGS

Scour Monitor # 2

	Total	Surf	SubSurf	Surf+L2	L2	L3	L4
D50.	27.	33.	23.	27.	22.	27.	
D75.	47.	55.	45.	42.	33.	56.	
D84.	58.	69.	55.	53.	41.	65.	
D90.	68.	76.	62.	63.	48.	74.	
D95.	78.	82.	74.	75.	56.	81.	

Scour Monitor # 3

	Total	Surf	SubSurf	Surf+L2	L2	L3	L4
D50.	29.	60.	18.				
D75.	53.	109.	33.				
D84.	97.	116.	39.				
D90.	108.	120.	44.				
D95.	117.	124.	52.				

Scour Monitor # 5

	Total	Surf	SubSurf	Surf+L2	L2	L3	L4
D50.	53.	53.	55.				
D75.	75.	67.	94.				
D84.	87.	75.	106.				
D90.	100.	80.	114.				
D95.	113.	85.	120.				

Scour Monitor # 10

	Total	Surf	SubSurf	Surf+L2	L2	L3	L4
D50.	33.	40.	27.				
D75.	65.	73.	58.				
D84.	74.	79.	69.				
D90.	79.	83.	76.				
D95.	84.	86.	82.				

Scour Monitor # 11

	Total	Surf	SubSurf	Surf+L2	L2	L3	L4
D50.	36.	47.	18.				
D75.	66.	60.	72.				
D84.	74.	67.	78.				
D90.	80.	75.	82.				
D95.	84.	82.	86.				

Scour Monitor # 3+10

	Total	Surf	SubSurf	Surf+L2	L2	L3	L4
D50.	30.	47.	22.				
D75.	61.	92.	43.				
D84.	78.	105.	55.				
D90.	90.	113.	65.				
D95.	107.	120.	77.				

Scour Monitor # 5+11

	Total	Surf	SubSurf	Surf+L2	L2	L3	L4
D50.	49.	50.	47.				
D75.	70.	63.	78.				
D84.	80.	72.	88.				
D90.	86.	78.	102.				
D95.	101.	84.	114.				

TRUNCATED (PARTICLES > 8 mm) MCNEIL SAMPLE

Site: ISSAQUAH CREEK

Scour Monitor # 2

	Total	Surf	SubSurf	Surf+L2	L2	L3	L4
D50.	36.	47.	32.	44.	40.	33.	27.
D75.	55.	59.	50.	62.	70.	45.	37.
D84.	64.	62.	66.	71.	77.	63.	41.
D90.	73.	68.	74.	78.	82.	72.	44.
D95.	81.	78.	82.	83.	85.	80.	53.

Scour Monitor # 5

	Total	Surf	SubSurf	Surf+L2	L2	L3	L4
D50.	36.	47.	31.	44.	40.	26.	31.
D75.	58.	70.	54.	69.	69.	40.	47.
D84.	70.	95.	65.	80.	77.	47.	57.
D90.	81.	107.	74.	88.	81.	53.	65.
D95.	93.	117.	81.	105.	85.	58.	76.

Scour Monitor # 7

	Total	Surf	SubSurf	Surf+L2	L2	L3	L4
D50.	34.	41.	31.	36.	28.	30.	33.
D75.	52.	64.	49.	50.	42.	52.	53.
D84.	61.	73.	58.	60.	47.	95.	59.
D90.	73.	79.	63.	69.	53.	106.	63.
D95.	88.	84.	96.	79.	58.	117.	74.

Scour Monitor # 9

	Total	Surf	SubSurf	Surf+L2	L2	L3	L4
D50.	40.	42.	37.	39.	31.	42.	
D75.	61.	54.	66.	60.	73.	62.	
D84.	72.	61.	78.	73.	89.	71.	
D90.	82.	67.	87.	85.	102.	78.	
D95.	93.	77.	104.	103.	114.	83.	

Scour Monitor # 5+9

	Total	Surf	SubSurf	Surf+L2	L2	L3	L4
D50.	38.	43.	33.	41.	36.	31.	31.
D75.	60.	59.	60.	64.	70.	53.	47.
D84.	71.	71.	72.	77.	80.	61.	57.
D90.	81.	87.	80.	87.	87.	70.	65.
D95.	93.	105.	87.	104.	102.	79.	76.

TRUNCATED (PARTICLES > 8 mm) MCNEIL SAMPLE

Site: N FK STILLI HAZEL

Scour Monitor # 6

	Total	Surf	SubSurf	Surf+L2	L2	L3	L4
D50.	58.	53.	61.	50.	47.	72.	
D75.	98.	103.	87.	85.	73.	146.	
D84.	125.	112.	143.	99.	79.	159.	
D90.	144.	118.	156.	109.	83.	167.	
D95.	162.	122.	168.	118.	86.	173.	

Scour Monitor # 9

	Total	Surf	SubSurf	Surf+L2	L2	L3	L4
D50.	111.	52.	160.	49.	45.	215.	
D75.	211.	63.	217.	90.	117.	237.	
D84.	227.	72.	231.	126.	140.	244.	
D90.	237.	78.	240.	145.	155.	248.	
D95.	246.	83.	247.	162.	167.	251.	

Scour Monitor # 11

	Total	Surf	SubSurf	Surf+L2	L2	L3	L4
D50.	35.	48.	26.	45.	40.	23.	
D75.	59.	100.	43.	85.	54.	32.	
D84.	90.	110.	52.	102.	57.	39.	
D90.	103.	116.	58.	111.	60.	44.	
D95.	115.	122.	66.	119.	62.	74.	

Scour Monitor # 15

	Total	Surf	SubSurf	Surf+L2	L2	L3	L4
D50.	44.	68.	35.	47.	33.	38.	
D75.	78.	107.	56.	91.	50.	62.	
D84.	95.	114.	68.	104.	63.	72:	
D90.	106.	119.	75.	112.	72.	78.	
D95.	117.	123.	82.	120.	80.	83.	

Scour Monitor # 16

	Total	Surf	SubSurf	Surf+L2	L2	L3	L4
D50.	82.	85.	80.	91.	96.	69.	
D75.	134.	139.	129.	142.	145.	100.	
D84.	150.	154.	147.	156.	158.	110.	
D90.	162.	164.	159.	165.	166.	116.	
D95.	171.	172.	170.	173.	173.	122.	

Scour Monitor # 11+16

	Total	Surf	SubSurf	Surf+L2	L2	L3	L4
D50.	58.	69.	50.	63.	60.	31.	
D75.	120.	125.	116.	132.	139.	83.	
D84.	141.	144.	138.	149.	154.	99.	
D90.	155.	157.	153.	161.	164.	109.	
D95.	167.	169.	166.	170.	172.	118.	

TRUNCATED (PARTICLES > 8 mm) MCNEIL SAMPLE

Site: N FK STILLI USGS

Scour Monitor # 2

	Total	Surf	SubSurf	Surf+L2	L2	L3	L4
D50.	100.	106.	91.				
D75.	137.	136.	138.				
D84.	153.	152.	153.				
D90.	163.	162.	163.				
D95.	171.	171.	172.				

Scour Monitor # 7

	Total	Surf	SubSurf	Surf+L2	L2	L3	L4
D50.	63.	63.	65.				
D75.	111.	93.	138.				
D84.	132.	105.	154.				
D90.	149.	113.	164.				
D95.	164.	120.	172.				

Scour Monitor # 9

	Total	Surf	SubSurf	Surf+L2	L2	L3	L4
D50.	50.	54.	45.				
D75.	118.	128.	117.				
D84.	143.	147.	140.				
D90.	157.	159.	155.				
D95.	168.	169.	167.				

Scour Monitor # 11

	Total	Surf	SubSurf	Surf+L2	L2	L3	L4
D50.	62.	61.	63.				
D75.	148.	154.	138.				
D84.	160.	164.	153.				
D90.	167.	170.	163.				
D95.	174.	175.	172.				

Scour Monitor # 2+7

	Total	Surf	SubSurf	Surf+L2	L2	L3	L4
D50.	81.	84.	74.				
D75.	125.	116.	138.				
D84.	144.	127.	153.				
D90.	157.	145.	163.				
D95.	169.	162.	172.				

TRUNCATED (PARTICLES > 8 mm) MCNEIL SAMPLE

Site: RAGING RIVER

Scour Monitor # 1

	Total	Surf	SubSurf	Surf+L2	L2	L3	L4
D50.	68.	66.	68.	68.	69.	128.	35.
D75.	130.	150.	119.	126.	85.	156.	95.
D84.	148.	161.	141.	146.	91.	165.	106.
D90.	160.	168.	155.	158.	104.	171.	114.
D95.	170.	174.	168.	169.	115.	176.	121.

Scour Monitor # 2

	Total	Surf	SubSurf	Surf+L2	L2	L3	L4
D50.	176.	198.	28.	187.	32.	23.	
D75.	219.	229.	46.	224.	54.	38.	
D84.	232.	239.	54.	235.	60.	44.	
D90.	240.	245.	59.	242.	65.	51.	
D95.	247.	249.	65.	248.	76.	57.	

Scour Monitor # 4

	Total	Surf	SubSurf	Surf+L2	L2	L3	L4
D50.	162.	170.	146.	150.	58.	213.	
D75.	210.	211.	210.	190.	139.	236.	
D84.	227.	227.	226.	213.	154.	243.	
D90.	237.	237.	237.	228.	164.	247.	
D95.	246.	246.	246.	241.	172.	251.	

Scour Monitor # 5

	Total	Surf	SubSurf	Surf+L2	L2	L3	L4
D50.	84.	72.	98.				
D75.	129.	101.	145.				
D84.	147.	111.	158.				
D90.	159.	117.	166.				
D95.	170.	122.	173.				

Scour Monitor # 7

	Total	Surf	SubSurf	Surf+L2	L2	L3	L4
D50.	124.	143.	25.				
D75.	207.	212.	46.				
D84.	224.	227.	61.				
D90.	236.	238.	71.				
D95.	245.	246.	80.				

Scour Monitor # 10

	Total	Surf	SubSurf	Surf+L2	L2	L3	L4
D50.	57.	46.	80.				
D75.	103.	96.	109.				
D84.	112.	107.	115.				
D90.	118.	115.	120.				
D95.	122.	121.	123.				

TRUNCATED (PARTICLES > 8 mm) MCNEIL SAMPLE

Site: RAGING RIVER

Scour Monitor # 11

	Total	Surf	SubSurf	Surf+L2	L2	L3	L4
D50.	65.	98.	38.				
D75.	119.	135.	57.				
D84.	139.	152.	63.				
D90.	154.	162.	72.				
D95.	167.	171.	80.				

Scour Monitor # 1+2+7

	Total	Surf	SubSurf	Surf+L2	L2	L3	L4
D50.	121.	166.	42.	144.	38.	58.	35.
D75.	195.	215.	88.	207.	69.	146.	95.
D84.	216.	230.	122.	225.	78.	158.	106.
D90.	230.	239.	143.	236.	85.	167.	114.
D95.	242.	247.	161.	245.	96.	173.	121.

Scour Monitor # 4+10

	Total	Surf	SubSurf	Surf+L2	L2	L3	L4
D50.	130.	145.	108.	113.	63.	213.	
D75.	195.	195.	195.	170.	119.	236.	
D84.	216.	216.	217.	195.	136.	243.	
D90.	231.	230.	231.	216.	152.	247.	
D95.	242.	242.	242.	235.	166.	251.	

Scour Monitor # 5+11

	Total	Surf	SubSurf	Surf+L2	L2	L3	L4
D50.	72.	91.	55.				
D75.	124.	124.	123.				
D84.	143.	142.	144.				
D90.	157.	156.	158.				
D95.	168.	168.	169.				

TRUNCATED (PARTICLES > 8 mm) MCNEIL SAMPLE

Site: S FK SNOQUALMIE

Scour Monitor # 2
```
        Total    Surf   SubSurf Surf+L2  L2      L3      L4
-----------------------------------------------------------------
D50.    48.      58.     36.
D75.    91.      101.    63.
D84.    104.     111.    87.
D90.    112.     117.    102.
D95.    120.     122.    114.
```

Scour Monitor # 4
```
        Total    Surf   SubSurf Surf+L2  L2      L3      L4
-----------------------------------------------------------------
D50.    119.     105.    139.
D75.    150.     117.    162.
D84.    161.     121.    169.
D90.    168.     123.    173.
D95.    174.     125.    177.
```

Scour Monitor # 6
```
        Total    Surf   SubSurf Surf+L2  L2      L3      L4
-----------------------------------------------------------------
D50.    59.      58.     65.
D75.    104.     94.     121.
D84.    122.     106.    142.
D90.    139.     114.    156.
D95.    159.     120.    168.
```

Scour Monitor # 8
```
        Total    Surf   SubSurf Surf+L2  L2      L3      L4
-----------------------------------------------------------------
D50.    44.      48.     35.
D75.    67.      69.     63.
D84.    75.      77.     72.
D90.    80.      81.     78.
D95.    85.      85.     84.
```

Scour Monitor # 9
```
        Total    Surf   SubSurf Surf+L2  L2      L3      L4
-----------------------------------------------------------------
D50.    80.      97.     58.
D75.    124.     202.    91.
D84.    202.     221.    104.
D90.    221.     234.    112.
D95.    238.     244.    120.
```

Scour Monitor # 11
```
        Total    Surf   SubSurf Surf+L2  L2      L3      L4
-----------------------------------------------------------------
D50.    33.      34.     32.     35.     35.     30.
D75.    51.      46.     54.     50.     53.     63.
D84.    61.      55.     64.     58.     59.     72.
D90.    70.      62.     73.     63.     65.     79.
D95.    79.      74.     81.     75.     76.     84.
```

TRUNCATED (PARTICLES > 8 mm) MCNEIL SAMPLE

Site: S FK SNOQUALMIE

Scour Monitor # 2+8

	Total	Surf	SubSurf	Surf+L2	L2	L3	L4
D50.	46.	54.	35.				
D75.	72.	79.	63.				
D84.	86.	92.	77.				
D90.	99.	104.	87.				
D95.	112.	115.	105.				

Scour Monitor # 4+9

	Total	Surf	SubSurf	Surf+L2	L2	L3	L4
D50.	100.	100.	99.				
D75.	145.	183.	146.				
D84.	171.	208.	158.				
D90.	196.	225.	167.				
D95.	224.	239.	173.				

TRUNCATED (PARTICLES > 8 mm) MCNEIL SAMPLE

Site: S FK WILLAPA

Scour Monitor # 3

	Total	Surf	SubSurf	Surf+L2	L2	L3	L4
D50.	35.						
D75.	45.						
D84.	52.						
D90.	56.						
D95.	60.						

Scour Monitor # 9

	Total	Surf	SubSurf	Surf+L2	L2	L3	L4
D50.	22.						
D75.	30.						
D84.	34.						
D90.	39.						
D95.	43.						

Scour Monitor # 11

	Total	Surf	SubSurf	Surf+L2	L2	L3	L4
D50.	17.						
D75.	24.						
D84.	28.						
D90.	31.						
D95.	36.						

339

TRUNCATED (PARTICLES > 8 mm) MCNEIL SAMPLE

Site: SQUIRE CREEK

Scour Monitor # 2

	Total	Surf	SubSurf	Surf+L2	L2	L3	L4
D50.	36.	44.	31.	41.	37.	28.	
D75.	55.	74.	43.	68.	54.	39.	
D84.	69.	86.	50.	80.	65.	43.	
D90.	81.	98.	59.	88.	73.	47.	
D95.	95.	112.	69.	105.	81.	55.	

Scour Monitor # 4

	Total	Surf	SubSurf	Surf+L2	L2	L3	L4
D50.	49.	45.	58.	37.	24.	52.	134.
D75.	93.	58.	132.	54.	39.	70.	159.
D84.	137.	62.	149.	61.	54.	77.	167.
D90.	152.	69.	161.	69.	71.	82.	172.
D95.	166.	78.	170.	79.	79.	85.	176.

Scour Monitor # 5

	Total	Surf	SubSurf	Surf+L2	L2	L3	L4
D50.	54.	78.	39.				
D75.	99.	108.	79.				
D84.	109.	115.	99.				
D90.	116.	120.	109.				
D95.	122.	123.	118.				

Scour Monitor # 8

	Total	Surf	SubSurf	Surf+L2	L2	L3	L4
D50.	71.	114.	26.	90.	23.	30.	
D75.	131.	150.	47.	141.	37.	57.	
D84.	148.	161.	58.	155.	46.	68.	
D90.	160.	168.	66.	165.	52.	76.	
D95.	170.	174.	77.	172.	58.	82.	

Scour Monitor # 10

	Total	Surf	SubSurf	Surf+L2	L2	L3	L4
D50.	54.	44.	74.	51.	75.	70.	
D75.	108.	58.	131.	117.	150.	105.	
D84.	132.	63.	149.	143.	161.	113.	
D90.	149.	102.	160.	157.	168.	119.	
D95.	164.	114.	170.	168.	174.	123.	

Scour Monitor # 12

	Total	Surf	SubSurf	Surf+L2	L2	L3	L4
D50.	54.	59.	42.				
D75.	73.	76.	61.				
D84.	79.	81.	70.				
D90.	83.	84.	77.				
D95.	86.	86.	83.				

TRUNCATED (PARTICLES > 8 mm) MCNEIL SAMPLE

Site: SQUIRE CREEK

Scour Monitor # 2+8

	Total	Surf	SubSurf	Surf+L2	L2	L3	L4
D50.	47.	84.	29.	64.	28.	29.	
D75.	93.	133.	44.	116.	45.	43.	
D84.	126.	150.	54.	140.	55.	54.	
D90.	145.	161.	62.	154.	61.	63.	
D95.	162.	171.	74.	167.	73.	75.	

Scour Monitor # 4+10

	Total	Surf	SubSurf	Surf+L2	L2	L3	L4
D50.	52.	44.	67.	45.	49.	59.	134.
D75.	104.	58.	132.	76.	138.	92.	159.
D84.	134.	63.	149.	124.	153.	104.	167.
D90.	151.	85.	161.	145.	163.	113.	172.
D95.	165.	105.	170.	162.	172.	120.	176.

Scour Monitor # 5+12

	Total	Surf	SubSurf	Surf+L2	L2	L3	L4
D50.	54.	63.	40.				
D75.	81.	85.	69.				
D84.	93.	96.	86.				
D90.	105.	107.	100.				
D95.	116.	117.	113.				

TRUNCATED (PARTICLES > 8 mm) MCNEIL SAMPLE

Site: TOLT RIVER 97

Scour Monitor # 7

	Total	Surf	SubSurf	Surf+L2	L2	L3	L4
D50.	21.	23.	20.				
D75.	30.	35.	28.				
D84.	35.	40.	31.				
D90.	39.	43.	35.				
D95.	43.	51.	40.				

TRUNCATED (PARTICLES > 8 mm) MCNEIL SAMPLE

Site: WILLAPA a ELK PRAIRIE

Scour Monitor # 6
	Total	Surf	SubSurf	Surf+L2	L2	L3	L4
D50.	41.	45.	35.				
D75.	53.	55.	51.				
D84.	57.	58.	56.				
D90.	60.	60.	59.				
D95.	62.	62.	61.				

Scour Monitor # 7
	Total	Surf	SubSurf	Surf+L2	L2	L3	L4
D50.	47.	72.	30.				
D75.	79.	97.	46.				
D84.	94.	108.	52.				
D90.	106.	115.	56.				
D95.	116.	121.	60.				

Scour Monitor # 67
	Total	Surf	SubSurf	Surf+L2	L2	L3	L4
D50.	44.	54.	31.				
D75.	61.	81.	48.				
D84.	74.	96.	54.				
D90.	92.	107.	58.				
D95.	108.	117.	61.				

TRUNCATED (PARTICLES > 8 mm) MCNEIL SAMPLE

Site: WILLAPA a TRAP ·

Scour Monitor # 2
	Total	Surf	SubSurf	Surf+L2	L2	L3	L4
D50.	39.	42.	38.	33.	28.	48.	
D75.	59.	60.	59.	49.	38.	69.	
D84.	69.	68.	69.	58.	42.	76.	
D90.	76.	75.	76.	65.	44.	81.	
D95.	82.	82.	83.	76.	53.	85.	

Scour Monitor # 3
	Total	Surf	SubSurf	Surf+L2	L2	L3	L4
D50.	33.	24.	46.	27.	33.	53.	
D75.	65.	37.	73.	45.	69.	75.	
D84.	73.	42.	79.	61.	76.	80.	
D90.	79.	45.	83.	71.	81.	83.	
D95.	84.	54.	86.	80.	85.	86.	

Scour Monitor # 7
	Total	Surf	SubSurf	Surf+L2	L2	L3	L4
D50.	31.	36.	27.				
D75.	47.	49.	45.				
D84.	54.	54.	55.				
D90.	59.	58.	62.				
D95.	64.	61.	74.				

TRUNCATED (PARTICLES > 8 mm) MCNEIL SAMPLE

Site: WILLAPA @ USGS

Scour Monitor # 2

	Total	Surf	SubSurf	Surf+L2	L2	L3	L4
D50.	30.	33.	28.	28.	24.	41.	
D75.	51.	55.	49.	43.	36.	61.	
D84.	61.	69.	58.	54.	43.	70.	
D90.	70.	76.	65.	64.	50.	77.	
D95.	79.	83.	76.	76.	57.	83.	

Scour Monitor # 3

	Total	Surf	SubSurf	Surf+L2	L2	L3	L4
D50.	37.	92.	27.				
D75.	91.	111.	38.				
D84.	104.	117.	43.				
D90.	112.	121.	48.				
D95.	120.	124.	55.				

Scour Monitor # 5

	Total	Surf	SubSurf	Surf+L2	L2	L3	L4
D50.	58.	55.	60.				
D75.	79.	69.	100.				
D84.	90.	76.	110.				
D90.	103.	81.	116.				
D95.	115.	85.	122.				

Scour Monitor # 10

	Total	Surf	SubSurf	Surf+L2	L2	L3	L4
D50.	42.	41.	42.				
D75.	69.	74.	65.				
D84.	77.	80.	74.				
D90.	81.	83.	79.				
D95.	85.	86.	84.				

Scour Monitor # 11

	Total	Surf	SubSurf	Surf+L2	L2	L3	L4
D50.	53.	51.	67.				
D75.	72.	62.	79.				
D84.	78.	70.	83.				
D90.	82.	77.	85.				
D95.	86.	83.	87.				

Scour Monitor # 3+10

	Total	Surf	SubSurf	Surf+L2	L2	L3	L4
D50.	39.	58.	32.				
D75.	70.	95.	52.				
D84.	84.	106.	62.				
D90.	97.	114.	71.				
D95.	111.	121.	80.				

Scour Monitor # 5+11

	Total	Surf	SubSurf	Surf+L2	L2	L3	L4
D50.	56.	53.	63.				
D75.	75.	65.	85.				
D84.	83.	74.	97.				
D90.	88.	79.	108.				
D95.	105.	84.	117.				

COMPARISONS OF PEBBLE COUNT AND MCNEIL
GRAIN SIZE DISTRIBUTION PERCENTILES

Four types of graphs are presented that show comparisons for D_{50}, D_{75}, D_{84}, and D_{90}:

(i) Quantiles calculated based on entire McNeil (bulk) sample, surface layer only

(ii) Quantiles calculated based on McNeil (bulk) sample truncated at 8 mm, surface layer only

(iii) Quantiles calculated based on entire McNeil (bulk) sample, surface plus subsurface layer (L1+L2)

(iv) Quantiles calculated based on McNeil (bulk) sample truncated at 8 mm, surface plus subsurface layer (L1+L2)
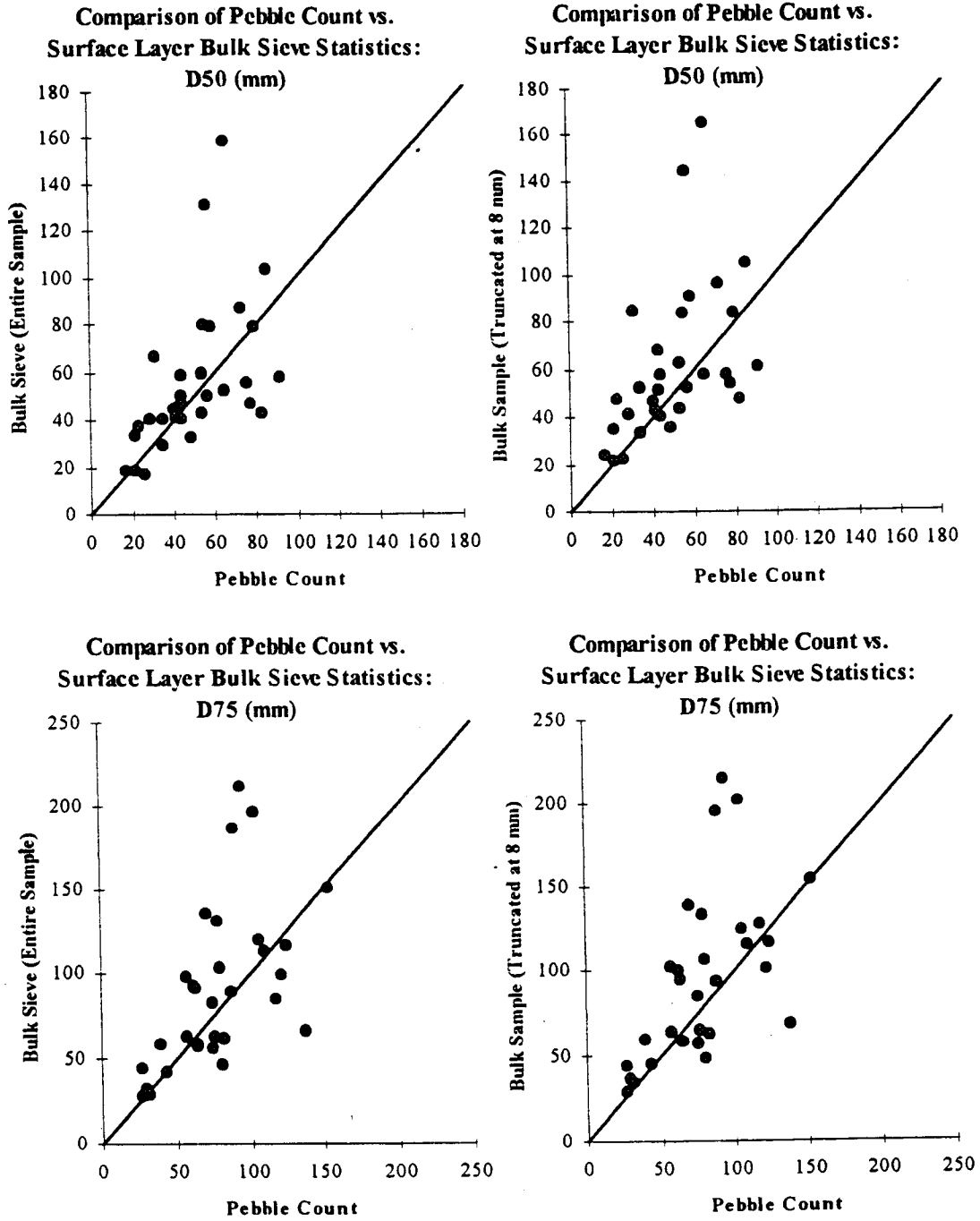
Figure G-1. Comparison of pebble count and bulk sample quantiles: Surface layer D_{50} and D_{75}, entire sample (left) and sample truncated at 8 mm (right).
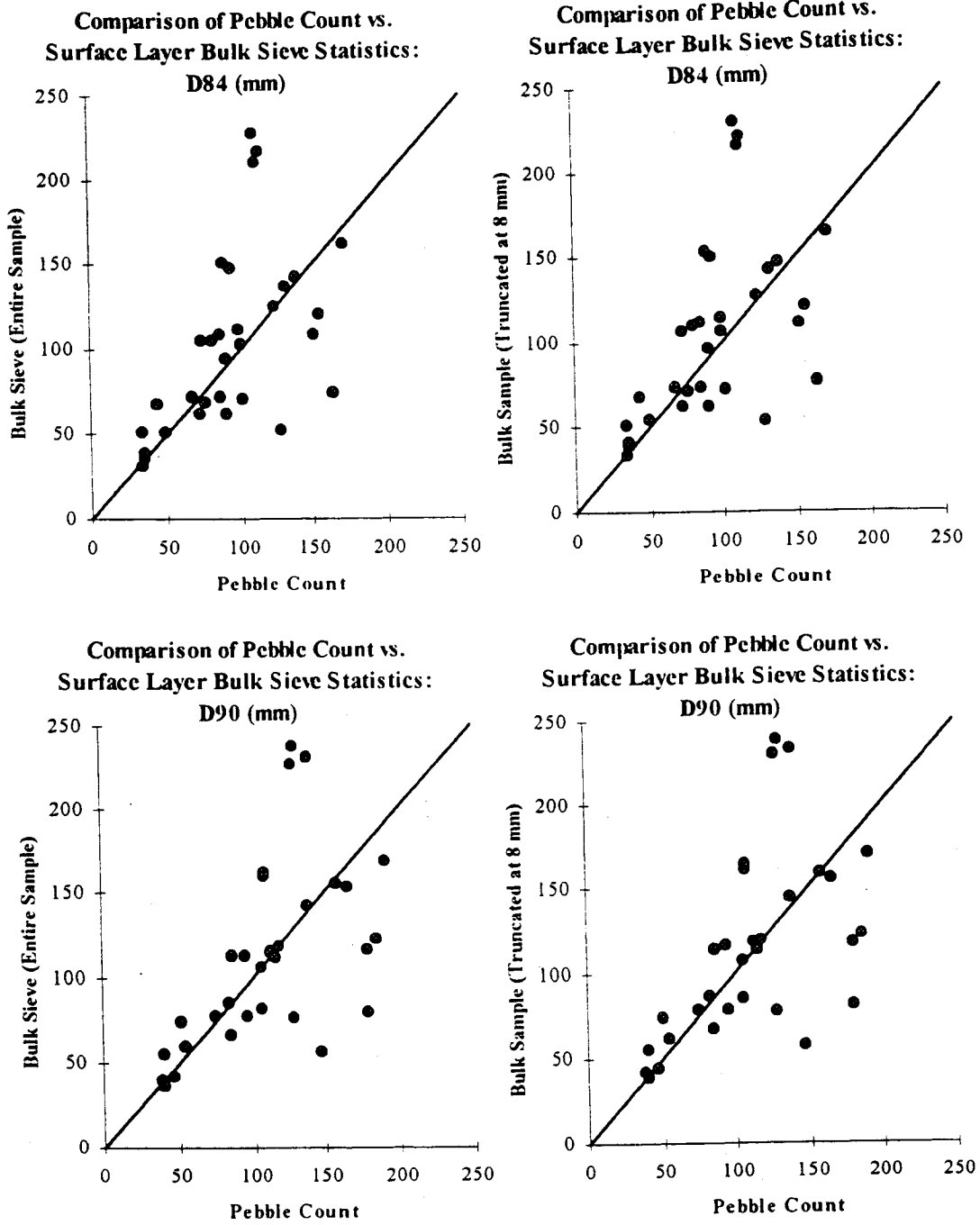
Figure G-2. Comparison of pebble count and bulk sample quantiles: Surface layer D_{84} and D_{90}, entire sample (left) and sample truncated at 8 mm (right).
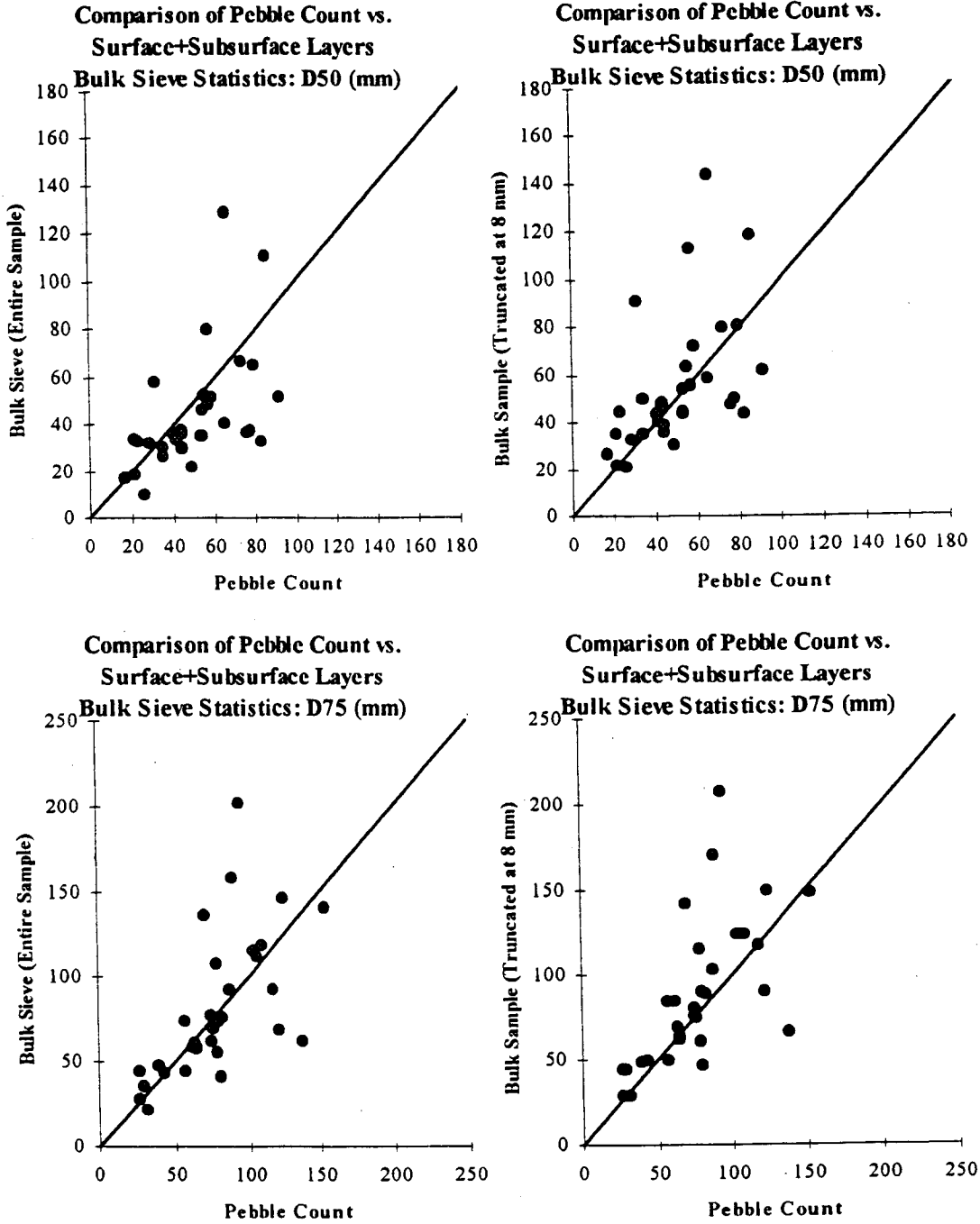
Figure G-3. Comparison of pebble count and bulk sample quantiles: Combined surface and subsurface layer D_{50} and D_{75}, entire sample (left) and sample truncated at 8 mm (right).
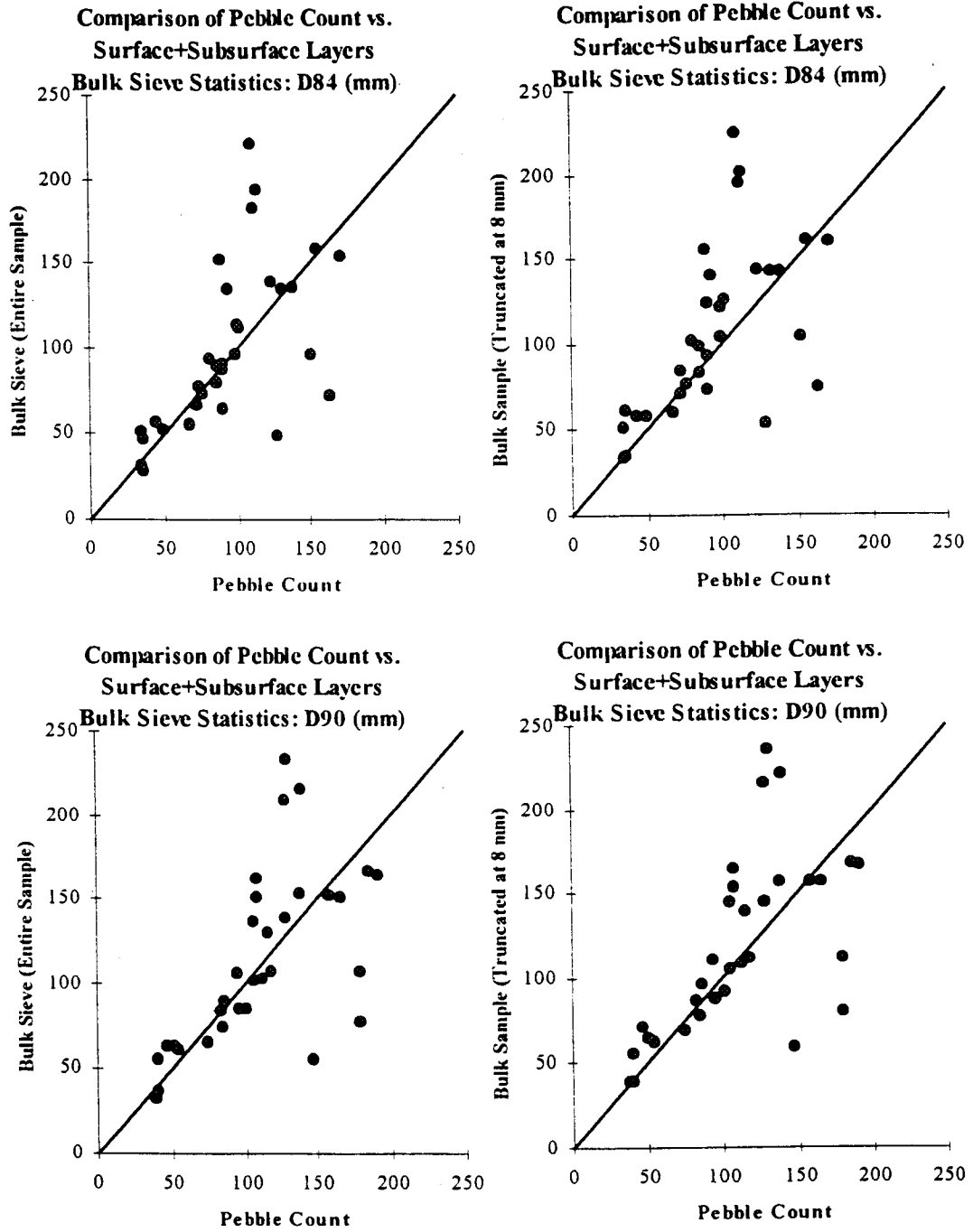
Figure G-4. Comparison of pebble count and bulk sample quantiles: Combined surface and subsurface layer D_{84} and D_{90}, entire sample (left) and sample truncated at 8 mm (right).

Appendix H

WATER SURFACE ELEVATION AND SLOPE PLOTS

Note: Friction slope estimate is indicated in slope plots by solid line and "Sf"
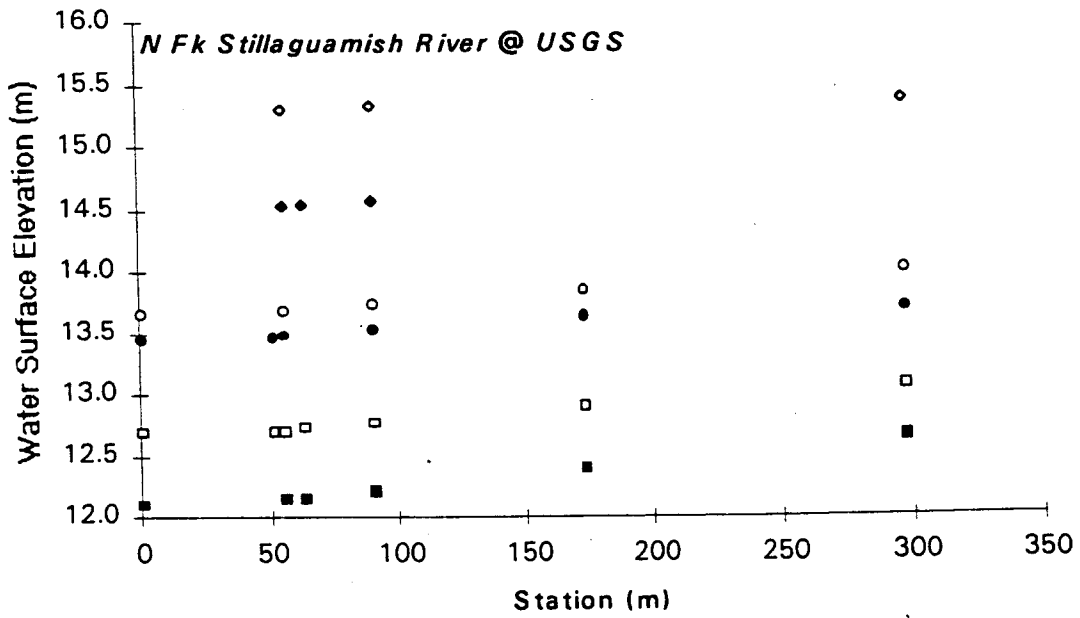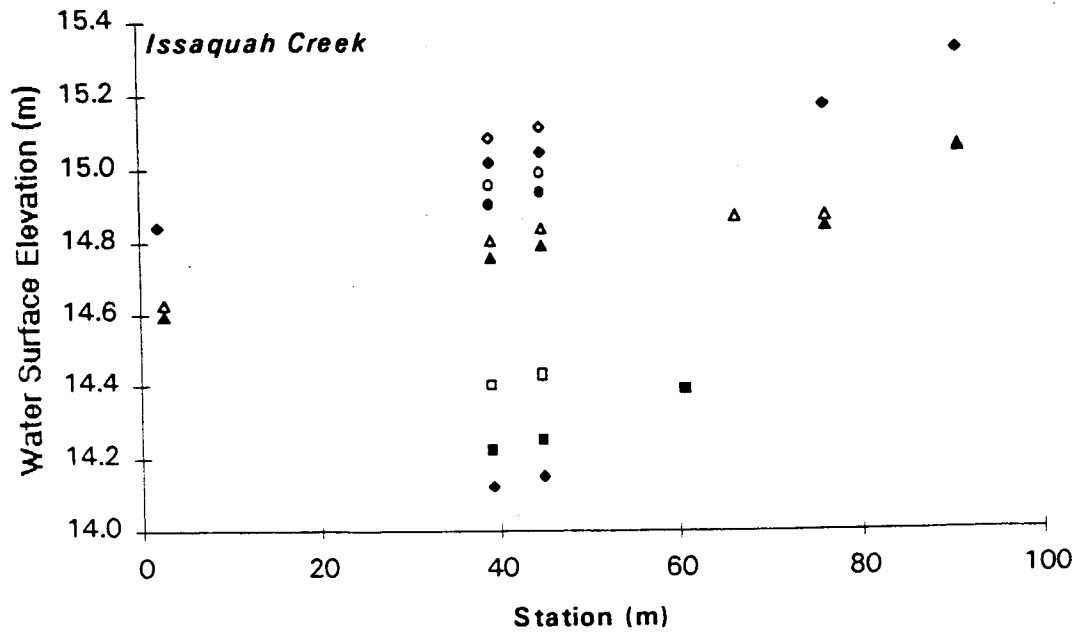
Figure H-1. Stream-wise (longitudinal) water surface elevations measured at the Issaquah Creek and North Fork Stillaguamish River at USGS sites.
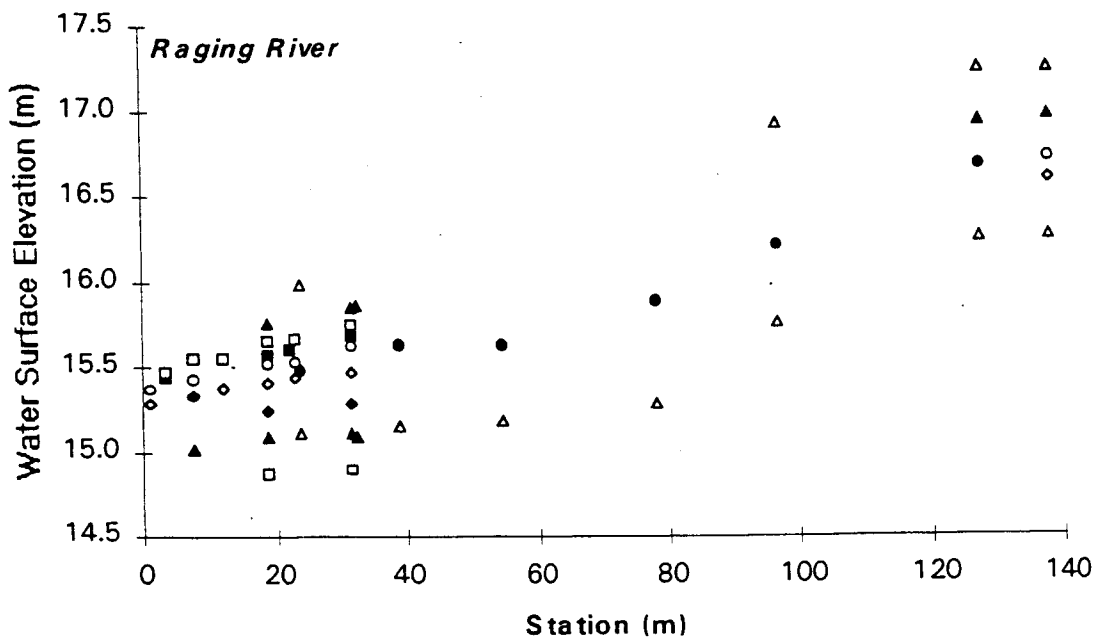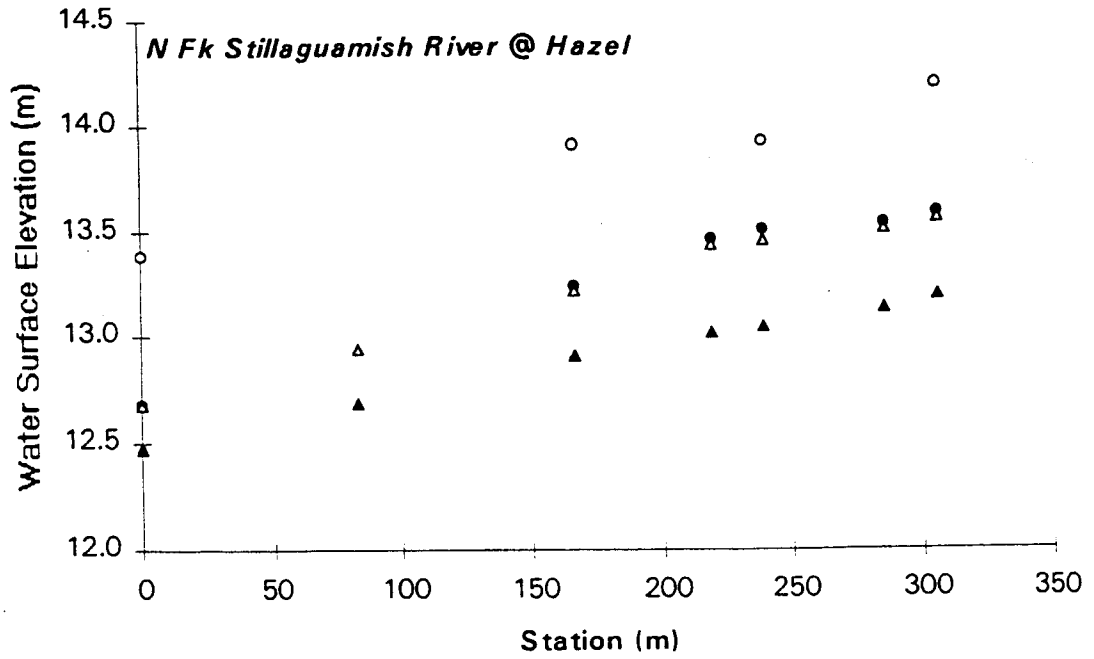
Figure H-2. Stream-wise (longitudinal) water surface elevations measured at the North Fork Stillaguamish River at Hazel and Raging River sites.

Figure H-3. Stream-wise (longitudinal) water surface elevations measured at the South Fork Snoqualmie River and South Fork Willapa River sites.
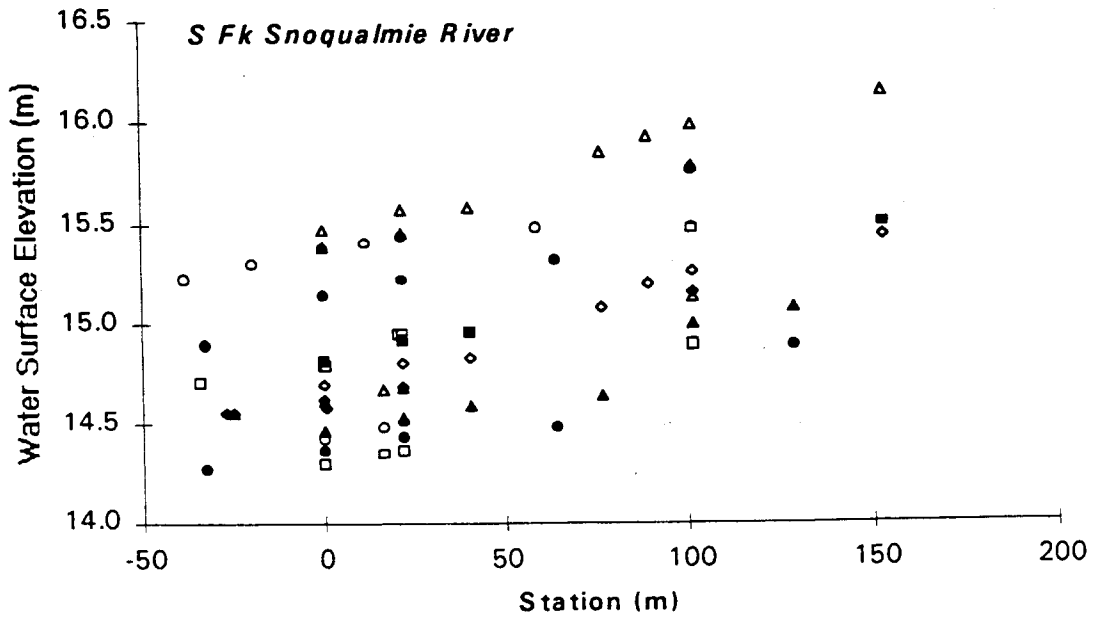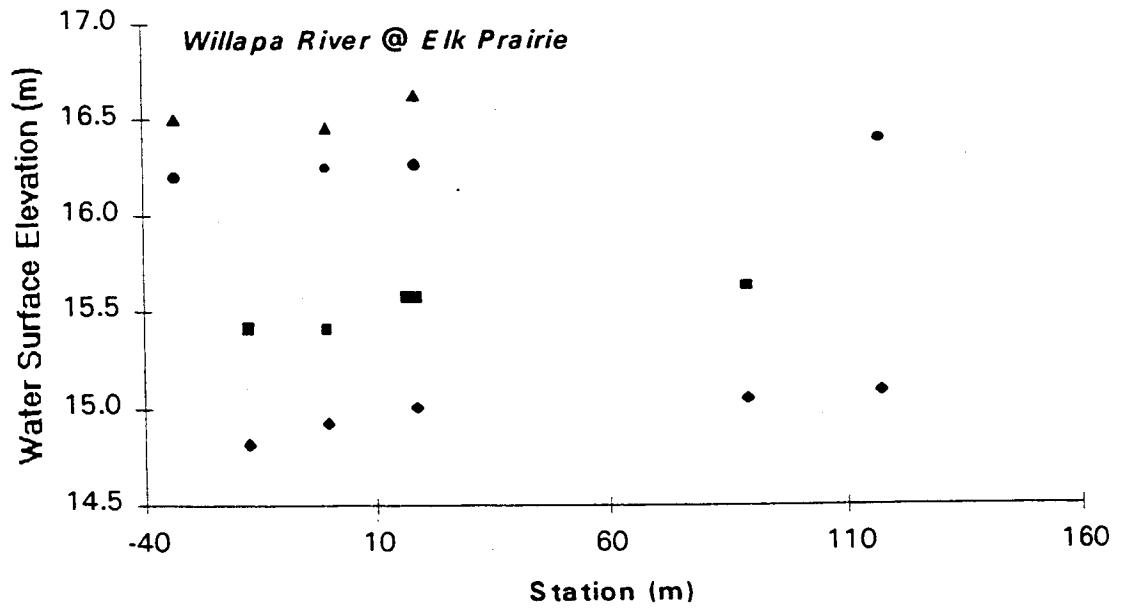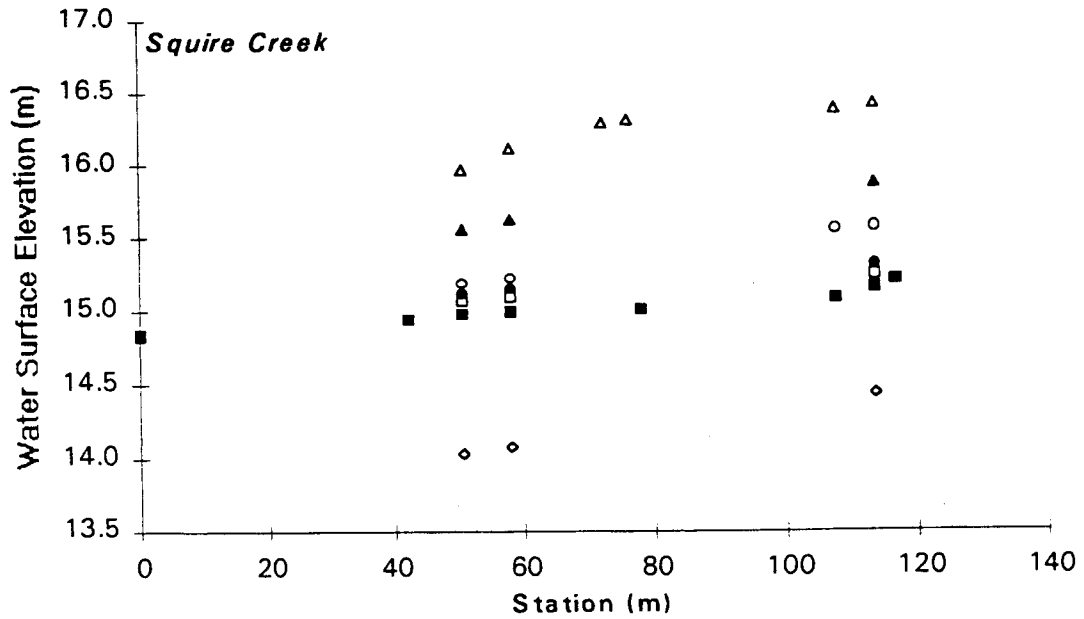
Figure H-4. Stream-wise (longitudinal) water surface elevations measured at the Squire Creek and Willapa River at Elk Prairie sites.
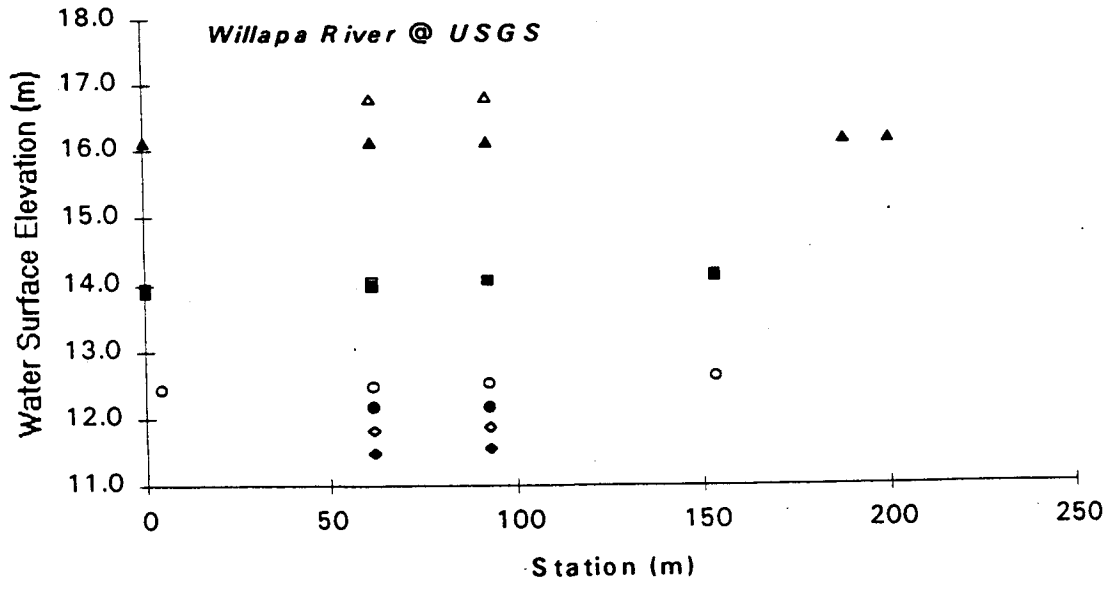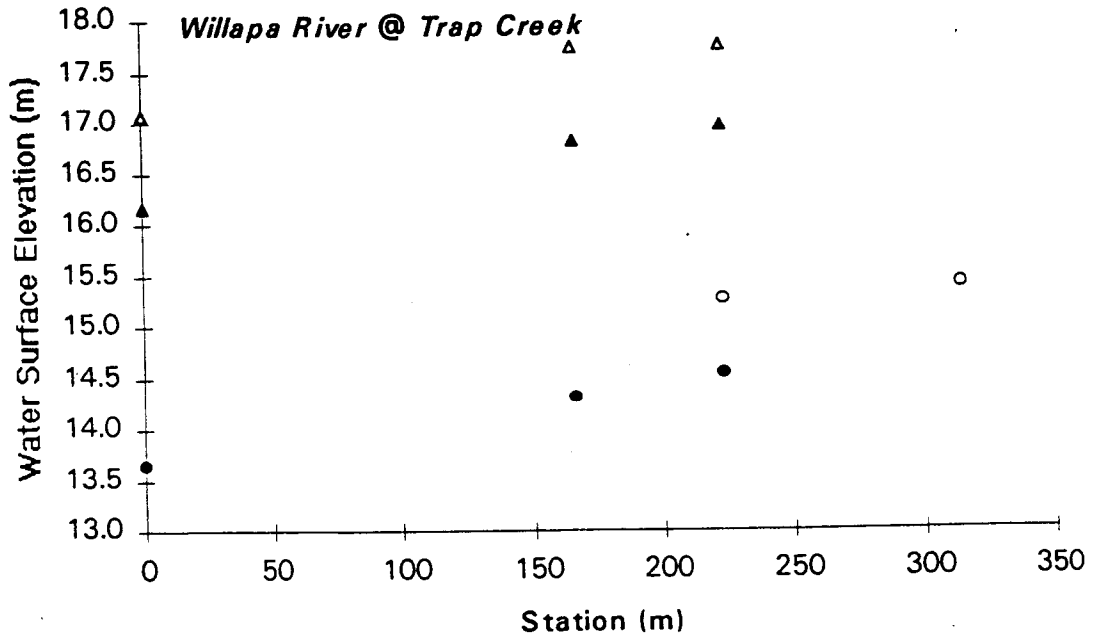
Figure H-5. Stream-wise (longitudinal) water surface elevations measured at the Willapa River sites near Trap Creek and the USGS station.
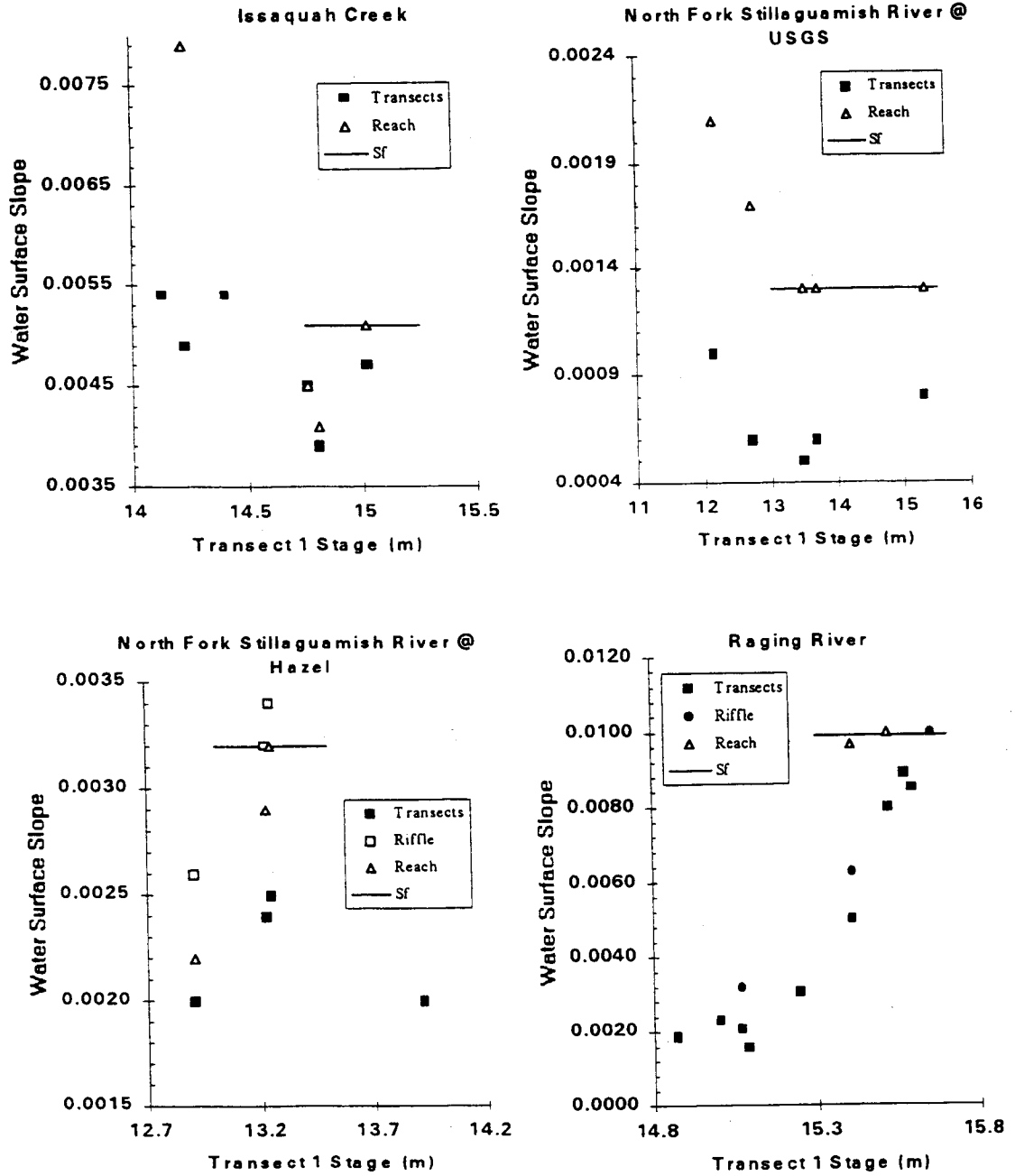
Figure H-6. Water surface slope measurements plotted against selected transect stage. Friction slope (Sf) estimate is indicated by line.
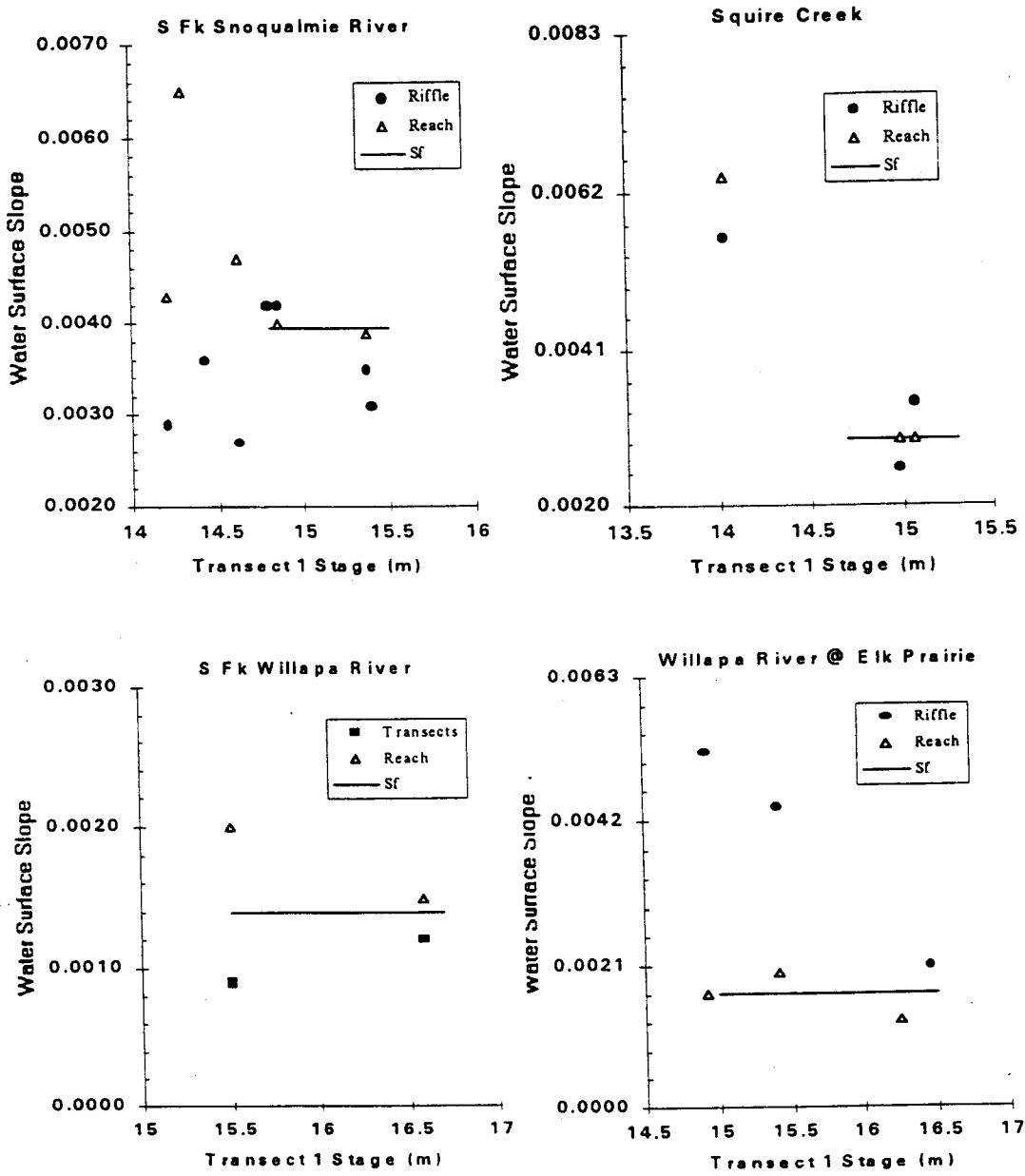
Figure H-7. Water surface slope measurements plotted against selected transect stage. Friction slope (Sf) estimate is indicated by line.
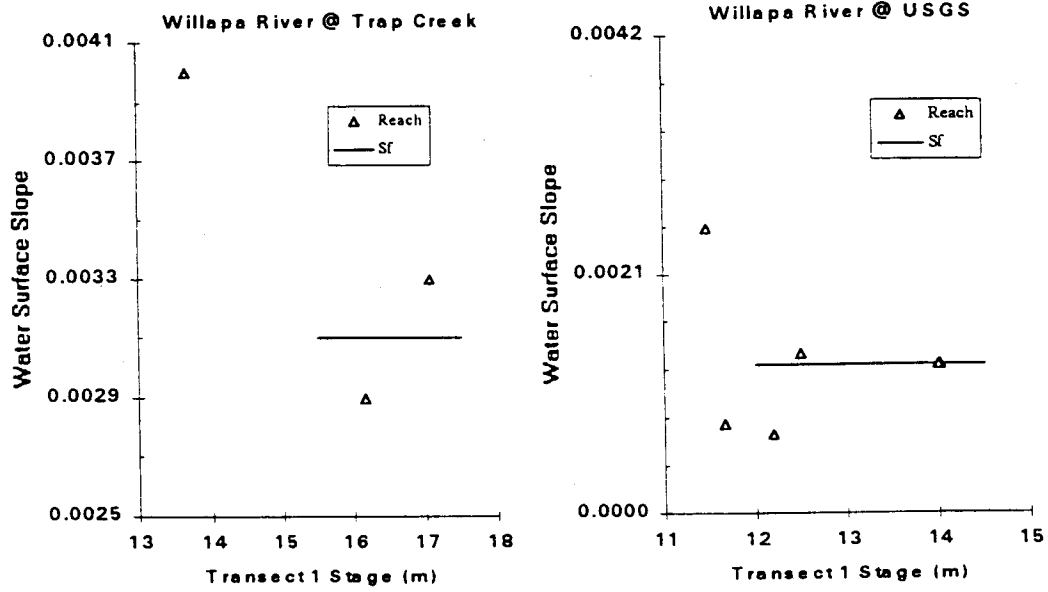
Figure H-8. Water surface slope measurements plotted against selected transect stage. Friction slope (Sf) estimate is indicated by line.
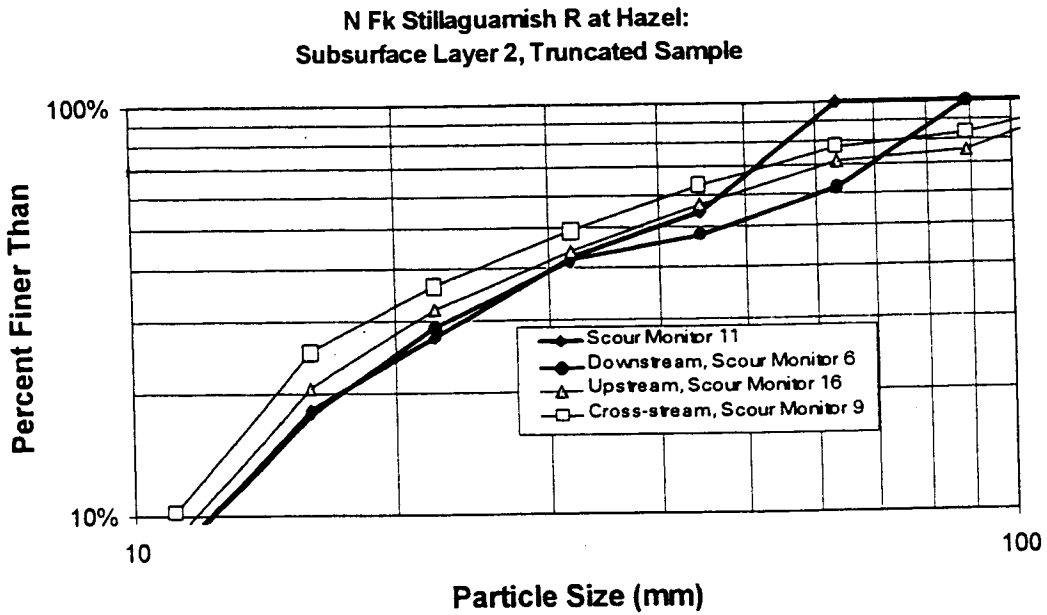
Appendix I

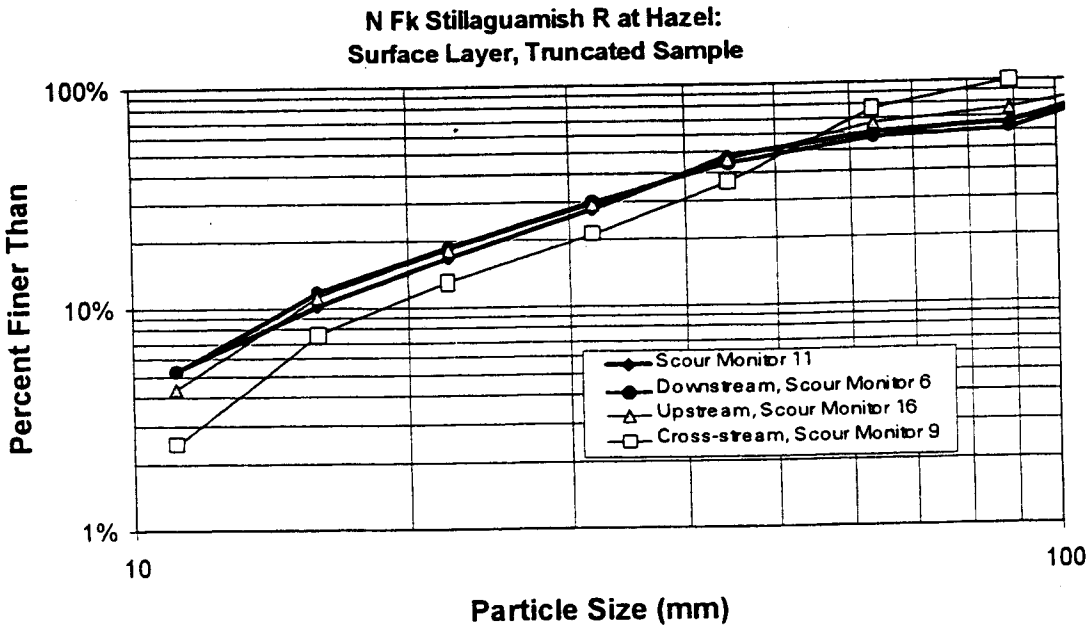## COMPARISONS OF STREAMBED LAYER
GRAIN SIZE DISTRIBUTIONS

Note: Grain size distributions are truncated at 8 mm and 127 mm to exclude influences of distribution tails (done because of bulk sample size requirements and biases). Layers follow same convention as before (1 = surface, 2 = first subsurface layer, 3 = next subsurface layer underneath layer 2, etc.).

N Fk Stillaguamish at USGS: Surface Layer, Truncated Sample

Legend:
- Downstream, Scour Monitor 2
- Scour Monitor 7
- Cross-stream, Scour Monitor 9
- Cross-stream, Scour Monitor 11

N Fk Stillaguamish at USGS: Subsurface Layer 2, Truncated Sample

Legend:
- Downstream, Scour Monitor 2
- Scour Monitor 7
- Cross-stream, Scour Monitor 9
- Cross-stream, Scour Monitor 11
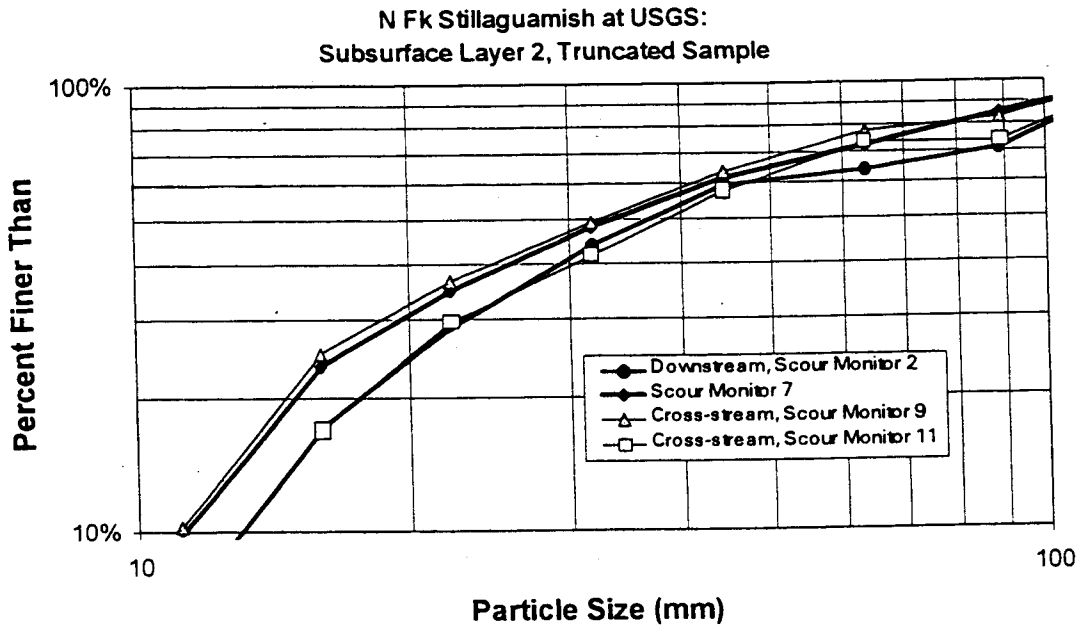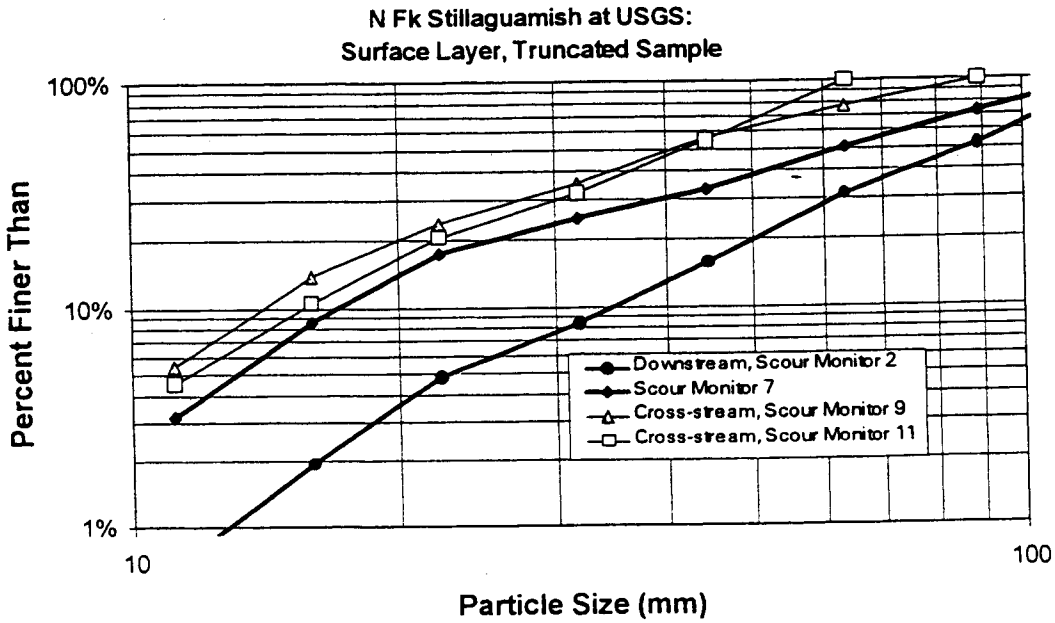
Figure I-1. Comparisons of grain size distributions (truncated at 8 mm and 127 mm) of the same layer at different locations of the streambed of the North Fork Stillaguamish River at USGS site.
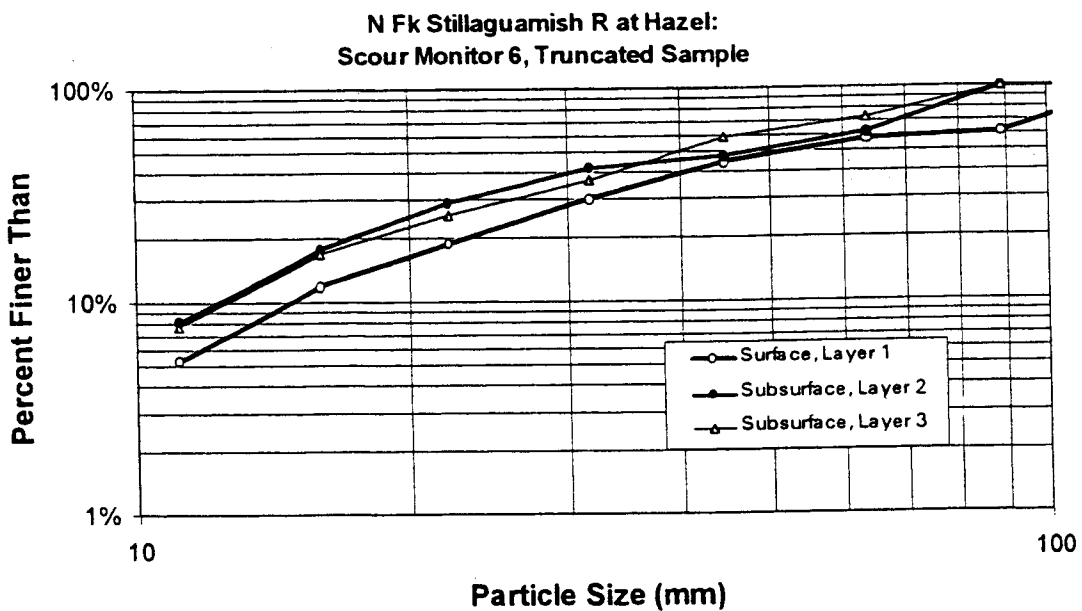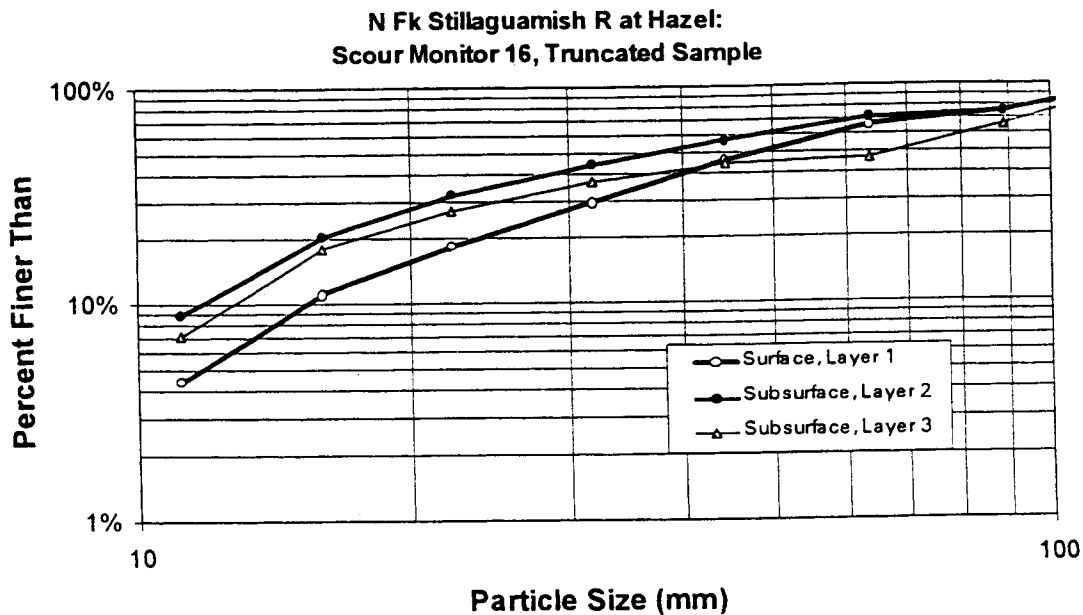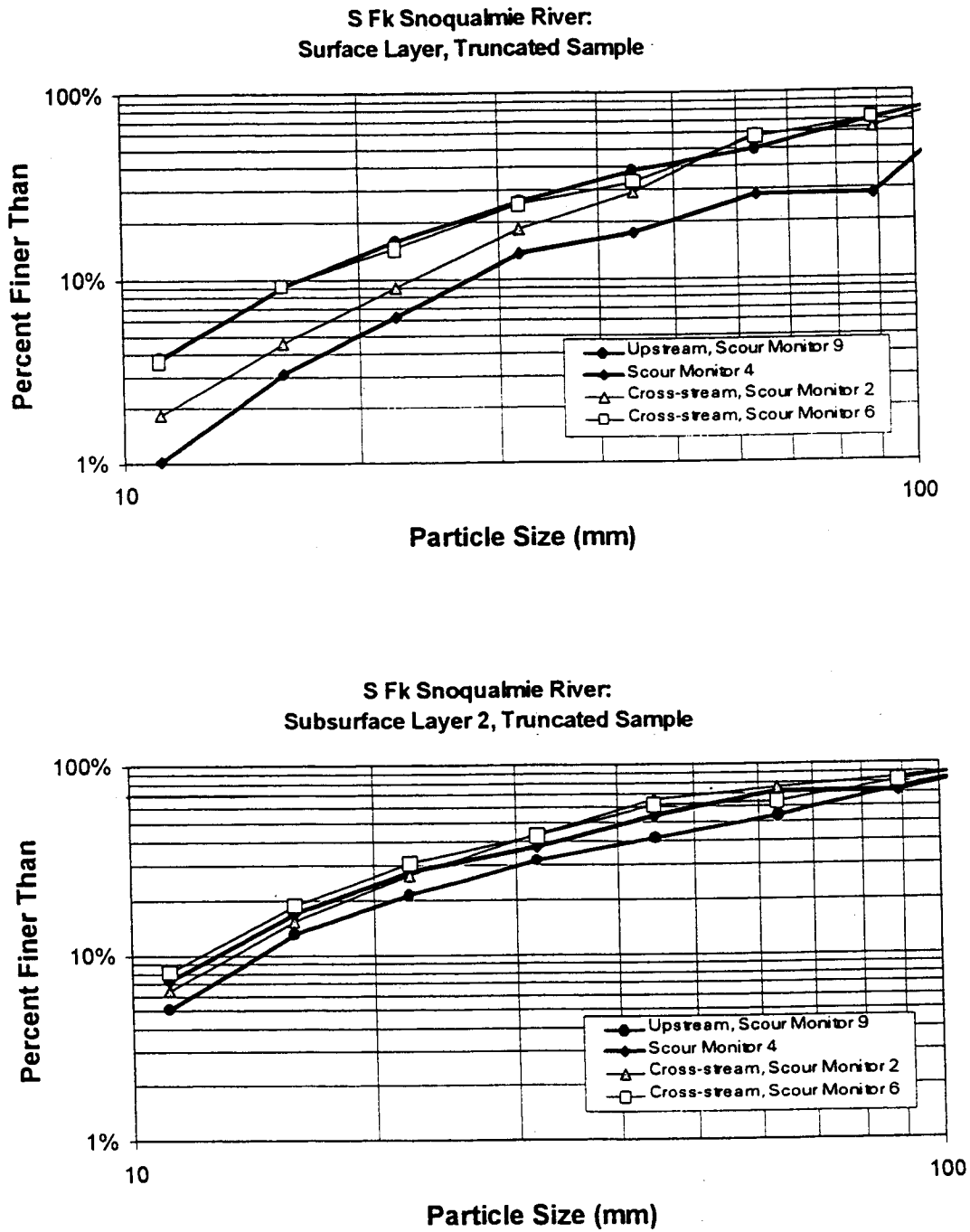
Figure I-2. Comparisons of grain size distributions (truncated at 8 mm and 127 mm) of different vertical layers of the streambed of the North Fork Stillaguamish River at Hazel site.

N Fk Stillaguamish R at Hazel:
Surface Layer, Truncated Sample

(Chart: Percent Finer Than vs. Particle Size (mm))

Legend:
- Scour Monitor 11
- Downstream, Scour Monitor 6
- Upstream, Scour Monitor 16
- Cross-stream, Scour Monitor 9

N Fk Stillaguamish R at Hazel:
Subsurface Layer 2, Truncated Sample

(Chart: Percent Finer Than vs. Particle Size (mm))

Legend:
- Scour Monitor 11
- Downstream, Scour Monitor 6
- Upstream, Scour Monitor 16
- Cross-stream, Scour Monitor 9

Figure I-3. Comparisons of grain size distributions (truncated at 8 mm and 127 mm) of the same layer at different of the streambed of the North Fork Stillaguamish River at Hazel site.
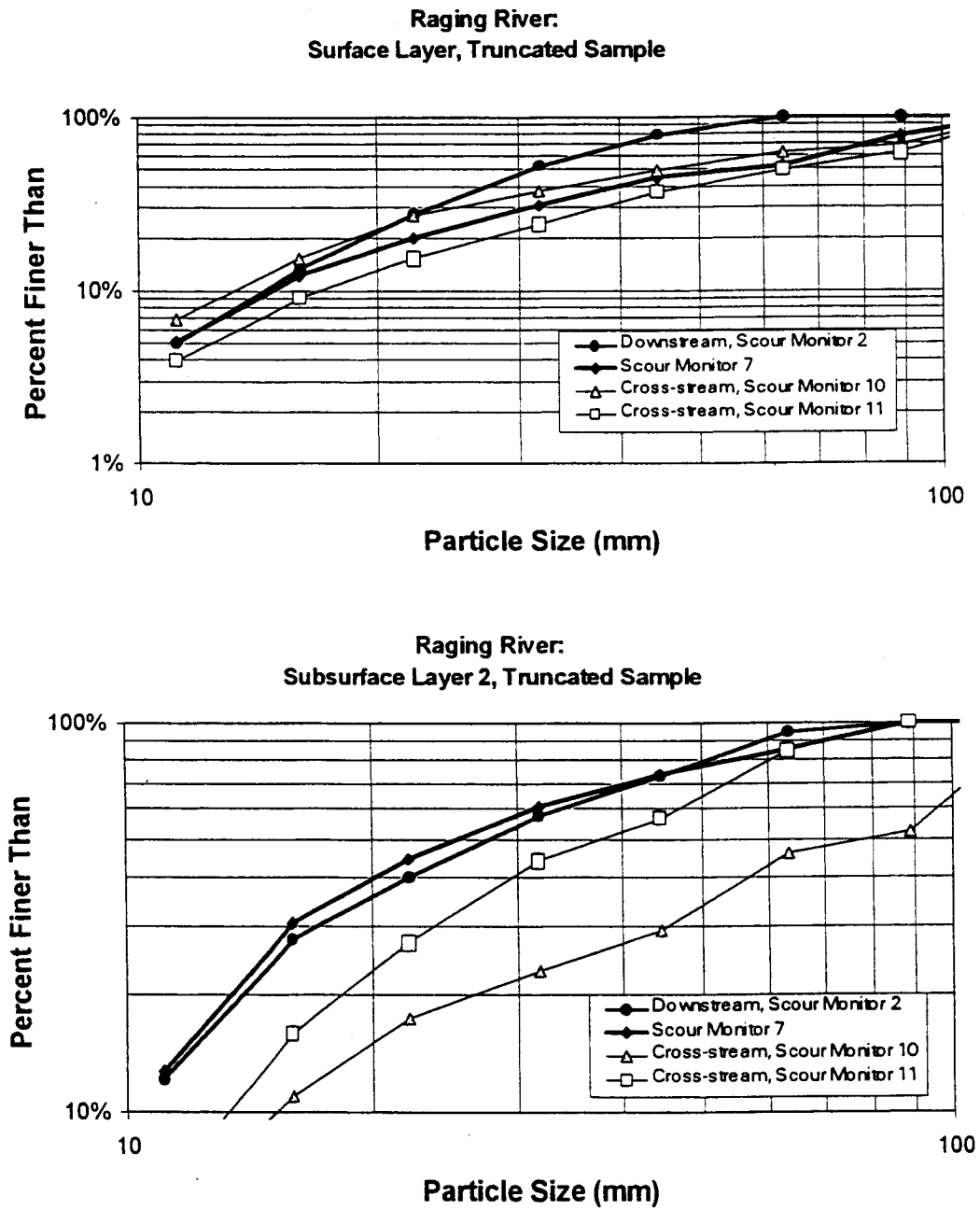
Figure I-4. Comparisons of grain size distributions (truncated at 8 mm and 127 mm) of different vertical layers of the streambed of the Raging River site.

S Fk Snoqualmie River:
Surface Layer, Truncated Sample

S Fk Snoqualmie River:
Subsurface Layer 2, Truncated Sample

Figure I-5. Comparisons of grain size distributions (truncated at 8 mm and 127 mm) of different vertical layers of the streambed of the South Fork Snoqualmie River site.
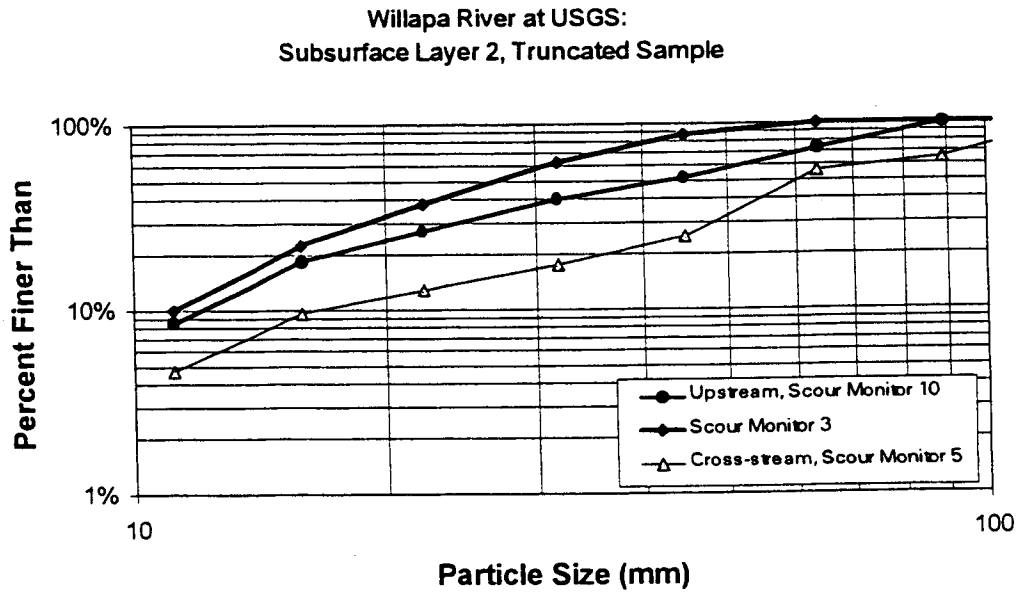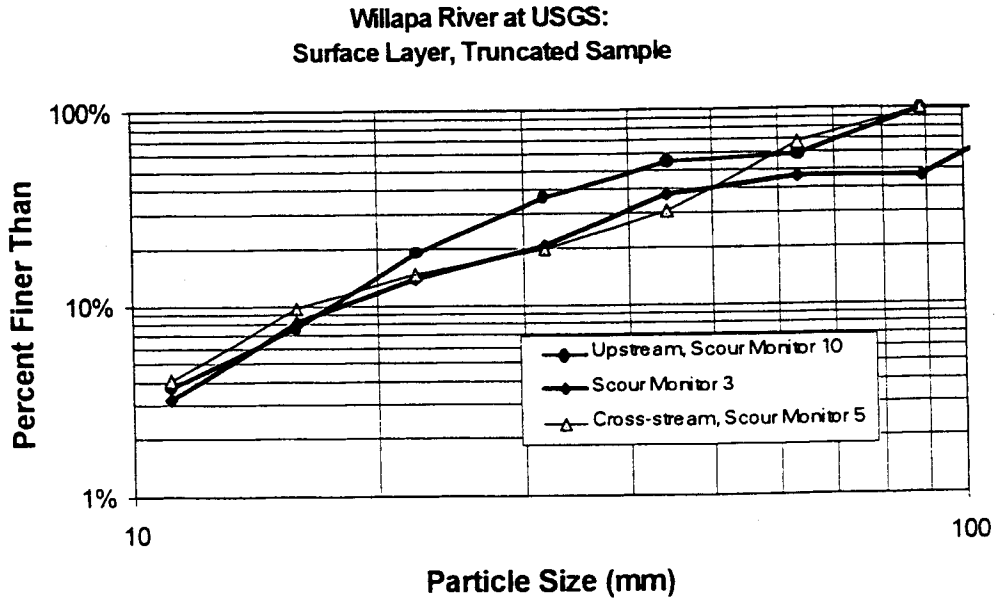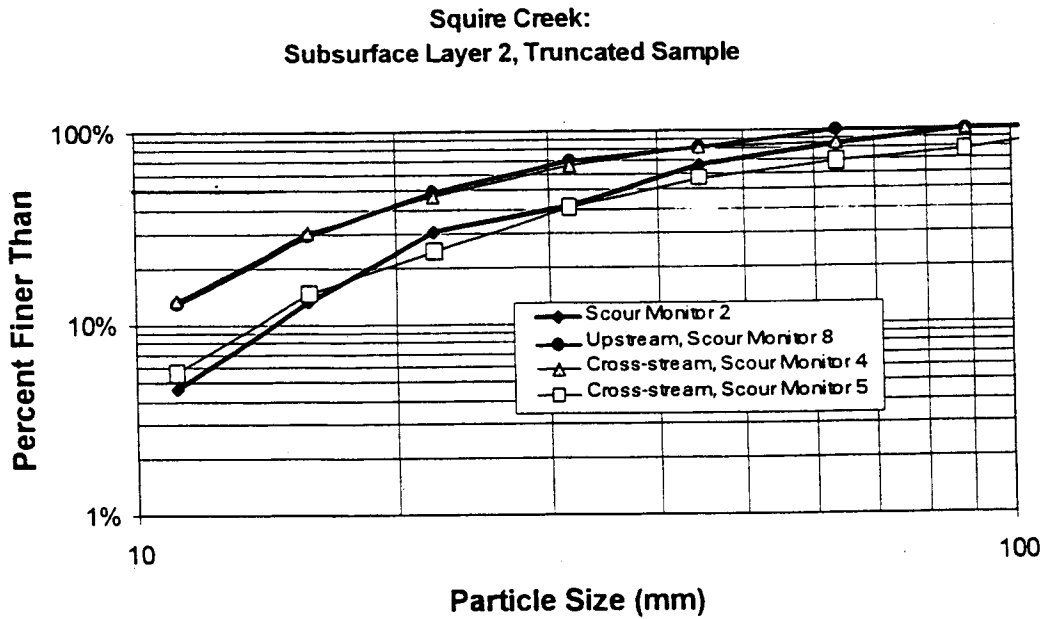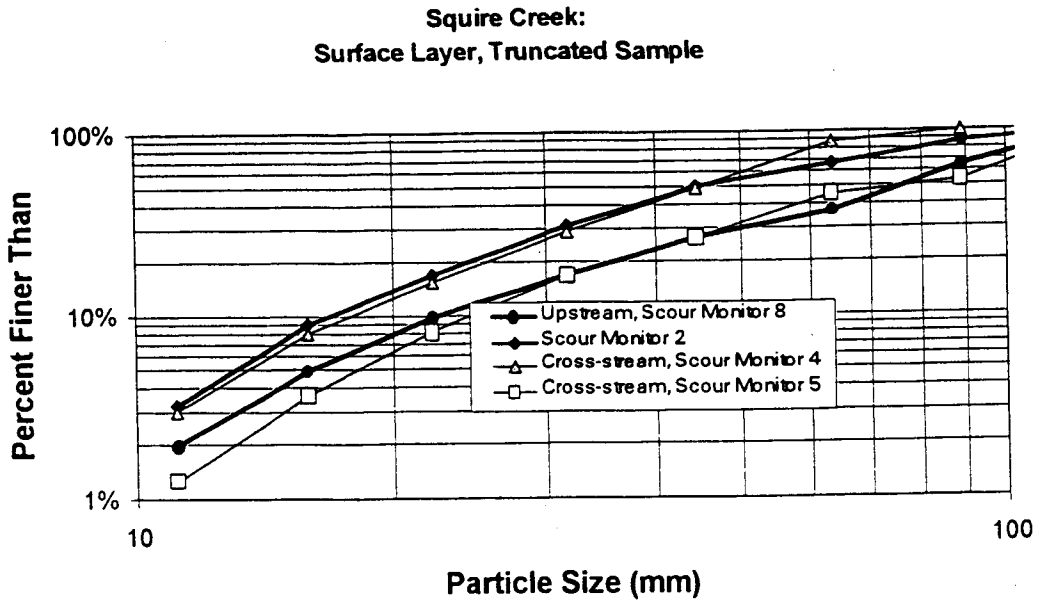
Figure I-8. Comparisons of grain size distributions (truncated at 8 mm and 127 mm) of different vertical layers of the streambed of the Willapa River at USGS site.

Squire Creek:
Scour Monitor 2, Truncated Sample

Squire Creek:
Scour Monitor 4, Truncated Sample
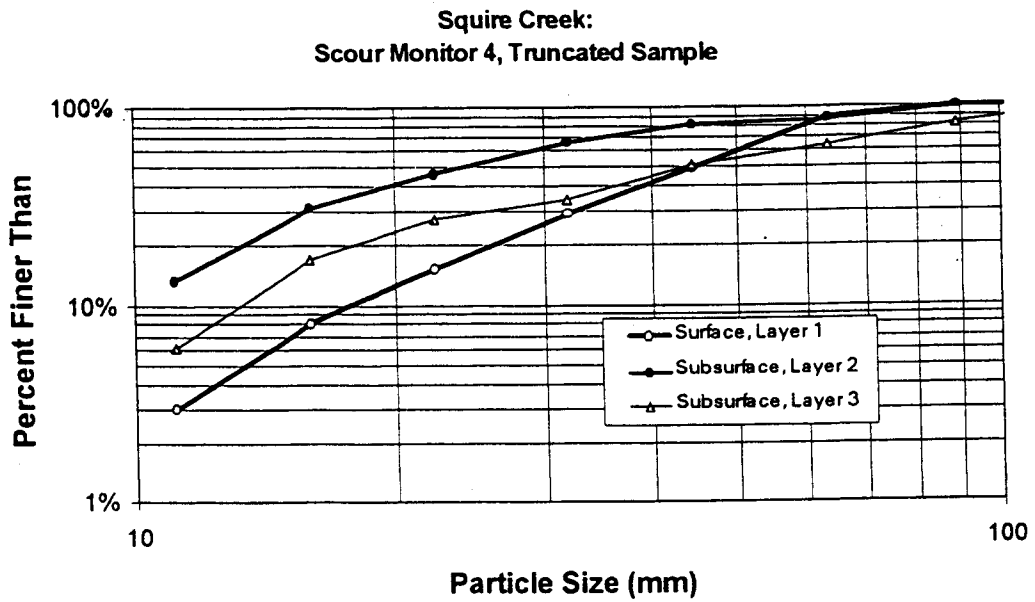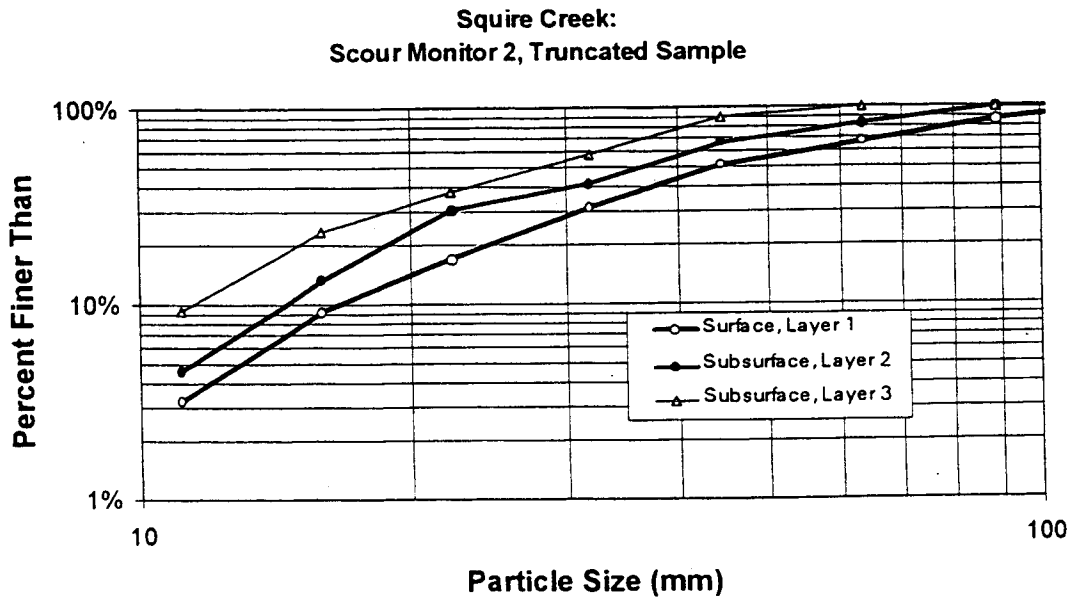
Figure I-6. Comparisons of grain size distributions (truncated at 8 mm and 127 mm) of different vertical layers of the streambed of the Squire Creek site.

Figure I-7. Comparisons of grain size distributions (truncated at 8 mm and 127 mm) of different vertical layers of the streambed of the Squire Creek site.